



Fate of Psychotropic Drugs in the Aquatic Environment: Assessment of Dead-End Photo-degradation Products Generated Under Varying Conditions by Combination of Experimental and *In-Silico* Methods

Kumulative Dissertationsschrift

von der Fakultät Nachhaltigkeit der Leuphana Universität Lüneburg zur Erlangung
des Grades

Doktor der Naturwissenschaften

(Dr. rer. nat.)

Angefertigt am Institut für nachhaltige Chemie und Umweltchemie

Leuphana Universität Lüneburg

genehmigte Dissertation von

Nareman Dahshan Henedaq Khaleel

geboren am 01. Jan. 1986, in Ismailia, Ägypten

Eingereicht am: 25.06.2020
Erstbetreuer und Erstgutachter: Prof. Dr. Klaus Kümmerer
(Leuphana Universität Lüneburg)
Zweitgutachter: Prof. Dr. Ralf Ebinghaus
(Helmholtz Zentrum, Geesthacht)
Drittgutachter: Prof. Dr. Carolin Floeter
(Hamburg University of Applied Sciences)

Die einzelnen Beiträge des kumulativen Dissertationsvorhabens sind wie folgt in Zeitschriften veröffentlicht:

1. **Nareman D.H. Khaleel, Waleed M.M. Mahmoud, Oliver Olsson, Klaus Kümmerer.** UV-photodegradation of desipramine: Impact of concentration, pH and temperature on formation of products including their biodegradability and toxicity. *Science of The Total Environment*. 566-567 (2016), pp. 826-840.
Doi: 10.1016/j.scitotenv.2016.05.095
2. **Nareman D.H. Khaleel, Waleed M.M. Mahmoud, Oliver Olsson, Klaus Kümmerer.** Initial fate assessment of teratogenic drug trimipramine and its photo-transformation products - role of pH, concentration and temperature. *Water Research* 108 (2017), pp. 197-211.
Doi: 10.1016/j.watres.2016.10.078
3. **Nareman D.H. Khaleel, Waleed M.M. Mahmoud, Oliver Olsson, Klaus Kümmerer.** Studying the fate of the drug Chlorprothixene and its photo transformation products in the aquatic environment: Identification, assessment and priority setting by application of a combination of experiments and various *in silico* assessments. *Water Research* 149 (2018), pp. 467-476.
Doi: 10.1016/j.watres.2018.10.075.

Nachdruck am Ende dieser Arbeit mit freundlicher Genehmigung der Elsevier B.V.



Fate of Psychotropic Drugs in the Aquatic Environment: Assessment of Dead-End Photo-degradation Products Generated Under Varying Conditions by Combination of Experimental and *In-Silico* Methods

This cumulative thesis
is submitted to the Faculty of Sustainability of Leuphana University Lüneburg to earn
the academic degree of
Doctor of Natural Science
(Dr. rer. nat.)

Carried out at the Institute of Sustainable and Environmental Chemistry
Leuphana University of Lüneburg

Dissertation submitted by
Nareman Dahshan Henedaq Khaleel
Born on 01. January 1986, in Ismailia, Egypt

Submitted on: 25.06.2020

Doctoral advisor and first reviewer: Prof. Dr. Klaus Kümmerer
(Leuphana Universität Lüneburg)

Second reviewer: Prof. Dr. Ralf Ebinghaus
(Helmholtz Zentrum, Geesthacht)

Third reviewer: Prof. Dr. Carolin Floeter
(Hamburg University of Applied Sciences)

The individual articles constituting this cumulative doctoral dissertation meet the formal requirements for a cumulative dissertation. The PhD thesis consists of the following publications:

1. **Nareman D.H. Khaleel, Waleed M.M. Mahmoud, Oliver Olsson, Klaus Kümmerer.** UV-photodegradation of desipramine: Impact of concentration, pH and temperature on formation of products including their biodegradability and toxicity. *Science of The Total Environment*. 566-567 (2016), pp. 826-840.
Doi: 10.1016/j.scitotenv.2016.05.095
2. **Nareman D.H. Khaleel, Waleed M.M. Mahmoud, Oliver Olsson, Klaus Kümmerer.** Initial fate assessment of teratogenic drug trimipramine and its photo-transformation products - role of pH, concentration and temperature. *Water Research* 108 (2017), pp. 197-211.
Doi: 10.1016/j.watres.2016.10.078
3. **Nareman D.H. Khaleel, Waleed M.M. Mahmoud, Oliver Olsson, Klaus Kümmerer.** Studying the fate of the drug Chlorprothixene and its photo transformation products in the aquatic environment: Identification, assessment and priority setting by application of a combination of experiments and various *in silico* assessments. *Water Research* 149 (2018), pp. 467-476.
Doi: 10.1016/j.watres.2018.10.075.

Reprinted at the end of this thesis with the permission of Elsevier B.V.

Acknowledgments

This thesis was supported by the Federal Ministry of Education within the framework of the RiSKWa joint project SAUBER⁺ (grant number: 02WRS1280AJ). I would like also to thank the Leuphana University in Lüneburg for their financial support (ProScience Forschungsförderfonds für Nachwuchswissenschaftlerinnen).

First, I would like to express my sincere gratitude to my great supervisor Prof. Dr. Klaus Kümmerer for the scientific support and for giving me the chance to work in his research group. I greatly appreciate the support I have gained from him, all the experience, advice and motivation I gained during my whole PhD studies. I also thank him for the valuable suggestions and discussions that have put me on the right way. Thankful and grateful to have him as a supervisor.

Many thanks go to Dr. Oliver Olsson for his help, advice, suggestions, and answering to my questions. I very much appreciate his support and his discussions that helped me in this thesis.

In general, I would like to thank all my colleagues and dear friends (Evgenia, Anette, Lamia, Tushar, Lukasz, Ewelina, Janin, Karen, Christoph and Kham Dieu Huynh) at the Institute of Sustainable and Environmental Chemistry in Lüneburg for the great cooperation and the helpful scientific discussions, advices and suggestions which helped me to complete this thesis.

I would like to thank Manuel Herrmann for the discussions and for his help in choosing the substances that I worked with.

I wish to say thank you to Marcello Wilde for all his support, help and advice in my work.

Heartfelt thanks to my husband and my colleague Waleed M. M. M. Ahmed for his support, his continuous inspiration and help on the scientific research work, sharing of my stresses and burdens and suffering from my bad temper, taking care of the children and giving me the strength to go through with this thesis. Without his help and support, I would not be able to achieve any step in my career. His Love, support, and patience have taught me so much about sacrifice, discipline, and compromise.

Many thanks from the bottom of my heart go to my sons; Mohamed, Omar und Yasin for being with me through my hard times. Their laughter, drawings, jokes and achievements softened my hard days.

I would like to thank my parents, who always supported, encouraged and believed in me, my brother Mohamed and my sisters Hayam and Shaimaa for standing behind me with their love and support.

Many thanks to my family and friends here and in Egypt for their countless support, encouragement and all the good time we had spent together.

Finally, no word can express my gratitude to Allah for providing me the blessings to complete this work.

Zusammenfassung

Das Vorhandensein von pharmazeutischen Arzneimitteln und ihren Nebenprodukten als organische Umweltkontaminanten in einer Vielzahl von Ökosystemen und ihre potenziellen Auswirkungen auf die Umwelt ist ein bekannter Aspekt, der in den letzten Jahren immer wieder angesprochen wurde. Die Untersuchung der Transformation von Arzneimitteln im aquatischen System ist sehr wichtig, da sie zur Bildung vieler neuer Transformationsprodukte (TPs) führen kann, die unterschiedlichen Eigenschaften haben können (z. B. mobiler, toxischer oder in höheren Konzentrationen vorhanden) und dadurch in die Umweltkompartimente gelangen können, die von ihren Ausgangsverbindungen nicht betroffen sind. Dennoch sind viele der pharmazeutischen Medikamente nicht gut reguliert oder kontrolliert und sie können viele negative Auswirkungen auf die Umwelt und/oder die menschliche Gesundheit haben. Darüber hinaus wird der Einfluss der kontinuierlichen Änderung der Umgebungsbedingungen wie pH-Wert, Temperatur und Ausgangskonzentration auf das Transformationsverhalten von Pharmazeutika in vielen Forschungen übersehen, obwohl er von hohem Interesse ist.

Psychopharmaka gehören zu den Arzneimitteln, deren Gefährdungspotenzial einschließlich des Verbleibs in der Umwelt und des Verhaltens im Vergleich zu anderen Arzneimitteln wie z. B. Antibiotika noch nicht gut verstanden ist. Psychopharmaka werden in hohem Maße verwendet, und ihr weltweiter Verbrauch ist heutzutage vor allem in den entwickelten Ländern wie Europa und den Vereinigten Staaten gestiegen. Darüber hinaus sind sie in verschiedenen Umweltkompartimenten in hohem Maße vorhanden und können eine Vielzahl von toxikologischen Problemen verursachen. Trimipramin (TMP), Desipramin (DMI) und Chlorprothixen (CPTX) sind drei Psychopharmaka mit eng verwandten chemischen Strukturen. Sie wurden für die Untersuchung in dieser Arbeit ausgewählt, da sie zu den weltweit an den häufigsten verschriebenen Psychopharmaka gehören und in der Umweltforschung nur wenige Daten zu ihrem Verbleib in der Umwelt (z.B. Abbau oder Transformation und Verbleib der TPs) vorliegen.

Um die ökologische Wirkung der Pharmazeutika auf Wasserorganismen zu untersuchen und ihren Verbleib im aquatischen System zu studieren, werden Labor-Bioabbau- und Photodegradationstests empfohlen. Die Verwendung der LC-MS/MS-Analyse mit der Kombination von Photolyse- und Biodegradationstests zur Identifizierung der gebildeten TPs und zur Untersuchung der biologischen Abbaubarkeit und der Persistenz der TPs ist ein hilfreicher neuer Einblick in das Umweltverhalten der Schadstoffe und ihrer TPs. Unterschiedliche Umweltbedingungen können den Verbleib von Pharmazeutika in der Umwelt beeinflussen. Daher kann die Beantwortung der Frage, wie verschiedene Variablen wie Temperatur, pH-Wert und Ausgangskonzentration das Abbaumuster von Pharmazeutika beeinflussen könnten, wertvolle Informationen über deren Verbleib in der Umwelt liefern. Toxizitätsbewertungen von Kontaminanten und ihren TPs mit Hilfe von In-silico-Software, die auf quantitativen Struktur-Aktivitäts-Beziehungsmodellen (QSAR) basiert, können besonders im Fall von

TPs eine gute Wahl sein, da die TP's meist nicht kommerziell verfügbar sind und IV meist nur in geringen Konzentrationen innerhalb komplexer Matrices gebildet werden, so dass eine Isolierung und Reinigung sehr schwierig sind.

Dementsprechend war das Prinzip dieser Arbeit, das Umweltschicksal von drei stark genutzten Psychopharmaka zu untersuchen, und dies wurde erreicht durch: 1) die Untersuchung der biologischen Abbaubarkeit von TMP, DMI und CPTX, 2) Untersuchung des Verhaltens von TMP, DMI und CPTX in Photodegradationstests unter Verwendung von Xe- und UV-Lampen mit Untersuchung des Einflusses verschiedener Umgebungsbedingungen auf ihr UV-Photodegradationsverhalten, 3) Überwachung der primären Eliminierung von TMP, DMI und CPTX während der Photodegradations- und Bioabbau-Tests mit HPLC und Messung ihres Mineralisierungsgrades mit Hilfe eines Analysators für gelösten organischen Kohlenstoff (DOC), 4) Aufklärung der Strukturen der TP's, die während des Abbaus von TMP, DMI und CPTX gebildet werden, mittels LC-MS/MS-Analyse, 5) die biologische Abbaubarkeit ihrer TP's durch Labortests und In-silico-Bewertungen zu analysieren, um den Verbleib und die Persistenz dieser TP's in der aquatischen Umwelt zu bestimmen, 6) Durchführung von in-silico-Toxizitätsvorhersagen für die ausgewählten Psychopharmaka und ihre TP's beim Menschen (Karzinogenität, Genotoxizität und Mutagenität) und im Ökosystem (Toxizität gegenüber Mikroorganismen und Toxizität in Regenbogenforellen).

TMP, DMI und CPTX erwiesen sich im Closed Bottle Test (CBT) und im Manometric Respiratory Test (MRT) als nicht leicht biologisch abbaubar. Sie zeigten keine signifikante Eliminierung oder Mineralisierung innerhalb von 128 Minuten nach Bestrahlung mit einer Xenon-Lampe. In den UV-photoabbau Proben zeigten die LC-MS/MS-Ergebnisse die Eliminierung der drei Psychopharmaka mit entsprechenden vergleichsweise geringeren Mineralisierungsgraden, was auf die Bildung von reichlich Photo-TP's hinweist.

Aus den UV-Photolyse-Tests, die unter verschiedenen Umgebungsbedingungen durchgeführt wurden, lässt sich schließen, dass die Abbaugeschwindigkeit von TMP, DMI und CPTX abnimmt, wenn ihre Ausgangskonzentrationen steigen. Der pH-Wert beeinflusste das Photodegradationsverhalten von TMP, DMI und CPTX mit unterschiedlichem Muster, abhängig von vielen Faktoren wie Löslichkeit, molarem Absorptionskoeffizienten (ϵ), Ionisierungsform und chemischer Struktur. Die Temperaturerhöhung zeigte keinen signifikanten Effekt auf die Photodegradationsleistung von DMI und CPTX, während sie einen erhöhten Effekt auf die Photodegradationsleistung von TMP zeigte. Dies könnte daran liegen, dass die Moleküle von DMI und CPTX die für den Abbau benötigte Energie bei niedriger Temperatur erreichen können. Während TMP's Moleküle noch etwas mehr Energie benötigen, um abgebaut zu werden und die Temperatur hilft ihnen, diese erforderliche Aktivierungsenergie leicht zu erreichen.

Die Aufklärung der TPs und die Untersuchung der Abbaupfade für TMP, DMI und CPTX während der UV-Bestrahlung zeigten, dass die Hydroxylierung der häufigste Pfad ist, gefolgt von Oxidation und Isomerisierung. Bei der UV-Umwandlung von CPTX wurde ein De-Chlorierungsweg beobachtet. Deaminierung und Verlust der aliphatischen Seitenkette wurden nur während der UV-Transformation von TMP beobachtet, während sie bei der DMI- und CPTX-Transformation nicht beobachtet wurden. Dies deutet darauf hin, dass die Bindung zwischen der Aminogruppe und der aliphatischen Seitenkette in DMI und CPTX im Vergleich zur gleichen Bindung in TMP widerstandsfähiger gegen Photodegradation sein kann. Dies könnte auf das Vorhandensein von zusätzlichen Methylgruppen im TMP-Molekül zurückzuführen sein, die die zuvor erwähnte Bindungsstärke verringern können.

Biologische Abbaubarkeitstests, die für Gemische durchgeführt wurden, die die Psychopharmaka und ihre TPs enthalten, zeigten geringe biologische Abbaubarkeitsergebnisse. Trotzdem wurde die Eliminierung einiger TPs in der LC-MS/MS-Analyse am Ende dieser biologischen Abbautests beobachtet. Dies deutet darauf hin, dass einige TPs wahrscheinlich biologisch abbaubar sind und diese Fähigkeit durch die vorherrschende Wirkung anderer nicht biologisch abbaubarer Verbindungen behindert wurde. In-silico-Vorhersagen zeigten, dass die Phototransformation für viele Endpunkte zu einer erhöhten Toxizität beim Menschen und für Wasserorganismen im Vergleich zur Ausgangsverbindung führen könnte.

Als Gesamtfazit zeigt die vorliegende Arbeit, dass eine Kombination aus Laborsimulationstests, LC-MS/MS-Analyse und In-silico-Tools zu wertvollen neuen Informationen über den Verbleib dreier wichtiger Psychopharmaka und ihrer TPs in der Umwelt führt. Diese Dissertation macht auch deutlich, dass unterschiedliche Umgebungsbedingungen wie Temperatur, anfängliche Wirkstoffkonzentration und pH-Wert das Abbauverhalten von Pharmazeutika unterschiedlich beeinflussen können, selbst wenn sie strukturell stark verwandt sind. Daher kann man nicht von einem Arzneimittel auf ein anderes schließen, sondern jedes muss einzeln untersucht werden, was eine große Herausforderung für die Risikobewertung der Kinetik von Chemikalien in der aquatischen Umwelt darstellt. Die hier vorgestellten Ergebnisse zeigten, dass die untersuchten Pharmazeutika und ihre TPs die Umwelt negativ beeinflussen können, was für das Ökosystem schädlich sein kann, da sie möglicherweise seit Jahrzehnten in der aquatischen Umwelt vorhanden sind, ohne dass ihr Umweltschicksal oder das damit verbundene Risiko bekannt ist. Daher müssen weitere Arbeiten durchgeführt werden, einschließlich der Analyse von Umweltproben (z. B. Oberflächengewässer) sowie Toxizitätstests im Labor, um das Wissen über ihre genauen Umweltauswirkungen zu erweitern.

Summary

The presence of pharmaceutical drugs and their by-products as environmental organic contaminants in a variety of eco-systems and their potential environmental impacts is a well-known aspect and has been raised in recent years. Studying the transformation of pharmaceutical drugs in the aquatic system is very important as it can lead to the formation of many new transformation products (TPs) that can have different properties (e.g. more mobile, toxic or present at higher concentrations) and this can enable them to reach the environmental compartments not affected by their parent compounds. Yet, many of the pharmaceutical drugs are not well regulated or controlled and they can cause a lot of adverse ecological and/or human health effects. In addition, impact of the continuous change in the environmental conditions such as pH, temperature and initial concentration on the transformation behaviour of pharmaceuticals is overlooked in many researches although it is of high interest.

Psychotropic drugs are among the pharmaceuticals which their potential hazards including environmental fate and behaviour is still not well understood compared to other drugs such as antibiotics. Psychotropic drugs are highly used, and their worldwide consumption has been increasing nowadays especially in developed countries such as Europe and the United States. Furthermore, they are highly found in different environmental compartments and can cause a lot of toxicological problems. Trimipramine (TMP), Desipramine (DMI) and Chlorprothixene (CPTX) are three psychotropic drugs with closely related chemical structures and they are selected to be studied in this thesis as they are among the worldwide commonly prescribed psychotropic drugs and data available on their environmental fate (e.g., degradation or transformation and fate of the TPs) is lacking in the environmental researches.

To investigate the ecological impact of the pharmaceuticals on water organisms and to study their fate in the aquatic system, laboratory biodegradation and photodegradation tests are recommended. The use of LC-MS/MS analysis with the combination of photolysis and biodegradation tests to identify the formed TPs and to study the biodegradability and the persistence of the TPs is a helpful new insight into the environmental behaviour of contaminants and their TPs. Different environmental conditions can affect the fate of pharmaceuticals in the environment, therefore answering the question how different variables such as temperature, pH and initial concentration could affect the degradation pattern of pharmaceuticals can provide valuable information regarding their environmental fate. Toxicity assessments of contaminants and their TPs using *in-silico* software based on quantitative structure activity relationship (QSAR) models can be a good choice especially in case of TPs because the TPs are mostly not available commercially and

are usually only formed in low concentrations within complex matrices so that isolation and purification are very difficult.

Accordingly, the principle of this thesis was to study the environmental fate of three highly used psychotropic drugs and this achieved through: 1) examining the biodegradability of TMI, DMI and CPTX, 2) studying the behaviour of TMP, DMI and CPTX in photodegradation tests using Xe and UV lamps with studying the effect of different environmental conditions on their UV-photodegradation behaviour, 3) monitoring the primary elimination of TMP, DMI and CPTX during photodegradation and biodegradation tests using HPLC, and measuring their degree of mineralization by means of dissolved organic carbon analyser (DOC), 4) elucidating the structures of the TPs which formed during the degradation of TMI, DMI and CPTX by using LC-MS/MS analysis, 5) analysing the biodegradability of their TPs by laboratory tests and *in-silico* assessments in order to determine the fate and persistence of these TPs in the aquatic environment, 6) conducting *in-silico* toxicity predictions for the selected psychotropic drugs and their TPs in human (carcinogenicity, genotoxicity and mutagenicity) and in eco-system (toxicity to microorganisms and toxicity in rainbow trouts).

TMP, DMI and CPTX were found to be not readily biodegradable in Closed Bottle test (CBT), and in Manometric Respiratory test (MRT). They did not show any significant elimination or mineralization within 128 minutes of irradiation using a xenon Lamp. In UV-photodegradation samples, LC-MS/MS results showed elimination of the three psychotropic drugs with corresponding comparatively lower degrees of mineralization indicating formation of abundant photo-TPs.

From the UV-photolysis tests, which were carried out under different environmental conditions, it can be concluded that the degradation rates of TMP, DMI and CPTX decreased when their initial concentrations increased. pH affected the photodegradation behaviour of TMP, DMI and CPTX with different pattern depending on many factors such as solubility, molar absorption coefficient (ϵ), ionisation form and chemical structure. Temperature elevation showed non-significant effect on the photodegradation performance of DMI and CPTX, while showed an enhanced effect on the photodegradation performance of TMP. This could be because the molecules of DMP and CPTX can reach the sufficient energy required for degradation at low temperature. While TMP's molecules still require some more energy to undergo degradation and temperature helps them to reach easily these required activation energy.

Elucidating the TPs and studying the degradation pathways for TMP, DMI and CPTX during UV irradiation indicated that hydroxylation is the most abundant pathway followed by oxidation and isomerization. De-chlorination pathway was observed during the UV-transformation of CPTX.

Deamination and loss of the aliphatic side chain were observed only during the UV-transformation of TMP, while not observed during DMI and CPTX transformation. This indicates that the bond between the amino- group and the aliphatic side chain in DMI and CPTX can be more resistant to photodegradation compared to the same bond in TMP. This could be due to the presence of extra methyl groups in TMP molecule which can decrease the previously mentioned bond strength.

Biodegradation tests performed for photodegradation mixtures, which contain the psychotropic drugs and their TPs, showed low biodegradation results. Despite that, elimination of some TPs was observed in the LC-MS/MS analysis at the end of these biodegradation tests. This indicates the probability of biodegradation ability for some TPs and this ability was hindered by the predominant effect of other non-biodegradable compounds. *In-silico* predictions showed that for many endpoints, photo-transformation might lead to an increased toxicity in humans and to water organisms compared with the parent compound.

As an overall conclusion, the present work demonstrates that a combination of laboratory simulation tests, LC-MS/MS analysis and *in-silico* tools result in valuable new information regarding environmental fate of three important psychotropic drugs and their TPs. This dissertation also highlights that different environmental conditions such as temperature, initial drug concentration and pH can differently affect the degradation behaviour of pharmaceuticals even when they are highly structurally related. Therefore, one cannot conclude from one pharmaceutical to another but each one needs to be investigated individually and this present a great challenge for risk assessment kinetics of chemicals in the aquatic environment. The results presented here showed that the investigated pharmaceuticals and their TPs can negatively affect the environment which may be harmful to the ecosystem as they might have been present for decades in the aquatic environment without any knowledge of their environmental fate or connected risk. Therefore, further work needs to be done including analysis of environmental samples (e.g., surface waters), as well as laboratory toxicity tests to further expand knowledge on their exact environmental impact.

List of Abbreviations

BOD	Biological oxygen demand
CBT	Closed Bottle Test
CFU	Colony forming unit
COD	Chemical oxygen demand
CPTX	Chlorprothixene
DOC	Dissolved organic carbon
DMI	Desipramine
EIC	Extracted ion chromatogram
HO•	Hydroxyl radical
HPLC	High performance liquid chromatography
LOD	Limit of detection
LC-MS/MS	Liquid Chromatographic tandem Mass Spectrometry
MRT	Manometric Respiratory Test
MS	Mass spectrometry
m/z	Mass-to-charge-ratio
OECD	Organization for Economic Co-operation and Development
PTP	Photo transformation product
QSAR	Quantitative structure activity relationship
RSD	Relative standard deviation
STPs	Sewage treatment plant
ThOD	Theoretical oxygen demand
TIC	Total ion chromatogram
TMP	Trimipramine
TP	Transformation product
t_R	Retention time
UV	Ultraviolet
<i>V. fischeri</i>	<i>Vibrio fischeri</i>

Table of contents

Acknowledgments	I
Zusammenfassung	III
Summary	VI
List of Abbreviations	IX
Table of Contents	X
1. Introduction and motivation	1
1.1 Psychotropic drugs	1
1.2 Transformation products	2
1.3 Research gap	3
2. Aims and objectives	3
3. Research approach and methods	3
3.1 Selection criteria	4
3.2 Environmental fate assessment	4
4. Results and discussion	5
5. Synopsis	21
6. Concluding remarks and outlook	22
7. References	23
Appendices	27

1. Introduction and motivation

1.1. Psychotropic drugs

During the past few decades, a growing world population along with better medical care have drastically increased the consumption of pharmaceuticals (Gómez-Canela et al., 2019; Santiago-Martín et al., 2020). Due to the increasing mental pressure in a meritocratic society and due to the rising environmental air pollution and water pollution, the prevalence of mental diseases and the importance of psychiatric hospitals were expected to increase (Janssens et al., 2014) and it is increasing. Depression was expected to be the second most serious illness, with respect to global disease burden (Lajeunesse et al., 2008; Trachta et al., 2004). The use of psychotic drugs has been increasing mainly in developed countries such as Europe and the United States (Lasserre et al., 2010; Optenberg et al., 2002). One in six adults in the USA reported taking a psychiatric drug in 2013. In Germany, the number of cases treated in psychiatric hospitals and people living in nursing homes has increased consecutively by about 13% between 2005 to 2011 (Langford and Thomas, 2009). The worldwide consumption of antipsychotics is increasing, and they have been found in different environmental compartments (Herrmann et al., 2016; Reichert et al., 2019; Writer et al., 2013; Yuan et al., 2013).

Psychotropic drugs are very harmful to the ecosystem because they affect not only the central nervous system but also are linked with reproduction, growth and immune functions. In addition, they can cause multiple physiological side effects in humans such as weight gain, fatigue and sexual dysfunction. Yet, there is a considerable lack in information about the fate of psychotropic drugs in the environment. Thus, their occurrence and fate in the aquatic system is an important environmental issue.

Three psychotropic drugs with very closely related chemical structures were selected to be investigated in this thesis: Trimipramine (TMP), Desipramine (DMI) and Chlorprothixene (CPTX). TMP is a worldwide commonly prescribed tricyclic antidepressant (TCA) and it was already detected in the sewage treatment plants in Germany (Fakhari et al., 2012). The presence of TMP in the aquatic environment could be harmful because TMP has teratogenic properties and may have eco-toxic effects. DMI is one of the highly used TCAs and it is at the same time the major metabolite of another two widely used TCAs named “Imipramine (IMI) and Lofepamine (LMI)” (Önal and Öztunç, 2011). CPTX is a widely used neuroleptic of the thioxanthene class and it is used mainly in nursing homes and in psychiatric hospitals (Herrmann et al., 2015b). CPTX has strong sedative effect; therefore, it is prescribed also for anxiety and agitation.

1.2. Transformation products

Transformations of any chemical compound such as pharmaceuticals are often described by detailed kinetic reaction mechanisms, which may include several hundred reaction steps. Transformation of chemicals and pharmaceuticals in the aquatic system is either biotic or abiotic degradation and it can lead to the formation of several transformation products (TPs). To understand and take into consideration these degradation processes and their resulting products, it is worthy to carry out a mean of simulation tests on the degradation of chemicals in the aquatic environment (Alexy et al., 2004; Lege et al., 2020). Biotic degradation is based exclusively on the activity of microorganisms such as bacteria and fungi. Abiotic degradation and transformation processes, such as photolysis and hydrolysis, are of great importance for the environmental fate of chemicals and pharmaceuticals. Photolysis is among the most important abiotic degradation mechanisms for many pollutants. The incomplete biotic and/or abiotic degradation of pharmaceuticals occurring in the environment or during treatment processes can lead to the formation of many TPs with significantly different physical, chemical and toxic properties. Most of the TPs have not been identified and little is known about their environmental relevance. The description of TPs' fate in the environment and the assessment of their effects on the aquatic ecosystems are impeded by the lack of data. In general, the TPs can strongly differ from their parent compounds as they could have for example a negative effect on environmental organisms and/or could be more persistent than their parent compounds (Illés et al., 2014; Mahmoud et al., 2014).

It is important to better understand the relevance and the rate of formation of the TPs in the environment, therefore, at least preliminary establishment of the structures of TPs by analytical methods such as LC-MS/MS is relevant as TPs are often formed as new molecules and are usually formed in low concentrations within complex matrices. This renders their isolation and purification very challenging, expensive and tedious or not possible at all. Further, most of these TPs being new chemicals are not commercially available, which makes the individual analysis of their environmental fate impossible. *In-silico* approaches can help to close or at least narrow data gaps if no experimental data are available or difficult or time consuming to get. Accordingly, *in-silico* approaches are gaining importance especially for providing data and knowledge for analysing environmental fate and impact of the TPs. Therefore, it is helpful to apply *in-silico* approaches such as quantitative structure activity relationships (QSARs) to model and assess the properties of TPs and of their parent compounds, such as the potential for biodegradation and toxicity in the environment. Based on this knowledge, a further risk assessment of the TPs can be done in first line.

1.3. Research gap

Although the consumption of psychotropic drugs is high and can cause several adverse effects on the ecosystem, their potential hazard including their environmental fate and behaviour is still not well understood compared to other drugs. Information and data regarding TMP, DMI and CPTX behaviour in the aquatic environment or during the application of water treatment technologies is still plainly lacking in the international scientific literature. Additionally, knowledge regarding a possible formation of TPs and the fate and effects of these TPs in aquatic environment is especially limited. Furthermore, the effect of environmental variables, such as temperature, pH and initial compound concentration, that can affect the photodegradation behaviour of pharmaceuticals in the environment was mostly overlooked. The influence of these variables on TMP, DMI and CPTX degradation and on the TP's formation kinetics and the comparison between the three pharmaceuticals is unknown.

2. Aims and objectives

The main objective of this PhD thesis was the initial environmental fate assessment for three highly used psychotropic drugs and have closely related chemical structures (TMP, DMI and CPTX). Accordingly, the research aims were:

1. Investigation of the photodegradability and biodegradability of the selected pharmaceuticals.
2. Development of analytical methods for the identification of the TPs and for the elucidation of the degradation reaction pathways.
3. Biodegradation study for the formed TPs.
4. Studying and comparing the effect of changing the initial concentration, pH and temperature on the degradation kinetics of the selected compounds.
5. Comparing the TPs formed during degradation under different concentrations, solution pH and temperature.
6. Prediction of the potential toxicity for the studied psychotropic drugs and their TPs against humans and organisms in the aquatic environment.

3. Research approach and methods for the three included articles

The research approach is an in-depth analysis of the fate of three psychotropic drugs and their TPs in the aquatic system through studying their bio- and photo degradation including formation kinetics and assessment of their possibly formed TPs (Figure 1).

The increasing worldwide consumption of psychotropic drugs and their high environmental risk which is associated with the lack of data about their fate in the environment lead to the following research approach

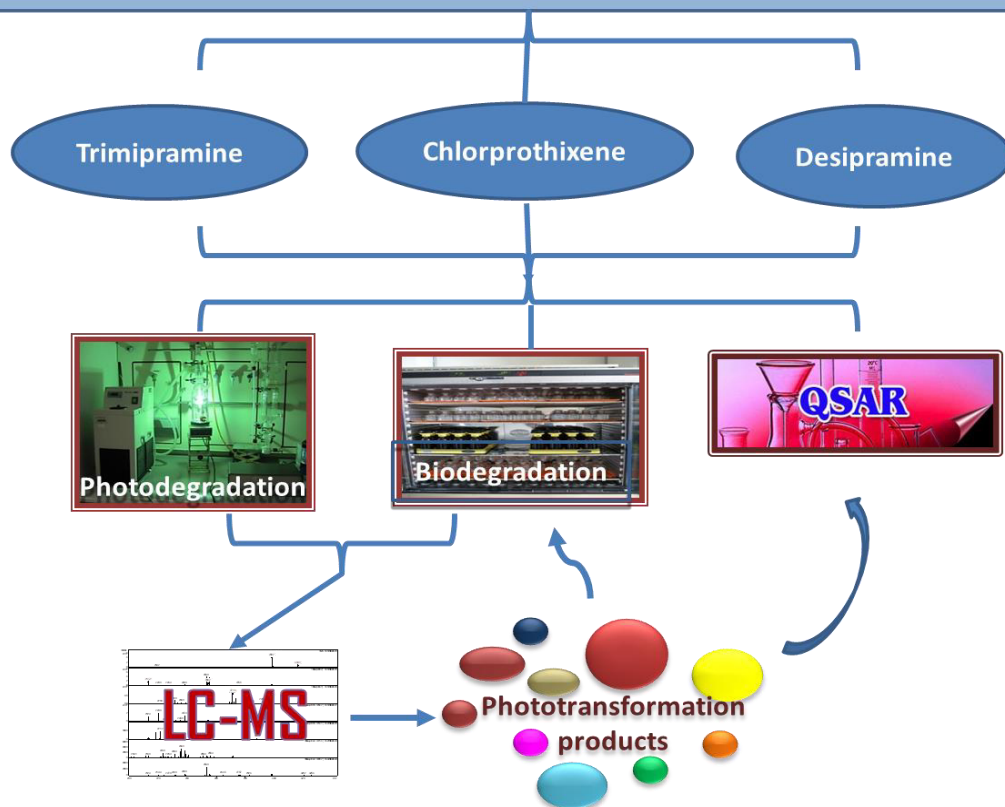


Figure 1: the research approach for the three articles in the thesis.

3.1. Selection criteria:

The first step to fulfil the main objectives of our research is the selection criteria for the investigated compounds which includes:

- I. Insufficient knowledge available up to now (TMP, DMP, and CPTX).
- II. High consumption worldwide (TMP, DMI, and CPTX).
- III. Possible high toxic effects to the ecosystem (TMP and CPTX).
- IV. Substance which is both a drug and a metabolite of other drugs (DMI).

3.2. Environmental fate assessment:

The environmental fate of the three selected psychotropic drugs and their connected risk were investigated through the application of the following tests:

1. Biodegradation tests were firstly studied using two tests from the Organization for Economic Cooperation and Development (OECD) series: Closed Bottle test (CBT; OECD 301 D) and Manometric Respiratory test (MRT; OECD 301 F).

2. Photodegradation tests in water using simulated sunlight (Xe-lamp) and UV-lamp were then performed according to the OECD guidelines (OECD-316, 2008). The effect of different conditions was studied through performing the UV photolysis tests under the following conditions:
 - (a) Four different starting concentrations: 5 mg L⁻¹, 10 mg L⁻¹, 50 mg L⁻¹ and 100 mg L⁻¹.
 - (b) Four different pH values: 3, 5, 7 and 9.
 - (c) Four different temperatures: 10, 20, 30 and 40 °C.
3. The primary elimination of TMP, DMI and CPTX during biodegradation and photodegradation tests was monitored by high-performance liquid chromatography ultraviolet analysis (HPLC-UV). The sufficient resolution, good sensitivity and acceptable analysis time for the developed liquid chromatographic separation of the studied compounds were obtained by adjusting different chromatographic factors mainly stationary-phase composition (column type and size), mobile phase compositions, column oven temperature and flow rate.
4. The degree of mineralization during photodegradation and biodegradation experiments were studied by DOC measurement using a Total Organic Carbon (TOC) Analyzer.
5. CBT and MRT were performed then for photolysis mixtures at different time points which contain the parent compounds with their TPs.
6. Structures of the newly formed TPs were elucidated and predicted using LC-MS/MS (ion trap, and orbitrap) analysis. LC-MS/MS analysis used also to follow the formation curves of the formed TPs during photodegradation and biodegradation tests.
7. QSAR models were used to predict the log P values for each newly identified TP. The predicted log P values were used in the preliminary differentiation between the TP isomers following the concept that the compound which has lower log P value, in case of using reversed phase C18 column, is more polar and therefore has relative lower retention time (t_R) and vice versa.
8. A set of *in-silico* prediction software package was applied for supporting biodegradation results, and for generating data for the ecotoxicity and the human toxicity (endpoints: carcinogenicity, genotoxicity and mutagenicity) assessment of the three studied psychotropic drugs and their TPs.

4. Results and Discussion

Before studying the biodegradability or the influence of pH value of the irradiated solution on the UV photodegradation performance of TMP, DMI and CPTX, the stability of the selected drugs in dark controls i.e. hydrolysis under the studied pH range was studied and showed the following results:

- 1- TMP was stable and showed no significant change in its concentration in dark control experiments performed at $\text{pH} \leq 7$. In dark control test at $\text{pH} 9$, 100 mg L^{-1} TMP solution showed slight turbidity and approximately 24% from its initial concentration precipitated. This happened because TMP solubility decreases in alkaline media (Tuckerman, 1984).
- 2- DMI was stable and showed no significant change in terms of stability in the studied pH range.
- 3- CPTX was found to be stable and completely soluble at $\text{pH} < 7$. At $\text{pH} 7$, CPTX dissolved concentration (100 mg L^{-1}) decreased and the solution became a little turbid and about 25% of the added CPTX precipitated. CPTX precipitates completely at $\text{pH} 9$ and a fluctuation in the concentration during the test was observed affecting the quality of the test. Therefore, photodegradation of CPTX at $\text{pH} 9$ was not studied.

Low biodegradation results after 28 days in CBT and MRT were found for TMP, DMI and CPTX, and the LC-MS/MS analysis of the biodegradation samples confirmed no elimination. No toxic effect was observed on the inoculum in the toxicity controls of their performed biodegradation tests. Therefore, they classified as being not readily biodegradable substances. The presence of three aromatic rings and chloride substituent in their structures can be the main reason of their low biodegradation results as these fragments were reported to retard biodegradation ability of compounds (Loonen et al., 1999).

Using a Xenon lamp (simulated sun light) for 128 min to the psychotropic drugs solutions at the initial concentration of 10 mg L^{-1} ($20 \text{ }^\circ\text{C}$ and $\text{pH} 5$), neither any elimination nor mineralization of TMP, DMI or CPTX was observed. This can be because the three psychotropics have high absorption in the UV-range with the absorption maximum at $260 \pm 10 \text{ nm}$, which means that they are expected to have a high degradation rate under the UV-radiation while a lower degradation rate under Xenon Lamp.

TMP, DMI and CPTX were efficiently degraded during UV-irradiation. With an initial concentration of 100 mg L^{-1} ($20 \text{ }^\circ\text{C}$ and $\text{pH} 5$), the HPLC analysis showed elimination of 91.8% of TMP, 67% of DMI and 99.8% of CPTX after 128 min of UV-irradiation (Figure 2). The corresponding mineralisation rates were found to be 23.9% (TMP), 5.6% (DMI) and 14.1% (CPTX) (Figure 2) as indicated by monitoring DOC. This indicates that these psychotropic drugs were transformed into TPs that were resistant to further UV-photolysis. Figure 2 shows that DMI degraded with the slowest rate compared to TMP and CPTX, while CPTX degraded with the highest rate. Although CPTX degraded faster than TMP, mineralization rate (%) of TMP was higher which means that TMP can be more easily mineralised in comparison to CPTX and therefore the

transformation of CPTX to other by-products was higher. So that TMP may be relatively more environmentally friendly compared to CPTX.

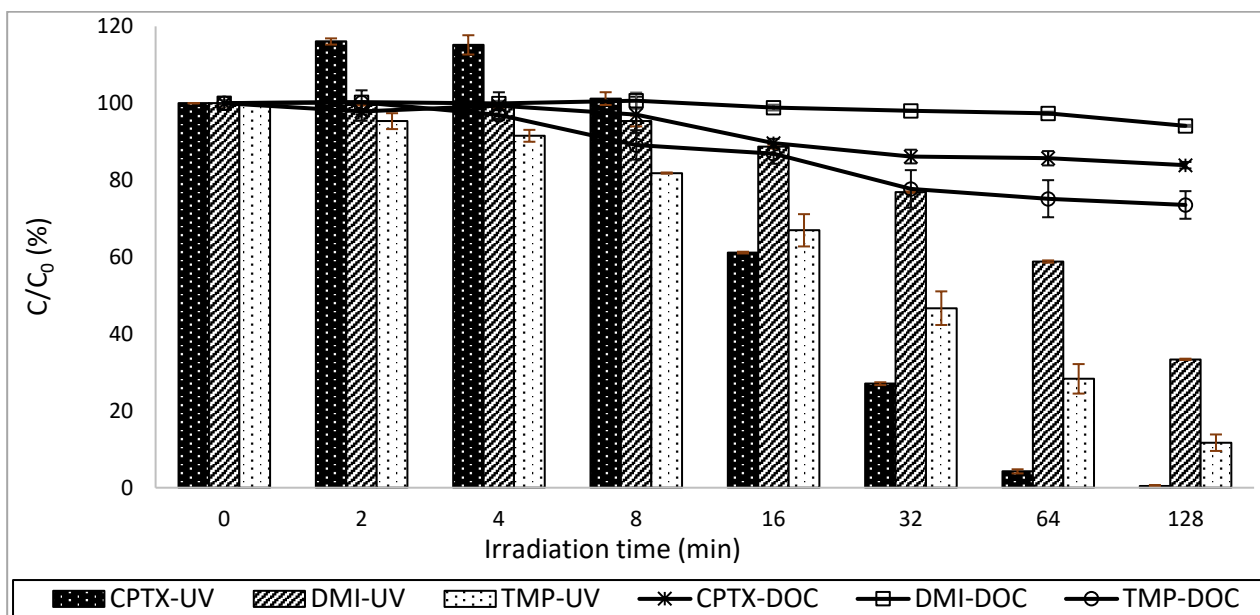


Figure 2: The UV-photolytic and DOC elimination for TMP, DMI, and CPTX at the concentration of 100 mg/L, pH = 5, and temperature = 20 °C during UV-photodegradation tests (n=3).

The degradation of TMP, DMI and CPTX under UV-irradiation using four initial concentration levels (5, 10, 50, and 100 mg L⁻¹) fit pseudo first-order kinetics with high linearity. In general, the photodegradation and mineralization rates increased as the initial concentration decreased and vice versa. Therefore, there is a possibility of complete mineralization at lower concentrations within a longer irradiation time. This means that photolysis might be quite fast under real world conditions as concentrations are low. However, it cannot be excluded that there will be other compounds, scavengers for radicals as well as photosensitizing compounds that can interfere with pharmaceuticals' photolysis in natural water (Hazime et al., 2012; Trovó et al., 2009). The observed decrease in the elimination kinetics and DOC removal rates by increasing the initial concentration is mostly because more parent compounds, more intermediates and TPs are present absorbing radiation and blocking others from the access to radiation "shadowing-effect" (Herrmann et al., 2015a).

Degradation and mineralization of TMP, DMI and CPTX during the UV-irradiation using different pH values showed that CPTX degraded with the fastest rate under the studied pH range (Figure 3). At pH 3, CPTX degraded with the fastest rate compared to its photodegradation at other pH conditions and compared to photodegradation rates of TMP and DMI at pH 3. CPTX photodegradation rate decreased slightly when pH of the solution increased to pH 5 and pH 7, but its photodegradation rates were still faster than TMP and DMI rates at pH 5 and pH 7, respectively.

The photodegradation rates of TMP and DMI were almost the same at pH3. When the pH increased, at pH 5 and pH 7, the photodegradation rate of TMP became faster, and of DMI became slower. At pH 9 experiments, the photodegradation of TMP continued in the increasing direction, while DMI degradation rate showed very little increase.

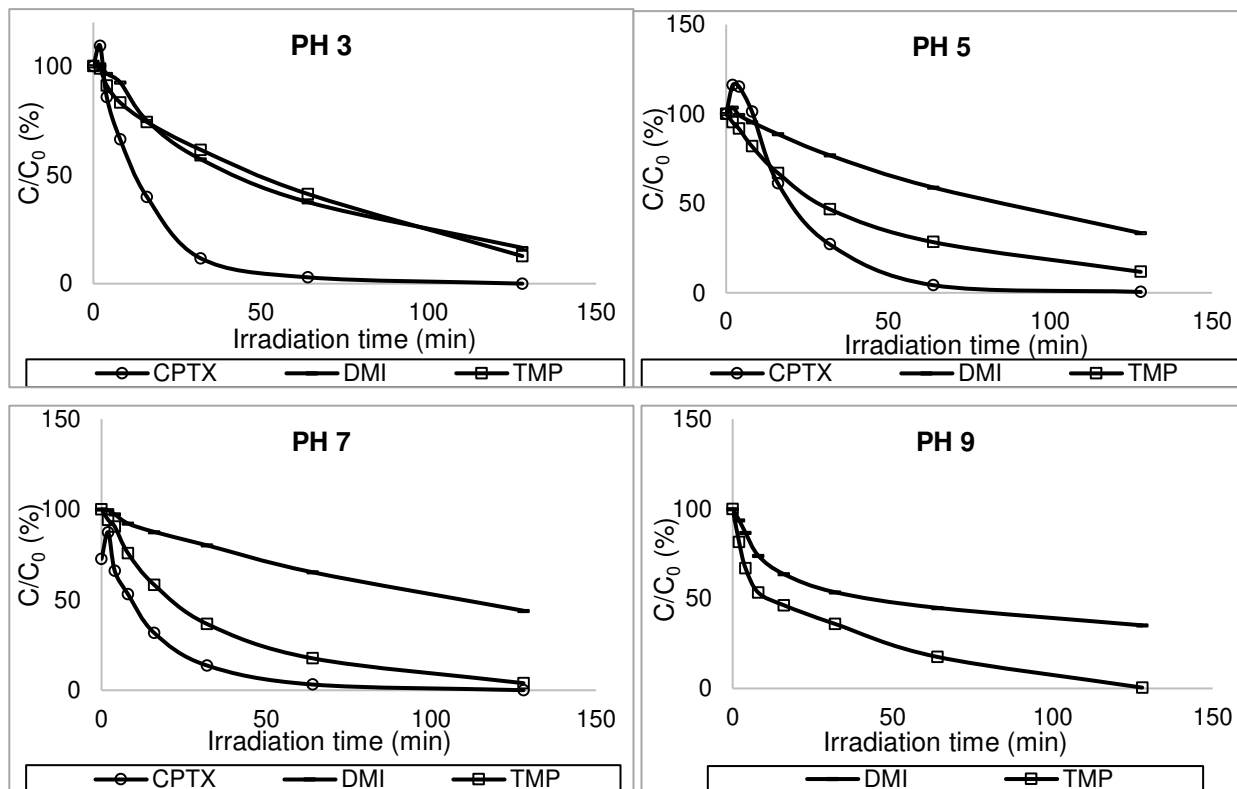


Figure 3: UV-photodegradation of TMP, DMI and CPTX at different pH values ($n=2$ with $SD \leq 4$).

TMP photodegradation and mineralization rates were found to be directly proportional to the pH value of the solution. After 128 min of irradiation, 87.6, 88.3, 96.2, and 99.5% of TMP were degraded at pH values of 3, 5, 7 and 9, respectively. The increase in the degradation and in the mineralization rates by the increase in pH values at $pH \leq 7$ can be due to the increase in the molar absorption coefficient (ϵ). The fastest degradation rate observed at pH 9 can be also due to the lower solubility and the different ionization form of TMP at pH 9. TMP degradation rate under pH 9 conditions showed a relative slowdown after 16 min of irradiation until the end of the test. The subsequent slowdown in degradation might be explained by the change in the solution pH value during the irradiation time, or by the formation of new TPs after 16 min, that are not formed at other pH values, which might absorb UV-radiation, thereby reducing the UV available for TMP degradation (Rastogi et al., 2014).

DMI degradation rate at $pH \leq 7$ was inversely proportional to the solution's pH value. At pH 9, the highest photodegradation rate was observed until 16 min of UV-irradiation, and then the photolysis rate slowed down from 16 min until 128 min. At the end of the test, DMI was eliminated

by 84%, 67%, 56% and 65% at pH 3, 5, 7 and 9, respectively. The degree of mineralization (in %), reached after 128 min of irradiation decreased with increasing the pH values of the irradiated solution. In case of pH 3 till pH 7 conditions, DOC results agree with the photolysis kinetic results. Whereas, at pH 9 experiment, the highest mineralization (in %) was seen during the entire photolysis experiment without showing the slowdown seen after 16 min in the photodegradation kinetic results. The changes in DMI photolysis rates at different pH values was likely related to the DMI species present at these pH values, which goes along with a change in the molar absorption coefficient (ϵ).

CPTX showed the highest degradation rate at pH 3, followed by pH 7 and the slowest rate at pH 5. The degradation rate at pH 7 is not only due to the pH effect but also due to the lower dissolved concentration. The rates of change in the degree of mineralization of CPTX during UV-irradiation at different pH experiments showed non-significant differences.

Temperature change showed negligible effect on the UV photodegradation behaviour of DMI and CPTX, as their photolysis and mineralization rates showed non-significant differences under the studied temperature range. In case of TMP, elimination and mineralization rates increased when the experimental temperature increased. Arrhenius plot is obtained by plotting $\ln k$ against $1/T$, and it was found to be linear in the studied temperature range. The activation energy was calculated from Arrhenius equation and it was found to be 12.6 kJ mol^{-1} .

LC-MS/MS analysis of the biodegradation samples of the three studied psychotropic drugs showed no new peaks, while their UV photo-treated samples showed the formation of new peaks that were gradually increasing at the beginning of the irradiation and mostly subsequently decreasing with the irradiation time. This demonstrates the formation of photo-transformation products (PTPs), and most of these PTPs showed retention time and log P results indicating that they are of higher polarity than their parent compounds themselves. The formed PTPs were named according to their m/z values.

- 1- In TMP UV-irradiated samples, 14 PTPs were observed with different m/z values except two PTPs that have the same m/z value (Figure 4). The most abundant photoproduct was PTP311, and it was probably formed from a mono-hydroxylation of TMP. A further hydroxylation step of PTP311 is proposed to explain the formation of the second highly formed product (PTP327). PTP313 and PTP329 differs by +2 Da from PTP311 and PTP327, respectively. It can be assumed that the formation of PTP313 and PTP329 were formed through a hydrogenation of PTP311 and PTP327, or through a hydration of TMP and PTP311, respectively. Two PTPs with m/z 309 (PTP309a and PTP309b) showed different molecular formula, different RDB value and different fragmentation pattern in their LC-MS results.

PTP309a is mostly formed from the oxidation of TMP. The structure of PTP309b could not be elucidated. The deamination of TMP lead to the formation of PTP250. PTP268 is suggested to be formed from PTP250 after a hydration process. The loss of the 3-(di-methylamino)-2-methylpropyl chain from TMP, PTP309a, and PTP311 result in the formation of PTP196, PTP210, and PTP212, respectively. PTP405 is assumed either to be formed by the dimerization of two molecules of PTP196 followed by mono-hydroxylation, or through the reaction between PTP196 and PTP212. PTP247 is assumed to come from the degradation of one benzene ring in TMP keeping the azepane cycle intact combined either with a mono-hydroxylation process in the benzene ring or with lactam formation in the azepane ring. PTP134 is the N,N,2-trimethylpropan-1-amine chain of TMP including further demethylation and di-hydroxylation processes.

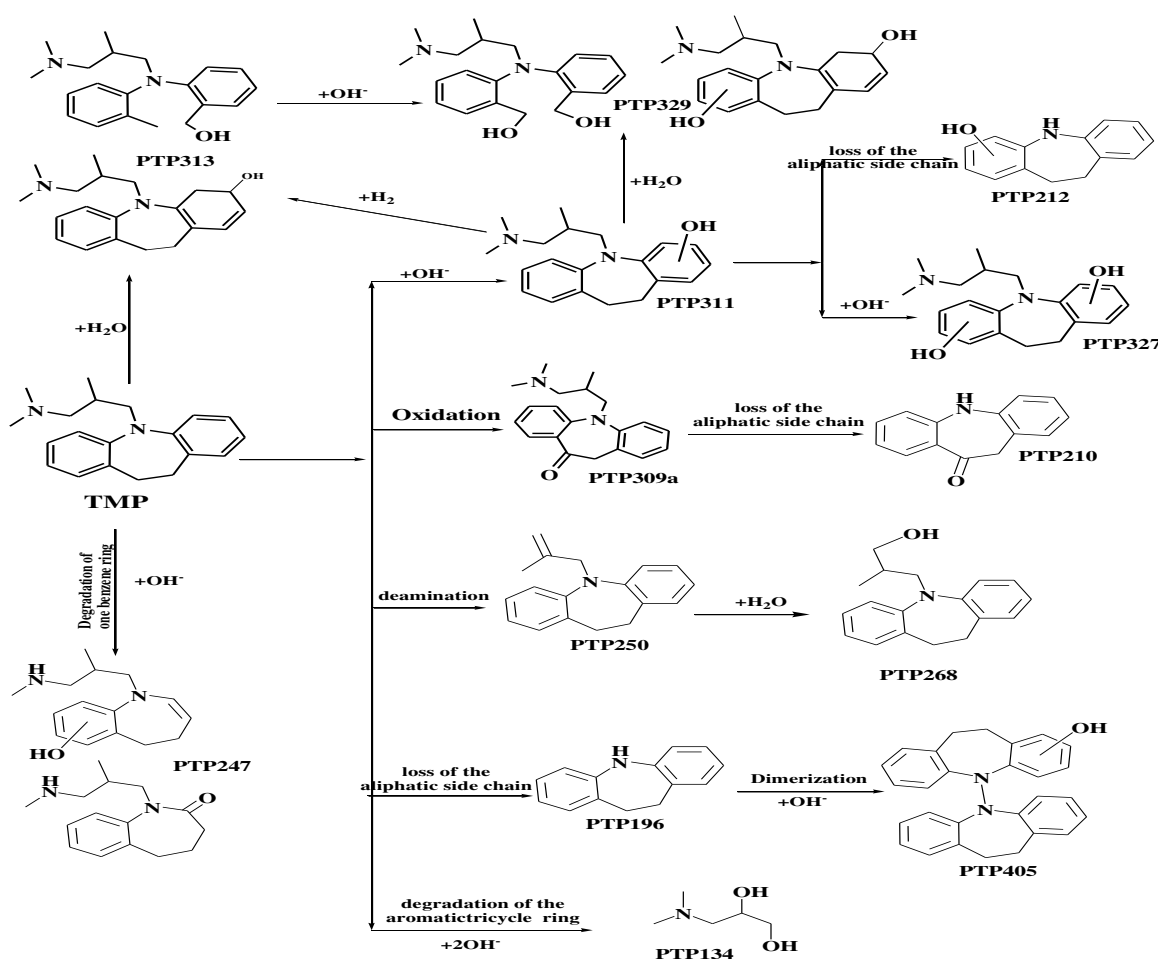


Figure 4: Photodegradation pathway of TMP under UV-irradiation

2- In DMI UV-irradiated samples, 18 new PTPs were observed with seven different m/z values indicating the formation of many isomers (Figure 5). The most intense precursor ion peaks (PTP267-1 and PTP267-2) are assumed to be isomers to DMI. The MS² spectrum and the fragmentation pattern of PTP267-1 and PTP267-2 indicated that they may differ only in the

position of the side chain methyl group. Two PTPs with m/z 281.17 (PTP281-1 and PTP281-2) were detected and they are isomers formed by oxidation of DMI. The MS² spectrum of PTP281-2 showed a key fragment at m/z 210, which indicates the oxidation in the azepane ring. The absence of the latter fragment in PTP281-1 suggests oxidation of the 1-methylaminopropyl chain. The suggested ion formula and fragmentation pattern of the five PTPs with m/z 283 pointed out that they are isomers formed through the hydroxylation of DMI at different positions. In the four PTPs with m/z 299, twofold hydroxylation took place. PTP299-2 and PTP299-3 showed MS² fragments with m/z 182 and 180, respectively, which indicated the position of the two hydroxyl groups either to be both in one of the benzene rings or one in the benzene ring and the other one in the azepane ring. Although PTP299-1 and PTP229-4 gave no key fragment indicating if the hydroxylation took place in the tricyclic part or in the 1-methylaminopropyl chain, their predicted log P values was used in predicting the position of the dihydroxylation (Figure 5). The PTPs with m/z 285.19 and 301.19 were most likely to be formed as a result of mono- and di-hydroxylation of DMI, mainly in the azepane ring, with subsequent ring cleavage. PTP219 could be formed from DMI after the degradation of one of the benzene rings keeping the azepane cycle intact combined with both oxidation and demethylation. PTP219 gave a fragment with m/z 160, which indicates that the oxidation occurs on the azepane ring.

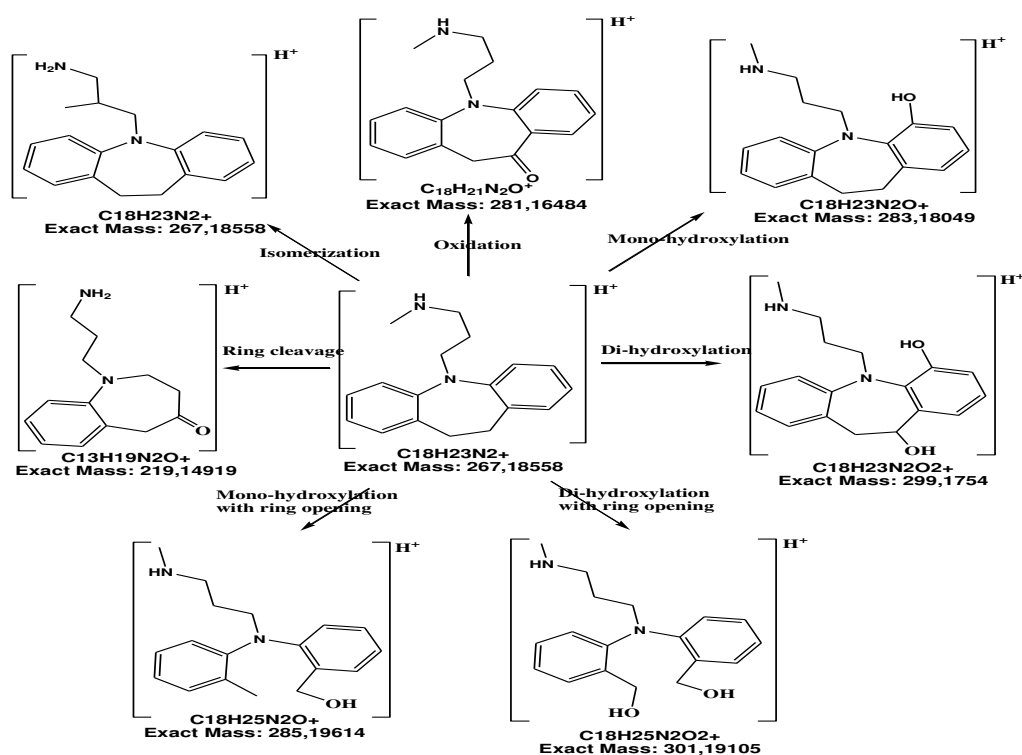


Figure 5: The proposed photo-transformation pathway of DMI during UV irradiation

3- In the UV-irradiated samples of CPTX, 14 PTPs containing many isomers are observed (Figure 6). In CPTX standard samples, before photolysis, one product at $m/z = 282.13$ was observed with a low peak intensity, and it degraded gradually during the UV-photodegradation tests. This TP could be either an impurity or a hydrolysis-transformation product. It is assumed to be a de-chlorinated derivative from CPTX. Two PTPs were detected with m/z 316. PTP316-1 (m/z 316.14) is suggested to be formed from CPTX after de-chlorination and di-hydroxylation processes. PTP316-2 (m/z 316.09) is assumed as an isomer to CPTX. Five precursor ion peaks with m/z 332 were observed and were divided into two groups: the first one has the exact m/z value of 332.13 with the suggested molecular formula of $C_{18}H_{22}O_3NS$. This group includes PTP332-1, PTP332-2, and PTP332-3, and they are suggested to be isomers that are generated from CPTX after de-chlorination and tri-hydroxylation processes. The second group has the m/z value of 332.09 with the suggested molecular formula of $C_{18}H_{19}ONClS$ and it includes PTP332-4 and PTP332-5. This group is identified as two isomers that formed by mono-hydroxylation of CPTX, where they differ in the position of the hydroxylation. One PTP with m/z 334.1 was observed and it could be formed through the hydration of CPTX. The PTP detected with m/z 348.13 is suggested to be formed from the de-chlorination of CPTX and the addition of four hydroxyl groups. With m/z 350.1, one PTP was observed that could have been generated from CPTX after hydration and mono-hydroxylation processes. Three PTP isomers with m/z 298.12 were produced from a de-chlorination of CPTX combined with a mono-hydroxylation process.

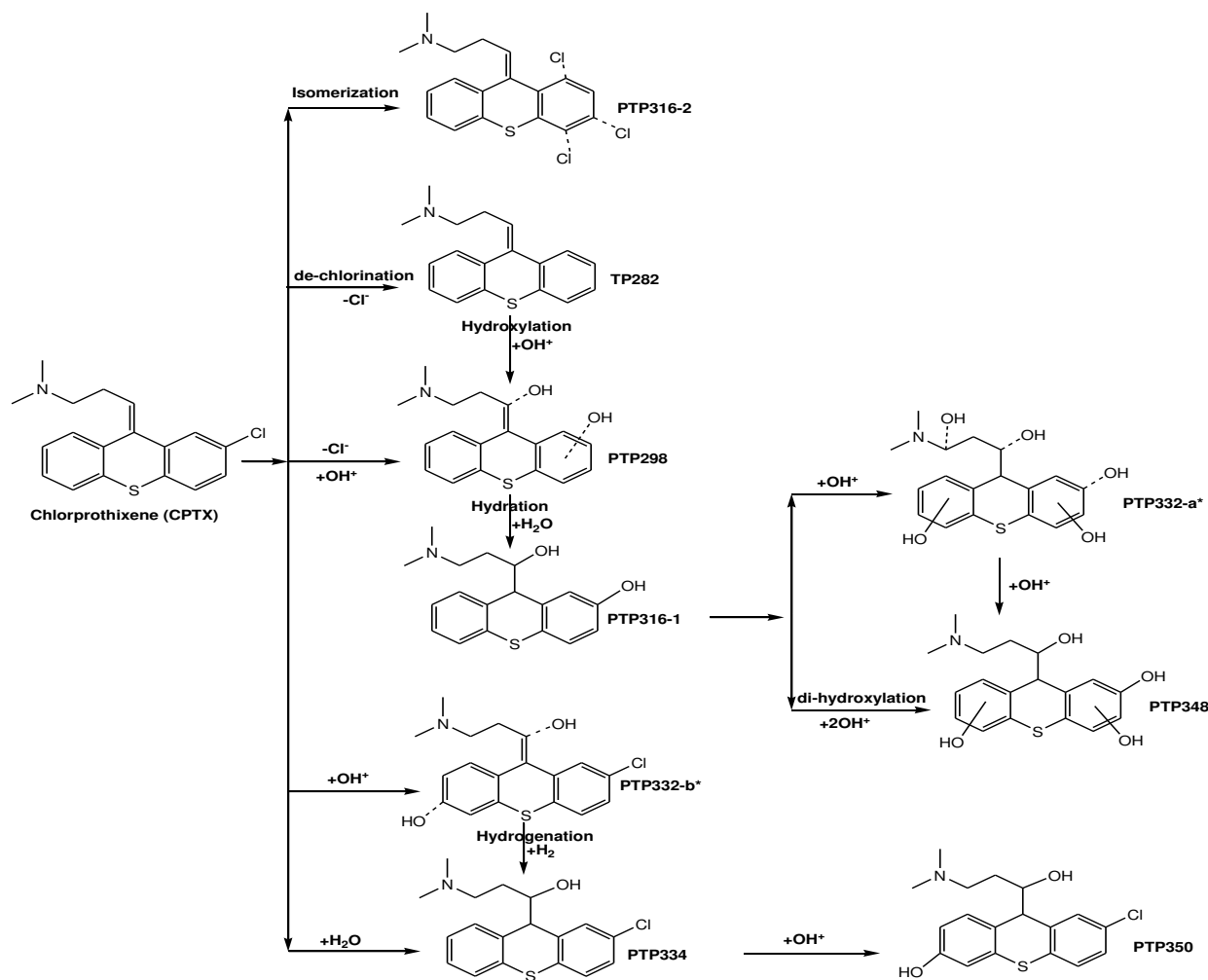


Figure 6: The proposed photo-transformation pathway of CPTX during UV irradiation

Initial drug concentration, temperature and pH can affect the PTPs formation kinetics and the following results were observed:

during the photolysis of TMP, DMI and CPTX at different concentration levels, most of the PTPs identified in the 100 mg L^{-1} UV-irradiated solutions were also formed during photolysis at other lower concentration levels but with different formation kinetics. Only at the initial concentration of 5 mg L^{-1} , a few of the formed PTPs were difficult to be detected which might be due to inadequate detection limits and/or low ionization rates. The formation/elimination kinetics of the PTPs during the experiments with initial lower concentrations were found to be faster than their kinetics at higher concentrations. The highest observed A/A_0 (%) values for most of the formed PTPs increased with increasing the initial concentrations of their parent compounds. A_0 is the peak area of the compound at time 0 or at Day 0, and A is the peak area of the TP at certain irradiation time or at Day 28 in either the photo-degradation or the biodegradation tests, respectively.

In the tests performed at different pH values, some PTPs showed an increase in A/A_0 (%) by increasing the pH; others showed a decrease in A/A_0 (%) when the pH increases; while the A/A_0 (%) value for other PTPs changed randomly at different pH values. So, it can be concluded that there is no rule to describe the effect of pH on the PTPs concentrations and formation kinetics.

In TMP photolysis samples: PTP250 and PTP268 showed an increase in the A/A_0 (%) by decreasing the pH value and therefore of less interest in the aquatic environment, this result could suggest that the loss of the dimethylamine group is favoured at acidic pH, in which this dimethylamine group is in its ionized form and can easily be removed. The time courses of PTP309a and PTP311 showed an increase of A/A_0 (%) in the following direction (pH9 > pH3 > pH7 > pH5). A/A_0 (%) of PTP210 and PTP212 increase with increasing pH value and they can hardly be seen in pH 3 condition, and therefore of interest in the aquatic environment. As it was mentioned before, PTP309a and PTP311 are formed by oxidation and hydroxylation of TMP, and PTP210 and PTP212 are formed from PTP309a and PTP311 by further loss of the 3-(dimethylamino)-2-methylpropyl chain. This suggests that oxidation and hydroxylation can occur extensively in the alkaline media followed by the acidic then the neutral ones (pH9 > pH3 > pH7 > pH5). While the loss of the 3-(dimethylamino)-2-methylpropyl chain preferably takes place in alkaline media and not in acidic media.

In DMI samples, the UV-photolysis behaviour is affected by the solution pH, as some PTPs were detectable at certain pH values and not at others. All the PTPs generated at pH 5 experiment are formed at the other pH experiments, except PTP283-5, which was uniquely formed at pH 5. One PTP, with m/z 235, was found only at pH 3 experiment; this is likely to be a secondary product from PTP299 after degradation of one benzene ring keeping the azepane cycle intact, with further dehydration and demethylation. At pH 9 experiment, three new PTPs with $m/z = 271$ were detected. These three PTPs can be assumed to be isomers formed through the oxidation of the azepane ring followed by multi-steps: ring cleavage, ring closing at another site, and demethylation reactions. The latter mechanism was described in detail elsewhere (Petrovic and Barceló, 2007).

In CPTX samples, it was observed that PTP316-1 was formed with the highest peak areas, as it showed A/A_0 (%) value equal 12.6 and 9.0 in experiments performed at pH 5 and pH 7, respectively. At pH 3, PTP316-1 was formed with very low A/A_0 (%) value. This means that the dechlorination of CPTX combined with di-hydroxylation processes could favourably occur in neutral and weakly acidic conditions and is unlikely to take place under strongly acidic conditions and therefore normally of high interest in the aquatic environment. A similar case was also observed for PTP316-2, which was formed with A/A_0 (%) value equal 3.7 and 7.1 at experiments performed at pH 5 and pH 7, respectively, corresponding to only 0.6% A/A_0 value in the pH 3 experiment. This can

lead to the conclusion that the isomerization of CPTX can favourably occur when the pH value increases and is less likely to take place in strongly acidic condition, and therefore PTP316-2 is of interest to the environment. PTP334 showed A/A_0 (%) values equal 10.6, 6.5, and 1.7 in experiments at pH 7, pH 5, and pH 3, respectively. This indicates that hydration of CPTX can more likely happen when the solution pH value increases, and that PTP334 is of further interest. PTPs (298-2 and 298-3) are formed with A/A_0 (%) values equal (9.0 and 10.8), (5.2 and 6.0), and (2.5 and 2.6) in pH 3, pH 5, and pH 7 experiments, respectively. This means that de-chlorination and hydroxylation of the tricyclic ring in CPTX molecule is favoured in strong acidic media and its occurrence% is inversely proportional to the pH value, and therefore they might be of less interest in the aquatic environment. The case was reversed in case of PTP298-1 which is of high interest in the environment as it formed with higher A/A_0 (%) values at pH 5 and pH 7 experiments equal 13.1 and 9.6, respectively, corresponding to 0.2 A/A_0 (%) at pH 3. It can be concluded that de-chlorination and hydroxylation of the aliphatic side chain in the CPTX molecule is difficult to occur at pH 3 and is likely to take place at weak acidic and neutral conditions. PTP332-3 was the one with the highest peak area formed compared with the five PTPs with m/z 332; its highest formation ratio was seen at pH 5 experiment (4.6%), followed by pH 3 with A/A_0 (%) value equal 2.4 and its concentration was lower at pH 7 with 0.6 A/A_0 (%), so it is normally of less interest to the environment. PTP332-5 showed A/A_0 (%) values of 1.2, 0.9, and 0.3 in experiments performed at pH 3, pH 5, and pH 7, respectively, indicating probable non-significant relevant to the environment. The pH showed non-significant effect on formation behaviour of PTP332-1, PTP332-2, and PTP332-4, as they showed very close A/A_0 (%) values in experiments performed at different pH values. The formation ratio of PTP350 is directly proportional to the solution pH, as it showed 3.7, 0.7, and 0.1 A/A_0 (%) in pH 7, pH 5, and pH 3 experiments, respectively. The previously mentioned case is similar to PTP334, and this confirmed the previous conclusion for PTP334. In addition, PTP348 was formed also with A/A_0 % values directly proportional to the pH of the solution. So, PTP350 and PTP348 could be relevant to the aquatic environment. TP282 was formed and eliminated with nearly the same ratio in the three compared pH experiments, indicating the probability that the pH has no effect on the elimination of the chloride atom from CPTX molecule.

Temperature change influenced the formation/elimination behaviour of TMP's PTPs. Some of the PTPs showed the highest A/A_0 (%) at 30°C and 40°C experiments like PTP134, PTP210, and PTP212. While others show the highest A/A_0 (%) at 10°C such as PTP311, PTP313, and PTP196. Although the temperature showed no effect on DMI photolysis rate, it influenced the formation/elimination kinetics of its PTPs. The formation/elimination curves of PTP219, PTP281-1, PTP283-1 and PTP281-2 were the fastest at 10°C and the slowest at 20°C experiments. While the

formation/elimination kinetics of other PTPs such as TP299-2 and TP283-2 increased with increasing temperatures. The formation/elimination of others PTPs increased when the temperature increased from 20°C to 40°C, while at 10°C, a broad variety of formation/elimination kinetics was observed. In CPTX samples, the temperature showed non-significant effect on the formation behaviour of the PTPs.

Biodegradation results of the photolysis samples from TMP, DMI and CPTX were low and this meant that all the PTPs should be classified as being not readily biodegradable. At the same time the obtained biodegradation results showed a relative slightly increased biodegradation rates in photolysis mixtures which were exposed longer to UV-irradiation. Therefore, the low concentration of the PTPs in the photodegradation mixtures should not be overlooked, as this finding suggests that there was one or more biodegradable PTPs, but their contribution to DOC is minimal and seems to be offset by the predominant effect of the other non-biodegradable PTPs and parent compounds themselves. LC-MS/MS analyses of the CBT and MRT samples at the start and at the end of the biodegradation tests for the photolysis mixtures confirmed the previous finding. LC-MS/MS analyses revealed the elimination of some PTPs combined with or without elimination in the sterile controls indicating probable biotic or abiotic degradation, respectively.

In TMP photolyzed samples (Figure 7); PTP210, PTP309b, and PTP212 showed elimination higher than 65% in biodegradation tests corresponding to 0% elimination in their sterile controls suggesting these PTPs as biodegradable. PTP327 and PTP329 showed elimination of 35% and 53% in CBT and MRT, and they can be partially biodegraded as they showed relative lower elimination rates in sterile samples. PTP134, PTP268, PTP250 and PTP196 were removed abiotically as they showed elimination between 39.4% and 98.4% in their test and sterile samples.

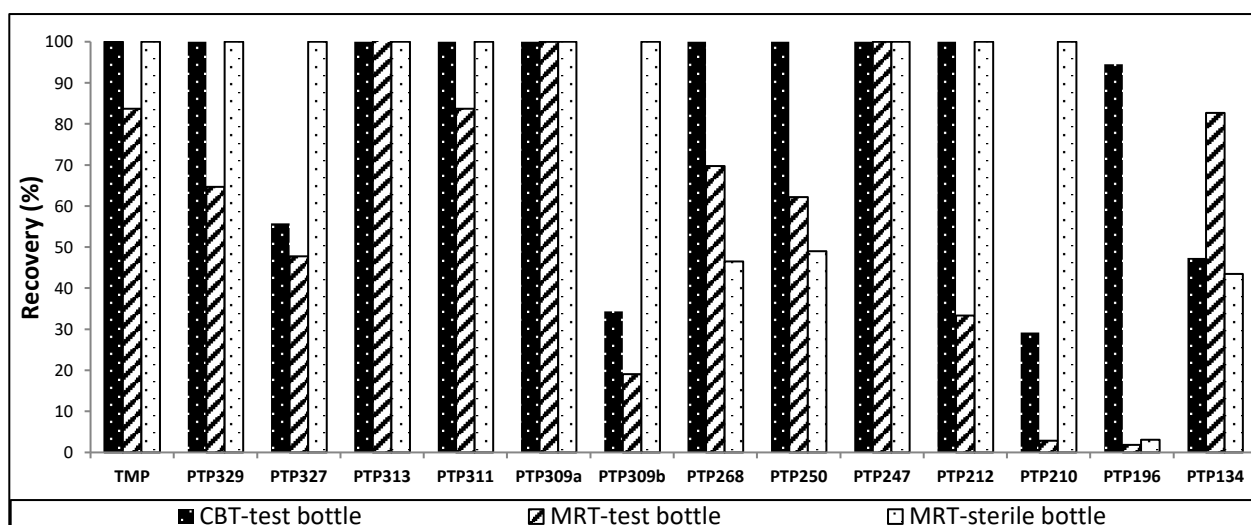


Figure 7: Recovery of TMP's PTPs after 28 days related to day 0 in CBT and MRT.

In DMI samples (Figure 8); PTP267–2, PTP281–2, PTP283–2, and PTP283–4 could be described as slightly biodegradable PTPs in MRT with higher degradation rates than that in CBT. The highest degradation rate was observed for PTP283–4 as it gave elimination of 78% and 19% in MRT and CBT, respectively. PTP283–4 could be considered as a partially biodegradable PTP as it is characterized by a lower elimination rate in the sterile sample (24%) than in the test sample (78%). The three PTPs (PTP267–2, PTP281–2, and PTP283–2) can be considered as abiotically degradable in MRT, because they showed the same elimination in both test and sterile samples. PTP299–4 was slightly degradable in CBT and MRT with about 31% elimination. PTP299–2 was almost eliminated in the test samples of CBT and MRT with degradation rates up to 93.8% at day 28. In this case, it is difficult to determine whether PTP299–2 was biotically or abiotically eliminated because it was eliminated in the sterile controls from the beginning of the test at day 0. One explanation might be a fast reaction with the added sodium azide.

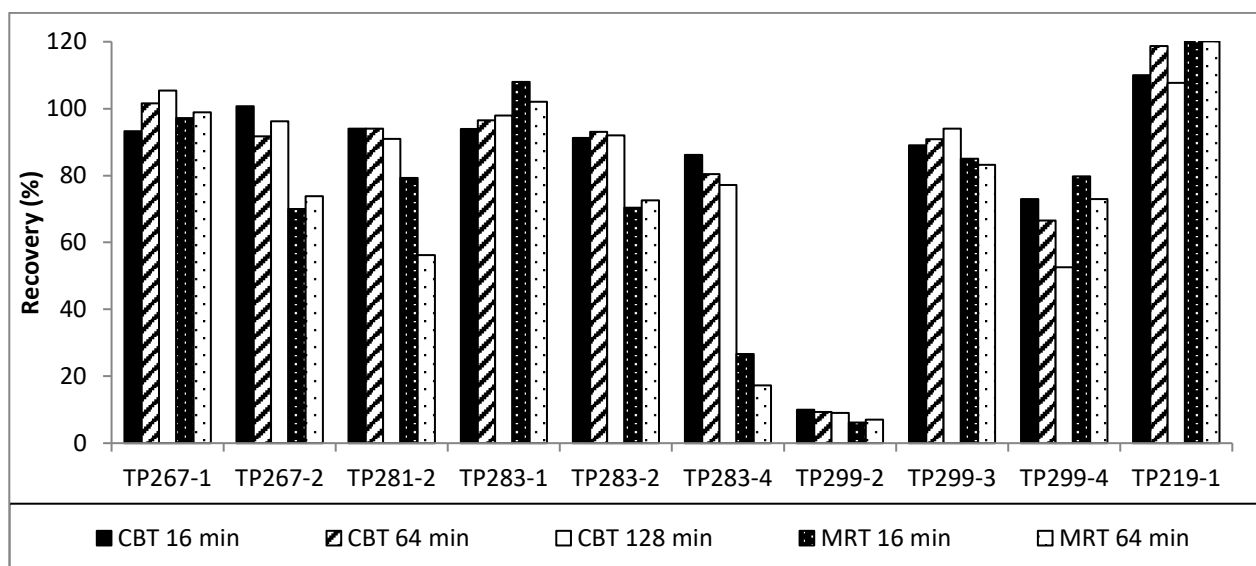


Figure 8: Recovery of DMI's PTPs after 28 days related to day 0 in CBT and MRT in different photolytic mixtures.

In CPTX samples (Figure 9): PTP334, PTP348, PTP332-1, PTP332-2, PTP332-3 and PTP332-4 were eliminated during the two biodegradation tests with elimination% ranged between 42.9% and 99.4%. They are biotically eliminated as they showed high elimination in test vessels without showing any corresponding elimination in the sterile controls. It is also noted that, although PTP332-4 and PTP332-5 are isomers, PTP332-4 is biodegradable one, and PTP332-5 is not. Therefore, it can be concluded that the position of the functional group in the compound can affect the ability of the bacteria to degrade these compounds, which is in agreement with the knowledge that stereochemistry can be of importance for biodegradability. It means that the isomerization is an

important factor that can affect the biodegradability of compounds in the environment and should be therefore considered.

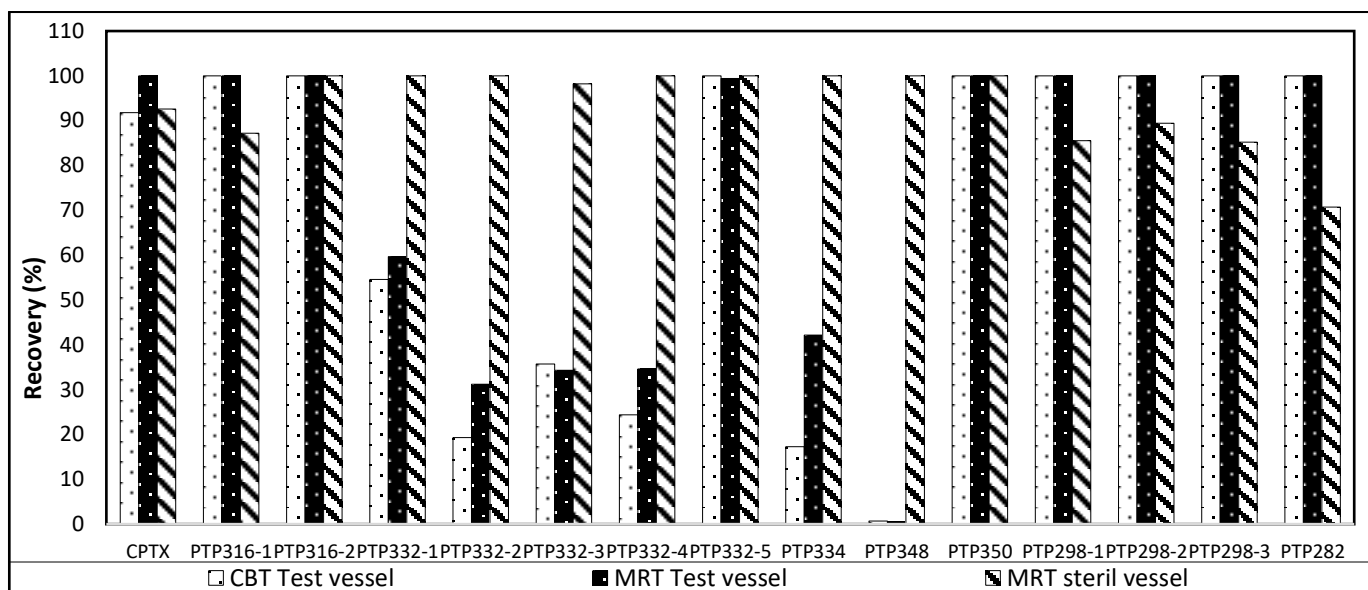


Figure 9: Recovery of CPTX's PTPs after 28 days (compared to day 0) in CBT and MRT in different photolytic mixtures.

QSAR results regarding the biodegradation assessment of the formed TPs showed the following results:

In case of TMP's PTPs: PTP313, PTP329 and PTP134 were predicted as readily biodegradable by the Case Ultra model. The Oasis Catalogic (OECD 301F) predicted PTP212 to be readily biodegradable, and EpiSuite models predicted PTP134 as readily biodegradable. The result from the Oasis Catalogic and EpiSuite were in agreement with the LC-MS/MS analysis results of the experimentally performed biodegradation tests, as PTP212 and PTP134 were found as probably biodegradable PTPs in both of them. While results from Case Ultra showed one probable false positive result in comparison with the LC-MS analysis results in which PTP313 is not eliminated at all.

In case of the PTPs of DMI: although Oasis Catalogic and EpiSuite models predicted all the PTPs as not readily biodegradable, Case Ultra model predicted some of the suggested structures for some PTPs as readily biodegradable such as PTP219, PTP301 und PTP299. In LC-MS/MS analysis results of the experimentally performed biodegradation tests, only PTP299-2 and PTP299-4 showed elimination.

In case of the PTPs of CPTX: they were all predicted to be not readily biodegradable with very few non-significant positive results in the five models used for ready biodegradability. These are

not in agreement with the LC-MS/MS analytical results which suggest some PTPs to be biodegradable. Therefore, laboratory tests for individual TPs are can confirm this result.

QSAR toxicity assessment using *in-silico* models were used to predict mutagenicity, genotoxicity, teratogenicity and ecotoxicity for the three studied psychotropics and their PTPs.

TMP, DMI, all TMP's PTPs and some of CPTX's PTPs (PTP332a, PTP348, PTP316, PTP334, and PTP350) showed no positive alert from the different models of the ICH M7 guideline conformal set from Case Ultra for mutagenicity or genotoxicity. Despite that it cannot be completely excluded that they might have a toxic effect in the environment, as some of them were out of domain in the applied Case Ultra models. CPTX and its PTP (PTP332b) were predicted to be carcinogenic in the GT Expert model, mutagenic in Salmonella (Module GT1 A7B) and in Salmonella mutagenicity (Pharm Salm), while predicted to be non-mutagenic in E-coli mutagenicity models. The toxicity results for PTP298 and TP282 are also the same as CPTX, except in the GTI A7B model for salmonella toxicity in which these PTPs, in contrast to CPTX, were mostly predicted as negatives. Some of the suggested structures for some PTPs of DMI (such as PTP299 and PTP301) were predicted to have mutagenic and genotoxic activities, because of the presence of an N-methylol group which leads to the formation of formaldehyde via hydrolysis, and the formaldehyde is a highly reactive genotoxic agent (Ashby and Tennant, 1988; BENIGNI and BOSSA, 2008).

TMP is known to be teratogenic and mostly all of its PTPs were predicted to be also teratogenic in all of the models used. CPTX is predicted to be non-teratogenic by the four applied models. Some of the PTPs of CPTX are predicted as non-teratogenic, while others (PTP332a, PTP348, and PTP350) are predicted positive teratogens in some of the applied modules.

The acute *V. fischeri* modules (Oasis Catalogic) predicted higher ecotoxicity results for all the PTPs formed during DMI photolysis, lower ecotoxic properties for all the PTPs formed during CPTX degradation, and lower ecotoxic properties for most of the PTPs formed during TMP photolysis except PTP309a and PTP250 which were predicted to be more ecotoxic than TMP.

The results from Case Ultra for Microtox Toxicity to Environmental Bacteria of DMI were out of domain, and of TMP were negative. Some DMI's PTPs (PTP285 and PTP301) were predicted to have Microtox Toxicity to environmental bacteria. In case of TMP's PTPs: PTP247-4 and PTP247-7 showed positive alerts in the Microtox Toxicity to Environmental Bacteria module. In Microtox Toxicity to Environmental Bacteria, CPTX and some of its PTPs (PTP298 and PTP282) were assessed as inconclusive and out of domain, indicating that probably no ecotoxicity prediction is possible for CPTX and the later mentioned PTPs, while most of the predicted structures for

PTP332b, PTP334 and PTP350 were predicted toxic in the Microtox Toxicity to Environmental Bacteria.

As a conclusion, some of the PTPs formed during the photodegradation of the three studied psychotropics were predicted to be toxic and at the same time were predicted to be not biodegradable in the *in-silico* and/or in the laboratory tests which indicate sound of environmental risk. These environmentally relevant products include: PTP309a and PTP247 in case of TMP, PTP285 in case of DMI, and PTP316, PTP350 in case of CPTX.

5. Synopsis

The main purpose of this thesis was an in deep environmental fate assessment of TMP, DMP and CPTX with comprehensive characterization and identification of the stable transformation products resulting from environmental degradation processes. Temperature, pH and concentration impact on their photodegradation behaviour was also considered. To achieve this purpose, laboratory degradation experiments were performed, then chemical-analytical methods with sensitive LC-MS/MS analysis were applied, and finally QSAR *in-silico* predictions for humans and eco-toxicity were assessed. Benefitted from this approach, the objectives addressed in the thesis have been achieved and the following conclusions can be drawn:

- a) The UV-photolysis is an important abiotic elimination process for the three investigated compounds, and it leads to the formation of many new PTPs and mostly without complete mineralization.
- b) The most abundant degradation pathways for the three studied psychotropic drugs during UV-photolysis are hydroxylation, followed by oxidation and isomerization. Deamination and loss of the aliphatic side chain were observed during TMP photo-transformation, and dechlorination was observed during CPTX transformation.
- c) The tested pharmaceuticals and their photodegradation mixtures showed low degradation results in the performed laboratory biodegradation tests. Despite that, LC-MS/MS analysis showed that some PTPs were eliminated significantly during the biodegradation tests. The effect of these possibly biodegradable PTPs was not seen in the biodegradation results due to their low concentrations in the mixtures.
- d) The UV degradation behaviour of the studied psychotropic drugs can be differently affected by variable conditions in the environment such as initial drug concentration, pH and temperature. Pharmaceuticals' degradation rates increase by decreasing their initial concentration. Higher temperature enhanced the degradation rate during TMP UV-photolysis, while showed no significant effect during DMI and CPTX degradation. pH affects the degradation rate and the TPs formation in different pattern depending on many factors such as pK_a of the substance, type of ionization and solubility.
- e) The applied techniques within this study emphasize the importance of *in-silico* approaches such as QSAR models as a tool for getting additional information on environmental fate of the psychotropic drugs and their TPs. The *in-silico* predictions confirmed that the TPs might have a different genotoxic, carcinogenic, mutagenic and eco-toxic potential compared to their parent compounds.

6. Concluding remarks and outlook

Although the use of psychotropic drugs is necessarily as human medicines, it is important to consider their environmental occurrence, fate and risk to better understand their behaviour in our aquatic environment. In this thesis, attention was drawn to the psychotropic drugs that are highly used and highly detected in the environment and can have toxic effect, and despite that their environmental fate is not well investigated. The results focused also on the elucidation, fate and relevance of the formed TPs, which are considered nowadays as environmental pollutants of high interest that could be as important as the parent pharmaceuticals themselves. The identification of TPs is one of the difficult and challenging aspects in the environmental chemical analysis of micro-pollutants, and it is still very limited especially in terms of predicting the TPs' formation pathways and the assessment of their environmental fate and toxicological properties. Therefore, the use of high-resolution analytical technique to identify the TPs, and the use of environmental simulation tests and *in-silico* prediction approaches to characterize the fate and risk of TPs are of high important. Good knowledge was gained due to combination of the UV photolysis with the biodegradation tests, especially to study the biodegradability of the photo-TPs which are difficulty to be isolated and very expensive if they available. Furthermore, it was found that different conditions during UV-analysis tests; such as initial concentration, pH and temperature; have an impact on the outcomes, especially the degradation rate of the parent compound and the formation rates of the TPs.

This research has led to many useful findings about the three psychotropic drugs and their TPs. Future studies should concentrate on the photo-TPs and their environmental fate and occurrence in the aquatic environment. Additionally, investigation of the eco- and human toxicity of TMP, DMI, CPTX and their TPs should be further investigated using laboratory tests as this study showed that some of them might have some toxicity using the *in-silico* models.

7. References

- Alexy, R., Kümpel, T., Kümmerer, K., 2004. Assessment of degradation of 18 antibiotics in the Closed Bottle Test. *Chemosphere* 57, 505–512.
- Ashby, J., Tennant, R.W., 1988. Chemical structure, *Salmonella* mutagenicity and extent of carcinogenicity as indicators of genotoxic carcinogenesis among 222 chemicals tested in rodents by the U.S. NCI/NTP. *Mutation Research/Genetic Toxicology* 204, 17–115.
- BENIGNI, R., BOSSA, C., 2008. Structure alerts for carcinogenicity, and the *Salmonella* assay system: A novel insight through the chemical relational databases technology. *Mutation Research/Reviews in Mutation Research* 659, 248–261.
- Fakhari, A.R., Tabani, H., Nojavan, S., Abedi, H., 2012. Electromembrane extraction combined with cyclodextrin-modified capillary electrophoresis for the quantification of trimipramine enantiomers. *Electrophoresis* 33, 506–515.
- Gómez-Canela, C., Pueyo, V., Barata, C., Lacorte, S., Marcé, R.M., 2019. Development of predicted environmental concentrations to prioritize the occurrence of pharmaceuticals in rivers from Catalonia. *Science of The Total Environment* 666, 57–67.
- Hazime, R., Ferronato, C., Fine, L., Salvador, A., Jaber, F., Chovelon, J.-M., 2012. Photocatalytic degradation of imazalil in an aqueous suspension of TiO₂ and influence of alcohols on the degradation. *Applied Catalysis B: Environmental* 126, 90–99.
- Herrmann, M., Menz, J., Gassmann, M., Olsson, O., Kümmerer, K., 2016. Experimental and in silico assessment of fate and effects of the antipsychotic drug quetiapine and its bio- and phototransformation products in aquatic environments. *Environmental pollution* 218, 66–76.
- Herrmann, M., Menz, J., Olsson, O., Kümmerer, K., 2015a. Identification of phototransformation products of the antiepileptic drug gabapentin: Biodegradability and initial assessment of toxicity. *Water research* 85, 11–21.
- Herrmann, M., Olsson, O., Fiehn, R., Herrel, M., Kümmerer, K., 2015b. The significance of different health institutions and their respective contributions of active pharmaceutical ingredients to wastewater. *Environment international* 85, 61–76.
- Illés, E., Szabó, E., Takács, E., Wojnárovits, L., Dombi, A., Gajda-Schranz, K., 2014. Ketoprofen removal by O₃ and O₃/UV processes: Kinetics, transformation products and ecotoxicity. *The Science of the total environment* 472, 178–184.

- Janssens, H., Clays, E., Clercq, B. de, Casini, A., Bacquer, D. de, Kittel, F., Braeckman, L., 2014. The relation between psychosocial risk factors and cause-specific long-term sickness absence. *European journal of public health* 24, 428–433.
- Lajeunesse, A., Gagnon, C., Sauvé, S., 2008. Determination of basic antidepressants and their N-desmethyl metabolites in raw sewage and wastewater using solid-phase extraction and liquid chromatography-tandem mass spectrometry. *Analytical chemistry* 80, 5325–5333.
- Langford, K.H., Thomas, K.V., 2009. Determination of pharmaceutical compounds in hospital effluents and their contribution to wastewater treatment works. *Environment international* 35, 766–770.
- Lasserre, A., Younès, N., Blanchon, T., Cantegreil-Kallen, I., Passerieux, C., Thomas, G., Chan-Chee, C., Hanslik, T., 2010. Psychotropic drug use among older people in general practice: Discrepancies between opinion and practice. *Br J Gen Pract* 60, e156-e162.
- Lege, S., Sorwat, J., Yanez Heras, J.E., Zwiener, C., 2020. Abiotic and biotic transformation of torasemide - Occurrence of degradation products in the aquatic environment. *Water research* 177, 115753.
- Loonen, H., Lindgren, F., Hansen, B., Karcher, W., Niemelä, J., Hiromatsu, K., Takatsuki, M., Peijnenburg, W., Rorije, E., Struijjs, J., 1999. Prediction of biodegradability from chemical structure: Modeling of ready biodegradation test data. *Environ Toxicol Chem* 18, 1763–1768.
- Mahmoud, W.M.M., Toolaram, A.P., Menz, J., Leder, C., Schneider, M., Kümmerer, K., 2014. Identification of phototransformation products of thalidomide and mixture toxicity assessment: An experimental and quantitative structural activity relationships (QSAR) approach. *Water research* 49, 11–22.
- OECD, 1992. Test No. 301: Ready biodegradability. OECD Publishing.
- OECD-2008, Test No. 316. Phototransformation of Chemicals in Water – Direct Photolysis. OECD Publishing
- Önal, A., Öztunç, A., 2011. A rapid and simple RP-HPLC method for quantification of desipramine in human plasma. *Reviews in Analytical Chemistry* 30, 2134.
- Optenberg, S.A., Lanctôt, K.L., Herrmann, N., Oh, P.I., 2002. Antidepressant Selection, Healthcare Resource Consumption and Costs in a Large Workplace Environment. *Clinical Drug Investigation* 22, 685–694.
- Petrovic, M., Barceló, D., 2007. LC-MS for identifying photodegradation products of pharmaceuticals in the environment. *TrAC Trends in Analytical Chemistry* 26, 486–493.

- Rastogi, T., Leder, C., Kümmerer, K., 2014. Qualitative environmental risk assessment of photolytic transformation products of iodinated X-ray contrast agent diatrizoic acid. *The Science of the total environment* 482-483, 378–388.
- Reichert, J.F., Souza, D.M., Martins, A.F., 2019. Antipsychotic drugs in hospital wastewater and a preliminary risk assessment. *Ecotoxicology and Environmental Safety* 170, 559–567.
- Santiago-Martín, A. de, Meffe, R., Teijón, G., Martínez Hernández, V., López-Heras, I., Alonso Alonso, C., Arenas Romasanta, M., Bustamante, I. de, 2020. Pharmaceuticals and trace metals in the surface water used for crop irrigation: Risk to health or natural attenuation? *Science of The Total Environment* 705, 135825.
- Trachta, G., Schwarze, B., Sägmüller, B., Brehm, G., Schneider, S., 2004. Combination of high-performance liquid chromatography and SERS detection applied to the analysis of drugs in human blood and urine. *Journal of Molecular Structure* 693, 175–185.
- Trovó, A.G., Nogueira, R.F.P., Agüera, A., Sirtori, C., Fernández-Alba, A.R., 2009. Photodegradation of sulfamethoxazole in various aqueous media: Persistence, toxicity and photoproducts assessment. *Chemosphere* 77, 1292–1298.
- Tuckerman, M.M., 1984. Analytical profiles of drug substances, Vol. 12. Edited by Klaus Florey. *Journal of Pharmaceutical Sciences* 73, 572.
- Writer, J.H., Ferrer, I., Barber, L.B., Thurman, E.M., 2013. Widespread occurrence of neuro-active pharmaceuticals and metabolites in 24 Minnesota rivers and wastewaters. *The Science of the total environment* 461-462, 519–527.
- Yuan, S., Jiang, X., Xia, X., Zhang, H., Zheng, S., 2013. Detection, occurrence and fate of 22 psychiatric pharmaceuticals in psychiatric hospital and municipal wastewater treatment plants in Beijing, China. *Chemosphere* 90, 2520–2525

Appendices

ARTICLE I

" UV-photodegradation of desipramine: Impact of concentration, pH and temperature on formation of products including their biodegradability and toxicity"

Science of The Total Environment. 566-567, pp. 826-840.

Doi: 10.1016/j.scitotenv.2016.05.095

AUTHORS:

Nareman D.H. Khaleel, Waleed M.M. Mahmoud, Oliver Olsson, Klaus Kümmerer



UV-photodegradation of desipramine: Impact of concentration, pH and temperature on formation of products including their biodegradability and toxicity



Nareman D.H. Khaleel^{a,b}, Waleed M.M. Mahmoud^{a,b}, Oliver Olsson^a, Klaus Kümmerer^{a,*}

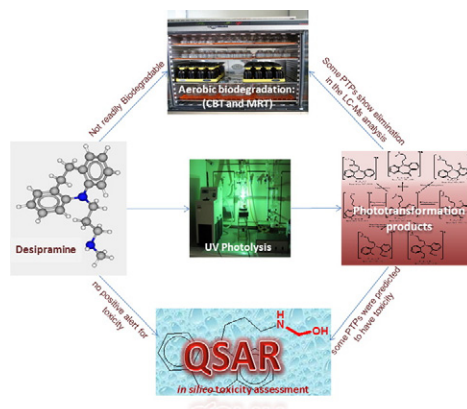
^a Sustainable Chemistry and Material Resources, Institute of Sustainable and Environmental Chemistry, Leuphana University of Lüneburg, Scharnhorststraße 1 C13, DE 21335 Lüneburg, Germany

^b Pharmaceutical Analytical Chemistry Department, Faculty of Pharmacy, Suez Canal University, Ismailia 41522, Egypt

HIGHLIGHTS

- Desipramine (DMI) is not readily biodegraded in the aquatic environment.
- UV photolysis rate and mechanism of DMI were affected by environmental conditions.
- UV Photolysis of DMI gives 18 new PTPs; their structures were elucidated.
- Some PTPs are eliminated in the biodegradation tests.
- Some PTPs are predicted as mutagenic, genotoxic and eco-toxic.

GRAPHICAL ABSTRACT



ARTICLE INFO

Article history:

Received 21 March 2016

Received in revised form 13 May 2016

Accepted 13 May 2016

Available online 30 May 2016

Editor: D. Barcelo

Keywords:

Tricyclic antidepressants

Mineralization

CBT and MRT

Photo-transformation product

QSAR

ABSTRACT

Desipramine (DMI) is a widely used tricyclic antidepressant, and it is the major metabolite of imipramine (IMI) and lofepramine (LMI); IMI and LMI are two of the most commonly used tricyclic antidepressants. If DMI enters the aquatic environment, it can be transformed by the environmental bacteria or UV radiation. Therefore, photolysis of DMI in water was performed using a simulated sunlight Xenon-lamp and a UV-lamp. Subsequently, the biodegradability of DMI and its photo-transformation products (PTPs) formed during its UV photolysis was studied. The influence of variable conditions, such as initial DMI concentration, solution pH, and temperature, on DMI UV photolysis behavior was also studied. The degree of mineralization of DMI and its PTPs was monitored. A Shimadzu HPLC-UV apparatus was used to follow the kinetic profile of DMI during UV-irradiation; after that, ion-trap and high-resolution mass spectrometry coupled with chromatography were used to monitor and identify the possible PTPs. The environmentally relevant properties and selected toxicity properties of DMI and the non-biodegradable PTPs were predicted using different QSAR models. DMI underwent UV photolysis with first-order kinetics. Quantum yields were very low. DOC values indicated that DMI formed new PTPs and was not completely mineralized. Analysis by means of high-resolution mass spectrometry revealed that the photolysis of DMI followed three main photolysis pathways: isomerization, hydroxylation, and ring opening.

* Corresponding author at: Nachhaltige Chemie und Stoffliche Ressourcen, Institut für Nachhaltige Chemie und Umweltchemie, Leuphana Universität Lüneburg, C.13, Scharnhorststraße 1, D-21335 Lüneburg, Germany.

E-mail address: klaus.kuemmerer@leuphana.de (K. Kümmerer).

The photolysis rate was inversely proportional to initial DMI concentration. The pH showed a significant impact on the photolysis rate of DMI, and on the PTPs in terms of both formation kinetics and mechanisms. Although temperature was expected to increase the photolysis rate, it showed a non-significant impact in this study. Results from biodegradation tests and QSAR analysis revealed that DMI and its PTPs are not readily biodegradable and that some PTPs may be human and/or eco-toxic, so they may pose a risk to the environment.

© 2016 Elsevier B.V. All rights reserved.

1. Introduction

Depression is expected to be the second most serious illness by the year 2020, with respect to global disease burden (Lajeunesse et al., 2008; Trachta et al., 2004). Accordingly, the use of antidepressant drugs should increase, and hence these drugs are expected to be present in increasingly high concentrations in the influents of sewage treatment plants (STPs). Tricyclic antidepressants (TCAs) are a group of antidepressants which inhibit nor-adrenaline reuptake. TCAs are much used in many countries such as Germany, Spain, and Austria. Their consumption has shown a steady increase during recent years (Bauer et al., 2008; Herrmann et al., 2015). This study focus on desipramine (DMI), which belongs to the TCA group and it is an example of the commonly used TCAs (Boonprasert et al., 2013). It is, at the same time, the major metabolite of other widely used TCAs, namely Imipramine (IMI) and Lofepamine (LMI) (Önal and Öztunç, 2011). DMI is extensively metabolized to 2-hydroxy DMI and desmethyl DMI in the liver, approximately 70% being excreted in urine, with an unchanged excreted fraction between 3 and 5% (Ramey et al., 2014; De Vane et al., 1981).

Antidepressants are among the many pharmaceutical substances that have been detected in drinking water in particular (Huerta-Fontela et al., 2011). Although DMI's parent compound (IMI) has already been detected in the aquatic environment, the presence of DMI in the aquatic environment has not been studied until now. IMI has been detected in four wastewater treatment plants in Beijing, China; the average detected concentration was 129 ng L^{-1} which is higher than the average concentration measured for the highly used carbamazepine (113 ng L^{-1}) (Petrovic and Barceló, 2007). IMI has also been detected in another place in Beijing, China (Sheng et al., 2014), and in the influent and the effluent in the STP of Vitoria-Gasteiz in Spain (Unceta et al., 2010). The ratio between the influent and effluent concentrations in the latter study indicates that IMI had not been eliminated by the sewage treatment. Although research on IMI has been carried out, LMI has not yet been checked in the aquatic environment.

When DMI, as an excreted drug or as a metabolite of IMI or LMI, reaches the aquatic environment, it can undergo various natural biotic and abiotic transformations. Transformations may also happen in technical treatment processes such as water disinfection by UV and other advanced oxidation processes used in STP effluent treatment and in drinking water (Arnold and McNeill, 2007; Khaleel et al., 2013; Santiago-Morales et al., 2014). These biotic and/or abiotic transformations can contribute to DMI degradation and elimination from the aquatic environment. They can also result in the production of transformation products (TPs). Some of these TPs have been shown to be more stable and more dangerous to humans and the eco-system than their parent pharmaceuticals. Therefore, it is important to study the fate of these TPs as (Gutowski et al., 2015; Illés et al., 2014; Mahmoud et al., 2014; Trautwein et al., 2014). In the literature concerning the biodegradability of TCAs, amitriptyline and nortriptyline were found to be dissipated in agricultural soils with dissipation times to dissipate 50% of material ranging from 34.1 to 85.3 days and can give bioactive TPs (Li 2013 #80). There are no data reported about biodegradation of DMI. Direct and indirect photolysis of some TCAs such as imipramine and clomipramine were studied (Calza 2008 #82) (Canudas 2002 #81). Regarding DMI, only the photolysis of DMI under simulated

solar irradiation has been investigated (Gros et al., 2015). These authors showed that DMI required a long irradiation time to be degraded using xenon lamp in pure water with $t_{1/2}$ of approximately 36 h, and showed that the toxicity of the received mixture of TPs and DMI increased. Therefore, photolysis of DMI using UV light and studying the biodegradability and the toxicity of the formed UV-photolysis transformation products (PTPs) is important.

Researching into the environmental impact of TPs is challenging, because isolation and purification of TPs are difficult tasks and because their structures and properties are often unknown. The use of *in silico* tools which are based for example on quantitative structure activity relationships (QSARs) allows some of these challenges to be circumvented (Rastogi et al., 2014). Once the structure of the TPs has been elucidated, the QSAR models can be applied to predict the environmental fate and toxicity of these TPs at different toxicological endpoints (Mahmoud et al., 2014).

So, the objective of this work was to study the environmental fate of DMI and its PTPs through: (i) the determination of the kinetics of the UV-photolysis and mineralization rates of DMI in pure water under variable conditions, (ii) the identification and structural elucidation of the PTPs by means of liquid chromatography coupled to high-resolution mass spectrometry and by studying their formation/elimination kinetics, (iii) studying the biodegradability of DMI and its photolytic mixtures, which contain the PTPs, by employing two tests standardized by the Organization for Economic Co-operation and Development (OECD), namely the Closed Bottle Test (CBT, OECD 301D) and the Manometric Respiratory Test (MRT, OECD 301F), to assess changes in biodegradability during UV photolysis, and (iv) a preliminary assessment of the toxicity and environmental fate of DMI and its PTPs using QSAR models.

DMI concentrations used in this study are high compared with the real environmental concentrations because this study aimed at a better general understanding of formation and properties of TPs such as some general trends for kinetics. Some aspects cannot be studied at low concentrations such as biodegradability of PTPs and the mineralization of DMI. However, the role of the concentration was assessed in this study. In the same manner, experimental design approach was not used here because it will be difficult to determine the effect of the studied variables on the type of the formed PTPs.

2. Experimental design and analytical methods

2.1. Materials

Desipramine (DMI), CAS number 58-28-6, of purity >98% was bought from Sigma-Aldrich (Steinheim, Germany). Acetonitrile, Methanol (HiPerSolv CHROMANORM, LC-MS grade, BDH Prolabo), and formic acid were obtained from VWR (Darmstadt, Germany). All reagents were used without further treatment or purification and the aqueous solutions were made using ultrapure (UP) water. In biodegradability testing, all the chemicals used as nutrients were of >98.5% purity.

2.2. Photolytic degradation experiments and quantum yield calculation

Photolysis experiments were performed under different conditions (initial drug concentrations of 5, 10, 50, and 100 mg L^{-1} ; temperatures

of 10, 20, 30, and 40 °C; and pH values of 3, 5, 7, and 9), in order to study the effect of these conditions on the UV-photolysis kinetics of DMI and on the formation kinetics and mechanism of the PTPs. The required pH value was adjusted using HCl and/or NaOH. In order to examine if DMI concentration was primarily affected by the different conditions studied, controls wrapped in aluminum foil were run simultaneously under the same conditions.

Photolytic experiments were performed using a 1 L batch photoreactor, filled with about 0.8 L of the working aqueous solution of DMI. Temperature was adjusted to the desired value using a cooling system (WKL230, LAUDA, Berlin), which ensured constant temperature throughout the experiment. The photoreactor was equipped with a magnetic stirrer to ensure a constant mixing of the solutions. During the photolysis, the pH was monitored using a laboratory pH meter (WTW pH/ION 735P inoLab®).

The light source used in UV photolysis tests was a TQ 150 W medium-pressure mercury lamp (UV Consulting Peschl, Mainz, Germany) with an ilmasil quartz immersion tube. The total photon flow rate of the polychromatic lamp used (200–440 nm) was assessed with a UV-pad Spectral Radiometer (Opsytec Dr. Gröbel GmbH, Ettlingen, Germany). The radiometer was placed at a distance of 4 cm from the emission source in an alumina box. The total photon flow rate of the lamp for all wavelengths was 5.71×10^6 (mol \times photons \times cm⁻² \times s⁻¹). The intensity of light emitted by the UV lamp and the molar absorbance of the DMI are summarized in Supplementary Fig. S1.

DMI was also subjected to simulated solar photolysis at initial concentrations of 10 mg L⁻¹ using a Xenon lamp (TXE 150, UV Consulting Peschl, Mainz, Germany). The Xenon lamp emits spectra similar to natural sunlight (200–800 nm), with the highest intensity in the visible range (200–280 nm: $1.61 \text{ e}^{-2} \text{ W/m}^2$, 280–315 nm: $1.16 \text{ e}^{-2} \text{ W/m}^2$, 315–380 nm: $3.75 \text{ e}^{-2} \text{ W/m}^2$, 380–780 nm: $5.58 \text{ e}^{-1} \text{ W/m}^2$; data provided by the manufacturer).

The photolysis experiments were conducted for 128 min. Samples were collected at 0, 2, 4, 8, 16, 32, 64 and 128 min of irradiation for HPLC-UV and LC-MSⁿ analyses, and dissolved organic carbon (DOC) determination. Collected samples were then filtered immediately through 0.45 μm membrane filters (CHROMAFIL® Xtra Typ: PES 45/25, Macherey-Nagel, Germany) and either analyzed immediately or stored in the dark at -20 °C until analyses. The DOC of the samples was measured to determine the extent of mineralization using a Shimadzu Total Organic Carbon Analyzer (TOC-Vcpn, Shimadzu GmbH, Duisburg, Germany) in three replicates.

For CBT and MRT of the photolytic mixture, samples were collected at 0 min and after 16, 64 and 128 min of UV irradiation. The initial concentration of DMI in the photolytic-treated samples was adjusted by measuring the DOC of the tested substance (0 min, i.e. before photolysis) and of the photolysed samples, to determine the required carbon content and to calculate the theoretical oxygen demand (ThOD), for each CBT and MRT.

A one-way ANOVA and Tukey's tests were performed to test the statistical significance of the difference in the photolysis rates of DMI under the variable environmental conditions studied during the photodegradation testing (Bosco and Larrechi, 2008; Gunasekar et al., 2013; Körbahti and Rauf, 2009).

The quantum yield (ϕ) for DMI was calculated from the determined photodegradation rate constant (k) assuming a wavelength-independent quantum yield in the wavelength interval (200–440 nm) (Prados-Joya et al., 2011; OECD-316, 2008; Zepp, 1978).

$$\phi = \frac{K_{\lambda}}{2.303 \times \left(\frac{A}{V}\right) \times L \times I_{\lambda} \times \varepsilon_{\lambda}} \quad (1)$$

where k_{λ} is the photodegradation rate constant (s⁻¹); I_{λ} is the photon flow rate emitted by the lamp (Einstein m⁻² s⁻¹); ε_{λ} is the molar extinction coefficient of the target compound for each wavelength (m² mol⁻¹);

ϕ is the quantum yield (mol Einstein⁻¹); A and V are the area and the volume of the solution in the photoreactor and L is the pathlength of the photolysis cell.

The photon flow rate was calculated from the irradiance of the lamp using Eq. (2):

$$I_{\lambda} = \frac{E \times \lambda \times 5.03 \times 10^{15}}{N_A} \quad (2)$$

where N_A is Avogadro's number ($N_A = 6.022 \cdot 10^{23} \text{ mol}^{-1}$); E is the irradiance of the lamp (W m⁻²); and λ is the wavelength (m).

2.3. Chemical analysis

2.3.1. HPLC/DAD

The kinetic profile of the DMI during irradiation was monitored using a Shimadzu Prominence HPLC-UV apparatus (Shimadzu, Duisburg, Germany) consisting of an LC-10AT binary pump, a CBM-10A communication interface, an SPD-M10A diode array detector (DAD), an SIL-10 auto sampler, a CTO-10 AS VP column oven, and Shimadzu Class LC10 software version (5.0). 10 μL of irradiated filtered samples were directly injected into the HPLC-UV apparatus. Analytical separation was performed using an RP-C18 column (EC 125/4 NUCLEODUR® 100–5 C18 ec, Macherey and Nagel, Düren, Germany), protected by an EC guard column (NUCLEODUR® 100–5 C18 ec, 4 \times 3 mm). The chromatographic separation was performed using a binary gradient of 0.1% formic acid in UP water (solution A) and 100% acetonitrile (solution B) as a mobile phase, with the following linear gradient: 0 min (5% B), 4 min (5% B), 6.5 min (20% B), 9 min (30% B), 12 min (40% B), 15 min (45% B), 18 min (50% B), 20 min (50% B), 23 min (5% B), and 28 min (5% B). The flow rate was 0.5 mL min⁻¹ and the oven temperature was set to 45 °C. The detection wavelength was 250 nm.

2.3.2. LC-MSⁿ

The separation and primary identification of the PTPs was performed using two LC-MSⁿ analysis systems. The first one was an Agilent 1100 series HPLC system (Agilent Technologies, Waldbronn, Germany) coupled with a Bruker Esquire 6000 plus ion trap mass spectrometer with electrospray ionization (ESI) source (Bruker Daltonics, Bremen, Germany) (LC-ITMS). This was used for an initial screening to elucidate and tentatively identify the structure of the PTPs formed. LC-ITMS was operated in full-scan MS^{1–4} modes to screen the structures of the PTPs. The second LC-MSⁿ system was a Dionex Ultimate 3000 UHPLC system (Dionex, Idstein, Germany) coupled to an LTQ Orbitrap-XL high-resolution mass spectrometer with H-ESI source (Thermo Scientific, Bremen, Germany) (LC-HRMS). This one was used for the further analysis and confirmation of the tentatively identified PTP structures. The structures of PTPs that resulted from the LC-ITMS analysis were checked by accurate mass measurements provided by the LC-HRMS, which gave the empirical ion formula, relative double bond equivalent values (RDB), and mass error calculations for the PTPs formed.

The same chromatographic column and method as described in Section 2.3.1, were used for both the LC-ITMS and the LC-HRMS analyses. Detailed information about the LC-MSⁿ systems used and their chromatographic conditions can be found in Supplementary text S1. Mass Frontier™ software (Thermo Scientific) was used to predict fragment ions for the proposed chemical structures and these fragments were matched to the ones obtained in the experimental product ion spectra.

Due to the lack of standards for the PTPs, their individual peak areas can only be used to monitor their relative course within the photolytic treatment. An absolute measurement of the individual concentrations is not possible. Furthermore, a peak of low intensity does not necessarily correspond to a high concentration of the related PTP and vice versa.

Therefore, the recovery % was calculated using the relation $A/A_0\%$, where A_0 is the peak area of the DMI at time 0 or at Day 0, and A is the peak area of the PTP at one of each sample's irradiation times or at Day 28, in either the photodegradation or biodegradation tests, respectively.

2.4. Aerobic biodegradation testing following OECD 301 D (closed bottle test (CBT))

Closed Bottle Test (CBT) is a simple test to evaluate the ready biodegradability of an organic compound in the environment. It was performed according to the OECD test guidelines (OECD, 1992a,b) using a low bacterial density (2 drops STP effluent/L), low nutrient content, and at room temperature (20 ± 1 °C) in the dark. The test system consisted of four different series, each series run in parallel (Supplementary Table S1a). The readily biodegradable sodium acetate and the test substance used in the test were adjusted to a concentration corresponding to 5 mg L^{-1} theoretical oxygen demand without nitrification (ThODNH₃). The concentration of standard DMI solution in the test bottle was 2.2 mg L^{-1} , corresponding to a ThOD of 5 mg L^{-1} . The final concentration of the photolytic mixtures after 16, 64 and 128 min, respectively, was adjusted according to the remaining DOC concentration to reach a comparable ThOD. All test bottles were inoculated with an aliquot from the effluent of the municipal STP in AGL Lüneburg, Germany (144,000 inhabitant equivalents). Throughout the test, the biochemical oxygen demand (BOD) was monitored by measuring the dissolved oxygen concentration (Friedrich et al., 2013). A test compound is classified as “readily biodegradable” if biodegradation, expressed as a percentage of oxygen consumed in the test bottle, exceeds 60% within a period of 10 days after the oxygen consumption reached 10% ThOD. Toxicity was assessed by comparing oxygen consumption, as measured in the toxicity controls, with the predicted level calculated based on the oxygen consumption in the quality control and in the test bottles, respectively. Toxicity controls allow for the recognition of false negative results caused by the toxicity of the test compound against the degrading bacteria. Samples taken at the beginning and at the end of the test (after 28 days) were stored at -20 °C for later HPLC-UV and LC-UV-MS/MS analyses.

2.5. Aerobic biodegradation testing following OECD 301 F (Manometric respiratory test (MRT))

The MRT was performed according to the OECD test guidelines (OECD, 1992a,b) using higher bacterial concentration (80 mL STP effluent/L) and higher concentrations of sodium acetate and of the test substance compared to the CBT. The concentration of DMI standard solution was 12.9 mg L^{-1} , corresponding to ThOD of 30 mg L^{-1} . MRT test consisted of five different series: the four series in the CBT and an additional sterile control bottle (Supplementary Table S1b). The sterile control contained sodium azide in order to account for abiotic degradation. All test bottles were inoculated with the same aliquot used in CBT. The OxiTop OC110-system (WTW GmbH, Weilheim, Germany) was used as measuring system. The bottles of the OxiTop OC110-system were firmly closed with measuring heads, which cover an exactly defined gas volume. The process of aerobic biodegradation was monitored by measuring carbon dioxide (CO₂) production. The measuring heads contained sodium hydroxide, which reacted with the CO₂ and converted it to sodium carbonate. In this manner, CO₂ was removed from the gas phase. The resulting decrease in pressure showed the corresponding oxygen consumption. Measurements were made in duplicate. By subtracting blank values from the quality control, toxicity control, and test compound values, the percentage of the final biodegradation was determined. Samples taken at the beginning and at the end of the test (after 28 days) were stored at -20 °C for later HPLC-UV and LC-UV-MS/MS analyses. DOC was also measured for Day 0 and Day 28 samples.

2.6. In silico prediction of toxicity and environmental fate

A set of software for *in silico* prediction was used because the software currently available on the market might have individual weaknesses due to different algorithms and training sets. The *in silico* software programs used here were: Case Ultra V 1.5.2.0 (MultiCASE Inc.) (Chakravarti et al., 2012; Saiakhov et al., 2013), EPI (Estimation Programs Interface) Suite (EPIWEB 4.1) from the U.S. Environmental Protection Agency (EPI Suite software (EPIWEB 4.1)), and Oasis Catalogic (V.5.11.6TB) from the Laboratory of Mathematical Chemistry, University Bourgas, Bulgaria (Laboratory of Mathematical Chemistry, 2012). Structure illustrations were done using Marvin Sketch 15.6.15.0, 2015, ChemAxon (<http://www.chemaxon.com>). Simplified molecular input line entry specification (SMILES) codes from the molecular PTP structures were used for the input of molecular structures. In addition, Oasis Catalogic software was used to predict the octanol-water partition coefficient value (log P) for both the DMI and the predicted structures of its PTPs (Supplementary materials Table S2).

2.6.1. In silico prediction of readily biodegradation

The ready biodegradability of DMI and its PTPs were predicted by various *in silico* models to compare them with the experimental results. The ready biodegradability values were predicted with Case Ultra, EPI Suite, and Oasis Catalogic according to OECD 301C MITI-I test guidelines (Ministry of International Trade and Industry, Japan) (OECD, 1992a). Oasis Catalogic also provides a biodegradation model according to OECD 301F, which is comparable to the experimental biodegradation test (MRT) used in this research (Dimitrov et al., 2011). In the Oasis Catalogic MITI-I and OECD 301F models, the ready biodegradability was predicted as a numerical value between 0 and 1, corresponding to 0% and 100% biodegradation, respectively. The experimental pass criterion for ready biodegradability is 60% biodegradation, which corresponds to the numeric value of 0.6. In EPI Suite, “readily biodegradable” was assigned a numeric value of 1, and “not readily biodegradable” was assigned a numeric value of 0 (0 to 1 is the probability range for a compound to undergo biodegradation). Results from EPI Suite, which are higher than 0.5, are indicative of readily biodegradability. Case Ultra provides positive (+), negative (−), out of domain (OD), and inconclusive (±) results. The latter “inconclusive” result indicates that a positive alert was found in the test compound but the calculated probability falls inside the grey zone of the model (10% around the classification threshold of the model) and therefore a concrete prediction cannot be made for the selected models.

2.6.2. In silico prediction of toxicity

In silico toxicity for DMI and its PTPs was predicted by a set of *in silico* models for toxicity predictions. Case Ultra was used to apply a combination of statistical and rule-based systems for bacterial mutagenicity according to the recently implemented ICH guideline M7 (International Conference on Harmonization (ICH), 2014). The following models of Expert rules for genotoxicity (GT Expert) were used: GT1 A7B (Mutagenicity for seven strains of *Salmonella typhimurium* (TA 97, 98, 100, and 1535–1538, FDA data source), GT1 AT Ecoli (A–T mutation in *E. coli* and *S. typhimurium* TA102, FDA data source), Pharm Ecoli (*E. coli* mutagenicity (all strains), public and proprietary sources), and Pharm Salm (*S. typhimurium* mutagenicity (TA 97, 98, 100, and 1535–1538), public and proprietary sources). Moreover, Case Ultra was used to predict ecotoxicity based on the effect of microtox toxicity on environmental bacteria (*V. fischeri*). For Case Ultra software, the predicted activities of the pharmaceuticals tested here were expressed as described in Section 2.6.1.

Oasis Catalogic was used to predict acute toxicity towards *V. fischeri* after 5, 15, and 30 min of exposure, and mutagenicity based on bacterial mutagenicity for *S. typhimurium* (module mutagenicity v.04). For Oasis Catalogic, the predicted activity of the pharmaceuticals tested in the three acute *V. fischeri* modules are expressed as mg L^{-1} for half maximal

inhibitory concentration (IC_{50}), and in the mutagenicity module are expressed as “mutagenic (+)” or “not mutagenic (-).”

3. Results and discussion

3.1. DMI photodegradation using different concentrations: elimination, mineralization and quantum yield calculation

The UV photolysis of DMI was performed in UP water at pH 5 and 20 °C using four concentration levels: 5, 10, 50, and 100 mg L⁻¹. In the controls without access to light, no significant loss of DMI was observed, indicating the absence of hydrolysis. Accordingly, DMI underwent photolysis only due to the effect of the used medium-pressure Hg lamp. Fig. 1a depicts the time-trend for the photolytic degradation of DMI and its dependence on the initial DMI concentration. The results of these processes fit first-order kinetics quite well ($R^2 > 0.97$), showing degradation rates (k) and half-lives ($t_{1/2}$) equal (0.1270&5.5), (0.6782&10.2), (0.0148&46.8), and (0.0085&81.5) min⁻¹ and min for DMI concentrations of 5, 10, 50, and 100 mg L⁻¹, respectively. The degree of DOC removal showed that after 128 min irradiation in the experiments at 100, 50, 10, and 5 mg L⁻¹, the mineralization observed was approximately 5.9, 12.1, 78.3, and 85%, respectively (Fig. 1b). Therefore, this UV-photolysis was accompanied by the formation of new PTPs, as no complete mineralization to CO₂ and water occurred. These results indicate the probability of faster degradation and of complete mineralization at lower concentrations, or even at high concentrations after a longer irradiation time. Therefore, better degradation is expected for realistic environmental concentrations. An ANOVA analysis indicated that the differences in photolysis rates as a function of DMI initial concentrations were statistically significant with $P < 0.001$. Tukey's test results confirmed that the differences in the photolysis rates between each pair of the studied concentrations are highly statistically significant ($P < 0.001$).

Supplementary Fig. S2 shows that the quantum yield and the degradation rate are inversely proportional to the DMI initial concentration. Two mechanisms likely explain the decrease in photolysis and mineralization rates of DMI, which are related to the increase in initial DMI concentration. The first relates the energy absorbed by each DMI molecule. Given that the radiation energy deposited in the medium per unit volume is constant, DMI molecules can absorb more radiant energy in the same time at lower concentrations (Prados-Joya et al., 2011). The second is the fact that more intermediates and PTPs were formed in response to irradiation with UV light at higher initial concentrations. These intermediates can compete with DMI and absorb UV light partially before the UV light can pass through the entire solution (Herrmann et al., 2015).

In contrast, no degradation or mineralization was observed in response to 128 min of irradiation using a xenon lamp (simulated sun light) at 10 mg L⁻¹ DMI concentration (Supplementary Fig. S3). This result agrees with the results of Gros et al. (Gros et al., 2015).

3.2. Identification of DMI PTPs and proposed degradation pathway

A large number of PTPs were present in the DMI photolytic mixtures; all of them can be assumed to be more polar than the DMI itself as they eluted earlier from the non-polar RP-C18 column. Supplementary Fig. S4a displays the total ion chromatogram (TIC) of the aqueous solution of 100 mg L⁻¹ DMI after 128 min of UV irradiation. Eight new peaks were detected in the TIC. Extracted ion chromatograms (EICs) for ions suspected to be present were also performed, as some PTPs in the TICs may have a low response in the chromatographic system and would be harder to detect. TIC and EICs results show that 18 new PTPs were formed during UV photolysis of DMI according to signals at different retention times (t_{RS}) with only seven different m/z values. The latter finding indicates the formation of isomers. The predicted log P values using QSAR models can help in the differentiation

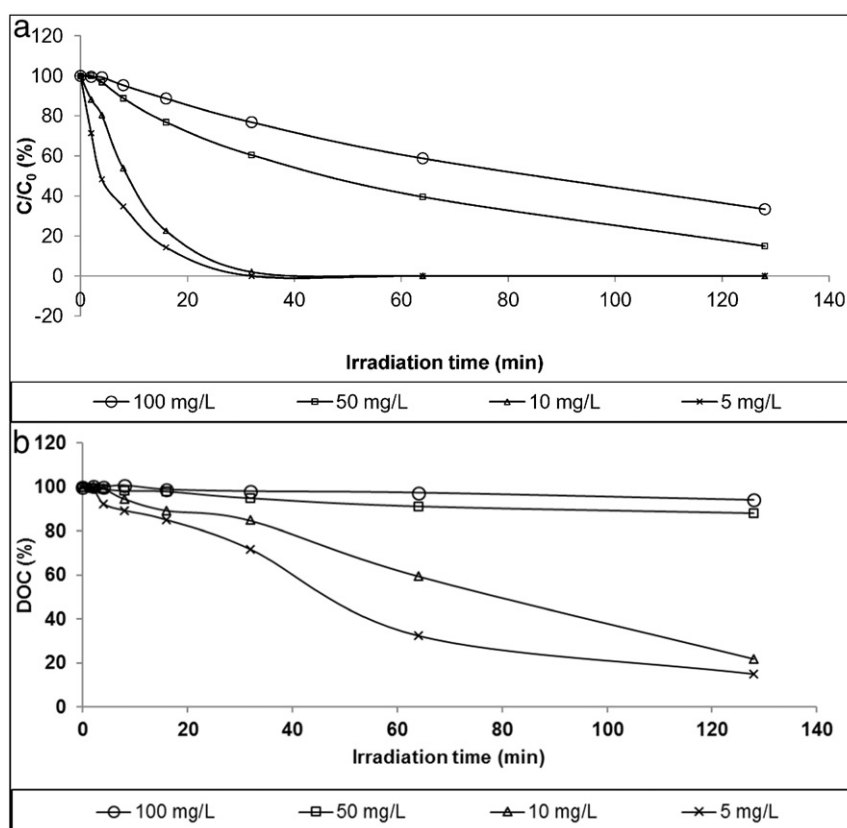


Fig. 1. The photolytic degradation (a), and the DOC recovery (b), of DMI by means of UV photodegradation at different concentrations. pH = 5, temperature = 20 °C.

between the isomers because the compound which has lower log P value is more polar and therefore has relative lower t_R (Supplementary Table S2). A tentative photolytic degradation pathway for DMI in UP water was proposed based on these results (Supplementary Fig. S4b).

For the 18 PTPs, up to MS³ spectra were generated. The accurate mass measurements for the PTPs were in agreement with the proposed elemental composition of $[M + H]^+$ ions with a low mass deviation of <2 mmu for most PTPs identified. All calculated RDB values for PTPs or fragments matched the respective predicted structures, increasing the likelihood that the proposed structures are correct (Table 1). Gros et al. found ten TPs produced from DMI photolysis using a xenon lamp after 72 min of irradiation. Only two of these TPs were found in our study using the UV irradiation; these two TPs are labelled as PTP₂₈₃ and PTP₂₉₉. The discrepancy might be because the TPs formed under Xe lamp irradiation were obviously not further degraded under Gros et al. conditions. However, under irradiation with UV light of higher energy as in our study, these PTPs are either not formed at all or else quickly transformed into the PTPs we did observe, which in turn were stable under UV irradiation. In addition, all of the other detected masses by Gros et al. were observed in our study but as main fragmentation products of the TPs in high resolution MS and not as photolysis TPs, indicating them to be preferred structures resulting from energy input.

The most intense precursor ion peaks, PTP₂₆₇₋₁ and PTP₂₆₇₋₂, have the suggested ion formula C₁₈H₂₃N₂, which is the same as the DMI formula. They are assumed to be isomers to the DMI, as they have also the same RDB value, and differ only in few of the MSⁿ fragments which however cannot be used to distinguish between the isomers. The MS² spectrum of the two PTPs shows fragment at m/z 239 (C₁₆H₁₉N₂), and PTP₂₆₇₋₁ gives a fragment at m/z 210 (C₁₅H₁₆N) and PTP₂₆₇₋₂ gives fragment at m/z 208 (C₁₅H₁₄N), indicating that these PTPs may differ only in the position of the sidechain methyl group (Supplementary Figs. S5 & S6 & S7).

Two PTPs with m/z 281.17 and with the suggested ion formula C₁₈H₂₁N₂O were detected and labelled as PTP₂₈₁₋₁ and PTP₂₈₁₋₂. These PTPs are formed by oxidation of DMI. The MS² spectrum of PTP₂₈₁₋₂ shows a key fragment at m/z 210 (C₁₄H₁₂NO). This key fragment originated through the loss of the 1-methylaminopropyl chain, indicating that the oxidation took place within the tricyclic part mainly in the azepane ring as oxidation at other positions is unlikely. The absence of the latter fragment in PTP₂₈₁₋₁ suggests oxidation of the 1-methylaminopropyl chain (Supplementary Figs. S8 & S9). According to the Log P predicted values, the PTP formed due to oxidation in the first carbon in the aminopropyl chain will be more polar than if oxidation had occurred in the other possible positions in the aminopropyl chain. Therefore, the oxidation in PTP₂₈₁₋₁ is likely to occur at the first carbon in the aminopropyl chain as it appears at lower t_R .

For the five PTPs with m/z 283, the suggested ion formula of C₁₈H₂₃N₂O points out that a hydroxylation of the molecule took place. Their MS² spectra showed no characteristic fragments that would reveal the position of the hydroxyl group. It is difficult to tell if the hydroxylation took place in the 1-methylaminopropyl chain or in the tricyclic part (Supplementary Figs. S10 & S11 & S12 & S13 & S14). According to the predicted Log P values, the PTPs formed due to hydroxylation in the 1-methylaminopropyl chain will be more polar than those formed due to hydroxylation in the tricyclic ring. As PTP₂₈₃₋₁, PTP₂₈₃₋₂, and PTP₂₈₃₋₃ appear at lower t_R , they should be hydroxylated in the 1-methylaminopropyl chain, whereas PTP₂₈₃₋₄ and PTP₂₈₃₋₅ seems to have the hydroxylation in the benzene ring of the tricyclic part as they appear at higher t_R . The TP found by Gros et al. in a previous study for the photolysis of DMI using Xenon lamp with m/z 283 is similar to PTP₂₈₃₋₄ or PTP₂₈₃₋₅. The MS² spectrum of PTP₂₈₃₋₂ shows a key fragment at m/z 226 (C₁₅H₁₆NO). This key fragment originated through the loss of the 1-methylaminoethyl chain, indicating that the hydroxylation took place within the first methyl in the 1-methylaminopropyl chain. In the same manner, PTP₂₈₃₋₃ and PTP₂₈₃₋₁ show key fragments at m/z 240 and m/z 255 (C₁₆H₁₈NO and C₁₆H₁₉N₂O) indicating that the

hydroxylation took place within the second and third methyl in the 1-methylaminopropyl chain, respectively.

In the four PTPs with m/z 299 (ion formula C₁₈H₂₃O₂N₂), twofold hydroxylation took place. PTP₂₉₉₋₂ and PTP₂₉₉₋₃ showed MS² fragments with m/z 182 (C₁₀H₁₆NO₂) and 180 (C₁₀H₁₄NO₂), respectively, that originated by the cleavage of one benzene ring and the loss of the 1-methyl aminopropyl chain keeping the two hydroxyl groups intact. These fragments indicate the position of the two hydroxyl groups either both in one of the benzene rings or else one in the benzene ring and the other one in the azepane ring (Supplementary Figs. S15 & S16 & S17 & S18). According to the predicted Log P values, the PTP formed due to di-hydroxylation in one benzene ring and in the azepane ring will be more polar than this formed due to dihydroxylation in one of the two benzene rings. Therefore, PTP₂₉₉₋₃ can be the di-hydroxylated product in one of the two benzene rings and PTP₂₉₉₋₂ is the di-hydroxylated product in the benzene and the azepane rings as PTP₂₉₉₋₂ has lower polarity and appears at lower t_R than PTP₂₉₉₋₃. From these results, PTP₂₉₉₋₃ seems to be like the suggested TP structure for the dihydroxylated product found by Gros et al. (Gros 2015 #49). Although PTP₂₉₉₋₁ and PTP₂₉₉₋₄ gave no key fragment indicating if the hydroxylation took place in the tricyclic part or in the 1-methylaminopropyl chain, their predicted log P values indicated that PTP₂₉₉₋₄ can have the two hydroxyl groups in the two benzene rings and that PTP₂₉₉₋₁ has one hydroxyl group in the benzene ring and the other one in the 1-methylaminopropyl chain. For PTP₂₉₉₋₁, the MS² spectrum of PTP₂₉₉₋₁ shows key fragment at m/z 240 (C₁₅H₁₄NO₂) which can indicate the exact position of the hydroxyl group in the 1-methylaminopropyl chain. This key fragment originated through the loss of the 1-methylaminoethyl chain, indicating that the sidechain hydroxylation took place on the first methyl in the 1-methylaminopropyl chain.

The PTPs with m/z 285.19 and 301.19 were most likely formed by mono- and di-hydroxylation of the DMI, mainly in the azepane ring, with subsequent ring cleavage (Supplementary Figs. S19 & S20 & S21). This cleavage has been discussed in a previous publication for a similar tricyclic ring of the anticonvulsant drug carbamazepine, but only as an intermediate product (Petrovic and Barceló, 2007). The structure of PTP₂₈₅₋₁ was not identified.

PTP₂₁₉ could be formed directly from DMI after the degradation of one of the benzene rings keeping the azepane cycle intact combined with both oxidation and demethylation from the aliphatic side chain. PTP₂₁₉ presented an increasing slope during the course of photolysis at 100 mg L⁻¹. It gave a fragment with m/z 160, which indicates that the oxidation occurs on the azepane ring (Supplementary Fig. S22).

Fig. 2 shows the formation/elimination kinetics of the PTPs, formed with A/A₀ (%) above 0.1% during the photolysis of DMI at an initial concentration of 100 mg L⁻¹ ($n = 3$). Most of the PTPs were formed immediately after starting the irradiation, increased in concentration constantly until a certain time point and were then eliminated, in favor of the formation of follow-up PTPs or mineralization. PTP₂₁₉, PTP₂₈₁₋₁, PTP₂₈₁₋₂, PTP₂₈₅₋₁, and PTP₂₉₉₋₁ were formed immediately after starting irradiation, but not further eliminated, presenting an increasing concentration throughout the entire photolysis. Thus, these PTPs could be considered to persist in the environment if they are not otherwise biodegradable. Supplementary Fig. S23 shows the formation/elimination kinetics of PTPs formed during the photolysis of DMI at different concentration levels. Most of the PTPs identified in the 100 mg L⁻¹ irradiated solution, also occurred during photolysis at other concentrations but with different degradation kinetics. Only at an initial concentration of 5 mg L⁻¹, a few of these PTPs were difficult to detect, which might be due to inadequate detection limits and/or low ionization rates. The PTPs from tests with initial lower concentrations showed faster formation/elimination kinetics than those formed at higher concentrations. This agrees with other finding in the literature (Herrmann et al., 2015; Mahmoud et al., 2014). It was observed that even PTPs that continuously increased over time during photolysis at

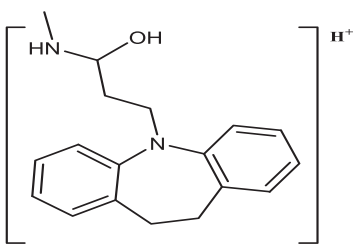
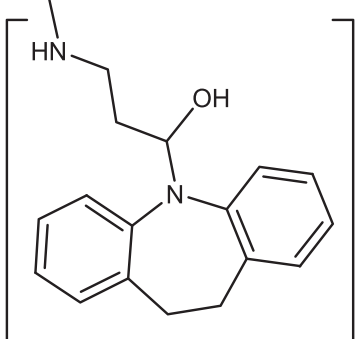
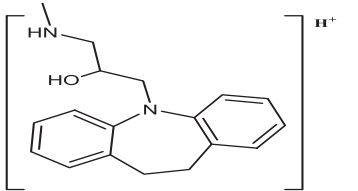
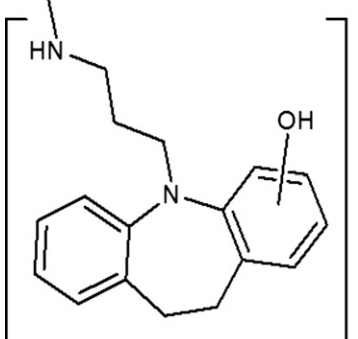
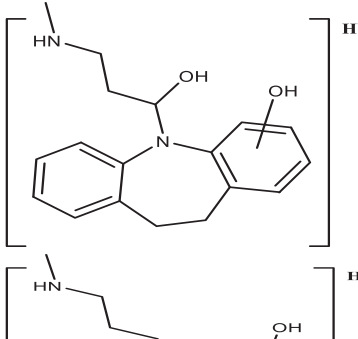
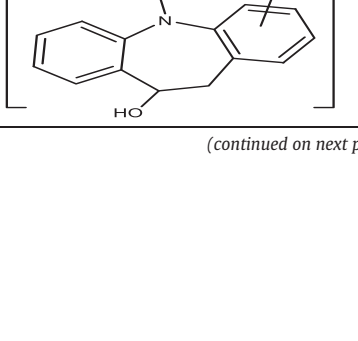

higher concentrations, behaved differently at lower concentrations, increasing up to a certain time point and then decreasing. This may be because at higher concentrations the required irradiation amount for these PTPs to begin to decrease was not reached, that is, they require a

longer irradiation time to begin to decrease. Therefore, certain PTPs cannot be categorized as environmentally dangerous substances as their formation depends on concentration which vary with irradiation time and intensity.

Table 1
Desipramine (DMI) and its possible photolysis transformation products (PTPs) showing the measured and the calculated masses, RDB, ion formula, relative error, and the proposed structures.

Compound	R _t	Measured mass [m/z]	Calculated mass [m/z]	RDB	Molecular formula	Relative error [ppm]	Precursor ion/product ion	Proposed structure of PTPs		
PTP ₂₆₇₋₁ MS ² : 267	12.12	267.18643	267.18612	8.5	C ₁₈ H ₂₃ N ₂	0.855	[M + H] ⁺			
		239.15402	239.15428	8.5	C ₁₆ H ₁₉ N ₂	-0.255	[M + H-C ₂ H ₄] ⁺			
		224.14514	224.14338	8.5	C ₁₆ H ₁₈ N	1.764	[M + H-C ₂ H ₅ N] ⁺			
		210.12802	210.12773	8.5	C ₁₅ H ₁₆ N	0.294	[M + H-C ₃ H ₇ N] ⁺			
		196.11238	196.11208	8.5	C ₁₄ H ₁₄ N	0.304	[M + H-C ₄ H ₉ N] ⁺			
		196.11238	196.11208	8.5	C ₁₄ H ₁₄ N	-0.166	[M + H-C ₂ H ₅ N] ⁺			
		MS ³ : 239 PTP ₂₆₇₋₂ MS ² : 267	12.9	267.18658	267.18612	8.5	C ₁₈ H ₂₃ N ₂		1.005	[M + H] ⁺
				239.15475	239.15428	8.5	C ₁₆ H ₁₉ N ₂		0.475	[M + H-C ₂ H ₄] ⁺
				238.1599	238.15903	8.5	C ₁₇ H ₂₀ N		0.874	[M + H-CH ₃ N] ⁺
				224.14284	224.14338	8.5	C ₁₆ H ₁₈ N		-0.536	[M + H-C ₂ H ₅ N] ⁺
208.10982	208.11208			9.5	C ₁₅ H ₁₄ N	-2.256	[M + H-C ₃ H ₉ N] ⁺			
196.11206	196.11208			8.5	C ₁₄ H ₁₄ N	-0.016	[M + H-C ₄ H ₉ N] ⁺			
MS ³ : 239		132.08104	132.08078	5.5	C ₉ H ₁₀ N	0.264	[M + H-C ₉ H ₁₃ N] ⁺			
		196.11247	196.11208	8.5	C ₁₄ H ₁₄ N	0.394	[M + H-C ₂ H ₅ N] ⁺			
DMI MS ² : 267)	13.49	267.18735	267.18612	8.5	C ₁₈ H ₂₃ N ₂	1.775	[M + H] ⁺			
		236.1436	236.14338	9.5	C ₁₇ H ₁₈ N	0.224	[M + H-C ₂ H ₄] ⁺			
		239.1528	239.15428	8.5	C ₁₆ H ₁₉ N ₂	-1.475	[M + H-CH ₃ N] ⁺			
		208.11247	208.11208	9.5	C ₁₅ H ₁₄ N	0.394	[M + H-C ₃ H ₉ N] ⁺			
		196.11226	196.11208	8.5	C ₁₄ H ₁₄ N	0.184	[M + H-C ₄ H ₉ N] ⁺			
MS ³ : 236)		208.1123	208.11208	9.5	C ₁₅ H ₁₄ N	0.224	[M + H-C ₂ H ₄] ⁺			
PTP ₂₈₁₋₁ MS ² : 281	9.76	281.16571	281.16484	9.5	C ₁₈ H ₂₁ ON ₂	0.87	[M + H] ⁺			
		238.12209	238.12264	9.5	C ₁₆ H ₁₆ ON	-0.551	[M + H-C ₂ H ₅ N] ⁺			
		196.11212	196.11208	8.5	C ₁₄ H ₁₄ N	0.044	[M + H-CO-C ₃ H ₇ N] ⁺			
		194.09657	194.09643	9.5	C ₁₄ H ₁₂ N	0.144	[M + H-CO-C ₃ H ₉ N] ⁺			
		196.11205	196.11208	8.5	C ₁₄ H ₁₄ N	-0.026	[M + H-CO-CH ₂] ⁺			
MS ³ : 238		220.11174	220.11208	10.5	C ₁₆ H ₁₄ N	-0.336	[M + H-H ₂ O] ⁺			
PTP ₂₈₁₋₂ MS ² : 281	11.12	281.16571	281.16484	9.5	C ₁₈ H ₂₁ ON ₂	0.87	[M + H] ⁺			
		250.12277	250.12264	10.5	C ₁₇ H ₁₆ ON	0.129	[M + H-CH ₃ N] ⁺			
		238.12276	238.12264	9.5	C ₁₆ H ₁₆ ON	0.119	[M + H-C ₂ H ₅ N] ⁺			
		224.10718	224.10699	9.5	C ₁₅ H ₁₄ ON	0.185	[M + H-C ₃ H ₇ N] ⁺			
		220.11261	220.11208	10.5	C ₁₆ H ₁₄ N	0.534	[M + H-C ₂ H ₇ NO] ⁺			
		210.09163	210.09134	9.5	C ₁₄ H ₁₂ ON	0.289	[M + H-C ₄ H ₉ N] ⁺			
		194.09644	194.09643	9.5	C ₁₄ H ₁₂ N	0.014	[M + H-C ₄ H ₉ NO] ⁺			
		MS ³ : 224		206.09578	206.09643	10.5	C ₁₅ H ₁₂ N		-0.646	[M + H-H ₂ O] ⁺
		MS ³ : 250		196.11284	196.11208	8.5	C ₁₄ H ₁₄ N		0.764	[M + H-CO] ⁺
				222.09131	222.09134	10.5	C ₁₅ H ₁₂ ON		-0.031	[M + H-C ₂ H ₄] ⁺
		182.09711	182.09643	8.5	C ₁₃ H ₁₂ N	0.684	[M + H-C ₄ H ₄ O] ⁺			

Table 1 (continued)

Compound	R _t	Measured mass [m/z]	Calculated mass [m/z]	RDB	Molecular formula	Relative error [ppm]	Precursor ion/product ion	Proposed structure of PTPs
PTP ₂₈₃₋₁ MS ² : 283 MS ³ : 265	10.64	283.18146	283.18049	8.5	C ₁₈ H ₂₃ ON ₂	0.97	[M + H] ⁺	
		265.17053	265.16993	9.5	C ₁₈ H ₂₁ N ₂	0.605	[M + H - H ₂ O] ⁺	
		255.14835	255.14919	8.5	C ₁₆ H ₁₉ ON ₂	-0.84	[M + H - C ₂ H ₄] ⁺	
		234.12804	234.12773	10.5	C ₁₇ H ₁₆ N	0.314	[M + H - CH ₅ N] ⁺	
		206.09641	206.09643	10.5	C ₁₅ H ₁₂ N	-0.016	[M + H - C ₃ H ₉ N] ⁺	
PTP ₂₈₃₋₂ MS ² : 283	11.19	283.18134	283.18049	8.5	C ₁₈ H ₂₃ ON ₂	0.85	[M + H] ⁺	
		265.17023	265.16993	9.5	C ₁₈ H ₂₁ N ₂	0.305	[M + H - H ₂ O] ⁺	
		252.13678	252.13829	9.5	C ₁₇ H ₁₈ ON	-1.511	[M + H - CH ₅ N] ⁺	
		240.13853	240.13829	8.5	C ₁₆ H ₁₈ ON	0.239	[M + H - C ₂ H ₅ N] ⁺	
		226.12241	226.12264	8.5	C ₁₅ H ₁₆ ON	-0.231	[M + H - C ₃ H ₇ N] ⁺	
		177.1391	177.13862	4.5	C ₁₁ H ₁₇ N ₂	0.475	[M + H - C ₇ H ₆ O] ⁺	
PTP ₂₈₃₋₃ MS ² : 283	11.81	283.18118	283.18049	8.5	C ₁₈ H ₂₃ ON ₂	0.69	[M + H] ⁺	
		265.16888	265.16993	9.5	C ₁₈ H ₂₁ N ₂	-1.045	[M + H - H ₂ O] ⁺	
		240.13576	240.13829	8.5	C ₁₆ H ₁₈ ON	-2.531	[M + H - C ₂ H ₅ N] ⁺	
PTP ₂₈₃₋₄ MS ² : 283	12.36	283.18124	283.18049	8.5	C ₁₈ H ₂₃ ON ₂	0.75	[M + H] ⁺	
		265.17249	265.16993	9.5	C ₁₈ H ₂₁ N ₂	2.565	[M + H - H ₂ O] ⁺	
		255.14738	255.14919	8.5	C ₁₆ H ₁₉ ON ₂	-1.81	[M + H - C ₂ H ₄] ⁺	
		240.13712	240.13829	8.5	C ₁₆ H ₁₈ ON	-1.171	[M + H - C ₂ H ₅ N] ⁺	
PTP ₂₈₃₋₅ MS ² : 283	13.49	283.18207	283.18049	8.5	C ₁₈ H ₂₃ ON ₂	1.58	[M + H] ⁺	
		252.13986	252.13829	9.5	C ₁₇ H ₁₈ ON	1.569	[M + H - CH ₅ N] ⁺	
		240.13605	240.13829	8.5	C ₁₆ H ₁₈ ON	-2.241	[M + H - C ₂ H ₅ N] ⁺	
		226.12407	226.12264	8.5	C ₁₅ H ₁₆ ON	1.429	[M + H - C ₃ H ₇ N] ⁺	
		165.13968	165.13917	3.5	C ₁₀ H ₁₇ N ₂	1.055	[M + H - C ₈ H ₆ O] ⁺	
		132.0802	132.08078	5.5	C ₉ H ₁₀ N	-0.576	[M + H - C ₉ H ₁₃ NO] ⁺	
PTP ₂₉₉₋₁ MS ² : 299 MS ³ : 281 MS ³ : 268	8.85	299.17615	299.1754	8.5	C ₁₈ H ₂₃ O ₂ N ₂	0.746	[M + H] ⁺	
		281.16528	281.16484	9.5	C ₁₈ H ₂₁ ON ₂	0.44	[M + H - H ₂ O] ⁺	
		268.13205	268.13321	9.5	C ₁₇ H ₁₈ O ₂ N	-1.155	[M + H - CH ₅ N] ⁺	
		250.12224	250.12264	10.5	C ₁₇ H ₁₆ ON	-0.401	[M + H - CH ₅ N] ⁺	
		240.10179	240.10191	9.5	C ₁₅ H ₁₄ O ₂ N	-0.115	[M + H - C ₂ H ₄] ⁺	
PTP ₂₉₉₋₂ MS ² : 299	9.84	299.17654	299.1754	8.5	C ₁₈ H ₂₃ O ₂ N ₂	1.136	[M + H] ⁺	
		281.16376	281.16484	9.5	C ₁₈ H ₂₁ ON ₂	-1.08	[M + H - H ₂ O] ⁺	
		255.18456	255.18558	7.5	C ₁₇ H ₂₃ N ₂	-1.015	[M + H - CO ₂] ⁺	
		182.11865	182.11756	3.5	C ₁₀ H ₁₆ O ₂ N	1.095	[M + H - C ₈ H ₇ N] ⁺	

(continued on next page)

Table 1 (continued)

Compound	R _t	Measured mass [m/z]	Calculated mass [m/z]	RDB	Molecular formula	Relative error [ppm]	Precursor ion/product ion	Proposed structure of PTPs
PTP ₂₉₉₋₃ MS ² : 299	11.12	299.17648	299.1754	8.5	C ₁₈ H ₂₃ O ₂ N ₂	1.076	[M + H] ⁺	
		281.16678	281.16484	9.5	C ₁₈ H ₂₁ ON ₂	1.94	[M + H-H ₂ O] ⁺	
		268.13525	268.13321	9.5	C ₁₇ H ₁₈ O ₂ N	2.045	[M + H-CH ₃ N] ⁺	
		256.13312	256.13375	8.5	C ₁₆ H ₁₈ O ₂ N	-0.085	[M + H-C ₂ H ₅ N] ⁺	
		242.11696	242.11756	8.5	C ₁₅ H ₁₆ O ₂ N	-0.595	[M + H-C ₃ H ₇ N] ⁺	
		224.10739	224.10699	9.5	C ₁₅ H ₁₄ ON	0.399	[M + H-H ₂ O-C ₃ H ₇ N] ⁺	
		180.10297	180.10191	4.5	C ₁₀ H ₁₄ O ₂ N	1.065	[M + H-C ₈ H ₉ N] ⁺	
PTP ₂₉₉₋₄ MS ² : 299	11.81	299.17624	299.1754	8.5	C ₁₈ H ₂₃ O ₂ N ₂	0.836	[M + H] ⁺	
		281.16675	281.16484	9.5	C ₁₈ H ₂₁ ON ₂	1.91	[M + H-H ₂ O] ⁺	
		268.13388	268.13321	9.5	C ₁₇ H ₁₈ O ₂ N	0.675	[M + H-CH ₃ N] ⁺	
		256.13287	256.13375	8.5	C ₁₆ H ₁₈ O ₂ N	-0.335	[M + H-C ₂ H ₅ N] ⁺	
		224.10748	224.10699	9.5	C ₁₅ H ₁₄ ON	0.489	[M + H-H ₂ O-C ₃ H ₇ N] ⁺	
		196.11227	196.11208	8.5	C ₁₄ H ₁₄ N	0.194	[M + H-CO ₂] ⁺	
		224.10648	224.10699	9.5	C ₁₅ H ₁₄ ON	0.351	[M + H-C ₃ H ₇ N] ⁺	
PTP ₂₈₅₋₁ MS ² : 285	9.6	285.1972	285.19614	7.5	C ₁₈ H ₂₅ ON ₂	1.06	[M + H] ⁺	
		227.15494		7.5	C ₁₅ H ₁₉ N ₂	0.665		
		199.123		7.5	C ₁₃ H ₁₅ N ₂	0.025		
		187.12347		6.5	C ₁₂ H ₁₅ N ₂	0.495		
		179.11809		4.5	C ₁₀ H ₁₅ ON ₂	0.2		
PTP ₂₈₅₋₂ MS ² : 285	12.67	285.19836	285.19614	7.5	C ₁₈ H ₂₅ ON ₂	0.58	[M + H] ⁺	
		254.15508	254.15394	8.5	C ₁₇ H ₂₀ ON	1.139	[M + H-CH ₃ N] ⁺	
PTP ₃₀₁₋₁ MS ² : 301	9.6	301.19196	301.19105	7.5	C ₁₈ H ₂₅ O ₂ N ₂	0.905	[M + H] ⁺	
		283.17877	283.18049	8.5	C ₁₈ H ₂₃ ON ₂	-1.72	[M + H-H ₂ O] ⁺	
		270.1514	270.1494	8.5	C ₁₇ H ₂₀ O ₂ N	2.545	[M + H-CH ₃ N] ⁺	
		252.14008	252.13829	9.5	C ₁₇ H ₁₈ ON	1.789	[M + H-CH ₇ NO] ⁺	
		242.11559	242.11756	8.5	C ₁₅ H ₁₆ O ₂ N	-1.965	[M + H-C ₂ H ₄] ⁺	
		301.19165	301.19105	7.5	C ₁₈ H ₂₅ O ₂ N ₂	0.595	[M + H] ⁺	
		270.14957	270.1494	8.5	C ₁₇ H ₂₀ O ₂ N	0.715	[M + H-CH ₃ N] ⁺	
PTP ₃₀₁₋₂ MS ² : 301	10.72	242.11682	242.11756	8.5	C ₁₅ H ₁₆ O ₂ N	-0.735	[M + H-C ₃ H ₉ N] ⁺	
		242.11803	242.11756	8.5	C ₁₅ H ₁₆ O ₂ N	0.475	[M + H-C ₂ H ₄] ⁺	
		132.08154	132.08078	5.5	C ₉ H ₁₀ N	0.764	[M + H-C ₆ H ₆ O ₂] ⁺	
		270.14957	270.1494	8.5	C ₁₇ H ₂₀ O ₂ N	0.715	[M + H-CH ₃ N] ⁺	
		242.11682	242.11756	8.5	C ₁₅ H ₁₆ O ₂ N	-0.735	[M + H-C ₃ H ₉ N] ⁺	
PTP ₂₁₉ MS ² : 219 MS ³ : 188	9	219.14966	219.14919	5.5	C ₁₃ H ₁₉ ON ₂	0.74	[M + H] ⁺	
		188.10735	188.10699	6.5	C ₁₂ H ₁₄ ON	0.359	[M + H-CH ₃ N] ⁺	
		160.07597	160.07569	6.5	C ₁₀ H ₁₀ ON	0.28	[M + H-C ₃ H ₉ N] ⁺	
		132.08102	132.08078	5.5	C ₉ H ₁₀ N	0.244	[M + H-C ₃ H ₄ O] ⁺	

*In case if PTP₂₆₇₋₁ and PTP₂₆₇₋₂, the position of the methyl group cannot be identified, so a suggested structure was added in between containing dotted bond which means that the methyl group may be one of these bonds.

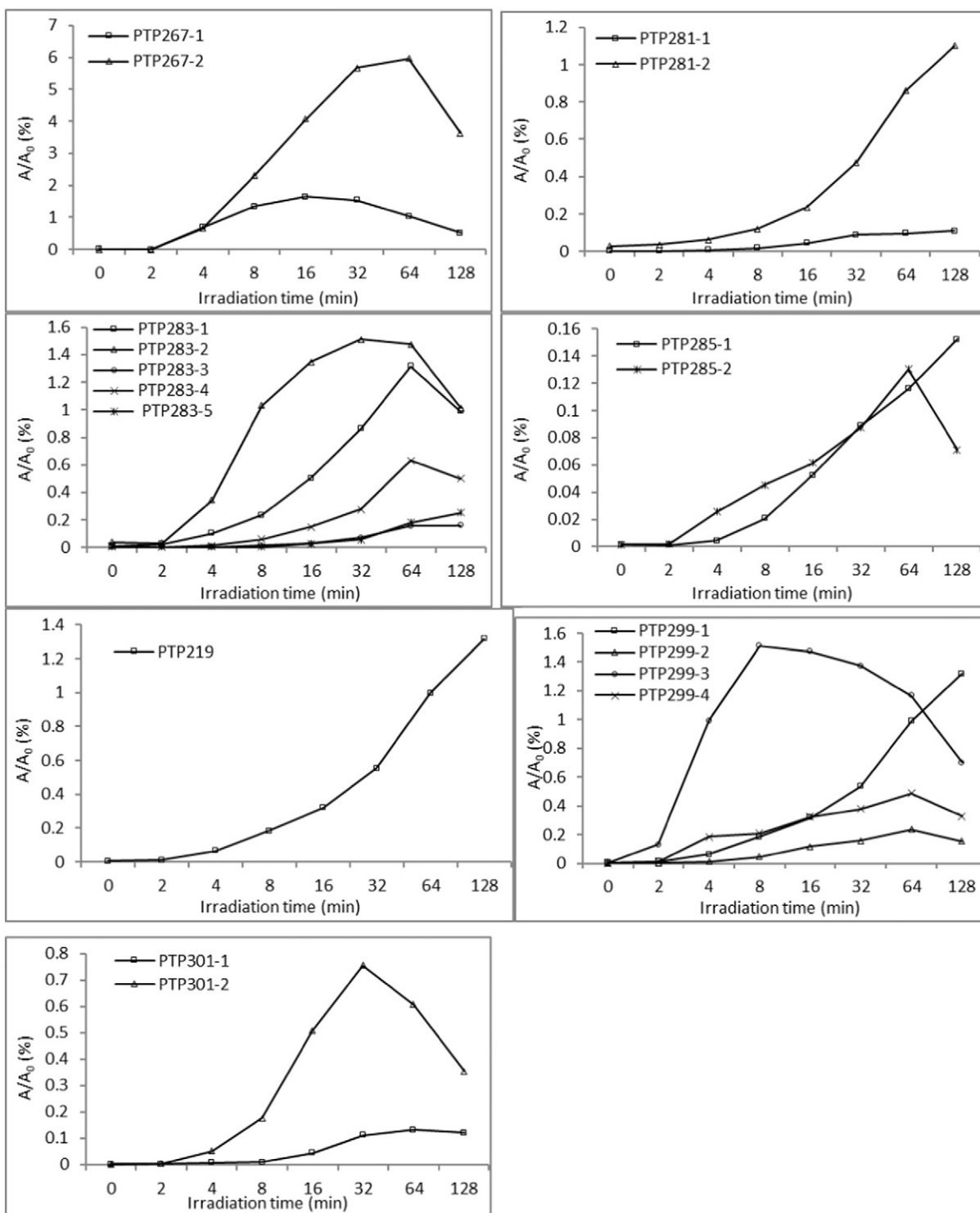


Fig. 2. Time curves of the relative peak area A/A_0 (%) of the PTPs during photolysis assigned to their m/z ratio (A is the peak area of the PTP at a specific time point, A_0 is the peak area of DMI (100 mg L^{-1}) at 0 min) ($n = 3$, with $SD < 0.13$ and $RSD < 9.7\%$).

3.3. Influence of pH and temperature on DMI photolysis kinetics and on PTPs formation/elimination kinetics and mechanism

3.3.1. Effect of pH

The influence of pH on the UV photolysis rate of 100 mg L^{-1} DMI and on the resulting PTPs was analyzed in experiments with pH 3, 5, 7, and 9 under UV irradiation at 20°C (Fig. 3a). DMI concentration in this pH range, in controls without access to light, showed no significant change

in terms of stability. As indicated by the results given in Fig. 3a, the degradation rate of DMI at $\text{pH} \leq 7$ is inversely proportional to the solution pH value. At pH 9, the highest photolysis rate was observed until 16 min of irradiation, and then the photolysis rate slowed down until 128 min. After 128 min of irradiation, the fastest degradation was seen at pH 3 as DMI was eliminated by 84%, 67%, 56%, and 65% at pH 3, 5, 7, and 9, respectively. An ANOVA analysis indicated that the differences in the photolysis rates as a function of the pH value are

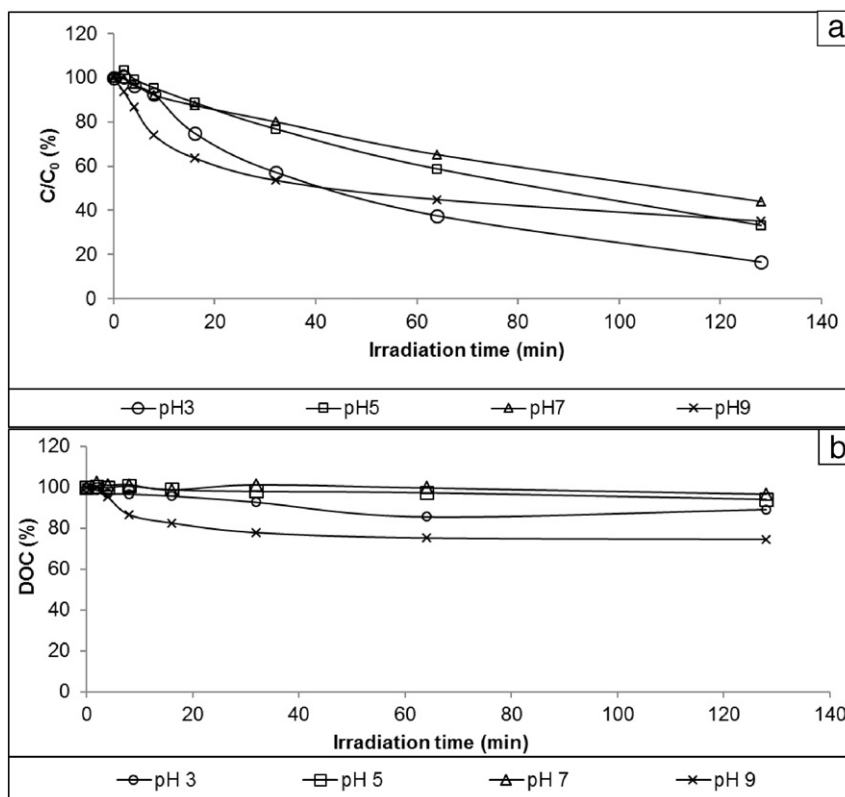


Fig. 3. The photolytic degradation (a), and the DOC recovery (b), of DMI by means of UV photodegradation at different pH values. DMI initial concentration = 100 mg L⁻¹, temperature = 20 °C.

statistically significant with $P < 0.001$. Tukey's test results confirmed that the differences in the photolysis rate between each two pH experiments are statistically significant ($P < 0.006$).

The degree of mineralization (in %), reached after 128 min of irradiation are decreased with increasing pH values from pH 3 to pH 7, which is in agreement with the photolysis kinetic results (Fig. 3b). However, at pH 9 experiment, the highest mineralization (in %) was seen during the entire photolysis experiment without showing the slowdown seen after 16 min in the photolysis kinetic results (Fig. 3b).

First-order reaction kinetics was used to describe the photolysis of DMI at pH 3, 5, and 7, with a photolysis rate constant (k) of 0.0145, 0.0085, and 0.0065 min⁻¹, respectively, R^2 ranged between 0.993 and 0.996. In the pH 9 experiment, DMI degradation followed two staged second-order kinetics; a faster one (from 0 min to 16 min) with $k = 0.0365 \text{ M}^{-1} \text{ min}^{-1}$ and $R^2 = 0.984$, and a slower one (from 16 min to 128 min) with $k = 0.011 \text{ M}^{-1} \text{ min}^{-1}$ and $R^2 = 0.988$. The difference between DMI photolysis rates at different pH values was likely related to the DMI species present at these pH values, which goes along with a change in the molar absorption coefficient (ϵ).

Supplementary Fig. S24 describes the variation in the DMI's (ϵ) as a function of the solution pH value. As shown in the figure, there is a slow increase in the ϵ values corresponding to the decrease in the pH values. According to Eq. (1), an increase in ϵ value would lead to an increase in k value. The results at pH ≤ 7 experiments are in agreement with the equation, as it showed an increase in k corresponding to the increase of ϵ . Result of the photolysis at pH 9 showed a variation of this trend, as a decrease in ϵ was accompanied by an increase in k . It can be concluded that there is no general rule describing the pH dependence of ϵ and k , as other parameters, such as the formed PTPs, could interfere with this effect (Canonica et al., 2008; Prados-Joya et al., 2011).

DMI is a strong basic substance with $pK_a = 10.02$ (Antal et al., 1980). DMI has three different species at different pH levels (Supplementary

Fig. S25). Each species carries a different electric charge, which has an influence on its photolytic degradation under different wavelengths, as UV spectra and electronic states are different. At pH = 3, 5, and 7, DMI is mostly protonated as HDMI⁺. At pH 9, DMI is in its neutral form, which might be more easily photolyzed than its protonated species (Kwon and Armbrust, 2004; Xu et al., 2014). This could be an explanation for the observed increase in the degradation rate within the first 16 min of irradiation in pH 9 experiment.

The slowdown seen after 16 min irradiation in pH 9 experiment could be explained by the change in pH values during the UV irradiation time. In pH 9 experiment, pH decreased from pH 9 to reach approximately pH 7 after 128 min of irradiation. In contrast, the pH did not change significantly during the entire irradiation time in case of the experiments performed at pH 3, 5, and 7 (Supplementary Fig. S26). When pH decreases, the amount of protonated DMI increases, and this can lead to variations in the degradation rates. Another explanation of this slowdown could be the presence of newly formed PTPs after 16 min, which might absorb radiation and hence decrease the photolysis rate (Khaleel et al., 2013; Rastogi et al., 2014).

Supplementary Fig. S27 shows the formation/elimination kinetics of the previously identified PTPs during the photolysis of the DMI at different pH values. Some PTPs showed an increase in A/A_0 (%) as the pH of the solution increases; others showed decreasing A/A_0 (%) with increasing pH; others varied independently of the solution pH value. Thus, there is no general rule that can describe the effect of pH on PTPs concentrations and formation kinetics. The UV-photolysis mechanism of DMI is also affected by the solution pH, as some PTPs were detectable at certain pH values and not at others. All of the PTPs generated at pH 5 experiment are formed at the other pH experiments too, except PTP₂₈₃₋₅, which uniquely of the PTPs previously identified, was formed only at pH 5. One PTP, with m/z 235, was found only at pH 3 experiment; this is likely to be a secondary product from PTP₂₉₉ after degradation of one benzene ring keeping the azepane cycle intact,

in combination with dehydration and demethylation (supplementary Fig. S28). At pH 9 experiment, three new PTPs (m/z 271) were detected. These three PTPs can be assumed to be isomers formed through the oxidation of the azepane ring followed by multiple steps: ring cleavage, ring closing at another site, and demethylation reactions (Supplementary Fig. S29). The latter mechanism was described in detail elsewhere (Petrovic and Barceló, 2007).

3.3.2. Effect of temperature

UV photolysis of 100 mg L⁻¹ DMI was performed in UP water with pH 5 at the following temperatures: 10 °C, 20 °C, 30 °C, and 40 °C. It was observed that the temperature has negligible effect on the UV photolysis process of DMI, as the photolysis and the mineralization rates are nearly the same at all the temperatures examined here (Fig. 4 & Supplementary Fig. S30). The degradation rate constants (k) according to first-order kinetics were 0.0078, 0.0085, 0.0086 and 0.0086 min⁻¹ at 10 °C, 20 °C, 30 °C, and 40 °C, respectively; with $R^2 > 0.997$. After 128 min of irradiation at different temperatures, the observed mineralization was approximately 12.4 ± 2%. ANOVA results confirmed that the differences in the photolysis rates as a function of the temperature were not statistically significant ($P = 0.121$).

Although the temperature had no effect on the DMI photolysis rate, it had an effect on the formation/elimination kinetics of the PTPs (Supplementary Fig. S31). For some PTPs (PTP₂₁₉, PTP₂₈₁₋₁, PTP₂₈₃₋₁, and PTP₂₈₁₋₂), the formation/elimination process was the fastest at 10 °C and the slowest at 20 °C experiments. While the formation/elimination kinetics of other PTPs such as TP₂₉₉₋₂ and TP₂₈₃₋₂ increased with increasing temperatures. The formation/elimination of other PTPs increased if the temperature was increased from 20 °C to 40 °C. While at 10 °C, a broad variety of formation/elimination kinetics was observed.

3.4. Aerobic biodegradation of DMI and its PTPs

3.4.1. Biodegradation of photolytic mixtures at pH 5 experiment

In the two biodegradation tests (CBT and MRT) used here, all validity criteria of the established OECD guidelines were met. The biodegradation values for the DMI and the resulting photolytic mixtures indicated that DMI and its PTPs are not readily biodegradable (Table 2 & Supplementary Fig. S32). In the toxicity controls, no toxic effect was seen against the bacteria employed. According to the OECD guidelines, the other pass criteria for MRT is a 70% removal of DOC value after 28 days, which was not seen in any of the samples studied here, confirming no biodegradation. The biodegradation rate (in %) increased slightly in photolysis mixtures when they were exposed longer to UV irradiation. This finding suggests that one or more biodegradable PTPs

Table 2

Results of the investigated aerobic biodegradation tests assay for DMI.

Biodegradation test	Test sample	Biodegradation after 28 day %	Parent compound elimination %	DOC removal %
CBT	0 min	0.74	5.69	
	16 min	-6.4	2.53	
	64 min	3.16	1.87	
	128 min	8.21	0.01	
MRT	0 min	-2.6	0.08	13
	16 min	-8.79	2.01	8.4
	64 min	3.6	1.95	21.2

were formed, but their contribution to DOC is minimal, and seems to be offset by the effect of the other non-biodegradable PTPs and DMI.

Samples from CBT and MRT were analyzed by means of LC-ITMS. The recoveries of DMI after 28 days in CBT and MRT were 99.6% and 95%, respectively. These findings confirmed that DMI is neither readily biodegradable nor abiotically degradable; neither was it eliminated by sorption onto the vessels glass surface or to the bacterial biomass. These results also indicate that no TPs were formed due to DMI biodegradation.

The peak areas of the most prevalent PTPs were compared at the start and the end of CBT and MRT. These PTPs were divided into three groups: stable PTPs, abiotically degraded PTPs, and biotically degraded PTPs (Fig. 5). The peak recoveries after 28 days for some PTPs were around 100% (PTP₂₆₇₋₁, PTP₂₈₃₋₁, PTP₂₉₉₋₃, and PTP₂₁₉) indicating that they are stable PTPs as they are neither biodegraded nor eliminated by sorption. Another group of PTP, including PTP₂₆₇₋₂, PTP₂₈₁₋₂, PTP₂₈₃₋₂, and PTP₂₈₃₋₄, could be described as slightly degradable PTPs in MRT with higher degradation rates than in CBT. The highest degradation rate in the latter group was observed for PTP₂₈₃₋₄ as it gave elimination of 78% and 19% in MRT and CBT, respectively. The PTP₂₈₃₋₄ could be considered a biodegradable PTP as it is characterized by a lower elimination rate in the sterile sample (24%) than in the test sample (78%). The other three PTPs (PTP₂₆₇₋₂, PTP₂₈₁₋₂, and PTP₂₈₃₋₂) can be considered partly abiotically degradable in MRT, because they showed the same elimination in both test and sterile samples. They showed an elimination of approximately 30% in MRT but only 6% elimination in CBT. PTP₂₉₉₋₄ was slightly degradable in both CBT and MRT with about 31% elimination. PTP₂₉₉₋₂ was almost completely eliminated in the test samples in both CBT and MRT with degradation rates up to 93.8%. In this case, it is difficult to determine whether PTP₂₉₉₋₂ was biotically or abiotically eliminated because it was completely eliminated in the sterile controls

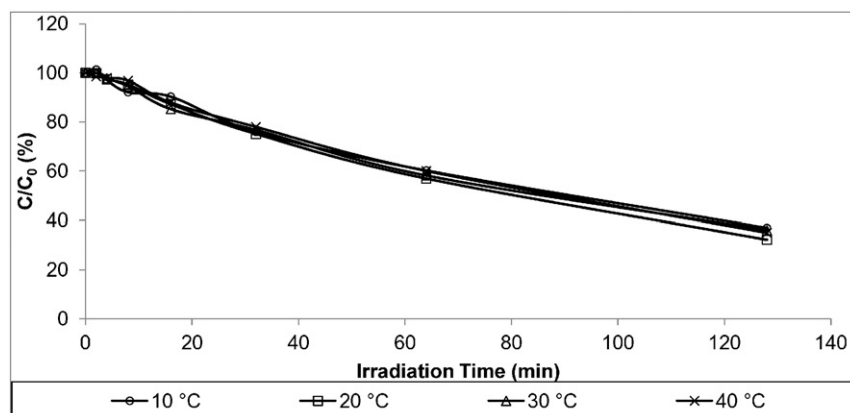


Fig. 4. The photolytic degradation of DMI by means of UV photodegradation at different temperatures. pH = 5, initial concentration = 100 mg L⁻¹.

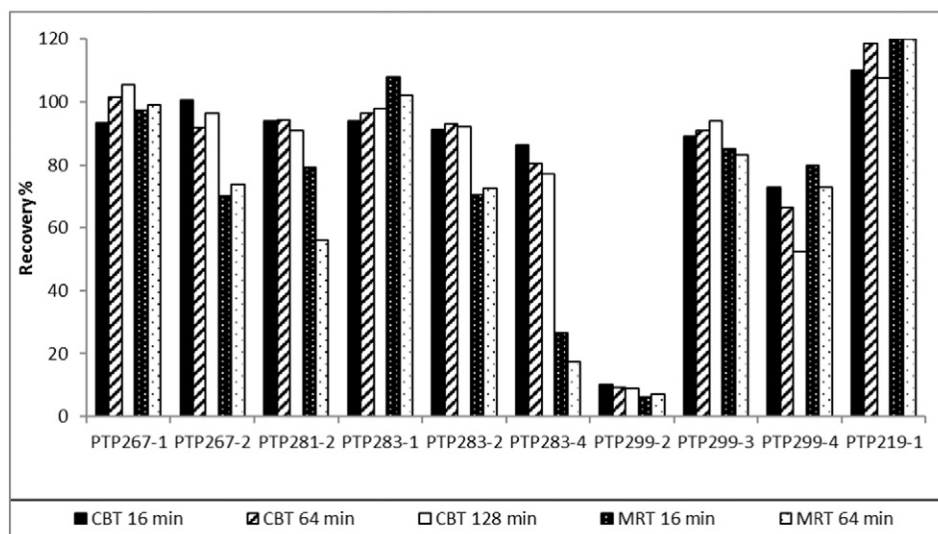


Fig. 5. Recovery of DMI's PTPs after 28 days related to day 0 in CBT and MRT in different photolytic mixtures.

at the beginning of the test. One explanation could be a fast reaction with sodium azide.

3.4.2. Biodegradation of photolysis mixtures at pH 3 and pH 9 experiments

As revealed by the results described at the beginning of Section 3, pH is the parameter with the greatest impact on the DMI photolysis mechanism, as new PTPs were detected in pH 3 and pH 9 experiments. For this reason, CBTs for UV-irradiated solutions of DMI at pH 3 and pH 9 at different time points (0 min, 32 min, and 128 min) were performed. The results for all of these tests showed no biodegradation as defined in the test guidelines, with biodegradation values equal to $8.4\% \pm 3.6\%$. The peak recoveries after 28 days of PTP₂₃₅, which was formed in pH 3 experiments, and PTP₂₇₁₋₁, PTP₂₇₁₋₂, and PTP₂₇₁₋₃, which were formed in pH 9 experiments, were checked, and they were 99.9%, 103.4%, 89.2%, and 90.1%, respectively. These findings indicate that they have to be classified as non-biodegradable and non-sorptive PTPs.

3.5. In silico fate prediction and qualitative risk assessment of DMI and its PTPs

Most of the readily biodegradability models are based on OECD 301C MITI-I test. MITI-I test is not directly comparable to CBT as the inoculum concentration (bacterial density) in CBT is much lower than in MITI-I test, thus false positive results of prediction from MITI-I are more likely than false negative ones. Therefore, the structure of DMI and its PTPs were analyzed to predict their ready biodegradability by using various *in silico* models in order to get more reliable results. As a consequence, these results were used in this study only as a rough orientation. A compound is classified as either biodegradable or non-biodegradable depending on certain predicted activating and deactivating alerts, which are identified by all QSAR models. Although DMI and its PTPs were out of domain in both models of Oasis Catalogic, certain output biodegradation values were predicted. Models of Oasis Catalogic software and EPI Suite software for ready biodegradability predicted the output values as <0.1 for DMI (Supplementary Table S3). These output values were below the pass criterion for ready biodegradability under MITI-I test and MRT conditions. Accordingly, DMI has been categorized as a non-readily biodegradable chemical. The results from Case Ultra for DMI biodegradability were out of domain and will therefore not be considered any further here. In summary, *in silico* prediction fitted well to the experimental biodegradation testing (CBT and MRT) confirming that DMI is not biodegradable in aquatic environments, and therefore, it is expected to be present in them. Some PTPs were predicted as readily biodegradable by the Case Ultra models, although

the Oasis Catalogic and Epi Suite models predicted that all PTPs were not readily biodegradable (Supplementary Table S3).

3.6. In silico toxicity predictions

The *in silico* toxicity assessment shows that the mutagenicity and genotoxicity of DMI and its PTPs can be altered after photodegradation (Supplementary Table S4). There was no positive alert from the different models of the ICHM7 guideline conformal set from Case Ultra for DMI. However, some of the PTPs were predicted to have mutagenic and genotoxic activities, because of the presence of an N-methylol group (Fig. 6). The potential toxicity of compounds containing this group (hemiaminal) is due to the formation of formaldehyde via hydrolysis, and the formaldehyde is a highly reactive genotoxic agent (Ashby and Tennant, 1988; Benigni and Bossa, 2008).

The three acute *V. fischeri* modules (Oasis catalogic) predicted a lower IC₅₀ for all the PTPs than for DMI itself. There were some positive alerts for the PTPs in the Microtox Toxicity to Environmental Bacteria module (Case Ultra) (Supplementary Table S5). The results from Case Ultra for Microtox Toxicity to Environmental Bacteria of DMI are out of domain. PTP₂₈₅ and PTP₃₀₁ were the PTPs predicted to have Microtox Toxicity to environmental bacteria. As mentioned above, the concentration of PTP₂₈₅₋₁ increased during the photolysis process, so this PTP could be a starting point for an experimental assessment of the predicted toxicities. Some of the structural moieties responsible for this alert are shown in Supplementary Fig. S33. Since some of the PTPs were out of domain in the applied Case Ultra models, it cannot be rolled out that these PTPs might have toxic effects in the environment.

The *in silico* toxicity assessment performed in this study provides a first indication that photodegradation might lead to PTPs that are more toxic than their respective parent compounds.

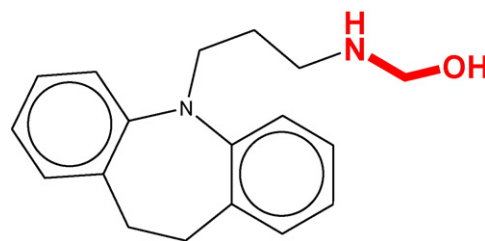


Fig. 6. The predicted structural moiety (hemiaminal) responsible for the genotoxic alert in PTP_{283_8} in model GT EXPERT Expert rules for genotoxicity using Case Ultra software are highlighted).

4. Conclusion

The results of this study showed that DMI is neither biodegradable nor is it degraded by sunlight in the environment, but it is degradable in response to UV-irradiation. It was eliminated to a considerable extent after 128 min of UV irradiation in UP water, with little elimination of DOC. This finding indicates the formation of new, more stable PTPs which were then found in chemical analysis. Therefore, UV treatment is likely to be not sufficient for the removal of DMI from the aquatic environment. Furthermore, the photolysis of DMI at different initial concentrations indicates that complete mineralization could be achieved at lower concentrations as the case under realistic environmental conditions, or after longer periods of irradiation (> 2 h), which could be used in technical treatment, although this would be highly expensive and time consuming.

It is important to consider the role of environmental variable conditions such as pH and temperature in studying the photodegradability of chemicals in the environment. The pH values of the irradiated solution showed a significant effect on the photolysis rate of DMI, and on the formation kinetics and mechanism of the PTPs. Furthermore, these results showed that, because of the numerous interdependencies of constraints during photolysis, the formation of PTPs varies, and therefore a sound risk assessment is impossible. This is also due to the fact that it is not known whether all of the PTPs formed have been detected by analytical means and that the real concentrations are unknown.

The results of biodegradation tests indicated that neither DMI nor most of its PTPs are readily biodegradable. Therefore, it can be expected that DMI and its PTPs may persist in surface and ground waters. QSAR results predicted some of the newly formed PTPs to be more human and eco-toxic than the parent compound. Our study demonstrated that combination of experimental and *in silico* predictions can be helpful in providing additional information on the environmental fate of pharmaceuticals and their PTPs and possibly associated risks.

Acknowledgements

The authors would like to thank the Federal Ministry of Research and Education for their financial support (Grant no. 02WRS1280A - J). The authors wish to thank Dr. Annette Haiss and Evgenia Logunova for planning the aerobic biodegradation tests, and to thank Dr. Marcelo L. Wilde and Janin Westphal for the analytical support. The authors also acknowledge Multicase Inc. for kindly providing the Case Ultra software.

Appendix A. Supplementary data

Supplementary data to this article can be found online at <http://dx.doi.org/10.1016/j.scitotenv.2016.05.095>.

References

- Antal, E., Mercik, S., Kramer, P.A., 1980. Technical considerations in the gas chromatographic analysis of desipramine. *J. Chromatogr. B Biomed. Sci. Appl.* 183 (2), 149–157.
- Arnold, W.A., McNeill, K., 2007. Chapter 3.2 transformation of pharmaceuticals in the environment: photolysis and other abiotic processes; analysis, fate and removal of pharmaceuticals in the water cycle. *Compr. Anal. Chem.* 50, 361–385.
- Ashby, J., Tennant, R.W., 1988. Chemical structure, *Salmonella* mutagenicity and extent of carcinogenicity as indicators of genotoxic carcinogenesis among 222 chemicals tested in rodents by the U.S. NCI/NTP. *Mutat. Res.* 204 (1), 17–115.
- Bauer, M., Monz, B.U., Montejó, A.L., Quail, D., Dantchev, N., Demyttenaere, K., et al., 2008. Prescribing patterns of antidepressants in Europe: results from the factors influencing depression endpoints research (FINDER) study. *Eur. Psychiatry* 23 (1), 66–73.
- Benigni, R., Bossa, C., 2008. Structure alerts for carcinogenicity, and the *Salmonella* assay system: a novel insight through the chemical relational databases technology. *Mutat. Res. Rev. Mutat. Res.* 659 (3), 248–261.
- Boonprasert, R., Tummarintra, P., Plabjuy, P., Kolladarungkri, T., 2013. Development of the method of the ultra performance liquid chromatography (UPLC) with photo diode array detector for determination of 7 tricyclic antidepressants' concentrations in human plasma. *Siriraj Med. J.* 65 (4), 100–104.
- Bosco, M., Larrechi, M.S., 2008. Rapid and quantitative evaluation of the effect of process variables on the kinetics of photocatalytic degradation of phenol using experimental design techniques and parallel factor (PARAFAC) analysis. *Anal. Bioanal. Chem.* 390 (4), 1203–1207.
- Canonica, S., Meunier, L., von Gunten, U., 2008. Phototransformation of selected pharmaceuticals during UV treatment of drinking water. *Water Res.* 42 (1–2), 121–128.
- Chakravarti, S.K., Saikhov, R.D., Klopman, G., 2012. Optimizing predictive performance of CASE ultra expert system models using the applicability domains of individual toxicity alerts. *J. Chem. Inf. Model.* 52 (10), 2609–2618.
- De Vane, C.L., Savett, M., Jusko, W.J., 1981. Desipramine and 2-hydroxy-desipramine pharmacokinetics in normal volunteers. *Eur. Clin. Pharmacol.* 19 (1), 61–64.
- Dimitrov, S., Pavlov, T., Dimitrova, N., Georgieva, D., Nedelcheva, D., Kesova, A., et al., 2011. Simulation of chemical metabolism for fate and hazard assessment. II CATALOGIC simulation of abiotic and microbial degradation. *SAR QSAR Environ. Res.* 22 (7–8), 719–755.
- EPI Suite software (EPIWEB 4.1), d. Estimation Program Interface <http://www.epa.gov/oppt/exposure/pubs/episuite.htm>.
- Friedrich, J., Längin, A., Kümmerer, K., 2013. Comparison of an electrochemical and luminescence-based oxygen measuring system for use in the biodegradability testing according to closed bottle test (OECD 301D). *Clean Soil Air Water* 41 (3), 251–257.
- Gros, M., Williams, M., Llorca, M., Rodriguez-Mozaz, S., Barceló, D., Kookana, R.S., 2015. Photolysis of the antidepressants amisulpride and desipramine in wastewaters: identification of transformation products formed and their fate. *Sci. Total Environ.* 530–531 434–44.
- Gunasekar, V., Divya, B., Brinda, K., Vijaykrishnan, J., Ponnusami, V., Rajan, K.S., 2013. Enzyme mediated synthesis of Ag-TiO₂ photocatalyst for visible light degradation of reactive dye from aqueous solution. *J. Sol-Gel Sci. Technol.* 68 (1), 60–66.
- Gutowski, L., Olsson, O., Leder, C., Kümmerer, K., 2015. A comparative assessment of the transformation products of 5-metolachlor and its commercial product Mercantor Gold® and their fate in the aquatic environment by employing a combination of experimental and *in silico* methods. *Sci. Total Environ.* 506–507, 369–379.
- Herrmann, M., Olsson, O., Fiehn, R., Herrel, M., Kümmerer, K., 2015. The significance of different health institutions and their respective contributions of active pharmaceutical ingredients to wastewater. *Environ. Int.* 85, 61–76.
- Huerta-Fontela, M., Galceran, M.T., Ventura, F., 2011. Occurrence and removal of pharmaceuticals and hormones through drinking water treatment. *Water Res.* 45 (3), 1432–1442.
- Illés, E., Szabó, E., Takács, E., Wojnárovits, L., Dombi, A., Gajda-Schranz, K., 2014. Ketoprofen removal by O₃ and O₃/UV processes: kinetics, transformation products and ecotoxicity. *Sci. Total Environ.* 472, 178–184.
- International Conference on Harmonization (ICH), 2014. ICH Guideline M7. http://www.ich.org/fileadmin/Public_Web_Site/ICH_Products/Guidelines/Multidisciplinary/M7/M7_Step_4.pdf (Accessed on 18.05.2016).
- Khaleel, N.D., Mahmoud, W.M., Hadad, G.M., Abdel-Salam, R.A., Kümmerer, K., 2013. Photolysis of sulfamethoxyppyridazine in various aqueous media: aerobic biodegradation and identification of photoproducts by LC-UV-MS/MS. *J. Hazard. Mater.* 244–245 (15), 654–661.
- Körbahti, B.K., Rauf, M.A., 2009. Determination of optimum operating conditions of carmine decoloration by UV/H₂O₂ using response surface methodology. *J. Hazard. Mater.* 161 (1), 281–286.
- Kwon, J., Armbrust, K.L., 2004. Hydrolysis and photolysis of paroxetine, a selective serotonin reuptake inhibitor, in aqueous solutions. *Environ. Toxicol. Chem.* 23 (6), 1394–1399.
- Laboratory of Mathematical Chemistry, 2012. OASIS Catalogic software V. 5.11.6TB. <http://oasis-lmc.org/>.
- Lajeunesse, A., Gagnon, C., Sauvé, S., 2008. Determination of basic antidepressants and their N-desmethyl metabolites in raw sewage and wastewater using solid-phase extraction and liquid chromatography–tandem mass spectrometry. *Anal. Chem.* 80 (14), 5325–5333.
- Mahmoud, W.M., Toolaram, A.P., Menz, J., Leder, C., Schneider, M., Kümmerer, K., 2014. Identification of phototransformation products of thalidomide and mixture toxicity assessment: an experimental and quantitative structural activity relationships (QSAR) approach. *Water Res.* 49 (1), 11–22.
- OECD. Organisation for Economic Co-operation and Development, 1992n. OECD Guideline for Testing of Chemicals 301: Ready Biodegradability.
- OECD. Organisation for Economic Co-operation and Development Guideline for Testing of Chemicals 301 D: Ready Biodegradability. Closed Bottle Test. OECD Publishing, Paris.
- OECD-316, 2008. Phototransformation of Chemicals in Water.
- Önal, A., Öztunç, A., 2011. A rapid and simple RP-HPLC method for quantification of desipramine in human plasma. *Rev. Anal. Chem.* 30 (3–4), 165–169.
- Petrovic, M., Barceló, D., 2007. LC-MS for identifying photodegradation products of pharmaceuticals in the environment. *TrAC Trends Anal. Chem.* 26 (6), 486–493.
- Prados-Joya, G., Sánchez-Polo, M., Rivera-Utrilla, J., Ferro-garcía, M., 2011. Photodegradation of the antibiotics nitroimidazoles in aqueous solution by ultraviolet radiation. *Water Res.* 45 (1), 393–403.
- Ramey, K., Ma, J.D., Best, B.M., Atayee, R.S., Morello, C.M., 2014. Variability in metabolism of imipramine and desipramine using urinary excretion data. *J. Anal. Toxicol.* 38 (6), 368–374.
- Rastogi, T., Leder, C., Kümmerer, K., 2014. Qualitative environmental risk assessment of photolytic transformation products of iodinated X-ray contrast agent diatrizoic acid. *Sci. Total Environ.* 482–483, 378–388.
- Saikhov, R., Chakravarti, S., Klopman, G., 2013. Effectiveness of CASE ultra expert system in evaluating adverse effects of drugs. *Mol. Inf.* 32 (1), 87–97.
- Santiago-Morales, J., Rosal, R., Hernando, M.D., Ulaszewska, M.M., García-Calvo, E., Fernández-Alba, A.R., 2014. Fate and transformation products of amine-terminated

- PAMAM dendrimers under ozonation and irradiation. *J. Hazard. Mater.* 266 (15), 102–113.
- Sheng, L., Chen, H., Huo, Y., Wang, J., Zhang, Y., Yang, M., et al., 2014. Simultaneous determination of 24 antidepressant drugs and their metabolites in wastewater by ultra-high performance liquid chromatography–tandem mass spectrometry. *Molecules* 19 (1), 1212–1222.
- Trachta, G., Schwarze, B., Sägmüller, B., Brehm, G., Schneider, S., 2004. Combination of high-performance liquid chromatography and SERS detection applied to the analysis of drugs in human blood and urine. *J. Mol. Struct.* 693 (1–3), 175–185.
- Trautwein, C., Berset, J., Wolschke, H., Kümmerer, K., 2014. Occurrence of the antidiabetic drug Metformin and its ultimate transformation product Guanylurea in several compartments of the aquatic cycle. *Environ. Int.* 70, 203–212.
- Unceta, N., Sampedro, M.C., Bakar, N.K.A., Gómez-Caballero, A., Goicolea, M.A., Barrio, R.J., 2010. Multi-residue analysis of pharmaceutical compounds in wastewaters by dual solid-phase microextraction coupled to liquid chromatography electrospray ionization ion trap mass spectrometry. *J. Chromatogr. A* 1217 (20), 3392–3399.
- Xu, J., Hao, Z., Guo, C., Zhang, Y., He, Y., Meng, W., 2014. Photodegradation of sulfapyridine under simulated sunlight irradiation: kinetics, mechanism and toxicity evolution. *Chemosphere* 99, 186–191.
- Zepp, R.G., 1978. Quantum yields for reaction of pollutants in dilute aqueous solution. *Environ. Sci. Technol.* 12 (3), 327–329.

Supporting Information for
UV-Photodegradation of Desipramine: Impact of Concentration, pH and Temperature on
Formation of Products Including their Biodegradability and Toxicity

Nareman D. H. Khaleel,^{1, 2} Waleed M. M. Mahmoud,^{1, 2} Oliver Olsson,¹ Klaus
Kümmerer,^{1*}

1- Sustainable Chemistry and Material Resources, Institute of Sustainable and Environmental Chemistry, Leuphana University of Lüneburg, Scharnhorststraße 1 C13, DE-21335 Lüneburg, Germany.

2- Pharmaceutical Analytical Chemistry Department, Faculty of Pharmacy, Suez Canal University, Ismailia 41522, Egypt.

Pages: 64

Texts: 1

Figures: 33

Tables:4

* Corresponding author. Address: Nachhaltige Chemie und Stoffliche Ressourcen, Institut für Nachhaltige Chemie und Umweltchemie, Leuphana Universität Lüneburg, C.13, Scharnhorststraße 1, D-21335 Lüneburg, Germany.

Tel.: +49 4131 677-2893

E-mail address: klaus.kuemmerer@leuphana.de (K. Kümmerer).

Table of content

Experimental methods:

Text S1 Supporting Information (SI): LC-MS Analytical method parameter for the elution and identification of the photo-transformation products (PTPs) of Desipramine (DMI).....**S5**

Figures:

Figure S1 SI: Emission spectrum for medium pressure Hg (mercury) lamp and the relative absorbance spectrum of 100 mg L⁻¹ desipramine (DMI).....**S6**

Figure S2 SI: Quantum yield and the photodegradation rate of the DMI UV photodegradation process as a function of the initial concentration; pH = 5, Temperature = 20 °C.....**S7**

Figure S3 SI: 10 mg L⁻¹ DMI LC-UV and Dissolved Organic Carbon (DOC) recovery during photolysis using Xenon lamp.....**S7**

Figure S4 SI: a) Total ion chromatogram (TIC) of 100 mg L⁻¹ DMI after 128 min of UV irradiation in UP water, and b) the proposed phototransformation pathway of DMI during UV irradiation**S8**

Figure S5: Fragmentation pattern of PTP₂₆₇₋₁ according to MSⁿ obtained from LC-HRMS.....**S9**

Figure S6: Fragmentation pattern of PTP₂₆₇₋₂ according to MSⁿ obtained from LC-HRMS.....**S10**

Figure S7: Fragmentation pattern of DMI according to MSⁿ obtained from LC-HRMS.....**S11**

Figure S8: Fragmentation pattern of PTP₂₈₁₋₁ according to MSⁿ obtained from LC-HRMS.....**S12**

Figure S9: Fragmentation pattern of PTP₂₈₁₋₂ according to MSⁿ obtained from LC-HRMS.....**S13**

Figure S10: Fragmentation pattern of PTP₂₈₃₋₁ according to MSⁿ obtained from LC-HRMS...**S14**

Figure S11: Fragmentation pattern of PTP₂₈₃₋₂ according to MSⁿ obtained from LC-HRMS...**S15**

Figure S12: Fragmentation pattern of PTP₂₈₃₋₃ according to MSⁿ obtained from LC-HRMS...**S16**

Figure S13: Fragmentation pattern of PTP₂₈₃₋₄ according to MSⁿ obtained from LC-HRMS...**S17**

Figure S14: Fragmentation pattern of PTP₂₈₃₋₅ according to MSⁿ obtained from LC-HRMS...**S18**

Figure S15: Fragmentation pattern of PTP₂₉₉₋₁ according to MSⁿ obtained from LC-HRMS...**S19**

Figure S16: Fragmentation pattern of PTP₂₉₉₋₂ according to MSⁿ obtained from LC-HRMS...**S20**

Figure S17: Fragmentation pattern of PTP₂₉₉₋₃ according to MSⁿ obtained from LC-HRMS...**S21**

Figure S18: Fragmentation pattern of PTP₂₉₉₋₄ according to MSⁿ obtained from LC-HRMS...**S22**

Figure S19: Fragmentation pattern of PTP₂₈₅₋₂ according to MSⁿ obtained from LC-HRMS...**S23**

Figure S20: Fragmentation pattern of PTP ₃₀₁₋₁ according to MS ⁿ obtained from LC-HRMS...	S24
Figure S21: Fragmentation pattern of PTP ₃₀₁₋₂ according to MS ⁿ obtained from LC-HRMS...	S25
Figure S22: Fragmentation pattern of PTP ₂₁₉ according to MS ⁿ obtained from LC-HRMS.....	S26
Figure S23: Time curves of the relative peak area A/A_0 (%) of products (PTPs) during photolysis at different concentrations.....	S27+28
Figure S24 SI: the change in the molar absorption coefficient (ϵ) as a function of the solution pH (DMI concentration = 100 mg L ⁻¹).....	S29
Figure S25 SI: DMI structure at different pH, pKa = 10.02.....	S29
Figure S26 SI: The changes in pH values during the UV-irradiation of DMI under different pH values.....	S30
Figure S27: Time curves of the relative peak area A/A_0 (%) of products (PTPs) during photolysis at different pH values.....	S31+32
Figure S28: Fragmentation pattern of PTP ₂₃₅ according to MS ⁿ obtained from LC-HRMS.....	S33
Figure S29: Fragmentation pattern of PTP ₂₇₁ according to MS ⁿ obtained from LC-HRMS.....	S34
Figure S30 SI: DOC Removal curves during the UV photodegradation process of DMI at different temperatures.....	S35
Figure S31: Time curves of the relative peak area A/A_0 (%) of products (PTPs) during photolysis at different temperatures.....	S36+37
Figure S32: Closed Bottle test and Manometric Respiratory Test results of DMI and its PTPs at different irradiation time points.....	S38
Figure S33: The structural moiety responsible for the positive alert (red color) and the unknown fragment in TP 301-31 predicted by Microtox Toxicity to Environmental Bacteria model using Case Ultra software.....	S39

Tables:

Table S1 SI: a) Test system of the Closed Bottle test (CBT), b) Test system of the manometric respiratory test (MRT).....	S40
Table S2 SI: Q-SAR predictions of log P for DMI and its suggested PTPs structures....	S41-S44

Table S3 SI: Q-SAR predictions for DMI and its TPs for ready biodegradability by different models: 1: Catalogic-BOD Kinetic (OECD 301F)_v.08.09, 2. Catalogic BOD 28 days MITI (OECD 301C) _v.06.07. 3: Case Ultra, MITI Ready biodegradation (AU6), 4: MITI Biodegradation probability Biowin 5 (linear model), 5: MITI Biodegradation probability Biowin 6 (MITI non-linear model), (Positive results are red, RB: Ready Biodegradable, NRB: non Ready Biodegradable).....**S45-54**

Table S4 SI: QSAR toxicity predictions for DMI and its TPs by different models (Models 1-5 (Case ultra software), Model 6 (Oasis catalogic)): (1) Salmonella mutagenicity TA 97, 98, 100, 1535–1538 (GT1 A7B), (2) A–T mutation E. coli and TA102 (GT1 AT E. coli), (3) Expert rules for genotoxicity (GT Expert), (4) E. coli mutagenicity (all strains) (Pharm E. coli), (5) Salmonella mutagenicity (TA97, 98, 100, 1535–1538) (Pharm Salm), 6. Mutagenicity v. 4.....**S55-59**

Table S5 SI: The predicted bacterial toxicity of DMI and its TPs with four acute toxicity models for *Vibrio fischeri* [Microtox Toxicity to Environmental Bacteria (AUA, Case Ultra) and three acute toxicity *Vibrio fischeri* models (Oasis Catalogic)].....**S60-64**

Text S1:

The LC-ITMS system comprising an HPLC 1100 series (Agilent Technologies, Böblingen, Germany) consisting of binary pumps (G1312A), column oven (G1316A), degasser (G1322A), and auto sampler (ALS G1329A + ALS Therm G1330), coupled to a Bruker data analysis system and atmospheric pressure electrospray ionization interface (Bruker Daltonic GmbH, Bremen, Germany). data acquisition and processing were performed using the associated Data analysis V.4 and Quant analysis V.2 software. The Esquire 6000 plus MS analysis was carried out in positive ionization mode using an ion spray voltage of 4160 V. The nebulizer (air) pressure was set at 30 psi. The Ion Spray source was operated at 350°C dry temperature with dry gas flow equal 12 L min⁻¹. The other operating conditions of the source were: - 500 V end plate, + 4160 V capillary voltage. The selected lens and block voltages were: +66.7 V capillary exit, +9.35 V octopole 1, +1.71 V octopole 2, 170.8 Vpp octopole reference amplitude, 33.4 V skimmer, 32.4 trap drive, -3.0 V lens 1 and -59.5 V lens 2. The scan range was determined from m/z 40 to 1000.

LITQ-Orbitrap XL mass spectrometer interfaced with heated electrospray ionization (HESI) source (Thermo Scientific, Bremen, Germany) was used for the determination of the accurate masses of DMI TPs. The LC-MS system comprising a Dionex UHPLC system (Ultimate 3000) consisting of two HPG-3400-RS binary pumps, a TCC-3000 column oven, a SRD-3600 degasser, and an auto sampler WPS-3000-TRS. UV detection was performed using a VWD-3400RS detector. The spectrometer was operated also in positive mode under the following conditions: spray voltage 4 kV, capillary voltage 19 V and tube lens voltage 75 V. The heated capillary and desolvation temperatures were 275 °C and 150 °C, respectively. Nitrogen served as sheath, auxiliary and sweep gas with flow rate equal 20, 5 and 0 arb, respectively. MS data were recorded in the full scan mode (m/z 100–400). Fragmentation to MS⁴ was achieved by setting collision induced dissociation (CID) on 35 eV. All data were processed using Xcalibur/Qual Browser 2.1.0 SP1 build 1160 (Thermo Scientific, Bremen, Germany).

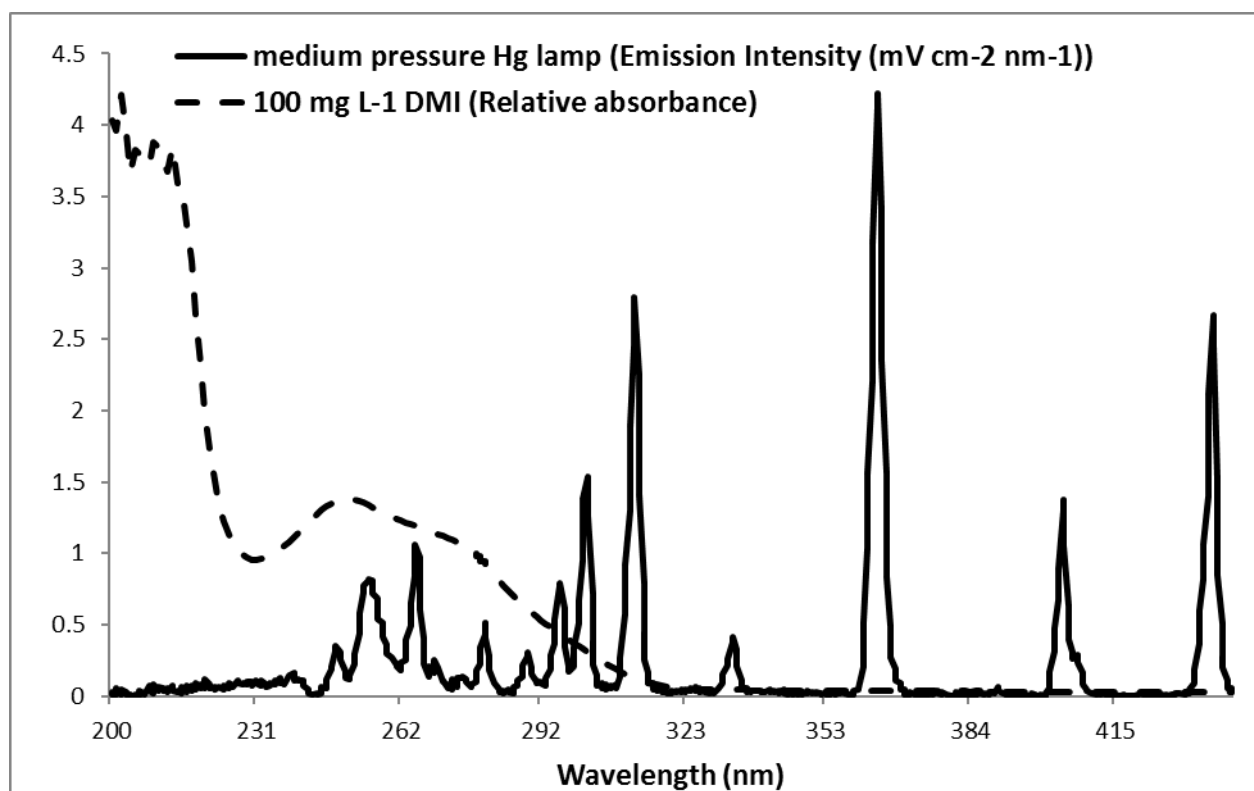


Figure S1: Emission spectrum for medium pressure Hg (mercury) lamp and the relative absorbance spectrum of 100 mg L⁻¹ desipramine (DMI)

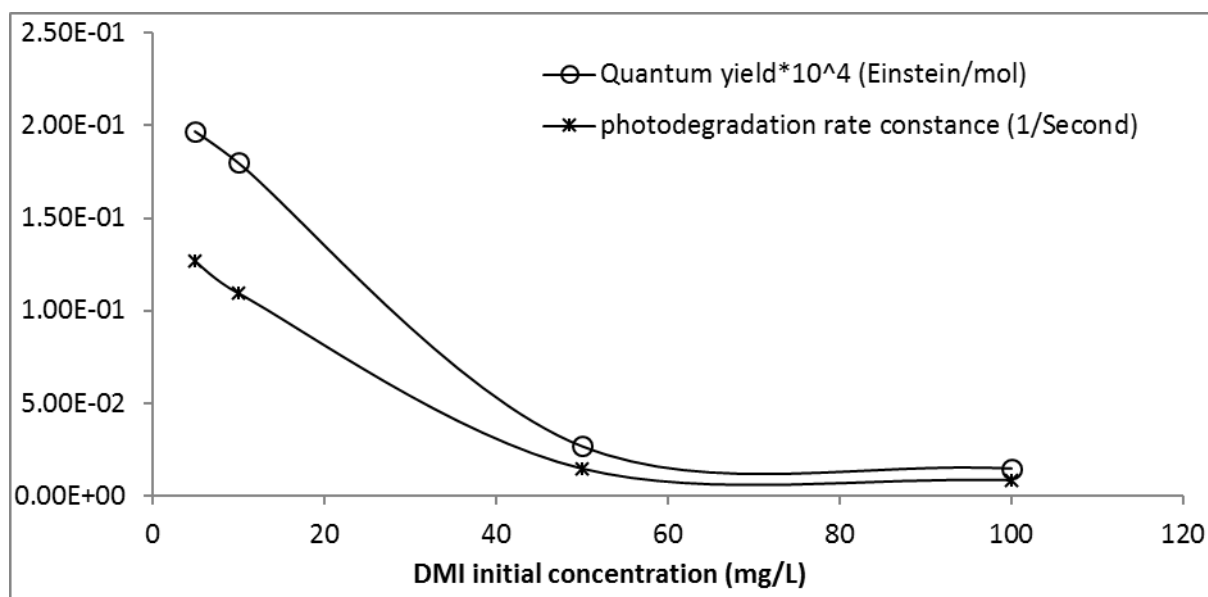


Figure S2: Quantum yield and the photodegradation rate of the DMI UV photodegradation process as a function of the initial concentration; pH = 5, Temperature = 20 °C.

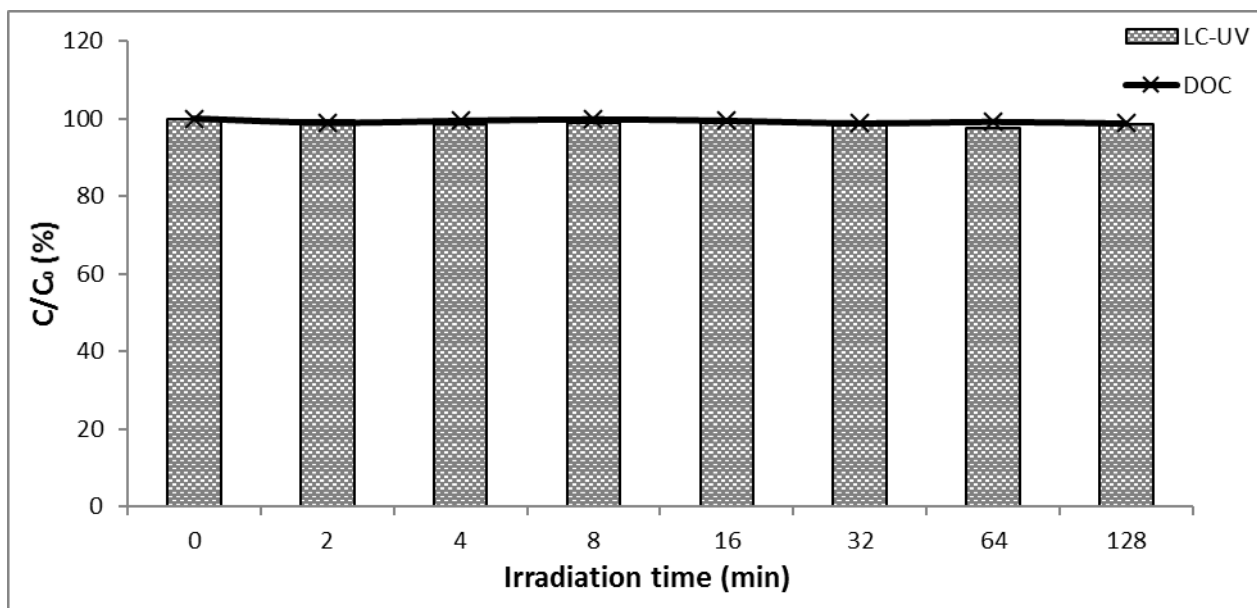


Figure S3: 10 mg L⁻¹ DMI LC-UV and Dissolved Organic Carbon (DOC) recovery during photolysis using Xenon lamp

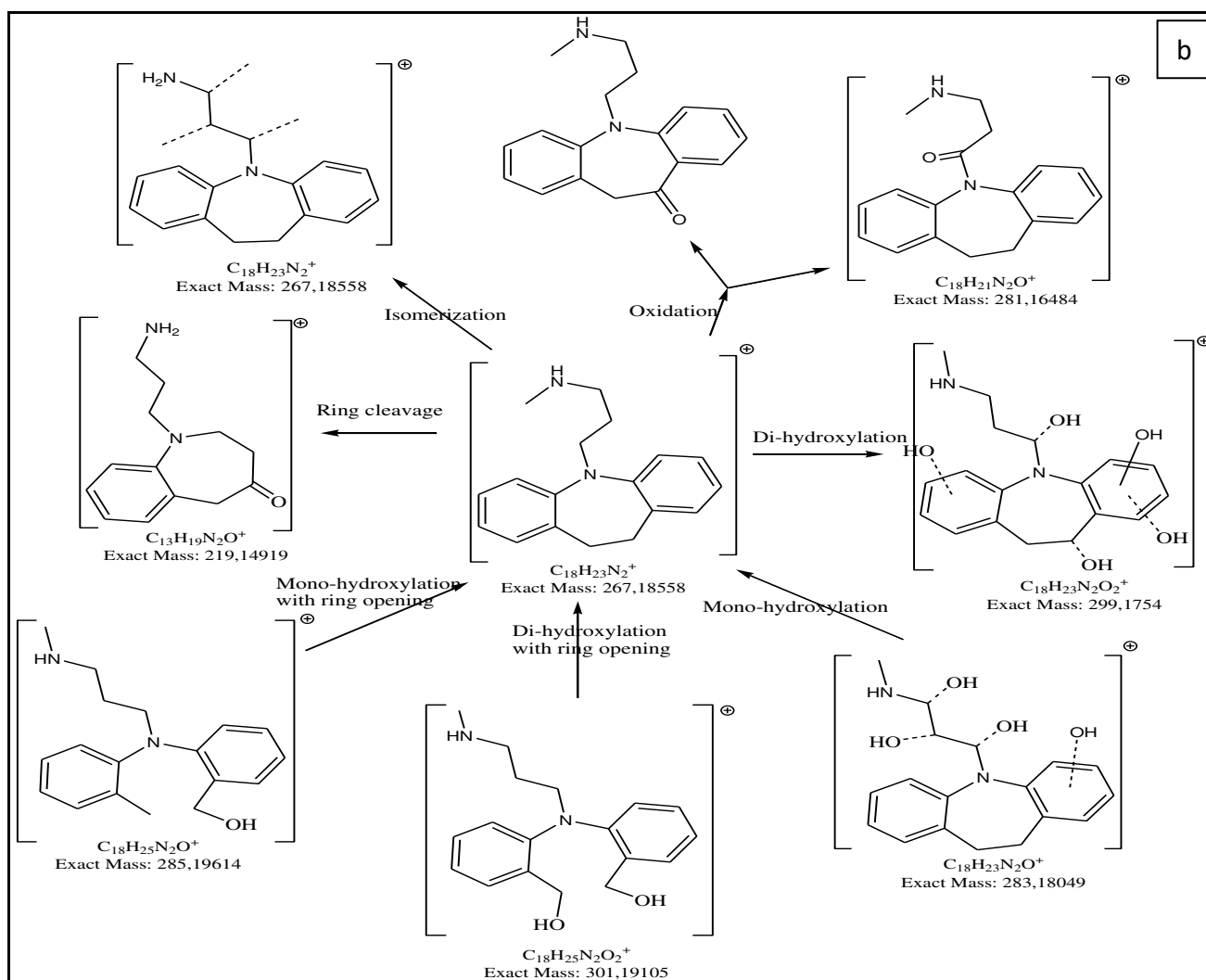
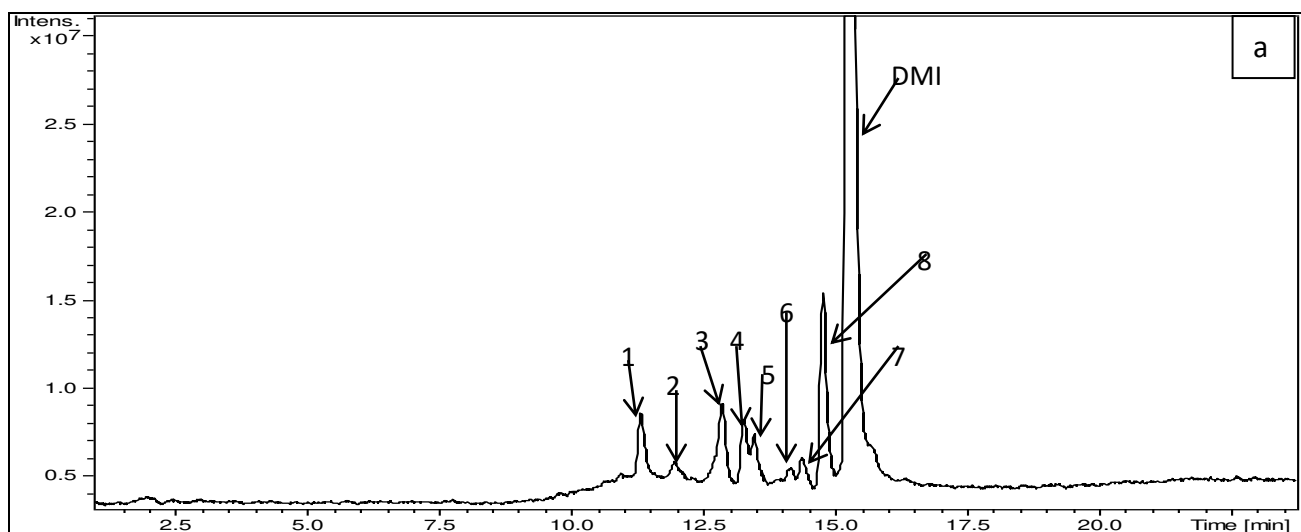


Figure S4: a) Total ion chromatogram (TIC) of 100 mg L⁻¹ DMI after 128 min of UV irradiation in UP water, and b) the proposed phototransformation pathway of DMI during UV irradiation.

1: PTP₂₁₉, 2: PTP₂₈₁₋₁, 3: PTP₂₈₃₋₁, 4: PTP₂₈₁₋₂, 5: PTP₂₈₃₋₂, 6: PTP₂₆₇₋₁, 7: PTP₂₈₃₋₄, 8: PTP₂₆₇₋₂.

PTP267-1

MS²/267

100DMI-LV-64min-normalC18column-130819b #945 RT: 12.22 AV: 1 NL: 7.25E4
T: FTMS + c ESI d Full ms2 267,19@cid35,00 [60,00-280,00]

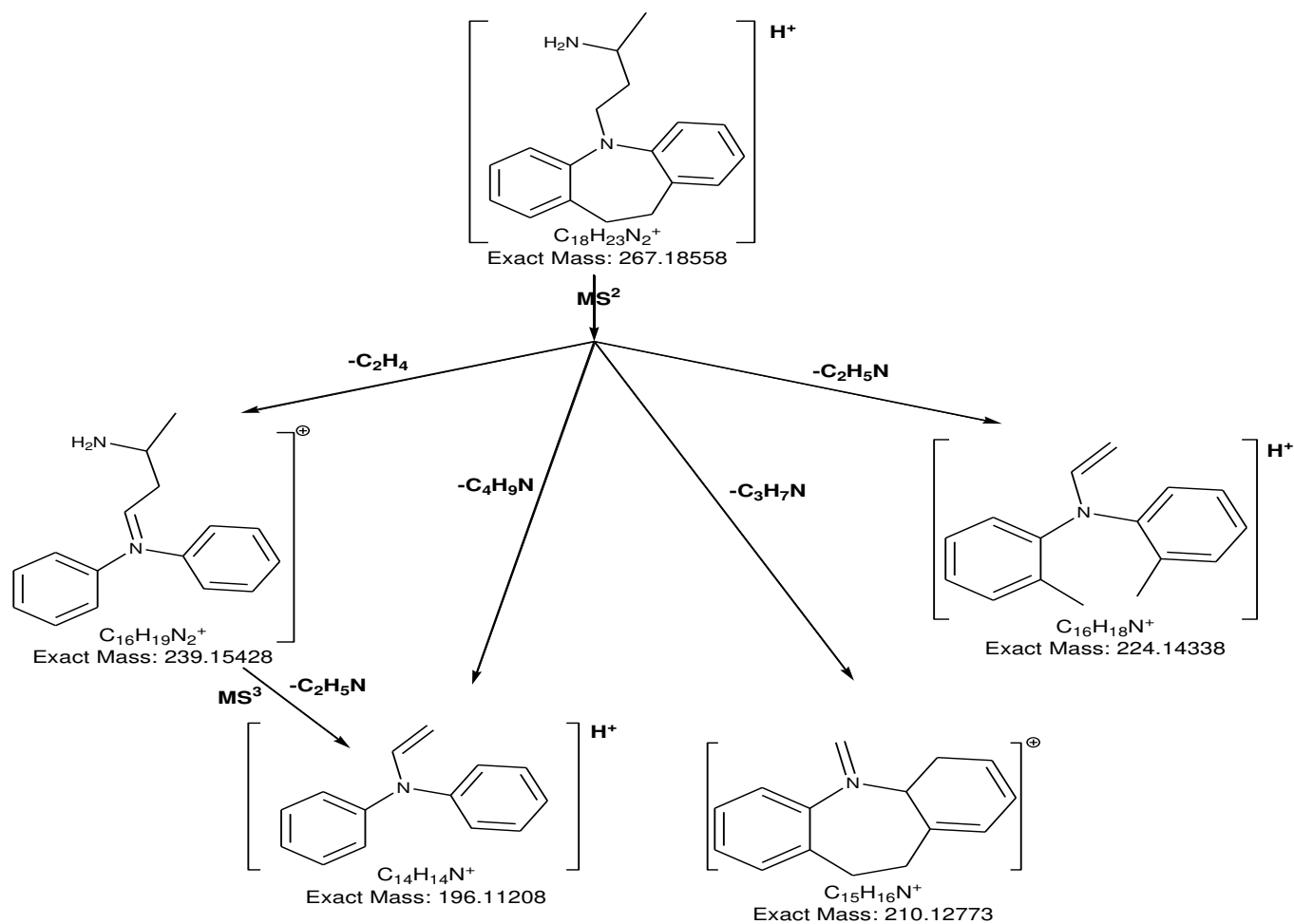
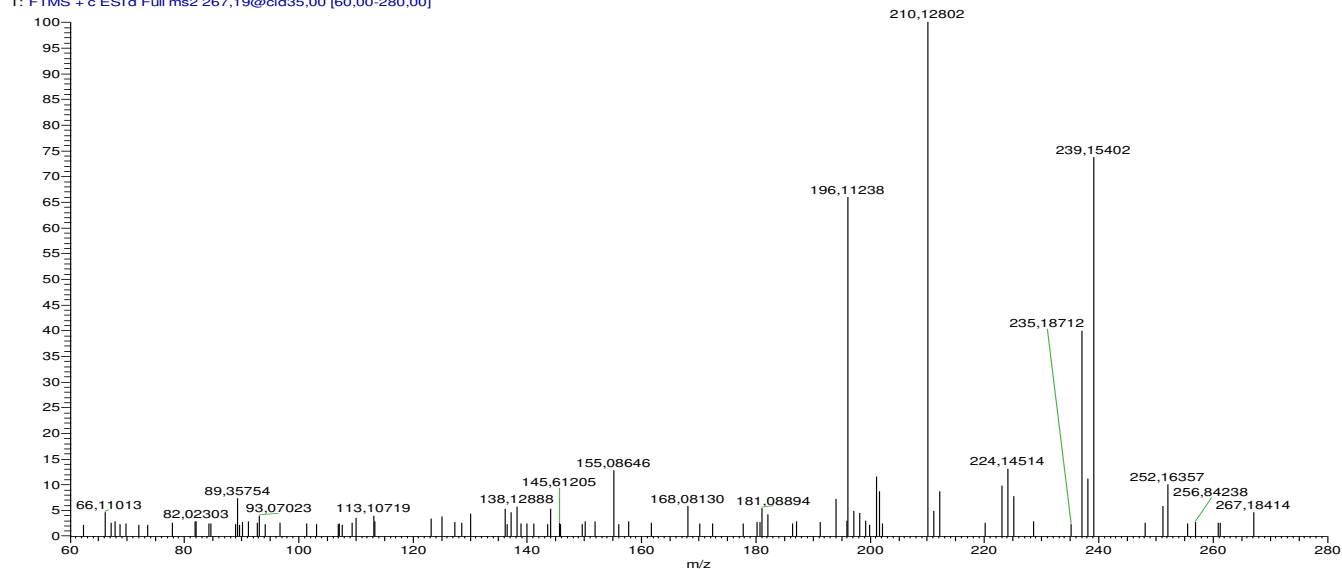


Figure S5: Fragmentation pattern of PTP₂₆₇₋₁ according to MSⁿ obtained from LC-HRMS

PTP267-2

MS²/267

100DMI-LV-128min-normalC18column-130819b #1003 RT: 12.93 AV: 1 NL: 4.40E6
T: FTMS + c ESI d Full ms2 267.19@cid35.00 [60.00-280.00]

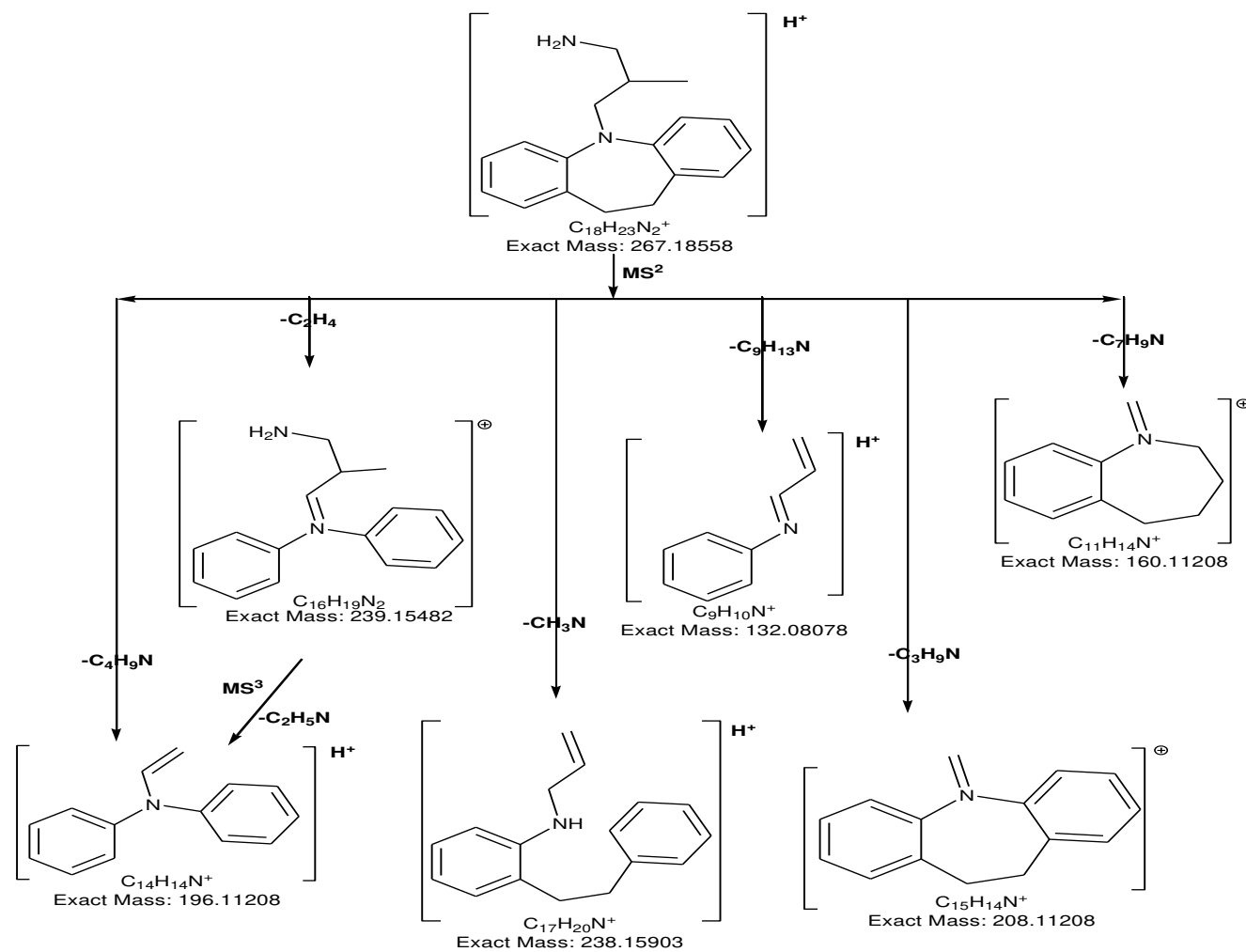
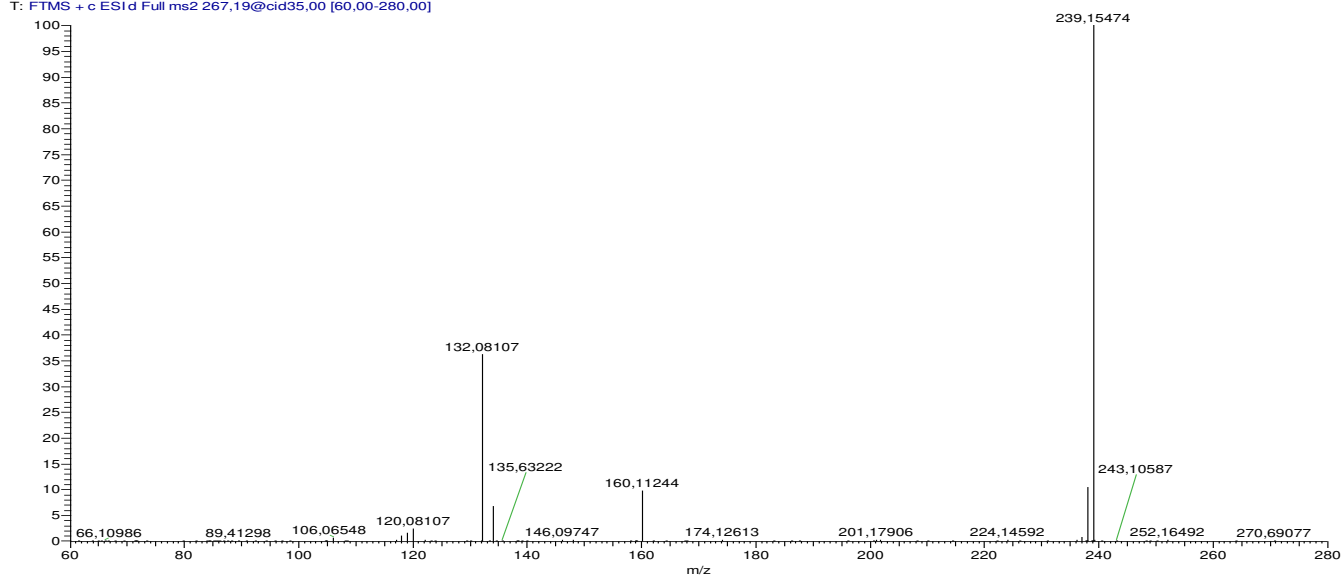


Figure S6: Fragmentation pattern of PTP₂₆₇₋₂ according to MSⁿ obtained from LC-HRMS

DMI

MS²/267

100DMI-UV-128min-normalC18column-130819b #1055 RT: 13.61 AV: 1 NL: 2.51E6
T: FTMS + c ESI d Full ms2 267,19@cid35,00 [60,00-280,00]

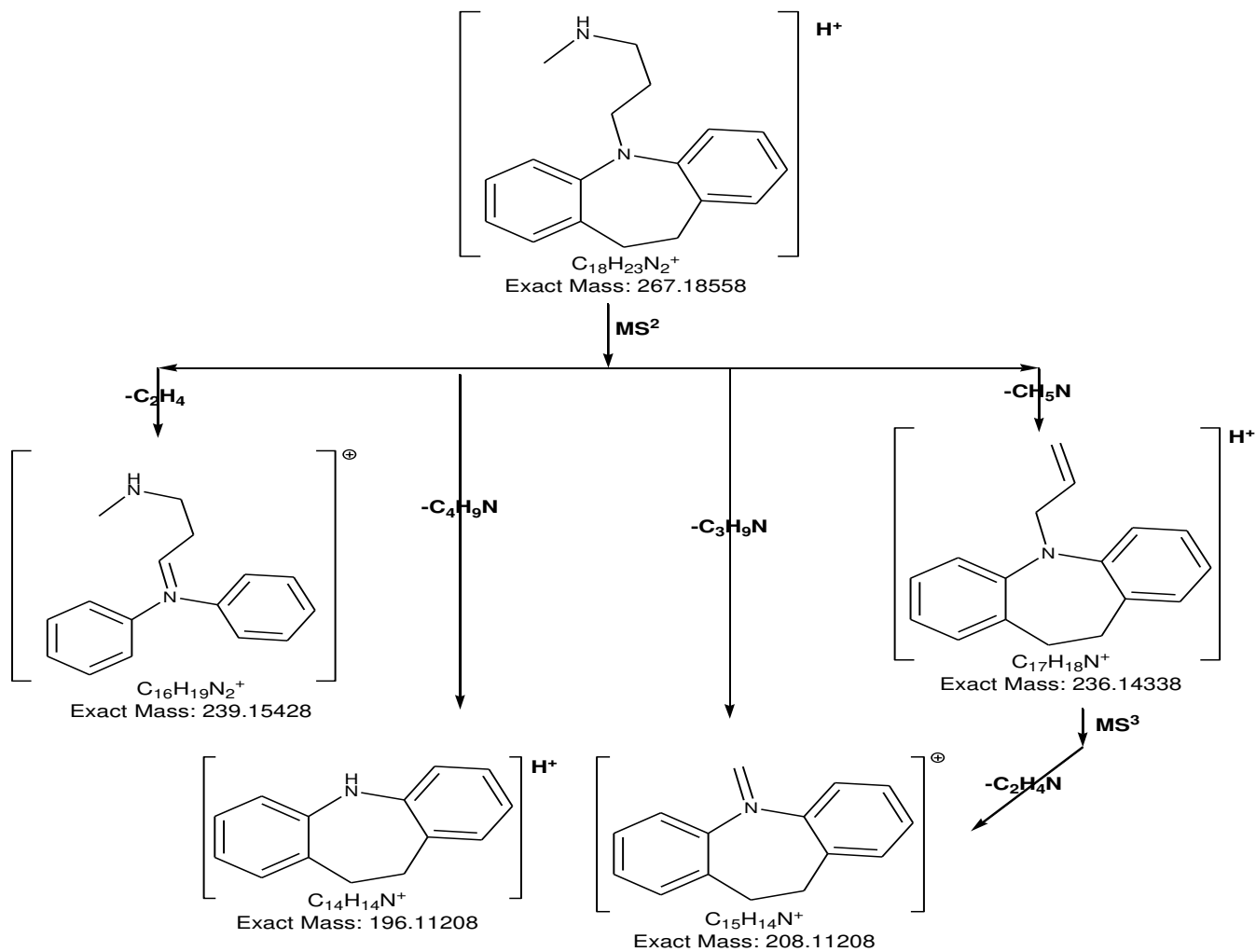
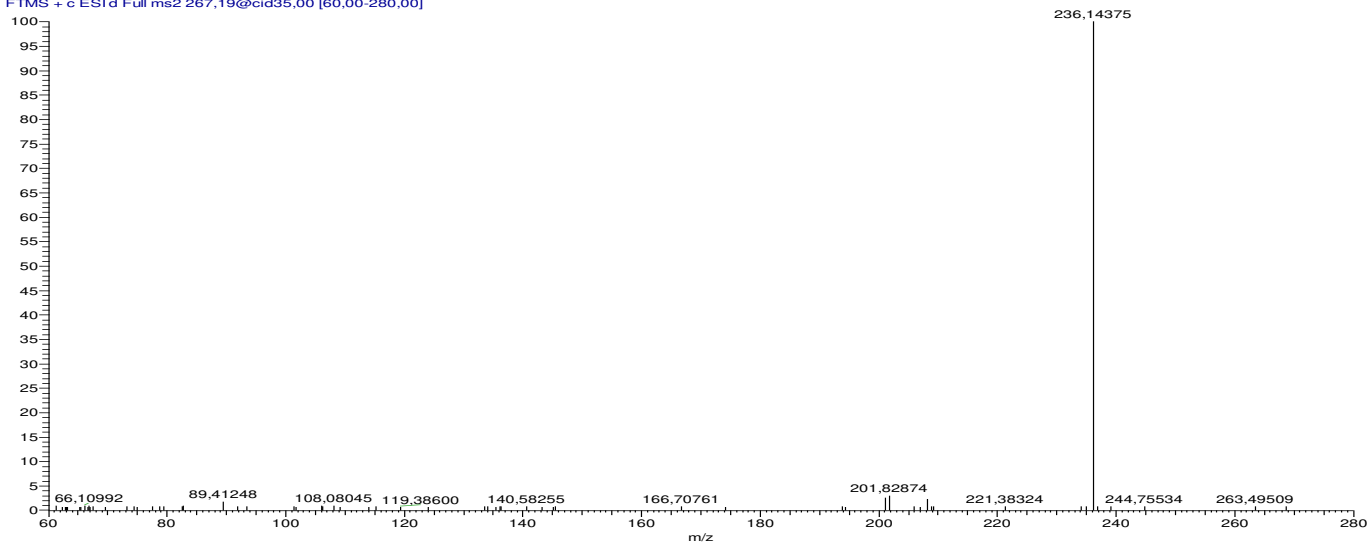


Figure S7: Fragmentation pattern of DMI according to MSⁿ obtained from LC-HRMS

PTP₂₈₁₋₁

MS²/281

100DMI-UV-64min-normalC18column-130819b #755 RT: 9.70 AV: 1 NL: 7.73E4
T: FTMS + c ESI d Full ms2 281.17@cid35.00 [65.00-295.00]

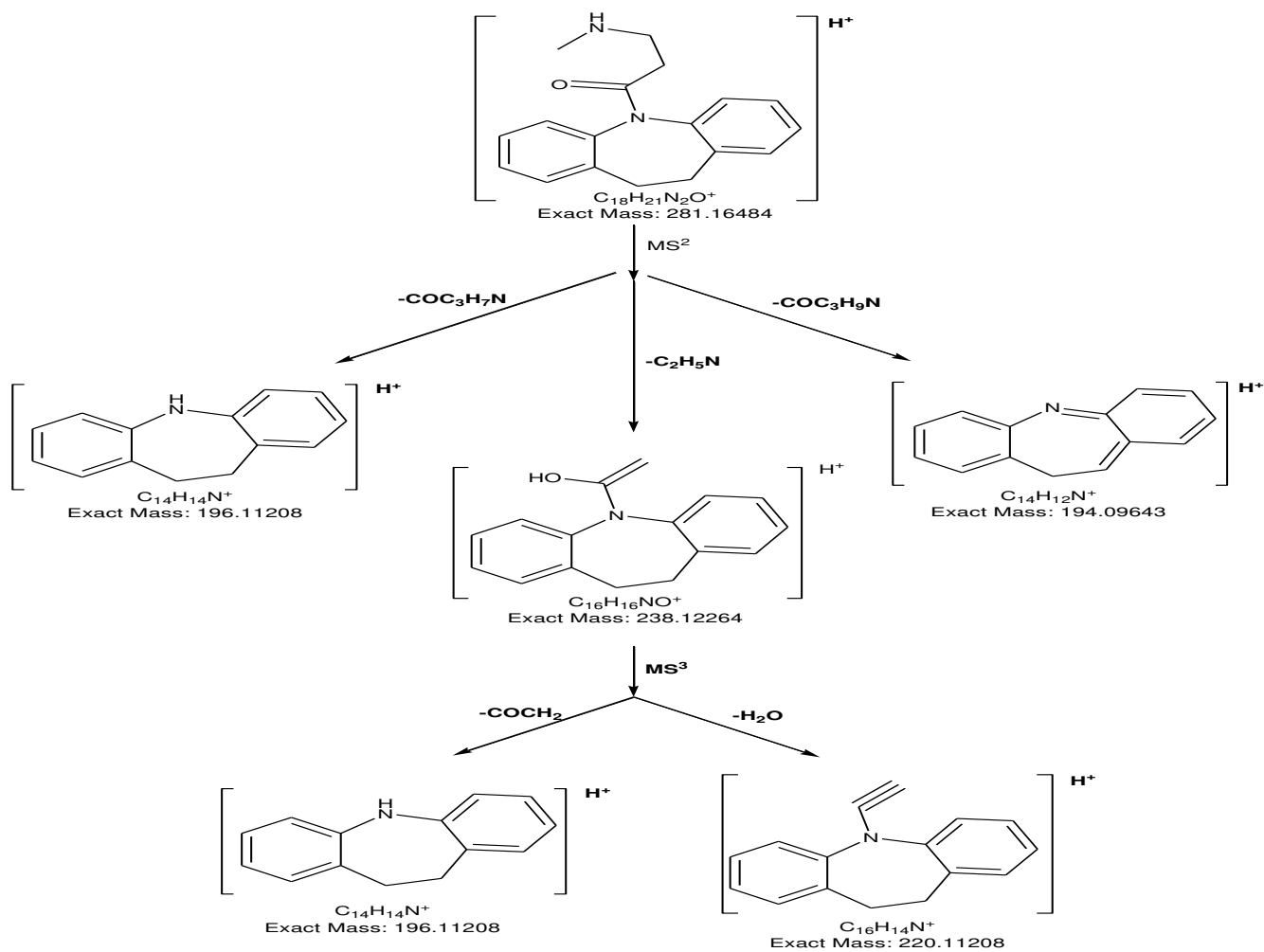
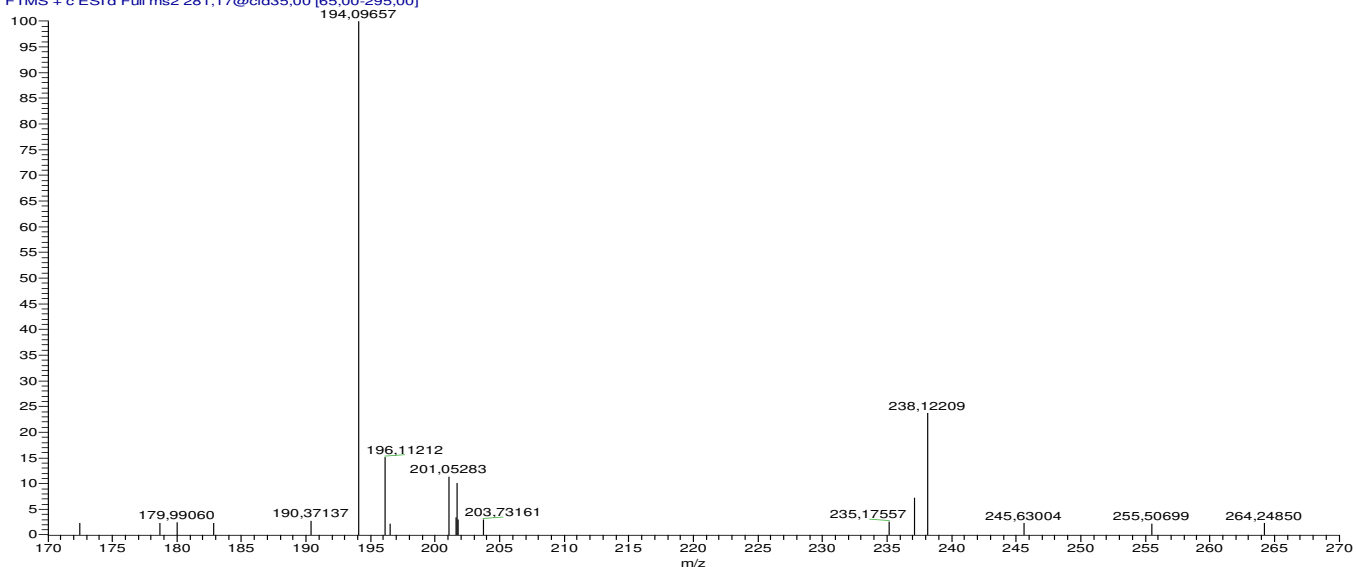


Figure S8: Fragmentation pattern of PTP₂₈₁₋₁ according to MSⁿ obtained from LC-HRMS

PTP₂₈₁₋₂

MS²/281

100DM-UV-64min-normalC18column-130819b #857 RT: 11.05 AV: 1 NL: 1.51E5
T: FTMS + c ESI d Full ms2 281.17@cid35.00 [65.00-295.00]

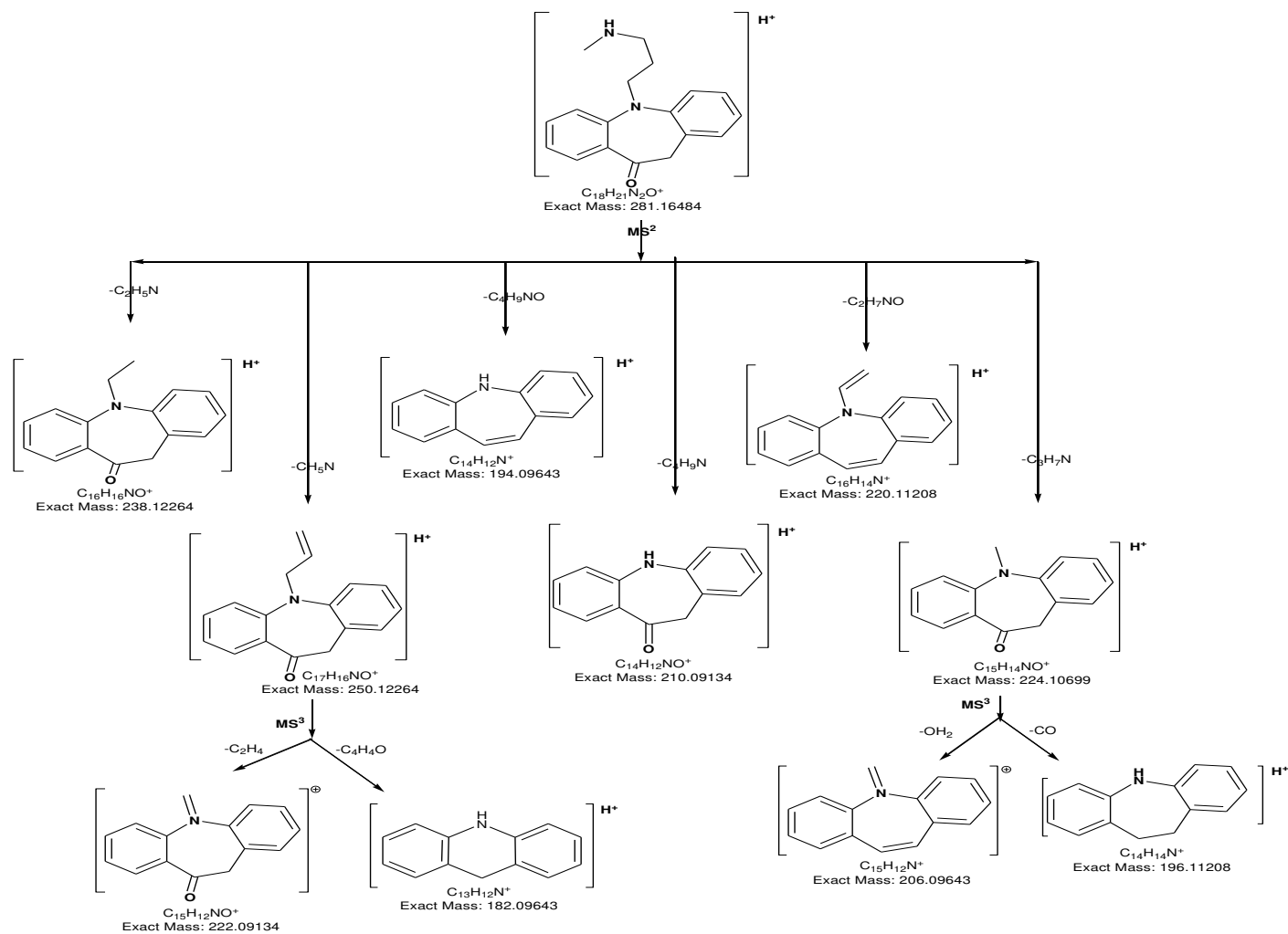
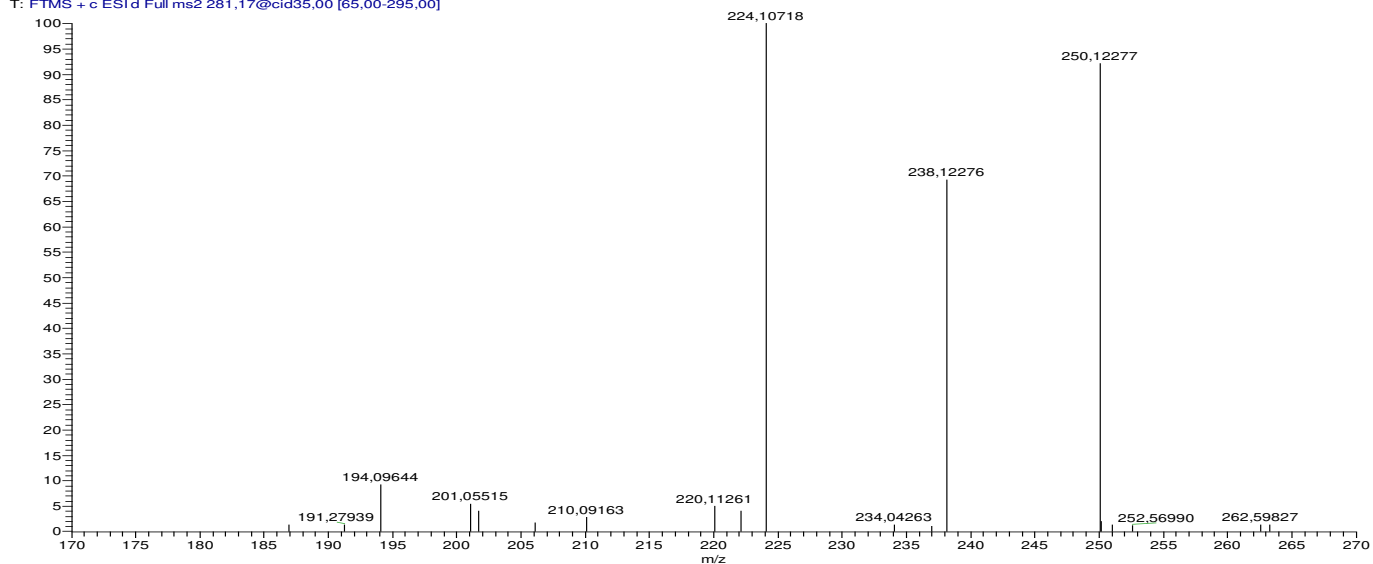


Figure S9: Fragmentation pattern of PTP₂₈₁₋₂ according to MSⁿ obtained from LC-HRMS

PTP₂₈₃₋₁

MS²/283

100DMI-LV-64min-normalC18column-130819b #821 RT: 10.58 AV: 1 NL: 2.62E6
T: FTMS + c ESI d Full ms2 283,18@cid35,00 [65,00-295,00]

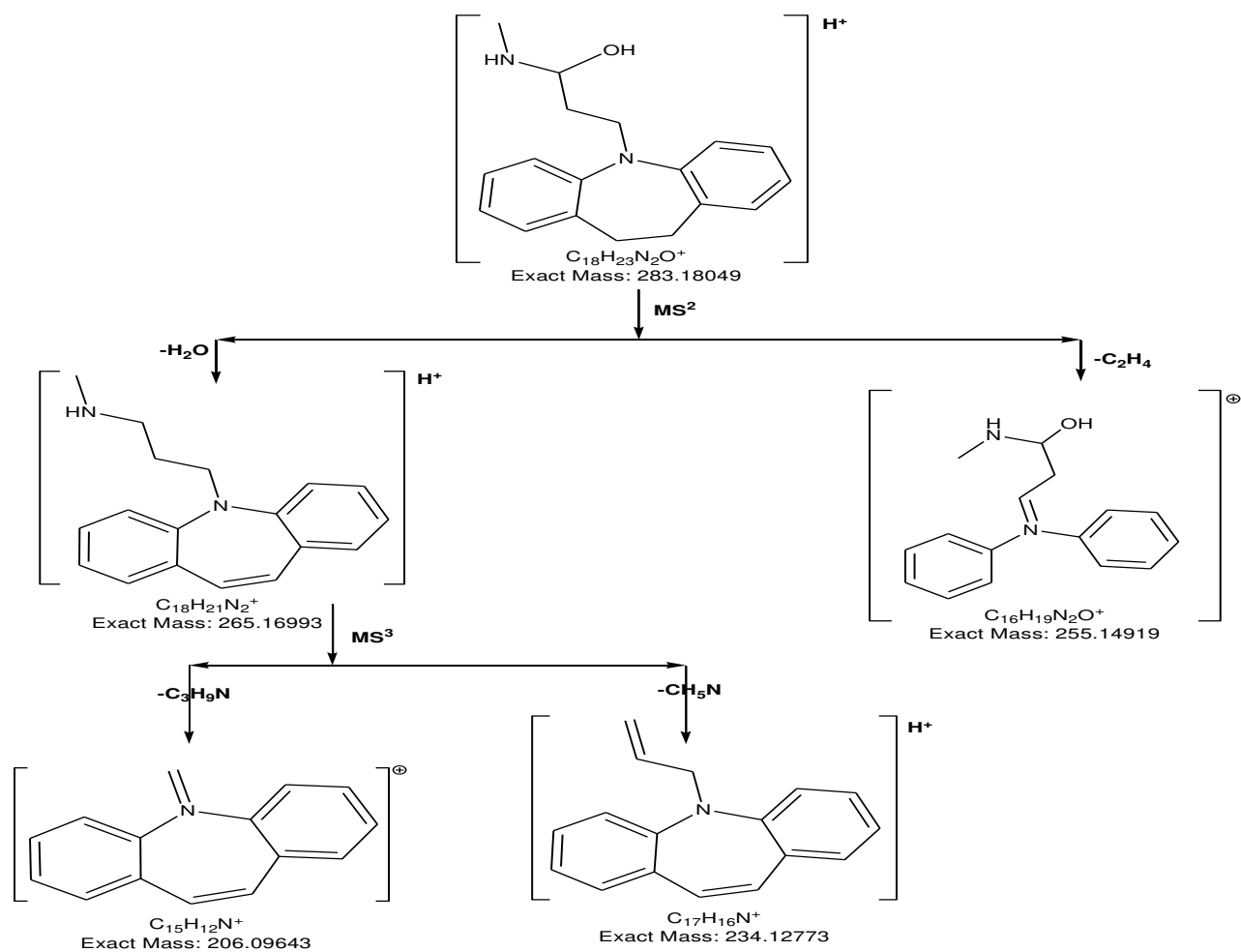
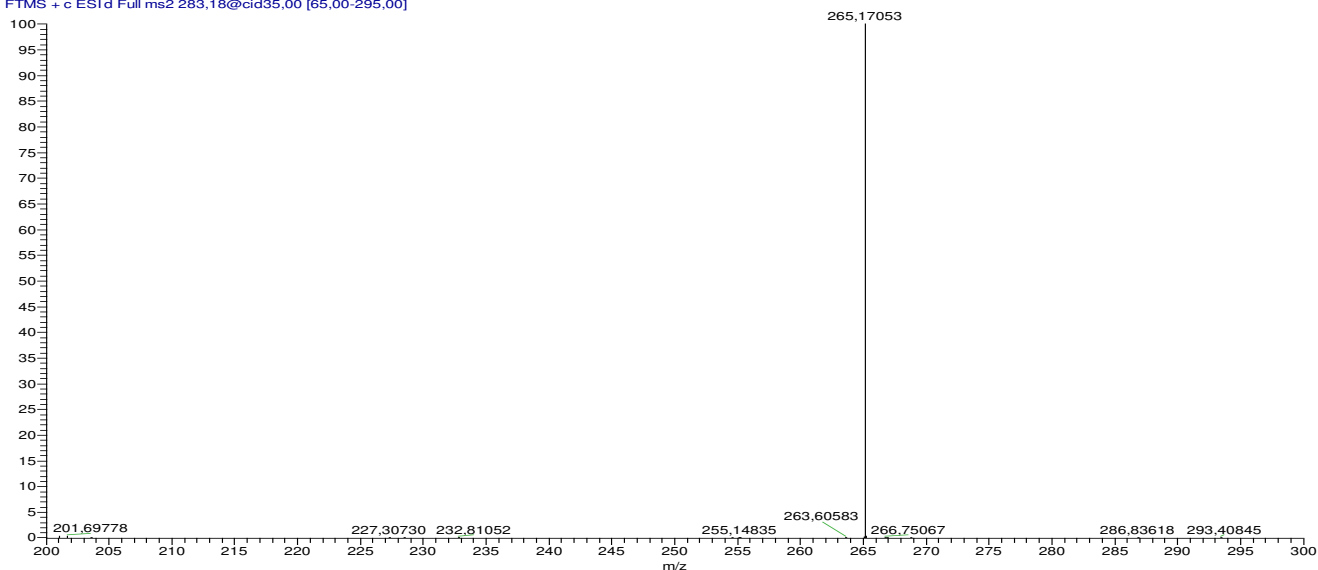


Figure S10: Fragmentation pattern of PTP₂₈₃₋₁ according to MSⁿ obtained from LC-HRMS

PTP₂₈₃₋₂

MS²/283

100DMI-LV-64min-normalC18column-130819b #863 RT: 11.13 AV: 1 NL: 1.64E5
T: FTMS + c ESI d Full ms2 283,18@cid35,00 [65,00-295,00]

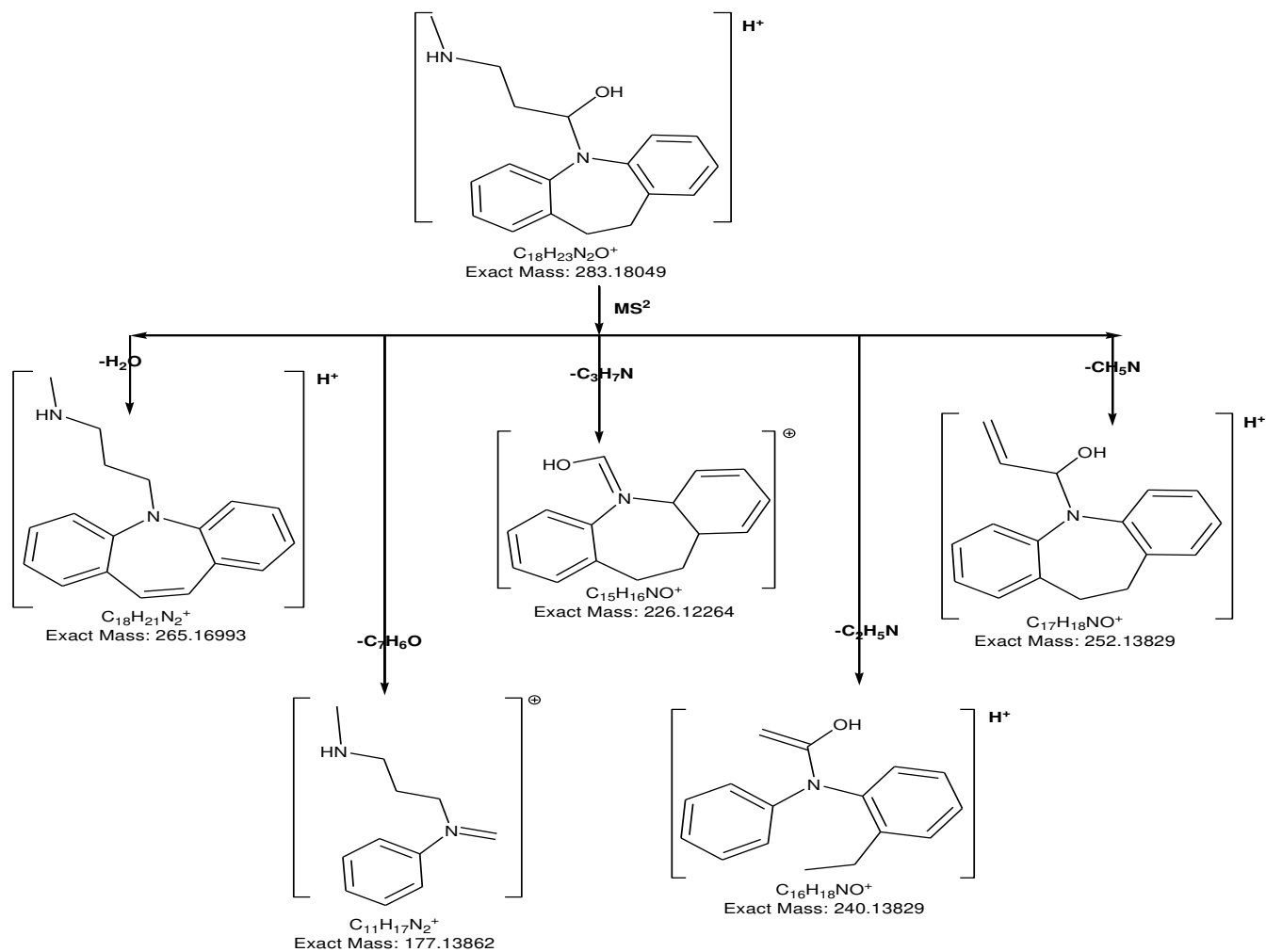
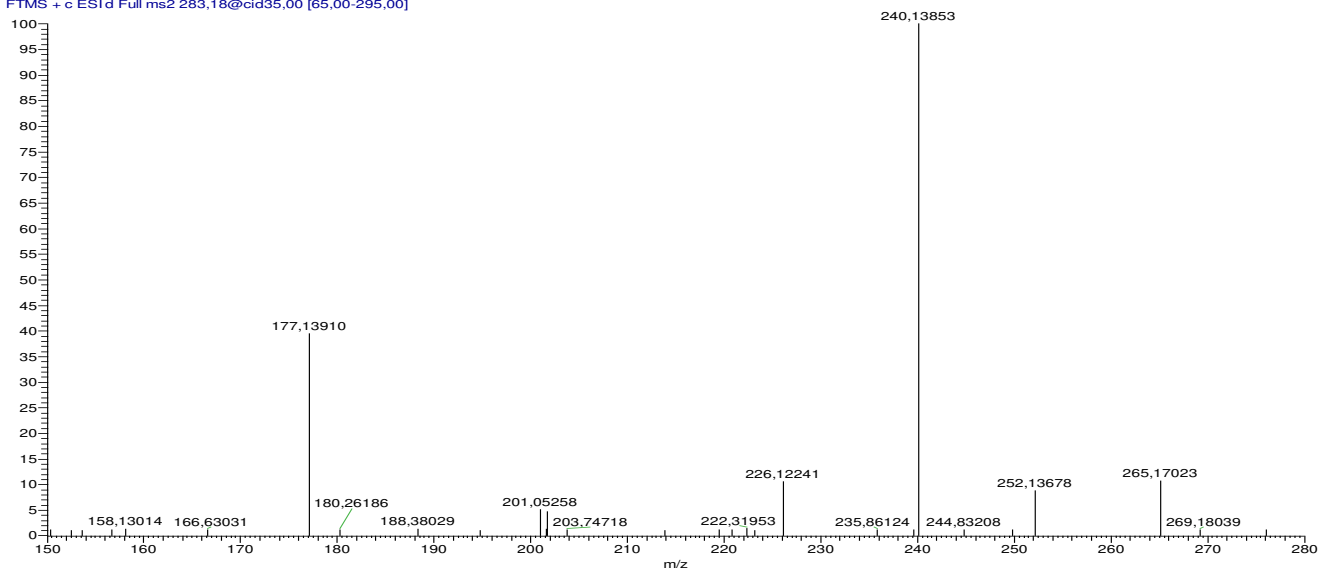


Figure S11: Fragmentation pattern of PTP₂₈₃₋₂ according to MSⁿ obtained from LC-HRMS

PTP₂₈₃₋₃

MS²/283

100DMI-UV-64min-normalC18column-130819b #899 RT: 11.60 AV: 1 NL: 9.90E3
T: FTMS + c ESI d Full ms2 283,18@cid35,00 [65,00-295,00]

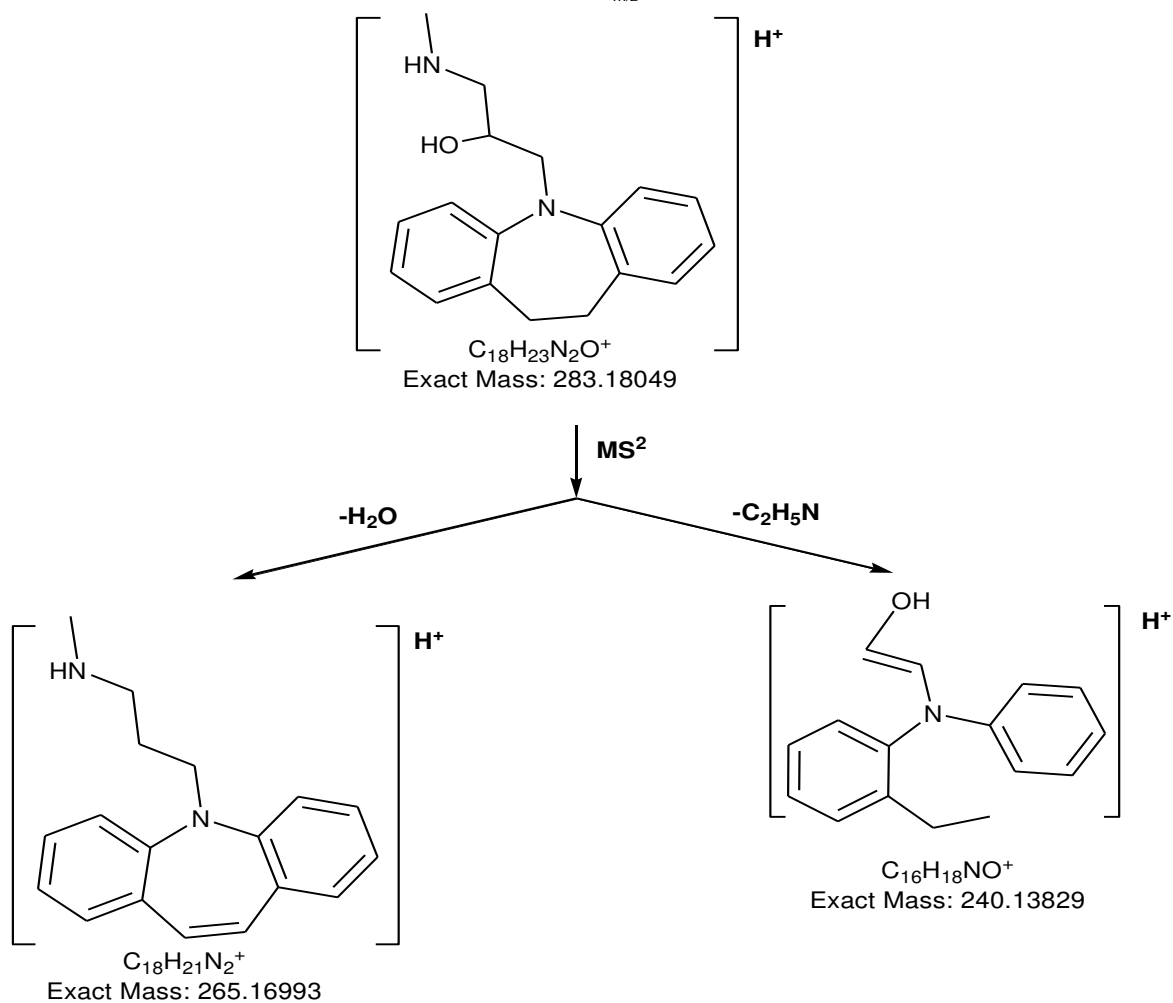
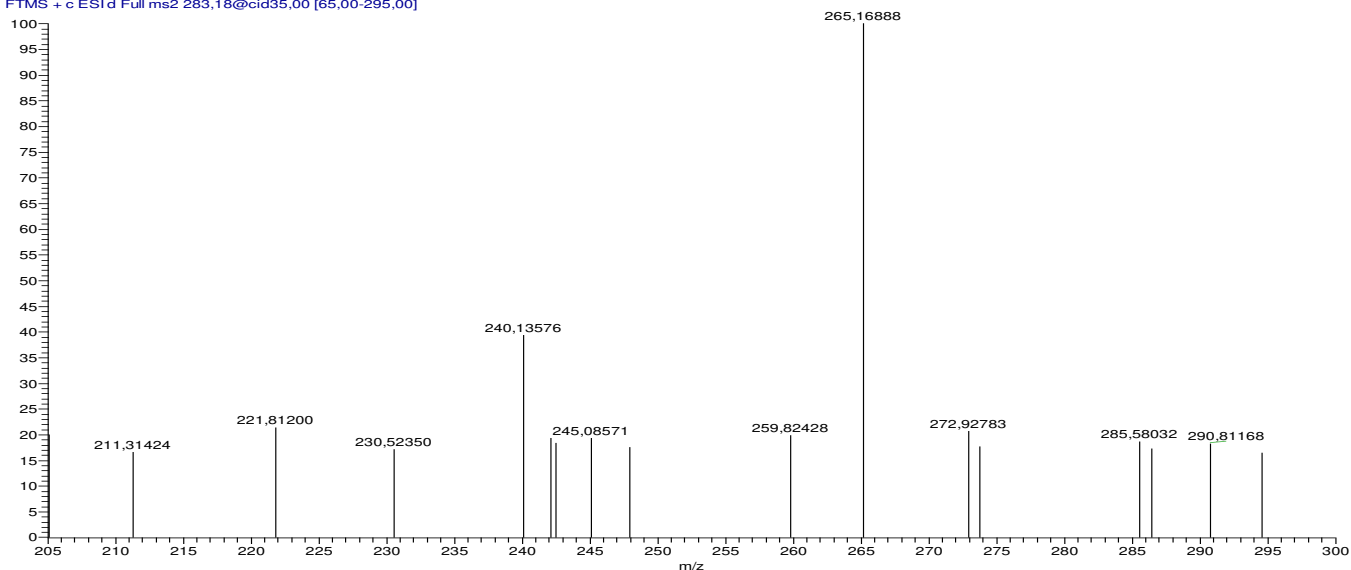


Figure S12: Fragmentation pattern of PTP₂₈₃₋₃ according to MSⁿ obtained from LC-HRMS

PTP₂₈₃₋₄

MS²/283

100DMH-UV-64min-normalC18column-130819b #951 RT: 12.30 AV: 1 NL: 1.05E4
T: FTMS + c ESI d Full ms2 283,18@cid35,00 [65,00-295,00]

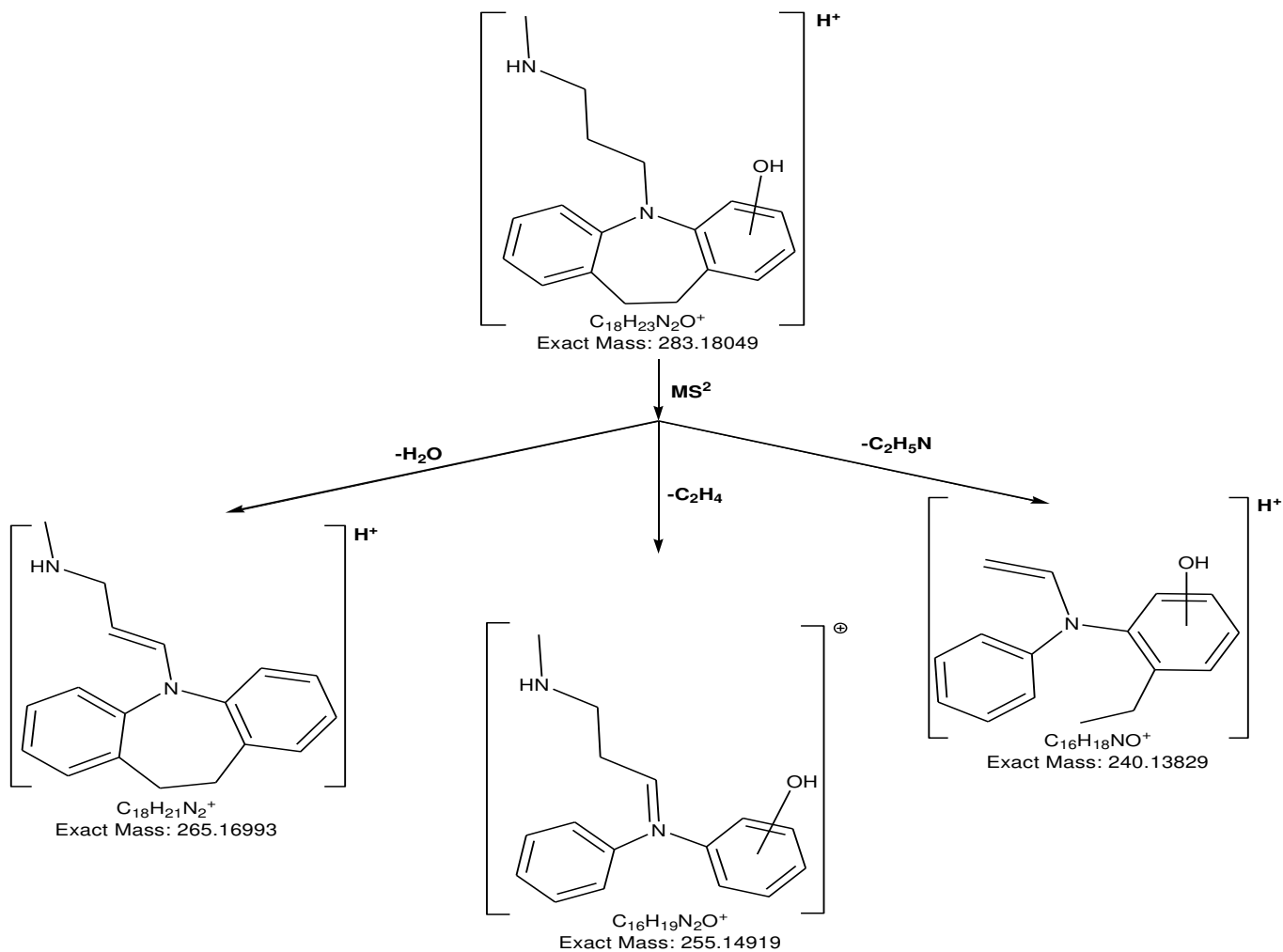
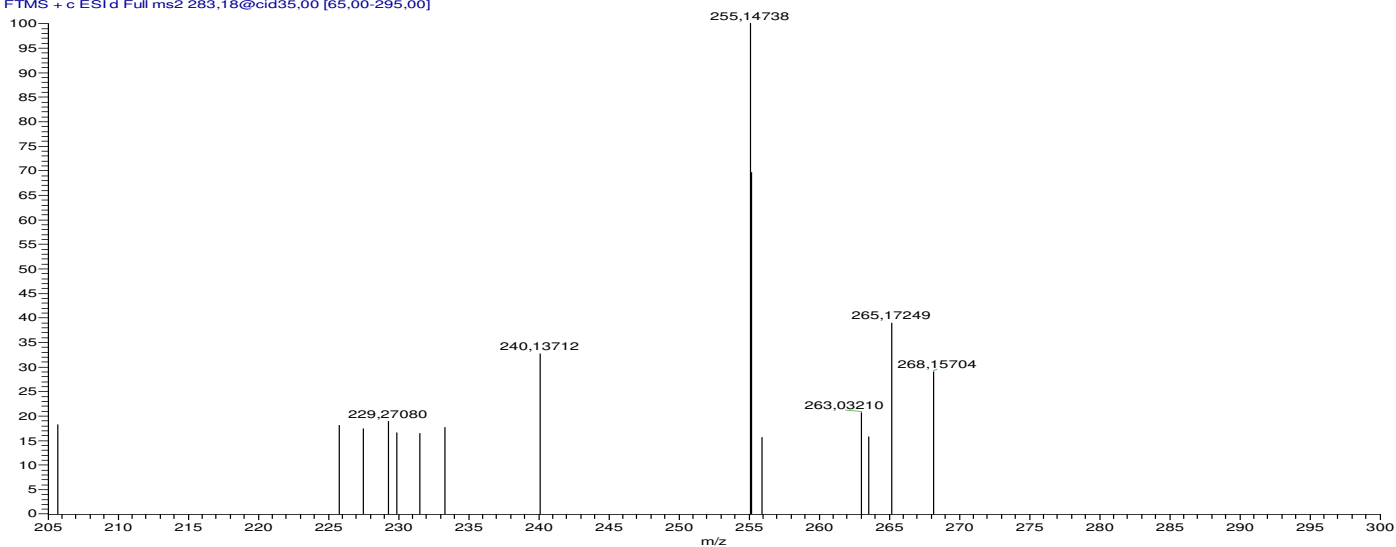


Figure S13: Fragmentation pattern of PTP₂₈₃₋₄ according to MSⁿ obtained from LC-HRMS

PTP₂₈₃₋₅MS²/283

100DMI-LV-64min-normalC18column-130819b #1044 RT: 13.50 AV: 1 NL: 2.18E4
 T: FTMS + c ESI d Full ms2 283,18@cid35,00 [65,00-295,00]

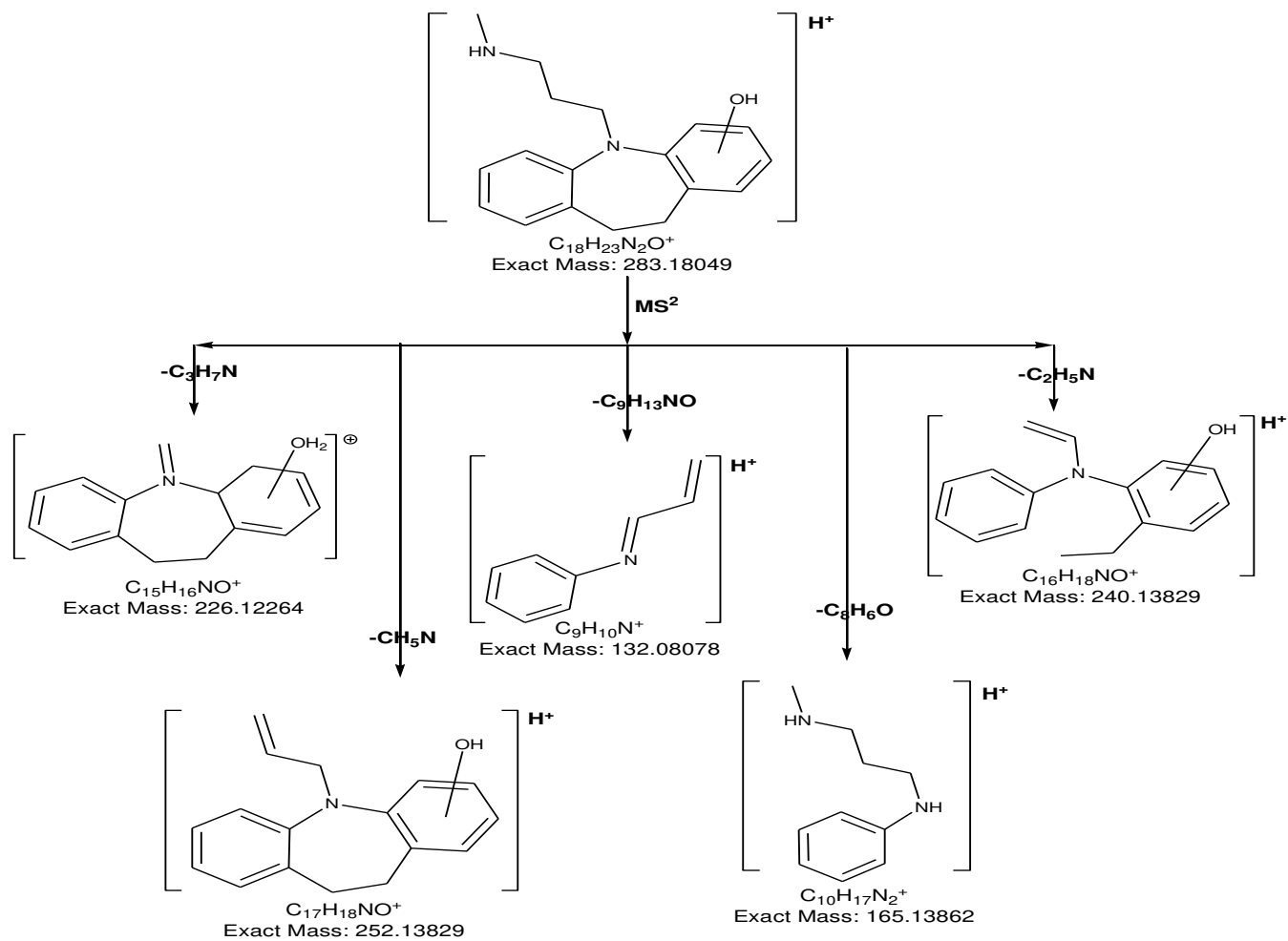
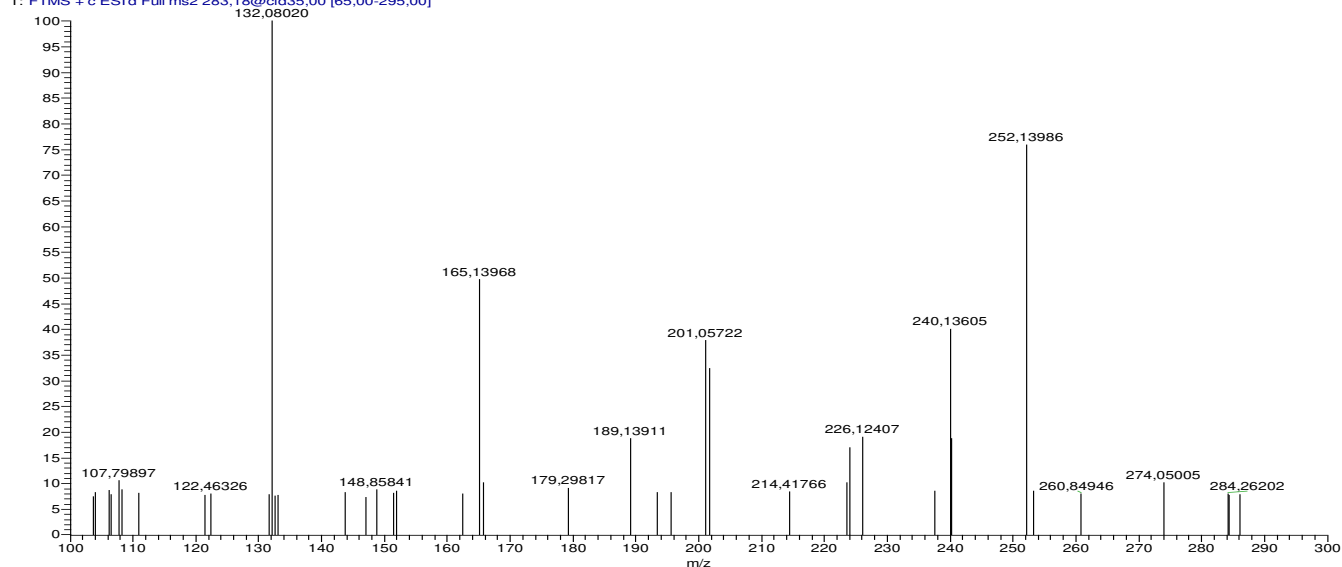


Figure S14: Fragmentation pattern of PTP₂₈₃₋₅ according to MSⁿ obtained from LC-HRMS

PTP₂₉₉₋₁

MS²/299

100DMI-LV-64min-normalC18column-130819b #703 RT: 9.02 AV: 1 NL: 3.07E4
T: FTMS + c ESI d Full ms2 299,18@cid35,00 [70,00-310,00]

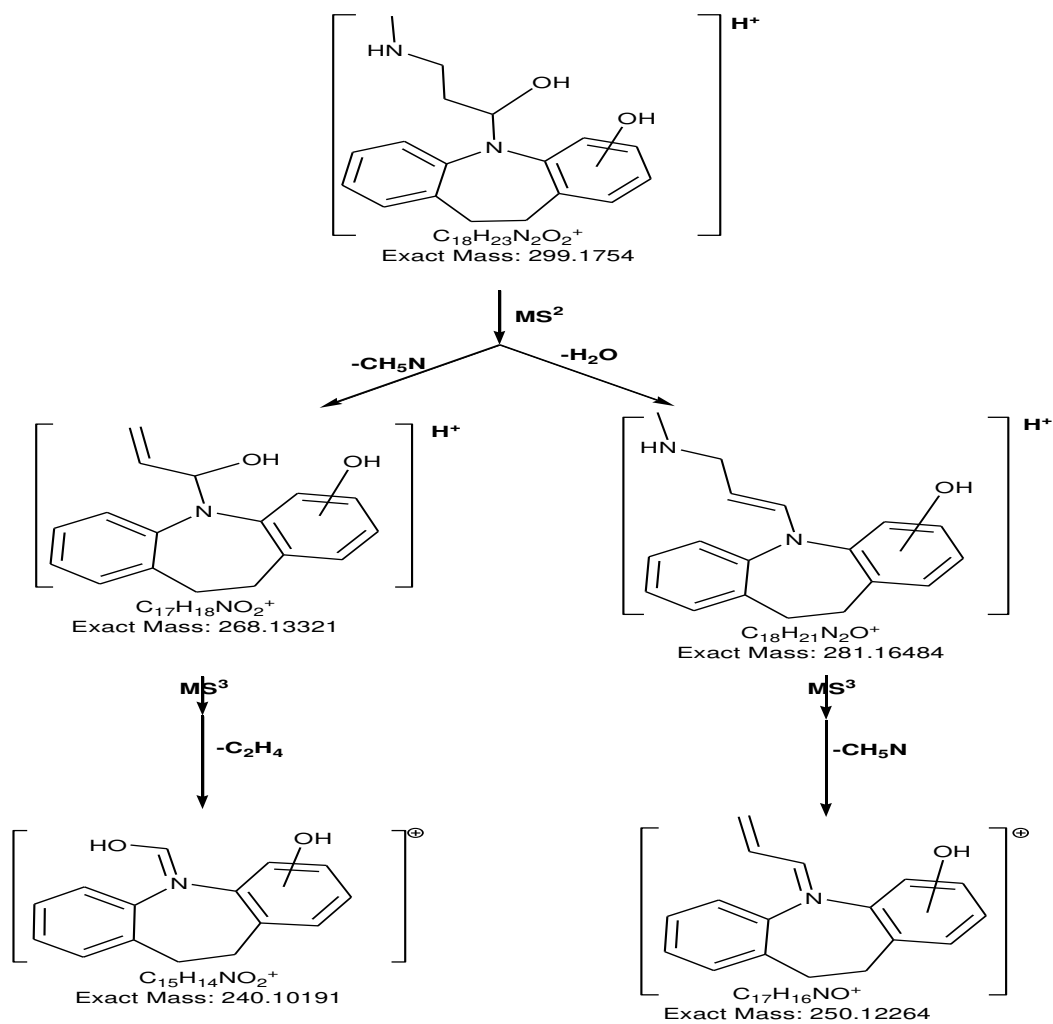
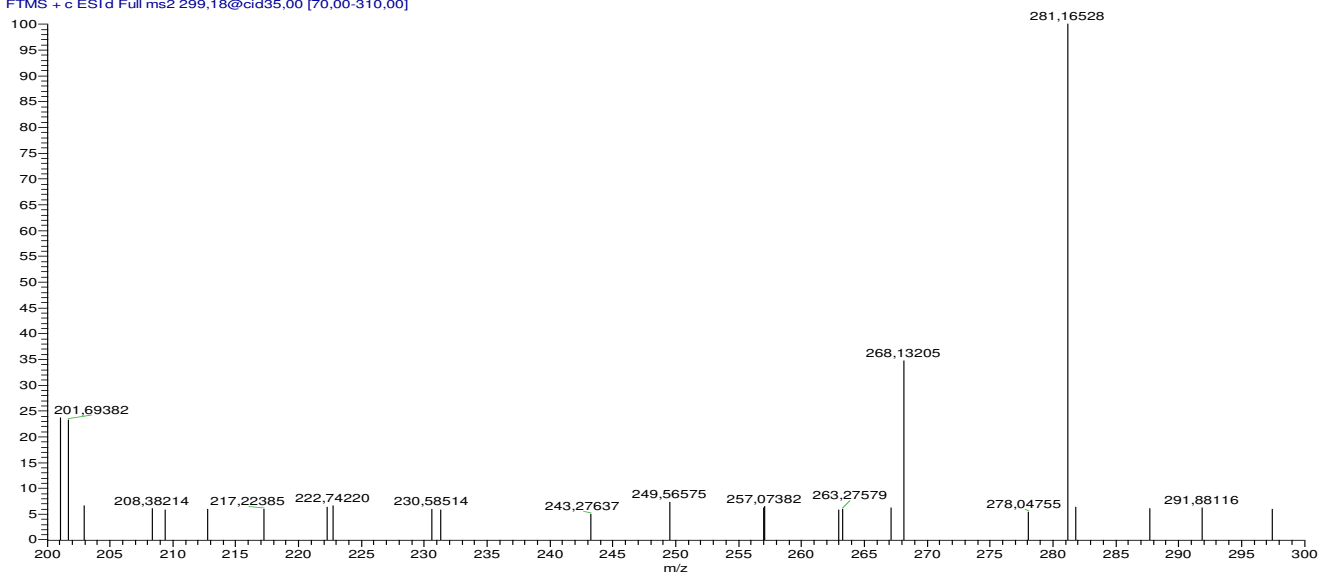


Figure S15: Fragmentation pattern of PTP₂₉₉₋₁ according to MSⁿ obtained from LC-HRMS

PTP₂₉₉₋₂

MS²/299

100DM-LV-64min-normalC18column-130819b #767 RT: 9.86 AV: 1 NL: 2.60E4
T: FTMS + c ESI d Full ms2 299,18@cid35,00 [70,00-310,00]

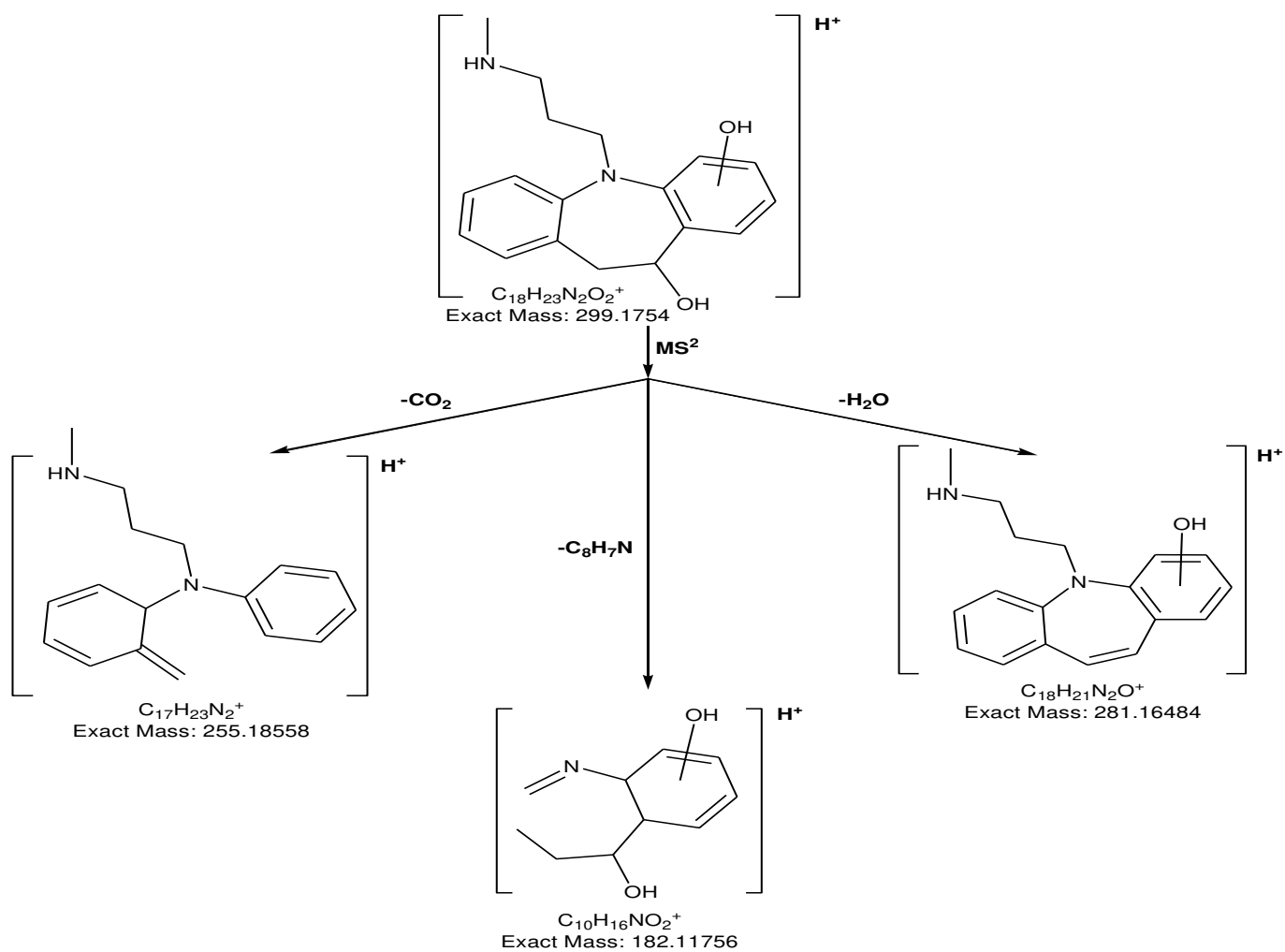
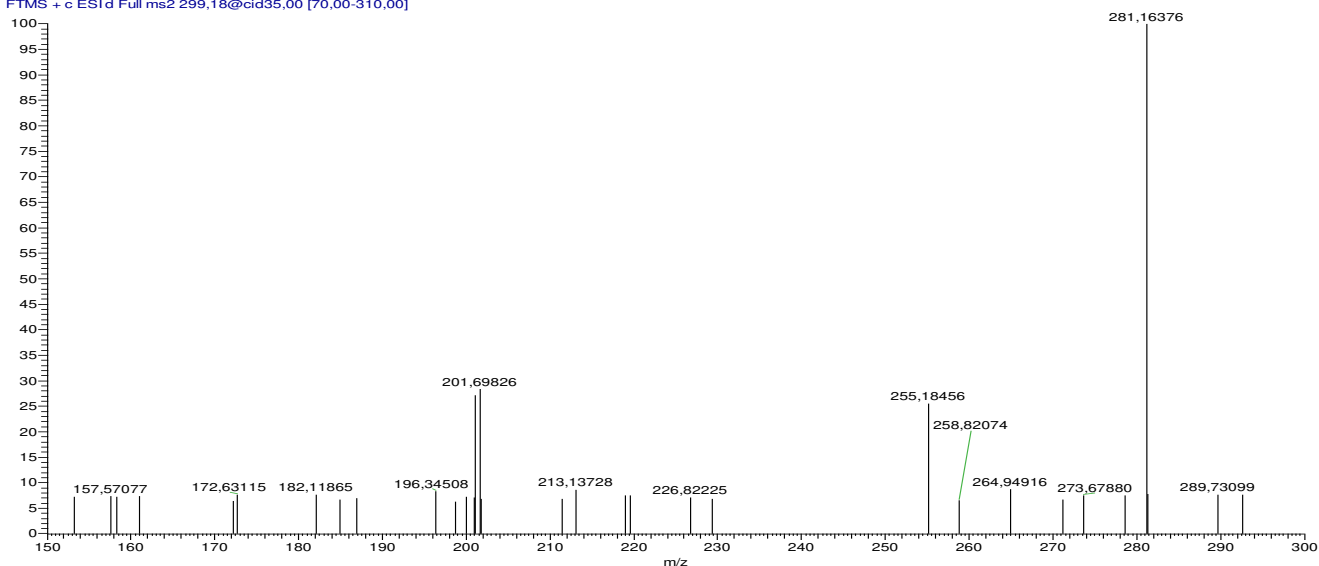


Figure S16: Fragmentation pattern of PTP₂₉₉₋₂ according to MSⁿ obtained from LC-HRMS

PTP₂₉₉₋₃

MS²/299

100DMI-LV-64min-normalC18column-130819b #869 RT: 11.21 AV: 1 NL: 2.13E5
T: FTMS + c ESI d Full ms2 299,18@cid35,00 [70,00-310,00]

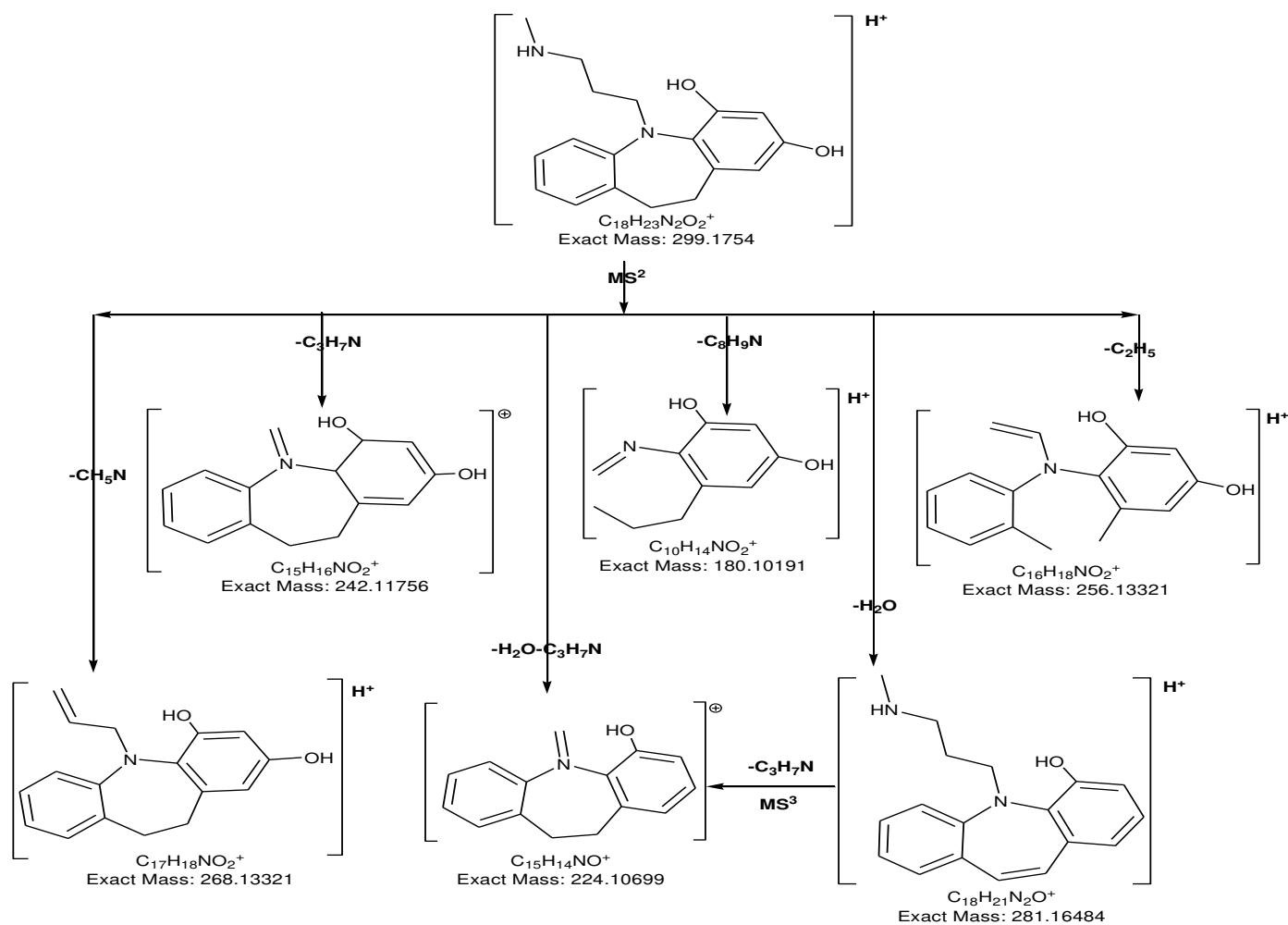
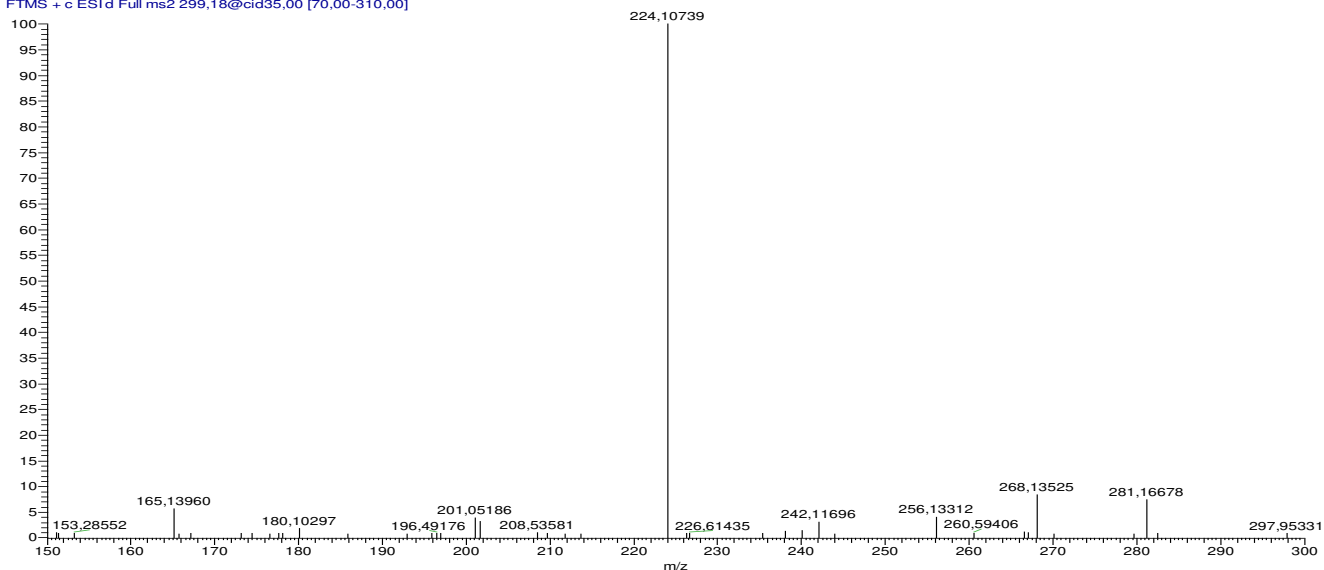


Figure S17: Fragmentation pattern of PTP₂₉₉₋₃ according to MSⁿ obtained from LC-HRMS

MS²/299

100DM-LV-64min-normalC18column-130819b #922 RT: 11.91 AV: 1 NL: 2.44E5
 T: FTMS + c ESI d Full ms2 299,18@cid35,00 [70,00-310,00]

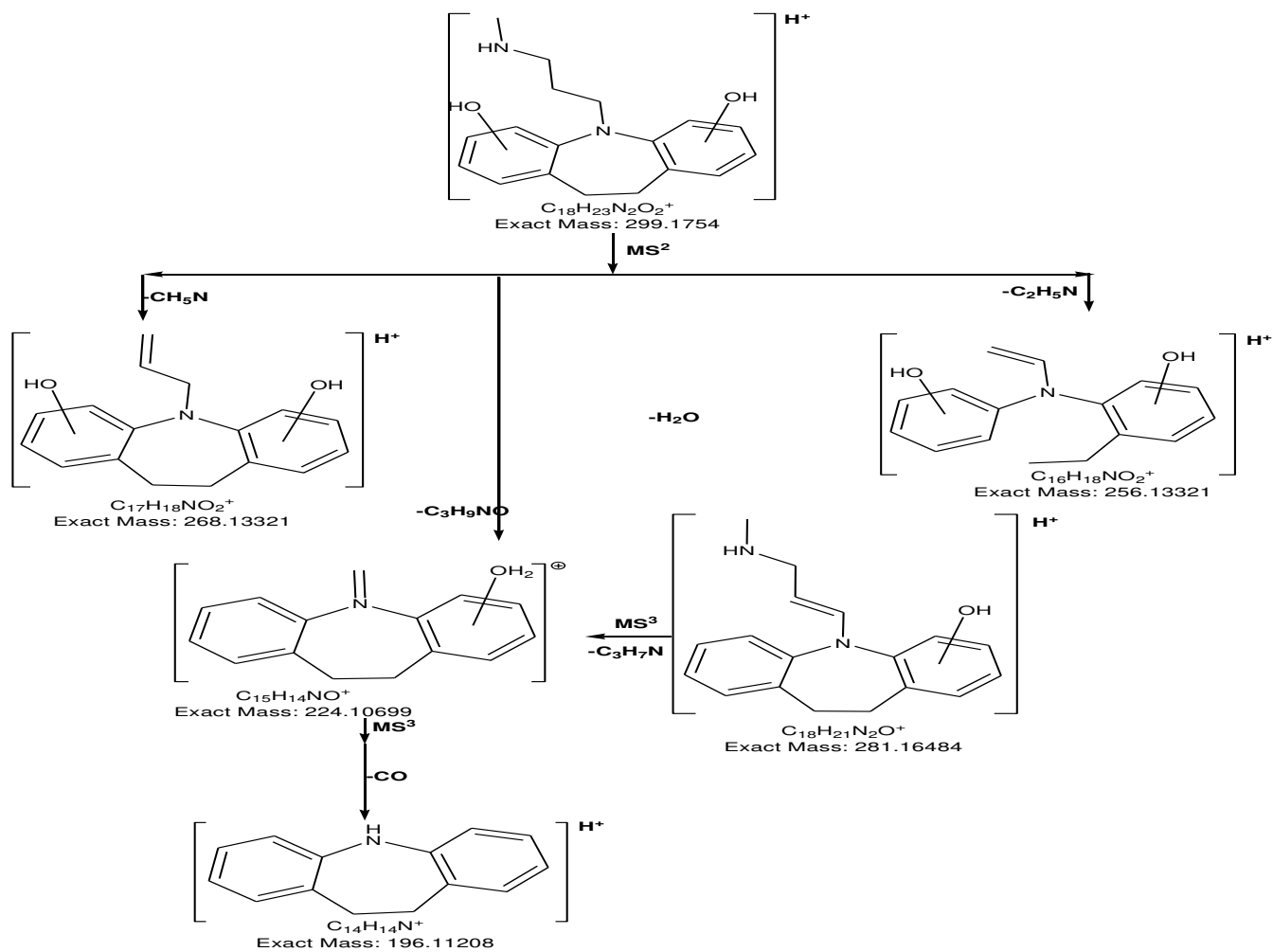
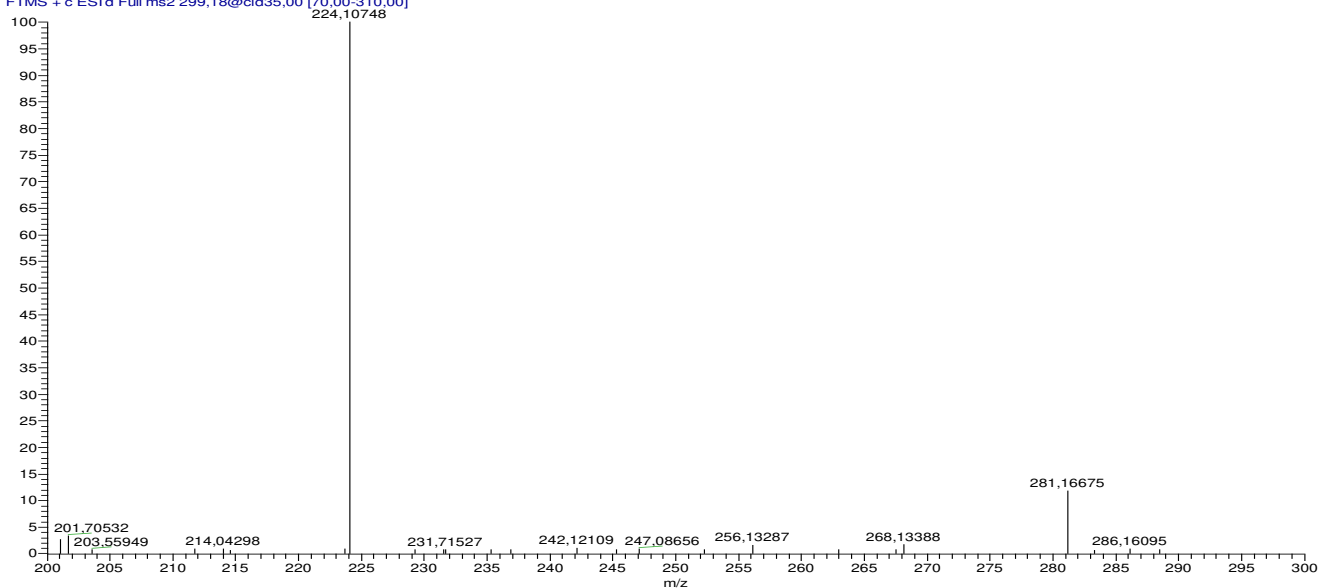


Figure S18: Fragmentation pattern of PTP₂₉₉₋₄ according to MSⁿ obtained from LC-HRMS

PTP₂₈₅₋₂

MS²/285

100DMI-LV-32min-normalC18column-130819d #980 RT: 12.64 AV: 1 NL: 6,55E3
T: FTMS + c ESI d Full ms2 285,20@cid35,00 [65,00-300,00]

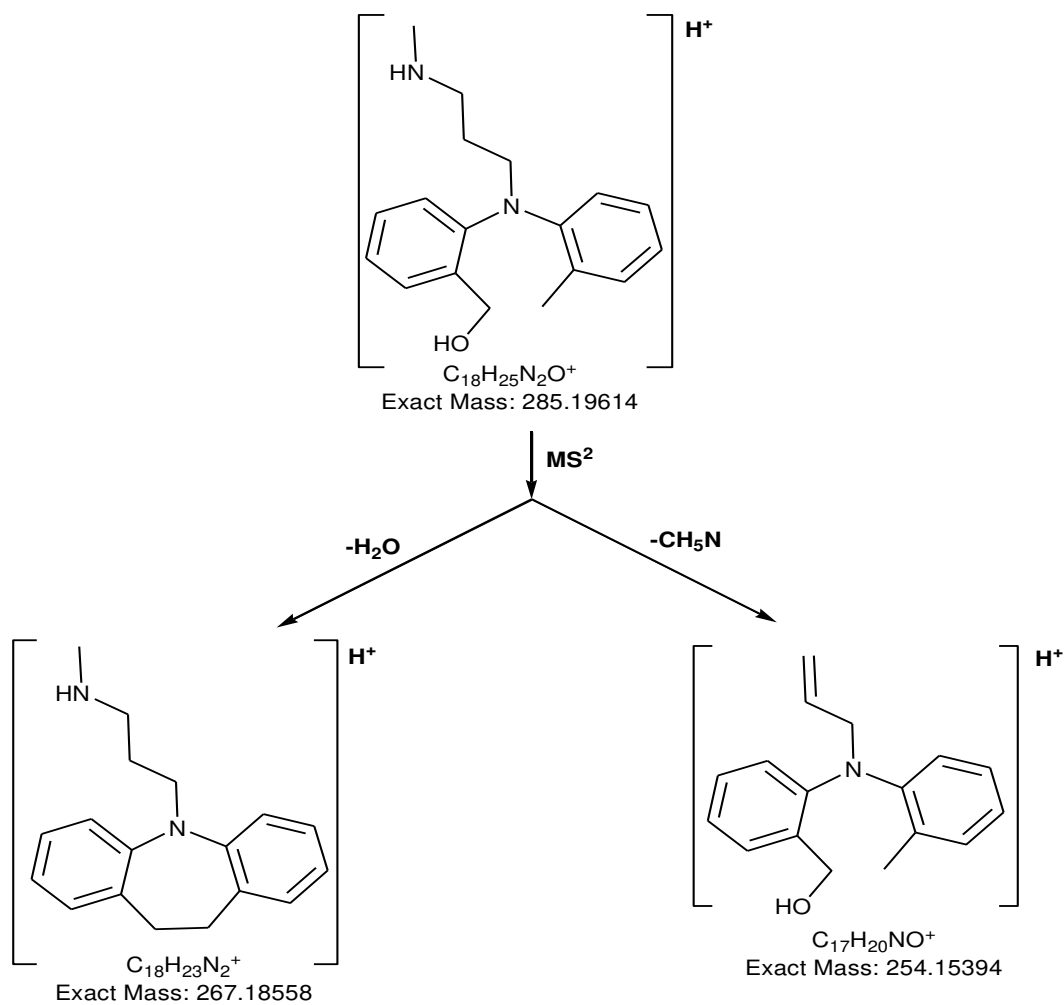
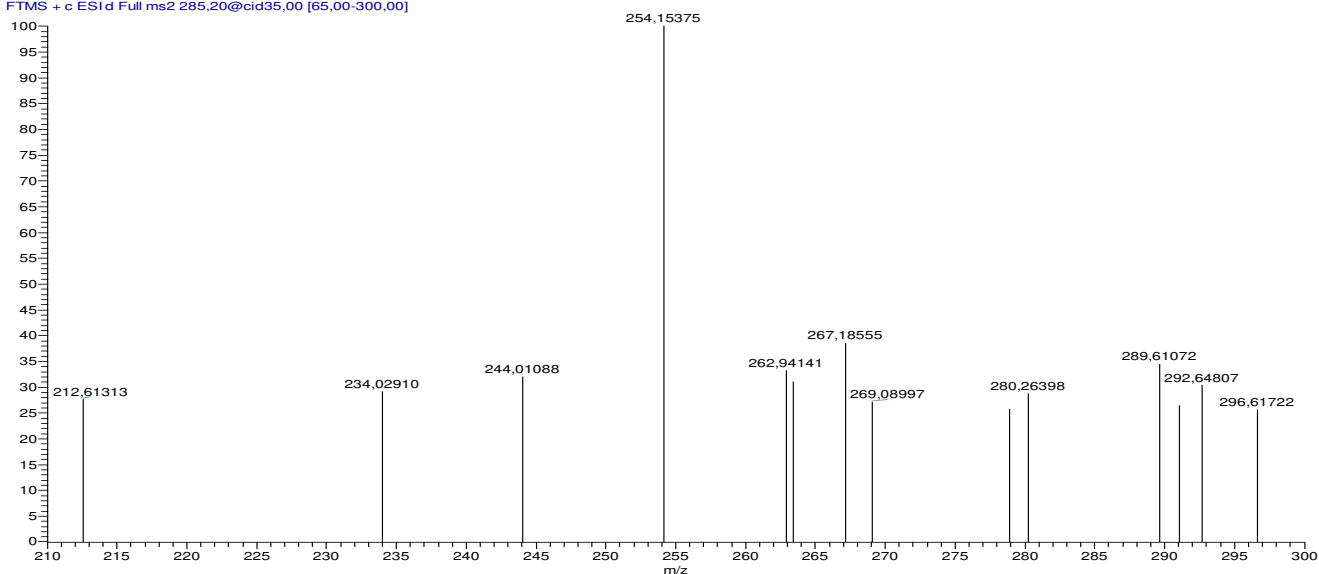


Figure S19: Fragmentation pattern of PTP₂₈₅₋₂ according to MSⁿ obtained from LC-HRMS

PTP₃₀₁₋₁

MS²/301

100DM-LV-64min-normalC18column-130819b #749 RT: 9.62 AV: 1 NL: 8,52E3
T: FTMS + c ESI d Full ms2 301,19@cid35,00 [70,00-315,00]

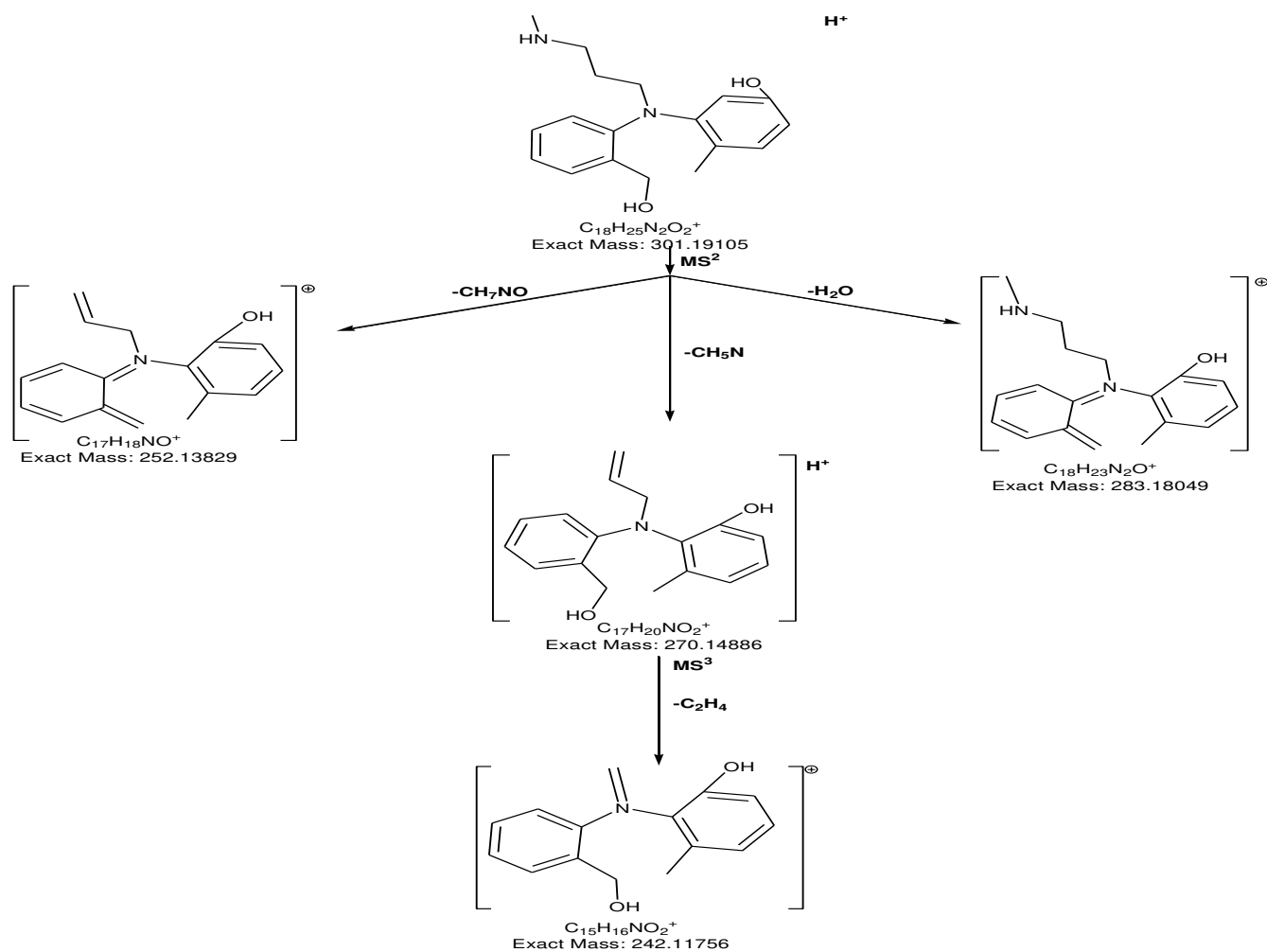
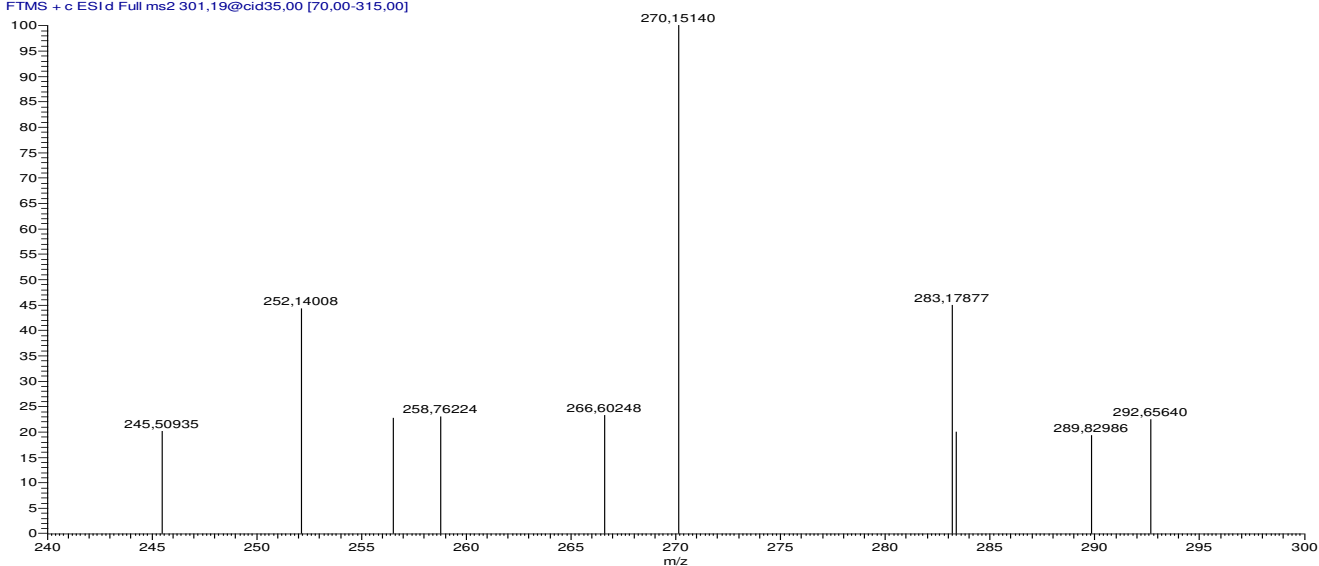


Figure S22: Fragmentation pattern of PTP₃₀₁₋₁ according to MSⁿ obtained from LC-HRMS

PTP₃₀₁₋₂

MS²/301

100DM-LV-64min-normalC18column-130819b #827 RT: 10.65 AV: 1 NL: 6,84E5
T: FTMS + c ES1d Full ms2 301,19@cid35,00 [70,00-315,00]

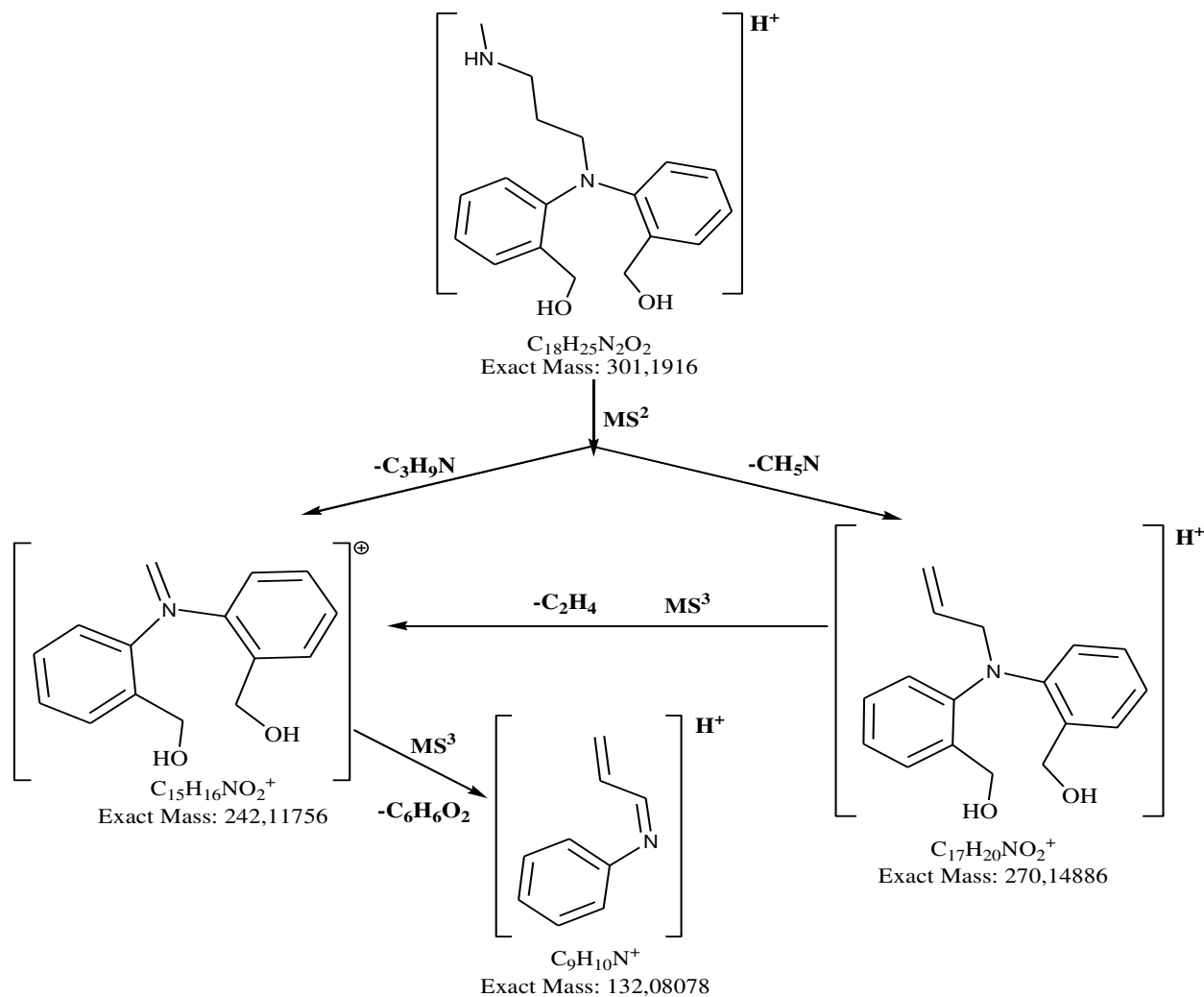
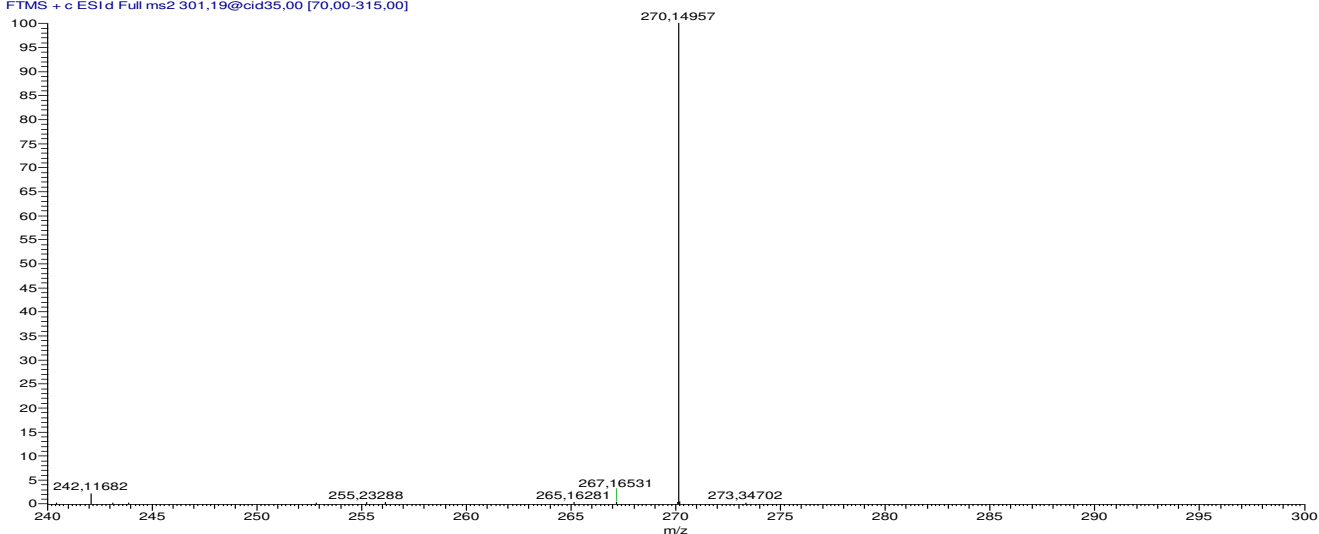


Figure S21: Fragmentation pattern of PTP₃₀₁₋₂ according to MSⁿ obtained from LC-HRMS

PTP₂₁₉

MS²/219

100DM-UV-64min-normalC18column-130819b #697 RT: 8.94 AV: 1 NL: 3.61E6
T: FTMS + c ESI d Full ms2 219,15@cid35,00 [50,00-230,00]

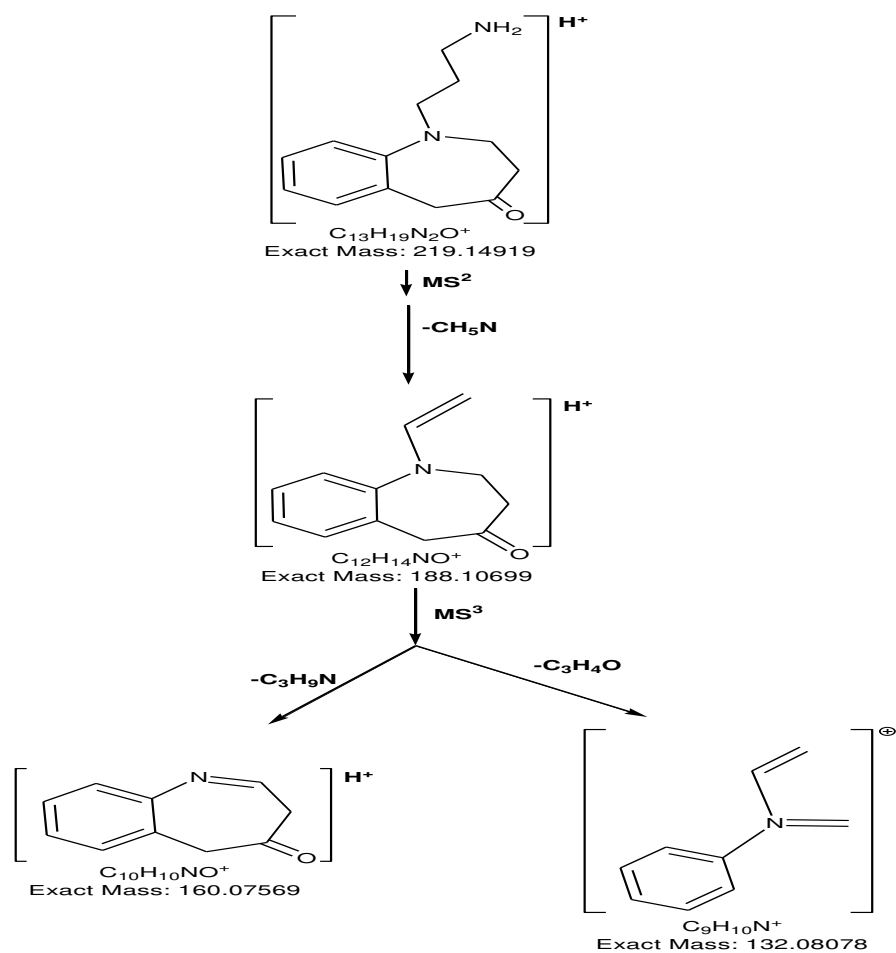
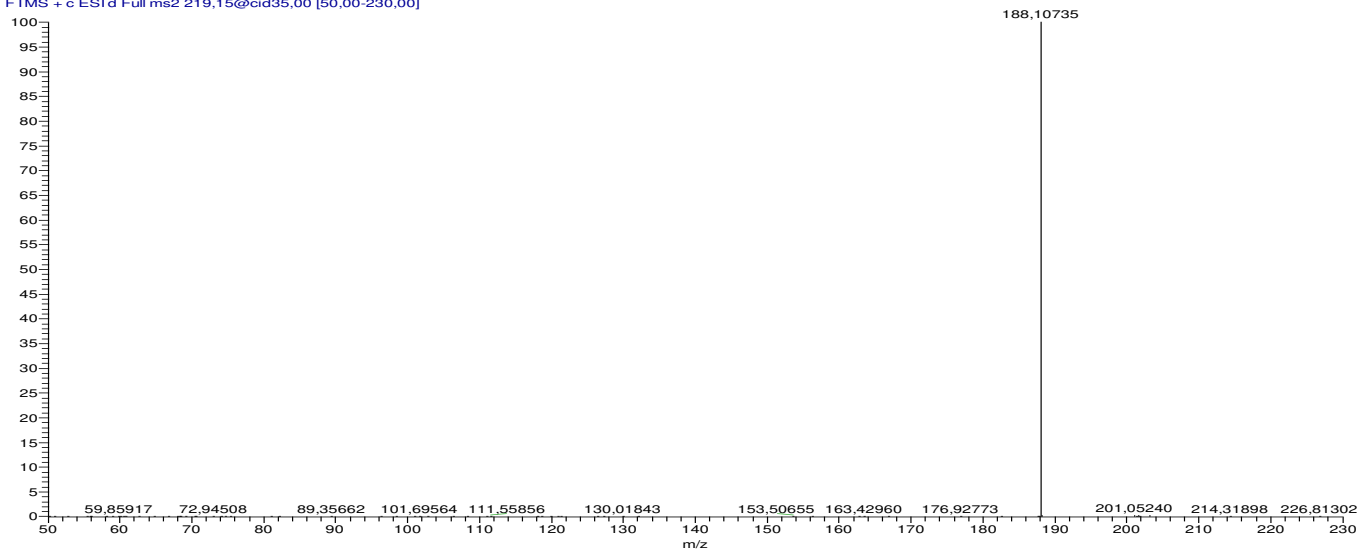
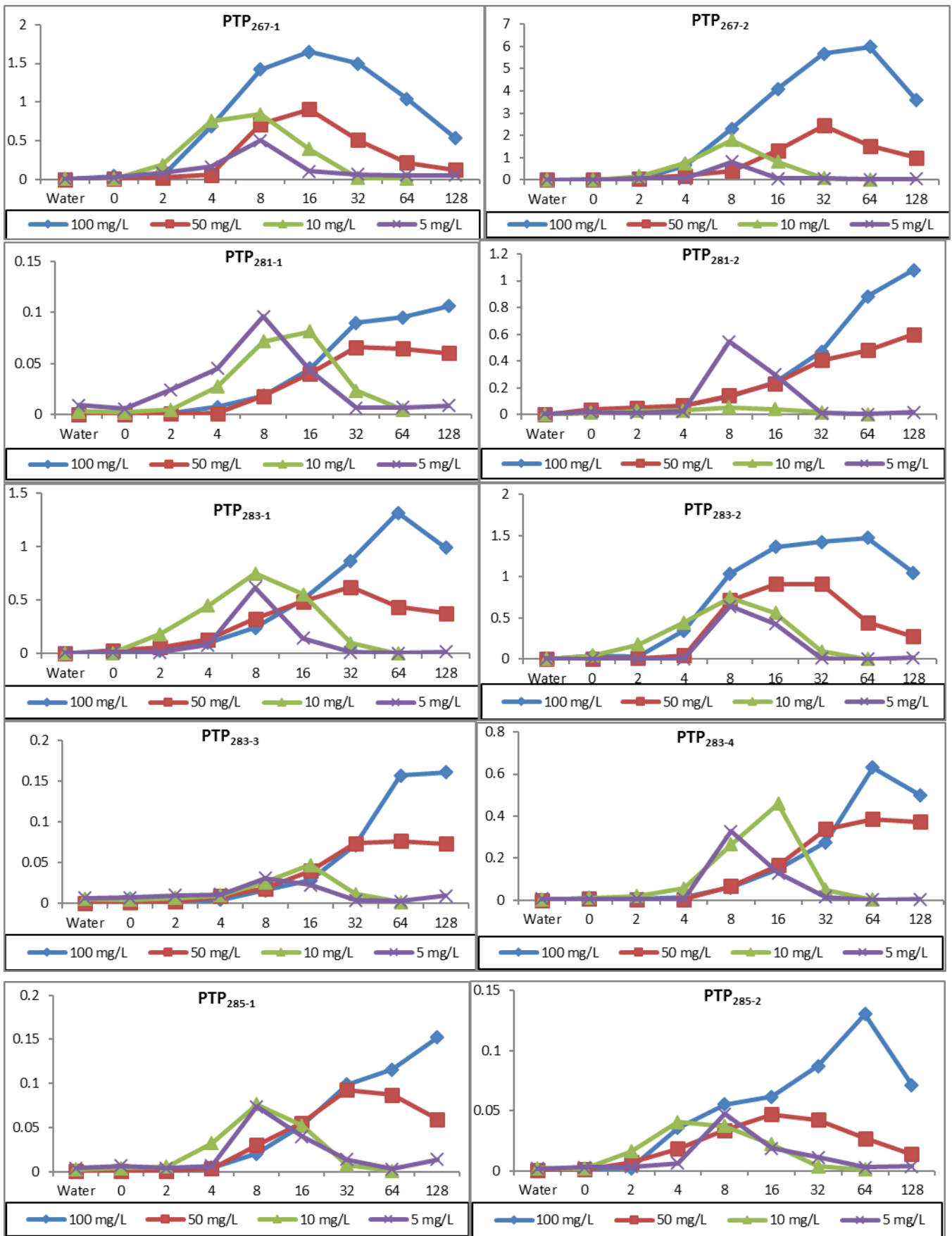


Figure S22: Fragmentation pattern of PTP₂₁₉ according to MSⁿ obtained from LC-HRMS



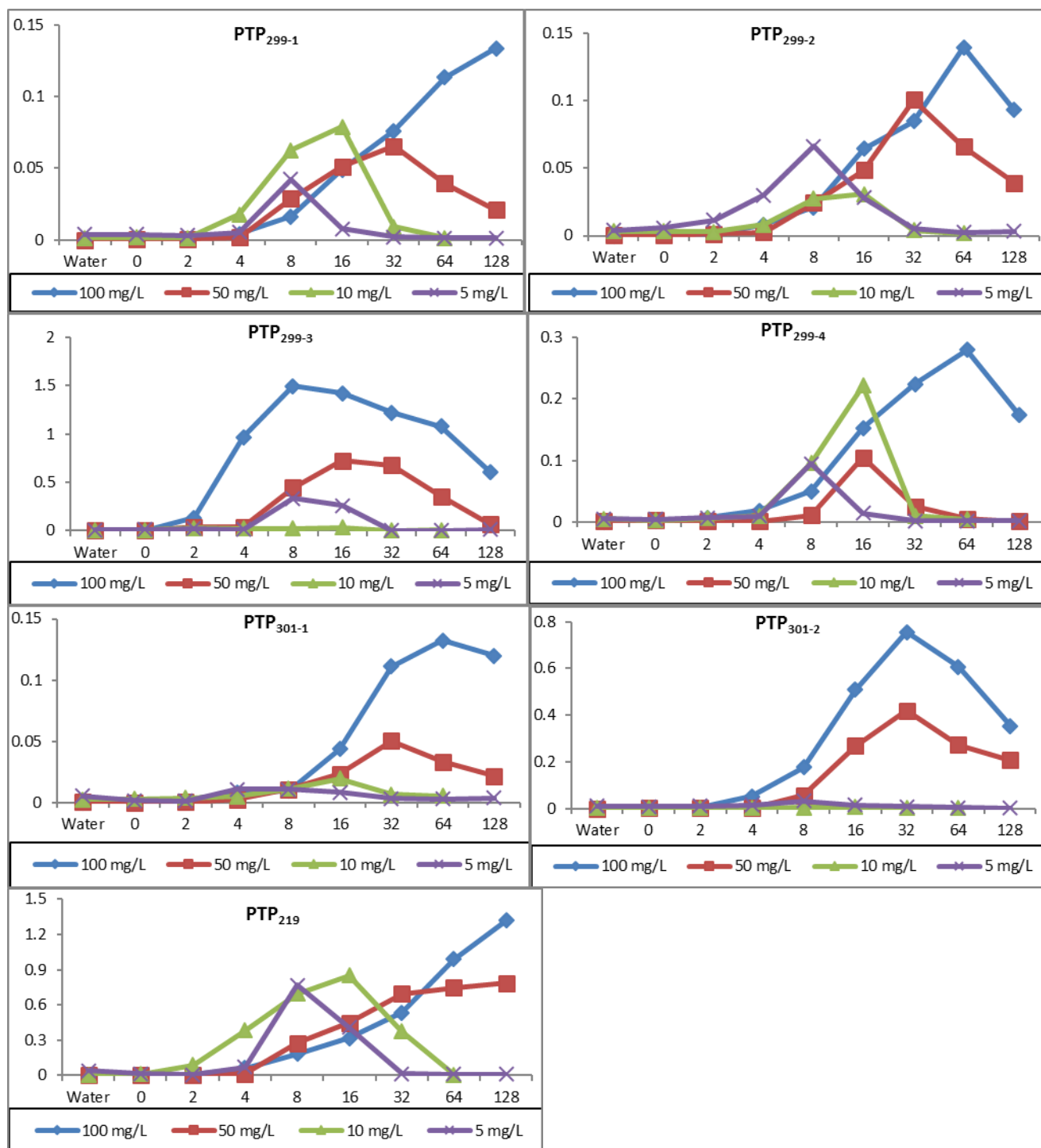


Figure S23: Time curves of the relative peak area A/A_0 (%) of products (PTPs) during photolysis at different concentrations.

*X axis is the irradiation time in min, and Y axis is the A/A_0 (%).

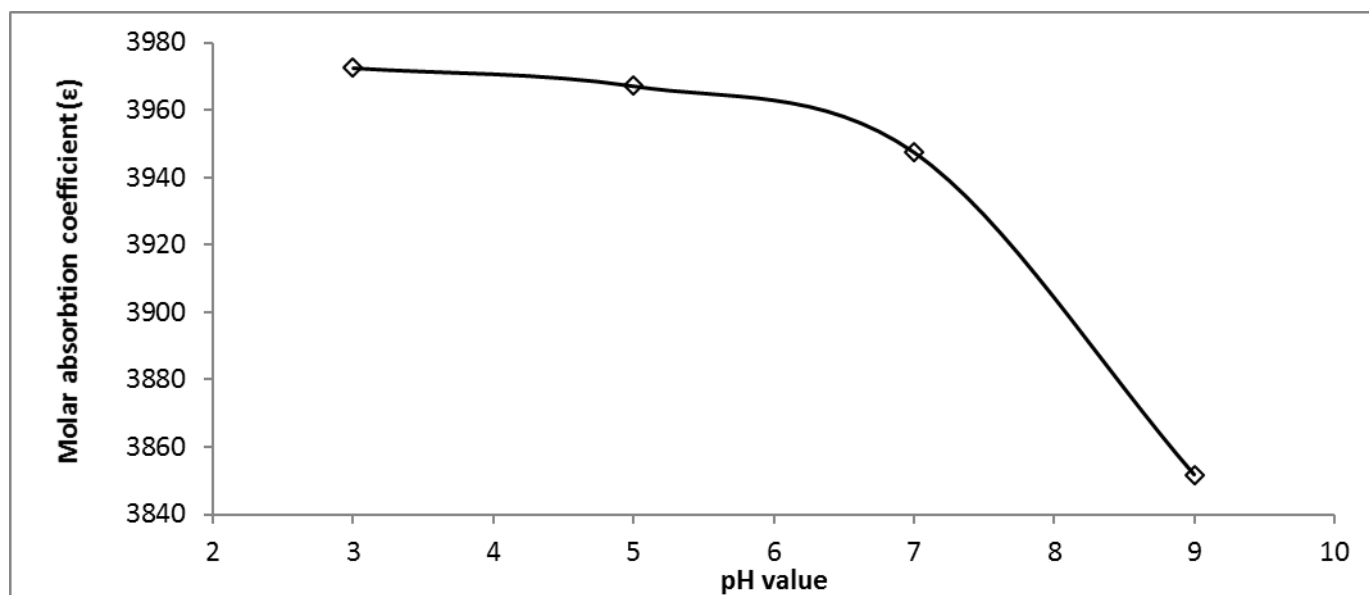


Figure S24: The change in the molar absorption coefficient (ϵ) as a function of the solution pH (DMI concentration = 100 mg L⁻¹).

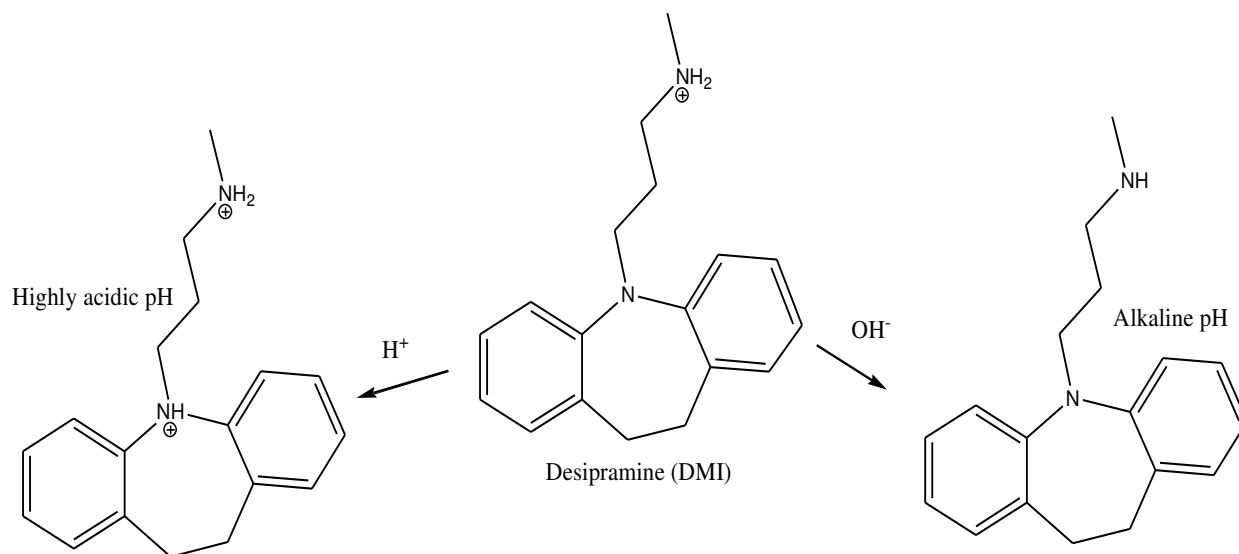


Figure S25: DMI structure at different pH, $pK_a = 10.02$.

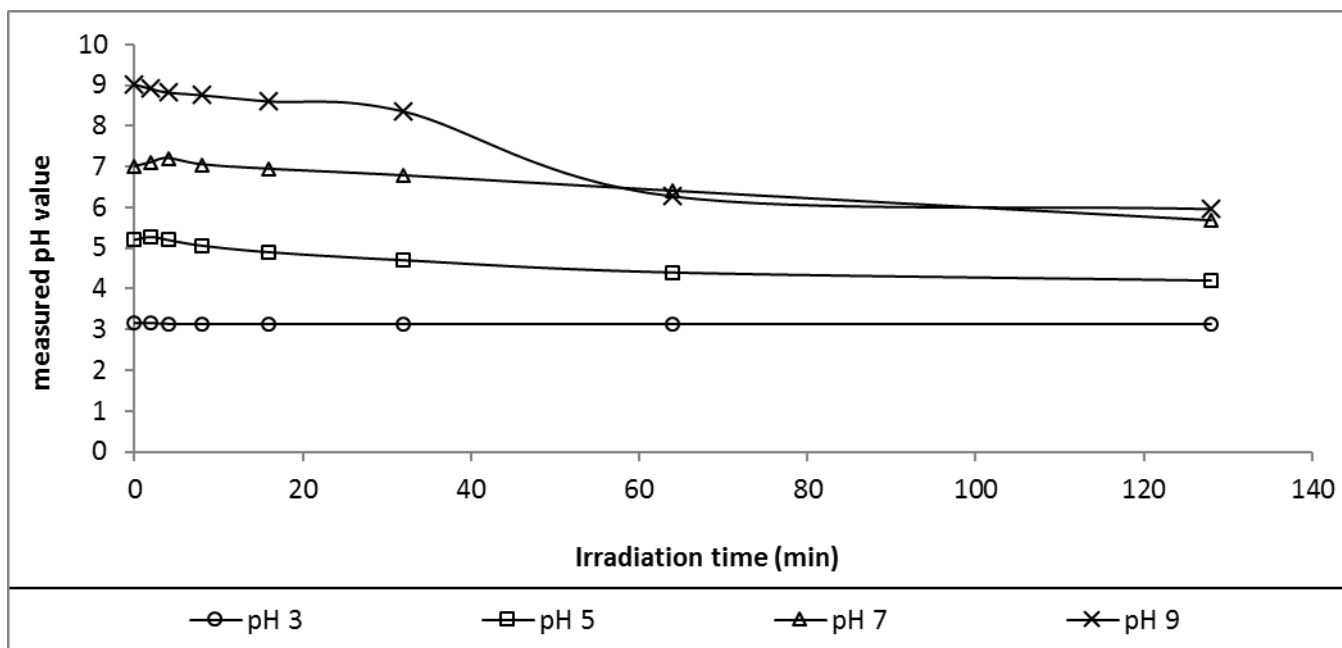
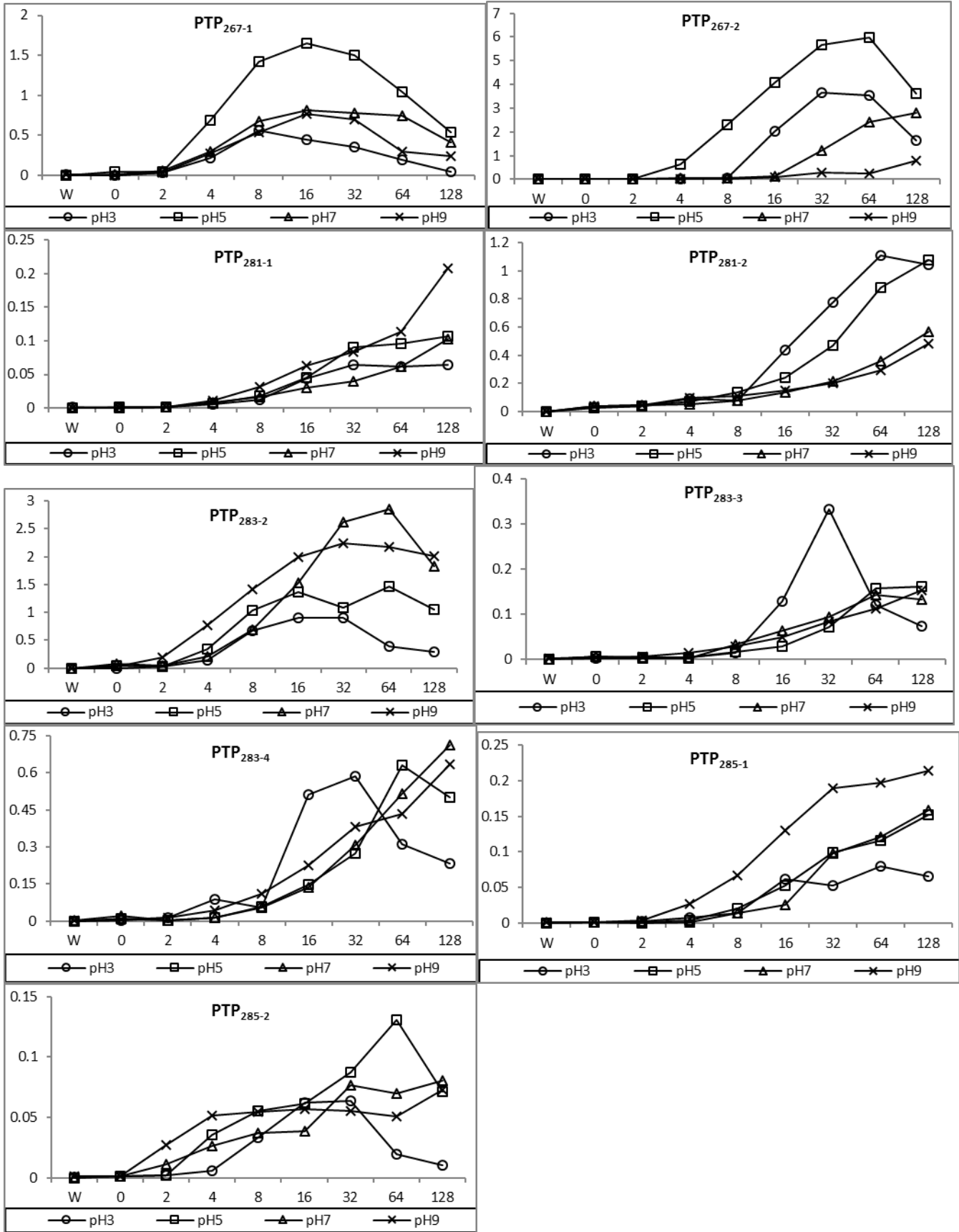


Figure S26: The changes in pH values during the UV-irradiation of DMI under different pH values.



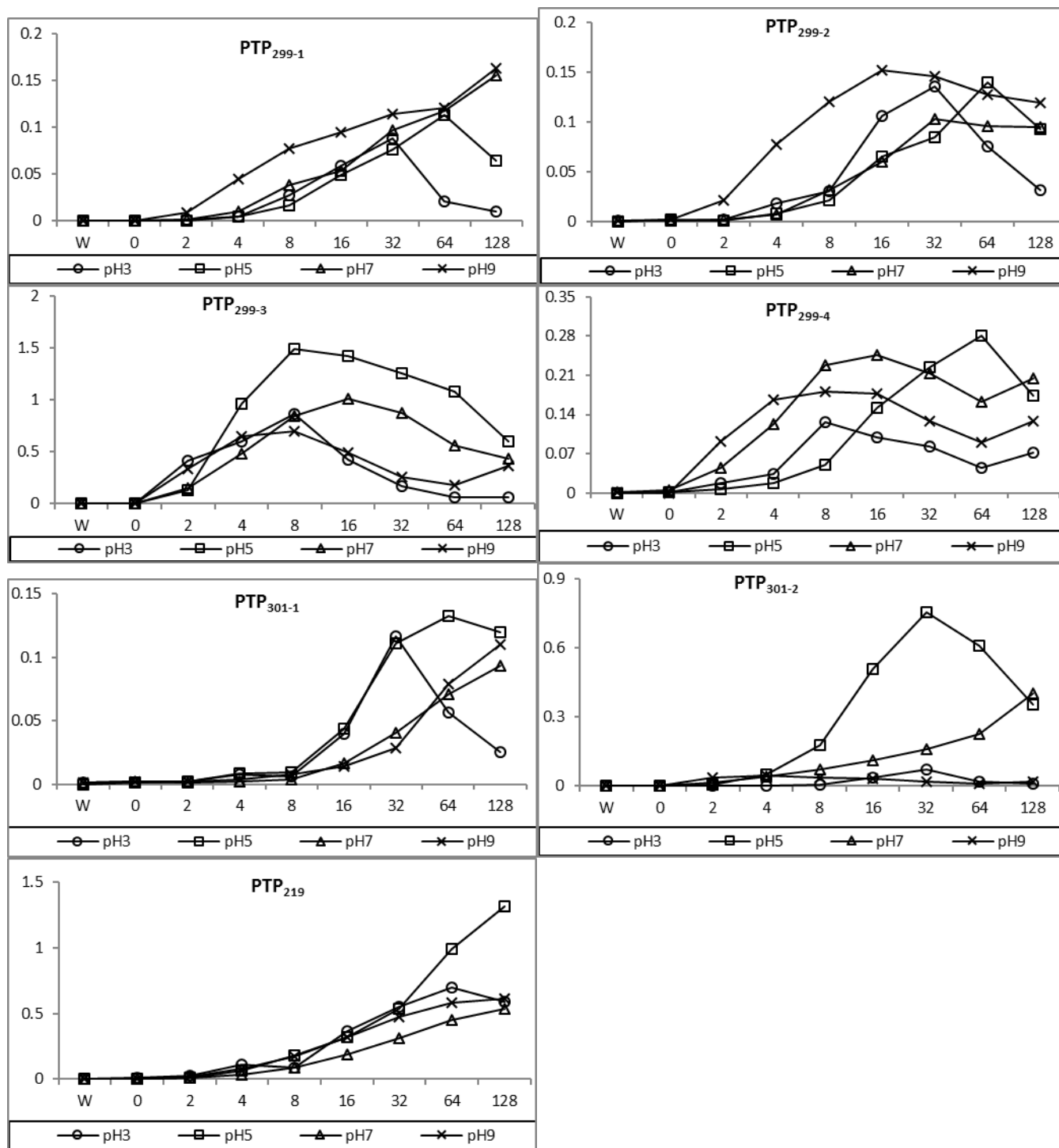


Figure S27: Time curves of the relative peak area A/A_0 (%) of products (PTPs) during photolysis at different pH values.

*X axis is the irradiation time in min, and Y axis is the A/A_0 (%).

PTP₂₃₅

MS²/235

100DMI-LV-64min-normalC18column-130819b #549 RT: 7.03 AV: 1 NL: 5.83E4
T: FTMS + c ESI d Full ms2 235,14@cid35,00 [50,00-250,00]

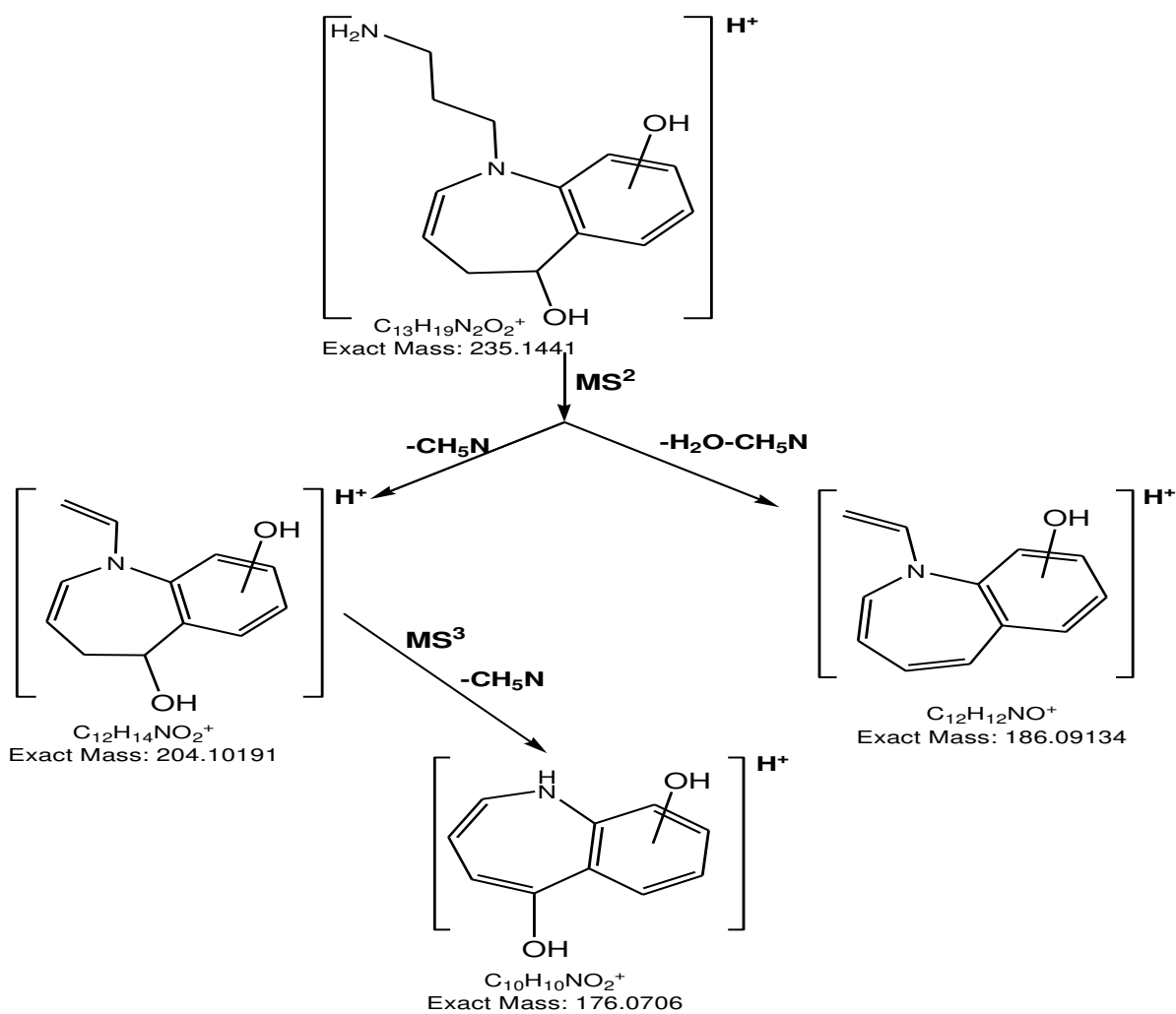
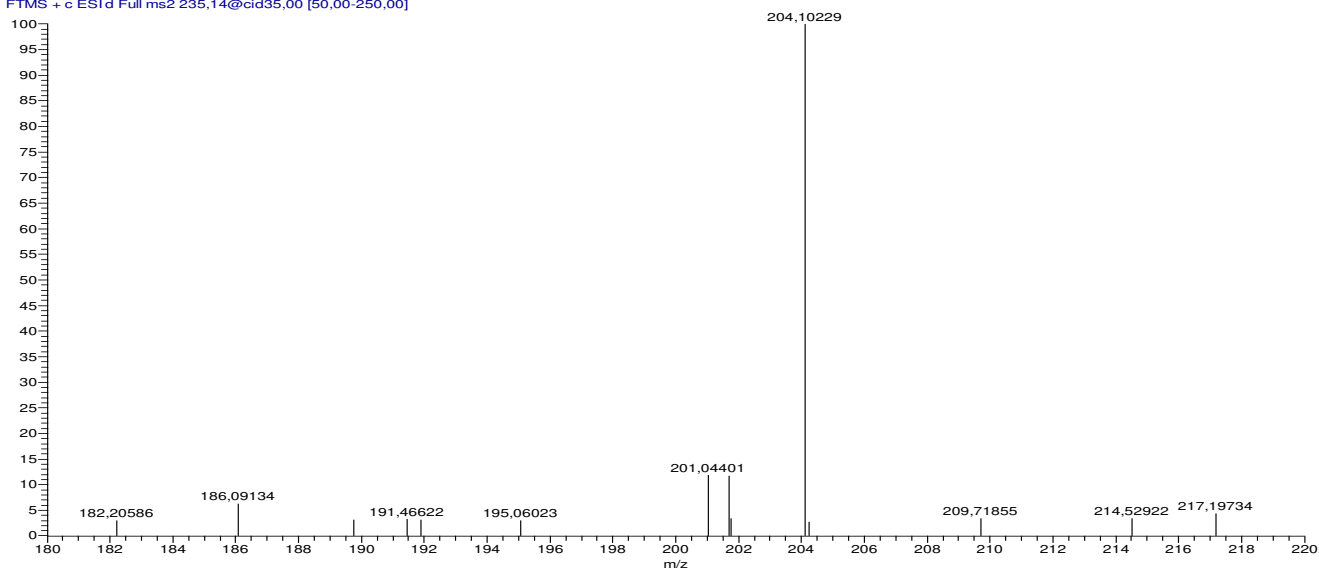


Figure S28: Fragmentation pattern of PTP₂₃₅ according to MSⁿ obtained from LC-HRMS

PTP₂₇₁

MS²/271

100DMI-LV-64min-normalC18column-130819b #1179 RT: 15.28 AV: 1 NL: 1.07E4
T: FTMS + c ESI d Full ms2 271.15@cid35.00 [60.00-285.00]

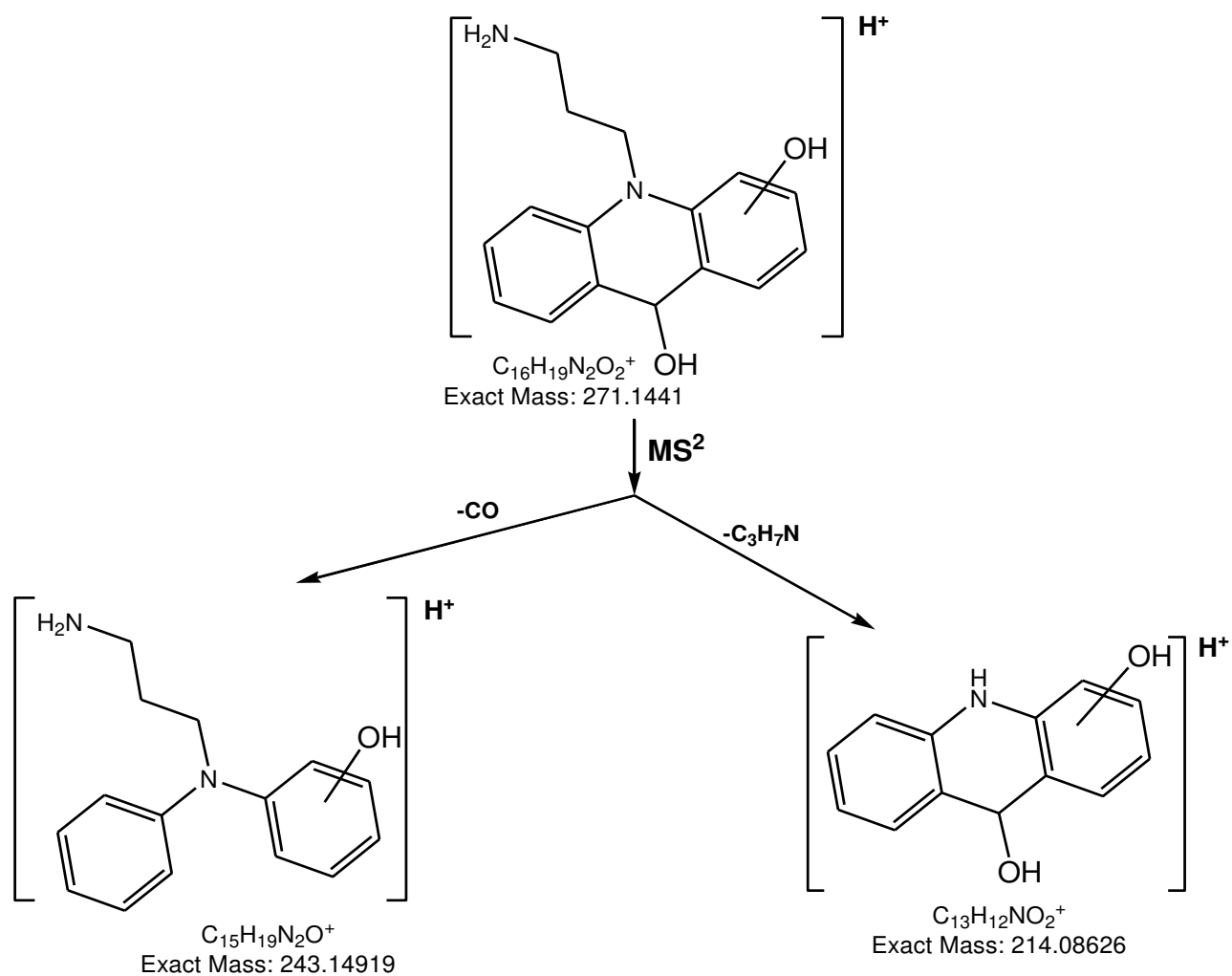
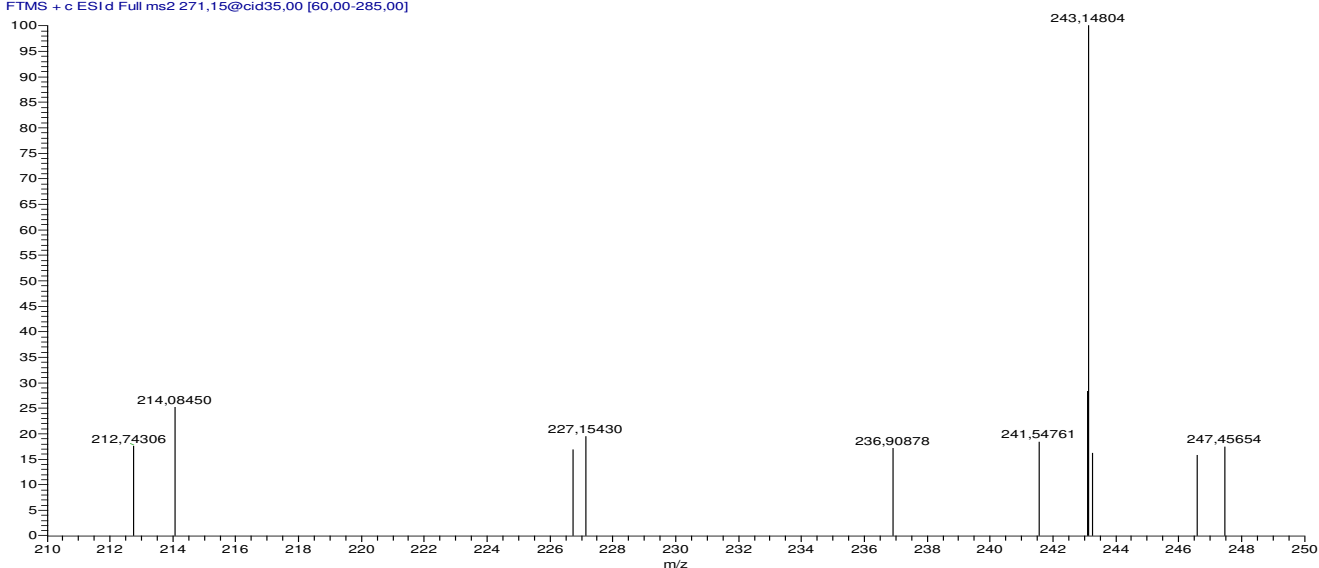


Figure S29: Fragmentation pattern of PTP₂₇₁ according to MSⁿ obtained from LC-HRMS

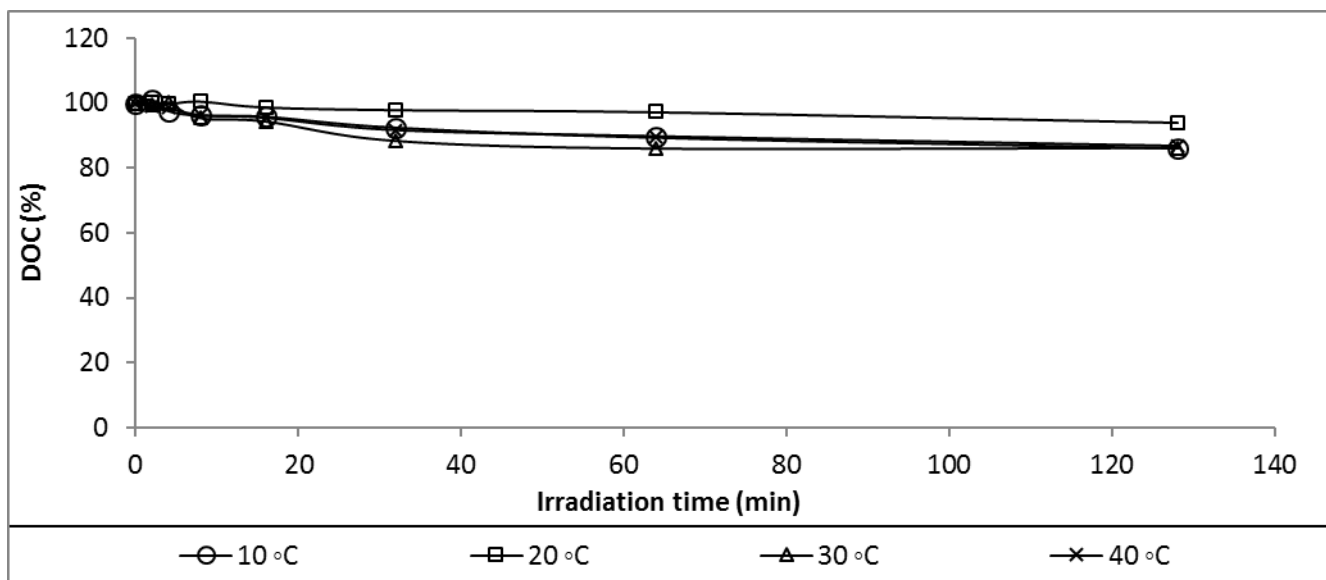
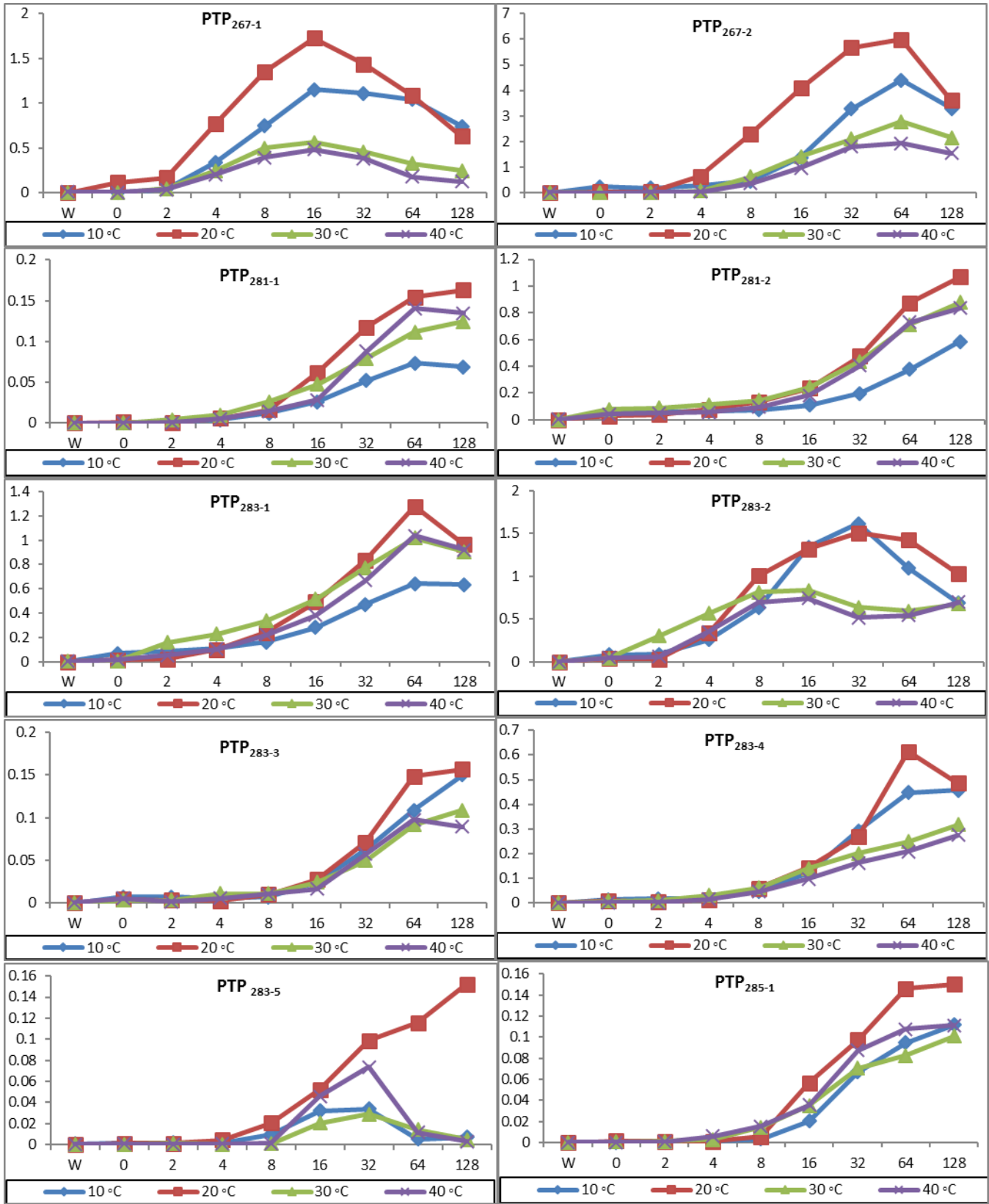


Figure S30: DOC **Recovery** curves during the UV photodegradation process of DMI at different temperatures.



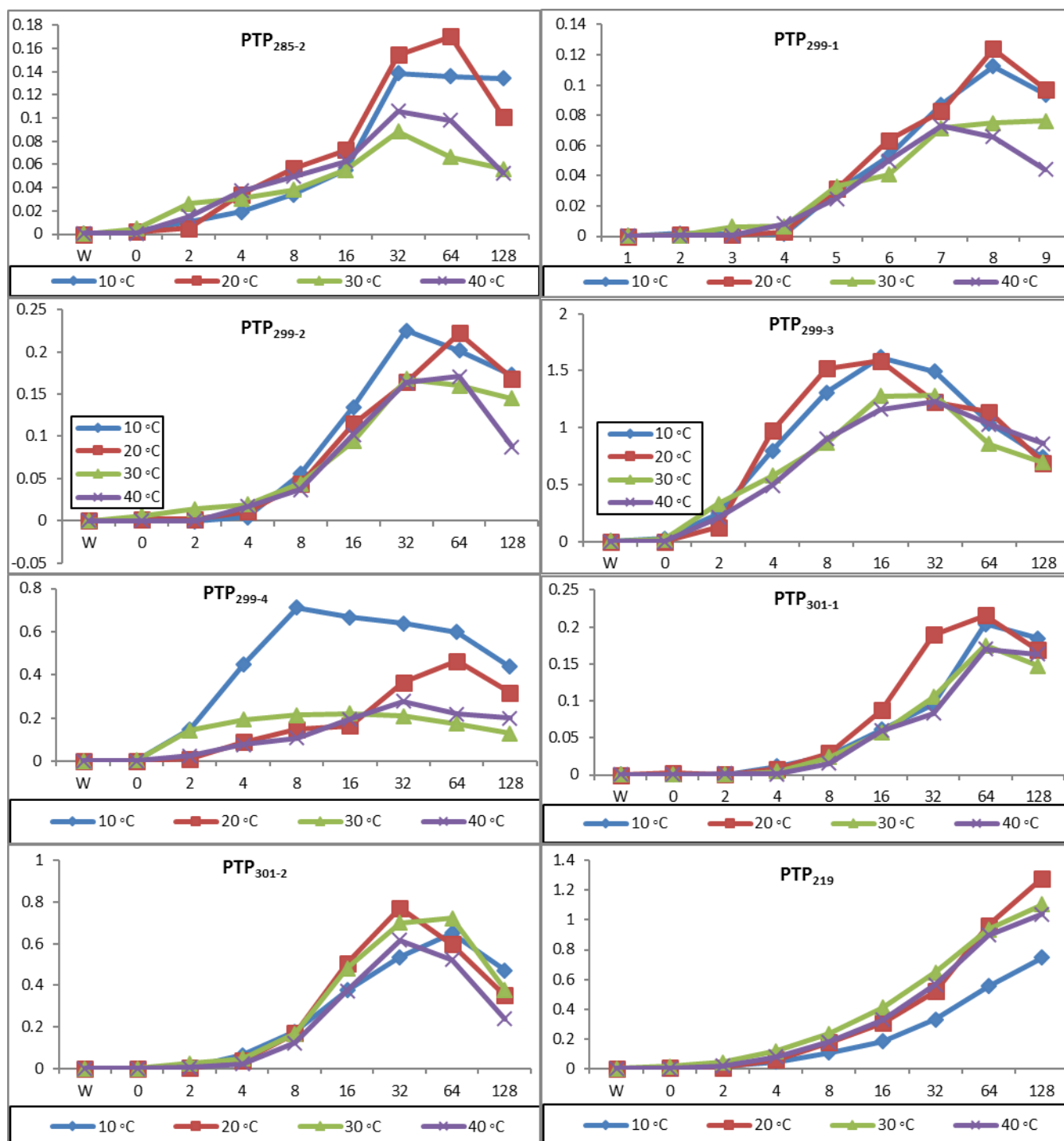


Figure S31: Time curves of the relative peak area A/A_0 (%) of products (PTPs) during photolysis at different temperatures.

*X axis is the irradiation time in min, and Y axis is the A/A_0 (%).

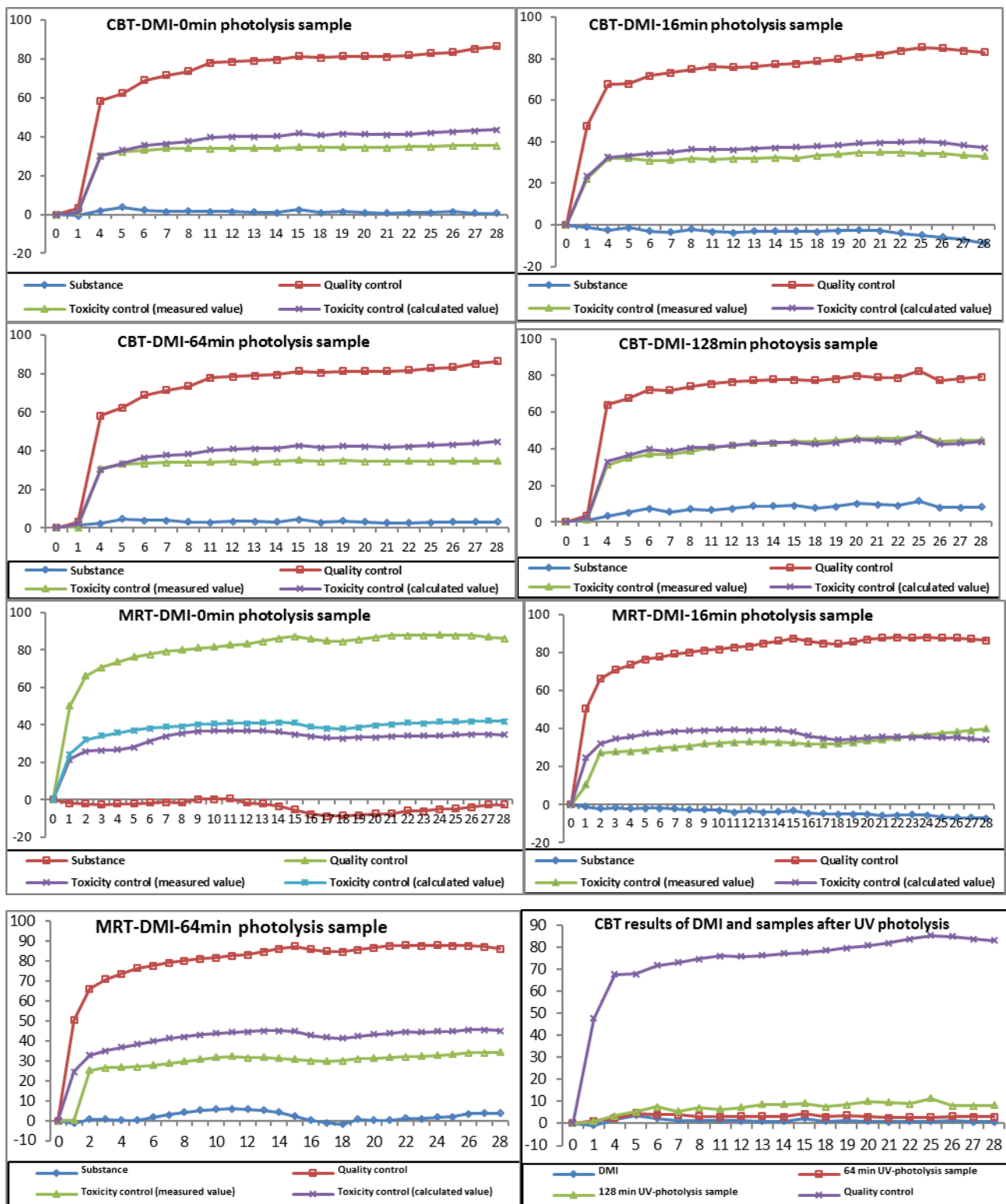


Figure S32. Closed Bottle test and Manometric Respiratory Test results of DMI and its PTPs at different irradiation time points.

*X axis is the time in days, and Y axis is the biodegradation (%).

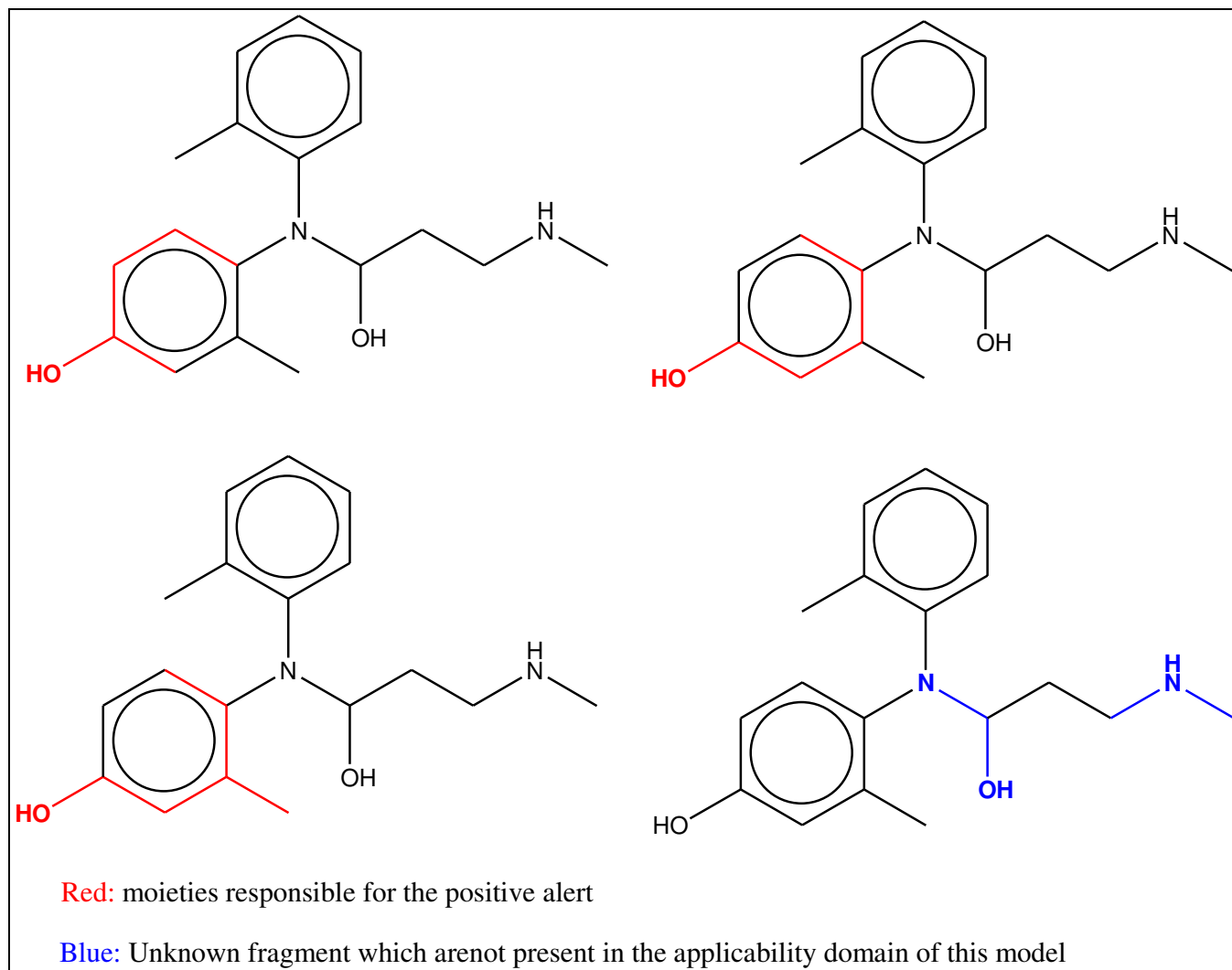


Figure S33: The structural moiety responsible for the positive alert (red color) and the unknown fragment in TP 301-31 predicted by Microtox Toxicity to Environmental Bacteria model using Case Ultra software.

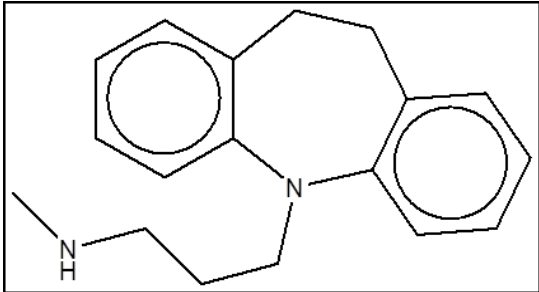
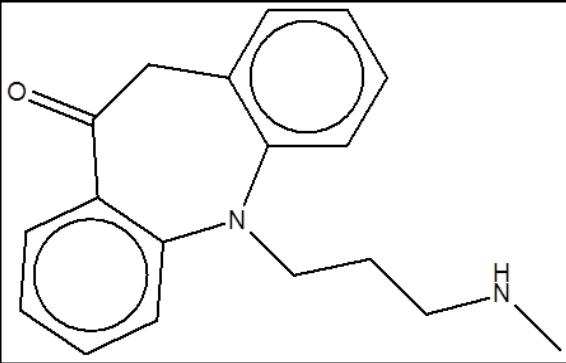
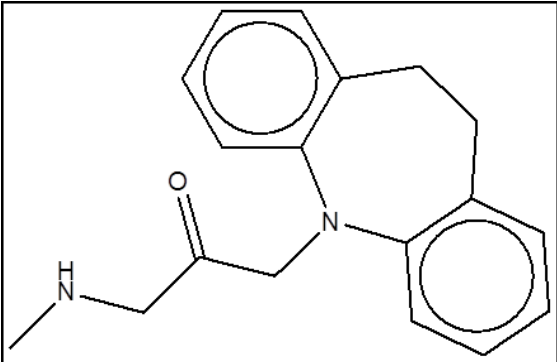
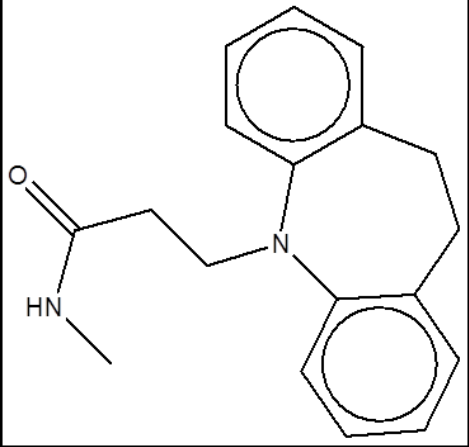
Table S1: a) Test system of the Closed Bottle test (CBT), b) Test system of the manometric respiratory test (MRT); “x” = addition, “- “= no addition.

a	Blank	Quality control	Test	Toxicity control
Mineral medium	x	x	x	x
Inoculum (2 drops L ⁻¹)	x	x	x	x
DMI (2.2 mg L ⁻¹ = 5 mg L ⁻¹ ThOD)	-	-	x	x
Sodium acetate (6.4 mg L ⁻¹) (ThOD = 5 mg L ⁻¹)	-	x	-	x

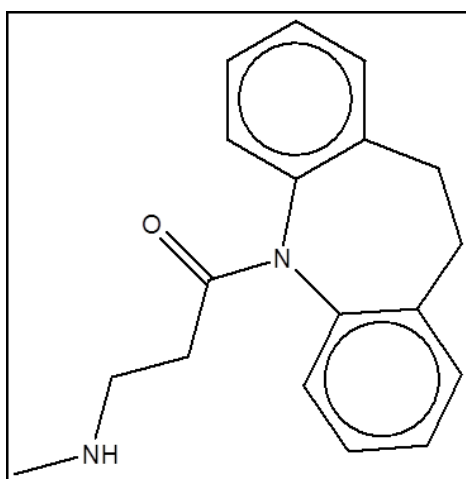
b	Blank	Quality control	Test	Toxicity control	Sterile control
Mineral medium	x	x	x	x	x
Inoculum (80 mL L ⁻¹)	x	x	x	x	-
DMI (12.9 mg L ⁻¹ = 30 mg L ⁻¹ ThOD)	-	-	x	x	x
Sodium acetate (ThOD = 30 mg L ⁻¹)	-	x	-	x	-
Sodium azide (160.09 mg L ⁻¹)	-	-	-	-	x

Table S2: Q-SAR predictions of log P for DMI and its suggested PTPs structures.

*dots means that when the functional group located in one of the dotted places.

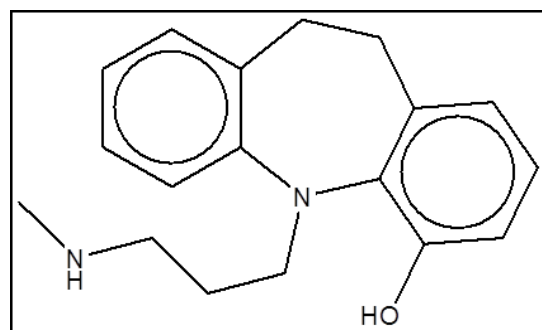
Molecular weight	Molecular structure	log P
267		4,7979
281		3,4401
281		4,3482
281		3,7832

281



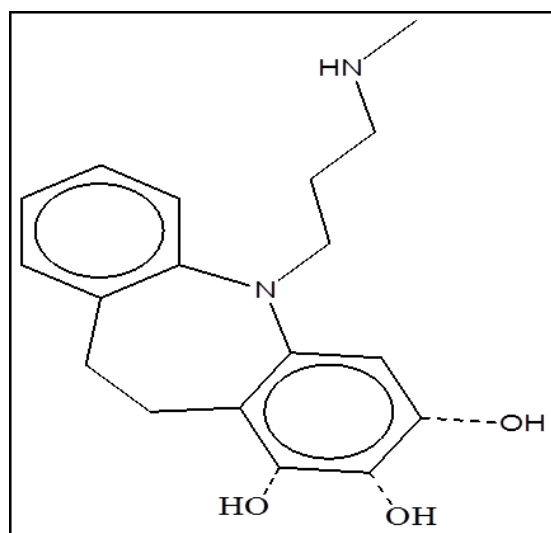
2,3426

283



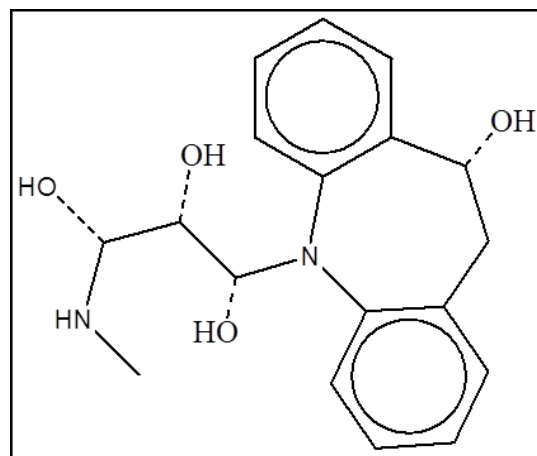
4,3177

283



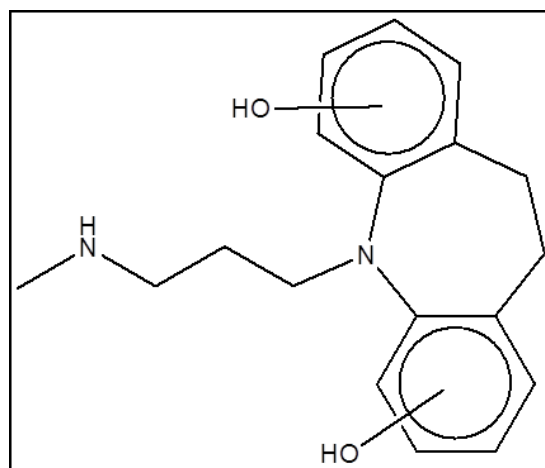
3,9667

283



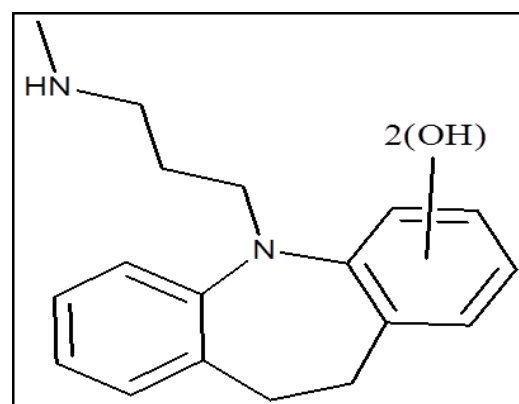
3,2596

299



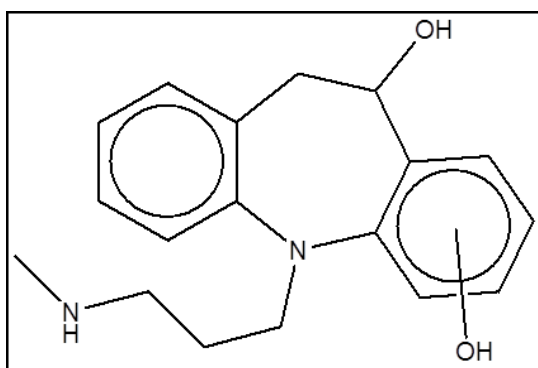
3,8375

299



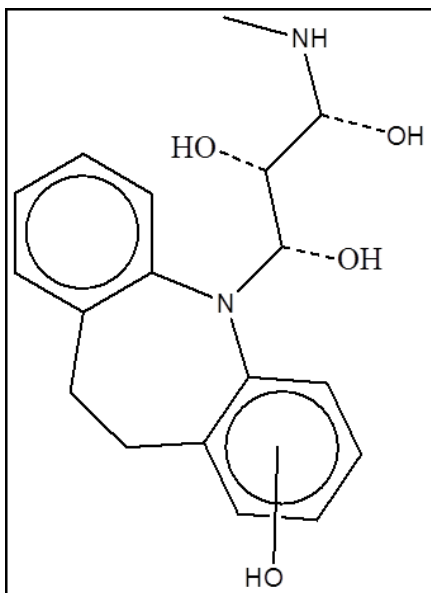
3,6971

299



2,4284-2,7794

299



2,4284

Table S3: Q-SAR predictions for DMI and its TPs for ready biodegradability by different models: 1: Catalogic-BOD Kinetic (OECD 301F)_v.08.09, 2. Catalogic BOD 28 days MITI (OECD 301C) _v.06.07. 3: Case Ultra, MITI Ready biodegradation (AU6), 4: MITI Biodegradation probability Biowin 5 (linear model), 5: MITI Biodegradation probability Biowin 6 (MITI non-linear model), (Positive results are red, RB: Ready Biodegradable, NRB: non Ready Biodegradable)

PTPs	Smiles	OASIS catalogic		Case Ultra	Episuite	
		Catalogic OECD 301F	Catalogic OECD 301C	AU6	Biowin 5	Biowin 6
DMI_267	<chem>c12c(cccc1)CCc1c(cccc1)N2CCCNC</chem>	0.0784	0.0917	OD	-0.0289	0.0138
PTP_219_1	<chem>c12c(cccc1)CC(=O)CN2CCCN</chem>	0.0486	0.0886	(+)	0.2938	0.1246
PTP_219_2	<chem>C1(=O)c2c(cccc2)N(CCCN)CCC1</chem>	0.0441	0.0646	(+)	0.3692	0.1696
PTP_219_3	<chem>c12c(cccc1)CCC(=O)CN2CCCN</chem>	0.0533	0.0419	(+)	0.2938	0.1246
PTP_219_4	<chem>c12c(cccc1)CCCC(=O)N2CCCN</chem>	0	0.1987	(+)	0.3875	0.2578
PTP_281_1	<chem>c12c(cccc1)CCc1c(cccc1)N2CCCNC=O</chem>	0.0224	0.0722	(±)	0.0224	0.0287
PTP_281_2	<chem>c12c(cccc1)CCc1c(cccc1)N2CCC(=O)NC</chem>	0.0796	0.056	(±)	-0.0266	0.0192
PTP_281_3	<chem>c12c(cccc1)CCc1c(cccc1)N2CC(=O)CNC</chem>	0.1225	0.0995	OD	-0.0022	0.0138
PTP_281_4	<chem>c12c(cccc1)CCc1c(cccc1)N2C(=O)CCNC</chem>	0.1217	0.1141	(±)	0.0915	0.033
PTP_281_5	<chem>C1(=O)c2c(cccc2)N(CCCNC)c2c(cccc2)C1</chem>	0.1838	0.0955	OD	0.1029	0.0238
PTP_283	<chem>c1(O)c2c(ccc1)CCc1c</chem>	0.1591	0.0917	OD	-0.0205	0.0126

_1	(cccc1)N2CCCNC					
PTP_283_2	c12c(cc(O)cc1)N(CCCNC)c1c(cccc1)CC2	0.1267	0.0937	OD	-0.0205	0.0126
PTP_283_3	c1(O)c2c(ccc1)N(CCCNC)c1c(cccc1)CC2	0.2056	0.0933	OD	-0.0205	0.0126
PTP_283_4	c12c(cc(O)cc1)CCc1c(cccc1)N2CCCNC	0.2056	0.0934	OD	-0.0205	0.0126
PTP_283_5	c12c(cccc1)CCc1c(cccc1)N2CC(O)CNC	0.1039	0.0995	(±)	-0.0155	0.014
PTP_283_6	c12c(cccc1)CCc1c(cccc1)N2C(O)CCNC	0.1081	0.1276	(±)	-0.0155	0.014
PTP_283_7	c12c(cccc1)CCc1c(cccc1)N2CCC(O)NC	0.0767	0.091	(±)	-0.0155	0.014
PTP_283_8	c12c(cccc1)CCc1c(cccc1)N2CCCNCO	0.0438	0.0836	(+)	0.1336	0.035
PTP_283_9	c12c(C(O)Cc3c(cccc3)N1CCCNC)cccc2	0.1769	0.0935	(±)	0.1306	0.0342
PTP_285_1	c1(O)c(N(c2c(C)cccc2)CCCNC)c(C)ccc1	0.2656	0.0916	OD	0.1678	0.0277
PTP_285_2	c1(C)c(N(c2c(C)cccc2)CCCNC)cc(O)cc1	0.2409	0.0999	OD	0.1678	0.0277
PTP_285_3	c1(N(c2c(C)cccc2)CCNC)c(C)cc(O)cc1	0.2251	0.0935	OD	0.1678	0.0277
PTP_285_4	c1(O)c(C)c(N(c2c(C)cccc2)CCCNC)ccc1	0.2251	0.0902	OD	0.1678	0.0277
PTP_285_5	c1(N(c2c(C)cccc2)CCNC)c(CO)cccc1	0.1948	0.1259	(+)	0.1758	0.0338
PTP_285_6	c1(N(c2c(C)cccc2)C(O)CCNC)c(C)cccc1	0.2261	0.1252	(±)	0.1729	0.0308
PTP_285_7	c1(N(c2c(C)cccc2)CC(O)CNC)c(C)cccc1	0.0973	0.093	(±)	0.1729	0.0308
PTP_285_8	c1(N(c2c(C)cccc2)CC	0.0719	0.0889	(±)	0.1729	0.0308

_8	C(O)NC)c(C)cccc1					
PTP_285_9	c1(N(c2c(C)cccc2)CCNCO)c(C)cccc1	0.0429	0.082	(+)	0.322	0.0751
PTP_299_1	c1(O)c2c(ccc1)CCc1c(O)cccc1N2CCCNC	0.2473	0.0935	OD	-0.0121	0.0115
PTP_299_2	c1(O)c2c(ccc1)CCc1c(ccc(O)c1)N2CCCNC	0.1982	0.0936	OD	-0.0121	0.0115
PTP_299_3	c1(O)c2c(ccc1)CCc1c(c(O)ccc1)N2CCCNC	0.1663	0.0937	OD	-0.0121	0.0115
PTP_299_4	c1(O)c2c(ccc1)CCc1c(cc(O)cc1)N2CCCNC	0.2384	0.0938	OD	-0.0121	0.0115
PTP_299_5	c1(O)c2c(ccc1)CCc1c(cccc1)N2CC(O)CNC	0.1253	0.0953	(±)	-0.007	0.0127
PTP_299_6	c1(O)c2c(ccc1)CCc1c(cccc1)N2C(O)CCNC	0.2257	0.1275	(±)	-0.007	0.0127
PTP_299_7	c1(O)c2c(ccc1)CCc1c(cccc1)N2CCC(O)NC	0.0984	0.0911	(±)	-0.007	0.0127
PTP_299_8	c1(O)c2c(ccc1)CCc1c(cccc1)N2CCCNC(O)	0.1916	0.0836	(+)	0.1421	0.032
PTP_299_9	c1(O)c2c(C(O)Cc3c(ccc3)N2CCCNC)ccc1	0.1442	0.0937	(±)	0.139	0.0313
PTP_299_10	c1(O)c2c(ccc1)CC(O)c1c(cccc1)N2CCCNC	0.1435	0.0938	(±)	0.139	0.0313
PTP_299_11	c1(O)c(O)c2c(cc1)CCc1c(cccc1)N2CCCNC	0.1767	0.1028	OD	-0.0121	0.0115
PTP_299_12	c1(O)c2c(cc(O)c1)CCc1c(cccc1)N2CCCNC	0.1961	0.0975	OD	-0.0121	0.0115
PTP_299_13	c1(O)c2c(c(O)cc1)CCc1c(cccc1)N2CCCNC	0.2395	0.0972	OD	-0.0121	0.0115
PTP_299_14	c1(O)c(O)cc2c(c1)CCc1c(cccc1)N2CCCNC	0.1232	0.1001	OD	-0.0121	0.0115
PTP_299	c1(O)c2c(cc(O)c1)N(0.1694	0.0936	OD	-0.0121	0.0115

_15	CCCNC)c1c(cccc1)C C2					
PTP_299 _16	c12c(C(O)Cc3c(cccc3)N1CCCNC)ccc(O)c2	0.1217	0.0937	(±)	0.139	0.0313
PTP_299 _17	c12c(C(O)Cc3c(cc(O) cc3)N1CCCNC)cccc2	0.2029	0.0957	(±)	0.139	0.0313
PTP_299 _18	c1(O)c2c(ccc1)N(CC CNC)c1c(ccc(O)c1)C C2	0.2359	0.0936	OD	-0.0121	0.0115
PTP_299 _19	c12c(cc(O)cc1)N(CC CNC)c1c(ccc(O)c1)C C2	0.2182	0.0939	OD	-0.0121	0.0115
PTP_299 _20	c12c(cc(O)cc1)CCc1c (cc(O)cc1)N2CCCNC	0.2242	0.0954	OD	-0.0121	0.0115
PTP_299 _21	c12c(cc(O)cc1)N(C(O))CCNC)c1c(cccc1)CC 2	0.1934	0.1302	(±)	-0.007	0.0127
PTP_299 _22	c12c(cc(O)cc1)N(CC C(O)NC)c1c(cccc1)C C2	0.1093	0.0931	(±)	-0.007	0.0127
PTP_299 _23	c12c(cc(O)cc1)N(CC(O)CNC)c1c(cccc1)CC 2	0.1136	0.0975	(±)	-0.007	0.0127
PTP_299 _24	c12c(cc(O)cc1)N(CC CNCO)c1c(cccc1)CC 2	0.1502	0.0853	(+)	0.1421	0.032
PTP_299 _25	c1(O)c(O)c2c(cc1)N(CCCNC)c1c(cccc1)C C2	0.2556	0.1017	OD	-0.0121	0.0115
PTP_299 _26	c12c(C(O)Cc3c(ccc(O))c3)N1CCCNC)cccc2	0.2678	0.0956	(±)	0.139	0.0313
PTP_299	c12c(C(O)Cc3c(cccc3	0.1835	0.0955	(±)	0.139	0.0313

_27)N1CCCNC)cc(O)cc2					
PTP_299_28	c1(O)c2c(ccc1)N(CC CNC)c1c(cc(O)cc1)C C2	0.2769	0.0952	OD	-0.0121	0.0115
PTP_299_29	c12c(cc(O)cc1)CCc1c (ccc(O)c1)N2CCCNC	0.2793	0.0952	OD	-0.0121	0.0115
PTP_299_30	c12c(cc(O)cc1)CCc1c (cccc1)N2CC(O)CNC	0.1709	0.1015	(±)	-0.007	0.0127
PTP_299_31	c12c(cc(O)cc1)CCc1c (cccc1)N2C(O)CCNC	0.2284	0.1302	(±)	-0.007	0.0127
PTP_299_32	c12c(cc(O)cc1)CCc1c (cccc1)N2CCC(O)NC	0.1211	0.0928	(±)	-0.007	0.0127
PTP_299_33	c12c(cc(O)cc1)CCc1c (cccc1)N2CCCNCO	0.2468	0.0851	(+)	0.1421	0.032
PTP_299_34	c1(O)c2c(ccc1)N(CC CNC)c1c(c(O)ccc1)C C2	0.2724	0.095	OD	-0.0121	0.0115
PTP_299_35	c1(O)c2c(ccc1)N(CC CNC)c1c(G(O)C2)ccc c1	0.2663	0.0954	(±)	0.139	0.0313
PTP_299_36	c1(O)c2c(ccc1)N(CC CNC)c1c(cccc1)CC2 O	0.1845	0.0954	(±)	0.139	0.0313
PTP_299_37	c1(O)c2c(ccc1)N(CC C(O)NC)c1c(cccc1)C C2	0.1211	0.0927	(±)	-0.007	0.0127
PTP_299_38	c1(O)c2c(ccc1)N(CC CNCO)c1c(cccc1)CC 2	0.2468	0.0851	(+)	0.1421	0.032
PTP_299_39	c1(O)c2c(ccc1)N(CC(O)CNC)c1c(cccc1)CC 2	0.1709	0.1012	(±)	-0.007	0.0127

PTP_299_40	c1(O)c2c(ccc1)N(C(O)CCNC)c1c(cccc1)CC2	0.2284	0.1302	(±)	-0.007	0.0127
PTP_299_41	c12c(C(O)C(O)c3c(cccc3)N1CCCNC)cccc2	0.0883	0.0952	(±)	0.2901	0.0824
PTP_299_42	c12c(C(O)Cc3c(cccc3)N1C(O)CCNC)cccc2	0.3896	0.1303	(±)	0.144	0.0347
PTP_299_43	c12c(C(O)Cc3c(cccc3)N1CC(O)CNC)cccc2	0.0985	0.1015	(±)	0.144	0.0347
PTP_299_44	c12c(C(O)Cc3c(cccc3)N1CCC(O)NC)cccc2	0.0737	0.0929	(±)	0.144	0.0347
PTP_299_45	c12c(C(O)Cc3c(cccc3)N1CCNCO)cccc2	0.3575	0.0853	(+)	0.2931	0.0841
PTP_299_46	c12c(cccc1)CCc1c(cccc1)N2C(O)C(O)CNC	0.1215	0.1167	(±)	-0.002	0.0142
PTP_299_47	c12c(cccc1)CCc1c(cccc1)N2C(O)CC(O)NC	0.1359	0.1793	(±)	-0.002	0.0142
PTP_299_48	c12c(cccc1)CCc1c(cccc1)N2C(O)CCNCO	0.0649	0.1193	(+)	0.1471	0.0354
PTP_299_49	c12c(cccc1)CCc1c(cccc1)N2CC(O)C(O)NC	0.0913	0.0969	(±)	-0.002	0.0142
PTP_299_50	c12c(cccc1)CCc1c(cccc1)N2CC(O)CNC	0.0927	0.091	(+)	0.1471	0.0354
PTP_299_51	c12c(cccc1)CCc1c(cccc1)N2CCC(O)NCO	0.068	0.0868	(+)	0.1471	0.0354
PTP_301_1	c1(O)c(N(c2c(C)c(O)ccc2)CCCNC)c(C)ccc1	0.3233	0.092	OD	0.1762	0.0253
PTP_301_2	c1(O)c(N(c2c(C)cc(O)ccc2)CCCNC)c(C)ccc1	0.2815	0.0955	OD	0.1762	0.0253
PTP_301_3	c1(O)c(N(c2c(O)cccc2)CCCNC)c(C)ccc1	0.2897	0.0935	OD	0.1762	0.0253
PTP_301	c1(O)c(N(c2c(C)ccc(0.3402	0.1022	OD	0.1762	0.0253

_4	O)c2)CCCNC)c(C)ccc 1					
PTP_301 _5	c1(O)c(N(c2c(C)cccc2)CC(O)CNC)c(C)ccc1	0.1778	0.095	(±)	0.1813	0.0281
PTP_301 _6	c1(O)c(N(c2c(C)cccc2)C(O)CCNC)c(C)ccc1	0.4715	0.1279	(±)	0.1813	0.0281
PTP_301 _7	c1(O)c(N(c2c(C)cccc2)CCC(O)NC)c(C)ccc1	0.1538	0.0907	(±)	0.1813	0.0281
PTP_301 _8	c1(O)c(N(c2c(C)cccc2)CCCNCO)c(C)ccc1	0.3971	0.0837	(+)	0.3304	0.0688
PTP_301 _9	c1(O)c(N(c2c(C)cccc2)CCCNC)c(CO)ccc1	0.148	0.1314	(+)	0.1842	0.0309
PTP_301 _10	c1(O)c(N(c2c(CO)ccc c2)CCCNC)c(C)ccc1	0.2347	0.1286	(+)	0.1842	0.0309
PTP_301 _11	c1(O)c(O)c(N(c2c(C)c ccc2)CCCNC)c(C)cc1	0.36	0.1048	OD	0.1762	0.0253
PTP_301 _12	c1(O)c(N(c2c(C)cccc2)CCCNC)c(C)cc(O)c1	0.2161	0.0912	OD	0.1762	0.0253
PTP_301 _13	c1(O)c(N(c2c(C)cccc2)CCCNC)c(C)c(O)cc1	0.1992	0.0977	OD	0.1762	0.0253
PTP_301 _14	c1(O)c(O)cc(N(c2c(C) cccc2)CCCNC)c(C)c1	0.2231	0.0981	OD	0.1762	0.0253
PTP_301 _15	c1(O)c(C)c(N(c2c(C)c ccc2)CCCNC)cc(O)c1	0.1217	0.0932	OD	0.1762	0.0253
PTP_301 _16	c1(CO)c(N(c2c(C)ccc c2)CCCNC)cc(O)cc1	0.1514	0.1144	(+)	0.1842	0.0309
PTP_301 _17	c1(C)c(N(c2c(CO)ccc c2)CCCNC)cc(O)cc1	0.2997	0.1405	(+)	0.1842	0.0309
PTP_301 _18	c1(O)c(C)c(N(c2c(C)c cc(O)c2)CCCNC)ccc1	0.3321	0.1004	OD	0.1762	0.0253
PTP_301 _19	c1(C)c(N(c2c(C)ccc(O))c2)CCCNC)cc(O)cc1	0.3486	0.1099	OD	0.1762	0.0253

PTP_301_20	c1(N(c2c(C)ccc(O)c2)CCCNC)c(C)cc(O)cc1	0.3216	0.0977	OD	0.1762	0.0253
PTP_301_21	c1(C)c(N(c2c(C)cccc2)C(O)CCNC)cc(O)cc1	0.3947	0.1398	(±)	0.1813	0.0281
PTP_301_22	c1(C)c(N(c2c(C)cccc2)CCC(O)NC)cc(O)cc1	0.1819	0.0992	(±)	0.1813	0.0281
PTP_301_23	c1(C)c(N(c2c(C)cccc2)CC(O)CNC)cc(O)cc1	0.1907	0.1041	(±)	0.1813	0.0281
PTP_301_24	c1(C)c(N(c2c(C)cccc2)CCCNCO)cc(O)cc1	0.3332	0.0915	(+)	0.3304	0.0688
PTP_301_25	c1(O)c(O)c(C)c(N(c2c(C)cccc2)CCCNC)cc1	0.2756	0.1011	OD	0.1762	0.0253
PTP_301_26	c1(N(c2c(CO)cccc2)CCNC)c(C)cc(O)cc1	0.2962	0.1315	(+)	0.1842	0.0309
PTP_301_27	c1(N(c2c(C)cccc2)CCNC)c(CO)cc(O)cc1	0.1981	0.137	(+)	0.1842	0.0309
PTP_301_28	c1(O)c(C)c(N(c2c(C)c(O)cc2)CCCNC)ccc1	0.3427	0.0939	OD	0.1762	0.0253
PTP_301_29	c1(N(c2c(C)cc(O)cc2)CCCNC)c(C)cc(O)cc1	0.3458	0.0977	OD	0.1762	0.0253
PTP_301_30	c1(N(c2c(C)cccc2)CC(O)CNC)c(C)cc(O)cc1	0.1709	0.0971	(±)	0.1813	0.0281
PTP_301_31	c1(N(c2c(C)cccc2)C(O)CCNC)c(C)cc(O)cc1	0.2284	0.1307	(±)	0.1813	0.0281
PTP_301_32	c1(N(c2c(C)cccc2)CC(O)NC)c(C)cc(O)cc1	0.1211	0.0927	(±)	0.1813	0.0281
PTP_301_33	c1(N(c2c(C)cccc2)CCCNCO)c(C)cc(O)cc1	0.3133	0.0855	(+)	0.3304	0.0688
PTP_301_34	c1(O)c(C)c(N(c2c(C)c(O)ccc2)CCCNC)ccc1	0.3371	0.0906	OD	0.1762	0.0253
PTP_301	c1(O)c(C)c(N(c2c(CO)ccc2)CCCNC)ccc1	0.2962	0.1264	(+)	0.1842	0.0309

_35)cccc2)CCCNc)ccc1					
PTP_301_36	c1(O)c(CO)c(N(c2c(C)cccc2)CCCNc)ccc1	0.1549	0.1286	(+)	0.1842	0.0309
PTP_301_37	c1(O)c(C)c(N(c2c(C)cccc2)CCC(O)NC)ccc1	0.1211	0.0892	(±)	0.1813	0.0281
PTP_301_38	c1(O)c(C)c(N(c2c(C)cccc2)CCCNCO)ccc1	0.3133	0.0824	(+)	0.3304	0.0688
PTP_301_39	c1(O)c(C)c(N(c2c(C)cccc2)CC(O)CNC)ccc1	0.1709	0.0936	(±)	0.1813	0.0281
PTP_301_40	c1(O)c(C)c(N(c2c(C)cccc2)C(O)CCNC)ccc1	0.2284	0.1254	(±)	0.1813	0.0281
PTP_301_41	c1(N(c2c(CO)cccc2)CCCNc)c(CO)cccc1	0.1848	0.16	(+)	0.1922	0.0376
PTP_301_42	c1(N(c2c(C)cccc2)C(O)CCNC)c(CO)cccc1	0.4446	0.1629	(+)	0.1893	0.0342
PTP_301_43	c1(N(c2c(C)cccc2)CC(O)CNC)c(CO)cccc1	0.1038	0.1315	(+)	0.1893	0.0342
PTP_301_44	c1(N(c2c(C)cccc2)CC(O)NC)c(CO)cccc1	0.0775	0.1273	(+)	0.1893	0.0342
PTP_301_45	c1(N(c2c(C)cccc2)CCCNCO)c(CO)cccc1	0.3971	0.1167	(+)	0.3383	0.0831
PTP_301_46	c1(N(c2c(C)cccc2)C(O)C(O)CNC)c(C)cccc1	0.2477	0.1143	(±)	0.1863	0.0311
PTP_301_47	c1(N(c2c(C)cccc2)C(O)CC(O)NC)c(C)cccc1	0.2543	0.1754	(±)	0.1863	0.0311
PTP_301_48	c1(N(c2c(C)cccc2)C(O)CCNCO)c(C)cccc1	0.188	0.1172	(+)	0.3354	0.076
PTP_301_49	c1(N(c2c(C)cccc2)CC(O)C(O)NC)c(C)cccc1	0.0864	0.0903	(±)	0.1863	0.0311
PTP_301	c1(N(c2c(C)cccc2)CC	0.0867	0.0852	(+)	0.3354	0.076

_50	(O)CNCO)c(C)cccc1					
PTP_301 _51	c1(N(c2c(C)cccc2)CC C(O)NCO)c(C)cccc1	0.0637	0.0846	(+)	0.3354	0.076

Table S4: QSAR toxicity predictions for DMI and its TPs by different models (Models 1-5 (Case ultra software), Model 6 (Oasis catalogic)): (1) Salmonella mutagenicity TA 97, 98, 100, 1535–1538 (GT1 A7B), (2) A–T mutation E. coli and TA102 (GT1 AT E. coli), (3) Expert rules for genotoxicity (GT Expert), (4) E. coli mutagenicity (all strains) (Pharm E. coli), (5) Salmonella mutagenicity (TA97, 98, 100, 1535–1538) (Pharm Salm), 6. Mutagenicity v. 4.

	1	2	3	4	5	6
DMI_267	(-)	(-)	known (-)	(-)	known (-)	(-)
PTP_219_1	(-)	(-)	(-)	(-)	(-)	(-)
PTP_219_2	(-)	(-)	(-)	(-)	(-)	(-)
PTP_219_3	(-)	(-)	(-)	(-)	(-)	(-)
PTP_219_4	(-)	(-)	(-)	(-)	(-)	(-)
PTP_281_1	(-)	OD	(-)	OD	(-)	(+)
PTP_281_2	(-)	(-)	(-)	(-)	(-)	(-)
PTP_281_3	(-)	(-)	(-)	(-)	(-)	(-)
PTP_281_4	(-)	(-)	(-)	(-)	(-)	(-)
PTP_281_5	(-)	(-)	(-)	(-)	(-)	(-)
PTP_283_1	(-)	(-)	(-)	(-)	(-)	(-)
PTP_283_2	(-)	(-)	(-)	(-)	(-)	(-)
PTP_283_3	(-)	(-)	(-)	(-)	(-)	(-)
PTP_283_4	(-)	(-)	(-)	(-)	(-)	(-)
PTP_283_5	(-)	(-)	(-)	(-)	(-)	(-)
PTP_283_6	(-)	OD	(-)	OD	(-)	(-)
PTP_283_7	(-)	OD	(-)	OD	(-)	(-)
PTP_283_8	(-)	(-)	(+)	(-)	(-)	(+)
PTP_283_9	(-)	(-)	(-)	(-)	(-)	(-)
PTP_285_1	(-)	(-)	(-)	(-)	(-)	(-)
PTP_285_2	(-)	(-)	(-)	(-)	(-)	(-)
PTP_285_3	(-)	(-)	(-)	(-)	(-)	(-)
PTP_285_4	(-)	(-)	(-)	(-)	(-)	(-)
PTP_285_5	(-)	(-)	(-)	(-)	(-)	(-)
PTP_285_6	(-)	OD	(-)	OD	(-)	(-)

PTP_285_7	(-)	(-)	(-)	(-)	(-)	(-)
PTP_285_8	(-)	OD	(-)	OD	(-)	(-)
PTP_285_9	(-)	(-)	(+)	(-)	(-)	(+)
PTP_299_1	(-)	(-)	(-)	(-)	(-)	(-)
PTP_299_2	(-)	(-)	(-)	(-)	(-)	(-)
PTP_299_3	(-)	(-)	(-)	(-)	(-)	(-)
PTP_299_4	(-)	(-)	(-)	(-)	(-)	(-)
PTP_299_5	(-)	(-)	(-)	(-)	(-)	(-)
PTP_299_6	(-)	OD	(-)	OD	(-)	(-)
PTP_299_7	(-)	OD	(-)	OD	(-)	(-)
PTP_299_8	(-)	(-)	(+)	(-)	(-)	(+)
PTP_299_9	(-)	(-)	(-)	(-)	(-)	(-)
PTP_299_10	(-)	(-)	(-)	(-)	(-)	(-)
PTP_299_11	(-)	(-)	(-)	(-)	(±)	(-)
PTP_299_12	(-)	(-)	(-)	(-)	(-)	(-)
PTP_299_13	(-)	(-)	(-)	(-)	(-)	(-)
PTP_299_14	(-)	(±)	(-)	(-)	(-)	(-)
PTP_299_15	(-)	(-)	(-)	(-)	(-)	(-)
PTP_299_16	(-)	(-)	(-)	(-)	(-)	(-)
PTP_299_17	(-)	(-)	(-)	(-)	(-)	(-)
PTP_299_18	(-)	(-)	(-)	(-)	(-)	(-)
PTP_299_19	(-)	(-)	(-)	(-)	(-)	(-)
PTP_299_20	(-)	(-)	(-)	(-)	(-)	(-)
PTP_299_21	(-)	OD	(-)	OD	(-)	(-)
PTP_299_22	(-)	OD	(-)	OD	(-)	(-)
PTP_299_23	(-)	(-)	(-)	(-)	(-)	(-)
PTP_299_24	(-)	(-)	(+)	(-)	(-)	(+)
PTP_299_25	(-)	(-)	(-)	(-)	(-)	(-)
PTP_299_26	(-)	(-)	(-)	(-)	(-)	(-)
PTP_299_27	(-)	(-)	(-)	(-)	(-)	(-)
PTP_299_28	(-)	(-)	(-)	(-)	(-)	(-)

PTP_299_29	(-)	(-)	(-)	(-)	(-)	(-)
PTP_299_30	(-)	(-)	(-)	(-)	(-)	(-)
PTP_299_31	(-)	OD	(-)	OD	(-)	(-)
PTP_299_32	(-)	OD	(-)	OD	(-)	(-)
PTP_299_33	(-)	(-)	(+)	(-)	(-)	(+)
PTP_299_34	(-)	(-)	(-)	(-)	(-)	(-)
PTP_299_35	(-)	(-)	(-)	(-)	(-)	(-)
PTP_299_36	(-)	(-)	(-)	(-)	(-)	(-)
PTP_299_37	(-)	OD	(-)	OD	(-)	(-)
PTP_299_38	(-)	(-)	(+)	(-)	(-)	(+)
PTP_299_39	(-)	(-)	(-)	(-)	(-)	(-)
PTP_299_40	(-)	OD	(-)	OD	(-)	(-)
PTP_299_41	(-)	(-)	(-)	(-)	(-)	(-)
PTP_299_42	(-)	OD	(-)	OD	(±)	(-)
PTP_299_43	(-)	(-)	(-)	(-)	(-)	(-)
PTP_299_44	(-)	OD	(-)	OD	(-)	(-)
PTP_299_45	(-)	(-)	(+)	(-)	(-)	(+)
PTP_299_46	(-)	OD	(-)	OD	(-)	(-)
PTP_299_47	(-)	OD	(-)	OD	(-)	(-)
PTP_299_48	(-)	OD	(+)	OD	(-)	(+)
PTP_299_49	(-)	OD	(-)	OD	(-)	(-)
PTP_299_50	(-)	(-)	(+)	(-)	(-)	(+)
PTP_299_51	(-)	OD	(+)	OD	(-)	(+)
PTP_301_1	(-)	(-)	(-)	(-)	(-)	(-)
PTP_301_2	(-)	(-)	(-)	(-)	(-)	(-)
PTP_301_3	(-)	(-)	(-)	(-)	(-)	(-)
PTP_301_4	(-)	(-)	(-)	(-)	(-)	(-)
PTP_301_5	(-)	(-)	(-)	(-)	(-)	(-)
PTP_301_6	(-)	OD	(-)	OD	(-)	(-)
PTP_301_7	(-)	OD	(-)	OD	(-)	(-)
PTP_301_8	(-)	(-)	(+)	(-)	(-)	(+)

PTP_301_9	(-)	(-)	(-)	(-)	(±)	(-)
PTP_301_10	(-)	(-)	(-)	(-)	(±)	(-)
PTP_301_11	(-)	(-)	(-)	(-)	(-)	(-)
PTP_301_12	(-)	(-)	(-)	(-)	(-)	(-)
PTP_301_13	(-)	(-)	(-)	(-)	(-)	(-)
PTP_301_14	(-)	(-)	(-)	(-)	(-)	(-)
PTP_301_15	(-)	(-)	(-)	(-)	(-)	(-)
PTP_301_16	(-)	(-)	(-)	(-)	(-)	(-)
PTP_301_17	(-)	(-)	(-)	(-)	(-)	(-)
PTP_301_18	(-)	(-)	(-)	(-)	(-)	(-)
PTP_301_19	(-)	(-)	(-)	(-)	(-)	(-)
PTP_301_20	(-)	(-)	(-)	(-)	(-)	(-)
PTP_301_21	(-)	OD	(-)	OD	(-)	(-)
PTP_301_22	(-)	OD	(-)	OD	(-)	(-)
PTP_301_23	(-)	(-)	(-)	(-)	(-)	(-)
PTP_301_24	(-)	(-)	(+)	(-)	(-)	(+)
PTP_301_25	(-)	(-)	(-)	(-)	(-)	(-)
PTP_301_26	(-)	(-)	(-)	(-)	(-)	(-)
PTP_301_27	(-)	(-)	(-)	(-)	(-)	(-)
PTP_301_28	(-)	(-)	(-)	(-)	(-)	(-)
PTP_301_29	(-)	(-)	(-)	(-)	(-)	(-)
PTP_301_30	(-)	(-)	(-)	(-)	(-)	(-)
PTP_301_31	(-)	OD	(-)	OD	(-)	(-)
PTP_301_32	(-)	OD	(-)	OD	(-)	(-)
PTP_301_33	(-)	(-)	(+)	(-)	(-)	(+)
PTP_301_34	(-)	(-)	(-)	(-)	(-)	(-)
PTP_301_35	(-)	(-)	(-)	(-)	(-)	(-)
PTP_301_36	(-)	(-)	(-)	(-)	(-)	(-)
PTP_301_37	(-)	OD	(-)	OD	(-)	(-)
PTP_301_38	(-)	(-)	(+)	(-)	(-)	(+)
PTP_301_39	(-)	(-)	(-)	(-)	(-)	(-)

PTP_301_40	(-)	OD	(-)	OD	(-)	(-)
PTP_301_41	(-)	(-)	(-)	(-)	(-)	(-)
PTP_301_42	(-)	OD	(-)	OD	(±)	(-)
PTP_301_43	(-)	(-)	(-)	(-)	(-)	(-)
PTP_301_44	(-)	OD	(-)	OD	(-)	(-)
PTP_301_45	(-)	(-)	(+)	(-)	(-)	(+)
PTP_301_46	(-)	OD	(-)	OD	(-)	(-)
PTP_301_47	(-)	OD	(-)	OD	(-)	(-)
PTP_301_48	(-)	OD	(+)	OD	(-)	(+)
PTP_301_49	(-)	OD	(-)	OD	(-)	(-)
PTP_301_50	(-)	(-)	(+)	(-)	(-)	(+)
PTP_301_51	(-)	OD	(+)	OD	(-)	(+)

(+) positive prediction for the respective endpoint, (-) negative prediction for the respective endpoint, and (OD) Out of domain

Table S5: The predicted bacterial toxicity of DMI and its TPs with four acute toxicity models for *Vibrio fischeri* [Microtox Toxicity to Environmental Bacteria (AUA, Case Ultra) and three acute toxicity *Vibrio fischeri* models (Oasis Catalogic)]

	AUA*	Acute tox 5min**	Acute tox 15min**	Acute tox 30min**
DMI_267	OD	0.4009	0.2914	0.1976
PTP_219_1	(-)	<=444.2873	<=575.6327	<=1113.7855
PTP_219_2	(±)	108.0898	129.9381	203.4946
PTP_219_3	OD	101.4346	117.1813	182.7967
PTP_219_4	(-)	236.2656	294.4838	518.8438
PTP_281_1	OD	<=2.6818	<=2.2674	<=2.0110
PTP_281_2	(-)	<=2.8962	<=2.4694	<=2.2141
PTP_281_3	OD	0.9652	0.759	0.5794
PTP_281_4	OD	<=45.7226	<=49.0702	<=65.6304
PTP_281_5	(±)	5.087	4.7593	4.5977
PTP_283_1	OD	<=1.0436	<=0.8202	<=0.6332
PTP_283_2	(±)	<=2.0904	<=1.7188	<=1.4703
PTP_283_3	OD	<=2.0511	<=1.6996	<=1.4478
PTP_283_4	(±)	<=2.0954	<=1.7212	<=1.4732
PTP_283_5	OD	8.1096	7.4546	7.7634
PTP_283_6	OD	8.1542	7.4788	7.798
PTP_283_7	OD	8.0964	7.4474	7.7532
PTP_283_8	OD	7.1351	6.4486	6.5986
PTP_283_9	OD	8.0389	7.4161	7.7084
PTP_285_1	OD	<=0.8470	<=0.6547	<=0.4897
PTP_285_2	(±)	<=1.6521	<=1.3497	<=1.1124
PTP_285_3	(+)	<=1.6827	<=1.3644	<=1.1290
PTP_285_4	OD	<=1.6681	<=1.3574	<=1.1211
PTP_285_5	OD	5.6014	5.0418	4.9634
PTP_285_6	OD	6.4131	5.8535	5.8742
PTP_285_7	OD	6.4812	5.8901	5.9248

PTP_285_8	OD	6.5539	5.9291	5.9786
PTP_285_9	OD	5.679	5.083	5.0192
PTP_299_1	OD	<=5.4367	<=4.8604	<=4.7314
PTP_299_2	(±)	<=5.5192	<=4.9039	<=4.7895
PTP_299_3	OD	<=2.7489	<=2.3338	<=2.0563
PTP_299_4	(±)	<=5.4953	<=4.8913	<=4.7727
PTP_299_5	OD	<=21.2366	<=21.1855	<=25.1415
PTP_299_6	OD	<=21.4417	<=21.3061	<=25.3383
PTP_299_7	OD	<=21.3726	<=21.2655	<=25.2720
PTP_299_8	OD	<=18.6171	<=18.2864	<=21.3057
PTP_299_9	OD	<=21.1442	<=21.1309	<=25.0527
PTP_299_10	OD	<=20.9353	<=21.0072	<=24.8516
PTP_299_11	OD	<=2.7534	<=2.3361	<=2.0591
PTP_299_12	OD	<=2.7950	<=2.3568	<=2.0843
PTP_299_13	OD	<=2.7460	<=2.3323	<=2.0546
PTP_299_14	OD	<=5.3891	<=4.8352	<=4.6977
PTP_299_15	OD	<=5.4336	<=4.8587	<=4.7291
PTP_299_16	(±)	<=41.4783	<=43.8238	<=57.2926
PTP_299_17	(±)	<=41.0452	<=43.5527	<=56.8067
PTP_299_18	(±)	<=10.7704	<=10.1362	<=10.9044
PTP_299_19	(±)	<=10.8539	<=10.1826	<=10.9729
PTP_299_20	(±)	<=10.7945	<=10.1496	<=10.9241
PTP_299_21	(±)	<=42.2322	<=44.2928	<=58.1361
PTP_299_22	(±)	<=42.3229	<=44.3490	<=58.2374
PTP_299_23	(±)	<=42.0881	<=44.2034	<=57.9751
PTP_299_24	(±)	<=36.3476	<=37.8177	<=48.5357
PTP_299_25	OD	<=5.4493	<=4.8671	<=4.7403
PTP_299_26	(±)	<=42.3170	<=44.3453	<=58.2308
PTP_299_27	(±)	<=41.7529	<=43.9950	<=57.6002
PTP_299_28	(±)	<=10.7441	<=10.1216	<=10.8827
PTP_299_29	(±)	<=10.9766	<=10.2505	<=11.0734

PTP_299_30	(±)	<=42.0389	<=44.1728	<=57.9201
PTP_299_31	(±)	<=42.7521	<=44.6143	<=58.7162
PTP_299_32	(±)	<=42.6346	<=44.5418	<=58.5852
PTP_299_33	(±)	<=37.2263	<=38.3554	<=49.4856
PTP_299_34	OD	<=10.6545	<=10.0716	<=10.8091
PTP_299_35	OD	<=41.5147	<=43.8464	<=57.3334
PTP_299_36	OD	<=41.2439	<=43.6772	<=57.0298
PTP_299_37	OD	<=42.8635	<=44.6829	<=58.8402
PTP_299_38	OD	<=36.0818	<=37.6540	<=48.2475
PTP_299_39	OD	<=41.4776	<=43.8233	<=57.2918
PTP_299_40	OD	<=41.8424	<=44.0507	<=57.7004
PTP_299_41	OD	73.4931	81.6158	115.8861
PTP_299_42	OD	73.6648	81.7284	116.1057
PTP_299_43	OD	74.3329	82.1657	116.9595
PTP_299_44	OD	74.4349	82.2323	117.0896
PTP_299_45	OD	64.4215	70.4424	98.1968
PTP_299_46	OD	75.2149	82.7406	118.0843
PTP_299_47	OD	74.1698	82.0591	116.7512
PTP_299_48	OD	65.0238	70.8309	98.941
PTP_299_49	OD	75.7607	83.0949	118.7791
PTP_299_50	OD	65.8126	71.3375	99.9138
PTP_299_51	OD	66.2882	71.6418	100.4993
PTP_301_1	OD	<=4.3567	<=3.8461	<=3.6186
PTP_301_2	(+)	<=4.3930	<=3.8650	<=3.6431
PTP_301_3	OD	<=2.2511	<=1.8710	<=1.6009
PTP_301_4	(±)	<=4.3988	<=3.8681	<=3.6470
PTP_301_5	OD	<=16.8067	<=16.6390	<=19.0327
PTP_301_6	OD	<=17.1164	<=16.8196	<=19.3168
PTP_301_7	OD	<=17.2696	<=16.9083	<=19.4569
PTP_301_8	OD	<=15.0552	<=14.5467	<=16.4141
PTP_301_9	OD	<=14.6798	<=14.3312	<=16.0812

PTP_301_10	OD	<=14.8079	<=14.4050	<=16.1950
PTP_301_11	OD	<=2.2477	<=1.8693	<=1.5990
PTP_301_12	(±)	<=2.2391	<=1.8651	<=1.5940
PTP_301_13	OD	<=2.1987	<=1.8451	<=1.5707
PTP_301_14	OD	<=4.4065	<=3.8721	<=3.6522
PTP_301_15	OD	<=4.4026	<=3.8700	<=3.6495
PTP_301_16	(±)	<=28.9775	<=29.8306	<=36.9618
PTP_301_17	(±)	<=29.2481	<=29.9950	<=37.2416
PTP_301_18	(±)	<=8.6606	<=8.0366	<=8.3626
PTP_301_19	(±)	<=8.6535	<=8.0327	<=8.3570
PTP_301_20	(+)	<=8.6626	<=8.0377	<=8.3641
PTP_301_21	(±)	<=33.7148	<=34.9662	<=44.3217
PTP_301_22	(±)	<=33.2906	<=34.7055	<=43.8687
PTP_301_23	(±)	<=33.8137	<=35.0268	<=44.4271
PTP_301_24	(±)	<=29.1352	<=29.9265	<=37.1249
PTP_301_25	OD	<=4.3942	<=3.8657	<=3.6439
PTP_301_26	(+)	<=29.3242	<=30.0411	<=37.3202
PTP_301_27	(±)	<=29.2442	<=29.9926	<=37.2375
PTP_301_28	(+)	<=8.7503	<=8.0857	<=8.4327
PTP_301_29	(+)	<=8.7598	<=8.0909	<=8.4402
PTP_301_30	(+)	<=33.8915	<=35.0745	<=44.5101
PTP_301_31	(+)	<=34.0148	<=35.1498	<=44.6415
PTP_301_32	(+)	<=33.5137	<=34.8428	<=44.1071
PTP_301_33	(+)	<=29.7938	<=30.3245	<=37.8043
PTP_301_34	OD	<=8.6068	<=8.0071	<=8.3204
PTP_301_35	OD	<=28.9954	<=29.8416	<=36.9803
PTP_301_36	OD	<=29.0395	<=29.8683	<=37.0259
PTP_301_37	OD	<=33.9867	<=35.1326	<=44.6115
PTP_301_38	OD	<=29.3633	<=30.0647	<=37.3605
PTP_301_39	OD	<=33.9505	<=35.1105	<=44.5729
PTP_301_40	OD	<=33.5423	<=34.8604	<=44.1376

PTP_301_41	OD	44.6208	47.7063	62.9097
PTP_301_42	OD	51.4517	55.6239	74.8896
PTP_301_43	OD	51.6855	55.7731	75.1656
PTP_301_44	OD	51.2179	55.4743	74.6133
PTP_301_45	OD	44.8844	47.8727	63.2111
PTP_301_46	OD	60.0036	65.2908	89.9733
PTP_301_47	OD	60.6586	65.7111	90.7694
PTP_301_48	OD	52.7799	56.4682	76.4545
PTP_301_49	OD	59.8413	65.1864	89.7758
PTP_301_50	OD	52.8628	56.5205	76.5518
PTP_301_51	OD	53.417	56.8701	77.2025

*Positive (+), negative (-), inconclusive ((±), the probability of being positive is around 50 ± 10%), out of domain (OD).

**the toxicity value is mg/l (IC 50).

ARTICLE II

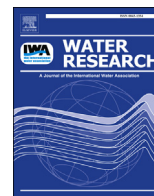
*“Initial fate assessment of teratogenic drug trimipramine and its
photo-transformation products –
role of pH, concentration and temperature”*

Water Research 108, pp. 197-211.

Doi: 10.1016/j.watres.2016.10.078

AUTHORS:

Nareman D.H. Khaleel, Waleed M.M. Mahmoud, Oliver Olsson, Klaus Kümmerer



Initial fate assessment of teratogenic drug trimipramine and its photo-transformation products – Role of pH, concentration and temperature



Nareman D.H. Khaleel ^{a, b}, Waleed M.M. Mahmoud ^{a, b}, Oliver Olsson ^a, Klaus Kümmerer ^{a, *}

^a Sustainable Chemistry and Material Resources, Institute of Sustainable and Environmental Chemistry, Leuphana University of Lüneburg, Scharnhorststraße 1 C13, DE-21335 Lüneburg, Germany

^b Pharmaceutical Analytical Chemistry Department, Faculty of Pharmacy, Suez Canal University, Ismailia 41522, Egypt

ARTICLE INFO

Article history:

Received 27 May 2016

Received in revised form

3 October 2016

Accepted 30 October 2016

Available online 2 November 2016

Keywords:

Photo-degradation

QSAR

Antidepressant

Biodegradability

Teratogenicity

Mutagenicity

ABSTRACT

Trimipramine (TMP) is an antidepressant drug used for the treatment of a variety of depressive states and other psychiatric disorders. It has been already detected in the aquatic environment. Currently, no further knowledge is available on fate and effects of TMP in the aquatic environment. Therefore, we studied the biodegradability of TMP and of its photolysis transformation products (PTPs) generated by irradiation with polychromatic UV light in aqueous solution. Different conditions including initial drug concentration, pH, and temperature were applied during TMP photolysis. Subsequently, the time courses of TMP and dissolved organic carbon (DOC) concentrations were monitored throughout the whole photo-degradation process. Then, high-resolution mass spectrometry was used to identify and elucidate the structures of the resulting PTPs. After that, the two standardized biodegradation tests, Closed Bottle test (CBT; OECD 301 D) and Manometric Respirometry test (MRT; OECD 301 F), were performed for TMP and its photolytic mixtures to assess the biodegradability of TMP and its PTPs. Finally, the toxicity of TMP and its photolytic mixtures was predicted using different quantitative structure activity relationship (QSAR) software. It was found that after 128 min of UV-irradiation, 91.8% of TMP at the initial concentration of 100 mg L⁻¹ was eliminated with only 23.9% removal in the DOC. So, it can be pointed out that more than 65% of the degraded TMP is transformed to new non-mineralized PTPs. 14 new PTPs were detected in TMP's photolytic mixtures. Their supposed structures indicate that the proposed photo-transformation pathway is mainly by hydroxylation. The statistical analysis confirms that the differences in the degradation rates of TMP as a function of concentration, pH, and temperature are statistically significant in most cases investigated here. In biodegradation testing, TMP and its PTPs are classified as not readily biodegradable, while LC-MS analysis revealed some PTPs to be eliminated more than TMP itself. Results from QSAR analysis confirmed that some of the PTPs could be biodegradable, and revealed that some of the non-biodegradable PTPs may be human and/or eco-toxic, posing a risk to the environment. Our findings show that TMP under UV-irradiation could lead to the formation of some more easily biodegradable PTPs and some others toxic and non-biodegradable PTPs. Therefore, further studies should be conducted regarding the fate and effects of TMP and its PTPs elucidated in this study on human health and on the environment.

© 2016 Elsevier Ltd. All rights reserved.

1. Introduction

Pharmaceutical drugs and their byproducts are increasingly

regarded as environmental pollutants, as indicated by the increasing number of reports on their occurrence in a variety of eco-systems and the growing concerns with regards to their potential environmental impacts.

Psychotropic drugs are among the pharmaceuticals highly to be found in the aquatic environment; their use has been increased mainly in developed countries such as Europe and the United States (Optenberg et al., 2002). Antidepressants are one of the

* Corresponding author. Nachhaltige Chemie und Stoffliche Ressourcen, Institut für Nachhaltige Chemie und Umweltchemie, Leuphana Universität Lüneburg, C13, Scharnhorststraße 1, DE-21335 Lüneburg, Germany.

E-mail address: klaus.kuemmerer@leuphana.de (K. Kümmerer).

most highly used psychotropic substances and they are correspondingly likely to be found in the environment (Huerta-Fontela et al., 2011). Trimipramine (TMP) is a commonly prescribed tricyclic antidepressant (TCA) worldwide (Fakhari et al., 2012). TMP was, for example, also highly used in psychiatric hospitals and nursing homes in Germany in the years of 2010, 2011, and 2012 (Herrmann et al., 2015b). In the year 2014, the consumption of prescribed TMP in Germany was 4.6 t (Schwabe and Paffrath, 2015). TMP is used for the treatment of a variety of depressive states and other psychiatric disorders, especially where sleep disturbance, anxiety or agitation is a presenting symptom. It is also frequently encountered in emergency toxicological screening, drug abuse testing and forensic medical examinations (Fakhari et al., 2012).

TMP is extensively metabolized to desmethyl TMP and 2-hydroxy TMP in the liver and excreted in urine, as unchanged and metabolized forms (Fraser et al., 1987). Metabolites of TCAs can quickly be cleaved back in wastewater to their free parent molecules by enzymatic or chemical decomposition (Reddy et al., 2005). Therefore, TMP is expected to be present in the influents of sewage treatment plants (STPs). In the year 2014, TMP was already detected in the sewage treatment plants (STPs) in Dresden, Germany in a concentration of 51.8 ng L⁻¹ (Gurke et al., 2015). In STPs, many pharmaceuticals are not eliminated and thus being able to reach surface waters, ground waters, and even drinking waters. The presence of TMP in the aquatic environment could be harmful because TMP has teratogenic properties (https://www.accessdata.fda.gov/drugsatfda_docs/label/2014/016792s0371bl.pdf) (Singh et al., 1978) and some studies showed also eco-toxic effects for psychotropic substances (Chiffre et al., 2016).

When TMP reaches the aquatic environment, it can undergo various biotic and abiotic transformations. In addition, transformations of psychotropic pharmaceuticals can also happen in technical treatment processes such as water disinfection by UV and in other advanced oxidation processes applied in STPs and in drinking water treatment (Herrmann et al., 2015a). However, to the author's best knowledge, no data is available considering the elimination or the transformation of TMP in the aquatic environment or by the application of water treatment technologies.

Incomplete biotic or abiotic degradation of pharmaceuticals occurring in the environment or during treatment can lead to the formation of transformation products (TPs) with significantly different physical, chemical, and toxic properties. These TPs could have a negative effect on the environmental organisms and/or could be more persistent than their parent compounds (Mahmoud et al., 2014). To the best of our knowledge, there has been no literature information on TPs formed from TMP.

Pharmaceuticals in the aquatic environment can cause toxic effects to humans and the ecosystem. In this study, QSAR is used as a screening tool for predicting the TPs fate and toxicity. Computational *in silico* QSAR predictive toxicology methods are accepted worldwide for the regulatory qualification of impurities, contaminants, and degradants in pharmaceuticals; this is because experimental testing is difficult as the TPs are rarely available and, even when obtainable, their cost is very high (Contrera, 2013).

In view of the considerations above, the main objectives of this study were to provide for the first time data about the fate and effects of TMP in the aquatic environment through: (i) studying its biodegradability and photo-degradability under different conditions, and (ii) obtaining information about the formation and the structure of the TPs, and their biodegradability and toxicity.

2. Experimental and analytical methods

2.1. Materials

Trimipramine maleate (TMP), CAS number 521-78-8, of purity higher than 98% was bought from Sigma-Aldrich (Steinheim, Germany). Acetonitrile (HiPerSolv CHROMANORM, LC-MS grade, BDH Prolabo) and formic acid were obtained from VWR (Darmstadt, Germany). In biodegradation tests, all the chemicals used as nutrients were of 98.5% purity, at least. All reagents were used without further treatment or purification. Aqueous solutions were prepared using ultrapure (UP) water.

2.2. Photo-degradation

2.2.1. Photo-degradation experimental setup

TMP photo-degradation experiments were performed in UP water under different conditions including: initial TMP concentrations of 5, 10, 50, and 100 mg L⁻¹; temperatures of 10, 20, 30, and 40 °C; and pH values of 3, 5, 7, and 9. In order to examine if the original TMP concentration is primarily affected by the different conditions studied, controls wrapped in aluminum foil were run simultaneously under the same conditions. The selected initial concentrations of TMP were considerably higher than the expected levels in the environment in order to ensure the elucidation of the potential PTPs formed and to allow biodegradation tests performing. Also, the differentiation between mineralization and transformation can only be done by employing DOC measurements which require concentrations in the mg L⁻¹ range and rule out the presence of organic matter other than the test compound.

The experiments were performed using a batch immersion tube photo-reactor (1 L) filled with about 0.8 L of TMP solution. The experiments were run under constant temperature and constant mixing of the solutions as the photo-reactor is provided with both a cooling system (WKL230, LAUDA, Berlin) and a magnetic stirrer. The light source used was a medium-pressure Hg lamp (TQ150W, UV Consulting Peschl, Mainz, Germany) with an ilmasil quartz immersion tube. The lamp emits polychromatic radiation in a range from 200 to 600 nm. The maximal intensities of the lamp were at 256, 265, 280, 301, 312, 334, 364, 414 and 436 nm. TMP shows a high absorption in the UV range, with its absorption maximum at 248 nm, which means that TMP was expected to have a high degradation rate under the UV-irradiation used (Fig. S1-1). The total photon flow rate of the polychromatic lamp used was estimated using a UV-pad Spectral Radiometer (Opsytec Dr. Gröbel GmbH, Ettlingen, Germany). The radiometer was placed at a distance of 4 cm from the emission source in an aluminum box. The total photon flow rate of the lamp for all wavelengths was 5.71 × 10⁶ (mol × photons × cm⁻² × s⁻¹). The photo-degradation experiments were conducted for 128 min. Aliquots of the reaction mixtures were periodically drawn from the photo-reactor at 0, 2, 4, 8, 16, 32, 64, and 128 min of irradiation for HPLC-UV and LC-MSⁿ analyses and for dissolved organic carbon (DOC) determination, in order to monitor the kinetics and the pathway of degradation and to follow the mineralization pattern of TMP. The collected samples were filtered immediately through 0.45 μm membrane filters (CHROMAFIL® Xtra Typ: PES 45/25, Macherey-Nagel, Germany), and either analyzed immediately or else stored in the dark at -20 °C until analysis. The required pH values for the TMP solution were adjusted using HCl and/or NaOH and the pH was monitored during the photolytic degradation experiments.

For the CBT and MRT, samples were collected at 0 min (i.e. a solution of the parent compound TMP only) and after 16 and 128 min of irradiation of 100 mg L⁻¹ TMP (pH 5, 20 °C). The final

concentration of TMP was adjusted by measuring the DOC of the tested substance (i.e. before photolysis) and of photo-treated samples, to determine the required carbon content and to calculate the theoretical oxygen demand (ThOD), for each CBT and MRT.

2.2.2. Quantum yield calculations and statistical analysis

In order to estimate the kinetics of degradation processes under the studied variable conditions, the following equations were applied (Khaleel et al., 2013):

$$\ln \frac{C}{C_0} = kt \quad (1)$$

$$t_{1/2} = \frac{\ln(2)}{k} \quad (2)$$

where k is the reaction rate constant, t is irradiation time, and $t_{1/2}$ is the half-lives.

The quantum yield (Φ) for TMP was calculated according to Equation (3) using the determined photolysis rate of TMP and the calculated absolute photon flux (Palm et al., 1997; Zepp, 1978).

$$\Phi_{\text{TMP}} = \frac{\frac{dc}{dt}}{\sum_{200 \text{ nm}}^{400 \text{ nm}} (2.303 \times J_{\text{abs}} \times \epsilon_{\text{TMP}} \times c_0 \times l)} \quad (3)$$

where Φ_{TMP} is the quantum yield of TMP, dc/dt is the elimination rate of TMP, J_{abs} is the absolute photon flux, ϵ_{TMP} is the molar absorption coefficient of TMP, c_0 is the initial concentration of TMP (mol L^{-1}), l is the path length (cm). Information about the absolute photon flux calculation was provided in supplementary materials text SI-1.

A one-way ANOVA and Tukey's tests were performed to test the statistical significance of the difference in the photo-degradation rates of TMP under the different environmental conditions studied during the photo-degradation testing (Gunasekar et al., 2013).

2.3. Chemical analysis

2.3.1. HPLC/DAD

A Shimadzu Prominence HPLC-UV apparatus (Shimadzu, Duisburg, Germany) was used to monitor the kinetic profile of TMP during UV-irradiation. The HPLC apparatus consists of an LC-10AT binary pump, a CBM-10A communication interface, an SPD-M10A diode array detector (DAD), an SIL-10 auto sampler, a CTO-10 AS VP column oven, and a Shimadzu Class LC10 software (version 5.0).

Analytical separation was performed using a NUCLEOSHELL® RP C18 ec column (2.7 μm , 100 \times 2 mm ID, Macherey and Nagel, Düren, Germany), protected by an EC guard column (NUCLEODUR® 100-5 C18 ec, 4 \times 3 mm). A gradient method was employed, using 0.1% formic acid in water (CH_2O_2 : solution A) and 100% acetonitrile (CH_3CN : solution B) as the mobile phase, and applying the following linear gradient: 0 min 10% B, 10 min 10% B, 18 min 90% B, 22 min 90% B, 25 min 10% B, and 30 min 10% B. The flow rate was 0.4 mL min^{-1} and the oven temperature was set to 40 °C. The detection wavelength was 250 nm. The injection volume was 10 μL of the irradiated filtered samples.

2.3.2. LC/MS/MS

The PTPs formed during the UV-irradiation of TMP after two LC-MSⁿ analysis systems, low resolution LC-MS ion trap (LC-MSIT) and high resolution LC-MS (HR-LC-MS). The LC-MSIT consisted of an Agilent 1100 series HPLC system (Agilent Technologies, Waldbronn, Germany) coupled with a Bruker Esquire 6000 plus ion trap

mass spectrometer with electrospray ionization (ESI) source (Bruker Daltonics, Bremen, Germany). Low mass resolution LC-MS was used as a first screening to elucidate and provisionally identify the structure of the PTPs formed. The LC-MSIT was operated in full-scan MSⁿ mode to screen the structures of the PTPs. The HR-LC-MS consisted of a Dionex Ultimate 3000 UHPLC system (Dionex, Idstein, Germany) coupled with an LTQ Orbitrap-XL high-resolution mass spectrometer with H-ESI source (Thermo Scientific, Bremen, Germany). The apparent structures of the PTPs were checked by accurate mass measurements provided by the HR-LC-MS, as it provides the empirical molecular formula, relative double bond equivalent values (RDB), and mass error calculations for the PTPs. Detailed information about both LC-MSⁿ systems used, and their chromatographic conditions, can be found in text SI-2. The same chromatographic column and method as described in Section 2.3.1 were used for both the LC-MSIT and the HR-LC-MS analyses.

Due to the lack of standards for the PTPs, their individual peak areas were used to monitor their relative course. The recovery percentage was calculated using the relation $A/A_0\%$, where A_0 is the peak area of the TMP at time 0 or at Day 0 and A is the peak area of the PTP at certain irradiation time or at Day 28 in either the photo-degradation or the biodegradation tests, respectively.

2.3.3. DOC analysis

In order to determine the extent of TMP's mineralization during the photo-degradation process, DOC was measured using a Total Organic Carbon (TOC) Analyzer Shimadzu 5000A (TOC-Vcpn, Shimadzu GmbH, Duisburg, Germany) in three replicates. Linear calibration for the measured range was performed with dried potassium phthalate.

2.4. Aerobic biodegradation testing: Closed Bottle test (CBT) and Manometric Respiratory test (MRT)

CBT and MRT were performed according to the OECD 301D and 301F guidelines, respectively. The basic experimental set-ups and validity criteria are described in detail elsewhere (Khaleel et al., 2013). The test system of CBT and MRT consisted of four and five different series, respectively, each series was run in parallel (Table S1). As an additional sterile bottle was used in MRT only, and it contained sodium azide in order to account for abiotic degradation. MRT uses higher bacterial concentrations and higher concentrations of sodium acetate and of the test substance compared to CBT. The concentration of TMP used was 2.3 mg L^{-1} , and 13.7 mg L^{-1} , corresponding to a theoretical oxygen demand (ThOD) of 5 mg L^{-1} and 30 mg L^{-1} in CBT and MRT, respectively. The final concentration of the photolytic mixtures after 16 and 128 min was adjusted according to the remaining DOC concentration to reach the comparable ThOD. All test bottles in the two tests were inoculated with an aliquot from the effluent of the municipal STP in AGL Lüneburg, Germany (144,000 inhabitant equivalents).

In CBT, biodegradability is expressed as the percentage of oxygen consumption based on ThOD and a test compound is classified as "readily biodegradable" if biodegradation exceeds 60% within a period of 10 days after the oxygen consumption reached 10% ThOD (OECD, 1992). In MRT, the process of aerobic biodegradation was monitored by the measurement of carbon dioxide (CO_2) production, where the resulting pressure decrease shows the corresponding oxygen consumption. Toxicity controls in CBT and MRT allow for the recognition of false negative results caused by the toxicity of the test compound reducing the numbers of the degrading bacteria. Samples taken at the beginning and at the end of the tests were stored at -20 °C for later HPLC and LC-MSⁿ analyses.

2.5. *In silico* prediction of toxicity and environmental fate

This prediction represents a snapshot intended to demonstrate the impact of using various QSAR models and illustrate the importance of the prediction rather than to compare the merits and limitations of each software models. The *in silico* software used here comprised: Case Ultra V.1.5.2.0 (MultiCASE Inc.), EPI Suite software (EPIWEB 4.1), and Oasis Catalogic software (V.5.11.6TB) (Table 1). Structure illustrations were performed using Marvin Sketch 15.6.15.0. The simplified molecular input line entry specification (SMILES) formats of the chemical structures of TMP and its PTPs were used as the entry. All the *in silico* models used in this study for the environmental fate predictions have validated databases and training sets. In general, the structures of the chemical species are scanned by the software against the validated databases of the model, and the software calculates the activity and predicts the output in the form of alerts for that corresponding activity. More information about their databases, training sets, and their validity criteria can easily be found elsewhere, following the references provided in Table 1 for each model.

2.5.1. *In silico* prediction of ready biodegradation

Various *in silico* models were used to predict if TMP and its PTPs were readily biodegradable or not (Table 1). *In silico* prediction of ready biodegradation of the PTPs has been applied here in order to support our analytical results from the biodegradation tests. As in biodegradation tests, we can only measure elimination not biodegradation of the PTPs using LC-MS methods. This prediction was made based on data for the OECD 301C MITI-I test (Ministry of International Trade and Industry, Japan, OECD, 2006) using Case Ultra, EPI Suite, and Oasis Catalogic software. By this approach, orientation is gained towards identifying the readily biodegradable and non-readily biodegradable molecules under different conditions. Oasis Catalogic software was also used to predict whether TMP and its PTPs were readily biodegradable or not based on data for the OECD 301F test (Oasis Catalogic software), which is directly comparable to the MRT. More details about the predicted values using *in silico* models were provided in Text SI-3.

2.5.2. *In silico* prediction of toxicity

Carcinogenicity, mutagenicity, and teratogenicity are among the toxicological endpoints that pose the highest concern for human health. Thus the International Conference on Harmonization (ICH) M7 guidance includes the use of *in silico* prediction as a part of the control and risk assessment of DNA reactive (mutagenic) impurities in pharmaceutical products (International Conference on Harmonization (ICH), 2014). *In silico* toxicity (toxicity to environmental bacteria, genotoxicity, mutagenicity, and teratogenicity) for TMP and its PTPs was predicted using a set of *in silico* prediction models for toxicity (Table 1). Case Ultra was used applying a combination of statistical and rule-based systems for bacterial mutagenicity according to the recently adopted ICH M7 guidance, using five GT Expert models. In addition, Case Ultra was used to predict teratogenicity based on A50, A51, A52, and A53 (Table 1). The toxicity to environmental bacteria was also predicted. Case Ultra software was used to predict bacterial toxicity based on microtox toxicity to environmental bacteria (*V. fischeri*). The Oasis Catalogic software was used to predict acute toxicity towards *V. fischeri* after 5, 15, and 30 min exposure. For Oasis Catalogic software, the predicted activity of the test chemicals in the three acute *V. fischeri* modules was expressed as mg L⁻¹ for half maximal inhibitory concentration (IC₅₀).

3. Results and discussion

3.1. UV photo-degradation of TMP in UP water

TMP primary elimination and mineralization were followed to evaluate the fate of TMP under UV-irradiation. With an initial concentration of 100 mg L⁻¹ (20 °C and pH 5), 77.2% of TMP was eliminated within the first one hour of UV-irradiation (Fig. 1). After 128 min of irradiation, at the end of the test, elimination was 91.8%. At the same time, there was no significant loss of TMP observed in dark controls, so TMP underwent photolytic degradation only by the effect of the UV Lamp used. Mineralization occurred slowly and DOC elimination at the end of the test was about 23.9%. The lower degree of DOC reduction and the primary elimination of 91.8% of

Table 1
List of used *in silico* models and software for the environmental fate predictions of TMP and its PTPs.

QSAR	Software models	End-points	References
Catalogic v 5.11.6 TB (OASIS)	Catalogic BOD Kinetic v.08.09	Ready biodegradability according to OECD 301F	(Laboratory of Mathematical Chemistry, 2012)
	Catalogic BOD 28 days OECD 301C v.06.07	Ready biodegradability according to MITI-I test	
	Vibrio fischeri pT5 v.01	Acute toxicity against <i>V. fischeri</i> after 5 min, IC50 [mg/L]	
	Vibrio fischeri pT15 v.01	Acute toxicity against <i>V. fischeri</i> after 15 min, IC50 [mg/L]	
	Vibrio fischeri pT30 v.01	Acute toxicity against <i>V. fischeri</i> after 30 min, IC50 [mg/L]	
Case Ultra v.1.4.5.1 (MultiCASE Inc.)	MITI-I test (OECD 301C, module AU6)	Ready biodegradability according to MITI-I test	(Chakravarti et al., 2012; Saiakhov et al., 2013)
	GT1 A7B	(Mutagenicity for 7 strains of <i>Salmonella typhimurium</i> TA 97, 98, 100, 1535–1538), FDA data source)	
	GT1 AT Ecoli Pharm Ecoli Pharm Salm	(A–T mutation in <i>E. coli</i> and <i>S. typhimurium</i> TA102, FDA data source) (<i>E. coli</i> mutagenicity (all strains) from public and proprietary sources) (<i>Salmonella typhimurium</i> mutagenicity (TA97, 98, 100, 1535–1538) from public and proprietary sources)	
	GT Expert	Expert rules for genotoxicity	
	Microtox toxicity environmental bacteria (AUA)	Bacterial toxicity	
	A50 v.1.5.2.0.795.300	Teratogenicity in Rabbits	
	A51 v.1.5.2.0.1232.500	Teratogenicity in Rat	
	A52 v.1.5.2.0.766.500	Teratogenicity in Mouse	
	A53 v.1.5.2.0.1350.550	Teratogenicity in misc. Mammals	
	EpiSuite (EPIWEB 4.1)	Biodegradation probability Biowin 5 (linear model) Biodegradation probability Biowin 6 (non-linear model)	

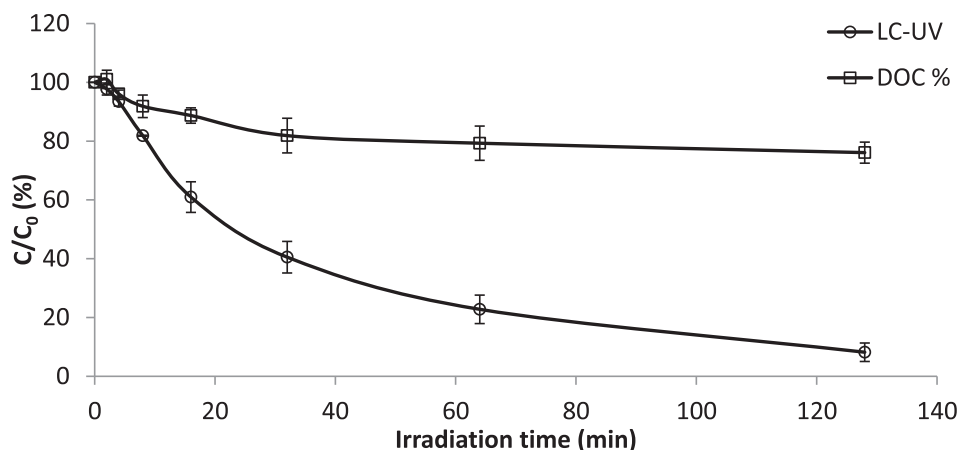


Fig. 1. Elimination of 100 mg L⁻¹ Trimipramine (TMP) by LC-UV at 250 nm and mineralization by dissolved organic carbon (DOC) recovery during direct UV-photolysis.

TMP indicate the formation of PTPs during the UV photo-degradation of TMP without complete mineralization into CO₂.

A first-order kinetic model was used, according to the OECD guidelines, to determine the photo-degradation rate constants (Herrmann et al., 2015b). UV photolysis of 100 mg L⁻¹ TMP in UP water fitted the first-order kinetic model with a 0.985 determination coefficient (R²), a 0.0169 min⁻¹ rate constant (k), and a 41.0 min half-life time (t_{1/2}).

3.2. Performance of UV-radiation in TMP degradation under different conditions

3.2.1. Effect of pH

The influence of the pH value of the solution on the UV photolysis and the mineralization rates of TMP was analyzed in experiments at pH 3, 5, 7, and 9 using the initial concentration of 100 mg L⁻¹ at 20 °C. The stability of TMP in dark controls under the pH range examined here showed no significant decrease in TMP concentration in experiments performed at pH ≤ 7. TMP solution at pH 9, in the dark control experiment, had shown slight turbidity and approximately 24% from its initial concentration was precipitated. This happened because TMP solubility decreases in alkaline media (Tuckerman, 1984). Fig. 2 shows TMP degradation and mineralization under the UV-irradiation for the different pH values. The photolysis and mineralization rates of TMP are directly proportional to the pH value of the solution. After 128 min of irradiation, 87.6, 88.3, 96.2, and 99.5% of TMP had degraded at pH values of 3, 5, 7, and 9, respectively.

Due to the lower solubility of TMP at pH 9, kinetics at pH 9 will be discussed separately. At pH values 3, 5, and 7, first-order reaction kinetics can be used to describe the photo-degradation of TMP; the corresponding photolysis rate constants (k) are 0.0156, 0.0169, and 0.0253 min⁻¹, respectively (R² > 0.98). The increase in the degradation and the mineralization rates by the increase in pH values at pH ≤ 7 can be due to the increase in the molar absorption coefficient (ε) (Fig. SI-2). As according to Equation (3), an increase in the ε value should produce an increase in the k value and vice versa. In the test at pH 9, the fastest degradation rate is seen but it shows also a relative slowdown after 16 min of irradiation until the end of the test. So TMP degradation at pH 9 followed two-stage first-order kinetics: a faster first stage with k = 0.077 and R² = 0.9758 (0–16 min of irradiation), and a slower second stage with k = 0.0199 and R² = 0.994 (16–128 min of irradiation). The fast kinetics at pH 9 can be explained either by the lower solubility or by the different ionization form of TMP at pH 9. Fig. SI-3 shows the

structures of the different resulting TMP species under different pH ranges; the structures obtained using Marvin Sketch 15.6.15.0 (Marvin Sketch, 2015). TMP is a strong basic substance with an experimental pK_a = 9.34 ± 0.22 (Llinas et al., 2008). At pH = 3, 5, and 7, TMP is mostly protonated as HTMP⁺. In alkaline solution (pH 9), TMP is around 50% in its neutral form, in which it might be more easily degradable and have more photo-reactivity than its protonated species (Gualano et al., 2014; Kwon and Armbrust, 2004). The subsequent slowdown in degradation at pH 9 after 16 min irradiation might be explained either by the change in the solution pH value during the irradiation time or by the presence of newly formed PTPs. During the UV-irradiation of TMP at pH 9, pH of the solution begins to decrease gradually after 16 min to reach the pH value of approximately 7 at 128 min of irradiation. In contrast, in the acidic and the neutral media, the pH did not show significant change during the entire course of the UV-irradiation (Fig. SI-4). The other possible explanation of the slowdown observed after 16 min of irradiation is the presence of newly formed PTPs after 16 min in the pH 9 experiment, that are not formed at other pH values, and which might absorb UV-radiation, thereby reducing the UV available for TMP degradation (Rastogi et al., 2014). Of course, these two explanations might also be in operation at the same time.

The ANOVA analysis indicates that the differences in the degradation rates as a function of the pH are statistically significant with P < 0.001. Tukey's test results confirm that the differences in the photolysis rates between each two pH experiments were statistically significant (P < 0.021), except for the difference between pH 3 and pH 5 experiments which is statistically non-significant. The non-significant difference between pH 3 and pH 5 could be because at these two pH values, TMP is mostly in its protonated form (99.88% and 100% at pH 3 and pH 5, respectively). At the same time, TMP has nearly the same absorption coefficient at these two pH values for the UV-range studied here.

3.2.2. Effect of TMP concentration

The photo-degradation kinetics of TMP in UP water at pH 5 and 20 °C using four different concentration levels (5, 10, 50, and 100 mg L⁻¹) are shown in Fig. 3a. The elimination kinetics for TMP's initial concentrations of 100 mg L⁻¹, 50 mg L⁻¹, 10 mg L⁻¹, and 5 mg L⁻¹ used in photolysis experiments fits first-order kinetics with high linearity (R² > 0.98) and half-lives equal to 41.0, 13.5, 4.1, and 2.0 min, respectively (Fig. SI-5). The photolysis rates increase as the initial TMP concentration decreases (Fig. SI-6). Although TMP photo-degradation followed first-order kinetics, the first-order rate constant (k) was affected by the initial concentration, which

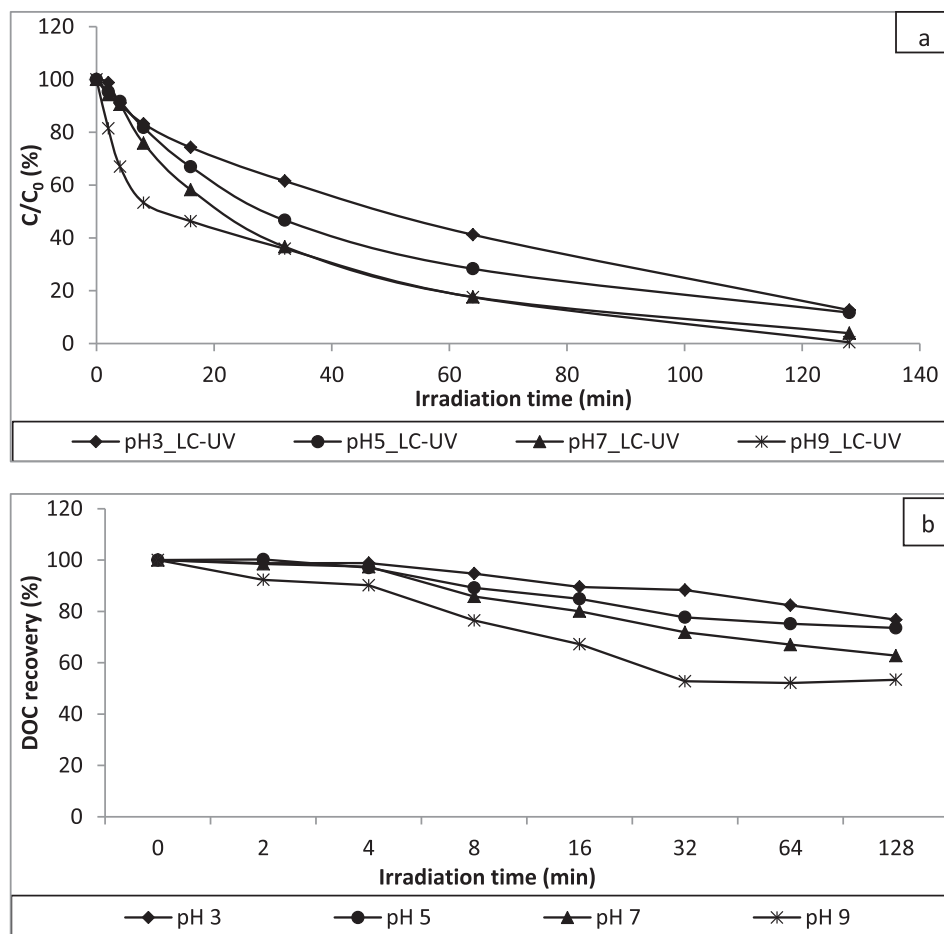


Fig. 2. The photolytic degradation (a) and the DOC Recovery (b) of TMP by mean of UV photo-degradation at different pH values. TMP initial concentration = 100 mg L⁻¹, temperature = 20 °C.

indicated that the kinetics were not clearly first-order (Li et al., 2014). Therefore, the data were plotted as $\ln(C/C_0)$ versus time to facilitate result analyses according to the OECD guidelines (OECD, 2008). The results for the degree of DOC removal show that, after 128 min of irradiation in the experiments at 100, 50, 10, and 5 mg L⁻¹, mineralization was about 23.9%, 30.7%, 75.4%, and 79.1%, respectively (Fig. 3b). It can be concluded that there is a possibility of complete mineralization at lower concentrations within a longer irradiation time. These results show that photolysis might be quite fast under real world conditions as concentrations are lower. However, it cannot be excluded that there will be other compounds present in the environmental water that may slow down the photo-transformation of TMP (Trovó et al., 2014). At the same time, scavengers for radicals as well as photosensitizing compounds can interfere with TMP in natural water (Hazime et al., 2012).

From the previously stated results, it is obvious that TMP elimination kinetics and the corresponding photo-degradation rate constant and DOC removal rate are decreasing by increasing TMP initial concentration. This is mostly because more parent compounds are present absorbing radiation and blocking others from the access to radiation. In addition, intermediates and PTPs that are formed with higher amount by the action of the UV light in case of higher concentrations may contribute to this shielding effect as such intermediates compete with TMP and can partially absorb the UV light before it can pass through the whole solution (Khaleel et al., 2016).

The ANOVA analysis confirms that the differences in the

degradation rates as a function of concentration are statistically significant with $P < 0.001$. Tukey's test results confirm that the differences in the photolysis rates between each pair of concentrations are highly statistically significant ($P < 0.001$).

According to the calculated k values (Equation (1)) using actinometer, the quantum yield (Equation (3)) of the direct photolysis process was calculated for TMP at concentrations of 5 and 10 mg L⁻¹ in the UP water and it was $3.44 \times 10^{-2} \text{ mol E}^{-1}$.

3.2.3. Effect of temperature

The photo-degradation of 100 mg L⁻¹ TMP was performed in UP water (pH 5) at the following temperatures: 10, 20, 30, and 40 °C (Fig. 4a and b). TMP elimination and mineralization rates are directly proportional to the experimental temperature. Arrhenius plot is obtained by plotting $\log k$ against $1/T$, and it is found to be linear in the studied temperature range (Fig. SI-7). The activation energy was calculated from Arrhenius equation and it is found to be 12.6 kJ mol⁻¹. According to first-order kinetics, the degradation rate constants (k) at 10, 20, 30, and 40 °C experiments are 0.0147, 0.0169, 0.0197 and 0.0248 min⁻¹, respectively ($R^2 > 0.986$). After 128 min of irradiation at different temperatures experiments, the observed mineralization (in %) amounted to 13.1, 23.9, 29.1, and 37.4 at 10, 20, 30, and 40 °C, respectively. This finding can be explained by the fact that only molecules with sufficient energy are able to react. So that, at a higher temperature, molecules can easily reach the required activation energy to undergo degradation and therefore it gives higher degradation rates.

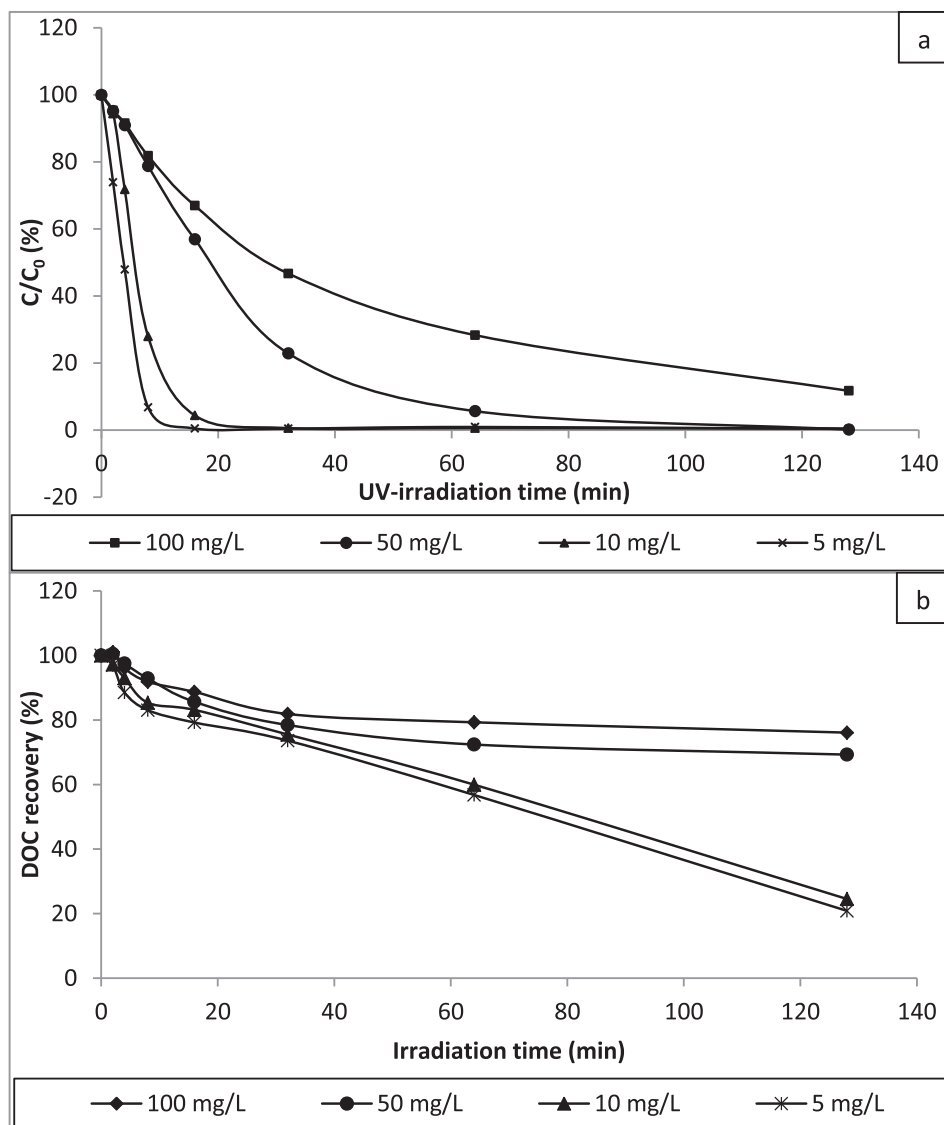


Fig. 3. The photolytic degradation (a) and the DOC Recovery (b) of TMP by mean of UV photo-degradation at different concentrations. pH = 5, temperature = 20 °C.

The ANOVA results indicate that the differences in the degradation rates, as a function of the temperature, had an acceptable statistical significance with $P = 0.002$. Tukey's test results confirmed that the differences in the photolysis rates, between each two temperatures' experiments, are of statistical significance ($P < 0.025$), except the differences between the experiments performed at 20 °C and 30 °C, and at 30 °C and 40 °C, that are statistically not significant where $P = 0.265$ and 0.150, respectively. Because of this temperature-dependent photo-degradation processes, different degradation rates in different regions (e.g. Europe and Africa) can be expected.

3.3. Identification of TMP's PTPs and degradation pathway

The LC-MS total ion chromatograms were checked for the UV-irradiated aqueous solution of TMP at all sampled time points. Then extracted ion chromatograms (EICs) of ions, that are suspected to be present, were executed. Based on the total ion chromatograms and EICs results, 14 PTPs are observed and elucidated with different m/z values, containing only two PTPs having the same m/z value (Table 2). The accurate mass measurements

provided by the HR-LC-MS are in agreement with the proposed elemental composition of $[M+H]^+$ ions with a low mass deviation of less than 1 mmu for all of the PTPs elucidated here. In addition, all calculated RDB values for the PTPs and their fragments matched the predicted structures, underlining the proposed structures (Table 2). Five from the detected PTPs named as PTP311, PTP327, PTP309a, PTP210, and PTP196 were reported before in the literature as metabolites of TMP in the rat (Hussain et al., 1991). MS² Fragmentation pattern of TMP according to HR-LC-MS data was provided in Fig. SI-8.

PTP311 (m/z value of 311.2 and with the suggested molecular formula $C_{20}H_{27}N_2O$) is primarily formed by a single hydroxylation of TMP. A key MS² fragment at m/z 226 ($C_{15}H_{16}NO$) suggests hydroxylation at the tricyclic ring. This key fragment originated through the loss of the 3-(dimethyl amino)-2-methylethyl chain (Fig. SI-9). A further hydroxylation step is proposed to explain the formation of the PTP327 (m/z 327.2) as a follow-up PTP from PTP311; PTP327 is a di-hydroxylated product from TMP. Also, the key MS² fragment at m/z 242 ($C_{15}H_{16}NO_2$) suggests di-hydroxylation at the tricyclic ring (Fig. SI-10). The same case was expected for PTPs with m/z 313 and 329. The latter two PTPs are

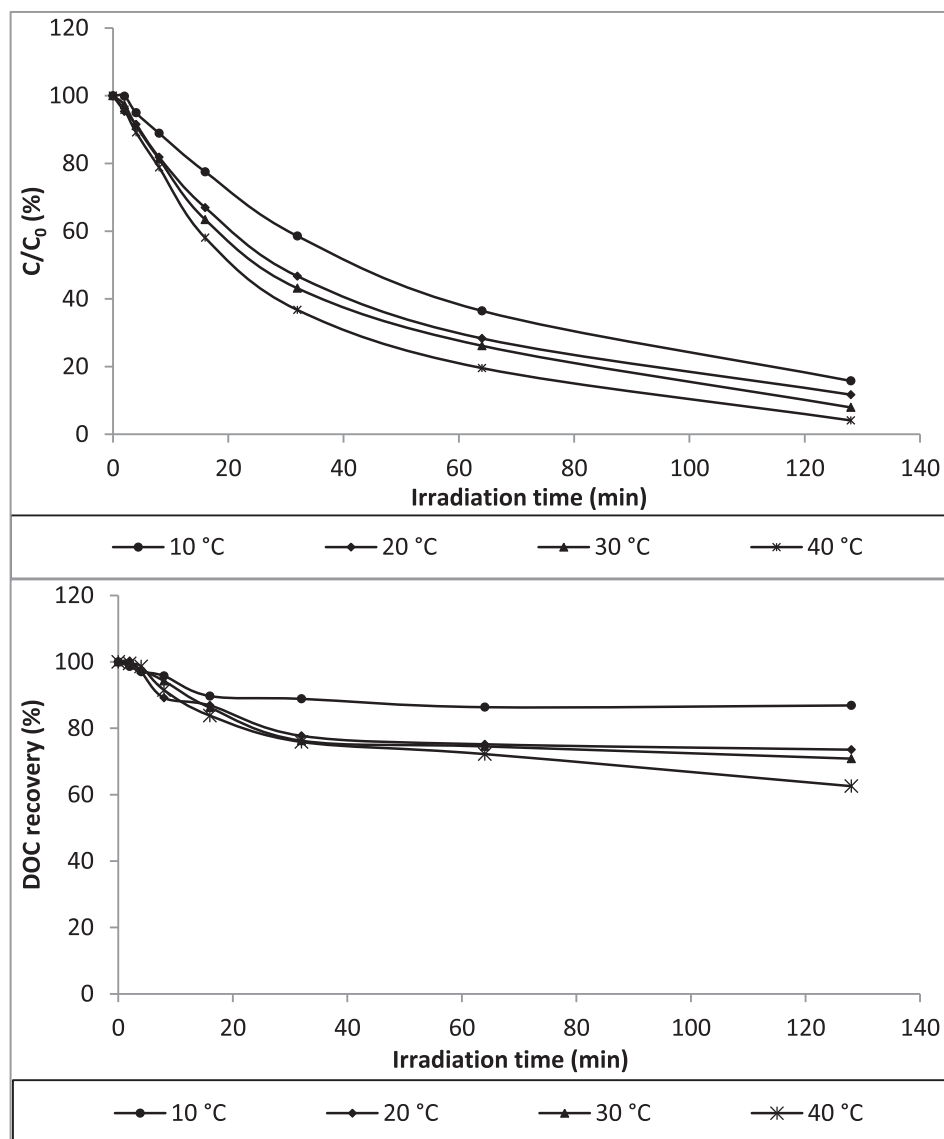


Fig. 4. The photolytic degradation (a) and the DOC Recovery (b) of TMP by mean of UV photo-degradation at different temperatures. TMP initial concentration = 100 mg L⁻¹, pH = 5.

formed after hydrogenation in the azepane ring of TMP accompanied with the previously mentioned mono- and di-hydroxylation processes (Figs. SI-11 & SI-12).

Two PTPs are formed with m/z 309.2 with two different formation mechanisms, as they gave different molecular formula, different RDB value, and different fragmentation pattern in their LC-MS results. PTP309a is proposed to be formed by the oxidation of TMP (Fig. SI-13), whereas PTP309b was not identified (Fig. SI-14).

PTP250 is suggested to be formed directly from TMP by deamination of the sidechain tertiary amine, which results in a loss of 45 Da accounting for the dimethylamine moiety. PTP286 is assumed to be formed from PTP250 after a single hydroxylation step (Fig. SI-15). MS² fragmentation pattern for PTP250 was not identified.

PTP196 (m/z 196.1) is formed directly from TMP, while PTP210 and PTP212 (m/z 210.1 and 212.1) are assumed to be PTPs derived from PTP309a and PTP311, respectively. These three PTPs are considered to be formed from the previously mentioned products, after the loss of the 3-(dimethylamino)-2-methylpropyl chain (Figs. SI-16 & SI-17). The loss of a side chain is a common

mechanism in the photolysis processes. Moreover, PTP210 and PTP212 have also been reported as PTPs formed through photo-degradation of Desipramine under xenon lamp irradiation; Desipramine is an antidepressant drug with structure highly related to TMP (Gros et al., 2015).

Dimerization is likely to happen mechanism during the photo-degradation of chemicals in the environment (Keen et al., 2013; Tiefenbacher et al., 1994; Vargas et al., 1995). PTP405 is assumed either to be formed by the dimerization of two molecules of PTP196 followed by mono-hydroxylation step or through the reaction between PTP196 and PTP 212 (Fig. SI-18).

PTP247 is assumed to come from a degradation of one benzene ring keeping the azepane cycle intact combined either with a mono-hydroxylation process in the benzene ring or with lactam formation in the azepane ring (Fig. SI-19). PTP134 is the N,N,2-trimethylpropan-1-amine chain of TMP including further di-hydroxylation (Fig. SI-20).

The time courses of the newly formed PTPs in TMP experiments performed at 100 mg L⁻¹ (pH 5, 20 °C) are shown in Fig. 5. Some of the formed PTPs were immediately formed after starting the

Table 2Accurate mass measurements of TMP and its PTPs determined by HRLCMS-LTQ Orbitrap in MS and MSⁿ mode.

Compound	RT	Measured mass [m/z]	Molecular formula	Calculated mass [m/z]	Relative error [mmu]	Precursor ion/product ion	RDB	Proposed structure
TMP	10.5	295.2178	C ₂₀ H ₂₇ N ₂	295.21688	1.265	[M + H] ⁺	8.5	
		224.14398	C ₁₆ H ₁₈ N	224.14338	0.604	[M + H - C ₄ H ₉ N] ⁺	8.5	
		210.12843	C ₁₅ H ₁₆ N	210.12773	0.704	[M + H - C ₅ H ₁₁ N] ⁺	8.5	
		100.11255	C ₆ H ₁₄ N	100.11208	0.474	[M + H - C ₁₄ H ₁₃ N] ⁺	0.5	
309a	10	309.19693	C ₂₀ H ₂₅ ON ₂	309.19614	0.79	[M + H] ⁺	9.5	
		100.11237	C ₆ H ₁₄ N	100.11208	0.294	[M + H - C ₁₄ H ₁₁ ON] ⁺	0.5	
		264.13834	C ₁₈ H ₁₈ ON	264.13829	0.049	[M + H - C ₂ H ₇ N] ⁺	10.5	
		224.10664	C ₁₅ H ₁₄ ON	224.10699	-0.351	[M + H - C ₅ H ₁₁ N] ⁺	9.5	
309b	10.6	309.23325	C ₂₁ H ₂₉ N ₂		0.725	[M + H] ⁺	8.5	
		224.1438	C ₁₆ H ₁₈ N		0.424	[M + H - C ₅ H ₁₁ N] ⁺	8.5	
		196.10921	C ₁₄ H ₁₄ N		-2.866	[M + H - C ₇ H ₁₅ N] ⁺	8.5	
311	10.4	311.21243	C ₂₀ H ₂₇ ON ₂	311.21179	0.64	[M + H] ⁺	8.5	
		293.2016	C ₂₀ H ₂₅ N ₂	293.2018	0.405	[M + H - H ₂ O] ⁺	9.5	
		100.1124	C ₆ H ₁₄ N	100.11208	0.324	[M + H - C ₁₄ H ₁₃ ON] ⁺	0.5	
		266.15216	C ₁₈ H ₂₀ ON	266.15394	-1.781	[M + H - C ₂ H ₇ N] ⁺	9.5	
		240.13689	C ₁₆ H ₁₈ ON	240.13829	-1.401	[M + H - C ₄ H ₉ N] ⁺	8.5	
		226.12314	C ₁₅ H ₁₆ ON	226.12264	0.499	[M + H - C ₅ H ₁₁ N] ⁺	8.5	
313	10.1	313.228	C ₂₀ H ₂₉ ON ₂	313.22744	0.56	[M + H] ⁺	7.5	
		295.2179	C ₂₀ H ₂₇ N ₂	295.21742	1.025	[M + H - H ₂ O] ⁺	8.5	
		268.17007	C ₁₈ H ₂₂ ON	268.16959	0.479	[M + H - C ₂ H ₇ N] ⁺	8.5	
		250.15981	C ₁₈ H ₂₀ N	250.15957	0.784	[M + H - C ₂ H ₉ ON] ⁺	9.5	
		100.11246	C ₆ H ₁₄ N	100.11208	0.384	[M + H - C ₁₄ H ₁₅ ON] ⁺	0.5	
327	10.1	327.20728	C ₂₀ H ₂₇ O ₂ N ₂	327.2067	0.575	[M + H] ⁺	8.5	
		309.19833	C ₂₀ H ₂₅ ON ₂	309.19614	2.19	[M + H - H ₂ O] ⁺	9.5	
		282.14954	C ₁₈ H ₂₀ O ₂ N	282.14886	0.685	[M + H - C ₂ H ₇ N] ⁺	9.5	
		242.11794	C ₁₅ H ₁₆ O ₂ N	242.11756	0.385	[M + H - C ₅ H ₁₁ N] ⁺	8.5	
		224.10664	C ₁₅ H ₁₄ ON	224.10699	-0.351	[M + H - C ₅ H ₁₃ ON] ⁺	9.5	
		193.17032	C ₁₂ H ₂₁ N ₂	193.16993	0.395	[M + H - C ₈ H ₆ O ₂] ⁺	3.5	
		132.08075	C ₉ H ₁₀ N	132.08078	-0.026	[M + H - C ₁₁ H ₁₇ O ₂ N] ⁺	5.5	
		100.11238	C ₆ H ₁₄ N	100.11208	0.304	[M + H - C ₁₄ H ₁₃ O ₂ N] ⁺	0.5	

(continued on next page)

Table 2 (continued)

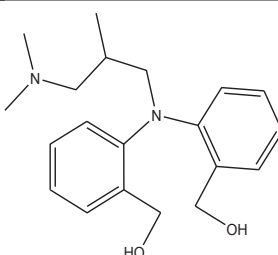
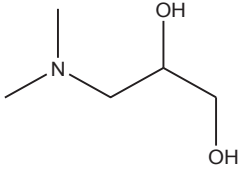
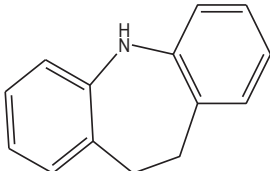
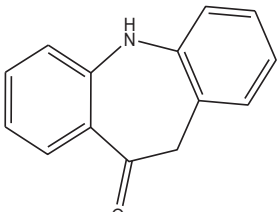
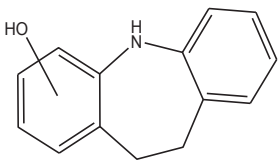
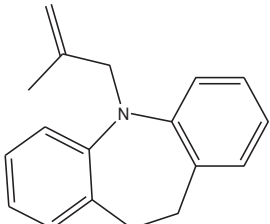
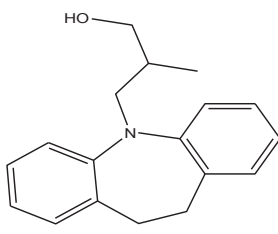
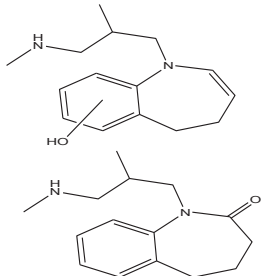
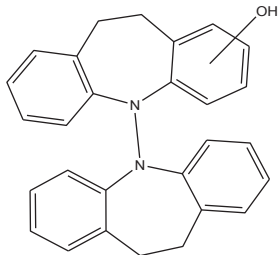
Compound	RT	Measured mass [m/z]	Molecular formula	Calculated mass [m/z]	Relative error [mmu]	Precursor ion/product ion	RDB	Proposed structure
329	9.92	329.22324	C ₂₀ H ₂₉ O ₂ N ₂	329.22235	0.885	[M + H] ⁺	7.5	
		284.16501	C ₁₈ H ₂₂ O ₂ N	284.16451	0.505	[M + H - C ₂ H ₇ N] ⁺	8.5	
		244.13351	C ₁₅ H ₁₈ O ₂ N	244.13321	0.305	[M + H - C ₅ H ₁₁ N] ⁺	7.5	
		100.11242	C ₆ H ₁₄ N	100.11208	0.344	[M + H - C ₁₄ H ₁₅ O ₂ N] ⁺	0.5	
134	0.7	134.11774	C ₆ H ₁₆ O ₂ N	134.11756	0.185	[M + H] ⁺	-0.5	
		116.10732	C ₆ H ₁₄ ON	116.10699	0.329	[M + H - H ₂ O] ⁺	0.5	
		58.06542	C ₃ H ₈ N	58.06513	0.294	[M + H - C ₃ H ₈ ON] ⁺	0.5	
196	12.1	196.11252	C ₁₄ H ₁₄ N	196.11208	0.444	[M + H] ⁺	8.5	
		180.08099	C ₁₃ H ₁₀ N	180.08078	0.214	[M + H - CH ₃] ⁺	9.5	
		168.08127	C ₁₂ H ₁₀ N	168.08078	0.494	[M + H - C ₂ H ₄] ⁺	8.5	
		118.06527	C ₈ H ₈ N	118.06513	0.144	[M + H - C ₆ H ₆] ⁺	5.5	
210	11.2	210.09166	C ₁₄ H ₁₂ ON	210.09134	0.319	[M + H] ⁺	9.5	
		192.08109	C ₁₄ H ₁₀ N	192.08078	0.314	[M + H - H ₂ O] ⁺	10.5	
		182.09677	C ₁₃ H ₁₂ N	182.09643	0.344	[M + H - CO] ⁺	8.5	
		165.07037	C ₁₃ H ₉	165.06988	0.493	[M + H - CH ₃ NO] ⁺	9.5	
212	11.2	212.10719	C ₁₄ H ₁₄ ON	212.10699	0.199	[M + H] ⁺	8.5	
250	11.7	250.15939	C ₁₈ H ₂₀ N	250.15903	0.364	[M + H] ⁺	9.5	
		172.11285	C ₁₂ H ₁₄ N	172.11285	0.774	[M + H - C ₆ H ₆] ⁺	6.5	
		158.09689	C ₁₁ H ₁₂ N	158.09689	0.464	[M + H - C ₇ H ₈] ⁺	6.5	
		146.0957	C ₁₀ H ₁₂ N	146.0957	0.726	[M + H - C ₈ H ₈] ⁺	5.5	

Table 2 (continued)

Compound	RT	Measured mass [m/z]	Molecular formula	Calculated mass [m/z]	Relative error [mmu]	Precursor ion/product ion	RDB	Proposed structure
268	11.7	268.1702	C ₁₈ H ₂₂ ON	268.16959	0.609	[M + H] ⁺	8.5	
		250.15939	C ₁₈ H ₂₀ N	250.15903	0.364	[M + H - H ₂ O] ⁺	9.5	
247	3.77	247.18068	C ₁₅ H ₂₃ ON ₂	247.18049	0.19	[M + H] ⁺	5.5	
		202.12296	C ₁₃ H ₁₆ ON	202.12264	0.319	[M + H - C ₂ H ₇ N] ⁺	6.5	
405	13.7	405.19522	C ₂₈ H ₂₅ ON ₂	405.19614	-0.92	[M + H] ⁺	17.5	
		313.13446	C ₂₁ H ₁₇ ON ₂	313.13354	0.92	[M + H - C ₇ H ₈] ⁺	14.5	
		210.09145	C ₁₄ H ₁₂ ON	210.09134	0.109	[M + H - C ₁₄ H ₁₃ N] ⁺	9.5	

experiment such as PTP196, PTP311, and PTP313. Other PTPs, which are mainly assumed to be secondary and tertiary products, are formed after a certain irradiation time such as PTP405, and PTP329. The curves for all of the PTPs increase constantly up to a specific time point and then decrease, in favor of the formation of follow-up PTPs or mineralization.

3.4. PTPs performance under different environmental conditions

This part aims to evaluate if the PTPs formed at higher initial concentration are identical to the ones detected at lower concentrations. Furthermore, the effect of the changes in the experimental pH and temperature on the PTPs was investigated.

Fig. SI-21 shows the kinetics of the formation/elimination of the PTPs formed during the photolysis of TMP at different pH values. Some PTPs show an increase in A/A₀(%) by increasing the pH; others show a decrease in A/A₀(%) when the pH increases; while the A/A₀(%) value for other PTPs differs randomly independent on the pH value. So it can be concluded that there is no rule to describe the effect of the pH on the PTPs concentrations and formation kinetics. For example, PTP250 and PTP268 show an increase in the A/A₀(%) by decreasing the pH value, which could suggest that the loss of the dimethylamine group is favored at acidic pH, in which this dimethylamine group is in its ionized form and can easily remove. The time courses of PTP309a and PTP311 show an increase of A/A₀(%) in the following direction (pH9 > pH3 > pH7 > pH5). Furthermore, A/A₀(%) of the PTP210 and the PTP212 increase with increasing pH

value and they can hardly be seen in pH 3 condition. As it was mentioned before, PTP309a and PTP311 are formed by oxidation and hydroxylation of TMP, and PTP210 and PTP212 are formed from PTP309a and PTP311 by further loss of the 3-(dimethylamino)-2-methylpropyl chain. This suggests the conclusion that oxidation and hydroxylation can occur extensively in the alkaline media followed by the acidic then the neutral ones (pH9 > pH3 > pH7 > pH5). While the loss of the 3-(dimethylamino)-2-methylpropyl chain preferably takes place in alkaline media, and not in acidic media.

The kinetics of formation/elimination of TMP's PTPs formed during the photolysis experiments at different concentration levels are shown in Fig. SI-22. As can be seen, each PTP detected at the initial concentration of 100 mg L⁻¹ also occurred during the photolysis at 50 and 10 mg L⁻¹ of TMP. At the initial concentration of 5 mg L⁻¹, some PTPs are hardly detectable, which might be due to non-sufficient detection limits. The PTPs at lower concentrations show faster formation/elimination kinetics than those at higher concentrations (Unceta et al., 2010). The highest A/A₀(%) value for most of the PTPs is directly proportional to the initial TMP concentration.

The kinetics of formation/elimination of TMP's PTPs formed during the photolysis experiments at different temperatures are shown in Fig. SI-23. Some of the PTPs show the highest A/A₀(%) at 30 °C and 40 °C experiments like PTP134, PTP210, and PTP212, while others show the highest at 10 °C such as PTP311, PTP313, and PTP196.

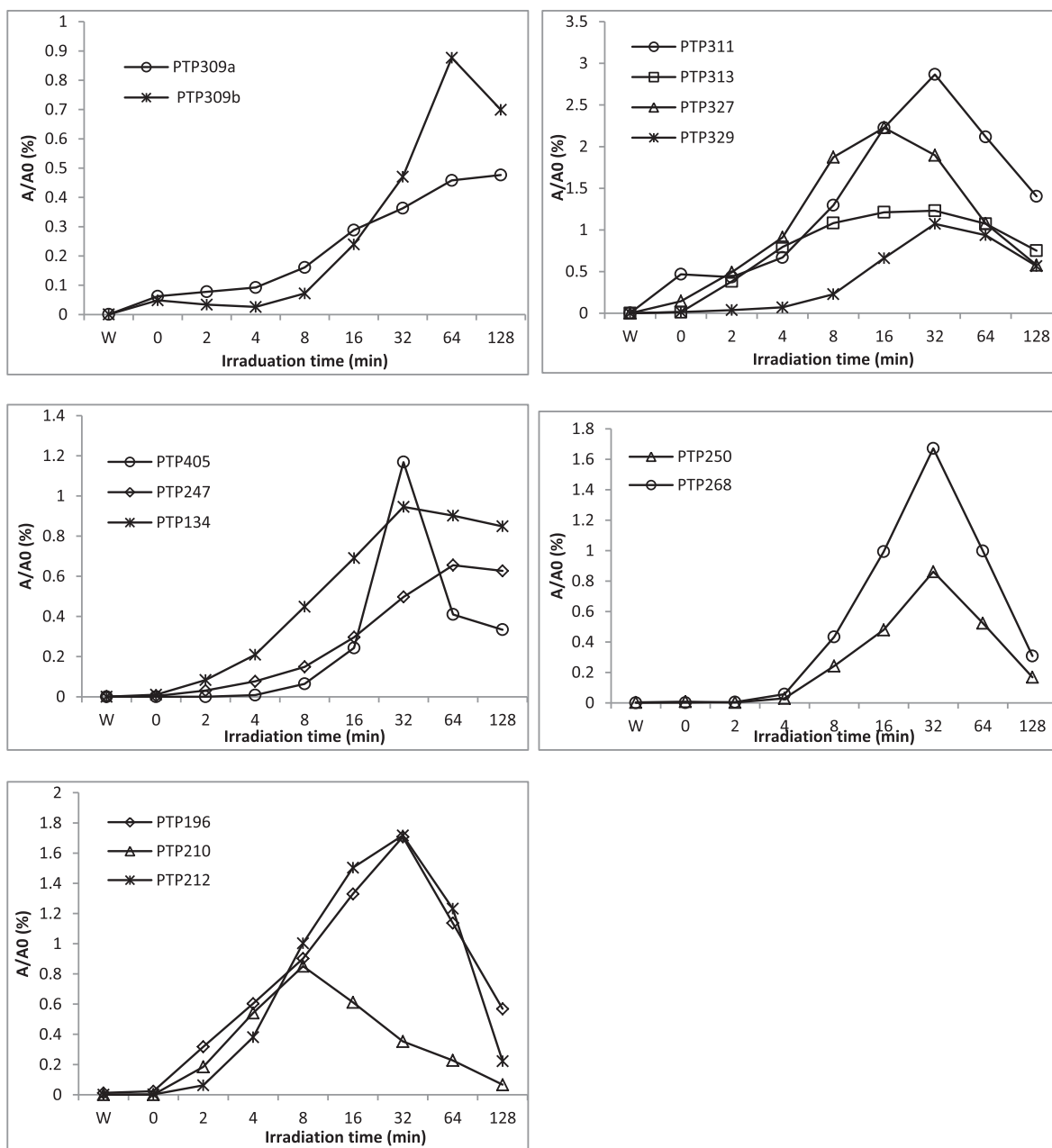


Fig. 5. Time curves of the relative peak area A/A_0 (%) of the PTPs during photolysis of TMP (pH 5, 20 °C) assigned to their m/z ratio (A is the peak area of the PTP at a specific time point, A_0 is the peak area of TMP (100 mg L⁻¹) at 0 min) (n = 3).

Table 3

Results of the investigated aerobic biodegradation test assays for TMP and its PTPs.

Biodegradation test	Test sample	Biodegradation% after 28 day	Parent compound elimination%	DOC removal%
CBT	0 min	10.6	0	
	16 min	15.8	2.4	
	128 min	27.0	11.0	
MRT	0 min	-8.1	0	6.0
	16 min	-3.9	3.5	24.4
	128 min	4.1	6.5	35.1

3.5. Aerobic biodegradation testing

In the two biodegradation tests performed, all validity criteria of the OECD guidelines were fulfilled. The activity of the inoculum in the quality controls was adequate and the test assays were valid according to the established guidelines. The results of the two test systems, CBT and MRT, for TMP and the samples taken after different times of irradiation are summarized in Table 3. TMP shows a low biodegradation regarding ThOD, amounted to 10.6% and –8.1% after 28 days in CBT and MRT, respectively. The recovery of TMP in CBT and MRT after 28 days were $95.5 \pm 5.8\%$ and $98.3 \pm 2.5\%$, respectively, based on LC–MS analysis. Therefore, TMP can be classified as a not readily biodegradable substance according to the test guidelines used. In MRT, the other pass criterion, according to the OECD guidelines, is a 70% removal of DOC value after 28 days, which is not reached in any of the tests performed. As TMP is not readily biodegradable substance, it could persist and accumulate in the environment. These results indicate that no bio-TPs of TMP were formed by biodegradation.

The biodegradation of photolysis samples taken after 16 and 128 min of UV-irradiation show a slight increase in the elimination in CBT and MRT compared to TMP (Table 3). At the same time, the slight increase in the DOC elimination during MRT after 28 days applied to the samples taken after 0 min, 16 min, and 128 min of photolysis indicate the possibility of biodegradation for some PTPs in biodegradation tests.

The samples from the start and the end of each biodegradation test assays were analyzed by the LC–MSⁿ. The peak areas of the PTPs at the start and end of CBT and MRT were compared as shown in Fig. 6. From Fig. 6, it can be observed that some of the formed PTPs are comparatively better biodegradable than TMP itself. In CBT and MRT, half of the detected PTPs showed recovery of approximately 100% after 28 days. Therefore, these PTPs are not biodegradable. Others PTPs show some degradation percentages. PTP210 is highly eliminated with 70.8% and 97.2% elimination in CBT and MRT, respectively. The second probably degradable one is PTP309b which gives 65.6% and 81.0% elimination in CBT and MRT,

respectively. Although, PTP212 is not degraded in the CBT at all, it shows elimination in MRT of 66.6%. The previously mentioned three PTPs (PTP210, PTP309b, and PTP212) show 0% elimination in their sterile samples in MRT, so they can be considered as biodegradable PTPs. PTP327 and PTP329 can be a partially biodegradable PTPs as they are not eliminated at all in the sterile samples. PTP327 shows 44.2% and 52.2% elimination in CBT and MRT, respectively, and PTP329 is eliminated with 35.3% in MRT. PTP134 is partially eliminated in CBT and MRT with 39.4% and 44.8%, respectively, combined with 56.6% elimination in the sterile sample. So PTP134 can be considered as a partially abiotically degradable PTP. PTP268, PTP250, and PTP196 show elimination during the MRT in both test and sterile samples indicating that they are removed abiotically in MRT. PTP196 is the highly abiotically removed one with 98.4% elimination, followed by PTP250 (53.5%), and finally comes PTP268 (51.0%).

3.6. QSAR

The predictive output of each software for TMP and its PTPs are summarized in Tables S1–S4.

3.6.1. *In silico* prediction of ready biodegradation

A compound is classified as either biodegradable or non-biodegradable depending on certain predicted activating and deactivating alerts, which are identified by all QSAR models. Most of the readily biodegradability models are based on OECD 301C MITI-I test. MITI-I test is not directly comparable to CBT as the inoculum concentration (bacterial density) in CBT is much lower than in MITI-I test, thus false positive results of prediction are more likely than false negative ones.

Both models of the Oasis Catalogic software and both models of EpiSuite software for ready biodegradability predicted the output values as < 0.03 for TMP (Tables S1–1). These output values are below the pass criterion for ready biodegradability under MITI-I test and MRT conditions. The result from Case Ultra about TMP biodegradability was negative. Accordingly, TMP has been

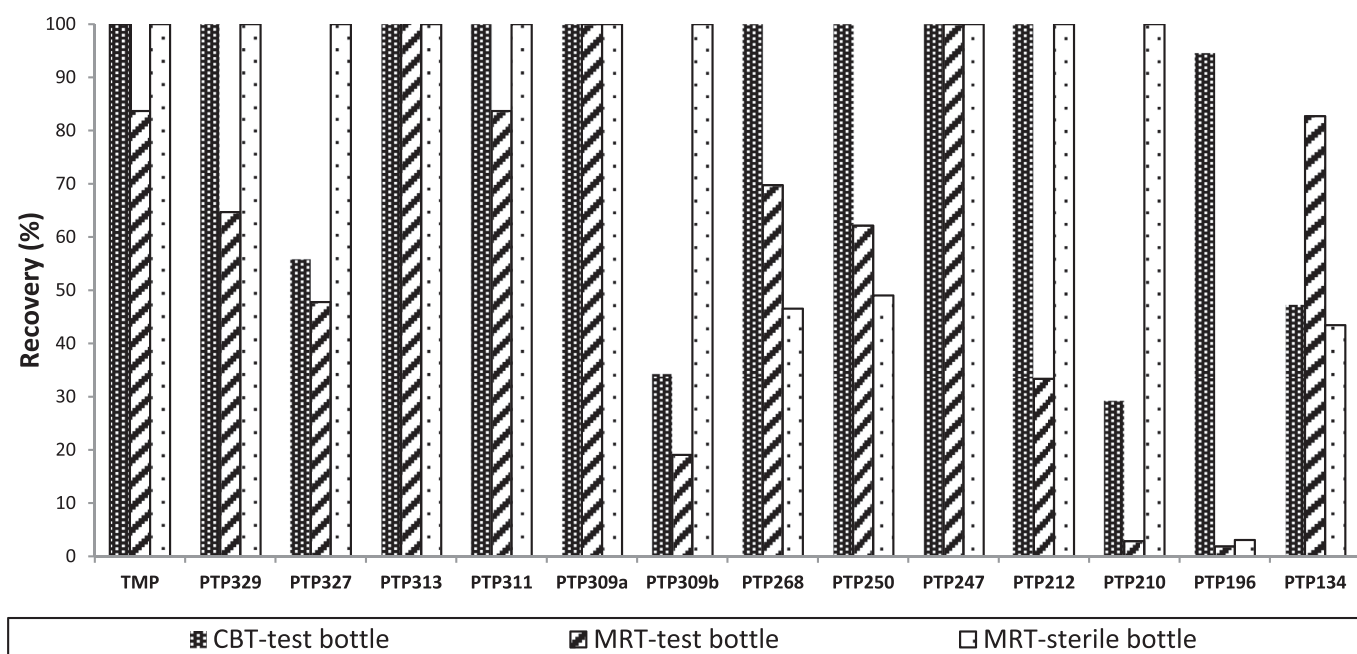


Fig. 6. Recovery of TMP's PTPs after 28 days related to day 0 in CBT and MRT.

categorized as a non-readily biodegradable chemical and this agrees with the results found experimentally in the CBT and MRT. In summary, *in silico* and the experimental performed biodegradation testing (CBT and MRT) confirmed that TMP is non-readily biodegradable, and therefore, it is expected to be present in the aquatic environments.

PTP313, PTP329, and PTP134 were predicted as readily biodegradable by the Case Ultra model, although the Oasis Catalogic (OECD 301F) predicted only PTP212 to be readily biodegradable (Table S1). EpiSuite models predicted PTP134 as readily biodegradable. The result from the Oasis Catalogic is in agreement with the LC-MS analysis results of the CBT and MRT samples, where PTP212 is found as a biodegradable PTP in all of them. While results from Case Ultra and EpiSuite shows some false positive results in comparison with the LC-MS analysis results. In the CBT and MRT, PTP313 and PTP212 are not eliminated at all and PTP329 and PTP134 are partially eliminated, although all of the previously mentioned PTPs are predicted to be readily biodegradable by Case Ultra and EpiSuite.

3.6.2. *In silico* toxicity predictions

The *in silico* assessment of the mutagenicity, teratogenicity, carcinogenicity, and genotoxicity of TMP and its PTPs are summarized in Table SI-2 & SI-3. TMP is known to be teratogenic and mostly all of its PTPs were predicted to be also teratogenic in all of the models used. On the contrary, there was no positive alert from the different models of the ICH M7 guideline conformal set from Case Ultra for TMP and its PTPs mutagenicity or genotoxicity. Although it cannot be completely excluded that these PTPs might have a toxic effect in the environment, as some of the PTPs were out of domain in the applied Case Ultra models.

The three acute *V. fischeri* modules (Oasis Catalogic) predicted PTP309a, and PTP250 more toxic than TMP because of their predicted lower IC₅₀ (mg/L) values. PTP247-4 and PTP247-8 showed positive alert in the Microtox Toxicity to Environmental Bacteria module (Case Ultra) (Tables SI-4). All of these predicted toxic PTPs are not biodegradable in both *in silico* and experimental tests, except PTP250 which is found to be a partially abiotically degradable product in MRT. The *in silico* QSAR assessment of the PTPs revealed significant increases in the potential aquatic toxicity against *V. fischeri* as compared to their parent compounds.

4. Conclusion

In the present study, the environmental fate and behavior of the teratogenic pharmaceutical TMP was assessed for the first time by studying its UV photo-degradability under different concentration levels. In addition, the biodegradability and the toxicity assessment of TMP and its PTPs were assessed. The solution pH and temperature affect both TMP degradation rate and the PTPs formation kinetics and mechanism, so they are important parameters that should be considered during studying the fate of pharmaceuticals in the environment. TMP was not completely eliminated or mineralized by UV photolysis at high initial concentrations in UP water. Even at lower concentrations, a long irradiation time was necessary to mineralize TMP. Additionally, 14 PTPs were proposed as UV products of TMP, few of them are previously reported as TMP metabolites. TMP and most of its PTPs are not eliminated after biodegradation testing, and therefore could be persistent in the environment. On the other hand, some PTPs such as PTP210 and PTP309b show better elimination in the biodegradation tests. The *in silico* QSAR toxicity assessment performed in this study provides a first indication that photo-degradation of TMP might lead to non-biodegradable PTPs that are more toxic than their respective parent compounds, so the risk assessment of these byproducts in aquatic

environments cannot be ignored.

Therefore, further investigations should be conducted regarding the environmental occurrence and the adverse effects of the formed PTPs of TMP.

Acknowledgement

The authors would like to thank the Federal Ministry of Research and Education for their financial support (grant no. 02WRS1280A - J). Financial supports from the Leuphana University Lüneburg (Project “KFP 73100004”) for WMMM are gratefully acknowledged. The authors wish to thank Dr. Annette Haiss and B.Sc. Evgenia Logunova for planning the aerobic biodegradation tests, and to thank Janin Westphal for the analytical support. The authors also acknowledge Multicase Inc. for kindly providing the Case Ultra software.

Appendix A. Supplementary data

Supplementary data related to this article can be found at <http://dx.doi.org/10.1016/j.watres.2016.10.078>.

References

- Chakravarti, S.K., Saiakhov, R.D., Klopman, G., 2012. Optimizing predictive performance of CASE Ultra Expert system models using the applicability domains of individual toxicity alerts. *J. Chem. Inf. Model.* 52 (10), 2609–2618.
- Chiffre, A., Clérandeau, C., Dwoinikoff, C., Le Bihanic, F., Budzinski, H., Geret, F., Cachot, J., 2016. Psychotropic drugs in mixture alter swimming behaviour of Japanese medaka (*Oryzias latipes*) larvae above environmental concentrations. *Environ. Sci. Pollut. Res.* 23 (6), 4964–4977.
- Contrera, J.F., 2013. Validation of Toxtree and SciQSAR *in silico* predictive software using a publicly available benchmark mutagenicity database and their applicability for the qualification of impurities in pharmaceuticals. *Regul. Toxicol. Pharmacol.* 67 (2), 285–293.
- Fakhari, A.R., Tabani, H., Nojavan, S., Abedi, H., 2012. Electromembrane extraction combined with cyclodextrin-modified capillary electrophoresis for the quantification of trimipramine enantiomers. *Electrophoresis* 33 (3), 506–515.
- Fraser, A.D., Isner, A.F., Perry, R.A., 1987. Distribution of trimipramine and its major metabolites in a fatal overdose case. *J. Anal. Toxicol.* 11.
- Gros, M., Williams, M., Llorca, M., Rodríguez-Mozaz, S., Barceló, D., Kookana, R.S., 2015. Photolysis of the antidepressants amisulpride and desipramine in wastewaters: identification of transformation products formed and their fate. *Sci. Total Environ.* 530–531, 434–444.
- Gualano, M.R., Bert, F., Mannocci, A., La Torre, G., Zeppengo, P., Siliquini, R., 2014. Consumption of antidepressants in Italy: recent trends and their significance for public health. *Psychiatr. Serv.* 65 (10).
- Gunasekar, V., Divya, B., Brinda, K., Vijaykrishnan, J., Ponnusami, V., Rajan, K.S., 2013. Enzyme mediated synthesis of Ag–TiO₂ photocatalyst for visible light degradation of reactive dye from aqueous solution. *J. Sol-Gel Sci. Technol.* 68 (1), 60–66.
- Gurke, R., Rossmann, J., Schubert, S., Sandmann, T., Rößler, M., Oertel, R., Fauler, J., 2015. Development of a SPE-HPLC–MS/MS method for the determination of most prescribed pharmaceuticals and related metabolites in urban sewage samples. *J. Chromatogr. B* 990, 23–30.
- Hazime, R., Ferronato, C., Fine, L., Salvador, A., Jaber, F., Chovelon, J.-M., 2012. Photocatalytic degradation of imazalil in an aqueous suspension of TiO₂ and influence of alcohols on the degradation. *Appl. Catal. B Environ.* 126, 90–99.
- Herrmann, M., Menz, J., Olsson, O., Kümmerer, K., 2015a. Identification of photo-transformation products of the antiepileptic drug gabapentin: biodegradability and initial assessment of toxicity. *Water Res.* 85, 11–21.
- Herrmann, M., Olsson, O., Fiehn, R., Herrel, M., Kümmerer, K., 2015b. The significance of different health institutions and their respective contributions of active pharmaceutical ingredients to wastewater. *Environ. Int.* 85, 61–76.
- Huerta-Fontela, M., Galceran, M.T., Ventura, F., 2011. Occurrence and removal of pharmaceuticals and hormones through drinking water treatment. *Water Res.* 45 (3), 1432–1442.
- Hussain, M.S., Coutts, R.T., Baker, G.B., Micetich, R.G., Daneshmand, M., 1991. Metabolism of antidepressants: urinary metabolites of trimipramine in the rat. *Prog. Neuro-Psychopharmacol. Biol. Psychiatry* 15 (2), 285–289.
- International Conference on Harmonization (ICH), 2014. ICH Guideline M7. http://www.ich.org/fileadmin/Public_Web_Site/ICH_Products/Guidelines/Multidisciplinary/M7/M7_Step_4.pdf (Accessed on 18 02 2014).
- Khaleel, N.D.H., Mahmoud, W.M., Hadad, G.M., Abdel-Salam, R.A., Kümmerer, K., 2013. Photolysis of sulfamethoxy-pyridazine in various aqueous media: aerobic biodegradation and identification of photoproducts by LC-UV–MS/MS. *J. Hazard. Mater.* 244–245, 654–661.

- Khaleel, N.D.H., Mahmoud, W.M.M., Olsson, O., Kümmerer, K., 2016. UV-photo-degradation of desipramine: impact of concentration, pH and temperature on formation of products including their biodegradability and toxicity. *Sci. Total Environ.* 826–840, 566–567.
- Keen, O.S., Thurman, E.M., Ferrer, I., Dotson, A.D., Linden, K.G., 2013. Dimer formation during UV photolysis of diclofenac. *Chemosphere* 93 (9), 1948–1956.
- Kwon, J.-W., Armbrust, K.L., 2004. Hydrolysis and photolysis of paroxetine, a selective serotonin reuptake inhibitor, in aqueous solutions. *Environ. Toxicol. Chem.* 23 (6), 1394–1399.
- Laboratory of Mathematical Chemistry, 2012. OASIS Catalogic Software V. 5.11.6 TB. <http://oasis-lmc.org/>.
- Li, K., Zhang, P., Ge, L., Ren, H., Yu, C., Chen, X., Zhao, Y., 2014. Concentration-dependent photodegradation kinetics and hydroxyl-radical oxidation of phenicol antibiotics. *Chemosphere* 111, 278–282.
- Llinas, A., Glen, R.C., Goodman, J.M., 2008. Solubility challenge: can you predict solubilities of 32 molecules using a database of 100 reliable measurements? *J. Chem. Inf. Model.* 48 (7), 1289–1303.
- Mahmoud, W.M.M., Toolaram, A.P., Menz, J., Leder, C., Schneider, M., Kümmerer, K., 2014. Identification of phototransformation products of thalidomide and mixture toxicity assessment: an experimental and quantitative structural activity relationships (QSAR) approach. *Water Res.* 49, 11–22.
- Marvin Sketch Version: 15.6.15.0, 2015. ChemAxon Ltd. <http://www.chemaxon.com>.
- Ministry of International Trade and Industry, Japan, OECD, 2006. Ready Biodegradability: Modified MITI Test (1).
- OECD, 1992. Guidelines for the Testing of Chemicals: Ready Biodegradability.
- OECD, 2008. Guidelines for Testing of Chemicals: Test No. 316: Phototransformation of Chemicals in Water Direct Photolysis. OECD Pub, Paris.
- Optenberg, S.A., Lancôt, K.L., Nathan, H., Oh, P.I., 2002. Antidepressant selection, healthcare resource consumption and costs in a large workplace environment resource consumption and cost a large workplace environment. *Clin. Drug Investig.* 22 (10), 685–694.
- Palm, W.-U., Millet, M., Zetzsch, C., 1997. Photochemical reactions of metamitron. *Chemosphere* 35 (5), 1117–1130.
- Rastogi, T., Leder, C., Kümmerer, K., 2014. Qualitative environmental risk assessment of photolytic transformation products of iodinated X-ray contrast agent diatrizoic acid. *Sci. Total Environ.* 482–483, 378–388.
- Reddy, S., Iden, C.R., Brownawell, B.J., 2005. Analysis of steroid conjugates in sewage influent and effluent by liquid chromatography-Tandem mass spectrometry. *Anal. Chem.* 77 (21), 7032–7038.
- Saiakhov, R., Chakravarti, S., Klopman, G., 2013. Effectiveness of CASE Ultra Expert system in evaluating adverse effects of drugs. *Mol. Inf.* 32 (1), 87–97.
- Schwabe, U., Paffrath, D., 2015. *Arzneiverordnungs-Report2015*.
- Singh, S., Basu, S., Sanyal, A.K., 1978. Trimipramine maleate induced malformations in chick embryos. *Indian J. Med. Res.* 67, 682–691.
- Tiefenbacher, E.-M., Haen, E., Przybilla, B., Kurz, H., 1994. Photodegradation of some quinolones used as antimicrobial therapeutics. *J. Pharm. Sci.* 83 (4), 463–467.
- Trovó, A.G., Paiva, V.A.B., Costa Filho, B.M., Machado, A.E.H., Oliveira, C.A., Santos, R.O., Daniel, D., 2014. Photolytic degradation of chloramphenicol in different aqueous matrices using artificial and solar radiation: reaction kinetics and initial transformation products. *J. Braz. Chem. Soc.* 25 (11), 2007–2015.
- Tuckerman, M.M., 1984. In: Florey, Klaus (Ed.), *Analytical Profiles of Drug Substances*, vol. 12. Academic Press, 111 Fifth Avenue, New York, NY 10003, 1983. 735pp. *Journal of Pharmaceutical Sciences* 73(4), 572.
- Unceta, N., Sampedro, M.C., Bakar, N.K.A., Gómez-Caballero, A., Goicolea, M.A., Barrio, R.J., 2010. Multi-residue analysis of pharmaceutical compounds in wastewaters by dual solid-phase microextraction coupled to liquid chromatography electrospray ionization ion trap mass spectrometry. *J. Chromatogr. A* 1217 (20), 3392–3399.
- US EPA, 2012. Estimation Programs Interface Suite™, V. 4.11. United States Environmental Protection Agency, Washington, DC, USA.
- Vargas, F., Matskevitch, V., Sarabia, Z., 1995. Photodegradation and in vitro phototoxicity of the antidiabetic drug chlorpropamide. *Arzneimittelforschung* 45 (10), 1079–1081.
- Zepp, R.G., 1978. Quantum yields for reaction of pollutants in dilute aqueous solution. *Environ. Sci. Technol.* 12 (3), 327–329.

Supporting Information for
Initial fate assessment of teratogenic drug trimipramine and its photo-
transformation products – role of pH, concentration and temperature

Nareman D. H. Khaleel,^{1, 2} Waleed M. M. Mahmoud,^{1, 2} Oliver Olsson,¹ Klaus
Kümmerer,^{1*}

1- Sustainable Chemistry and Material Resources, Institute of Sustainable and Environmental Chemistry, Leuphana University of Lüneburg, Scharnhorststraße 1 C13, DE-21335 Lüneburg, Germany.

2- Pharmaceutical Analytical Chemistry Department, Faculty of Pharmacy, Suez Canal University, Ismailia 41522, Egypt.

Pages: 41

Texts: 3

Figures: 23

Tables:4

* Corresponding author. Address: Nachhaltige Chemie und Stoffliche Ressourcen, Institut für Nachhaltige Chemie und Umweltchemie, Leuphana Universität Lüneburg, C.13, Scharnhorststraße 1, D-21335 Lüneburg, Germany.

Tel.: +49 4131 677-2893

E-mail address: klaus.kuemmerer@leuphana.de (K. Kümmerer).

Table of content

Texts:

Text SI-1: Quantum yield calculation using actinometer.....	S4
Text SI-2: LC-MS Analytical method parameter for the elution and identification of the photo-transformation products (PTPs) of Trimipramine (TMP).....	S4
Text SI-3: <i>In silico</i> prediction values interpretation.....	S5

Figures:

Figure SI-1: Emission spectrum for medium pressure Hg (mercury) lamp and the relative absorbance spectrum of 100 mg L ⁻¹ Trimipramine (TMP).....	S6
Figure SI-2: the change in the molar absorption coefficient (ϵ) as a function of the solution pH (TMP concentration = 100 mg L ⁻¹).....	S7
Figure SI-3: TMP structure at different pH, pKa = 9.42.....	S7
Figure SI-4: The changes in pH values during the UV-irradiation of DMI under different pH values.....	S8
Figure SI-5: First-order plot of UV-photodegradation of TMP for different initial concentrations.....	S8
Figure SI-6: The changes in the UV-photodegradation rate of MP as a function of the initial concentration; pH = 5, Temperature = 20 °C.....	S9
Figure SI-7: Arrhenius plot for degradation of TMP by UV irradiation at different temperatures.....	S9
Figure SI-8: Fragmentation pattern of TMP according to MS ⁿ obtained from LC-HRMS.....	S10
Figure SI-9: Fragmentation pattern of PTP ₃₁₁ according to MS ⁿ obtained from LC-HRMS.....	S11
Figure SI-10: Fragmentation pattern of PTP ₃₁₃ according to MS ⁿ obtained from LC-HRMS..	S12
Figure SI-11: Fragmentation pattern of PTP ₃₂₇ according to MS ⁿ obtained from LC-HRMS...	S13
Figure SI-12: Fragmentation pattern of PTP ₃₂₉ according to MS ⁿ obtained from LC-HRMS...	S14
Figure SI-13: Fragmentation pattern of PTP _{309a} according to MS ⁿ obtained from LC-HRMS..	S15
Figure SI-14: Fragmentation pattern of PTP _{309b} according to MS ⁿ obtained from LC-HRMS..	S16
Figure SI-15: Fragmentation pattern of PTP ₂₆₈ according to MS ⁿ obtained from LC-HRMS...	S17
Figure SI-16: Fragmentation pattern of PTP ₁₉₆ according to MS ⁿ obtained from LC-HRMS...	S18
Figure SI-17: Fragmentation pattern of PTP ₂₁₀ according to MS ⁿ obtained from LC-HRMS...	S19

Figure SI-18: Fragmentation pattern of PTP₄₀₅ according to MSⁿ obtained from LC-HRMS... **S20**

Figure SI-19: Fragmentation pattern of PTP₂₄₇ according to MSⁿ obtained from LC-HRMS... **S21**

Figure SI-20: Fragmentation pattern of PTP₁₃₄ according to MSⁿ obtained from LC-HRMS... **S22**

Figure SI-21: Time curves of the relative peak area A/A_0 (%) of products (PTPs) during photolysis at different pH values..... **S23+24**

Figure SI-22: Time curves of the relative peak area A/A_0 (%) of products (PTPs) during photolysis at different concentrations..... **S25+26**

Figure SI-23: Time curves of the relative peak area A/A_0 (%) of products (PTPs) during photolysis at different temperatures..... **S27+28**

Tables:

Table SI-1: a) Q-SAR predictions for TMP and its PTPs for ready biodegradability by different models **S29-33**

Table SI-2: QSAR toxicity predictions according to ICH M7 guidance for TMP and its PTPs using Case Ultra software **S34-S36**

Table SI-3: QSAR teratogenicity predictions for TMP and its PTPs by different models (Case Ultra software)..... **S37-38**

Table SI-4: . The predicted bacterial toxicity of DMI and its PTPs with four acute toxicity models for *Vibrio fischeri* **S39-41**

Text SI-1:

The fluence rate under Hg lamp irradiation was determined by chemical actinometry using metamitron as an actinometer assuming a wavelength-independent quantum yield and using the emission spectrum of the lamp (data measured by BLACK-Comet UV-VIS spectroradiometer (StellarNet Inc., Florida, USA)).

The relative photon flux ($J_{\lambda\text{rel}}$) was measured in terms of relative counts using a Black Comet UV-VIS spectrometer. The conversion factor f was calculated to characterize the actual intensity of the lamp. The absolute photon flux ($J_{\lambda\text{abs}}$) could be calculated by means of f and $J_{\lambda\text{rel}}$ (Eq. (2)).

$$\text{Faktor } F = \frac{\frac{dc}{dt}}{\Phi_{\text{Act}} \times \sum_{200\text{nm}}^{400\text{nm}} (2.303 \times J_{\lambda\text{rel}} \times \epsilon_{\lambda} \times c \times l)} \quad (1)$$

$$J_{\lambda\text{abs}} = J_{\lambda\text{rel}} \cdot F \quad (2)$$

Where F is the conversion factor, dc/dt is the photolysis rate of the actinometer, Φ_{Act} is the quantum yield of the actinometer, $J_{\lambda\text{rel}}$ is the relative photon flux of each wavelength (counts); ϵ_{λ} is the molar absorption coefficient ($\text{L mol}^{-1} \text{cm}^{-1}$), c is the initial concentration (mol L^{-1}), l is the path length of the (cm).

Text SI-2:

The LC-ITMS system comprising an HPLC 1100 series (Agilent Technologies, Böblingen, Germany) consisting of binary pumps (G1312A), column oven (G1316A), degasser (G1322A), and auto sampler (ALS G1329A + ALS Therm G1330), coupled to a Bruker data analysis system and atmospheric pressure electrospray ionization interface (Bruker Daltonic GmbH, Bremen, Germany). data acquisition and processing were performed using the associated Data analysis V.4 and Quant analysis V.2 software. The Esquire 6000 plus MS analysis was carried out in positive ionization mode using an ion spray voltage of 4160 V. The nebulizer (air) pressure was set at 30 psi. The Ion Spray source was operated at 350 °C dry temperature with dry gas flow equal 12 L min⁻¹. The other operating conditions of the source were: - 500 V end plate, + 4160 V capillary voltage. The selected lens and block voltages were: +50.0 V capillary exit, +9.29 V octopole 1, +1.89 V octopole 2, 204.2 Vpp octopole reference amplitude, 39.1 V skimmer, 36.4 trap drive, -3.5 V lens 1 and -65.5 V lens 2. The scan range was determined from m/z 40 to 1000.

LTQ-Orbitrap XL mass spectrometer interfaced with heated electrospray ionization (HESI) source (Thermo Scientific, Bremen, Germany) was used for the determination of the

accurate masses of TMP's PPTPs. The LC–MS system comprising a Dionex UHPLC system (Ultimate 3000) consisting of two HPG-3400-RS binary pumps, a TCC-3000 column oven, a SRD-3600 degasser, and an auto sampler WPS-3000-TRS. UV detection was performed using a VWD-3400RS detector. The spectrometer was operated also in positive mode under the following conditions: spray voltage 4 kV, capillary voltage 19 V and tube lens voltage 75 V. The heated capillary and desolvation temperatures were 275 °C and 150 °C, respectively. Nitrogen served as sheath, auxiliary and sweep gas with flow rate equal 20, 5 and 0 arb, respectively. MS data were recorded in the full scan mode (m/z 100–400). Fragmentation to MS^4 was achieved by setting collision induced dissociation (CID) on 35 eV. All data were processed using Xcalibur/Qual Browser 2.1.0 SP1 build 1160 (Thermo Scientific, Bremen, Germany).

Text SI-3:

The Oasis Catalogic models predicted the ready biodegradability as a numerical value between 1 and 0, corresponding to 100% and 0% biodegradation, respectively. The numeric value of 0.6 corresponds to 60% biodegradation, which is a pass criterion for ready biodegradability under MITI-I test conditions. In EPI Suite models (Biodegradation probability Biowin 5 and 6), “Readily biodegradable” was assigned a numeric value of 1 and “not readily biodegradable” was assigned a numeric value of 0 (0 to 1 is the range of probability of undergoing biodegradation). The Case Ultra provides positive (+), negative (–), out of domain (OD) and inconclusive (\pm) results. An inconclusive result indicates that a positive alert was found in the test compound but the calculated probability falls within the grey zone of the model (10% around the classification threshold of the model) and, therefore, a concrete alert prediction cannot be provided for the given models.

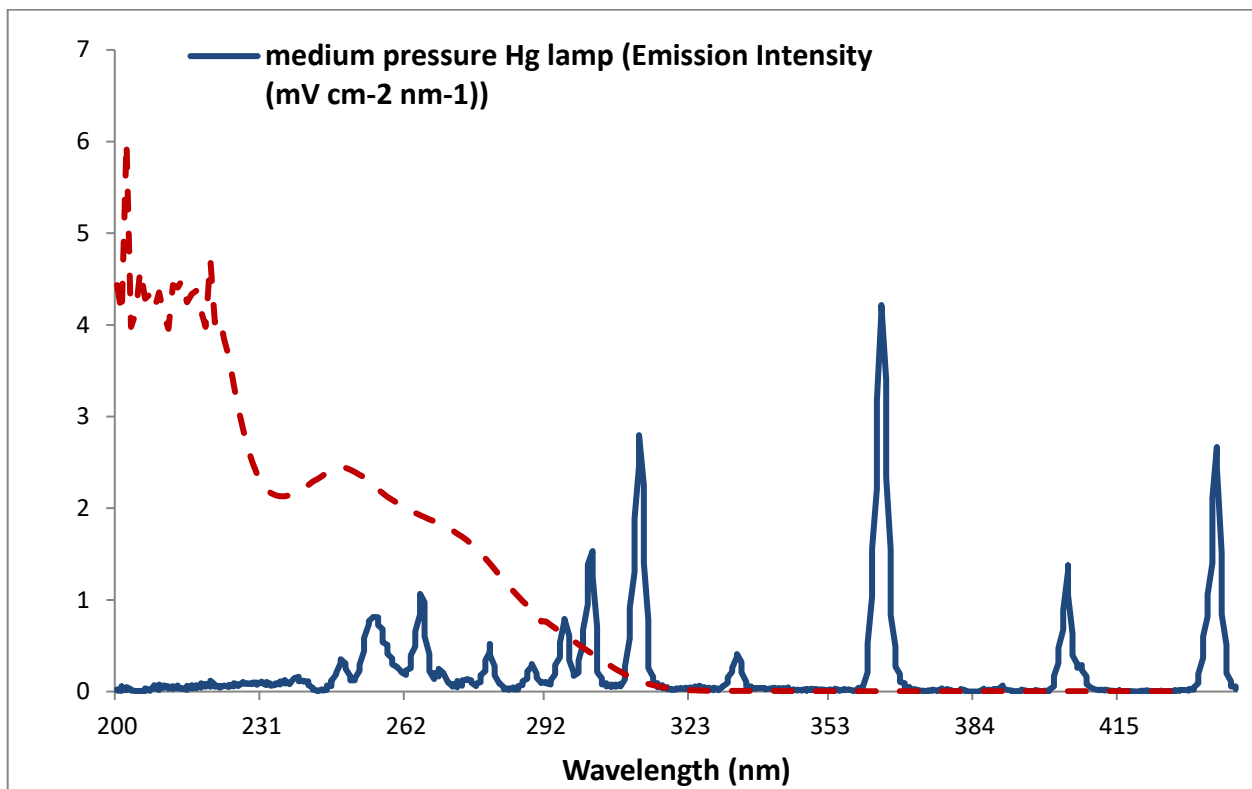


Figure SI-1: Emission spectrum for medium pressure Hg (mercury) lamp and the relative absorbance spectrum of 100 mg L⁻¹ trimipramine (TMP)

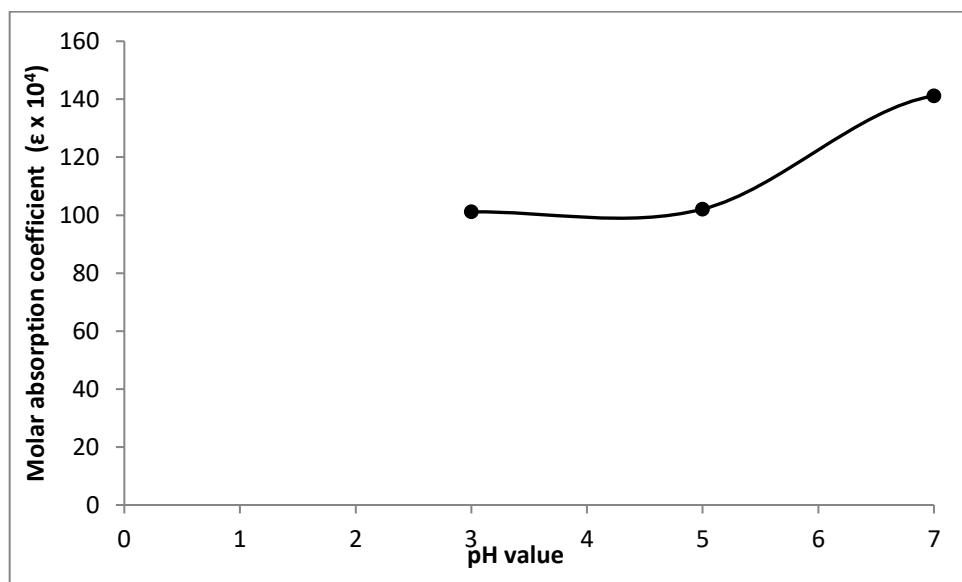


Figure SI-2: the change in the molar absorption coefficient (ϵ) as a function of the solution pH (TMP concentration = 100 mg L^{-1}).

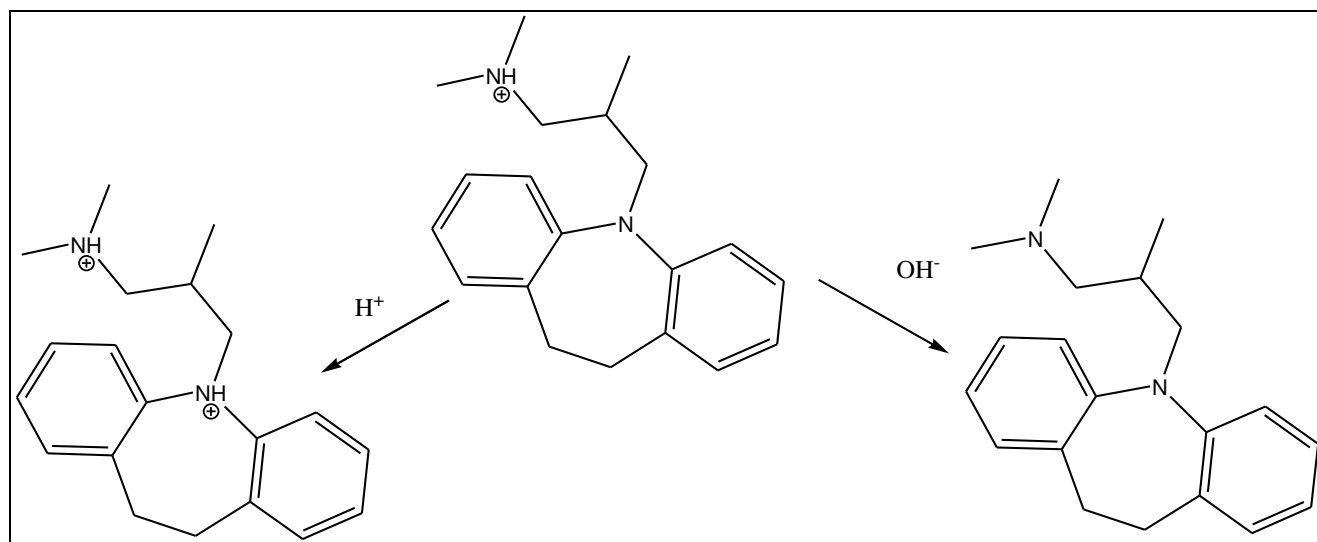


Figure SI-3: TMP structure at different pH, $\text{pK}_a = 9.42$.

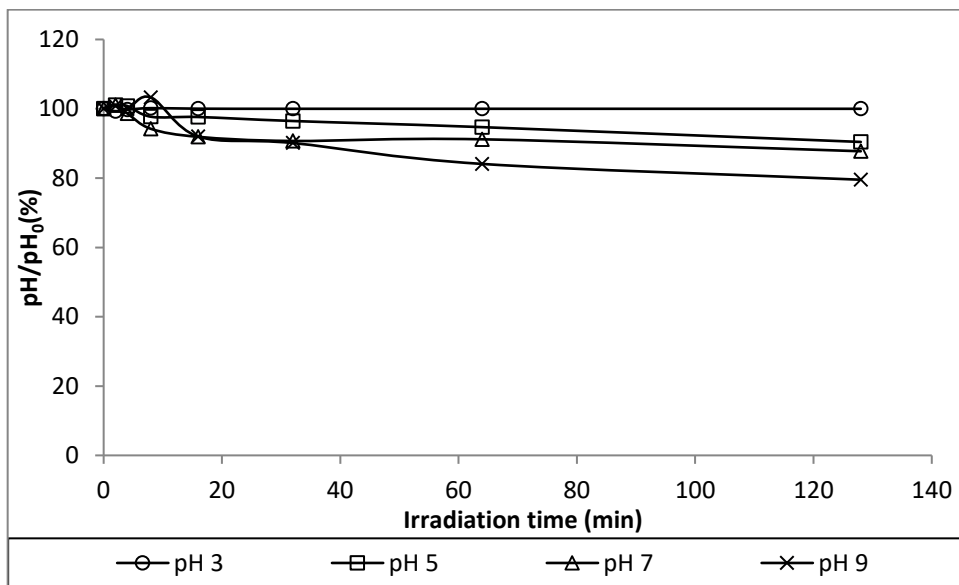


Figure SI-4: The changes in pH values during the UV-irradiation of TMP under different pH values (pH : is the pH value at certain UV irradiation time point, pH₀ is the pH value at time 0).

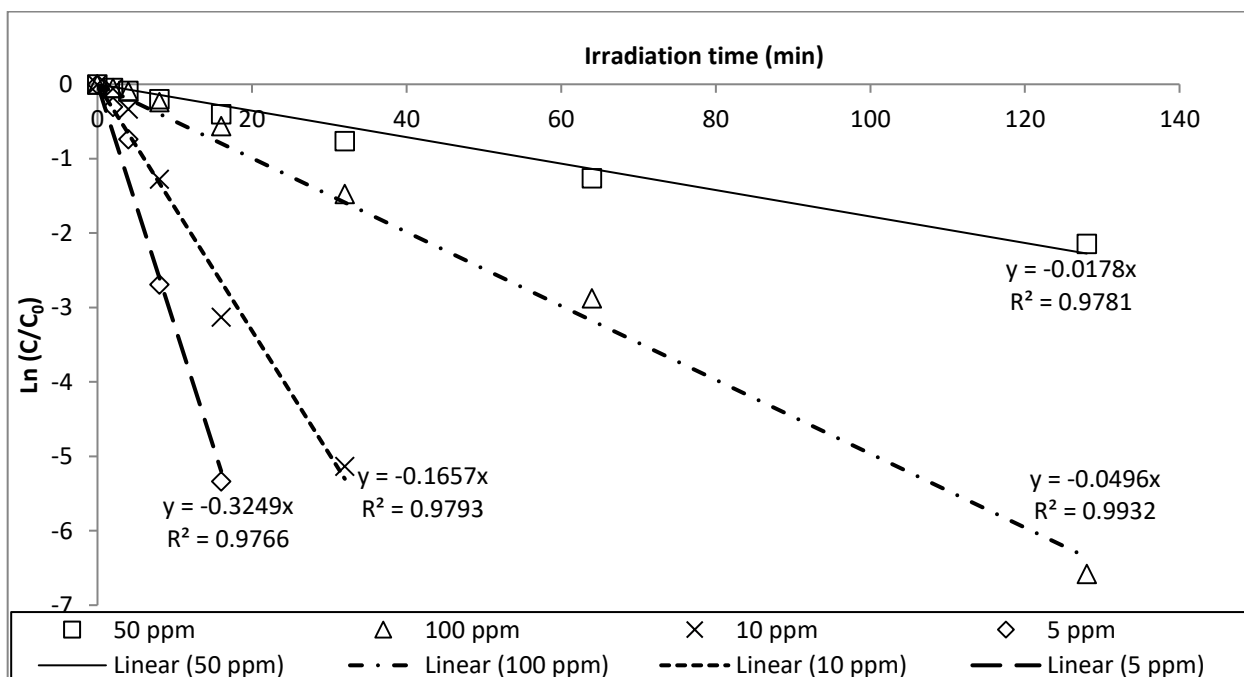


Figure SI-5: First-order plot of UV-photodegradation of TMP for different initial concentrations.

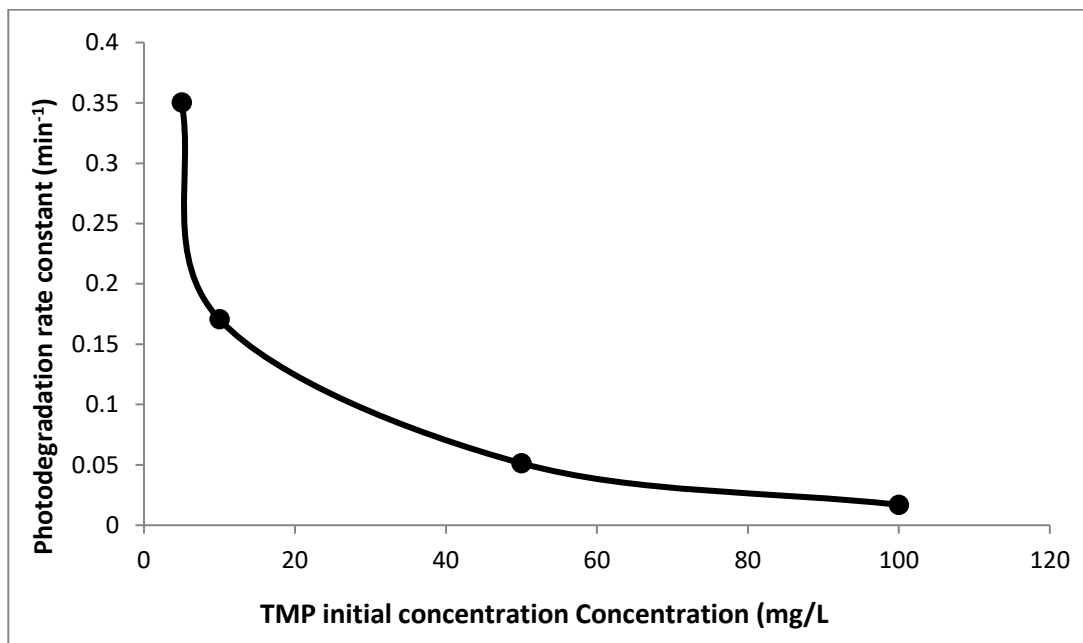


Figure SI-6: The changes in the UV-photodegradation rate of MP as a function of the initial concentration; pH = 5, Temperature = 20 °C.

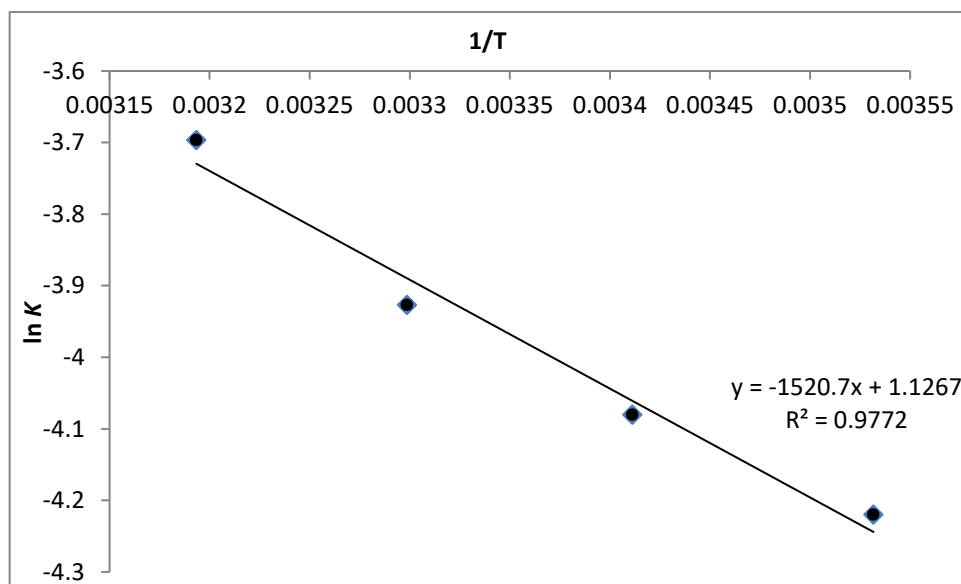


Figure SI-7: Arrhenius plot for degradation of TMP by UV irradiation at different temperatures.

Trimipramine (TMP)

100TMP-UV-32min-C18nucleoshell-140617b #931 RT: 10.44 AV: 1 NL: 5.46E7
T: FTMS + c ESI d Full ms2 295.22@cid35.00 [7]

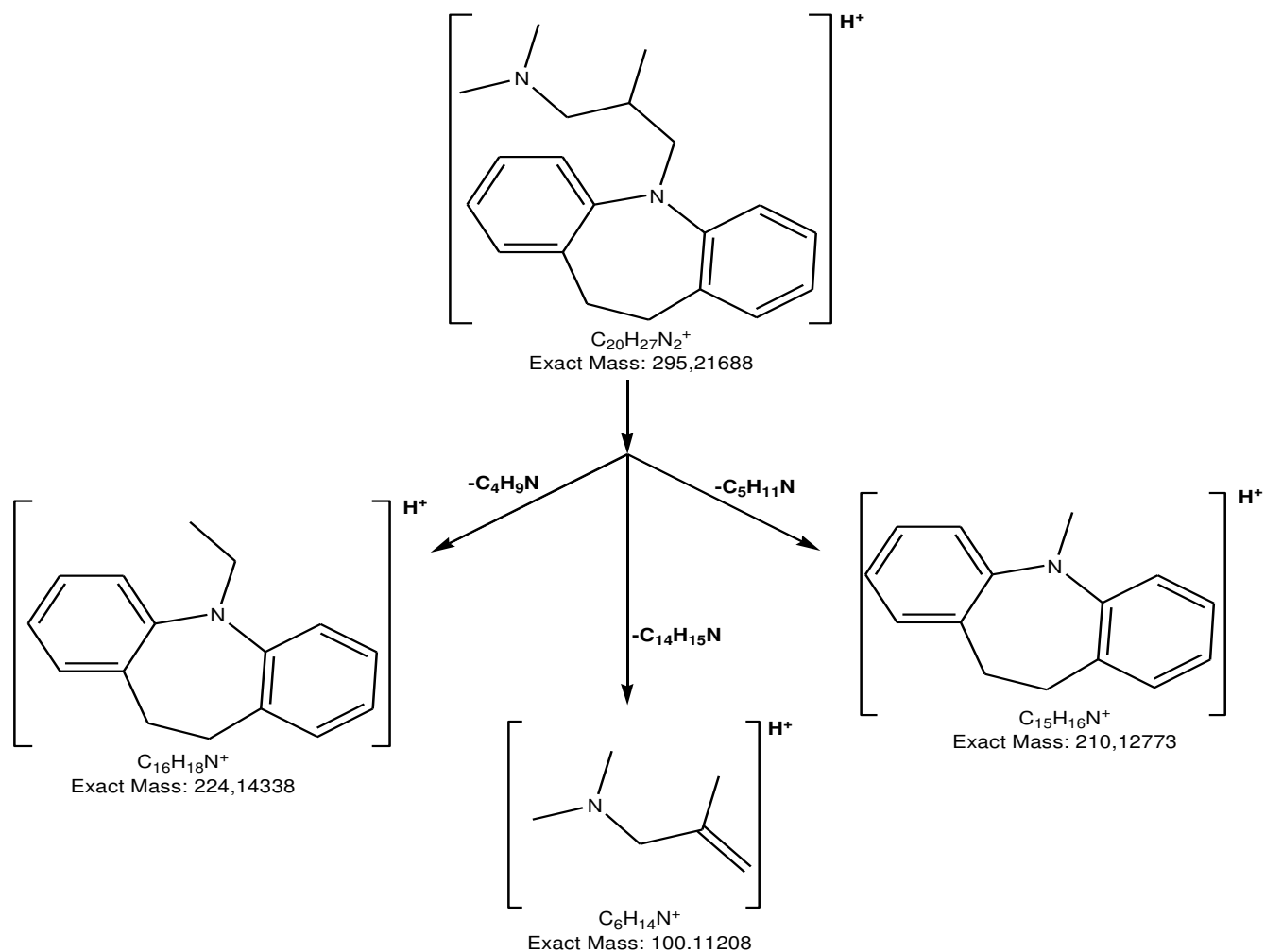
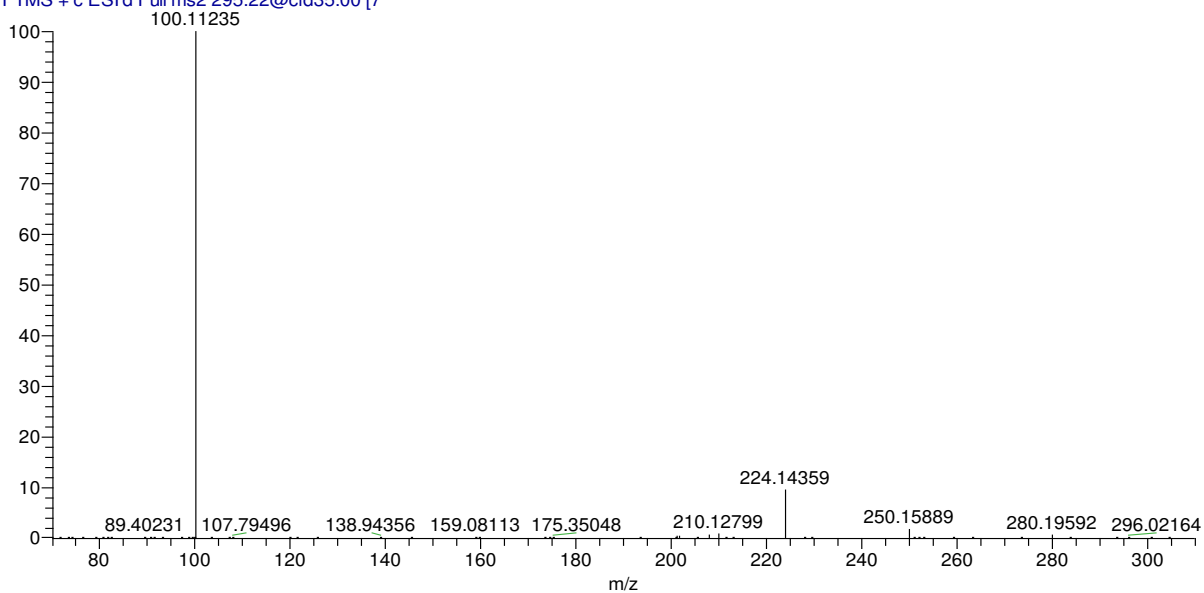


Figure SI-8: Fragmentation pattern of TMP according to MS² obtained from LC-HRMS

PTP311

100TMP-UV-64min-C18nucleoshell-140617b #906 RT: 10.15 AV: 1 NL: 1.97E5
T: FTMS + c ESI d Full ms2 311.21@cid35.00 [7]

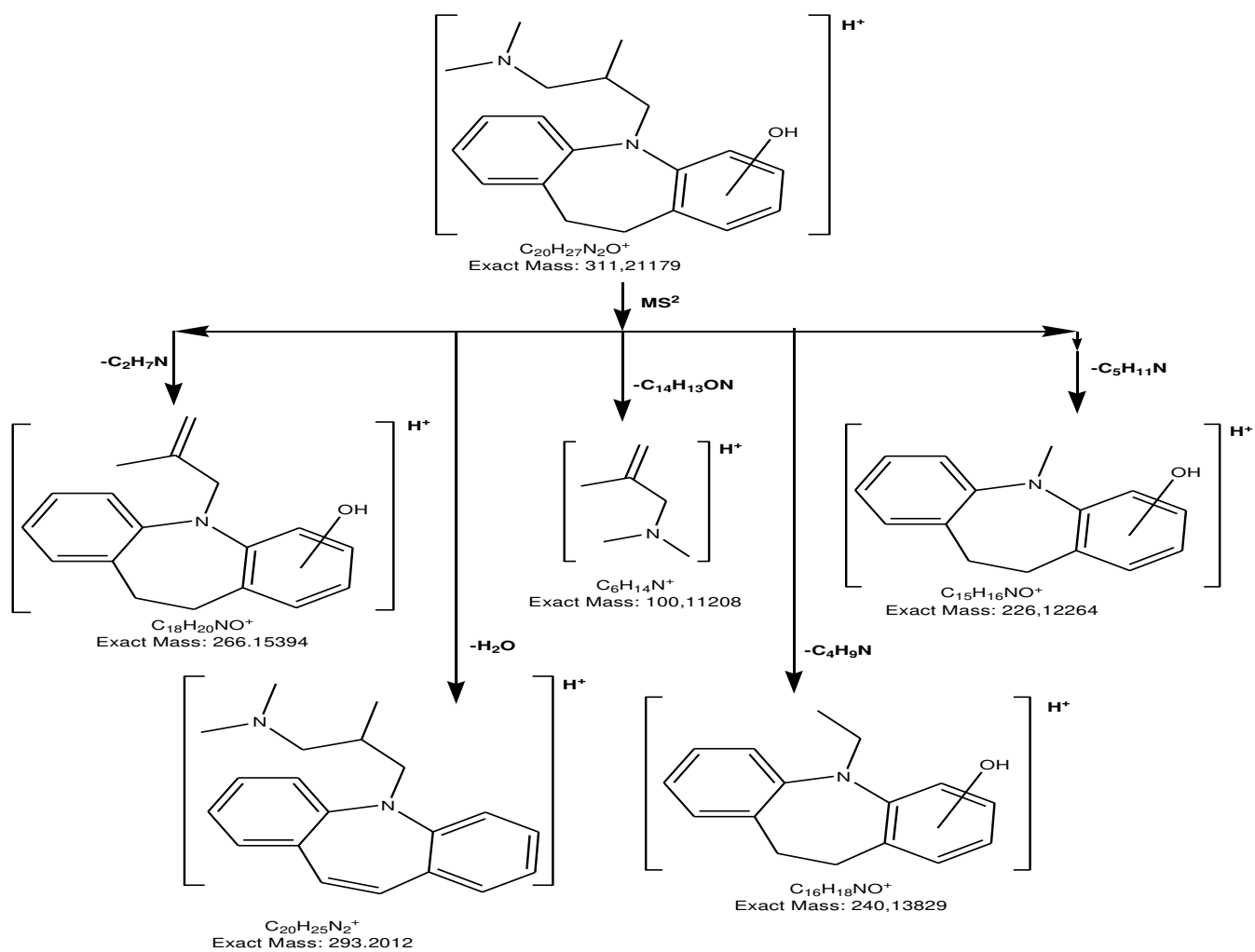
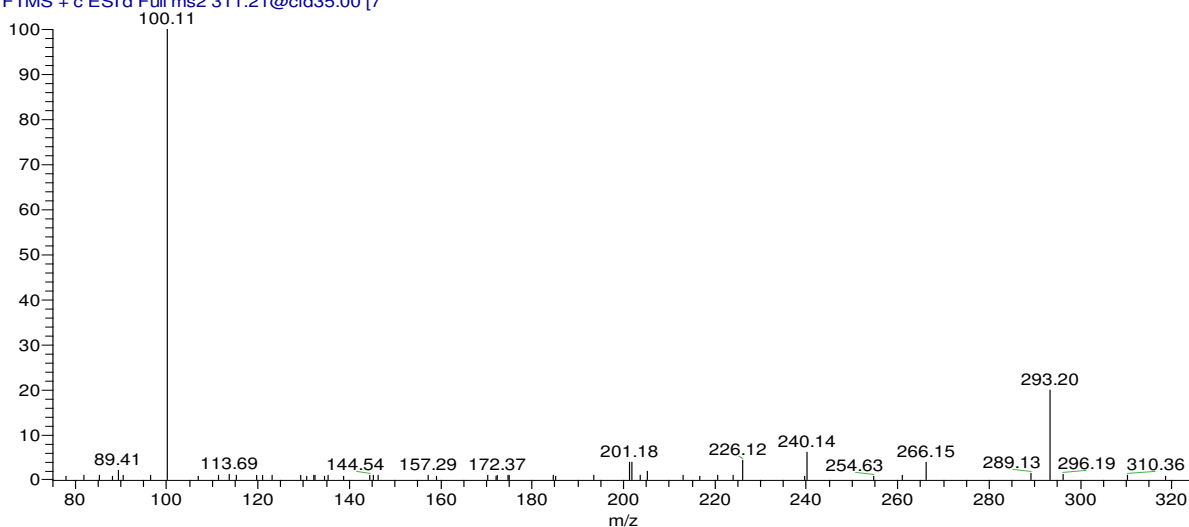


Figure SI-9: Fragmentation pattern of PTP311 according to MS² obtained from LC-HRMS

PTP313

100TMP-UV-32min-C18nucleoshell-140617b #913 RT: 10.23 AV: 1 NL: 3.94E5
T: FTMS + c ESI d Full ms2 313.23@cid35.00 [7]

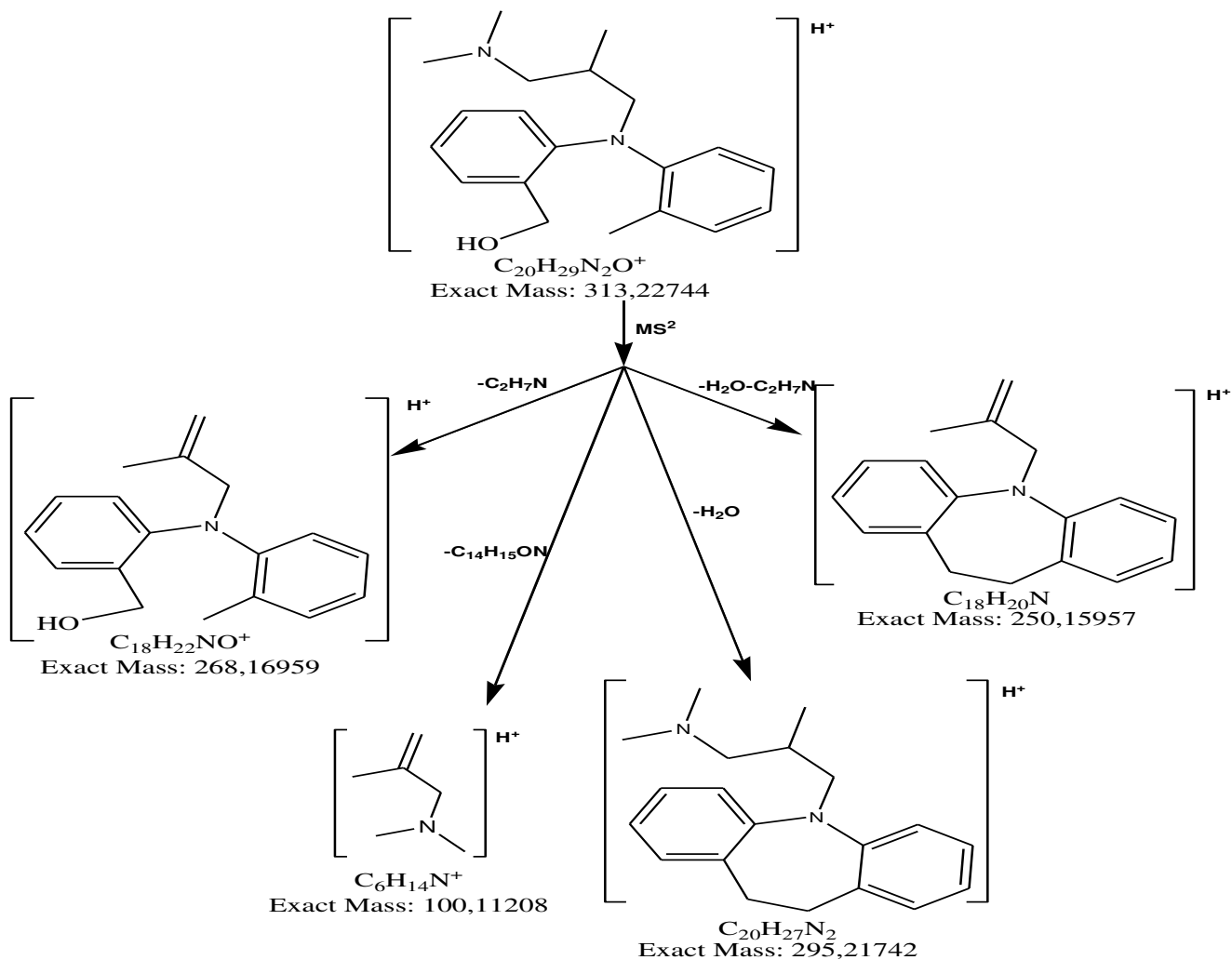
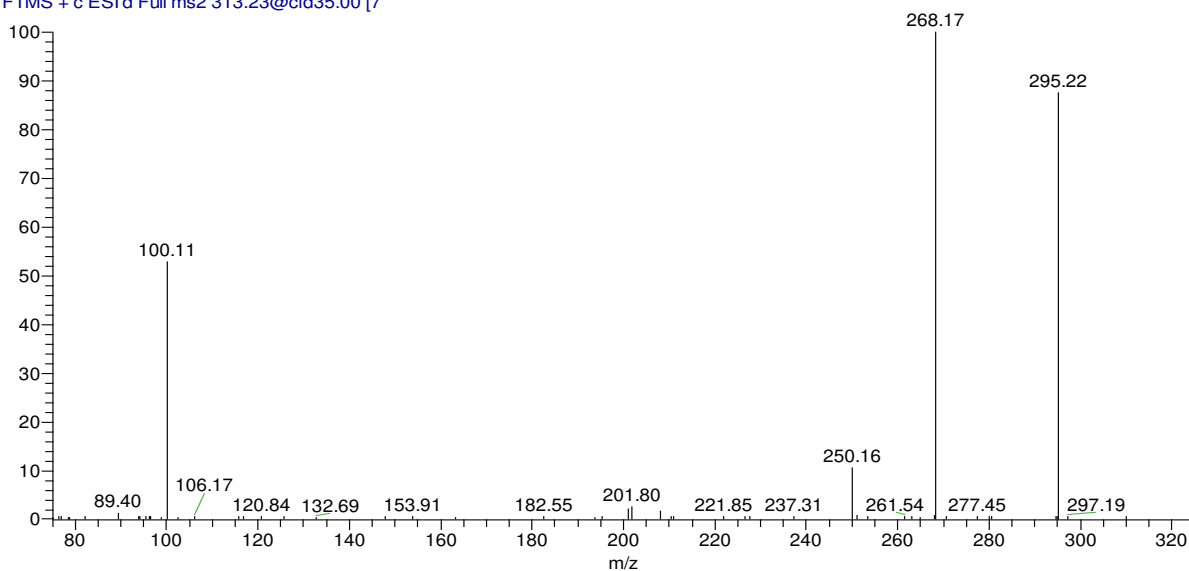


Figure SI-10: Fragmentation pattern of PTP313 according to MS² obtained from LC-HRMS

PTP327

100TMP-UV-32min-C18nucleoshell-140617b #901 RT: 10.08 AV: 1 NL: 1.72E5
T: FTMS + c ESI d Full ms2 327.21@cid35.00 [8]

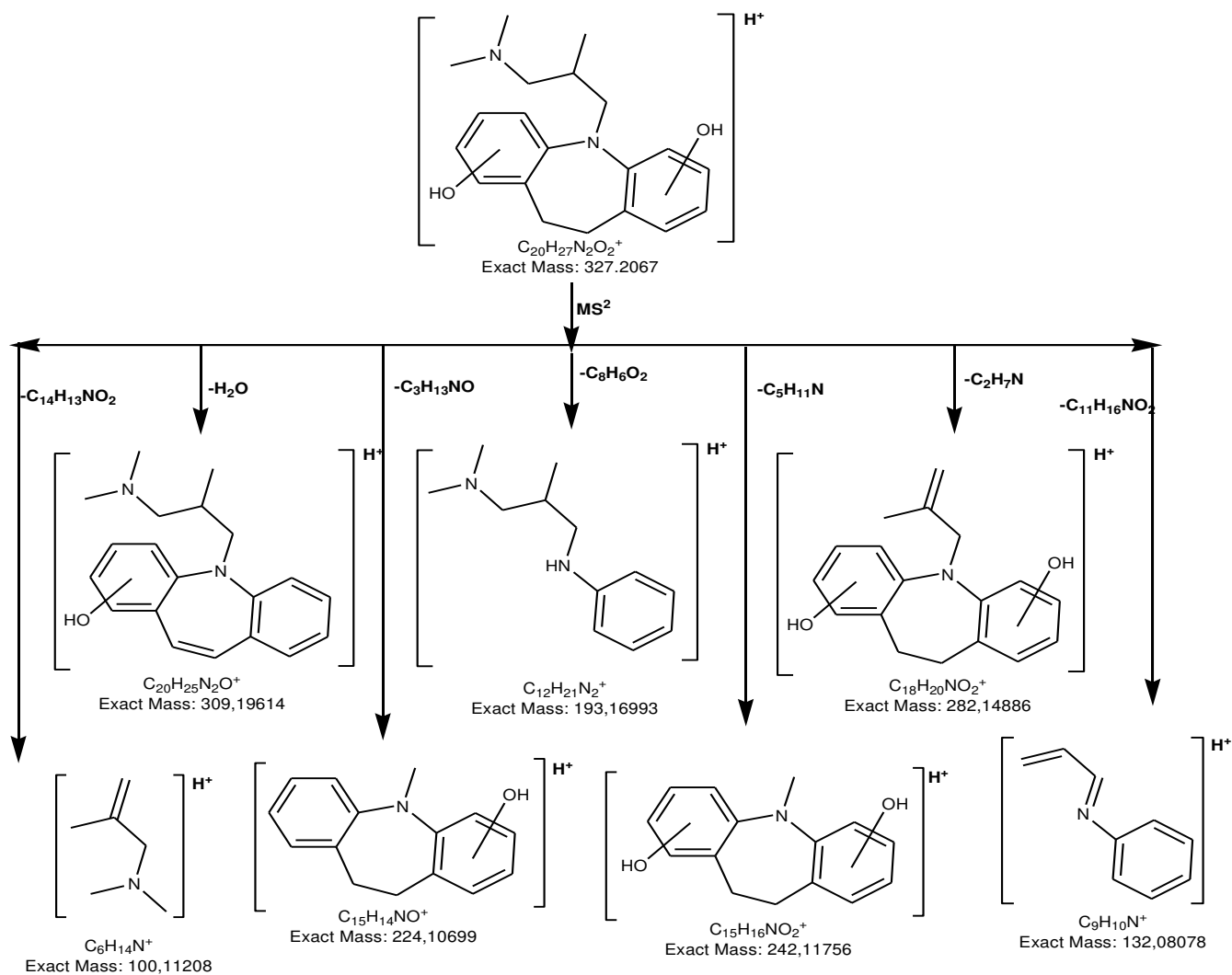
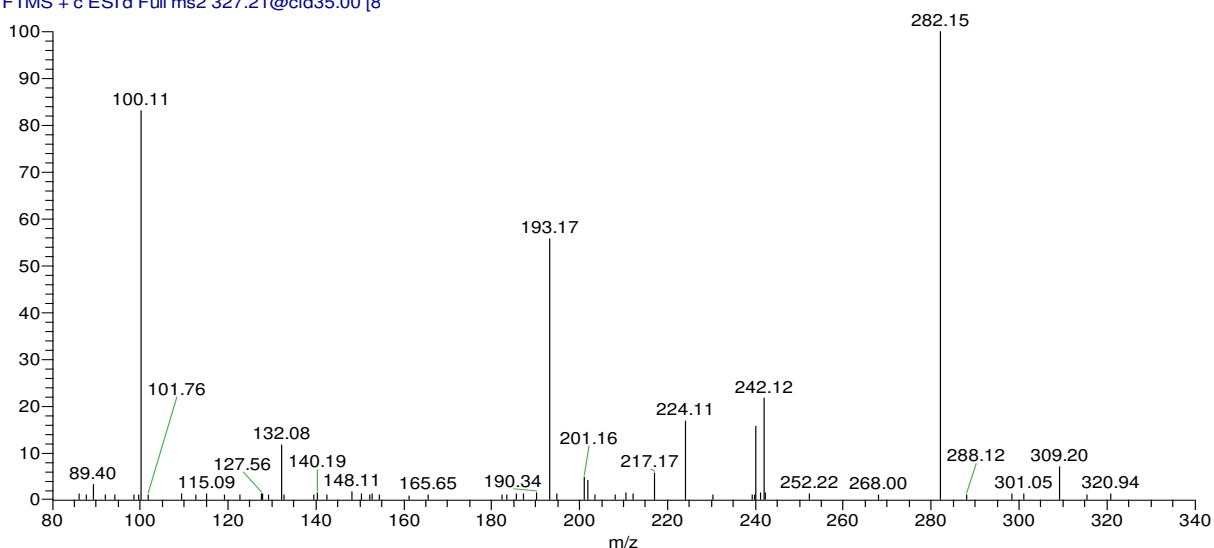


Figure SI-11: Fragmentation pattern of PTP327 according to MS² obtained from LC-HRMS

PTP329

100TMP-UV-64min-C18nucleoshell-140617b #894 RT: 10.00 AV: 1 NL: 1.20E5
T: FTMS + c ESI d Full ms2 329.22@cid35.00 [8]

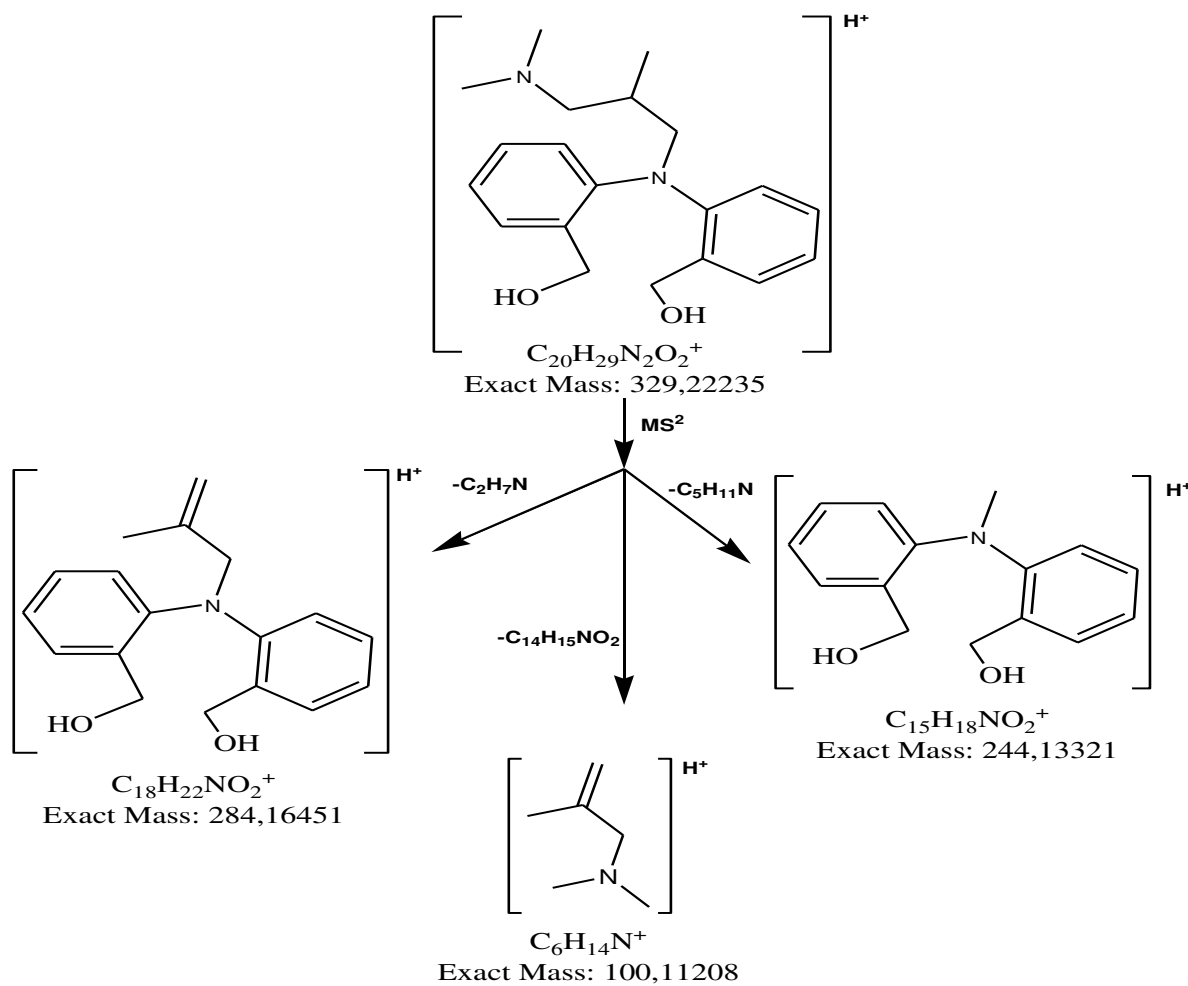
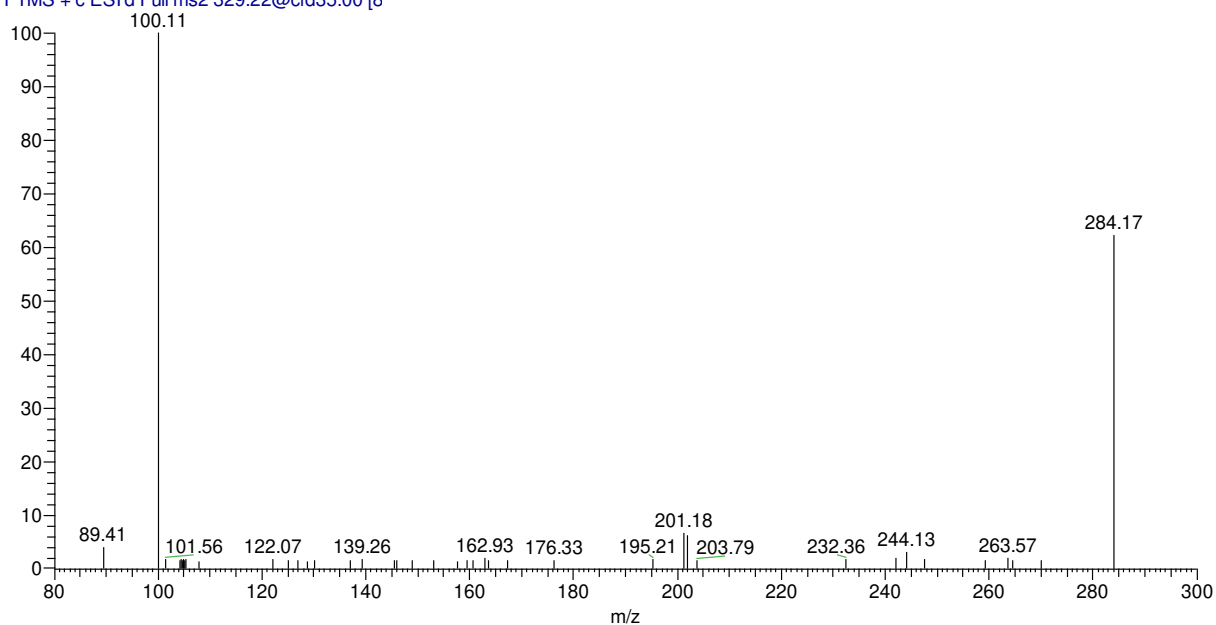


Figure SI-12: Fragmentation pattern of PTP329 according to MS^2 obtained from LC-HRMS

PTP309a

100TMP-UV-32min-C18nucleoshell-140617b #895 RT: 10.01 AV: 1 NL: 4.23E5
T: FTMS + c ESI d Full ms2 309.20@cid35.00 [7]

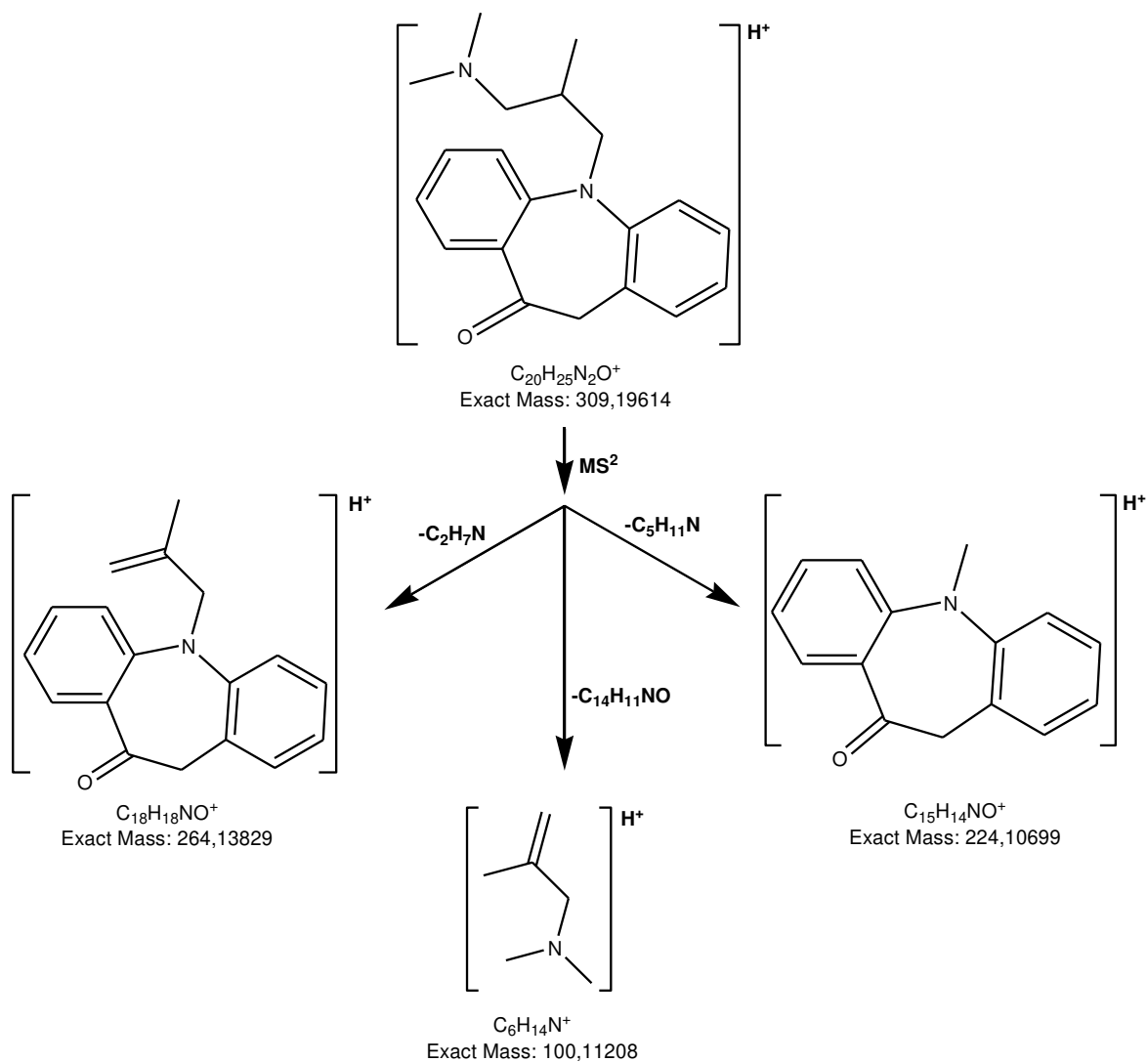
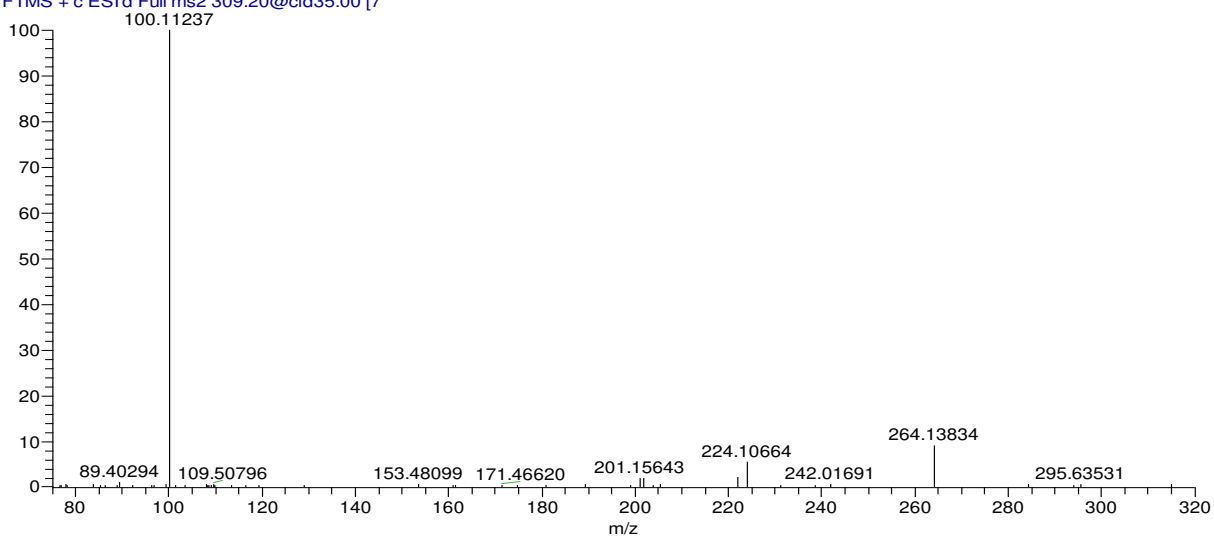


Figure SI-13: Fragmentation pattern of PTP309a according to MS² obtained from LC-HRMS;

PTP309b

100TMP-UV-32min-C18nucleoshell-140617b #943 RT: 10.57 AV: 1 NL: 6.15E6
T: FTMS + c ESI d Full ms2 309.23@cid35.00 [7]

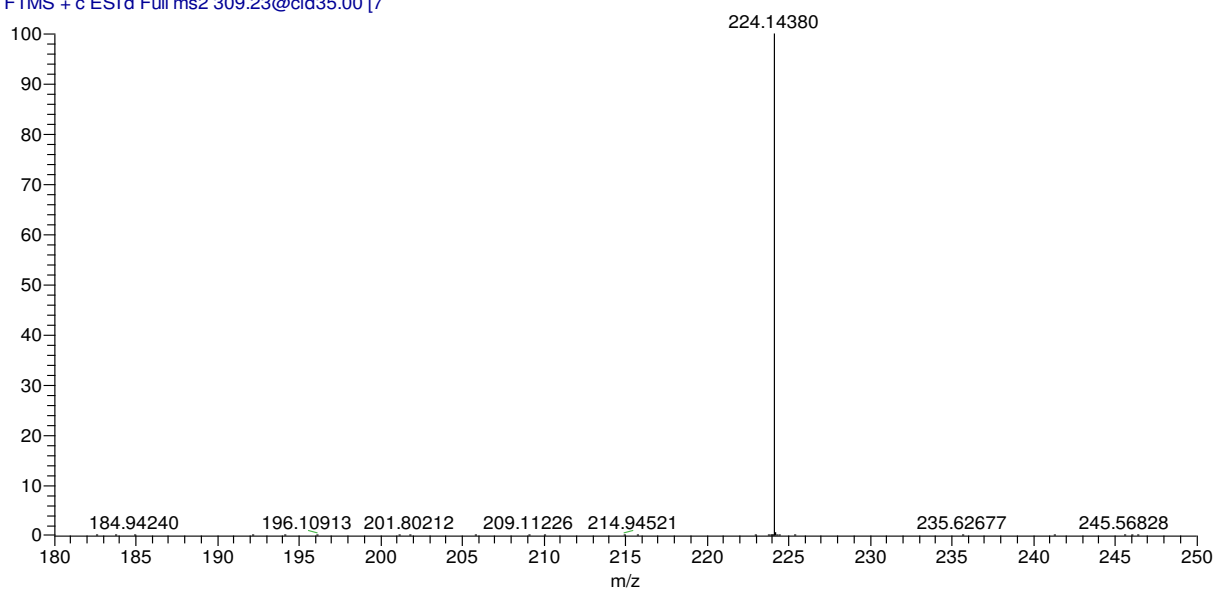
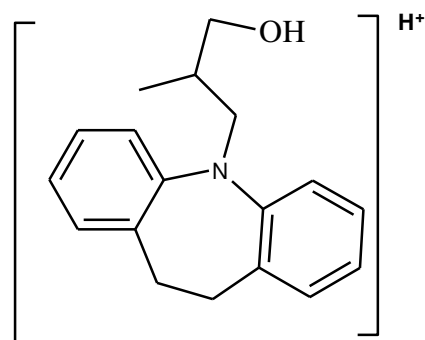
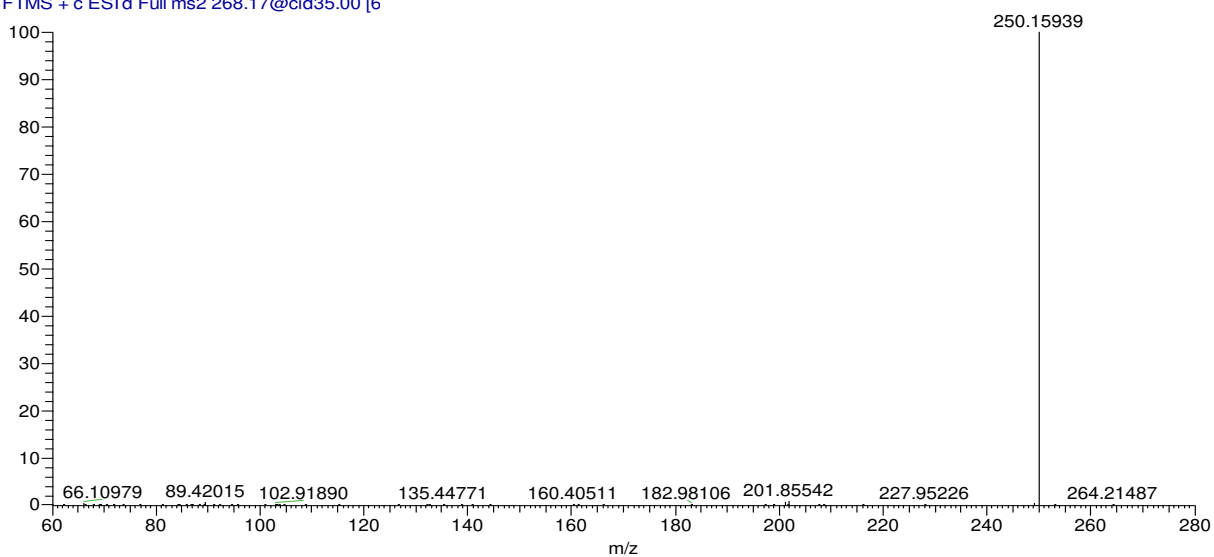


Figure SI-14: LC-HRMS-MS² Fragmentation of PTP309b

PTP268

100TMP-UV-64min-C18nucleoshell-140617b #1042 RT: 11.72 AV: 1 NL: 1.09E6
T: FTMS + c ESI d Full ms2 268.17@cid35.00 [6]

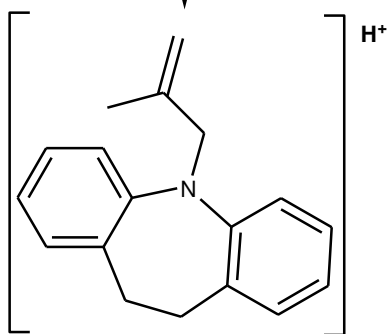


$C_{18}H_{22}NO^+$

Exact Mass: 268,16959

MS²

-H₂O



$C_{18}H_{20}N^+$

Exact Mass: 250,15903

Figure SI-15: Fragmentation pattern of PTP268 according to MS² obtained from LC-HRMS

PTP196

100TMP-UV-32min-C18nucleoshell-140617b #1079 RT: 12.14 AV: 1 NL: 5.61E5
T: FTMS + c ESI d Full ms2 196.11@cid35.00 [5]

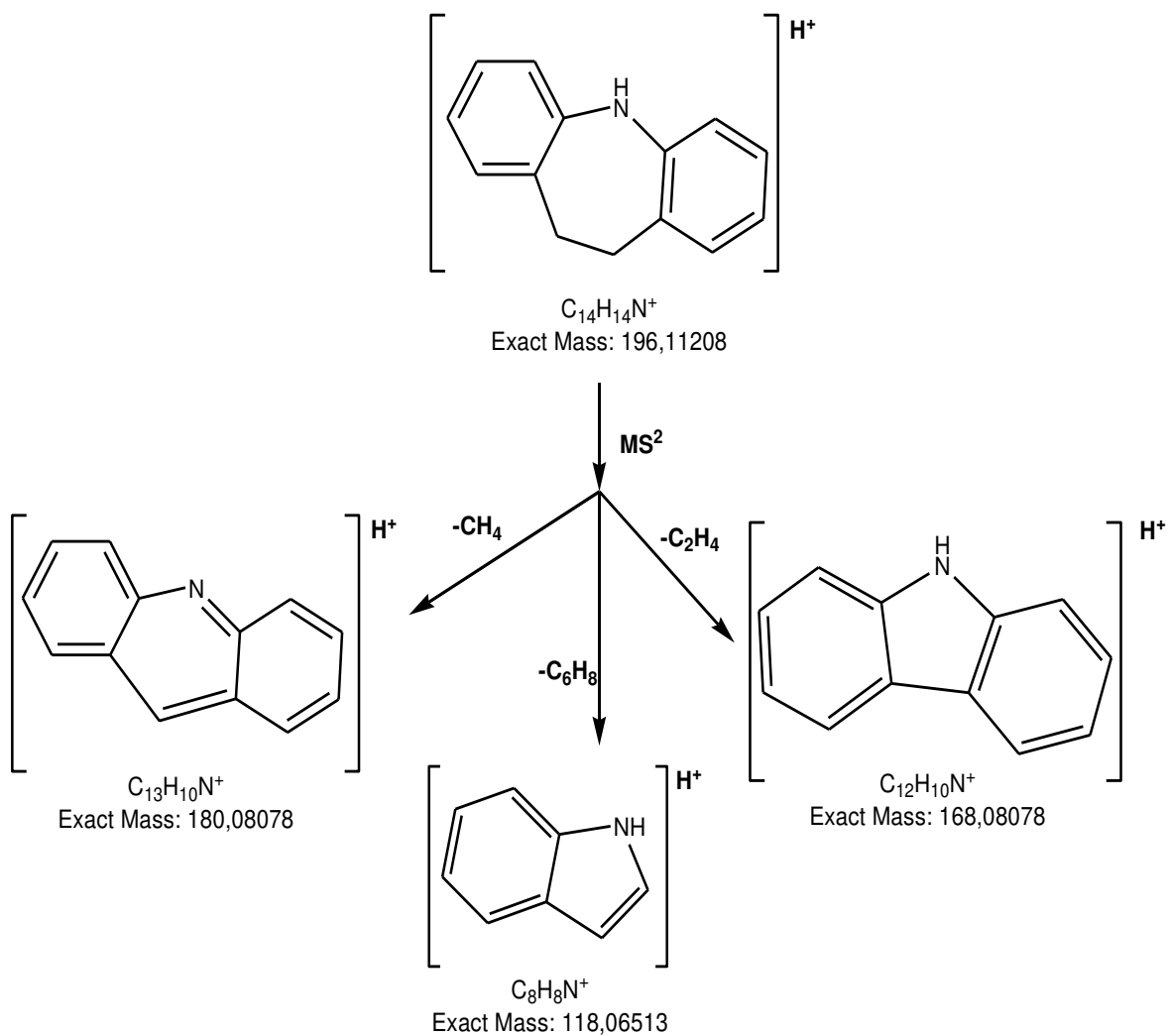
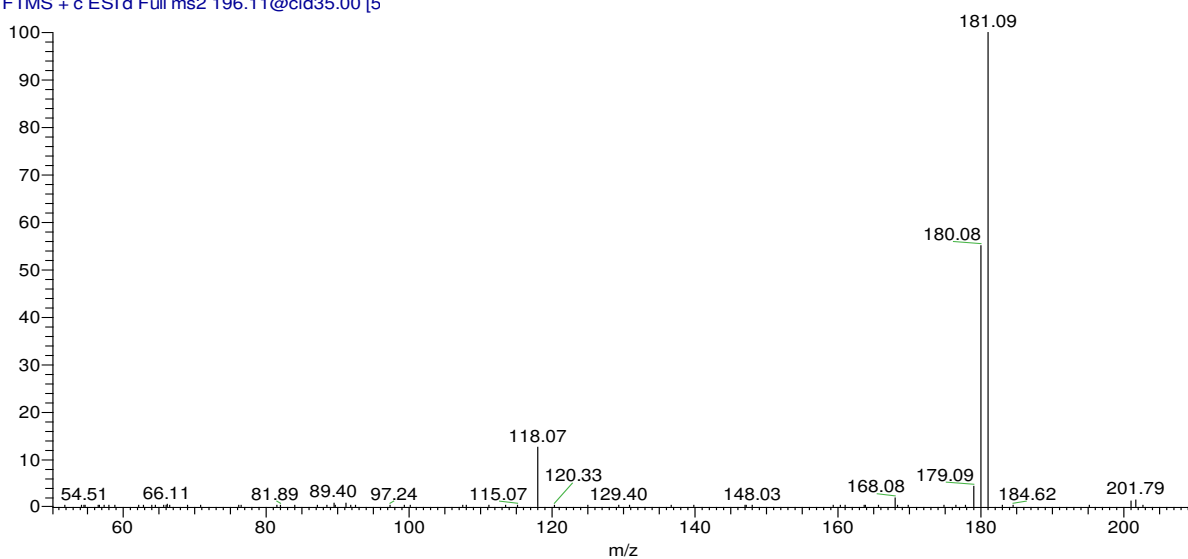


Figure SI-16: Fragmentation pattern of PTP196 according to MS^2 obtained from LC-HRMS

PTP210

100TMP-UV-64min-C18nucleoshell-140617b #996 RT: 11.20 AV: 1 NL: 3.19E5
T: FTMS + c ESI d Full ms2 210.09@cid35.00 [5]

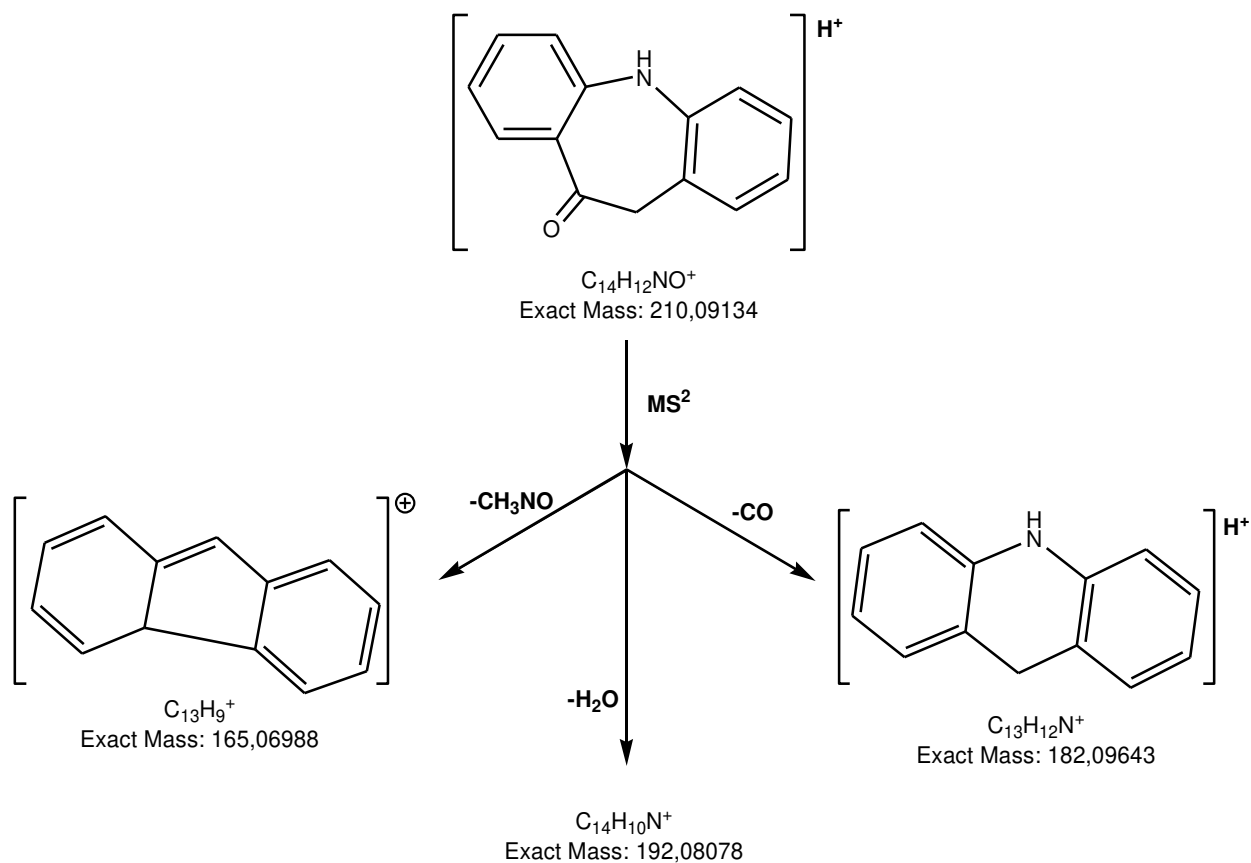
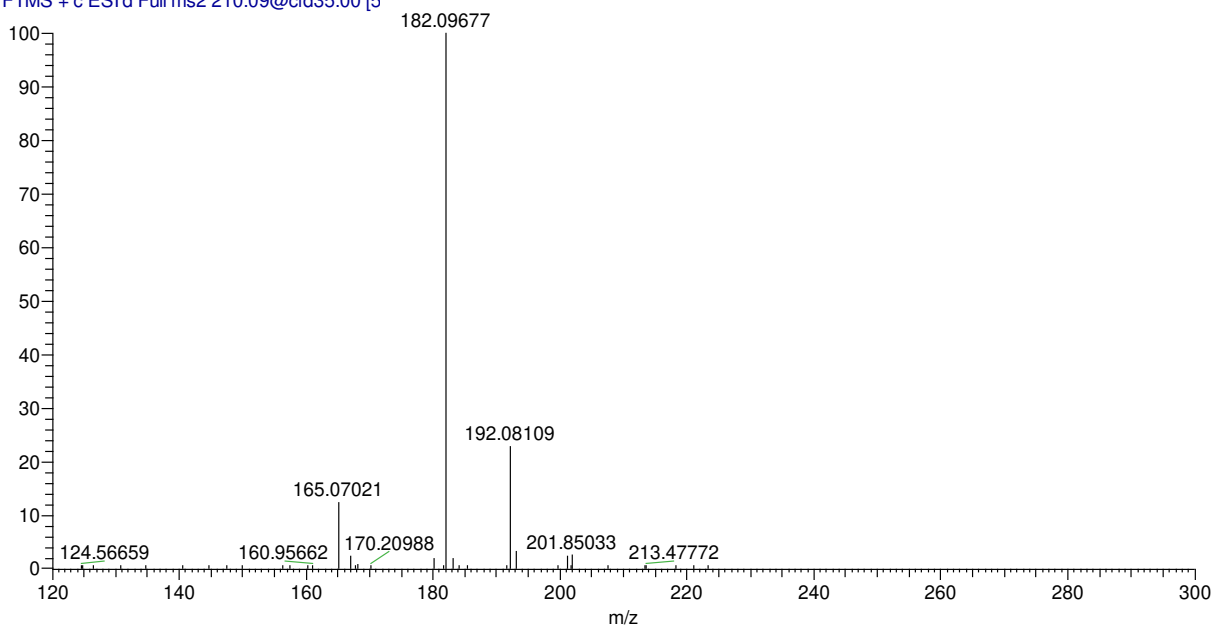


Figure SI-17: Fragmentation pattern of PTP210 according to MS² obtained from LC-HRMS

PTP405

100TMP-UV-64min-C18nucleoshell-140617b #1207 RT: 13.60 AV: 1 NL: 5.39E4
T: FTMS + c ESI d Full ms2 405.20@cid35.00 [1]

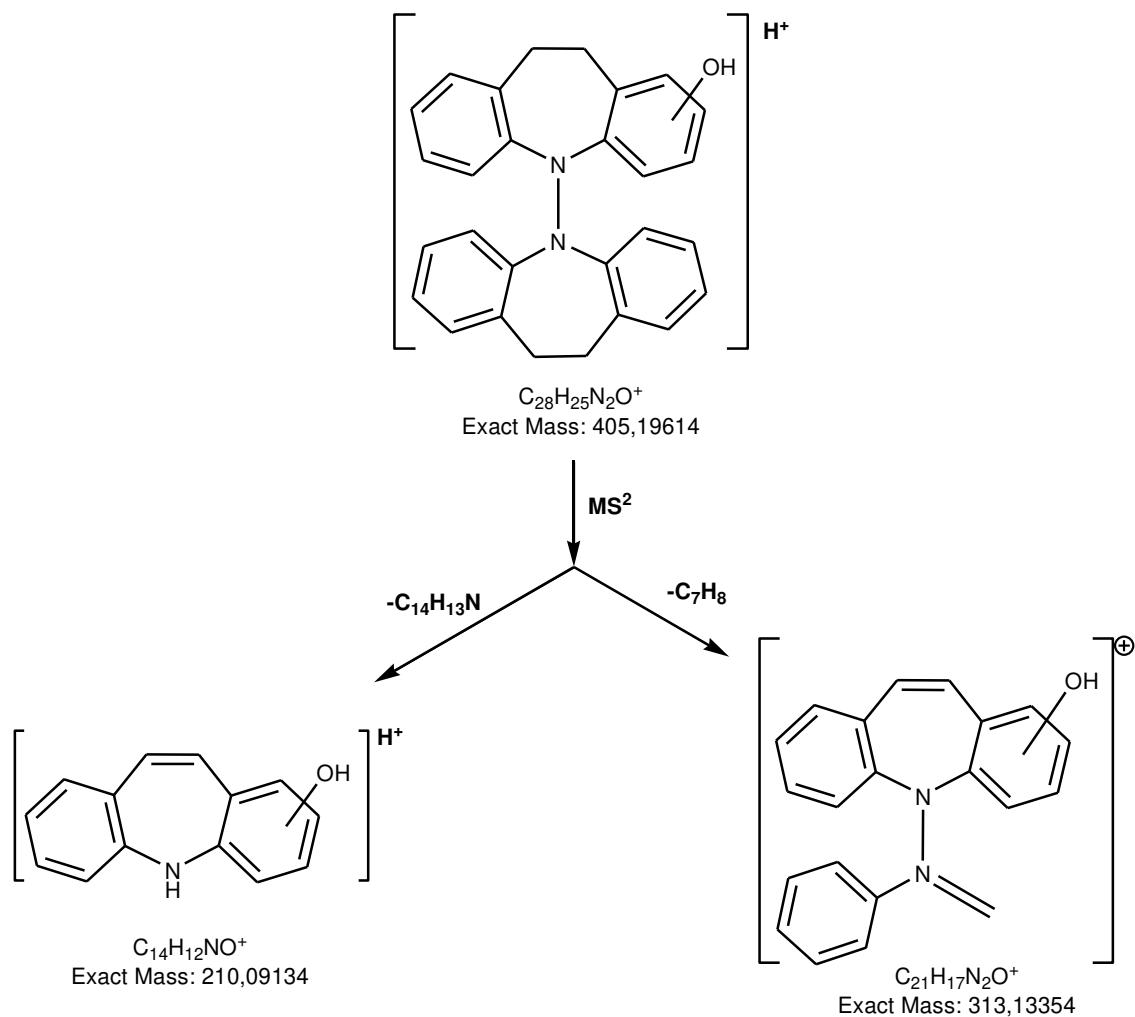
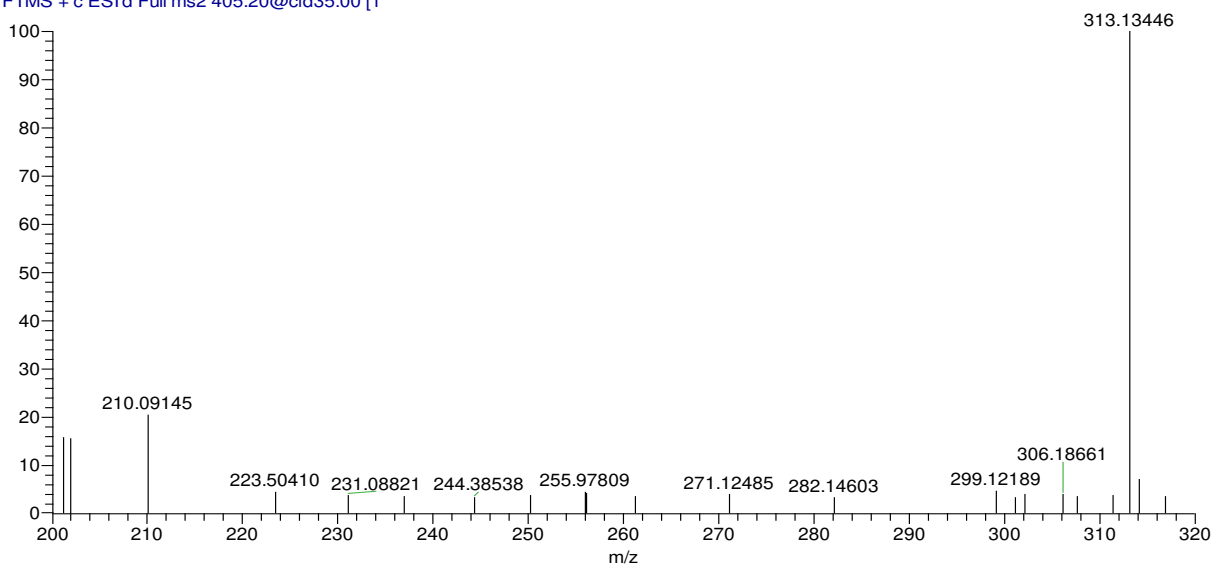


Figure SI-18: Fragmentation pattern of PTP405 according to MS^2 obtained from LC-HRMS

PTP247

100TMP-UV-64min-C18nucleoshell-140617b #329 RT: 3.66 AV: 1 NL: 7.87E5
T: FTMS + c ESI d Full ms2 247.18@cid35.00 [5]

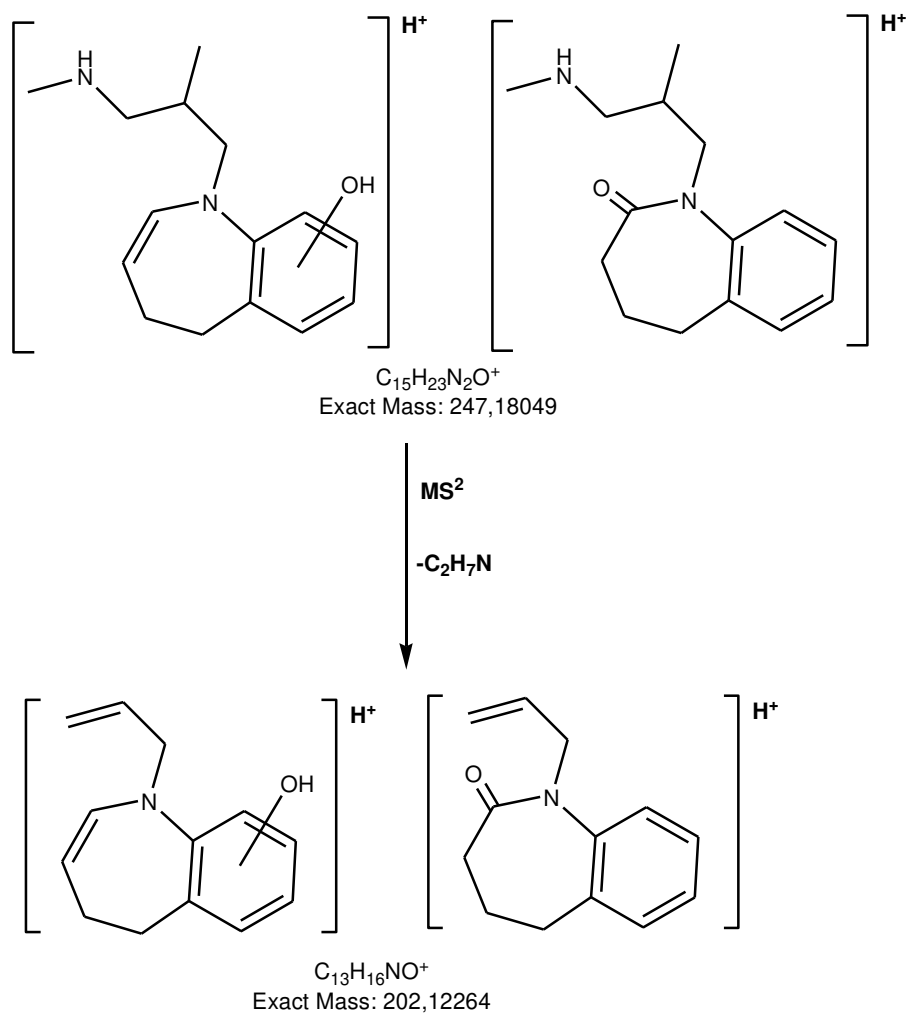
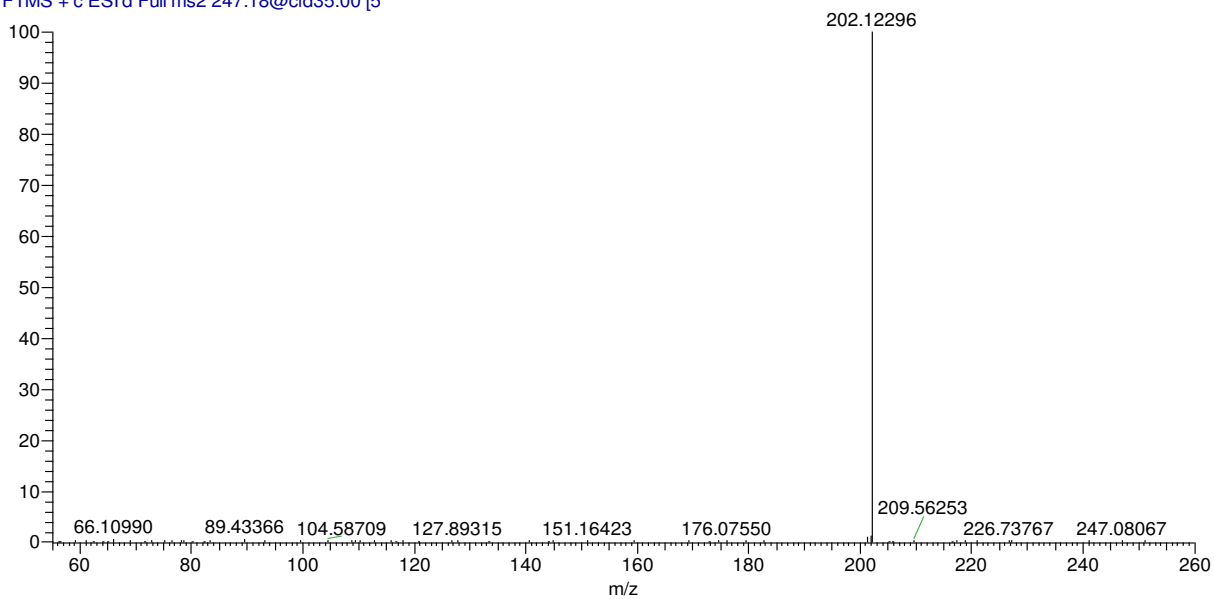


Figure SI-19: Fragmentation pattern of PTP247 according to MS^2 obtained from LC-HRMS

PTP134

100TMP-UV-64min-C18nucleoshell-140617b #64 RT: 0.71 AV: 1 NL: 2.95E6
T: FTMS + c ESI d Full ms2 134.12@cid35.00 [5]

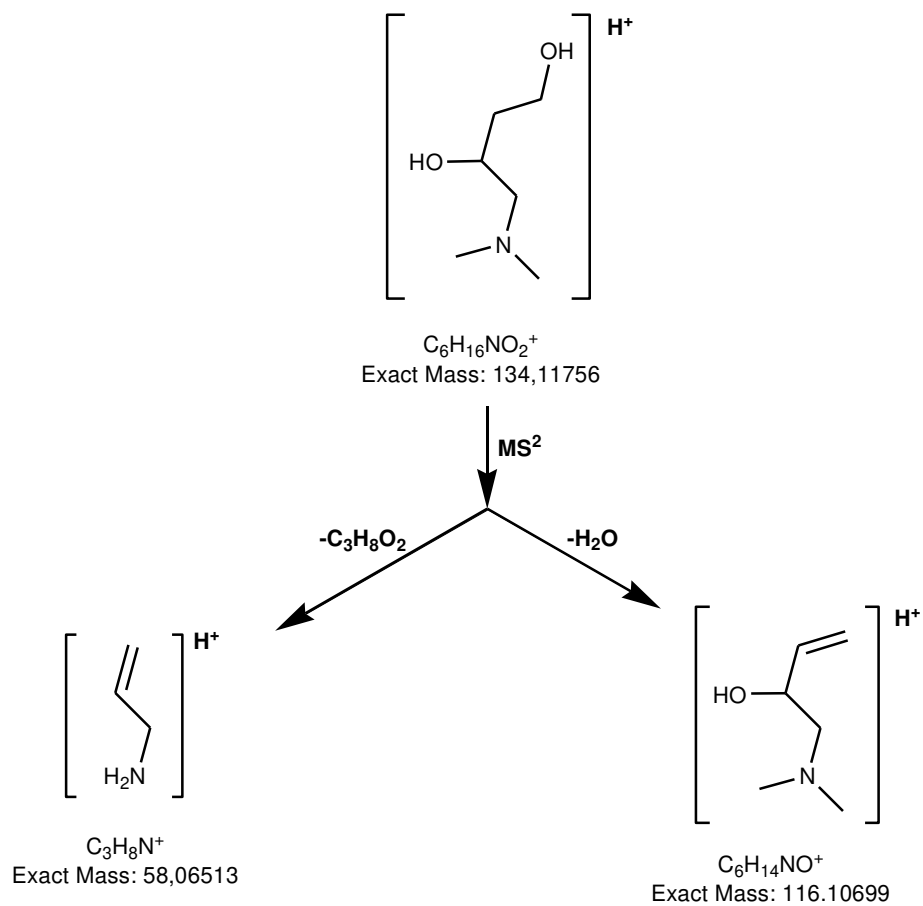
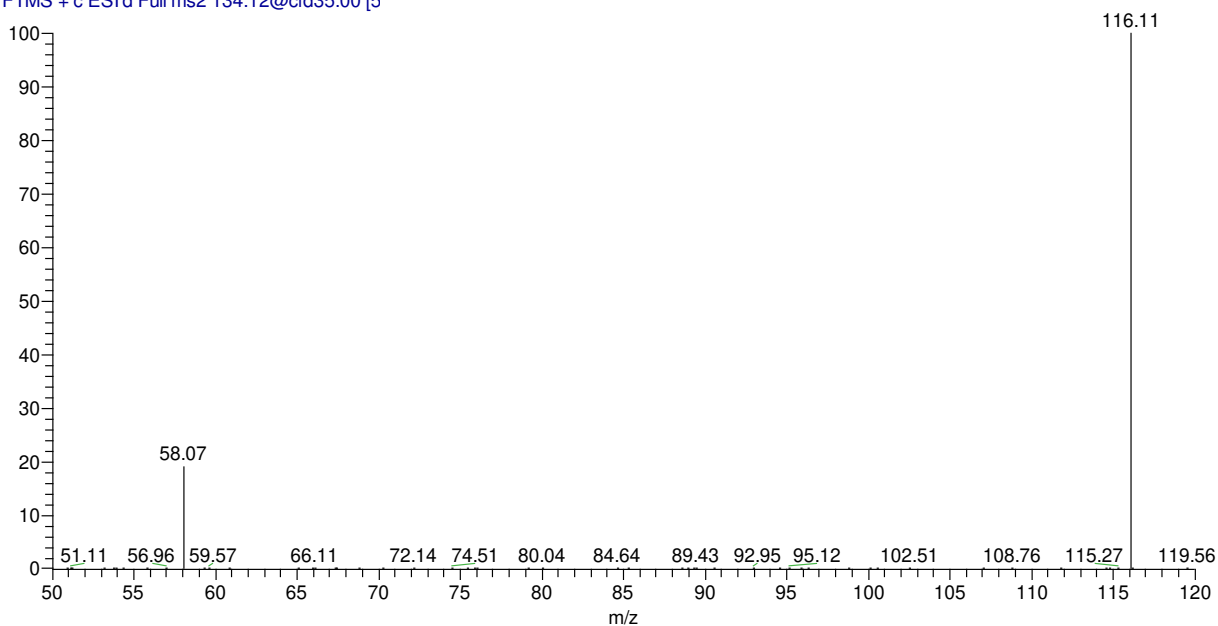
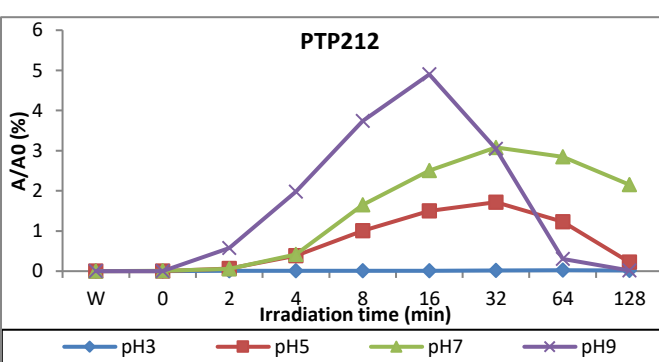
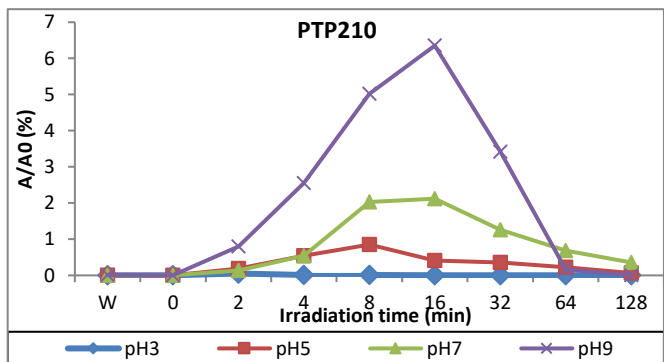
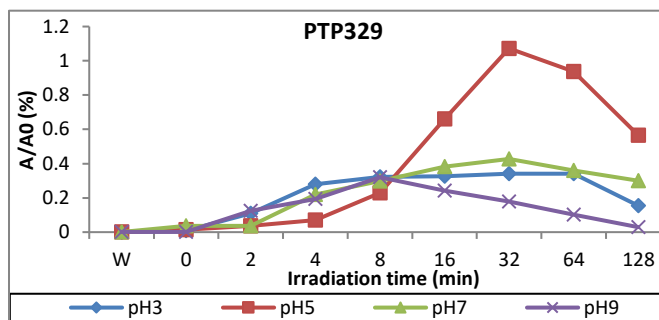
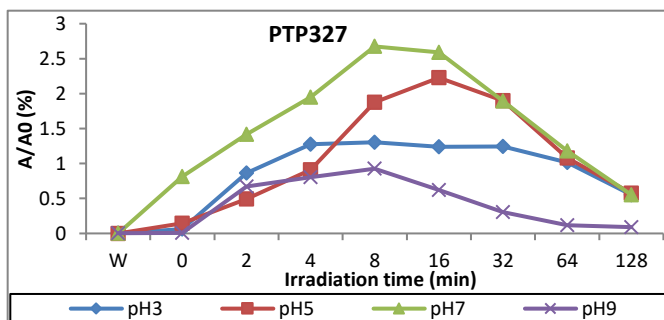
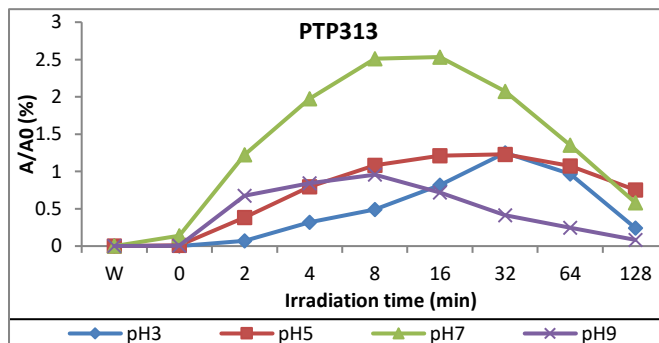
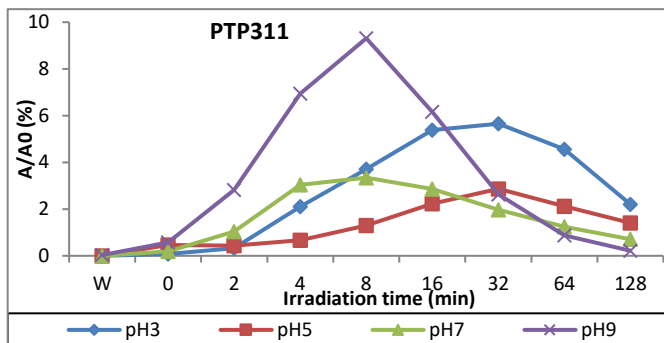
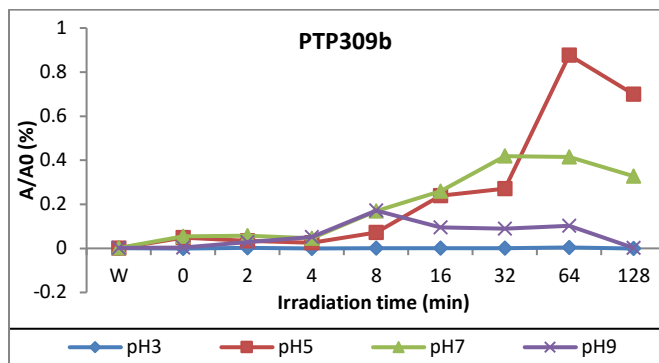
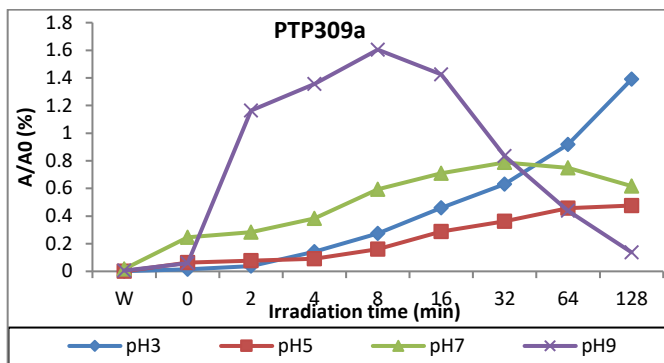


Figure SI-20: Fragmentation pattern of PTP134 according to MS² obtained from LC-HRMS



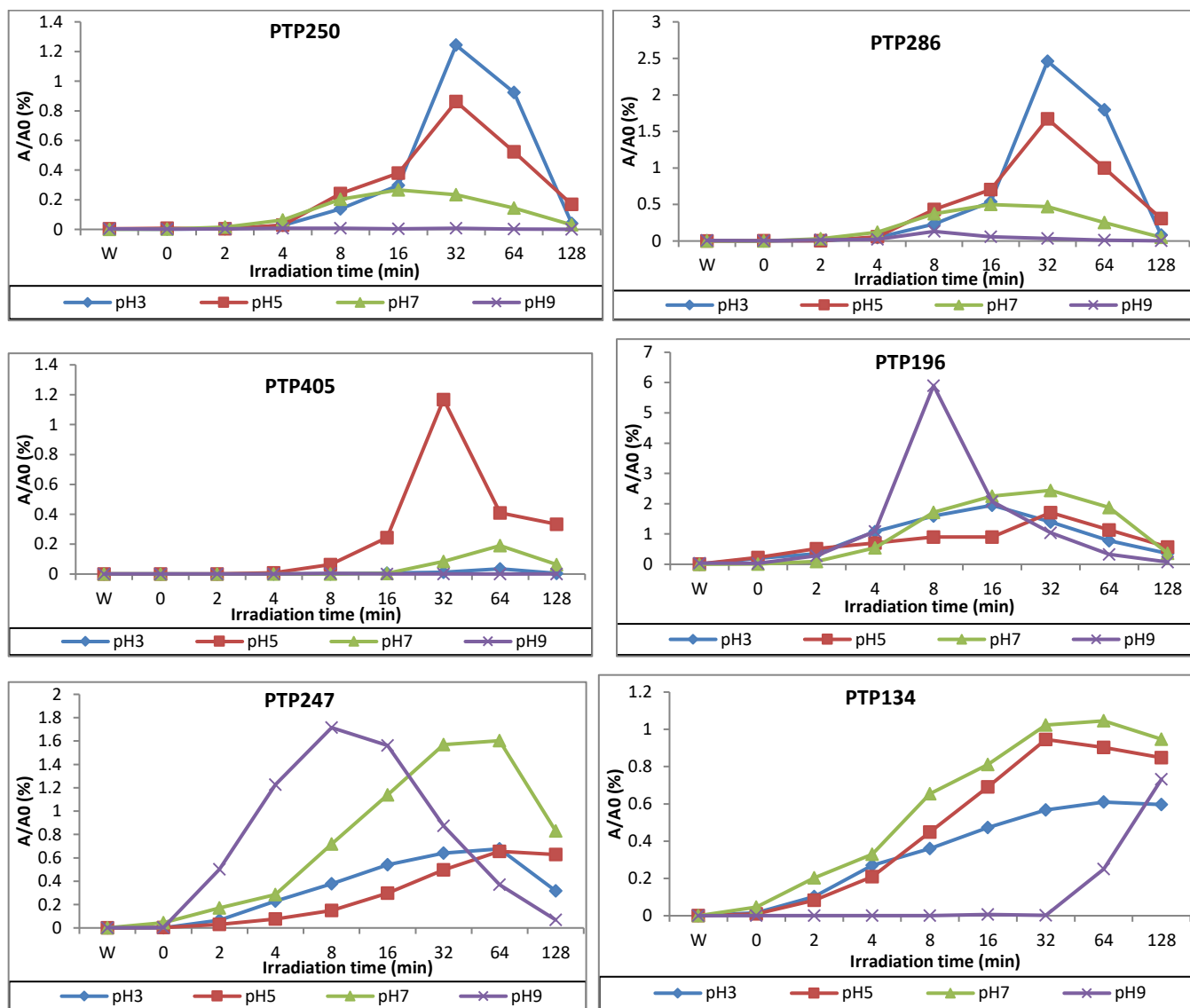
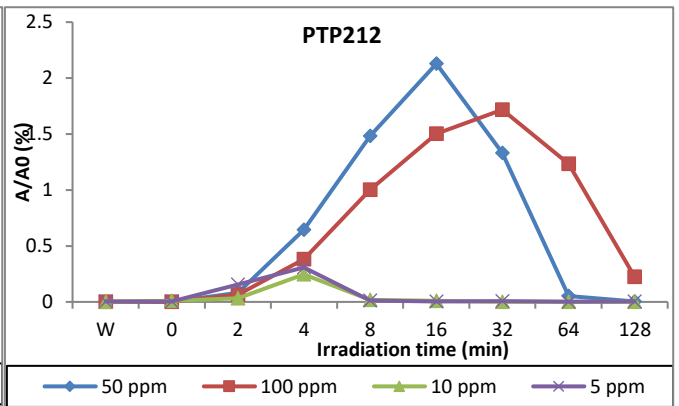
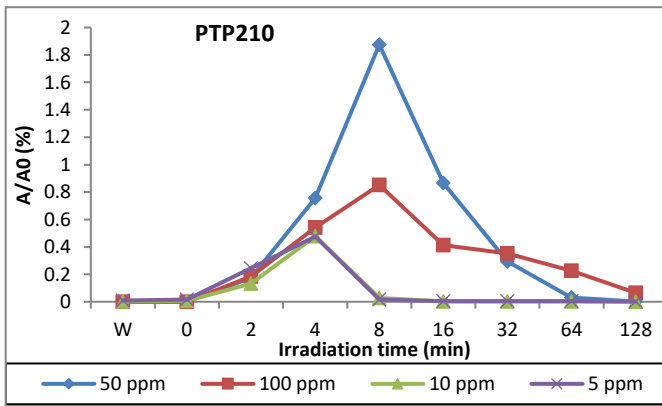
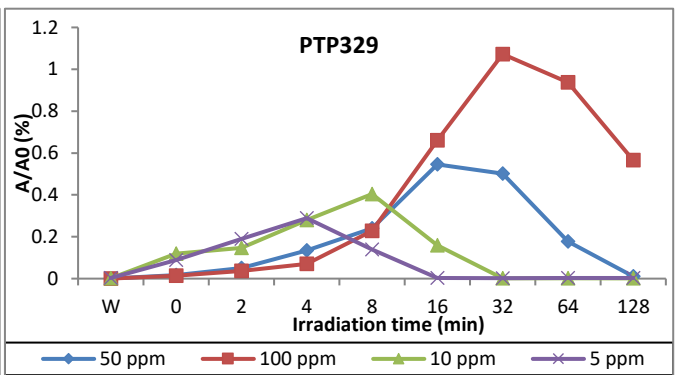
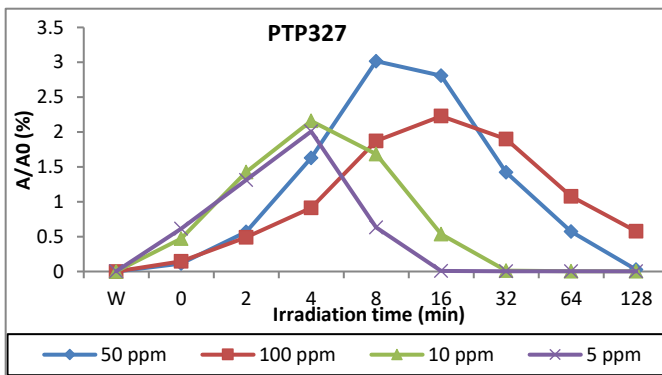
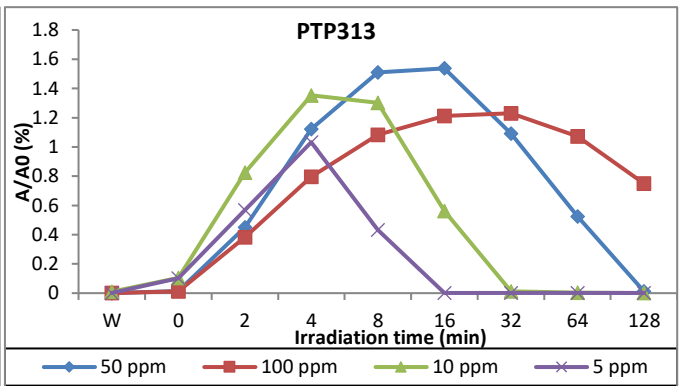
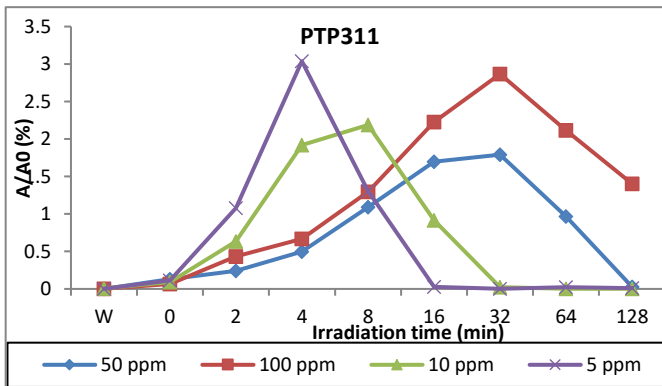
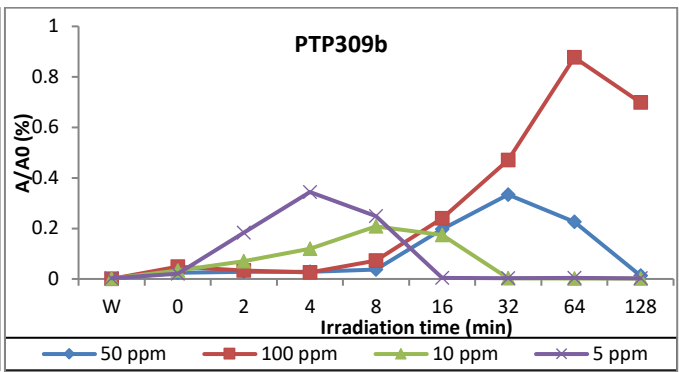
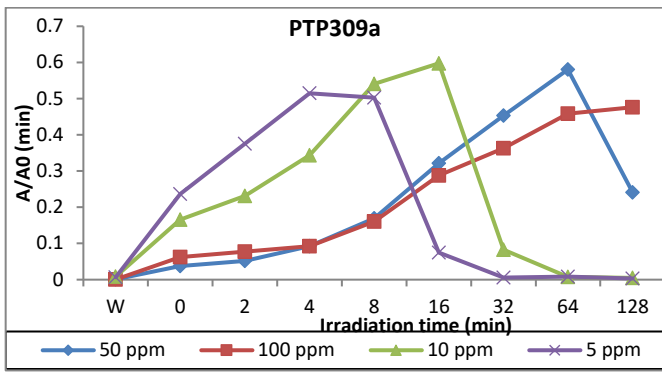


Figure SI-21: Time curves of the relative peak area A/A_0 (%) of TMP PTPs during photolysis at different pH values.



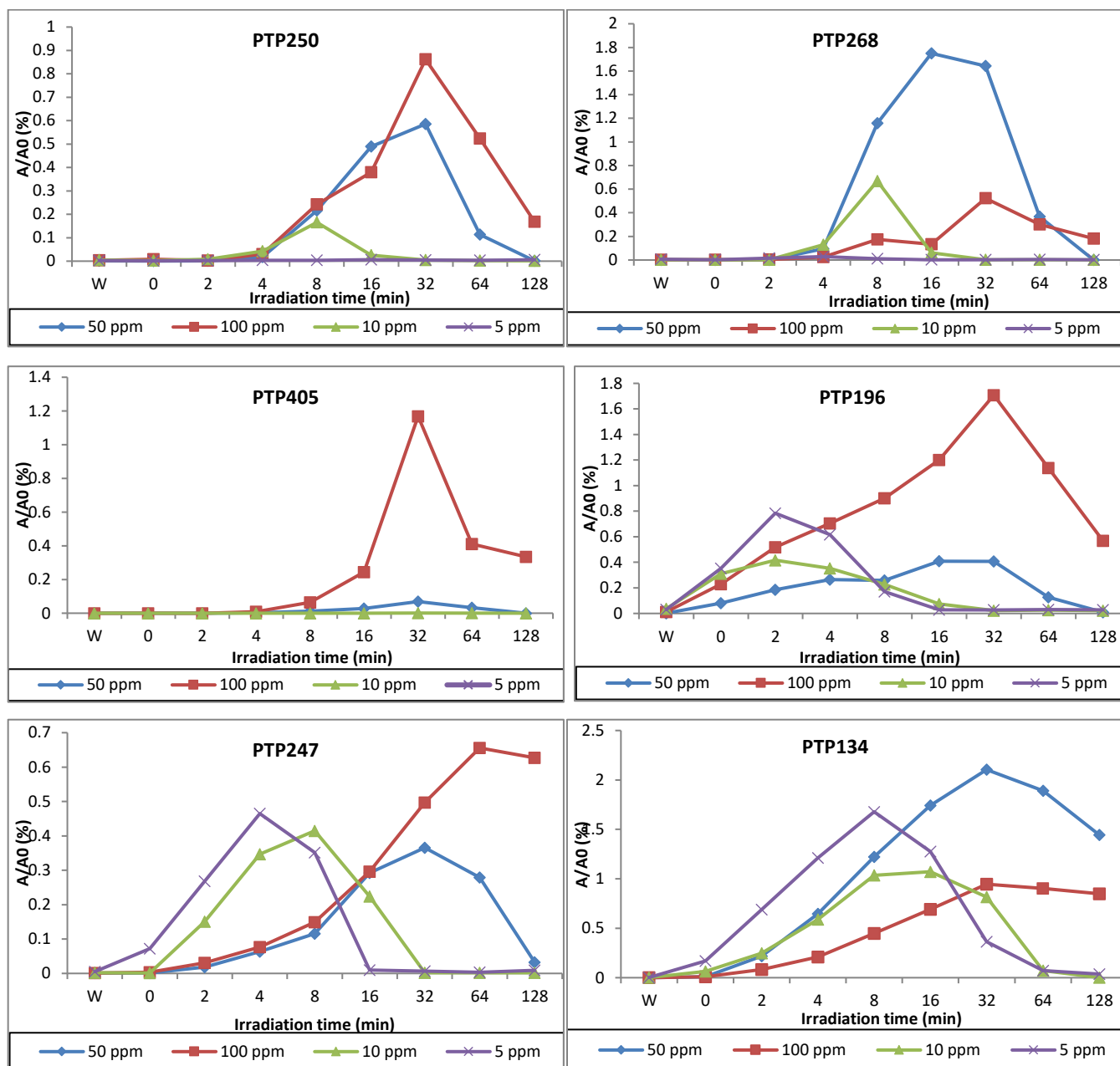
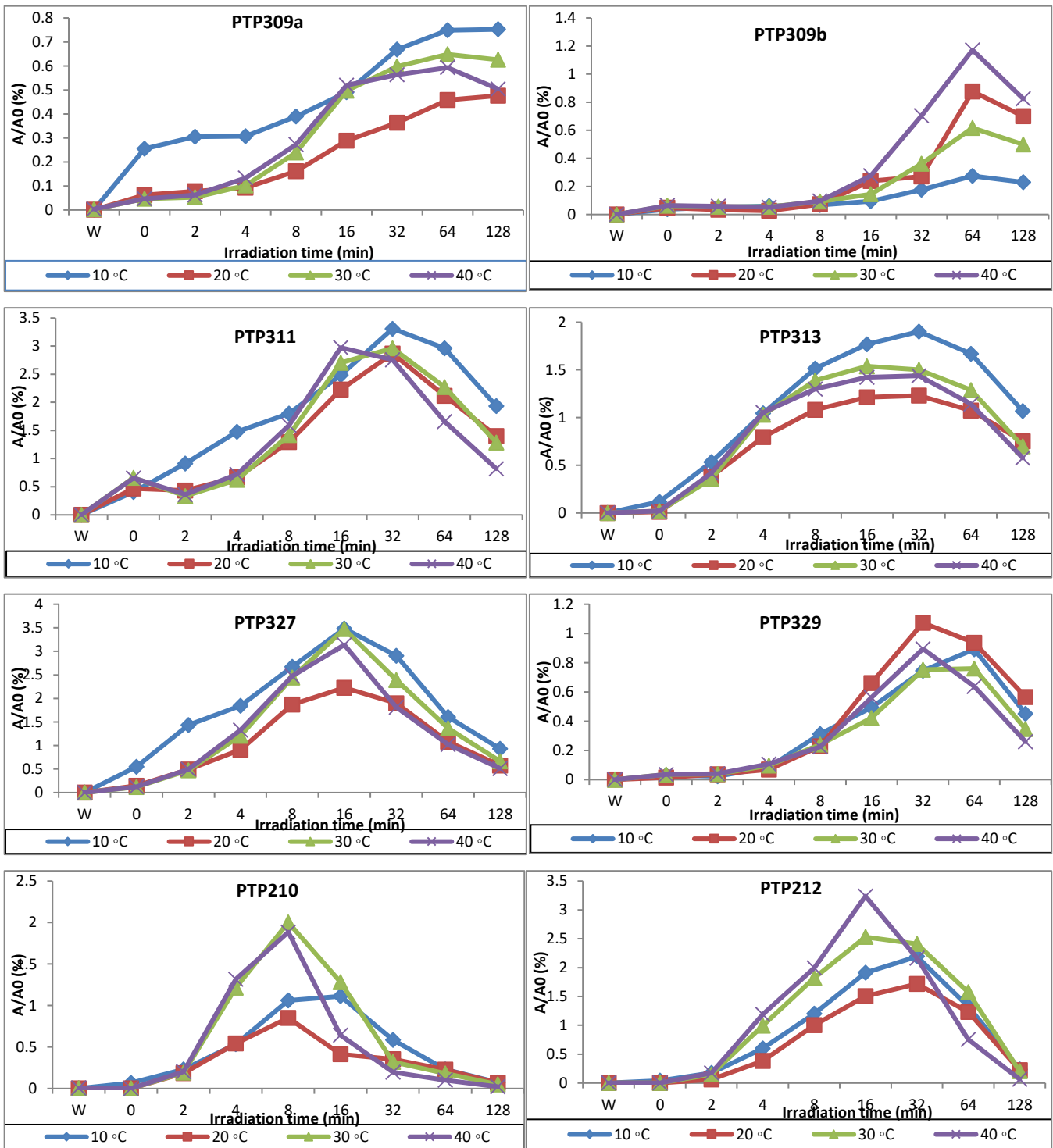


Figure SI-22: Time curves of the relative peak area A/A_0 (%) of TMP PTPs during photolysis at different concentrations.



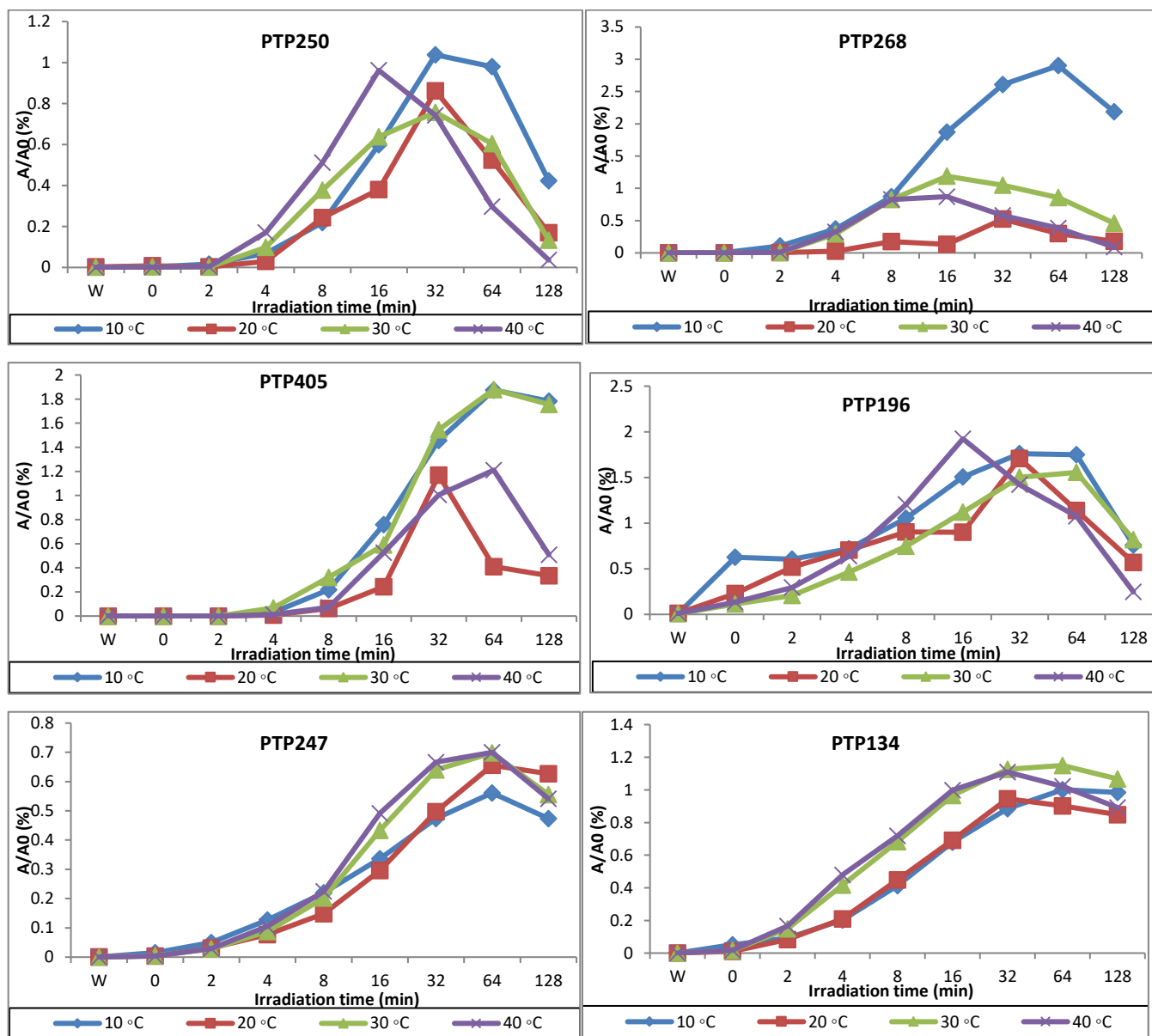


Figure SI-23: Time curves of the relative peak area A/A_0 (%) of products (PTPs) during photolysis at different temperatures.

Table SI-1: Q-SAR predictions for TMP and its PTPs for ready biodegradability by different models: 1. Catalogic-BOD Kinetic (OECD 301F)_v.08.09, 2. Catalogic BOD 28 days MITI (OECD 301C) _v.06.07. 3: Case Ultra, MITI Ready biodegradation (AU6), 4: MITI Biodegradation probability Biowin 5 (linear model), 5: MITI Biodegradation probability Biowin 6 (MITI non-linear model), (Positive results are red, RB: Ready Biodegradable, NRB: non Ready Biodegradable) (**Red is positive result (readily biodegradable)**)

Compounds	Smiles	OASIS catalogic		Case Ultra	Epi Suite	
		Catalogic OECD 301F*	Catalogic OECD 301C*	AU6	Biowin 5**	Biowin 6**
TMP	<chem>CC(CN(C)C)CN1c2c cccc2CCc3ccccc13</chem>	0.0013	0.0227	(-)	-0.3297	0.0022
PTP309a	<chem>CC(CN(C)C)CN1c2c cccc2CC(=O)c3ccccc13</chem>	0.0175	0.022	(-)	-0.1979	0.0038
PTP311-1	<chem>CC(CN(C)C)CN1c2c cccc2CC(O)c3ccccc13</chem>	0.0026	0.023	(±)	-0.1703	0.0055
PTP313-1	<chem>CC(CN(C)C)CN(c1c cccc1)c2ccccc2CCO</chem>	0.0204	0.0414	(+)	-0.1089	0.0069
PTP313-2	<chem>CC(CN(C)C)CN(c1c cccc1C)c2ccccc2CO</chem>	0.0205	0.0635	(+)	-0.1250	0.0054
PTP327-1	<chem>CC(CN(C)C)CN1c2c ccc(O)c2CCc3ccccc(O)c13</chem>	0.168	0.0232	(-)	-0.3129	0.0018
PTP327-2	<chem>CC(CN(C)C)CN1c2c cc(O)cc2CCc3ccccc(O)c13</chem>	0.1704	0.0238	(-)	-0.3129	0.0018
PTP327-3	<chem>CC(CN(C)C)CN1c2c c(O)ccc2CCc3ccccc(O)c13</chem>	0.2273	0.0245	(-)	-0.3129	0.0018
PTP327-4	<chem>CC(CN(C)C)CN1c2c (O)cccc2CCc3ccccc(O)c13</chem>	0.1497	0.0239	(-)	-0.3129	0.0018

PTP327-5	CC(CN(C)C)C(O)N1 c2ccccc2CCc3cccc(O)c13	0.2113	0.0479	(±)	-0.3079	0.0020
PTP327-6	CC(CN(C)C)CN1c2c ccc(O)c2CCc3ccc(O) cc13	0.1926	0.0237	(-)	-0.3129	0.0018
PTP327-7	CC(CN(C)C)CN1c2c c(O)ccc2CCc3ccc(O) cc13	0.2024	0.0249	(-)	-0.3129	0.0018
PTP327-8	CC(CN(C)C)CN1c2c cc(O)cc2CCc3ccc(O) cc13	0.1944	0.0244	(-)	-0.3129	0.0018
PTP327-9	CC(CN(C)C)C(O)N1 c2ccccc2CCc3ccc(O)cc13	0.1865	0.0489	(±)	-0.3079	0.0020
PTP327-10	CC(CN(C)C)CN1c2c cc(O)cc2CCc3c(O)cc cc13	0.1872	0.0232	(-)	-0.3129	0.0018
PTP327-11	CC(CN(C)C)CN1c2c cc(O)cc2CCc3cc(O)c cc13	0.1898	0.0237	(-)	-0.3129	0.0018
PTP327-12	CC(CN(C)C)C(O)N1 c2ccccc2CCc3cc(O) ccc13	0.2153	0.0486	(±)	-0.3079	0.0020
PTP327-13	CC(CN(C)C)CN1c2c ccc(O)c2CCc3c(O)cc cc13	0.1846	0.0227	(-)	-0.3129	0.0018
PTP327-14	CC(CN(C)C)C(O)N1 c2ccccc2CCc3c(O)c ccc13	0.2153	0.0485	(±)	-0.3079	0.0020
PTP327-15	CC(CN(C)C)CN1c2c cccc2C(O)C(O)c3ccc cc13	0.0028	0.0274	(±)	-0.0108	0.0138

PTP327-16	CC(CN(C)C)CN1c2c cccc2C(O)Cc3c(O)cc cc13	0.095	0.0232	(±)	-0.1619	0.0050
PTP327-17	CC(CN(C)C)CN1c2c cc(O)cc2CC(O)c3ccc cc13	0.0959	0.0238	(±)	-0.1619	0.0050
PTP327-18	CC(CN(C)C)CN1c2c cccc2CC(O)c3c(O)cc cc13	0.0968	0.0231	(±)	-0.1619	0.0050
PTP327-19	CC(CN(C)C)CN1c2c cccc2C(O)Cc3cccc(O)c13	0.0751	0.0236	(±)	-0.1619	0.0050
PTP327-20	CC(CN(C)C)CN1c2c cccc2C(O)Cc3ccc(O) cc13	0.1488	0.0244	(±)	-0.1619	0.0050
PTP327-21	CC(CN(C)C)CN1c2c cccc2CC(O)c3cc(O)c cc13	0.0959	0.0236	(±)	-0.1619	0.0050
PTP327-22	CC(CN(C)C)CN1c2c cccc2CC(O)c3ccc(O) cc13	0.0712	0.024	(±)	-0.1619	0.0050
PTP327-23	CC(CN(C)C)CN1c2c cccc2CC(O)c3cccc(O)c13	0.0758	0.0236	(±)	-0.1619	0.0050
PTP327-24	CC(CN(C)C)C(O)N1 c2cccc2CC(O)c3cc ccc13	0.3665	0.0488	(±)	-0.1568	0.0056
PTP329-1	CC(CN(C)C)CN(c1c cccc1CO)c2cccc2C O	0.0207	0.0961	(+)	-0.1087	0.0061
PTP134	CN(C)CC(O)CCO	0.3472	0.4647	(+)	0.6517	0.7459
PTP196	C1Cc2cccc2Nc3ccc cc13	0	0.0048	(-)	-0.0721	0.0259

PTP210-1	<chem>O=C1Cc2ccccc2Nc3ccccc13</chem>	0.629	0.0029	(-)	0.0597	0.0443
PTP212-1	<chem>OC1Cc2ccccc2Nc3ccccc13</chem>	0.5542	0.005	(±)	0.0874	0.0632
PTP212-2	<chem>Oc1cccc2Nc3ccccc3CCc12</chem>	0.2695	0.0042	(-)	-0.0637	0.0237
PTP212-3	<chem>Oc1cccc2CCc3ccccc3Nc12</chem>	0.2765	0.0054	(-)	-0.0637	0.0237
PTP212-4	<chem>Oc1ccc2CCc3ccccc3Nc2c1</chem>	0.1878	0.0061	(-)	-0.0637	0.0237
PTP212-5	<chem>Oc1ccc2Nc3ccccc3CCc2c1</chem>	0.2695	0.0049	(-)	-0.0637	0.0237
PTP212-6	<chem>ON1c2ccccc2CCc3ccccc13</chem>	0	0.0049	OD	0.0380	0.0541
PTP250	<chem>CC(C)CN1c2ccccc2C=Cc3ccccc13</chem>	0.0204	0.0275	(-)	-0.0368	0.0159
PTP268-1	<chem>CC(C)CN1c2ccccc2CC(O)c3ccccc13</chem>	0	0.0062	(±)	-0.0071	0.0276
PTP268-2	<chem>CC(C)CN1c2ccccc2CCc3c(O)ccccc13</chem>	0.1255	0.0058	(-)	-0.1582	0.0101
PTP268-3	<chem>CC(C)CN1c2ccccc2CCc3cccc(O)c13</chem>	0.1025	0.0066	(-)	-0.1582	0.0101
PTP268-4	<chem>CC(C)CN1c2ccccc2CCc3ccc(O)cc13</chem>	0.1029	0.0071	(-)	-0.1582	0.0101
PTP268-5	<chem>CC(C)CN1c2ccccc2CCc3cc(O)ccc13</chem>	0.1255	0.0062	(-)	-0.1582	0.0101
PTP268-6	<chem>CC(C)C(O)N1c2cccc2CCc3ccccc13</chem>	0.1288	0.2313	(±)	-0.1532	0.0112
PTP405-1	<chem>OC1Cc2ccccc2N(N3c4ccccc4CCc5ccccc35)c6ccccc16</chem>	0.2778	0.0046	(±)	-0.3755	0.0018

PTP405-2	<chem>Oc1cccc2N(N3c4cccc4CCc5cccc35)c6cccc6CCc12</chem>	0.1303	0.0043	OD	-0.5266	0.0006
PTP405-3	<chem>Oc1ccc2N(N3c4cccc4CCc5cccc35)c6cccc6CCc2c1</chem>	0.1303	0.0046	OD	-0.5266	0.0006
PTP405-4	<chem>Oc1ccc2CCc3cccc3N(N4c5cccc5CCc6cccc46)c2c1</chem>	0.1727	0.0051	OD	-0.5266	0.0006
PTP405-5	<chem>Oc1cccc2CCc3cccc3N(N4c5cccc5CCc6cccc46)c12</chem>	0.2969	0.0048	OD	-0.5266	0.0006
PTP247-1	<chem>CNCC(C)CN1C=CC(O)Cc2cccc12</chem>	0.0935	0.1379	(±)	0.1398	0.0260
PTP247-2	<chem>CNCC(C)CN1C=CC(C(O)c2cccc12</chem>	0.0958	0.1392	(±)	0.1930	0.0536
PTP247-3	<chem>CNCC(C)CN1C=C(O)CCc2cccc12</chem>	0.0958	0.096	OD	0.1409	0.0360
PTP247-4	<chem>CNCC(C)CN1C=CCc2cc(O)ccc12</chem>	0.1973	0.1406	OD	0.0420	0.0199
PTP247-5	<chem>CNCC(C)CN1C=CCc2c(O)cccc12</chem>	0.1973	0.1344	OD	0.0420	0.0199
PTP247-6	<chem>CNCC(C)CN1C(O)=CCc2cccc12</chem>	0.0338	0.2056	OD	0.1409	0.0360
PTP247-7	<chem>CNCC(C)CN1C=CCc2ccc(O)cc12</chem>	0.2043	0.1374	OD	0.0420	0.0199
PTP247-8	<chem>CNCC(C)CN1C=CCc2cccc(O)c12</chem>	0.2266	0.1376	OD	0.0420	0.0199

* "100% biodegradation" was assigned a numeric value of 1 and "0% biodegradation" was assigned a numeric value of 0.

**A Probability greater than or equal to 0.5 indicates readily biodegradable substance and a probability Less than 0.5 indicates not readily biodegradable

Table SI-2: QSAR toxicity predictions according to ICH M7 guidance for TMP and its PTPs using Case Ultra software: (1) Salmonella mutagenicity TA 97. 98. 100. 1535–1538 (GT1 A7B). (2) A–T mutation E. coli and TA102 (GT1 AT E. coli). (3) Expert rules for genotoxicity (GT Expert). (4) E. coli mutagenicity (all strains) (Pharm E. coli). (5) Salmonella mutagenicity (TA97. 98. 100. 1535–1538) (Pharm Salm).

Compounds	1	2	3	4	5
TMP	(-)	(-)	(-)	(-)	(-)
PTP309a	(-)	(-)	(-)	(-)	(-)
PTP311-1	(-)	(-)	(-)	(-)	(-)
PTP313-1	(-)	(-)	(-)	(-)	(-)
PTP313-2	(-)	(-)	(-)	(-)	(-)
PTP327-1	(-)	(-)	(-)	(-)	(-)
PTP327-2	(-)	(-)	(-)	(-)	(-)
PTP327-3	(-)	(-)	(-)	(-)	(-)
PTP327-4	(-)	(-)	(-)	(-)	(-)
PTP327-5	(-)	OD	(-)	OD	(-)
PTP327-6	(-)	(-)	(-)	(-)	(-)
PTP327-7	(-)	(-)	(-)	(-)	(-)
PTP327-8	(-)	(-)	(-)	(-)	(-)
PTP327-9	(-)	OD	(-)	OD	(-)
PTP327-10	(-)	(-)	(-)	(-)	(-)
PTP327-11	(-)	(-)	(-)	(-)	(-)
PTP327-12	(-)	OD	(-)	OD	(-)
PTP327-13	(-)	(-)	(-)	(-)	(-)
PTP327-14	(-)	OD	(-)	OD	(-)
PTP327-15	(-)	(-)	(-)	(-)	(-)

PTP327-16	(-)	(-)	(-)	(-)	(-)
PTP327-17	(-)	(-)	(-)	(-)	(-)
PTP327-18	(-)	(-)	(-)	(-)	(-)
PTP327-19	(-)	(-)	(-)	(-)	(-)
PTP327-20	(-)	(-)	(-)	(-)	(-)
PTP327-21	(-)	(-)	(-)	(-)	(-)
PTP327-22	(-)	(-)	(-)	(-)	(-)
PTP327-23	(-)	(-)	(-)	(-)	(-)
PTP327-24	(-)	OD	(-)	OD	(±)
PTP329-1	(-)	(-)	(-)	(-)	(-)
PTP134	(-)	(-)	(-)	(-)	(-)
PTP196	(-)	(-)	(-)	(-)	(-)
PTP210-1	(-)	(-)	(-)	(-)	(-)
PTP212-1	(-)	(-)	(-)	(-)	(-)
PTP212-2	(-)	(-)	(-)	(-)	(-)
PTP212-3	(-)	(-)	(-)	(-)	(-)
PTP212-4	(-)	(-)	(-)	(-)	(-)
PTP212-5	(-)	(-)	(-)	(-)	(-)
PTP212-6	(±)	(-)	(-)	(-)	(±)
PTP250	(-)	(±)	(-)	(-)	(-)
PTP268-1	(-)	(-)	(-)	(-)	(-)
PTP268-2	(-)	(-)	(-)	(-)	(-)
PTP268-3	(-)	(-)	(-)	(-)	(-)
PTP268-4	(-)	(-)	(-)	(-)	(-)
PTP268-5	(-)	(-)	(-)	(-)	(-)

PTP268-6	(-)	OD	(-)	OD	(-)
PTP405-1	(-)	(-)	(-)	(-)	(-)
PTP405-2	(-)	(-)	(-)	(-)	(-)
PTP405-3	(-)	(-)	(-)	(-)	(-)
PTP405-4	(-)	(-)	(-)	(-)	(-)
PTP405-5	(-)	(-)	(-)	(-)	(-)
PTP247-1	(-)	(-)	(-)	(-)	(-)
PTP247-2	(-)	(-)	(-)	(-)	(-)
PTP247-3	(-)	(-)	(-)	(-)	(-)
PTP247-4	(-)	(-)	(-)	(-)	(-)
PTP247-5	(-)	(-)	(-)	(-)	(-)
PTP247-6	OD	OD	(-)	(-)	(-)
PTP247-7	(-)	(-)	(-)	(-)	(-)
PTP247-8	(-)	(-)	(-)	(-)	(-)

(+) positive prediction for the respective endpoint. (-) negative prediction for the respective endpoint. inconclusive ((±). the probability of being positive is around the model's current classification threshold \pm 10%). and (OD) Out of domain

Table SI-3: QSAR teratogenicity predictions for TMP and its PTPs by different models (Case Ultra software): A50 (Teratogenicity in Rabbits), A51 (Teratogenicity in Rats), A52 (Teratogenicity in Mouse), and A53 (Teratogenicity in misc. Mammals). (Red is positive result)

Compounds	A50	A51	A52	A53
TMP	known (+)	known (+)	known (+)	known (+)
PTP309a	(-)	(±)	(+)	(±)
PTP311-1	(-)	(±)	(+)	(±)
PTP313-1	(-)	(-)	(-)	(-)
PTP313-2	(-)	(-)	(+)	(-)
PTP327-1	(-)	(-)	(-)	(±)
PTP327-2	(-)	(-)	(-)	(±)
PTP327-3	(-)	(-)	(-)	(±)
PTP327-4	(+)	(-)	(-)	(±)
PTP327-5	(+)	(-)	(-)	(±)
PTP327-6	(-)	(-)	(-)	(-)
PTP327-7	(-)	(-)	(-)	(-)
PTP327-8	(-)	(-)	(-)	(-)
PTP327-9	OD	(-)	(+)	(-)
PTP327-10	(-)	(-)	(-)	(-)
PTP327-11	(-)	(-)	(-)	(-)
PTP327-12	OD	(-)	(+)	(-)
PTP327-13	(-)	(-)	(-)	(-)
PTP327-14	OD	(-)	(-)	(-)
PTP327-15	(-)	(±)	(+)	(±)
PTP327-16	(-)	(±)	(-)	(-)
PTP327-17	(-)	(-)	(+)	(-)
PTP327-18	(-)	(±)	(-)	(-)
PTP327-19	(-)	(-)	(-)	(+)
PTP327-20	(-)	(-)	(+)	(±)
PTP327-21	(-)	(-)	(+)	(-)
PTP327-22	(-)	(-)	(+)	(±)
PTP327-23	(-)	(-)	(-)	(±)
PTP327-24	OD	(-)	(+)	(-)
PTP329-1	(-)	(-)	(-)	(-)
PTP134	(-)	(-)	(-)	(-)
PTP196	(+)	(-)	(-)	(-)
PTP210-1	(-)	(-)	(-)	(-)
PTP212-1	(-)	(-)	(-)	(-)
PTP212-2	(-)	(-)	(-)	(-)
PTP212-3	(+)	(-)	(-)	(±)
PTP212-4	(-)	(-)	(-)	(-)
PTP212-5	(-)	(-)	(-)	(-)

PTP212-6	(+)	OD	(+)	OD
PTP250	(-)	(-)	(+)	(±)
PTP268-1	(-)	(-)	(+)	(±)
PTP268-2	(-)	(-)	(-)	(-)
PTP268-3	(+)	(-)	(-)	(+)
PTP268-4	(-)	(-)	(+)	(±)
PTP268-5	(-)	(-)	(+)	(-)
PTP268-6	(+)	(-)	(+)	(-)
PTP405-1	(+)	(-)	(+)	(-)
PTP405-2	(+)	(-)	(+)	(-)
PTP405-3	(+)	(-)	(+)	(-)
PTP405-4	(+)	(-)	(+)	(-)
PTP405-5	(+)	(-)	(+)	(±)
PTP247-1	(-)	(-)	(±)	(±)
PTP247-2	(-)	(-)	(±)	(±)
PTP247-3	OD	(-)	(+)	(+)
PTP247-4	(-)	(-)	(±)	(±)
PTP247-5	(-)	(-)	(±)	(±)
PTP247-6	OD	(±)	OD	(±)
PTP247-7	(-)	(-)	(±)	(±)
PTP247-8	(-)	(-)	(±)	(+)

Table SI-4. The predicted bacterial toxicity of DMI and its PTPs with four acute toxicity models for *Vibrio fischeri* [Microtox Toxicity to Environmental Bacteria (AUA. Case Ultra) and three acute toxicity *Vibrio fischeri* models (Oasis Catalogic)] (**Red is positive result**)

Compounds	AUA*	Acute tox 5min**	Acute tox 15min**	Acute tox 30min**
TMP	(-)	0.14	0.09	0.05
PTP309a	(±)	1.66	1.41	1.15
PTP311-1	OD	2.59	2.18	1.90
PTP313-1	(-)	2.06	1.69	1.42
PTP313-2	(-)	1.84	1.50	1.24
PTP327-1	(-)	<=1.7744	<=1.4398	<=1.1754
PTP327-2	(±)	<=1.7958	<=1.4500	<=1.1869
PTP327-3	(±)	<=1.7955	<=1.4498	<=1.1868
PTP327-4	(-)	<=0.9078	<=0.6977	<=0.5168
PTP327-5	OD	<=6.9721	<=6.2883	<=6.2682
PTP327-6	(±)	<=3.5292	<=3.0066	<=2.7155
PTP327-7	(±)	<=3.4733	<=2.9783	<=2.6805
PTP327-8	(±)	<=3.5563	<=3.0202	<=2.7324
PTP327-9	(±)	<=13.8099	<=13.1135	<=14.4450
PTP327-10	(±)	<=3.5085	<=2.9962	<=2.7025
PTP327-11	(±)	<=3.5746	<=3.0294	<=2.7437
PTP327-12	(±)	<=13.8543	<=13.1383	<=14.4827
PTP327-13	(-)	<=3.4968	<=2.9903	<=2.6952
PTP327-14	OD	<=13.6387	<=13.0171	<=14.2996
PTP327-15	OD	23.60	23.91	28.37
PTP327-16	OD	<=13.5465	<=12.9651	<=14.2211
PTP327-17	(±)	<=13.7247	<=13.0656	<=14.3727

PTP327-18	OD	<=13.4426	<=12.9062	<=14.1325
PTP327-19	OD	<=6.8798	<=6.2390	<=6.2008
PTP327-20	(±)	<=13.4218	<=12.8944	<=14.1148
PTP327-21	(±)	<=13.6804	<=13.0407	<=14.3351
PTP327-22	(±)	<=13.6740	<=13.0370	<=14.3296
PTP327-23	OD	<=6.8747	<=6.2362	<=6.1970
PTP327-24	OD	24.35	24.35	29.11
PTP329-1	(-)	14.60	14.12	15.63
PTP134	(-)	<=26962.5273	<=39895.7969	<=156250.9219
PTP196	(-)	0.80	0.63	0.49
PTP210-1	(±)	10.65	10.71	12.04
PTP212-1	OD	16.53	16.54	19.92
PTP212-2	(-)	<=4.2292	<=3.7929	<=3.7456
PTP212-3	(-)	<=2.1588	<=1.8313	<=1.6404
PTP212-4	(±)	<=4.2033	<=3.7791	<=3.7269
PTP212-5	(±)	<=4.2585	<=3.8084	<=3.7666
PTP212-6	OD	0.92	0.73	0.58
PTP250	(±)	0.05	0.03	0.01
PTP268-1	OD	0.49	0.37	0.26
PTP268-2	(-)	<=0.1369	<=0.0914	<=0.0530
PTP268-3	(-)	<=0.0781	<=0.0496	<=0.0265
PTP268-4	(±)	<=0.1372	<=0.0915	<=0.0531
PTP268-5	(±)	<=0.1383	<=0.0920	<=0.0534
PTP268-6	OD	0.50	0.37	0.26
PTP405-1	OD	<=0.1025	<=0.0666	<=0.0347

PTP405-2	OD	<=0.3447	<=0.2444	<=0.1521
PTP405-3	(±)	<=0.3454	<=0.2446	<=0.1523
PTP405-4	(±)	<=0.3423	<=0.2433	<=0.1512
PTP405-5	OD	<=0.6523	<=0.4902	<=0.3343
PTP247-1	(±)	51.92	55.84	77.74
PTP247-2	(±)	<=52.8947	<=56.4629	<=78.9311
PTP247-3	OD	15.08	14.53	16.93
PTP247-4	(+)	<=13.5689	<=12.9651	<=14.8744
PTP247-5	(±)	<=13.5216	<=12.9384	<=14.8323
PTP247-6	OD	14.98	14.47	16.83
PTP247-7	(+)	<=13.4634	<=12.9055	<=14.7805
PTP247-8	(±)	<=6.7857	<=6.1820	<=6.4046

*Positive (+). negative (-). inconclusive ((±). the probability of being positive is around 50 ± 10%). out od domain (OD).

**the toxicity value is mg/l (IC 50).

ARTICLE III

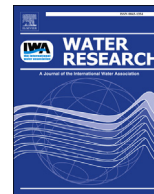
“Studying the fate of the drug Chlorprothixene and its photo transformation products in the aquatic environment: Identification, assessment and priority setting by application of a combination of experiments and various in silico assessments”

Water Research 149, pp. 467-476.

Doi: 10.1016/j.watres.2018.10.075.

AUTHORS:

Nareman D.H. Khaleel, Waleed M.M. Mahmoud, Oliver Olsson, Klaus Kümmerer



Studying the fate of the drug Chlorprothixene and its photo transformation products in the aquatic environment: Identification, assessment and priority setting by application of a combination of experiments and various *in silico* assessments

Nareman D.H. Khaleel^{a, b}, Waleed M.M. Mahmoud^{a, b}, Oliver Olsson^a, Klaus Kümmerer^{a, *}

^a Sustainable Chemistry and Material Resources, Institute of Sustainable and Environmental Chemistry, Leuphana University of Lüneburg, Universitätsallee 1 C13, DE-21335, Lüneburg, Germany

^b Pharmaceutical Analytical Chemistry Department, Faculty of Pharmacy, Suez Canal University, Ismailia, 41522, Egypt

ARTICLE INFO

Article history:

Received 14 July 2018

Received in revised form

28 September 2018

Accepted 28 October 2018

Available online 8 November 2018

Keywords:

Thioxanthene

Photodegradation

Transformation

ABSTRACT

Chlorprothixene (CPTX) is an antipsychotic drug of the thioxanthene class. Although it is widely used as a tranquillizer in psychiatry, anesthesiology, pediatrics, and in general medical practice, there is a gap in knowledge regarding its occurrence and fate in the environment. Therefore, we provide for the first-time data on the environmental fate and ecotoxicity of CPTX and its potential photo-transformations products (PTPs).

Firstly, two standardized biodegradation tests (Closed Bottle test (CBT) and Manometric Respiratory test (MRT)) were performed to assess CPTX's environmental biodegradability. Then, its photo-degradability was studied using Xenon and UV lamps. Effects of different conditions (initial drug concentration, pH, and temperature) were applied during UV-photodegradation. Subsequently, the time courses of CPTX and dissolved organic carbon (DOC) concentrations were monitored throughout the photodegradation tests. After that, high-resolution mass spectrometry was employed to elucidate the structures of the formed photo-transformation products (PTPs). In addition, biodegradation tests were performed for the photolytic mixtures to assess the biodegradability of the PTPs. Finally, the (eco)toxicity assessment for CPTX and its photolytic mixtures was predicted using different (quantitative) structure-activity relationship ((Q)SAR) software.

CPTX was found to be not readily biodegradable in CBT and MRT. CPTX was not eliminated by irradiation with the Xenon lamp, however primarily eliminated using the UV-lamp. The CPTX elimination during UV-irradiation was faster at lower concentrations. CPTX UV-photodegradation was affected by pH value, while not affected by the temperature of the irradiated solution. 13 PTPs were detected in UV-photolysis mixtures. One additional product was detected in CPTX standard solution, and it was degraded simultaneously with CPTX during UV-irradiation. On one hand, Biodegradation assays revealed that UV-photolytic mixtures of CPTX, containing its PTPs, were not better biodegradable than CPTX itself. On the other hand, LC-MS analysis showed some PTPs which were eliminated after the biodegradation tests indicating possible biodegradability of these PTPs. This because those PTPs are present in low concentrations in the photolysis mixture and their effect can be hindered by the effect of CPTX and other non-biodegradable PTPs. QSAR analysis revealed that CPTX and some of its PTPs may have some human and/or eco-toxic properties.

In conclusion, the release of CPTX into aquatic environments could be harmful. Therefore, further research focusing on CPTX and its PTPs are strongly recommended.

© 2018 Elsevier Ltd. All rights reserved.

* Corresponding author. Nachhaltige Chemie und Stoffliche Ressourcen, Institut für Nachhaltige Chemie und Umweltchemie, Leuphana Universität Lüneburg, C.13, Universitätsallee 1, D-21335, Lüneburg, Germany.

E-mail address: klaus.kuemmerer@leuphana.de (K. Kümmerer).

1. Introduction

The occurrence of emerging organic contaminants in the aquatic environment has been raised in recent years. Pharmaceuticals and their byproducts, from incomplete mineralization, are an important part of these contaminants and may cause adverse ecological and/or human health effects (Rastogi et al., 2014; Santos et al., 2010). Most of these contaminants were not regulated or controlled. Pharmaceuticals in general and neurological drugs in particular have been found in different environmental compartments such as rivers, psychiatric hospitals effluent, and wastewater treatment plants in the concentration range of ng/L to µg/L (Herrmann et al., 2016; Writer et al., 2013; Yuan et al., 2013). Although the consumption of neurological drugs is high, their potential hazard including their environmental fate and behaviour is still not well understood compared to other drugs such as antibiotics.

Chlorprothixene (CPTX, C₁₈H₁₈ClNS, CAS Nr. 6469-93-8) is a neuroleptic of the thioxanthene class. CPTX is widely used as a major tranquillizer in psychiatry, anesthesiology, pediatrics and in general medical practice (Huus and Khan, 1967; Santiago et al., 2011). It is also prescribed for anxiety and agitation because of its strong sedative effect (Chen et al., 2012). In the year 2016, the consumption of prescribed CPTX in Germany was 1.8 tons (Schwabe et al., 2017). In addition, it was reported by Herrmann et al. that CPTX is highly used in nursing homes and in psychiatric hospitals in Germany (Herrmann et al., 2015b).

CPTX is metabolized in human bodies mainly to nor-chlorprothixene and chlorprothixene-sulfoxide. CPTX and its metabolites are excreted in urine and feces (Käferstein et al., 2013). Like other pharmaceuticals, CPTX will reach the influents of sewage treatment plants (STPs) either through excretion or through improperly drug disposal. If no effluent treatment is in place, CPTX and its metabolites will directly enter surface water. In aquatic systems, CPTX can undergo biotic degradation by microorganisms (Henning et al., 2018; Herrmann et al., 2016), and photodegradation by sunlight or UV-irradiation which is used in drinking water purification systems and is discussed for advanced wastewater treatment (Herrmann et al., 2015a; Khaleel et al., 2016, 2017; Kovalova et al., 2013). Despite that, nothing is known about the occurrence and fate of CPTX in the aquatic environment. Therefore, more data in this respect is needed for a sound environmental risk assessment.

Incomplete mineralization of pharmaceuticals in the environment results in the formation of new chemicals i.e. transformation products (TPs). In general, environmental fate and hazardous properties of TPs can strongly differ from their parent compounds (Illés et al., 2014; Mahmoud et al., 2014). Therefore, it is important to identify the structure of the possibly formed TPs and to study their fate and toxic properties. The research about TPs is a huge and difficult task. Most often they are not commercially available, and their synthesis or their isolation and enrichment are tedious, expensive and time-consuming, if possible at all. Also, there are often many TPs generated from one parent compound. Therefore, experimental investigation of individual TPs is most often impossible. (Quantitative) structure-activity-relationships ((Q)SARs) are increasingly used to identify hazardous structural features, therefore. Consequently, QSAR methodologies were recently suggested to be used for the risk assessment of pharmaceuticals and their TPs (Mahmoud et al., 2013; Menz et al., 2017).

The main objectives of this research were to provide for the first-time data about the fate and effects of CPTX and possibly within a treatment or the aquatic environment formed TPs through studying biodegradability, photo-degradability under different conditions, and toxicity.

2. Materials and methods

2.1. Chemicals

Chlorprothixene (CAS Number: 6469-93-8) of analytical reagent grade was supplied by Sigma–Aldrich (Steinheim, Germany). Acetonitrile (LiChrosolv[®], LC–MS grade) and formic acid were purchased from VWR (Darmstadt, Germany). Aqueous mobile phase, standard solutions, and solutions for photolysis (UV and Xenon) and biodegradation (CBT and MRT) treatments were prepared with ultrapure water obtained from a SG Ultra-Clear UV TM Water Purification System with TOC monitoring from SG Wasser-aufbereitung und Regenerierstation (Barsbüttel, Germany). All the nutrients used in biodegradation tests have a purity of 98.5% at least.

2.2. Photo-degradation experimental setup

Photo-degradation experiments were performed at concentrations higher than the ones to be expected in the environment in order to be able to perform subsequently biodegradation tests which demand at least a concentration of test compound (theoretical oxygen demand, ThOD) around 5 mg/L. In addition, higher concentrations are also required to good identify the PTPs and to follow their formation curves. The effect of starting concentration on photolysis was addressed by testing the following range of concentrations (5, 10, 50, and 100 mg/L). Xenon lamp and UV-lamp were employed in order to simulate sunlight (environment) and UV disinfection (potable water treatment). The Xenon lamp (TXE 150, UV Consulting Peschl, Mainz, Germany) emits a spectrum similar to natural sunlight (200–800 nm). The UV-lamp is a medium-pressure mercury lamp (TQ150, UV Consulting Peschl, Mainz, Germany) with ilmasil quartz immersion tube. The UV-lamp emits polychromatic radiation and its total photon flow rate for all wavelengths was 5.71×10^6 (mol \times photons \times cm⁻² \times s⁻¹) (more information in text S1(SM)). CPTX shows high absorption in the UV-range with the absorption maximum at 270 nm, which means that CPTX was expected based on its absorption spectrum to have a high accessibility for UV-radiation used here (Fig. S1(SM)).

In photodegradation experiments, about 800 mL of the working solution was used in a 1000 mL laboratory batch glass photoreactor. During the entire experiments, mixtures were magnetically stirred to ensure a constant mixing of the solutions. The temperature was maintained to the desired value by a circulating cooler (WKL230, LAUDA, Berlin), and pH was monitored throughout the test. During the experiments, samples were drawn from the reactor at different time intervals (0, 2, 4, 8, 16, 32, 64, and 128 min) to assess concentration change of CPTX and dissolved organic carbon (DOC) using HPLC-UV, LC-MSⁿ, and DOC analyses. Before analyses, all samples were filtered by 0.45 µm filter membranes (CHROMAFIL[®] Xtra. Typ: PES 45/25, Macherey-Nagel, Germany). Samples were analyzed directly or stored in the dark at –20 °C until analysis. For more details, see text S1(SM).

Photolysis experiments using the Xenon lamp were performed with an initial CPTX concentration of 10 mg/L at 20 °C and pH value of 5. Photolysis experiments using the UV-lamp were performed under different conditions (initial CPTX concentrations of 5, 10, 50, and 100 mg/L; temperatures of 10, 20, 30, and 40 °C; and pH values of 3, 5, 7, and 9), in order to study the effect of these parameters on the degradation kinetics and on the PTPs formed.

For CBT and MRT of the photolytic mixture, samples were collected at 0 min and after 4, 16, and 128 min of UV-irradiation. The initial concentration of CPTX in the photolytic treated samples was adjusted by measuring the DOC of the tested substance (0 min, i.e. before photolysis) and of the photolyzed samples, to

determine the required carbon content and to calculate the theoretical oxygen demand (ThOD), for each CBT and MRT.

A pseudo-first-order kinetic model was used, according to the OECD guidelines, to determine the photo-degradation rate constants (OECD, 2008).

2.3. Analytical methods

CPTX concentration was determined by using a high-performance liquid chromatography (HPLC) (Shimadzu, Duisburg, Germany) consisting of an LC-10AT binary pump, a CBM-10A communication interface, an SPD-M10A diode array detector (DAD), an SIL-10 autosampler, a CTO-10 AS VP column oven, and Shimadzu Class LC10 software version (5.0). The chromatographic column used was an RP-C18 column (EC 125/4 NUCLEODUR® 100-5 C18 ec, Macherey and Nagel, Düren, Germany), protected by an EC guard column (NUCLEODUR® 100-5 C18 ec, 4 × 3 mm). The mobile phase consisted of 0.1% formic acid in water (CH₂O₂: solution A) and 100% acetonitrile (CH₃CN: solution B). A linear gradient method was applied: 0 min 1% B, 4 min 10% B, 11.50 min 20% B, 13 min 30% B, 15 min 45% B, 18 min 50% B, 20 min 30%, 23 min 1% B, 28 min 1% B. Detection wavelength was set to 270 nm. The elution flow rate was 0.5 mL min⁻¹, the oven temperature was set to 45 °C, and the injection volume was 10 µL in all samples.

The degree of mineralization in photolysis experiments and biodegradation tests was studied by DOC measurement using a Total Organic Carbon (TOC) Analyzer Shimadzu 5000A (TOC 5000, Shimadzu GmbH, Duisburg, Germany) in three replicates.

An LC-MSⁿ analysis was performed a) for screening on an Agilent 1100 series HPLC system (Agilent Technologies, Waldbronn, Germany) coupled to a Bruker Esquire 6000 plus low-resolution mass spectrometer with an ESI source (Bruker Daltonics, Bremen, Germany) (LC-ITMS), and b) for confirmation of the derived chemical structure of the TPs using a Dionex Ultimate 3000 UHPLC system (Dionex, Idstein, Germany) coupled with a LTQ Orbitrap-XL high-resolution mass spectrometer with a H-ESI source (Thermo Scientific, Bremen, Germany) (LC-HRMS). The chromatographic method described above was also used for LC-MSⁿ analysis (for more information about the used LC-MSⁿ systems, see Text S2(SM)).

An absolute measurement of the individual concentrations of the TPs is not possible, due to the lack of standards for these TPs. Furthermore, a peak of low intensity does not necessarily correspond to a low concentration of the related TP and vice versa. Therefore, the peak area of TPs (A) was related to the peak area of CPTX at time point 0 min (A₀) to calculate the recovery% of each TP. Every TP exceeding 0.5% of A/A₀ was structurally elucidated. Structures were analyzed using Auto-MS Mode and, to improve the reliability of results, the LC-HRMS up to MS³ was studied. Moreover, the occurrence of TPs in different conditions was studied to confirm their formation.

Samples from the biodegradation tests were analyzed with LC-ITMS using recovered peak areas of CPTX and its TPs S/S₀ (S is the peak area of the TP at day 28, and S₀ is the peak area of the TP at day 0).

2.4. Biodegradation testing: Closed Bottle test (CBT) and Manometric Respiratory test (MRT)

CBT and MRT were performed according to the OECD 301D and 301F guidelines, respectively. The basic experimental set-ups and validity criteria are described in detail elsewhere (Calisto and Esteves, 2009). The standard test period for both CBT and MRT is 28 days, and they are performed at room temperature (20 ± 1 °C) in the dark at pH of 7.5. Temperature and pH were monitored during

the test. The test systems, in CBT and MRT, contain four different series: (test substance, toxicity control, blank, and quality control). MRT contains an additional fifth series named sterile control. Sterile control vessel contains sodium azide to account for abiotic degradation. Toxicity controls allow for the recognition of false negative results caused by the toxicity of the test compound against the degrading bacteria used in the tests. All test vessels were inoculated with an aliquot from the effluent of the municipal STP of AGL in Lüneburg, Germany (144,000 inhabitant equivalents). Comparing CBT and MRT, MRT was performed with higher bacterial density and higher sodium acetate and test compound concentrations (Table S1(SM)). Samples at day 0 and day 28 were taken and stored at -20 °C for subsequent HPLC-UV, and LC-MSⁿ analyses.

Measurements were performed in duplicates, respectively. The final biodegradation in percentage was calculated, after subtracting the blank values, from the quality control, toxicity control, and test compound values. In both tests, the chemical is classified as readily biodegradable if the measured biochemical oxygen demand (BOD) reaches at least 60% of the theoretical oxygen demand (ThOD) or DOC of 70% (OECD, 1992). For more information about biodegradation measurements, see Text S3(SM).

2.5. In-silico prediction of toxicity and environmental fate

The software for *in-silico* prediction of properties of TPs were: Case Ultra V 1.5.2.0 (MultiCASE Inc.) (ChemAxon, 2015; Marvin Sketch 15.6.15.0; International Conference on Harmonization (ICH), 2014), EPI Suite (EPIWEB 4.1) from the U.S. Environmental Protection Agency (<http://www.epa.gov/oppt/exposure/pubs/episuite.htm>), and Oasis Catalogic (V.5.11.6TB) from Laboratory of Mathematical Chemistry, University Bourgas, Bulgaria (Rastogi et al., 2014). All the *in-silico* models used in our study have validated databases and training sets as well as information on applicability domains. More details can be found elsewhere (Menz et al., 2017; Calisto and Esteves, 2009).

2.5.1. In-silico prediction of ready biodegradability

The biodegradability for CPTX and its TPs was predicted by *in-silico* models shown in Table 1. *In silico* prediction of ready biodegradation of TPs was used to support analytical results from the biodegradation tests. As in biodegradation tests, elimination of the TPs using LC-MS methods can only be measured while not attributed to their biodegradation. The ready biodegradability values in most of the used models were predicted according to OECD 301C MITI-I test (Ministry of International Trade and Industry, Japan) (OECD, 1992). Only the Oasis Catalogic software provides one biodegradation model according to OECD 301F which is comparable to the experimentally performed biodegradation test (MRT) (Trautwein and Kümmerer, 2012). More details about the predicted values using *in silico* models were provided in Text S4(SM).

2.5.2. In-silico prediction of toxicity

Carcinogenicity, mutagenicity, and teratogenicity are among the toxicological endpoints that pose the highest concern for human health. *In-silico* toxicity for CPTX and its TPs was predicted by a set of *in-silico* prediction models for toxicity (Table 1). Case Ultra was used applying a combination of statistical and rule-based systems for bacterial mutagenicity according to the recently adopted ICH M7 guideline (International Conference on Harmonization (ICH), 2014). In addition, Case Ultra was used to predict teratogenicity based on the models A50, A51, A52, and A53. Case Ultra software was used also to predict acute bacterial toxicity based on microtox tests (toxicity to bacterium *V. fischeri*), and on Rainbow Trout Toxicity (toxicity to fish). Oasis Catalogic software was also used to

Table 1
List of *in-silico* models and software used for the log P, biodegradability and toxicity predictions of CPTX and its TPs.

QSAR	software Models	End-points	References
Catalogic v 5.11.6 TB (OASIS)	Catalogic BOD Kinetic v.08.09	Ready biodegradability according to OECD 301F	(Laboratory of Mathematical Chemistry, 2012)
	Catalogic BOD 28 days OECD 301C v.06.07	Ready biodegradability according to MITI-I test	
Case Ultra v.1.4.5.1 (MultiCASE Inc.)	Vibrio fischeri pT30 v.01	Acute toxicity against <i>V. fischeri</i> after 30 min, IC50 [mg/L]	(Chakravarti et al., 2012; Saiakhov et al., 2013)
	MITI-I test (OECD 301C, module AU6)	Ready biodegradability according to MITI-I test	
	GT1 A7B	(Mutagenicity for 7 strains of <i>Salmonella typhimurium</i> TA 97, 98, 100, 1535–1538), FDA data source)	
	GT1 AT Ecoli	(A–T mutation in <i>E. coli</i> and <i>S. typhimurium</i> TA102, FDA data source)	
	Pharm Ecoli	(<i>E. coli</i> mutagenicity (all strains) from public and proprietary sources)	
	Pharm Salm	(<i>Salmonella typhimurium</i> mutagenicity (TA97, 98, 100, 1535–1538) from public and proprietary sources)	
	GT Expert	Expert rules for genotoxicity	
	Microtox toxicity environmental bacteria (AUA)	Bacterial toxicity	
	Rainbow trout toxicity (AUE)	Bacterial toxicity	
	A50 v.1.5.2.0.795.300	Teratogenicity in Rabbits	
A51 v.1.5.2.0.1232.500	Teratogenicity in Rat		
A52 v.1.5.2.0.766.500	Teratogenicity in Mouse		
A53 v.1.5.2.0.1350.550	Teratogenicity in misc. Mammals		
EpiSuite (EPIWEB 4.1)	Biodegradation probability Biowin 5 (linear model)	Ready biodegradability according to MITI-I test	(U.S. EPA, 2012)
	Biodegradation probability Biowin 6 (non-linear model)		

predict acute toxicity towards *V. fischeri* (30 min exposure time), in which the predicted activity of the test chemicals was expressed as mg/L for half maximal inhibitory concentration (IC₅₀).

3. Results and discussion

3.1. CPTX photodegradation

The direct photo-degradation and mineralization results of 10 mg/L CPTX (20 °C and pH 5) using Xe-lamp and UV-lamp were followed to evaluate the fate of CPTX under sunlight and UV-irradiation (Fig. 1). With Xe-lamp, CPTX showed no significant elimination or mineralization during 128 min of irradiation. That is in agreement with expectation as absorbance spectrum of CPTX does not significantly overlap with the emission spectrum of the Xenon light source. With UV-lamp, 10 mg/L CPTX was primarily eliminated and partially mineralized. Within the first 16 min of UV-irradiation, 99.6 ± 0.4% of CPTX was eliminated. At the same time, there was no significant loss of CPTX observed in dark controls, so CPTX underwent photolytic degradation only by the effect of the UV-Lamp used. Slower mineralization was observed, and DOC elimination at 16 min of UV-radiation was not more than 20%. After 16 min of UV-radiation, the DOC elimination% continued to increase and it reached the value of about 70% elimination after 128 min of radiation. The incomplete removal of DOC and the primary elimination of CPTX indicate the formation of PTPs during the UV-irradiation. At the beginning of 10 mg/L CPTX UV-experiment, the pH of the solution was 5.2 ± 0.4, and it decreased gradually to reach the value of 3.9 ± 0.5 at the end of the test (128 min). This might indicate that the formed PTPs can have acidic nature.

The UV-photolysis curves of CPTX using different initial concentrations are shown in Fig. 2. Experiments performed at different initial concentrations fit pseudo-first-order kinetics with high linearity ($R^2 > 0.98$) with k values equal to 0.054, 0.094, 0.386, and 0.702 min⁻¹ at concentrations of 100, 50, 10, and 5 mg/L, respectively (Fig. S2(SM)). The degree of DOC removal results showed that, after 128 min of irradiation in the experiments at 100, 50, 10, and 5 mg/L, mineralization% was about 14.1, 19.9, 69.8, and 87.1,

respectively (Fig. 2). The quantum yield was only possible to be calculated for the initial concentration of 5 mg/L, and it was determined to be 0.064. From the above-mentioned results, it is obvious that CPTX elimination kinetics and the corresponding DOC removal were faster at lower initial concentration. This because more CPTX molecules and more intermediates and PTPs at higher concentrations do compete to absorb the radiant energy in the irradiated solution (Gutowski et al., 2015). Therefore, degradation of CPTX might be quite fast under real-world conditions, but it cannot be also excluded that there will be other compounds present in the environmental water (i.e. quenching compounds as well as radiation absorbing compounds) that may slow down the photo-transformation process (Oliveira et al., 2019; Trovó et al., 2014).

In photodegradation tests of 100 mg/L CPTX at different temperatures (10 °C, 20 °C, 30 °C, and 40 °C; in UP water (pH = 5.0)), the photolysis and the mineralization rate values are very close (Fig. S3(SM)). So, the temperature showed not a highly remarkable effect on the UV-photolysis of CPTX. The degradation kinetic rates at 10 °C and 40 °C are slightly faster than that at 20 °C, and the slowest degradation rate was observed at 30 °C experiments (Fig. S4(SM)).

3.2. Influence of pH on photo-degradation of CPTX

The pH influence on the photo-degradation of 100 mg/L CPTX was investigated by performing tests at pH values ranging from 3.0 to 7.0 (Fig. 3). In the dark controls, CPTX was found to be soluble at pH < 7. At pH 7, CPTX dissolved concentration (100 mg/L) decreased and the solution became a little turbid because about 25% of the added CPTX precipitated. Photodegradation in highly alkaline pH was not studied here, because CPTX precipitates at higher pH and a fluctuation in the concentration at the test beginning was observed affecting the quality of the test. Fig. S5(SM) shows the soluble part (in %) of 100 mg/L CPTX at different pH values.

The pK_a value of CPTX is 9.76 and it has two forms in aqueous solution (Fig. S6(SM)) (ChemAxon, 2015. Marvin Sketch 15.6.15.0). Photodegradation of CPTX at pH 3, 5, and 7 fitted first-order kinetics. CPTX shows the highest degradation rate at pH 3 in which

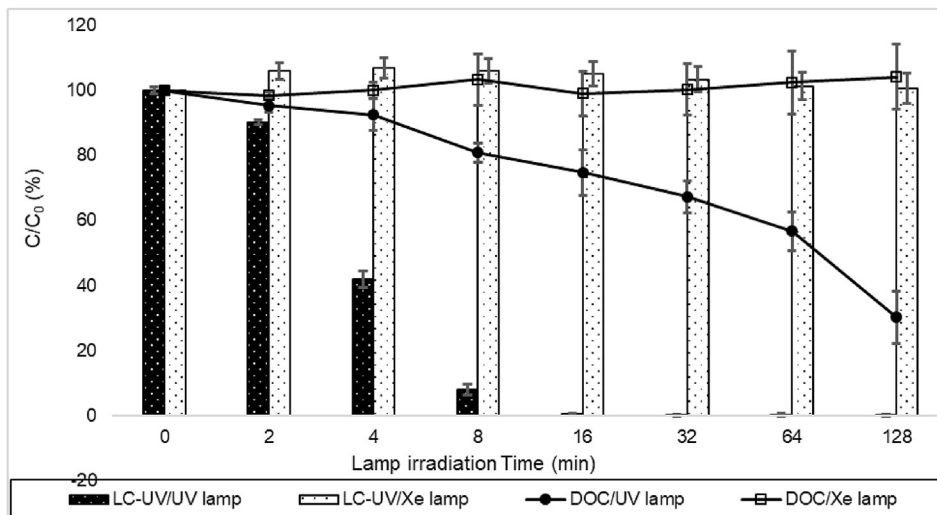


Fig. 1. Elimination of Chlorprothixene (CPTX) by UV- and Xe-photolysis (10 mg L^{-1} CPTX) monitored by LC-UV and Dissolved Organic Carbon (DOC) ($n = 3$).

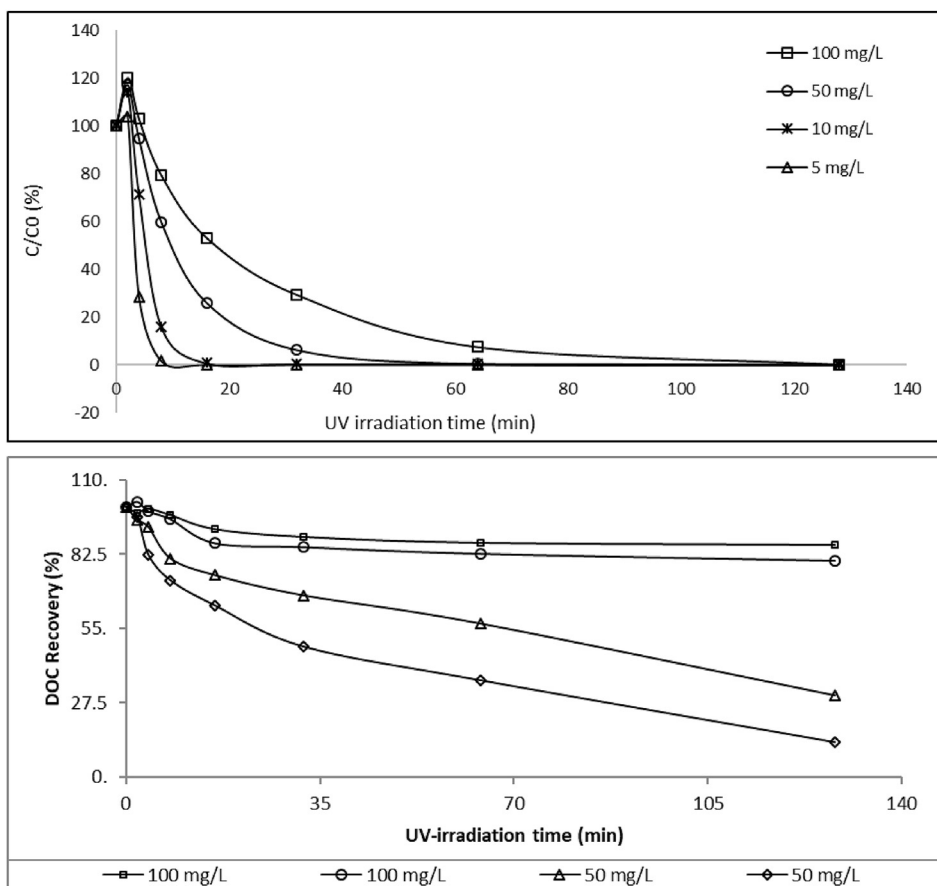


Fig. 2. The photolytic elimination (a) and the DOC (b) of CPTX by means of UV-photodegradation at different concentrations. PH = 5, temperature = 20°C ($n = 2$, $\text{SD} < 3.5$ at all points).

CPTX is in its protonated form (HCPTX^+). The slowest degradation rate was observed at pH 5 conditions which followed first order kinetic with k value equal 0.0544 (Fig. S7(SM)). Under pH 3 and pH 7 conditions, the degradation of CPTX showed two staged degradation rates; a first faster rate till 32 min of UV-irradiation with k values equal 0.071 and 0.0596, respectively, followed by a slower

rate with k values equal 0.0434 and 0.0456 at pH 3 and pH 7 experiments, respectively (Fig. S7(SM)). The degradation rate at pH 7 could be not only due to the pH effect but also due to the lower dissolved concentration. Fig. 3b shows the DOC removal kinetics of CPTX at studied pH values. The rates of change in the degree of mineralization during irradiation at different pH experiments are

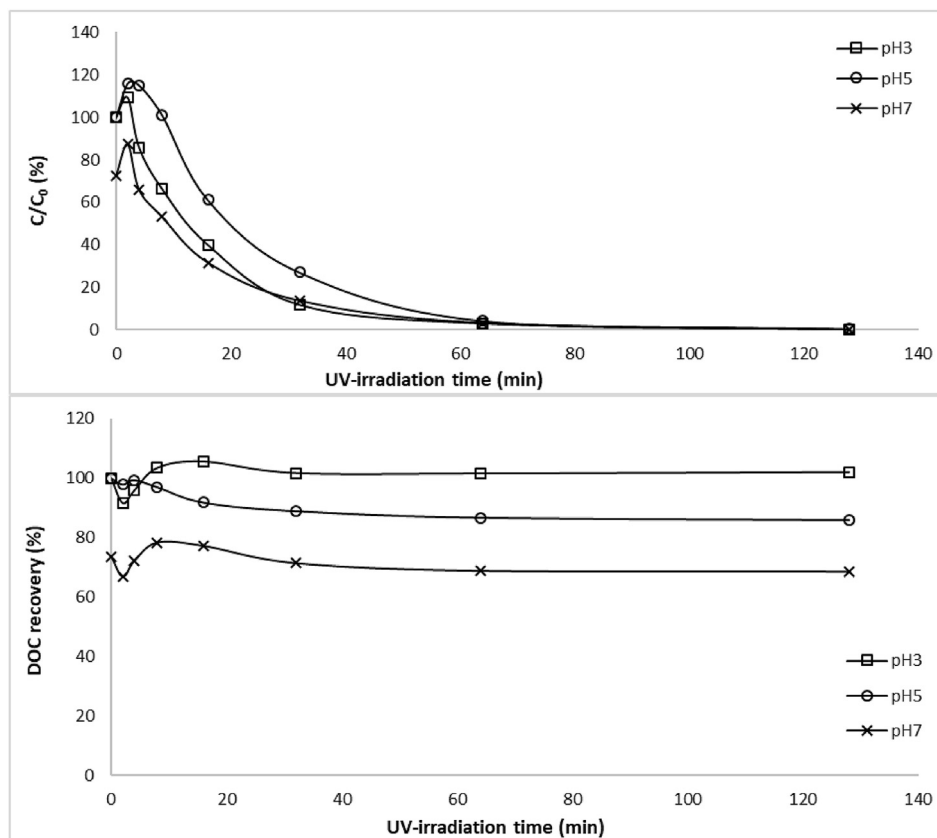


Fig. 3. The photolytic elimination (a) and the DOC (b) of CPTX by means of UV photodegradation at different pH values. CPTX initial concentration = 100 mg L⁻¹, temperature = 20 °C (n = 2, SD < 2.3 at all points).

nearly the same. Which means that pH could have a non-remarkable effect on the mineralization rate of CPTX.

3.3. Identification of CPTX transformation products

The LC-MS total and extracted ion chromatograms were checked for samples of the UV-irradiated aqueous solution of CPTX. 14 TPs were observed, and their chemical structure could be assigned, respectively. The log P values for the TPs were predicted using QSAR models (Table S4(SM)), and it helped in the differentiation between the isomers because the compound which has lower log P value is more polar and therefore should appear at relative lower t_R on the applied non-polar analytical column. Fig. 4 shows the tentative photodegradation pathway of CPTX according to our results. Table S2(SM) shows CPTX and its TPs, which are labeled according to their m/z values. It is obvious from Table S2(SM) that all the formed TPs appear at lower t_R than CPTX itself and therefore showed lower log P values in Table S4(SM). So, the formed TPs are expected to show higher mobility and persistence in the aquatic environment. In addition, CPTX's TPs can be harder removed from water by sorption processes due to their higher polarity than CPTX and thus higher water solubility (Reemtsma et al., 2016). The fragmentation pattern for each TP can be found in Figs. S8–S20(SM). All the observed TPs had not been observed in any earlier studies.

In CPTX standard samples, before photolysis, one product at (m/z: 282.13) was observed with a low peak intensity, and it degraded gradually during the UV-irradiation. This TP could be either an impurity or a hydrolysis-transformation product, and it is labeled as TP282. It has the suggested molecular formula of C₁₈H₂₀NS and

predicted to be a de-chlorinated derivative from CPTX (Fig. S9(SM)).

Two PTPs were detected with m/z 316 and they were labeled as PTP316-1 and PTP316-2. PTP316-1 (m/z 316.14) is suggested to be formed from CPTX after de-chlorination and di-hydroxylation processes (Fig. S10(SM)). PTP316-2 (m/z = 316.09) has suggested molecular formula and relative double bond (RDB) value similar to CPTX. In addition, its MSⁿ fragmentation pattern was mostly as CPTX with little differences which cannot be used to suggest the difference between the two substances. Therefore, PTP316-2 is assumed as an isomer to CPTX (Fig. S8&S11(SM)).

Five precursor ion peaks with m/z 332 were observed and can be divided into two groups: the first one has the exact m/z value of 332.13 and the suggested molecular formula: C₁₈H₂₂O₃NS. This group includes PTP332-1, PTP332-2, and PTP332-3, which are suggested to be isomers generated from CPTX after de-chlorination and tri-hydroxylation. These three PTPs gave MSⁿ fragmentation patterns that are mostly the same with very little differences which allow not to differentiate them (Figs. S12–14(SM)). Combining the obtained fragmentation pattern and the log P values, PTP332-1 can have two hydroxyl groups on the tricyclic ring and one on the first or second carbon atom of the aliphatic side chain. PTP332-2 can have two hydroxyl groups on the tricyclic ring and one on the third carbon atom of the aliphatic side chain. PTP332-3 can have the three hydroxyl groups on the tricyclic ring. The second group has the m/z value of 332.09 with the suggested molecular formula of C₁₈H₁₉ONCIS and it includes PTP332-4 and PTP332-5. They differ only in their retention time and have the same RDB values and their MSⁿ fragmentation pattern is almost the same. Therefore, this group is identified as isomers formed by mono-hydroxylation of CPTX where they differ in the position of the hydroxylation

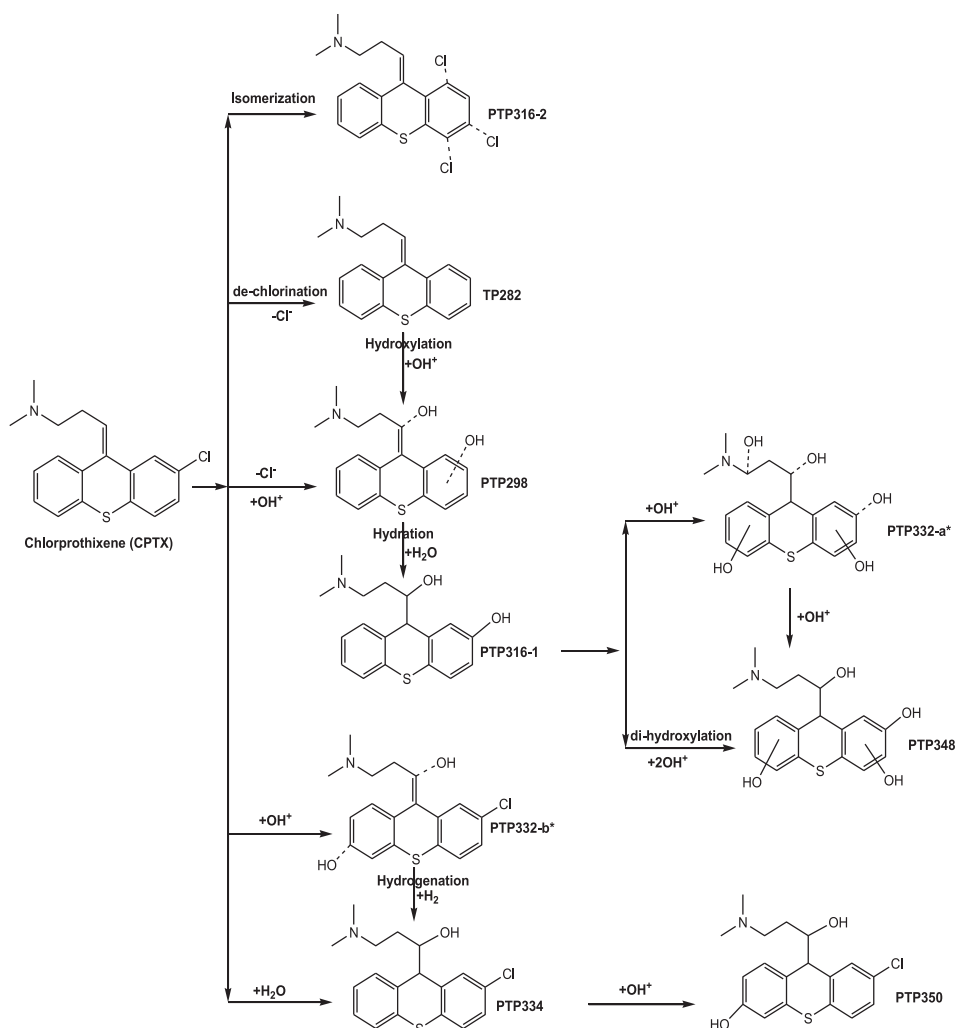


Fig. 4. Proposed tentative scheme of degradation pathways of CPTX and formation of PTPs during photolysis under Medium pressure UV-lamp.

(Figs. S15–16(SM)). According to the log P values, PTP332-4 is hydroxylated on the aliphatic sidechain and PTP332-5 on the tricyclic ring.

The PTP with m/z 334.1 could be formed through the hydration of CPTX (Fig. S17(SM)).

The PTP detected with m/z 348.13 is suggested to be formed from the de-chlorination of CPTX and the addition of four hydroxyl groups (Fig. S18(SM)).

With m/z 350.1, one PTP was observed that could have been generated from CPTX after hydration and mono-hydroxylation processes (Fig. S19(SM)).

Three PTP isomers with m/z 298.12 were produced from a de-chlorination of CPTX followed by a mono-hydroxylation process (Fig. S20(SM)). According to the Log P predicted values, the hydroxylation in PTP298-1 is likely to occur at the aliphatic sidechain as it appears at lower t_R . PTP298-2 and PTP298-3 are probably hydroxylated on the tricyclic ring.

In a study with chlorpromazine which is a structurally highly related substance (Trautwein and Kümmerer, 2012), most of the photolysis products were formed by sulfoxidation. In our study, the sulfoxide product was excluded because the MS^2 fragment which indicates the extrusion of the SO moiety ($-48 m/z$) was not detected. In addition, Our LC-MS results showed a loss of water which confirms the hydroxylation at a carbon atom, not at the sulfur atom. Furthermore, the RDB values of our PTPs excluded any

sulfoxidation.

Fig. S21(SM) shows the appearance/disappearance of the TPs formed with A/A_0 (%) above 0.5% during the photolysis of CPTX (initial concentration of CPTX is 100 mg/L, pH 5, and temperature 20 °C; $n = 3$). PTP316-1, PTP298-1, and PTP334-4 are the main transformation intermediate during CPTX photolysis. Their yields reached up to 12.6, 10.5, and 6.5 (A/A_0 %), respectively. Concentration of products (PTP316-1, PTP332-1, PTP332-3, PTP32-4, PTP332-5, PTP348, PTP298-1, PTP298-2, and PTP298-3) increased quickly during the first 16 or 32 min of reaction and then decreased slowly. The concentration of PTP332-2 increased slowly during the first hour and then decreased quickly. While, the concentration of products (PTP316-2, PTP334, and PTP350) increased quickly during the first 8 min of reaction and decreased also quickly during the next 8 min.

At lower initial concentration, the TPs formed and eliminated faster than at higher concentrations (Fig. S22(SM)). Some TPs were not detected at lower concentrations such as PTP332-3, PTP332-5, PTP348, and TP282 which are not detected at experiments performed with 5 mg/L CPTX. This finding agrees with many other findings (Herrmann et al., 2015a; Herrmann et al., 2016; Khaleel et al., 2017). On the other hand, the temperature showed no highly significant effect on the formation behavior of the TPs (Fig. S23(SM)).

3.4. Influence of solution pH value on PTP formation

The behavior of the identified TPs is compared in UV-photolysis experiments performed at different pH values of 3, 5, and 7 (Fig. S24(SM)). As the pH of the real water samples is mostly slightly alkaline, so the PTPs that formed with higher A/A_0 (%) value, in the pH 7 experiment, could be more relevant to the environment. It was observed that PTP316-1 was detected with the highest peaks, as it showed A/A_0 % value equal 12.6 and 9.0 in experiments performed at pH 5 and pH 7, respectively. At pH 3 PTP316-1 was formed with very low A/A_0 % value. This means that the de-chlorination of CPTX combined with di-hydroxylation processes could favorably occur in neutral and weakly acidic conditions and is unlikely to take place under strongly acidic conditions and therefore normally of high interest in the aquatic environment. A similar case was also observed for PTP316-2, which was formed with A/A_0 % value equal 3.7 and 7.1 at experiments performed at pH 5 and pH 7, respectively corresponding to only 0.6% A/A_0 value in the pH 3 experiment. This can lead to the conclusion that the isomerization of CPTX can favorably occur when the pH value increases until pH 7 and is less likely to take place in strongly acidic condition, and that PTP316-2 is of interest to the environment. PTP334 showed A/A_0 % values equal 10.6, 6.5, and 1.7 in experiments at pH 7, pH 5, and pH 3, respectively. This indicates that hydration of CPTX can more likely happen when the solution pH value increases till pH 7, and that this PTP is of further interest. PTPs (298-2 and 298-3) are formed with A/A_0 % values equal (9.0 and 10.8), (5.2 and 6.0), and (2.5 and 2.6) in pH 3, pH 5, and pH 7 experiments, respectively. This means that de-chlorination and hydroxylation of the tricyclic ring in CPTX molecule are favored in strongly acidic media and its occurrence% is inversely proportional to the pH value, and therefore they are normally of less interest in the aquatic environment. The case was reversed in case of PTP298-1 which is of high interest in the environment as it formed with higher A/A_0 % values at pH 5 and pH 7 experiments equal 13.1 and 9.6, respectively, corresponding to 0.2 A/A_0 % at pH 3. It can be concluded that de-chlorination and hydroxylation of the aliphatic side chain in the CPTX molecule is difficult to occur at pH 3 and is likely to take place at weak acidic and neutral conditions. PTP332-3 was the one with the highest peak area formed compared with the five PTPs with m/z 332; its highest formation ratio was seen at pH 5 experiment (4.6%), followed by pH 3 with A/A_0 % value equal to 2.4 and its concentration was lower at pH 7 with 0.6 A/A_0 %, so it is of less interest to the environment. PTP332-5 showed A/A_0 % values of 1.2, 0.9, and 0.3 in experiments performed at pH 3, pH 5, and pH 7, respectively, indicating probable non-significant relevant to the environment. The pH had no effect on formation behavior of PTP332-1, PTP332-2, and PTP332-4, as they showed nearly similar A/A_0 % values in experiments performed at different pH values. The formation ratio of PTP350 is directly proportional to the solution pH, as it showed 3.7, 0.7, and 0.1 A/A_0 % in pH 7, pH 5, and pH 3 experiments, respectively. The previously mentioned case is similar to PTP334, and this confirmed the previous conclusion for PTP334. In addition, PTP348 has formed also with A/A_0 % values directly proportional to the pH of the solution. So, PTP350 and PTP348 could be relevant to the aquatic environment. TP282 was formed and eliminated with nearly the same ratio in the three compared pH experiments, indicating the probability that the pH has no effect on the elimination of the chloride atom from CPTX molecule.

3.5. Aerobic biodegradation of CPTX and its TPs

According to the criteria of the OECD guideline, all performed tests were valid (Fig. S25(SM)). In comparison with the CBT, MRT showed similar or only a little higher biodegradation rates

(Table S3(SM)). No significant change in pH was observed in all the test vessels.

The biodegradation values of CPTX were very low in both CBT and MRT. The LC-MS recoveries of CPTX after 28 days in CBT and MRT were $95.8 \pm 5.3\%$ and 99.9 ± 7.6 , respectively. In agreement, no TPs from CPTX's biodegradation was observed. Accordingly, CPTX is neither readily biodegradable nor abiotically degradable nor was it eliminated by sorption.

The results of the toxicity controls showed an inhibitory effect in the investigated MRT assays within the first 2 and 9 days in CPTX's photodegraded samples taken at 16 and 128 min of photo-treatment, respectively. This indicates that the inoculum's bacteria were not degrading readily biodegradable sodium acetate (reference substance) within the first days. In the CBT, this effect was not observed, which can be due to the lower concentrations of the TPs applied in this test. The same observation was reported by Rastogi et al. in studying the biodegradability of diatrizoic acid photodegradation samples (Rastogi et al., 2014).

In CBT and MRT tests of CPTX's irradiated samples taken after 4, 16, and 128 min, the oxygen consumption indicated that the formed TPs are not readily biodegradable. The DOC elimination in these samples showed a slight increase when compared to that in CPTX standard sample (Table S3(SM)). This indicates that only a few TPs could be biodegradable to a certain degree or alternatively some more but only incompletely. Therefore, the peak areas of the detected TPs were compared for the start and the end of the two tests performed (Fig. 5). The peak recoveries of LC-MS analysis of samples after 28 days for some of the formed TPs were around 100%, thereby excluding any microbial biotransformation for these products: PTP316-1, PTP316-2, PTP332-5, PTP350, PTP298-1, PTP298-2, PTP298-3, PTP282. Concluding these products and the parent compound CPTX to persist in the environment. On the other hand, some PTPs showed better elimination in biodegradation tests than CPTX. PTP334 is biotically eliminated during the two biodegradation tests (70.3%). PTP348 was mostly eliminated (99.4%) with no elimination in the sterile control, indicating biotic degradation. Four PTPs with m/z 332 (PTP332-1, PTP332-2, PTP332-3, and PTP332-4) show high elimination in test vessels with no elimination in sterile samples indicating biotic elimination. Although PTP332-4 and PTP332-5 are isomers, PTP332-4 is biodegradable, and PTP332-5 is not. Therefore, it can be concluded that the position of the functional group in the compound can affect the ability of the bacteria to degrade these compounds, which mean that the isomerization is an important factor that can affect the biodegradability of compounds in the environment (Hao et al., 2009).

3.6. *In silico* prediction of properties of CPTX and its TPs

3.6.1. Biodegradability

The structure of CPTX and its TPs were analyzed for predicting their ready biodegradability by using *in silico* models. The compound is classified as biodegradable or not according to certain predicted activating and deactivating alerts which are identified by all QSAR models. *In silico* prediction of ready biodegradation of the TPs has been applied here in order to support our analytical results from the biodegradation tests. As in biodegradation tests, biodegradation of each TP was not possible as it measures the biodegradability of the mixture as all, and then we measure the elimination, not biodegradation, of each TP using LC-MS method. Table S4(SM) summarizes the *in-silico* models used for the predictions of the ready biodegradability of CPTX and its TPs.

The two models of Oasis Catalogic software and the two models of EpiSuite software for ready biodegradability predicted the output values as < 0.14 for CPTX (Table S4(SM)). These output values are below the pass criterion for ready biodegradability under

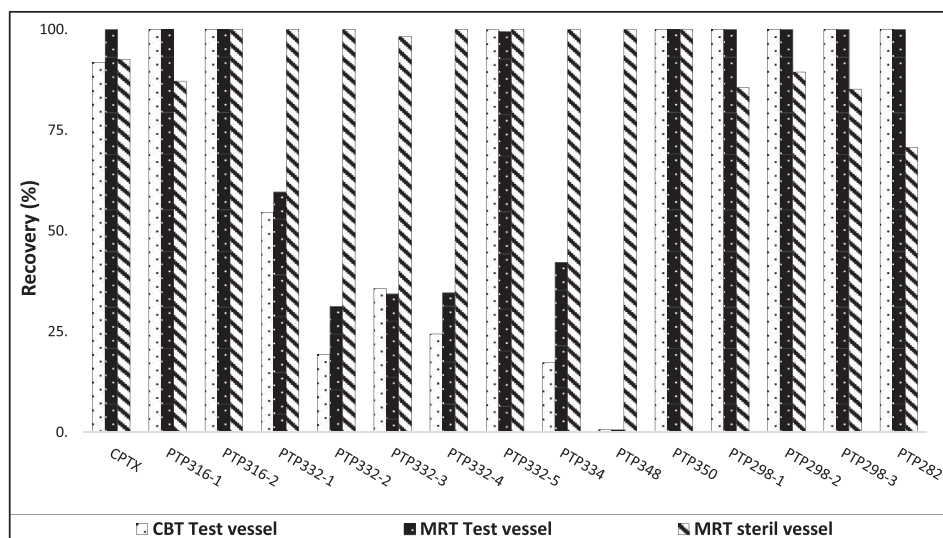


Fig. 5. Recovery of CPTX's PTPs after 28 days (compared to day 0) in CBT and MRT in different photolytic mixtures.

MITI-I test and MRT conditions. The result from Case Ultra about CPTX biodegradability was negative. That confirmed the experimental results. The five models used for ready biodegradability predicted the formed TP to be not readily biodegradable with very few non-significant positive results which are not in agreement with the analytical results. In addition, the Catalogic OECD 301F model predicted biodegradation availability values for the TPs relatively higher than that predicted by Catalogic OECD 301C model.

Accordingly, CPTX and its TPs can be categorized as a non-readily biodegradable which is in agreement with the results found experimentally in the CBT and MRT. On the other hand, these results are not in agreement with the LC-MS analytical results which suggest some TPs to be biodegradable. In summary, *in-silico* and the experimental biodegradation and analytical testing indicated that CPTX and some of its TPs are not readily biodegradable, and that some other TPs could be biodegradable. Therefore, if CPTX and its non-biodegradable TPs reach the aquatic systems like surface waters, they are expected to persist in the aquatic environment. This would lead to an increase in the number of hazardous substances in the aquatic environment. In addition, further research focusing on the biodegradability of the TPs are recommended.

3.6.2. Toxicity

The *in-silico* prediction models for toxicity were used to assess the toxicity of the TPs compared to CPTX. The *in-silico* assessment of the mutagenicity and genotoxicity of CPTX and its TPs are summarized in Table S5(SM) using the different models of the ICHM7 guideline conformal set from Case Ultra. The QSAR teratogenicity predictions are summarized in Table S6(SM) and the ecotoxicity prediction results are shown in Table S7(SM).

Ecotoxicity: The *V. fischeri* modules (Oasis catalogic) have predicted higher IC_{50} for all the TPs than for CPTX itself, indicating higher ecotoxicity for CPTX. In addition, most of the TPs formed with m/z 332b, 334, 350, and 282 showed lower IC_{50} values compared with other TPs. Therefore, the previously mentioned products could be relatively more ecotoxic than the others. In Microtox Toxicity to Environmental Bacteria (AUA) (*V. fischeri*) and Rainbow Trout Toxicity (AUE) modules, CPTX was assessed as inconclusive and out of domain, respectively, indicating that no ecotoxic prediction is possible for CPTX. All the suggested

structures of PTP298 and PTP282 showed the same ecotoxic results as CPTX in both AUA and AUE tests. On the other hand, most of the suggested structures for PTP316, PTP332a, and PTP348 are predicted to be toxic to *rainbow trout* in the AUE model only, and some of the predicted structures for PTP332b are predicted toxic in the AUA model (*Vibrio fischeri*) only. Most of the established structures for PTP334 and PTP350 are predicted to be toxic against rainbow trout and *Vibrio fischeri*. The predicted active PTPs is due to the presence of two or three of the positive alerts shown in Fig. S23(SM).

Mutagenicity, carcinogenicity, and teratogenicity: CPTX is predicted to be a mutagen in *Salmonella* (Module GT1 A7B) due to the presence of two alerts: ID 161 and ID 661 (Fig. S23 (SM)). CPTX was active also in *Salmonella* mutagenicity (Pharm Salm) because of the alerts ID 38 and ID 3230. In *E-coli* mutagenicity models, CPTX gives negative results. CPTX is predicted to be carcinogenic in the GT Expert model, because of the presence of a polycyclic aromatic and polycyclic conjugated system (ID A3.1 and ID A3.9) (Fig. S23 (SM)). CPTX is predicted to be no teratogen by the four applied models. PTP332b gave mostly the same results as CPTX, based on the same positive alerts as CPTX. The toxicity results for PTP298 and TP282 are also the same as CPTX, except in the GTI A7B model for *salmonella* toxicity in which these PTPs, in contrast to CPTX, were mostly predicted as negatives. This is because in PTP298 and TP282, all the alerts as CPTX are present except the alert ID 661. Most of the established structures of PTP332a, PTP348, and PTP350 are predicted non-mutagenic and non-carcinogenic, while predicted positive teratogens in some of the applied modules. The presence of many hydroxyl functional groups that give positive alerts (Fig. S26(SM)) is the reason. On the other hand, PTP316 and PTP334 are mostly predicted to be non-mutagenic, non-teratogenic, and non-carcinogenic in the used models due to the absence of positive alerts.

Summarizing: the obtained results provide indications that the activities of various TPs related to the toxic endpoints studied here may be altered by photolysis of CPTX. In general, there were indications that some TPs of CPTX can be toxic and these TPs showed receive more attention in future studies. On the other hand, some TPs such as PTP332a, PTP334, and PTP348 are expected to be less toxic and more biodegradable than CPTX, and this provides a first hint for further studies on potential substitutes of CPTX.

4. Conclusions

In this study, the environmental fate and behaviour of CPTX were assessed for the first time by studying its biodegradability, photo degradability, and toxicity including possibly formed TPs. The obtained results showed that CPTX was neither readily biodegradable nor photolyzed by Xe-lamp, but it was primarily eliminated by UV-irradiation. The UV-photodegradation rate of CPTX was affected by CPTX initial concentration and pH value of the solution, while not affected by the temperature. Moreover, it was shown that the photodegradation pathway was only slightly affected by the initial concentration and some TPs were difficultly appeared at lower concentrations. Therefore, it was possible to use a comparably high initial concentration of CPTX under experimental conditions to identify and determine the characteristic fate and effects of TPs. UV-photodegradation of CPTX lead to the formation of 13 PTPs, none of them were reported before. The main UV-degradation pathway of CPTX is hydroxylation combined with or without de-chlorination. The results of biodegradation tests showed that the TPs were not readily biodegradable, while LC-MS analysis showed six probably biodegradable TPs. The *in-silico* toxicity assessment combined with biodegradation tests provides a first indication that photodegradation of CPTX by UV-treatment might lead to some non-biodegradable TPs that are more toxic than CPTX, and some others possibly biodegradable TPs that are less toxic than CPTX. Therefore, further investigations should be conducted regarding the environmental occurrence, risk assessment, and pharmacological activity of the formed PTPs from CPTX. For this, the combination of *in silico* methods and experimental work turned out to be very supportive.

Acknowledgments

The authors would like to thank the Federal Ministry of Research and Education for financial support (grant no. 02WRS1280A - J). The authors wish to thank Dr. Annette Haiss and B.Sc. Evgenia Logunova for planning the aerobic biodegradation tests and to Janin Westphal for the analytical support. The authors also acknowledge Multicase Inc. for kindly providing the Case Ultra software.

Appendix A. Supplementary data

Supplementary data to this article can be found online at <https://doi.org/10.1016/j.watres.2018.10.075>.

References

- Calisto, V., Esteves, V.I., 2009. Psychiatric pharmaceuticals in the environment. *Chemosphere* 77 (10), 1257–1274.
- Chakravarti, S.K., Saiakhov, R.D., Klopman, G., 2012. Optimizing predictive performance of CASE ultra expert system models using the applicability domains of individual toxicity alerts. *J. Chem. Inf. Model* 52 (10), 2609–2618.
- ChemAxon, 2015. Marvin Sketch 15.6.15.0. <http://www.chemaxon.com>.
- Chen, Y.-W., Chu, C.-C., Chen, Y.-C., Leung, Y.-M., Wang, J.-J., 2012. Intrathecal chlorprothixene, *cis*-(*z*)-flupenthixol, chlorpromazine and fluphenazine for prolonged spinal blockades of sensory and motor functions in rats. *Eur. J. Pharmacol.* 693 (1–3), 31–36.
- Gutowski, L., Baginska, E., Olsson, O., Leder, C., Kümmerer, K., 2015. Assessing the environmental fate of S-metolachlor, its commercial product Mercantor Gold® and their photoproducts using a water-sediment test and *in silico* methods. *Chemosphere* 138, 847–855.
- Hao, R., Li, J., Zhou, Y., Cheng, S., Zhang, Y., 2009. Structure-biodegradability relationship of nonylphenol isomers during biological wastewater treatment process. *Chemosphere* 75 (8), 987–994.
- Henning, N., Kunkel, U., Wick, A., Ternes, T.A., 2018. Biotransformation of gabapentin in surface water matrices under different redox conditions and the occurrence of one major TP in the aquatic environment. *Water Res.* 137, 290–300.
- Herrmann, M., Menz, J., Gassmann, M., Olsson, O., Kümmerer, K., 2016. Experimental and *in silico* assessment of fate and effects of the antipsychotic drug quetiapine and its bio- and phototransformation products in aquatic environments. *Environ. Pollut.* 218, 66–76. Barking, Essex: 1987.
- Herrmann, M., Menz, J., Olsson, O., Kümmerer, K., 2015a. Identification of photo-transformation products of the antiepileptic drug gabapentin: biodegradability and initial assessment of toxicity. *Water Res.* 85, 11–21.
- Herrmann, M., Olsson, O., Fiehn, R., Herrel, M., Kümmerer, K., 2015b. The significance of different health institutions and their respective contributions of active pharmaceutical ingredients to wastewater. *Environ. Int.* 85, 61–76.
- Huus, I., Khan, A.R., 1967. Studies on the metabolism of chlorprothixene (Truxal) in rats and dogs. *Acta Pharmacol. Toxicol.* 25 (4), 397–404.
- Illés, E., Szabó, E., Takács, E., Wojnárovits, L., Dombi, A., Gajda-Schrantz, K., 2014. Ketoprofen removal by O₃ and O₃/UV processes: kinetics, transformation products and ecotoxicity. *Sci. Total Environ.* 472, 178–184.
- International Conference on Harmonization (ICH), 2014. ICH Guideline M7. http://www.ich.org/fileadmin/Public_Web_Site/ICH_Products/Guidelines/Multidisciplinary/M7/M7_Step_4.pdf. (Accessed 18 February 2014).
- Käferstein, H., Sticht, G., Madea, B., 2013. Chlorprothixene in bodies after exhumation. *Forensic Sci. Int.* 229 (1–3), e30–e34.
- Khaleel, N.D.H., Mahmoud, W.M.M., Olsson, O., Kümmerer, K., 2016. UV-photodegradation of desipramine: impact of concentration, pH and temperature on formation of products including their biodegradability and toxicity. *Sci. Total Environ.* 566–567, 826–840.
- Khaleel, N.D.H., Mahmoud, W.M.M., Olsson, O., Kümmerer, K., 2017. Initial fate assessment of teratogenic drug trimipramine and its photo-transformation products - role of pH, concentration and temperature. *Water Res.* 108, 197–211.
- Kovalova, L., Siegrist, H., Gunten, U. von, Eugster, J., Hagenbuch, M., Wittmer, A., Moser, R., McArdell, C.S., 2013. Elimination of micropollutants during post-treatment of hospital wastewater with powdered activated carbon, ozone, and UV. *Environ. Sci. Technol.* 47 (14), 7899–7908.
- Laboratory of Mathematical Chemistry, 2012. OASIS Catalogic software V. 5.11.6 TB. <http://oasis-lmc.org/>.
- Mahmoud, W.M.M., Toolaram, A.P., Menz, J., Leder, C., Schneider, M., Kümmerer, K., 2014. Identification of phototransformation products of thalidomide and mixture toxicity assessment: an experimental and quantitative structural activity relationships (QSAR) approach. *Water Res.* 49, 11–22.
- Mahmoud, W.M.M., Trautwein, C., Leder, C., Kümmerer, K., 2013. Aquatic photochemistry, abiotic and aerobic biodegradability of thalidomide: identification of stable transformation products by LC-UV-MS(n). *Sci. Total Environ.* 463–464, 140–150.
- Menz, J., Toolaram, A.P., Rastogi, T., Leder, C., Olsson, O., Kümmerer, K., Schneider, M., 2017. Transformation products in the water cycle and the unsolved problem of their proactive assessment: a combined *in vitro/in silico* approach. *Environ. Int.* 98, 171–180.
- OECD, 1992. Test No. 301: Ready Biodegradability. OECD Publishing.
- OECD, 2008. Test Nr. 316: Phototransformation of Chemicals in Water – Direct Photolysis. OECD Publishing.
- Oliveira, C., Lima, D.L., Silva, C.P., Calisto, V., Otero, M., Esteves, V.I., 2019. Photodegradation of sulfamethoxazole in environmental samples: the role of pH, organic matter and salinity. *Sci. Total Environ.* 648, 1403–1410.
- Rastogi, T., Leder, C., Kümmerer, K., 2014. Qualitative environmental risk assessment of photolytic transformation products of iodinated X-ray contrast agent diazotric acid. *Sci. Total Environ.* 482–483, 378–388.
- Reemtsma, T., Berger, U., Arp, H.P.H., Gallard, H., Knepper, T.P., Neumann, M., Quintana, J.B., Voogt, P.d., 2016. Mind the gap: persistent and mobile organic compounds-water contaminants that slip through. *Environ. Sci. Technol.* 50 (19), 10308–10315.
- Saiakhov, R., Chakravarti, S., Klopman, G., 2013. Effectiveness of CASE ultra expert system in evaluating adverse effects of drugs. *Mol. Inf.* 32 (1), 87–97.
- Santiago, L.E.P., García, C., Lhiaubet-Vallet, V., Miranda, M.A., Oyola, R., 2011. Solvent dependence of the photophysical properties of 2-chlorothioxanthone, the principal photoproduct of chlorprothixene. *Photochem. Photobiol.* 87 (3), 611–617.
- Santos, L.H.M.L.M., Araújo, A.N., Fachini, A., Pena, A., Delerue-Matos, C., Montenegro, M.C.B.S.M., 2010. Ecotoxicological aspects related to the presence of pharmaceuticals in the aquatic environment. *J. Hazard Mater.* 175 (1–3), 45–95.
- Schwabe, U., Paffrath, D., Ludwig, W.-D., Klauber, J., 2017. *Arzneiverordnungs-report 2017*. Springer Berlin Heidelberg, Berlin, Heidelberg.
- Trautwein, C., Kümmerer, K., 2012. Degradation of the tricyclic antipsychotic drug chlorpromazine under environmental conditions, identification of its main aquatic biotic and abiotic transformation products by LC-MSⁿ and their effects on environmental bacteria. *J. Chromatogr B Analyt Technol Biomed Life Sci* 889–890, 24–38.
- Trovó, A.G., Paiva, V.A.B., Costa Filho, B.M., Machado, A.E.H., Oliveira, C.A., Santos, R.O., Daniel, D., 2014. Photolytic degradation of chloramphenicol in different aqueous matrices using artificial and solar radiation: reaction kinetics and initial transformation products. *J. Braz. Chem. Soc.* 25 (11), 2007–2015.
- US EPA, 2012. Estimation Programs Interface Suite™, v 4.11. United States Environmental Protection Agency, Washington, DC, USA.
- Writer, J.H., Ferrer, I., Barber, L.B., Thurman, E.M., 2013. Widespread occurrence of neuro-active pharmaceuticals and metabolites in 24 Minnesota rivers and wastewaters. *Sci. Total Environ.* 461–462, 519–527.
- Yuan, S., Jiang, X., Xia, X., Zhang, H., Zheng, S., 2013. Detection, occurrence and fate of 22 psychiatric pharmaceuticals in psychiatric hospital and municipal wastewater treatment plants in Beijing, China. *Chemosphere* 90 (10), 2520–2525.

Supplementary Materials (SM) for:
**Environmental fate of Chlorprothixene in the aquatic environment with
studying the environmental behavior of its byproducts.**

Nareman D. H. Khaleel,^{1, 2} Waleed M. M. Mahmoud,^{1, 2} Oliver Olsson,¹ Klaus
Kümmerer,^{1*}

1- Sustainable Chemistry and Material Resources, Institute of Sustainable and Environmental Chemistry, Leuphana University of Lüneburg, Scharnhorststraße 1 C13, DE-21335 Lüneburg, Germany.

2- Pharmaceutical Analytical Chemistry Department, Faculty of Pharmacy, Suez Canal University, Ismailia 41522, Egypt.

Pages: 70

Texts: 4

Figures: 26

Tables: 7

* Corresponding author. Address: Nachhaltige Chemie und Stoffliche Ressourcen, Institut für Nachhaltige Chemie und Umweltchemie, Leuphana Universität Lüneburg, C.13, Scharnhorststraße 1, D-21335 Lüneburg, Germany.

Tel.: +49 4131 677-2893

E-mail address: klaus.kuemmerer@leuphana.de (K. Kümmerer).

Table of content

Texts (Supplementary Materials (SM)):

Text S1: Photodegradation set up: more informations about the used lamps and the calculations o the photodegradation kinetics	S4
Text S2: LC-MS Analytical method parameter for the elution and identification of the photo-transformation products (PTPs) of chlorprothixene	S5
Text S2: Biodegradation tests (CBT-MRT)	S6
Text S4: <i>In silico</i> prediction values interpretation.....	S7

Figures (Supplementary Materials (SM)):

Figure S1: Emission spectrum for medium pressure Hg (mercury) lamp and the relative absorbance spectrum of 100 mg L ⁻¹ Chlorprothixene (CPTX)	S8
Figure S2: First-order kinetics plot of photodegradation of CPTX for different initial concentrations.....	S9
Figure S3: The photolytic degradation (a) and the DOC Recovery (b) of CPT by mean of UV photodegradation at different temperatures. CPTX initial concentration = 100 mg L ⁻¹ , pH = 5.....	S10
Figure S4: First-order kinetics plot of photodegradation of CPTX for different Temperatures.....	S11
Figure S5: The change in the dissolved concentration of CPTX as a function of the solution pH (CPTX added concentration = 100 mg L ⁻¹).....	S12
Figure S6: The two forms of CPTX in aqueous solution according to pH value, pK _a = 9.76	S12
Figure S7: First-order kinetics plot of photodegradation of CPTX for different pH values.....	S13
Figure S8: Fragmentation pattern of E/Z CPTX according to MS ⁿ obtained from LC-HRMS	S14
Figure S9: Fragmentation pattern of HTP282 according to MS ⁿ obtained from LC-HRMS	S15
Figure S10: Fragmentation pattern of PTP316-1 according to MS ⁿ obtained from LC-HRMS	S16
Figure S11: Fragmentation pattern of PTP316-2 according to MS ⁿ obtained from LC-HRMS	S17
Figure S12: Fragmentation pattern of PTP332-1 according to MS ⁿ obtained from LC-HRMS	S18
Figure S13: Fragmentation pattern of PTP332-2 according to MS ⁿ obtained from LC-HRMS	S19
Figure S14: Fragmentation pattern of PTP332-3 according to MS ⁿ obtained from LC-HRMS	S20
Figure S15: Fragmentation pattern of PTP332-4 according to MS ⁿ obtained from LC-HRMS	S21

Figure S16: Fragmentation pattern of PTP332-5 according to MSn obtained from LC-HRMS	S22
Figure S17: Fragmentation pattern of PTP334 according to MSn obtained from LC-HRMS	S23
Figure S18: Fragmentation pattern of PTP348 according to MSn obtained from LC-HRMS	S24
Figure S19: Fragmentation pattern of PTP350 according to MSn obtained from LC-HRMS	S25
Figure S20: Fragmentation pattern of PTP289 according to MSn obtained from LC-HRMS	S26
Figure S21: Time curves of the relative peak area A/A_0 (%) of the PTPs during photolysis assigned to their m/z ratio (A is the peak area of the PTP at a specific time point, A_0 is the peak area of CPTX (100 mg L ⁻¹) at 0 min) (n = 3, with SD < 0.27 and RSD < 13.6%)	S27
Figure S22: Time curves of the relative peak area A/A_0 (%) of CPTX PTPs during photolysis at different concentrations	S28-29
Figure S23: Time curves of the relative peak area A/A_0 (%) of CPTX PTPs during photolysis at different Temperature	S30+31
Figure S24: Time curves of the relative peak area A/A_0 (%) of CPTX PTPs during UV-photolysis at different pH values	S32+33
Figure S25: Closed Bottle test and Manometric Respiratory Test results of CPTX and its photolytic mixtures at different irradiation time points	S34+35
Figure S26: Structural alerts (in bold) in CPTX and its TPs for environmental toxicity by different QSAR models	S36

Tables (Supplementary Materials (SM)):

Table S1: a) Test system of the Closed Bottle test (CBT), b) Test system of the manometric respiratory test (MRT)	S37
Table S2: Accurate mass measurements of CPTX and its TPs determined by HRLCMS-LTQ Orbitrap in MS and MS ⁿ mode	S38-41
Table S3: Results of the investigated aerobic biodegradation test assays for CPTX and its photolytic mixtures	S42
Table S4: Q-SAR predictions for CPTX and its TPs for ready biodegradability by different models	S43-S55
Table S5: QSAR toxicity predictions according to ICH M7 guidance for CPTX and its TPs using Case Ultra software	S56-60
Table S6: QSAR teratogenicity predictions for CPTX and its TPs by different models (Case Ultra software)	S61-65
Table S7: The predicted bacterial toxicity of CPTX and its TPs	S66-70

Texts

Text S1:

The Xenon one (TXE 150, UV Consulting Peschl, Mainz, Germany) emits spectra similar to natural sunlight (200–800 nm). It shows the highest intensity in the visible range (200–280 nm: $1.61 \text{ e}^{-2} \text{ W/m}^2$, 280–315 nm: $1.16 \text{ e}^{-2} \text{ W/m}^2$, 315–380 nm: $3.75 \text{ e}^{-2} \text{ W/m}^2$, 380–780 nm: $5.58 \text{ e}^{-1} \text{ W/m}^2$) (data provided by the manufacturer). The UV-lamp is a medium-pressure mercury lamp (TQ150, UV Consulting Peschl, Mainz, Germany) with ilmasil quartz immersion tube. The UV-lamp emits polychromatic radiation in the range from 200 to 600 nm. The maximal intensities were at 254, 265, 302, 313, 366, 405/408, 436, 546, and 577/579 nm. The total photon flow rate of the polychromatic UV-lamp was estimated using a UV-pad Spectral Radiometer (Opsytec Dr. Gröbel GmbH, Ettlingen, Germany). The radiometer was placed at a distance of 4 cm from the emission source in an alumina box. The total photon flow rate of the lamp for all wavelengths was $5.71 \times 10^6 \text{ (mol} \times \text{photons} \times \text{cm}^{-2} \times \text{s}^{-1})$.

UV photodegradation tests performed under different concentrations, temperature and pH values. The required pH value was adjusted using HCl and/or NaOH. Controls wrapped in aluminum foil were run simultaneously under the same conditions to examine if CPTX concentration is primary affected by the different conditions studied.

The photodegradation experiment first-order rate constants (k) for CPTX was obtained as a very good fit of the data by a linear regression of logarithmic concentration values ($\ln C_0/C$) determined as a function of time (t) (supplementary Figure S). The first-order linear relationship of $\ln C_0/C$ versus t (from 2 min to 64 min) was found based on the obtained results for CPTX in UP water.

Text S2:

The LC-ITMS system comprising an HPLC 1100 series (Agilent Technologies, Böblingen, Germany) consisting of binary pumps (G1312A), column oven (G1316A), degasser (G1322A), and auto sampler (ALS G1329A + ALS Therm G1330), coupled to a Bruker data analysis system and atmospheric pressure electrospray ionization interface (Bruker Daltonic GmbH, Bremen, Germany). data acquisition and processing were performed using the associated Data analysis V.4 and Quant analysis V.2 software. The Esquire 6000 plus MS analysis was carried out in positive ionization mode using an ion spray voltage of 4240 V. The nebulizer (air) pressure was set at 30 psi. The Ion Spray source was operated at 350 °C dry temperature with dry gas flow equal 12 L min⁻¹. The other operating conditions of the source were: - 500 V end plate, + 4160 V capillary voltage. The selected lens and block voltages were: +79.2 V capillary exit, +8.44 V octopole 1, +1.81 V octopole 2, 237.5 Vpp octopole reference amplitude, 33.4 V skimmer, 36.0 trap drive, -3.0 V lens 1 and -62.5 V lens 2. The scan range was determined from m/z 50 to 1000.

LTDQ-Orbitrap XL mass spectrometer interfaced with heated electrospray ionization (HESI) source (Thermo Scientific, Bremen, Germany) was used for the determination of the accurate masses of TMP's PTPs. The LC-MS system comprising a Dionex UHPLC system (Ultimate 3000) consisting of two HPG-3400-RS binary pumps, a TCC-3000 column oven, a SRD-3600 degasser, and an auto sampler WPS-3000-TRS. UV detection was performed using a VWD-3400RS detector. The spectrometer was operated also in positive mode under the following conditions: spray voltage 4 kV, capillary voltage 19 V and tube lens voltage 75 V. The heated capillary and desolvation temperatures were 275 °C and 150 °C, respectively. Nitrogen served as sheath, auxiliary and sweep gas with flow rate equal 20, 5 and 0 arb, respectively. MS data were recorded in the full scan mode (m/z 100-400). Fragmentation to MS⁴ was achieved by setting collision induced dissociation (CID) on 35 eV. All data were processed using Xcalibur/Qual Browser 2.1.0 SP1 build 1160 (Thermo Scientific, Bremen, Germany).

Text S3:

Comparing CBT and MRT, MRT was performed with higher bacterial density and higher sodium acetate and test compound concentrations. The concentrations of CPTX was 2.4 mg/L, and 14.4 mg/L corresponding to a theoretical oxygen demand (ThOD) of 5 mg/L and 30 mg/L in CBT and MRT, respectively. Two drops or 80 ml of inoculum were added to 1 L of medium, which results in approximately $((5-10) \times 10^2)$ CFU ml⁻¹ or $((5-10) \times 10^6)$ CFU ml⁻¹, in CBT and MRT, respectively. The final concentrations of the photolytic mixtures after 4, 16, and 128 min were adjusted according to the remaining DOC concentration to reach a comparable ThOD.

In CBT, to monitor the process of aerobic biodegradation, sensor spots in the bottles were used to measure oxygen concentration in the bottles. Biodegradability is expressed as the percentage of oxygen consumption based on ThOD and a test compound is classified as “readily biodegradable” if biodegradation exceeds 60% within a period of 10 days after the oxygen consumption reached 10% ThOD {OECD 1992 #22}. In MRT, the bottles of the OxiTop OC110-system were firmly closed with measuring heads which cover an exactly defined gas volume. The process of aerobic biodegradation was monitored by the measurement of carbon dioxide (CO₂) production where the resulting pressure decrease shows the corresponding oxygen consumption. The validity criterion in MRT is a removal of 60% ThOD within 14 days window for the quality control.

Text S4:

In the used *in-silico* software, structure illustrations were performed by using Marvin Sketch 15.6.15.0, and a simplified molecular input line entry specification (SMILES) codes were used for input of molecular structures. The structures of the chemical species are scanned by the software against the validated databases of the model, and the software calculates the activity and predicts the output in the form of alerts for that corresponding activity.

In the Oasis Catalogic MITI-I and OECD 301F models, the ready biodegradability was predicted as a numerical value between 0 and 1 which corresponds to 0% and 100% biodegradation, respectively. The pass criterion for ready biodegradability is 60% biodegradation which corresponds to the numeric value of 0.6. In EPI Suite, “Readily biodegradable” was assigned a numeric value of 1 and “not readily biodegradable” was assigned a numeric value of 0 (0 to 1 is the probability range to undergo biodegradation). Case Ultra models provide positive (+), negative (-), out of domain (OD) and inconclusive (\pm) results. Inconclusive indicate that a positive alert was found in the test compound but the calculated probability falls inside the gray zone of the model (10 % around the classification threshold of the model) and therefore a concrete prediction cannot be provided alerts for the selected models.

Case Ultra was used to apply a combination of statistical and rule-based systems for bacterial mutagenicity according to the recently implemented ICH guideline M7 (ref, International Conference on Harmonization (ICH), 2014) using the following models (GT Expert (Expert rules for genotoxicity)); GT1 A7B (Mutagenicity for 7 strains of Salmonella typhimurium TA 97, 98, 100, 1535–1538, FDA data source), GT1 AT Ecoli (A–T mutation in E. coli and S. typhimurium TA102, FDA data source), Pharm Ecoli (E. coli mutagenicity (all strains) from public and proprietary sources), Pharm Salm (Salmonella typhimurium mutagenicity (TA97, 98, 100, 1535-1538) from public and proprietary sources).

Figures

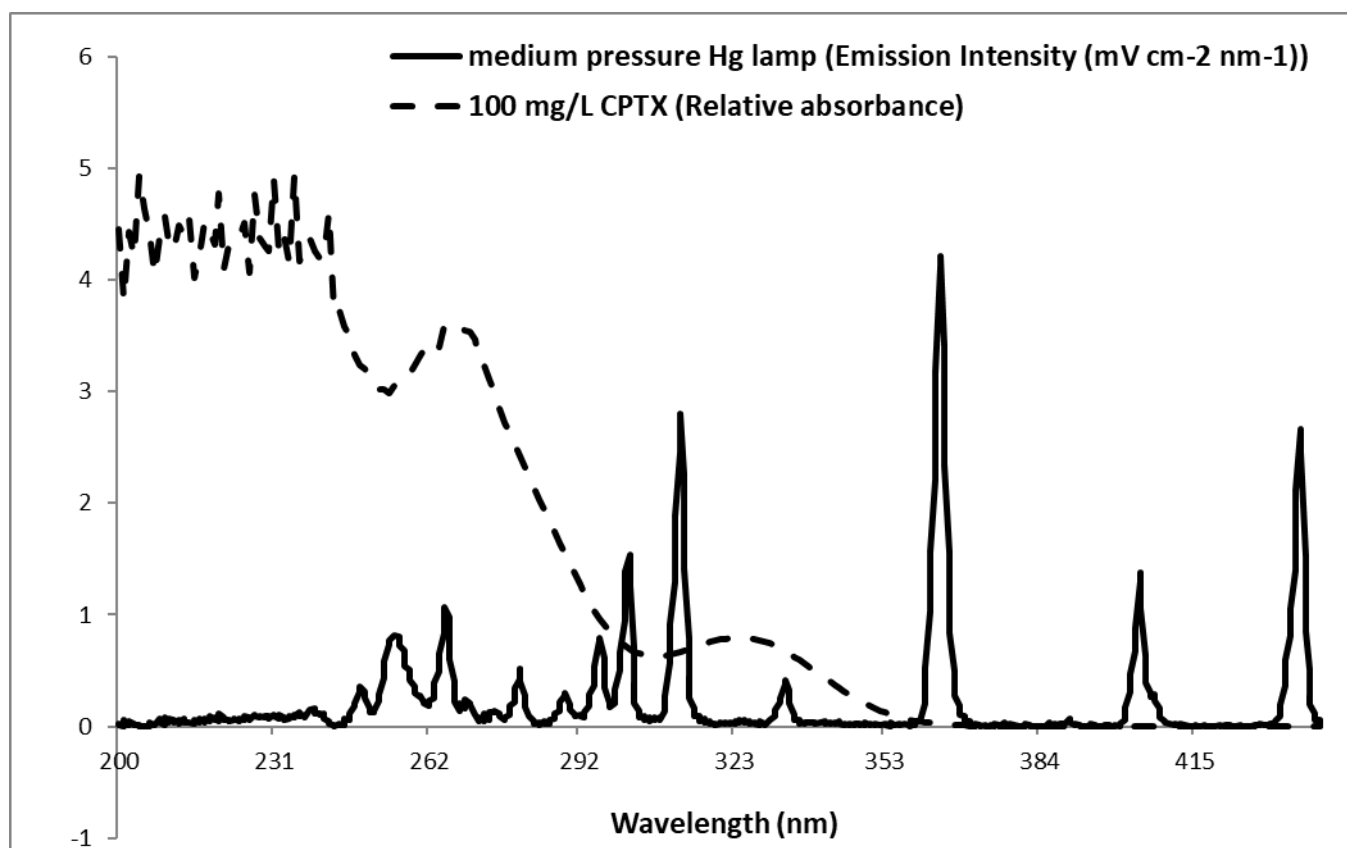


Figure S1: Emission spectrum for medium pressure Hg (mercury) lamp and the relative absorbance spectrum of 100 mg L⁻¹ Chlorprothixene (CPTX).

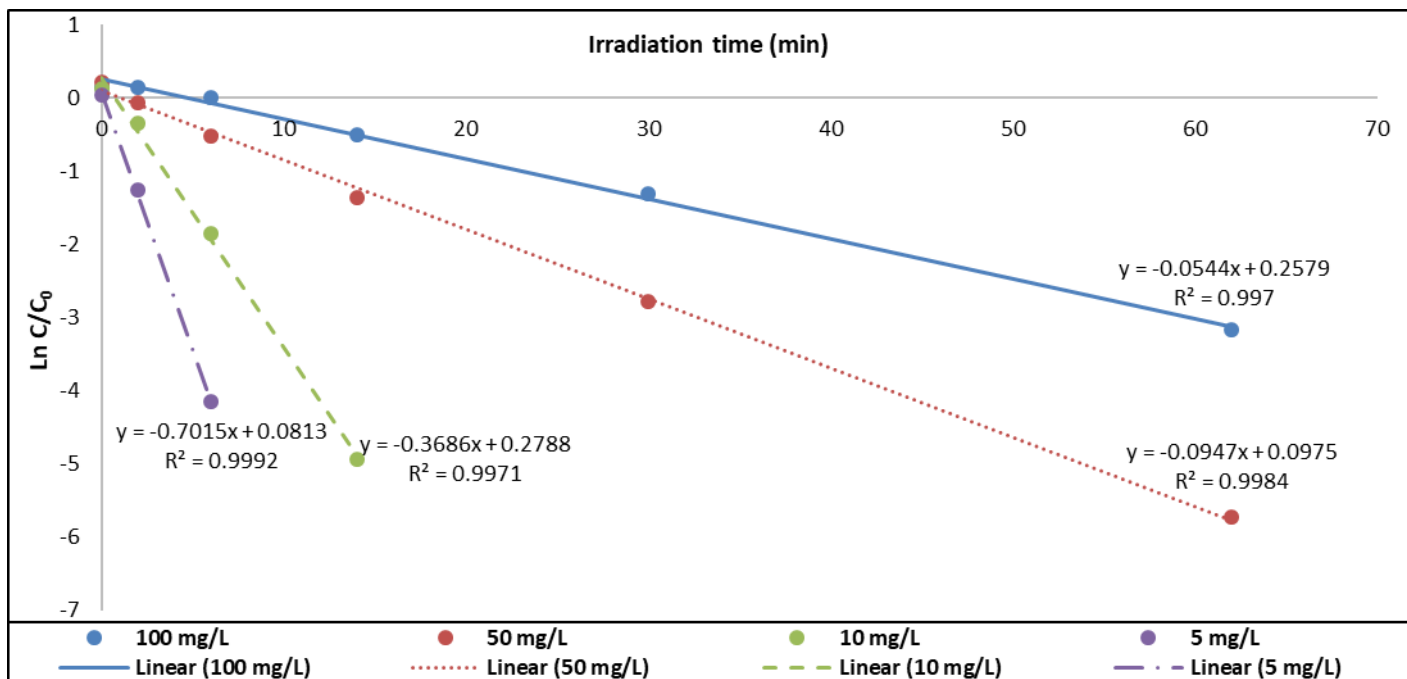


Figure S2: First-order kinetics plot of photodegradation of CPTX for different initial concentrations.

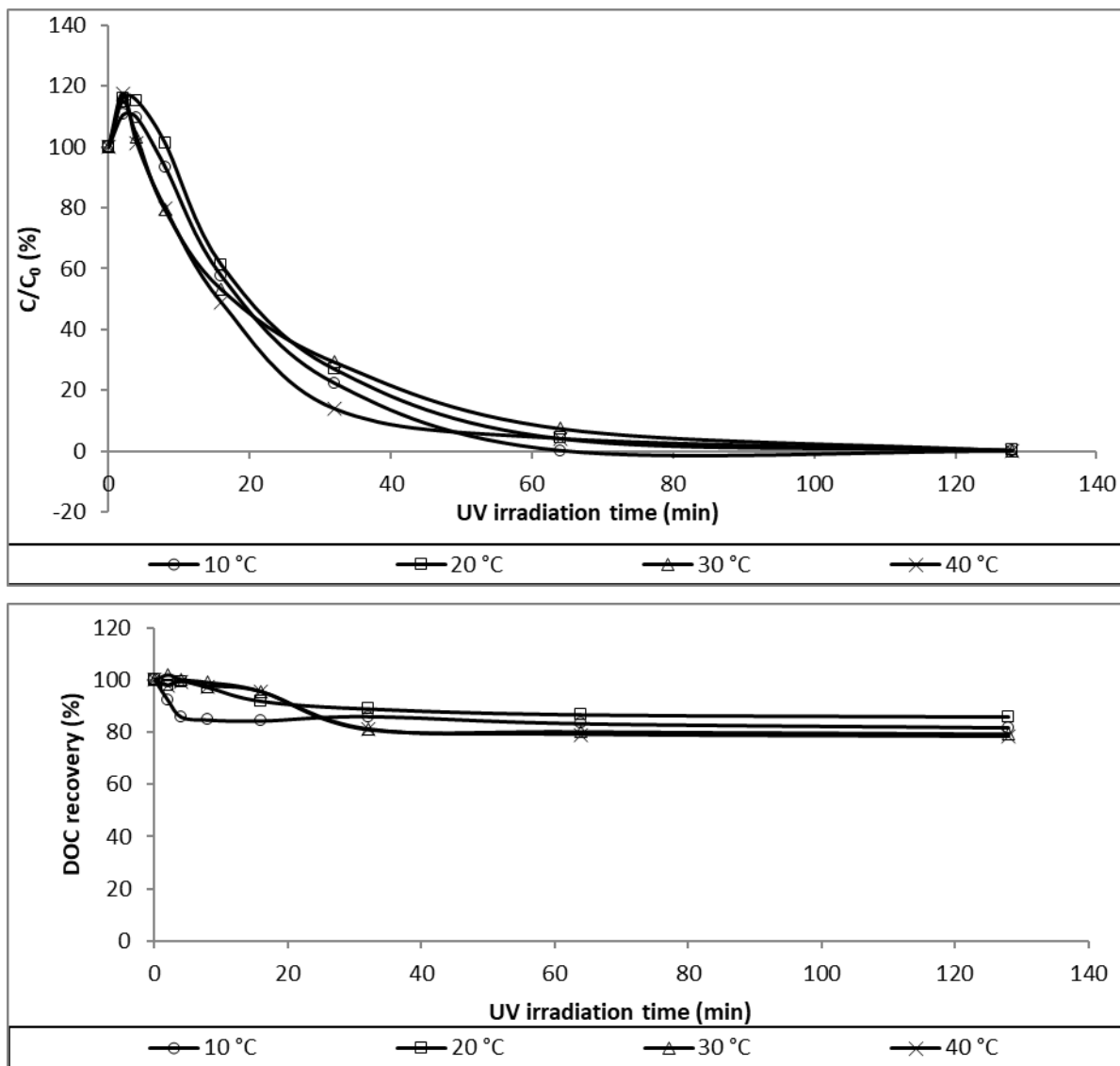


Figure S3: The photolytic degradation (a) and the DOC Recovery (b) of CPT by mean of UV photodegradation at different temperatures. CPTX initial concentration = 100 mg L⁻¹, pH = 5.

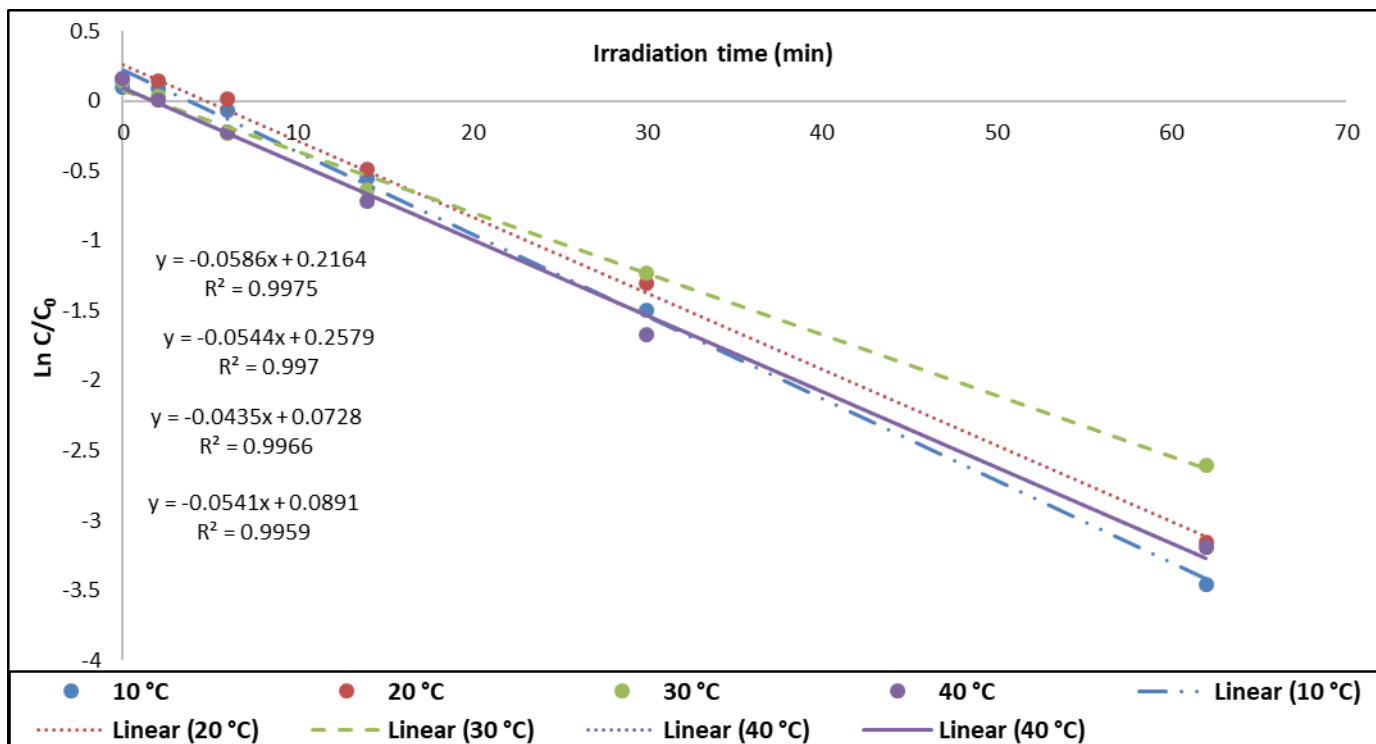


Figure S4: First-order kinetics plot of photodegradation of CPTX for different Temperatures.

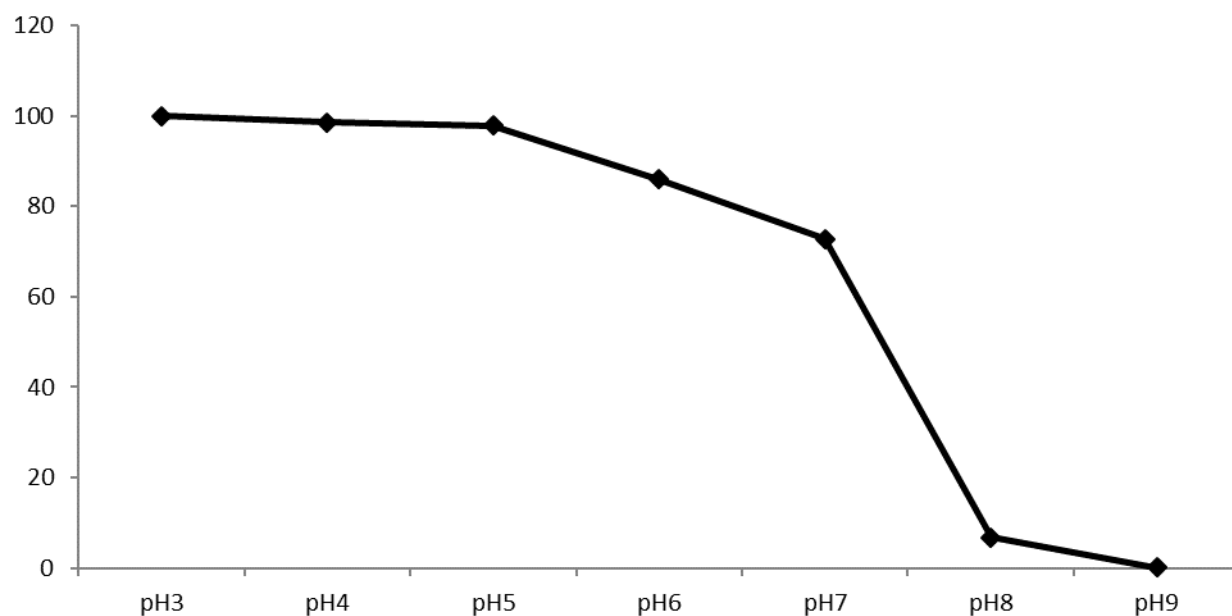


Figure S5: The change in the dissolved concentration of CPTX as a function of the solution pH (CPTX added concentration = 100 mg L⁻¹).

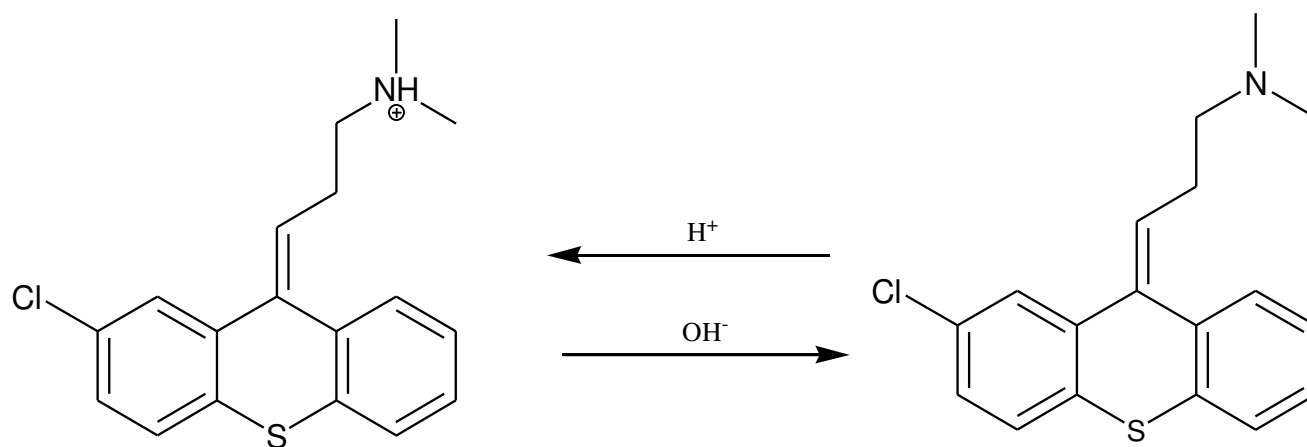


Figure S6: The two forms of CPTX in aqueous solution according to pH value, pK_a = 9.76.

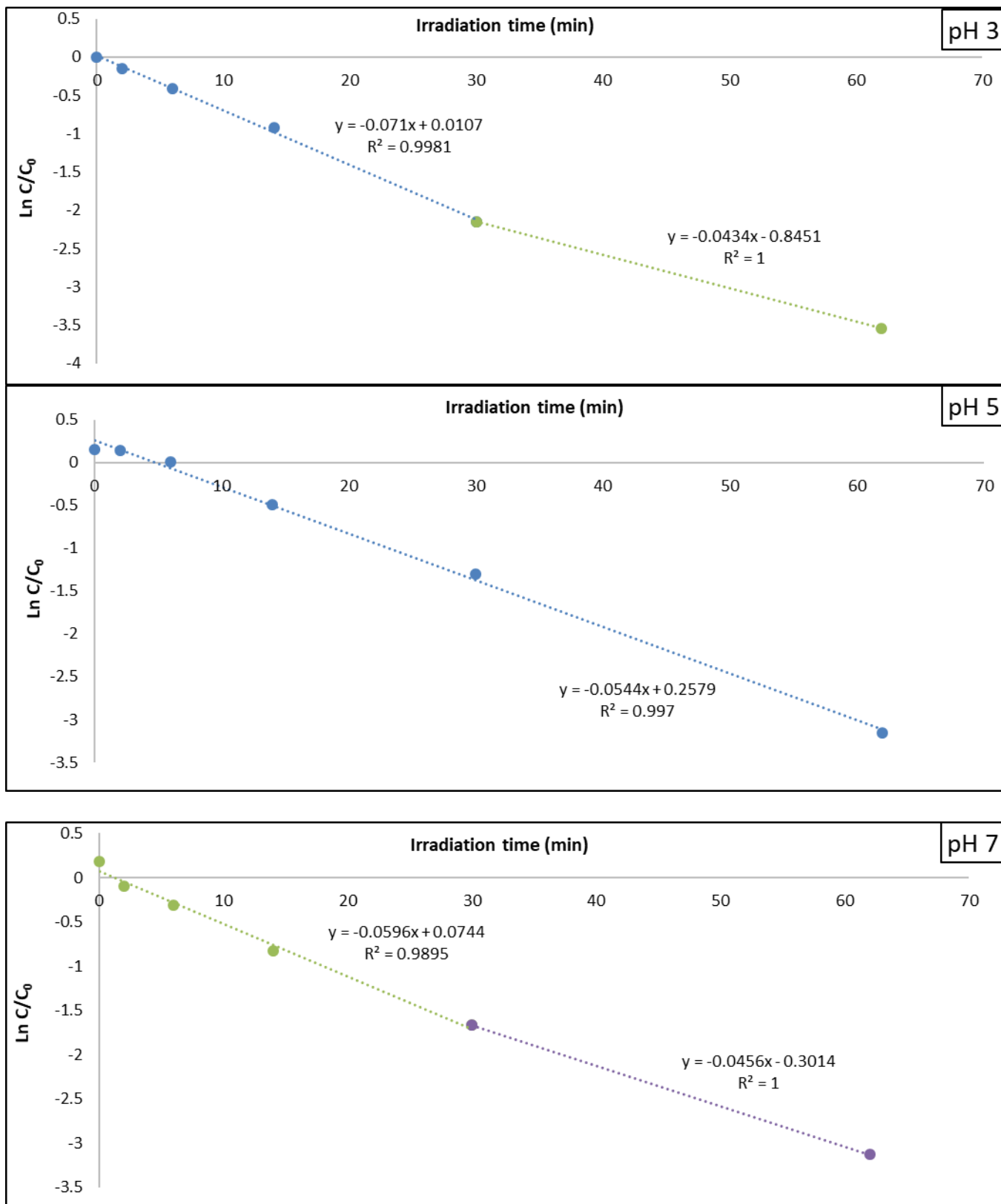


Figure S7: First-order kinetics plot of photodegradation of CPTX for different pH values.

Chlorprothixene_100PPmUV8min30C140725b #1171 RT: 15.13 AV: 1 NL: 7.48E7
T: FTMS + c ESI d Full ms2 316.09@cid35.00 [7]

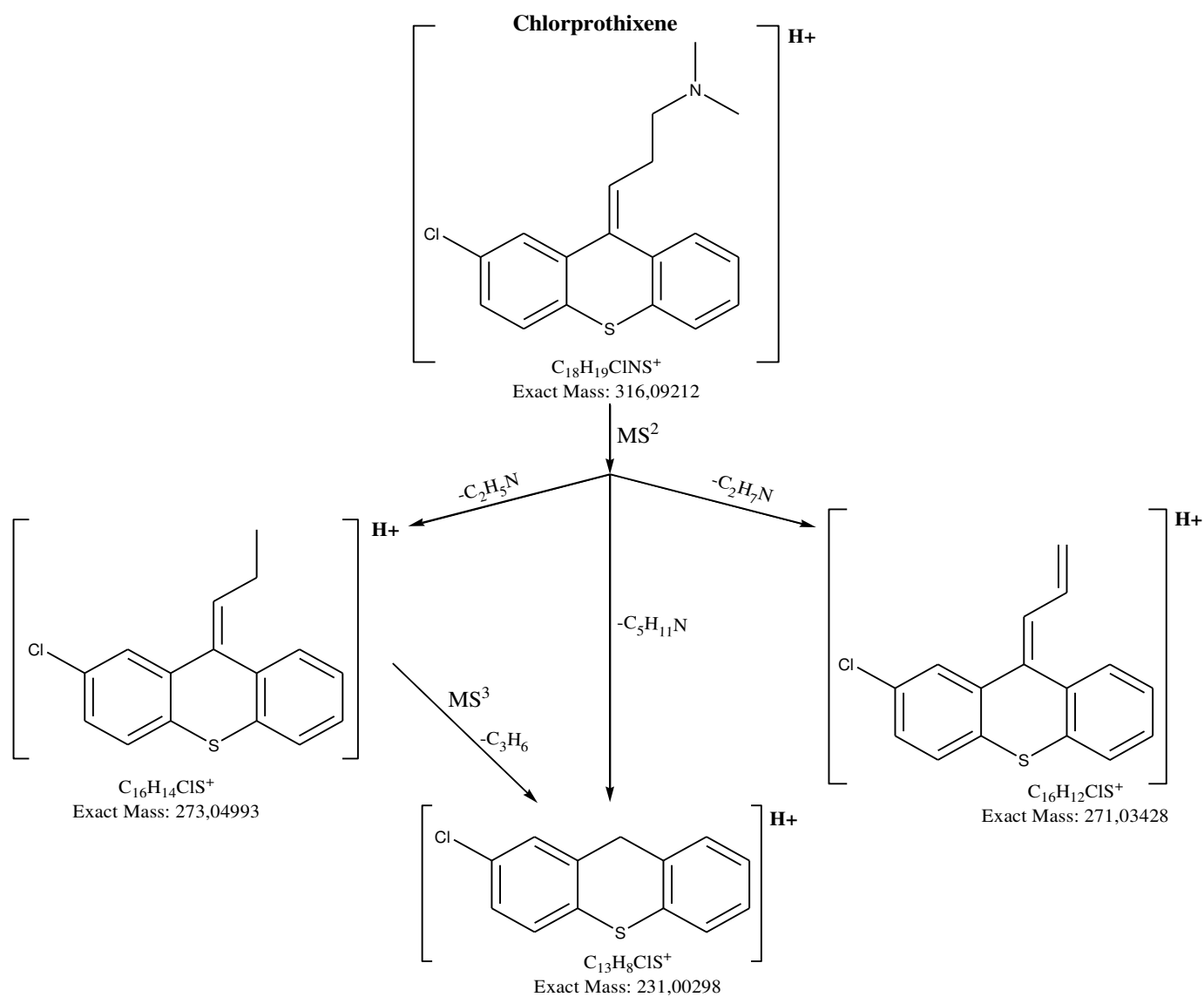
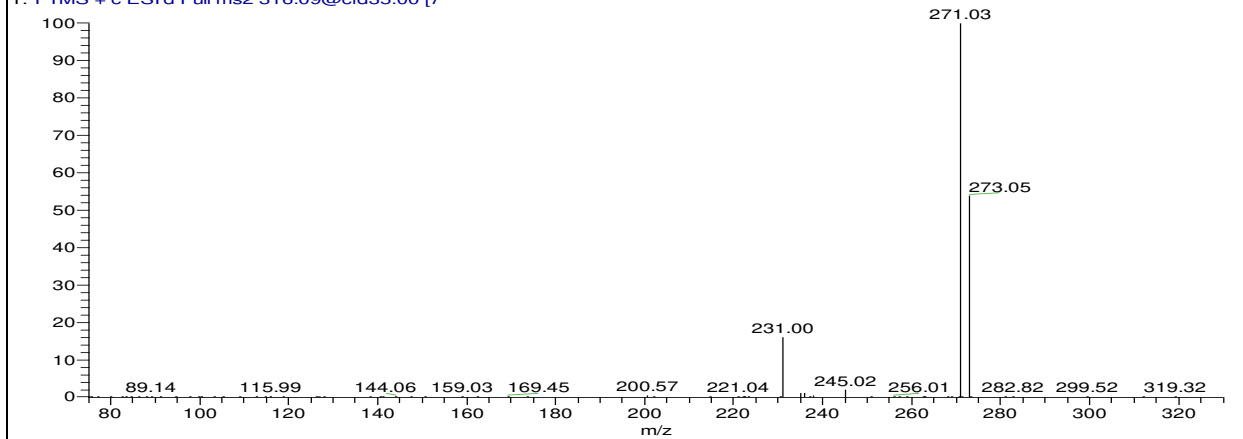


Figure S8: Fragmentation pattern of E/Z CPTX according to MSⁿ obtained from LC-HRMS

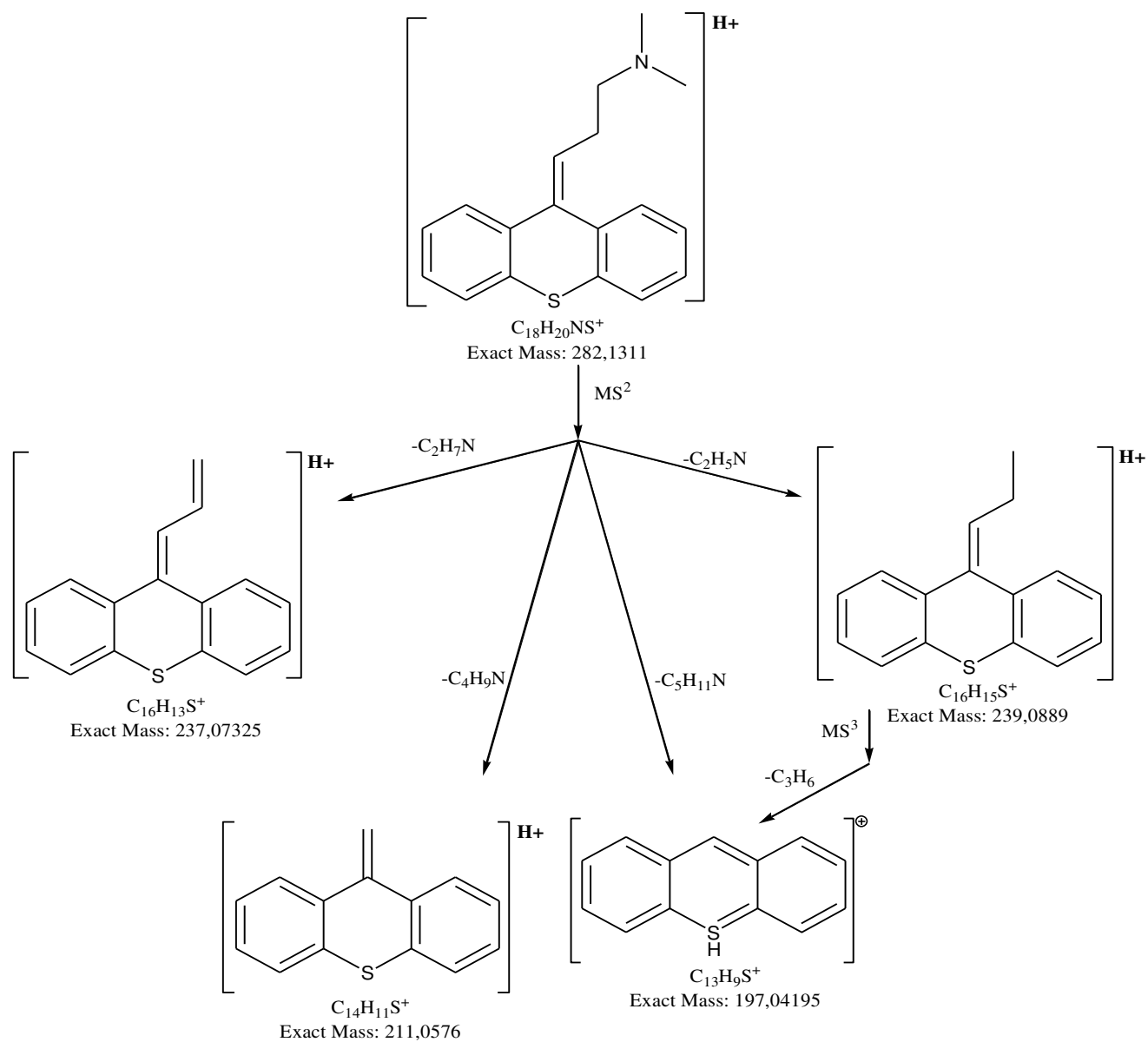
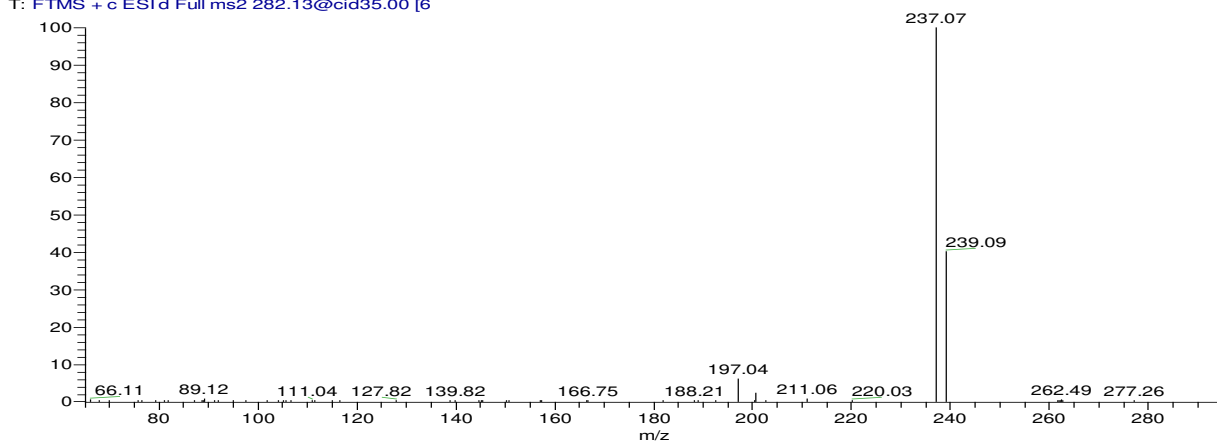


Figure S9: fragmentation pattern of HTP282 according to MS_n obtained from LC-HRMS

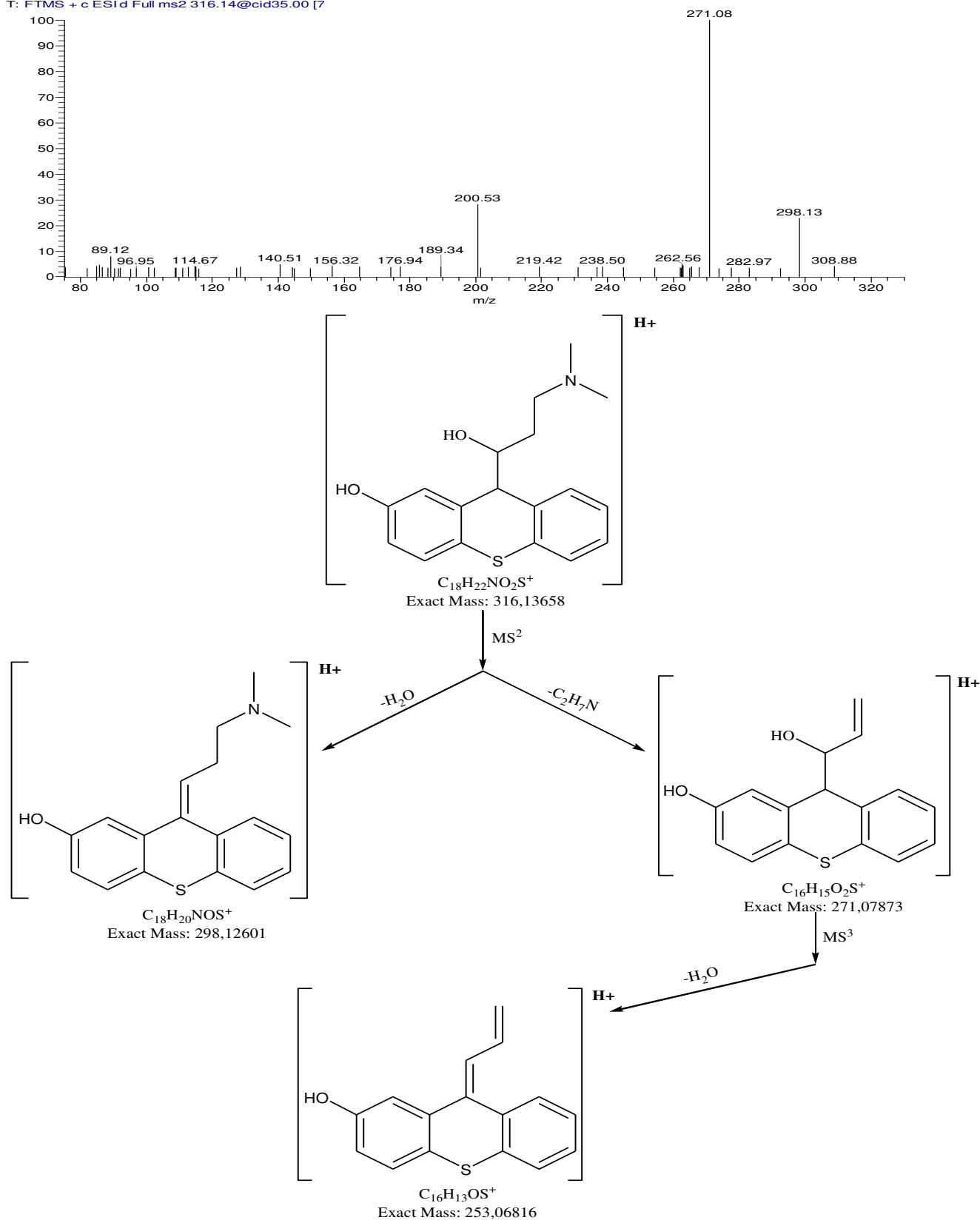


Figure S10: fragmentation pattern of PTP316-1 according to MSⁿ obtained from LC-HRMS

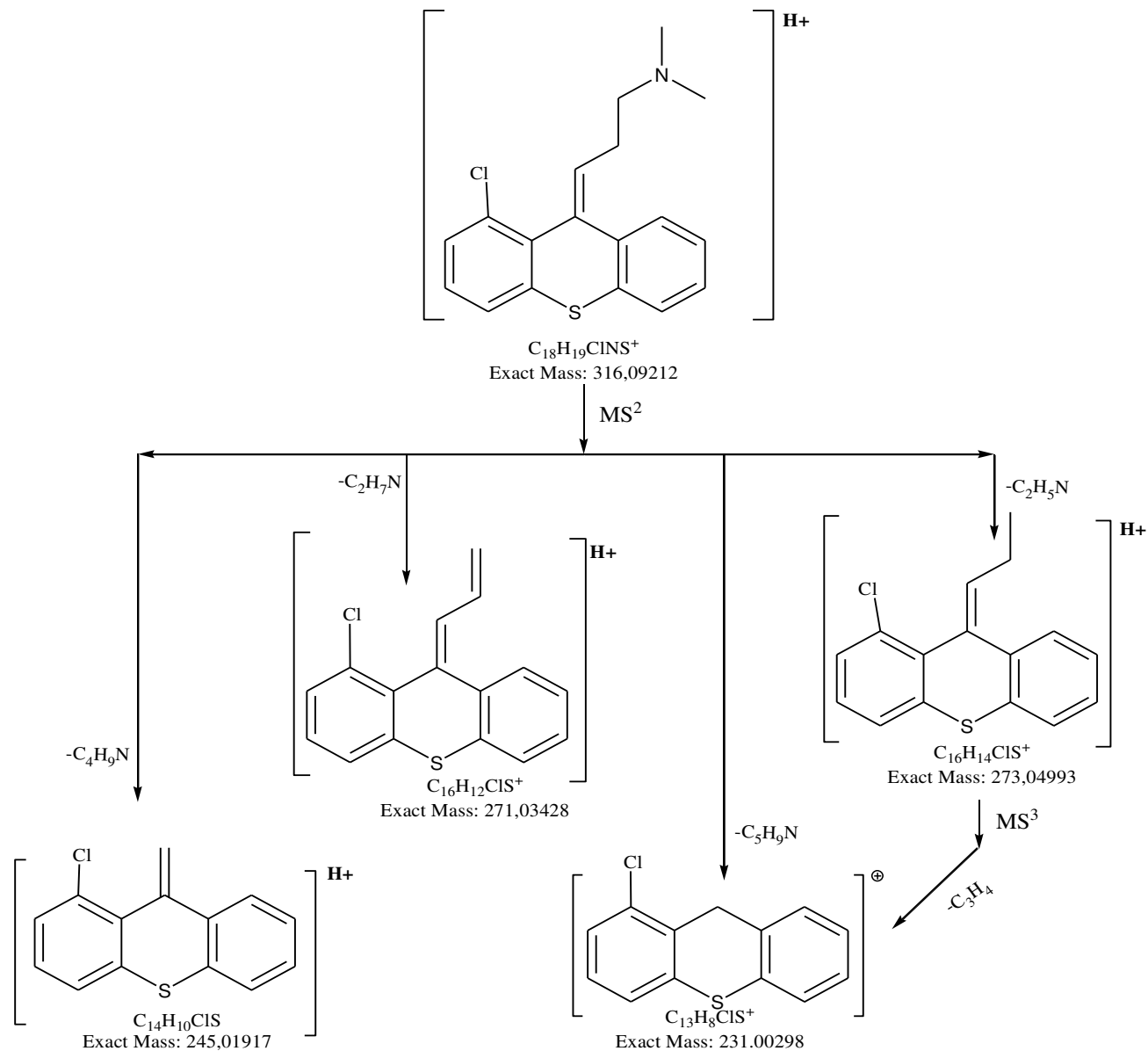
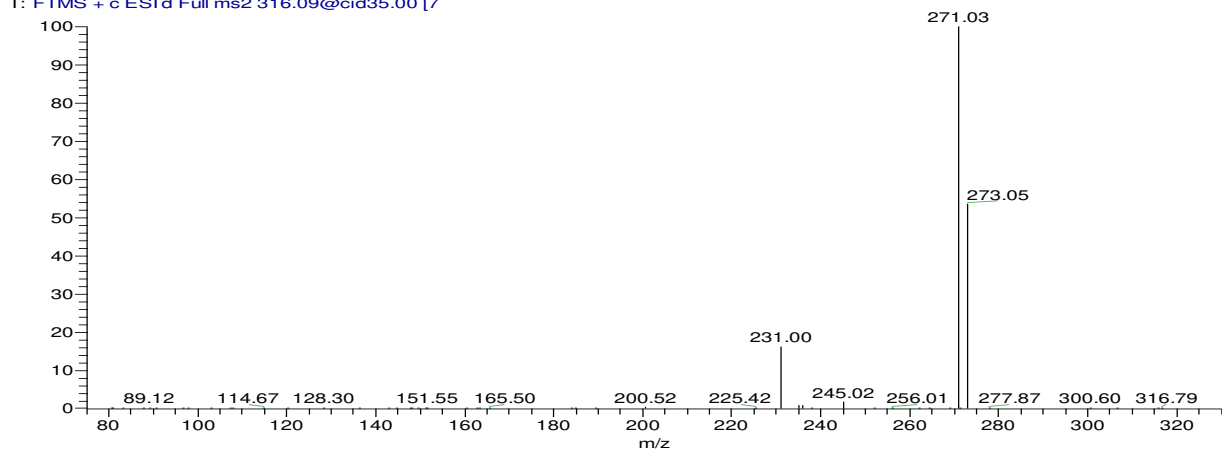
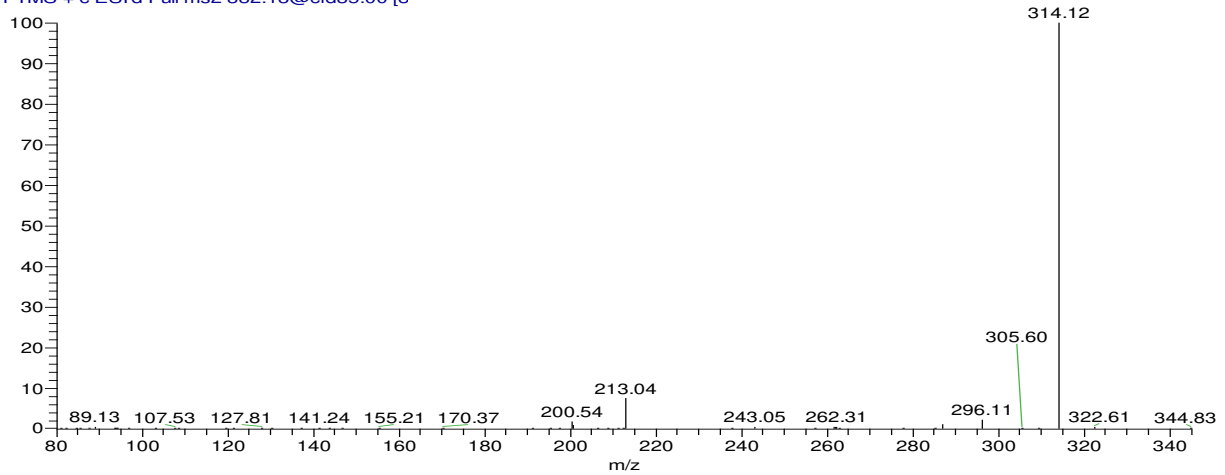


Figure S11: fragmentation pattern of PTP316-2 according to MS_n obtained from LC-HRMS



O

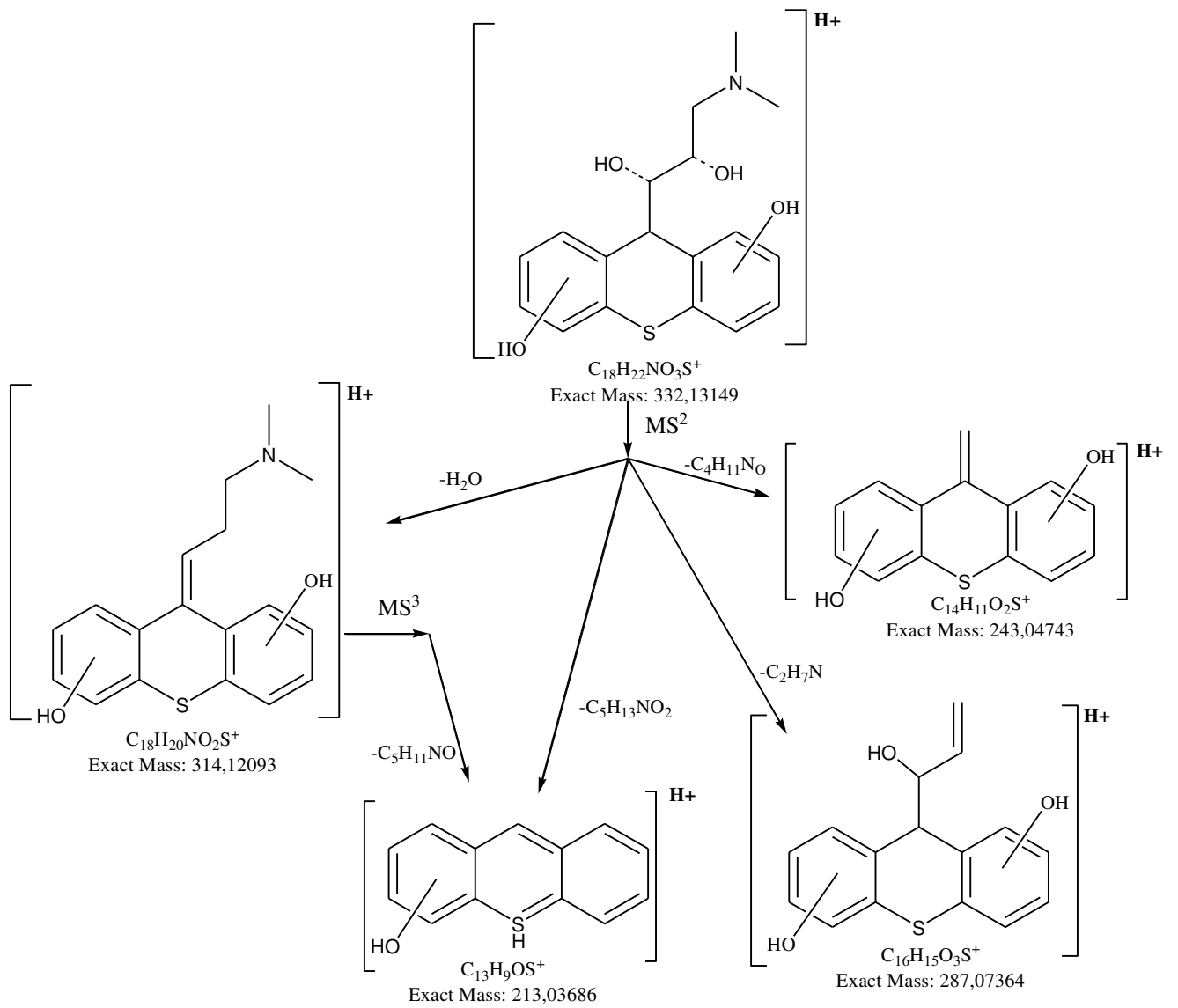


Figure S12: fragmentation pattern of PTP332-1 according to MS_n obtained from LC-HRMS

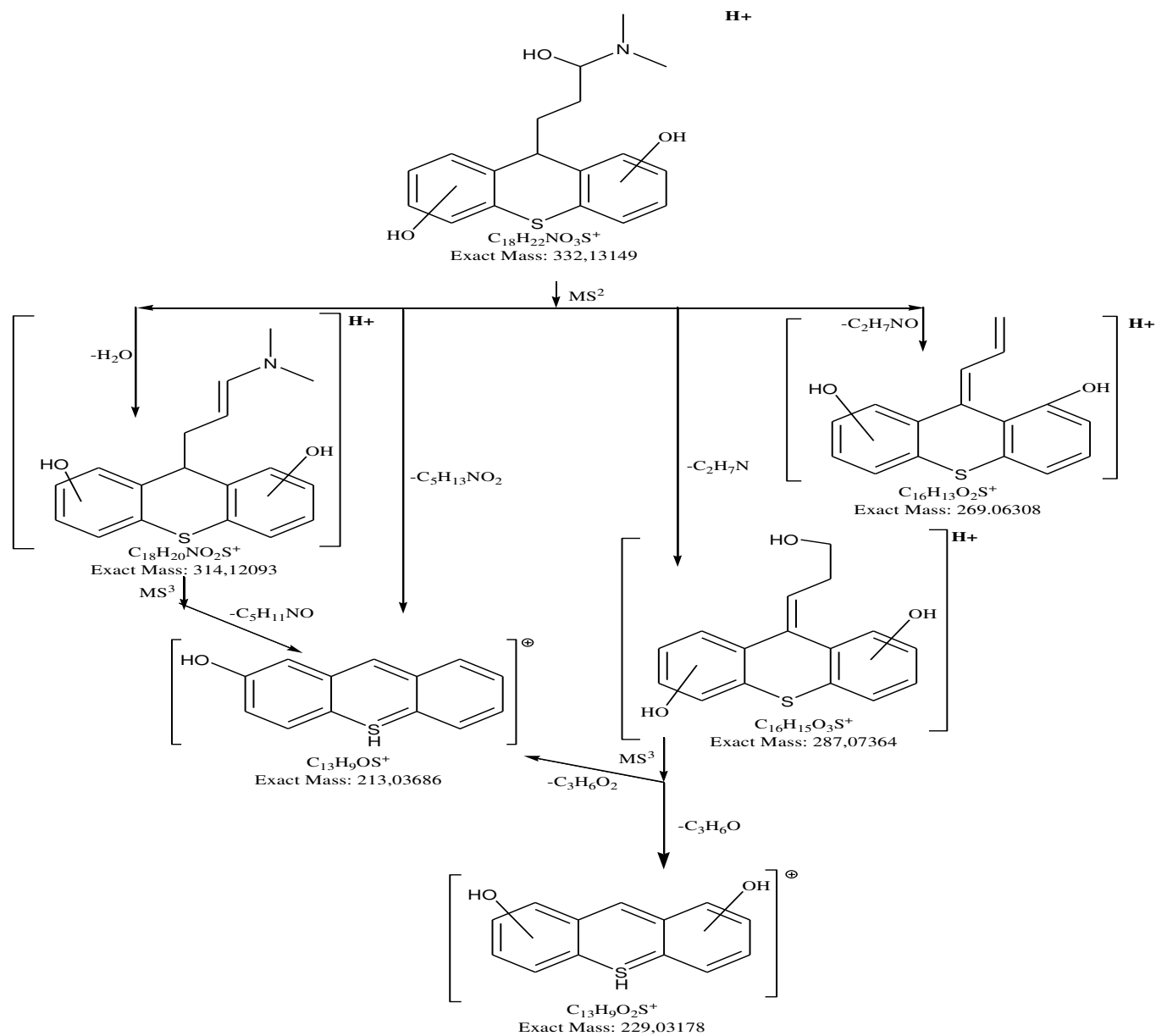
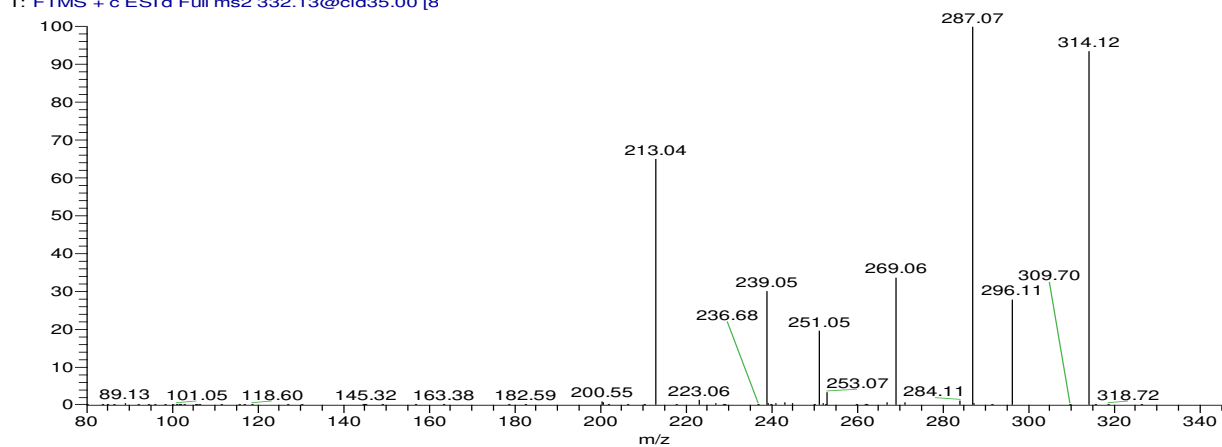


Figure S13: fragmentation pattern of PTP332-2 according to MSⁿ obtained from LC-HRMS

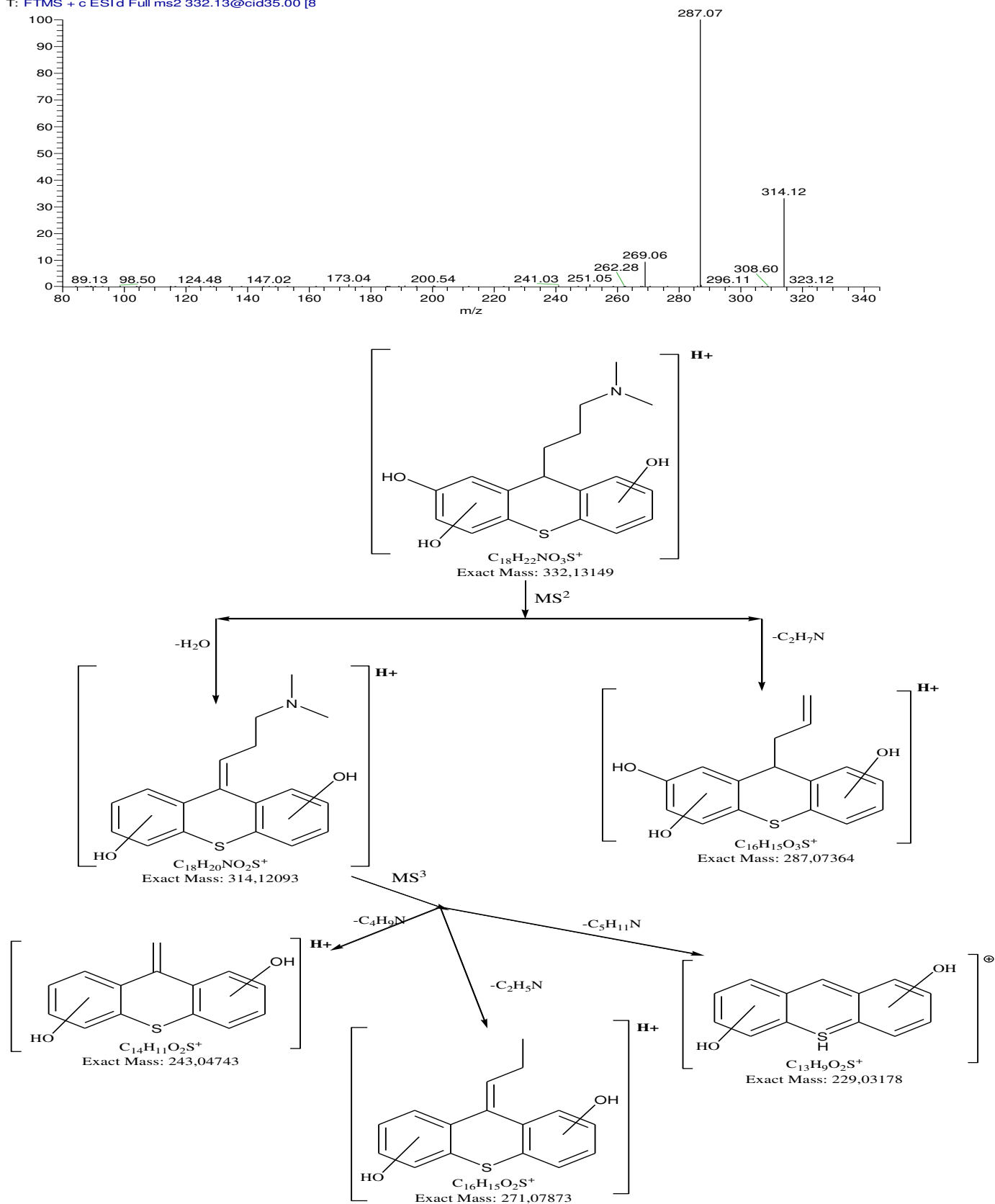


Figure S14: fragmentation pattern of PTP332-3 according to MSn obtained from LC-HRMS

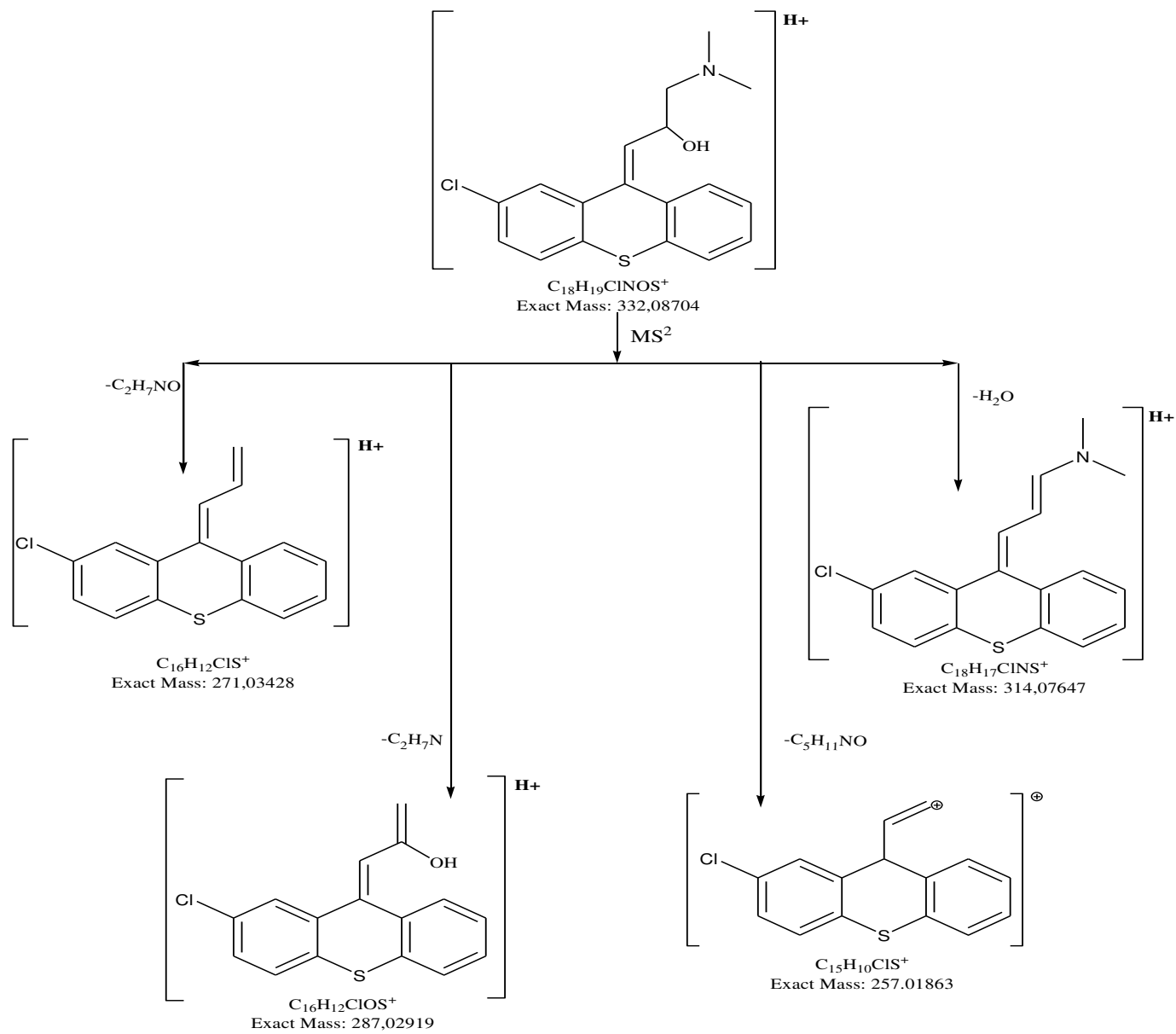
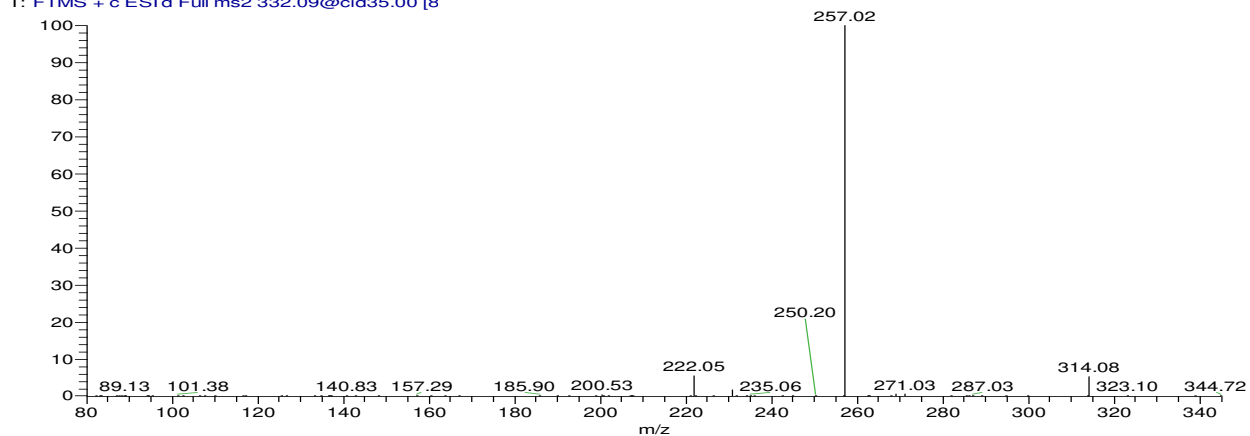


Figure S15: fragmentation pattern of PTP332-4 according to MSn obtained from LC-HRMS

Chlorprothixene 100PPmUV32min30C140726b #1081 RT: 13.98 AV: 1 NL: 7.44E4
T: FTMS + c ESI d Full ms2 332.09@cid35.00 [8]

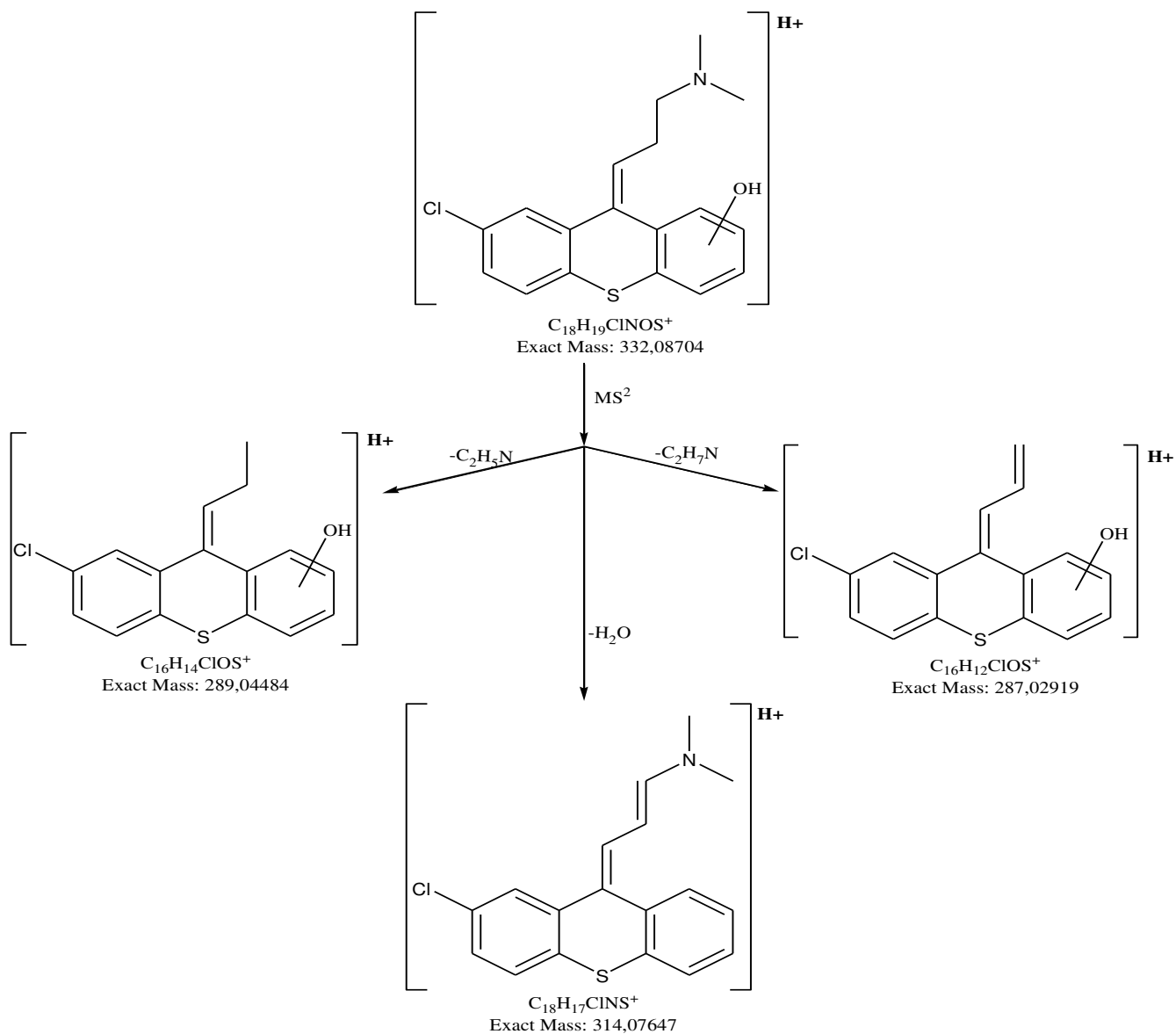
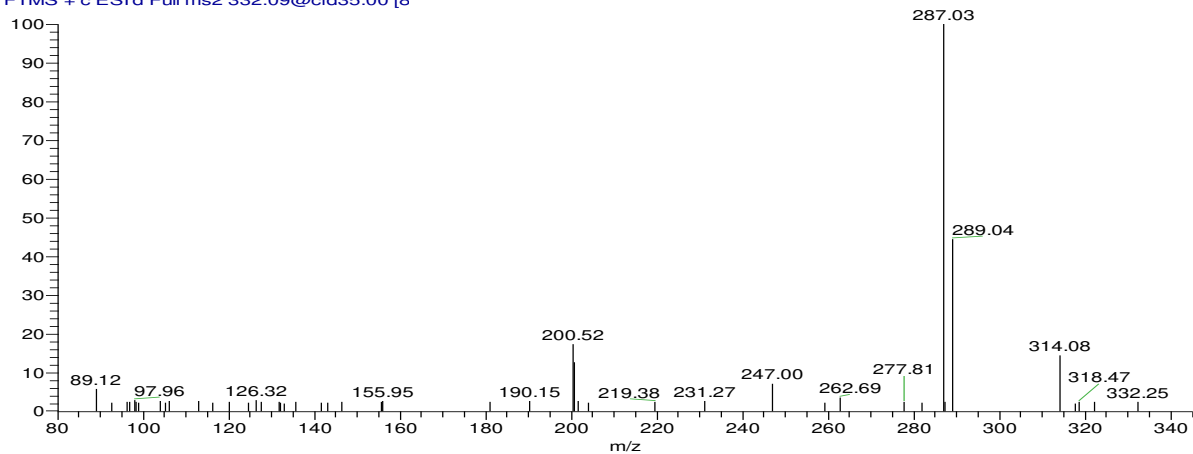


Figure S16: fragmentation pattern of PTP332-5 according to MS_n obtained from LC-HRMS

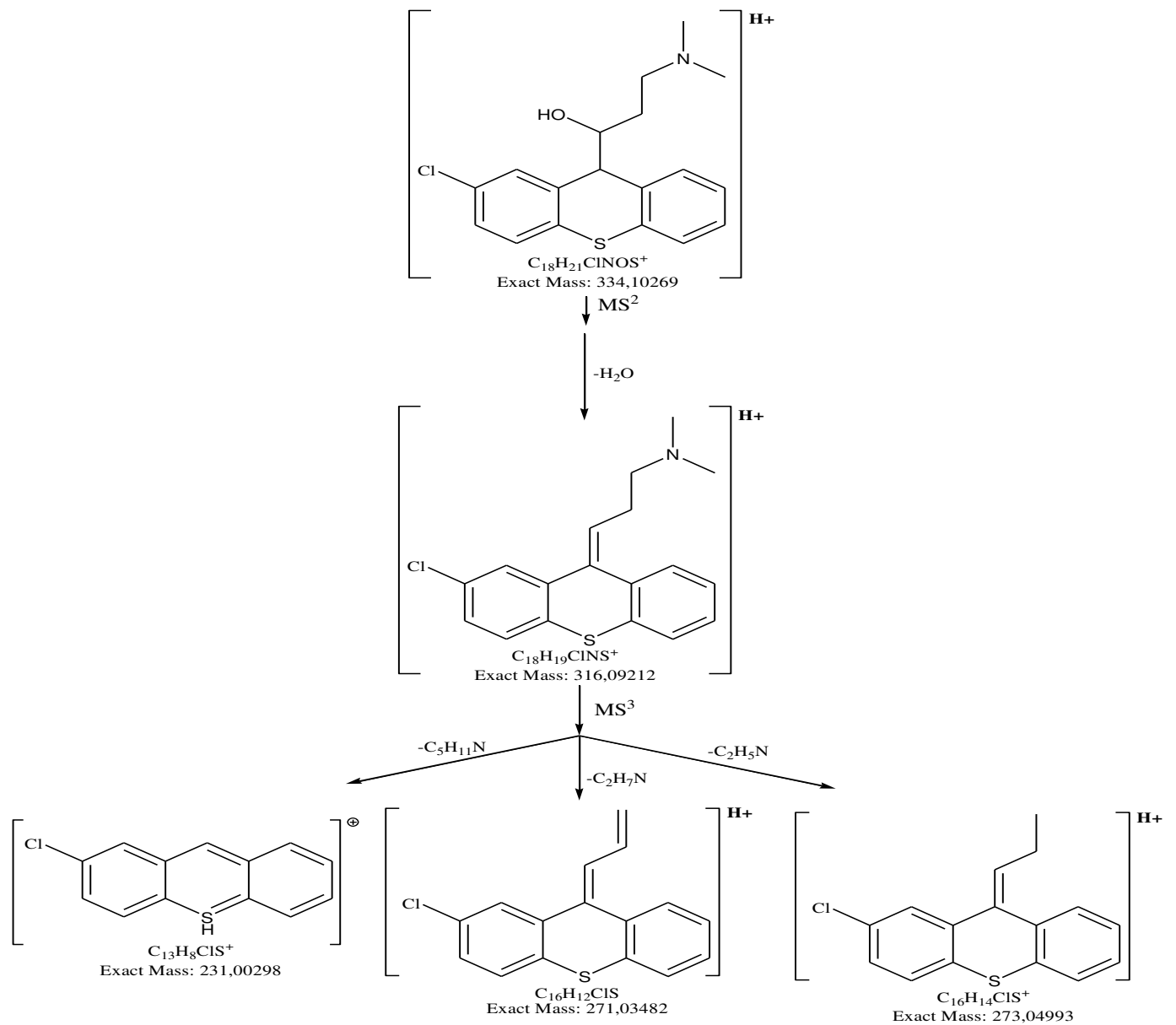
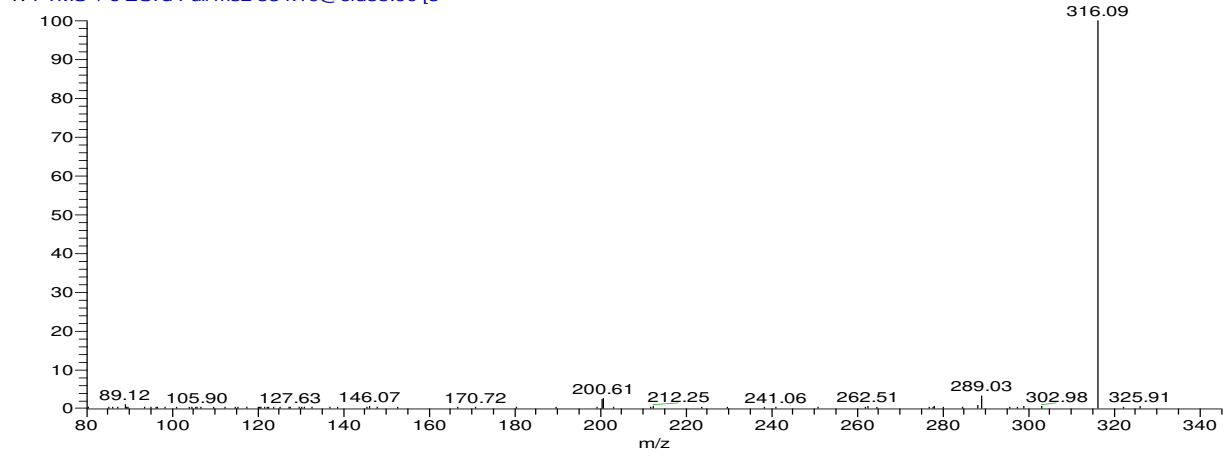


Figure S17: fragmentation pattern of PTP334 according to MSⁿ obtained from LC-HRMS

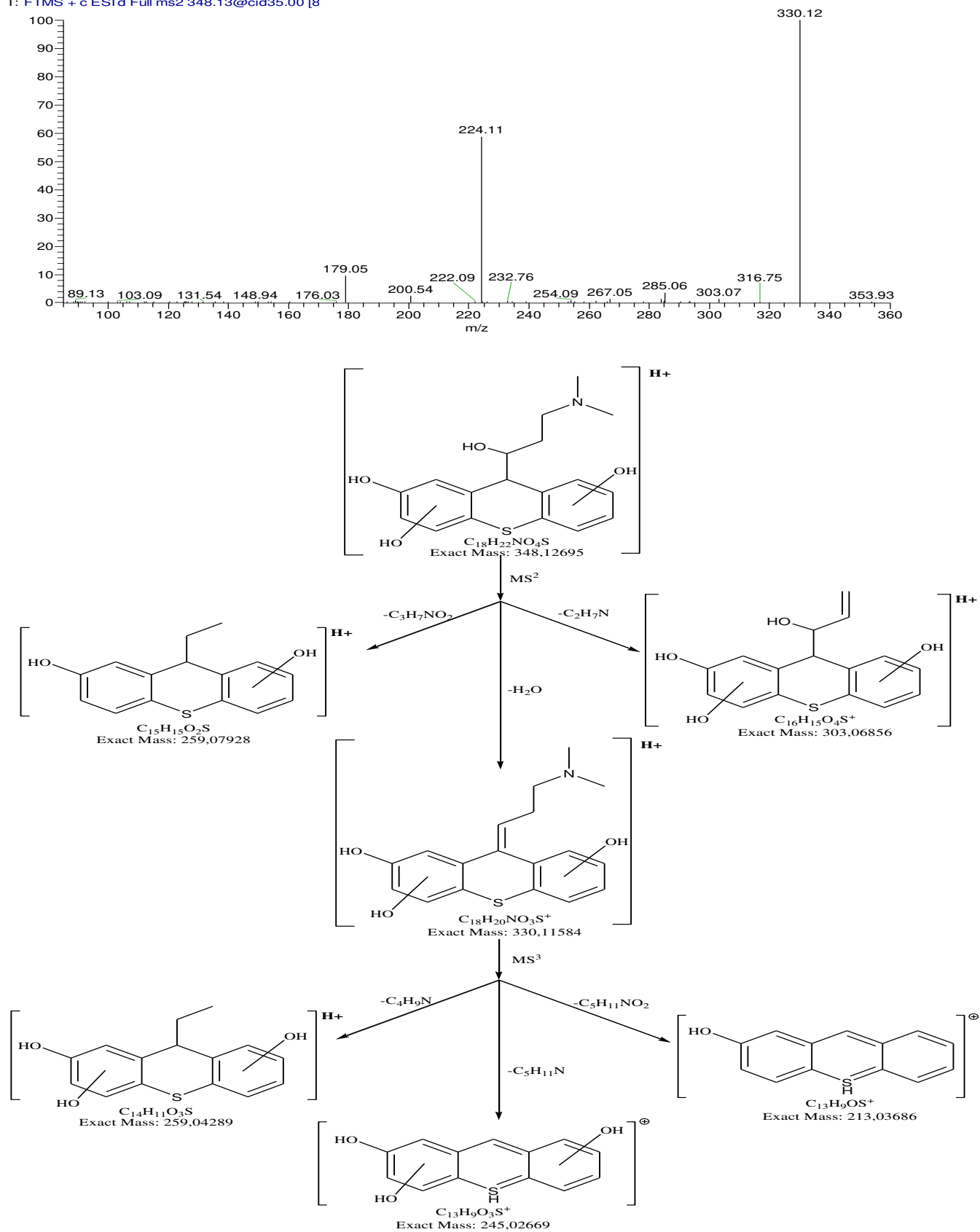


Figure S18: fragmentation pattern of PTP348 according to MSn obtained from LC-HRMS

Chlorprothixene_100PPmUV32min30C140726b #944 RT: 12.17 AV: 1 NL: 2.31E6
T: FTMS + c ESI d Full ms2 350.10@cid35.00 [8]

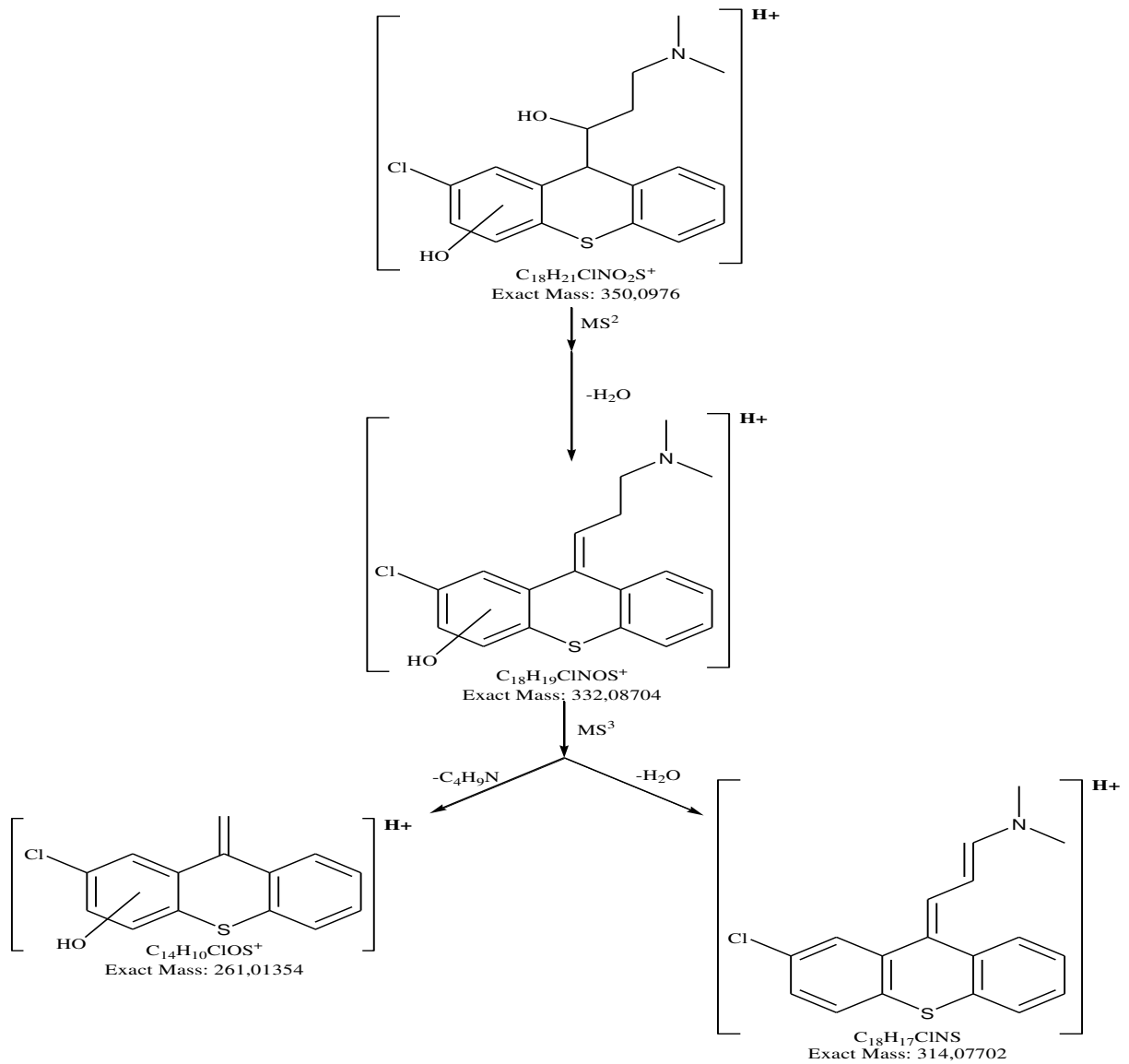
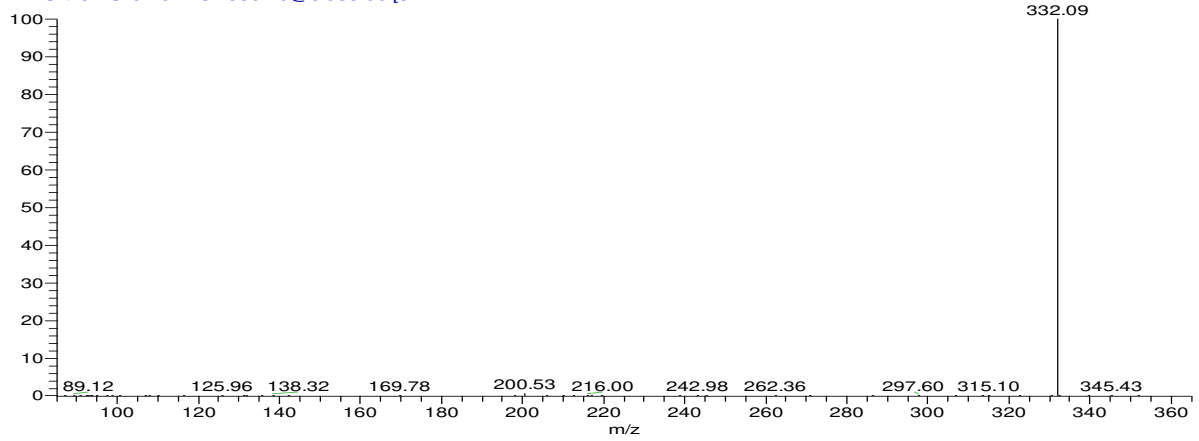


Figure S19: fragmentation pattern of PTP350 according to MS_n obtained from LC-HRMS

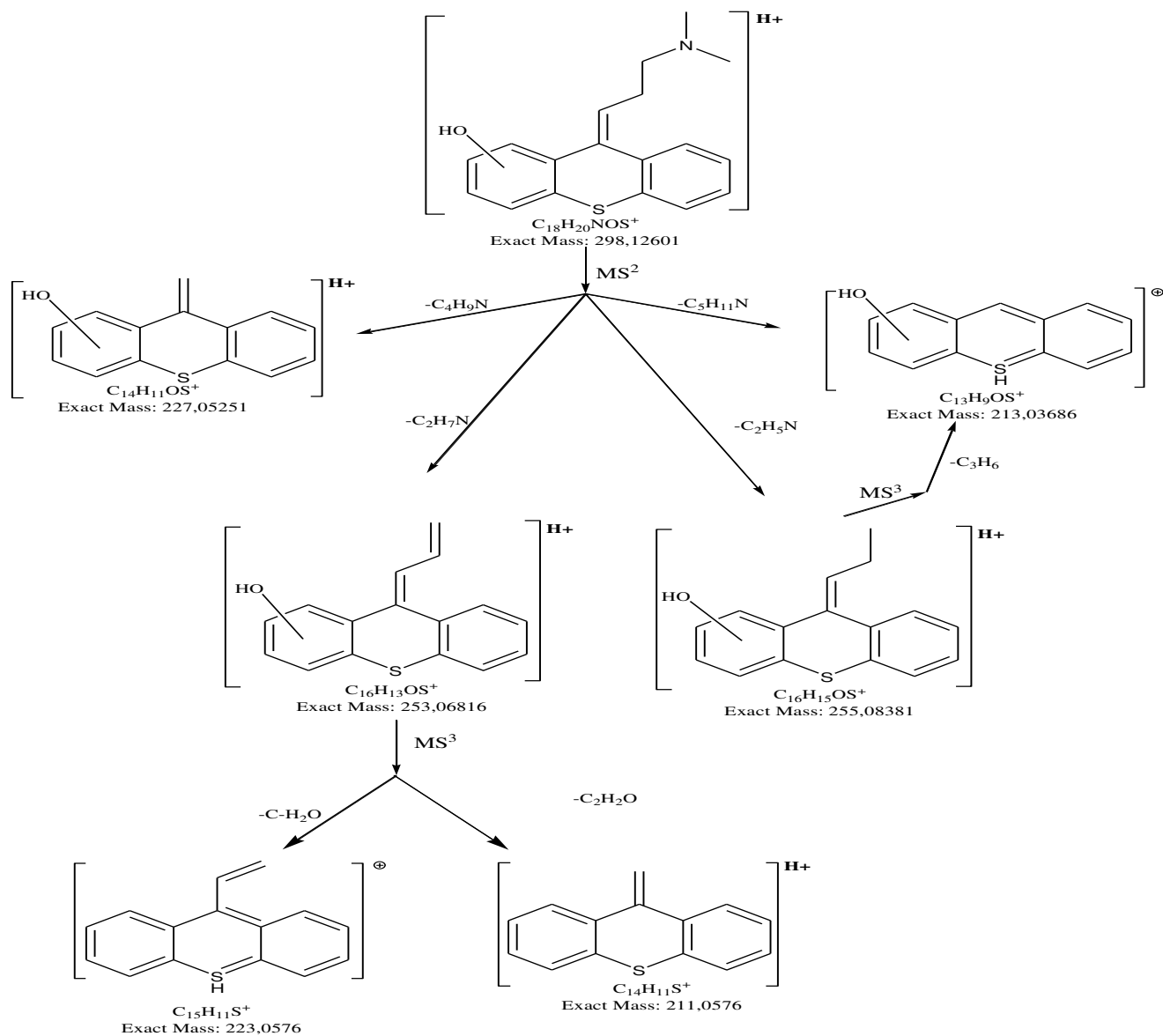
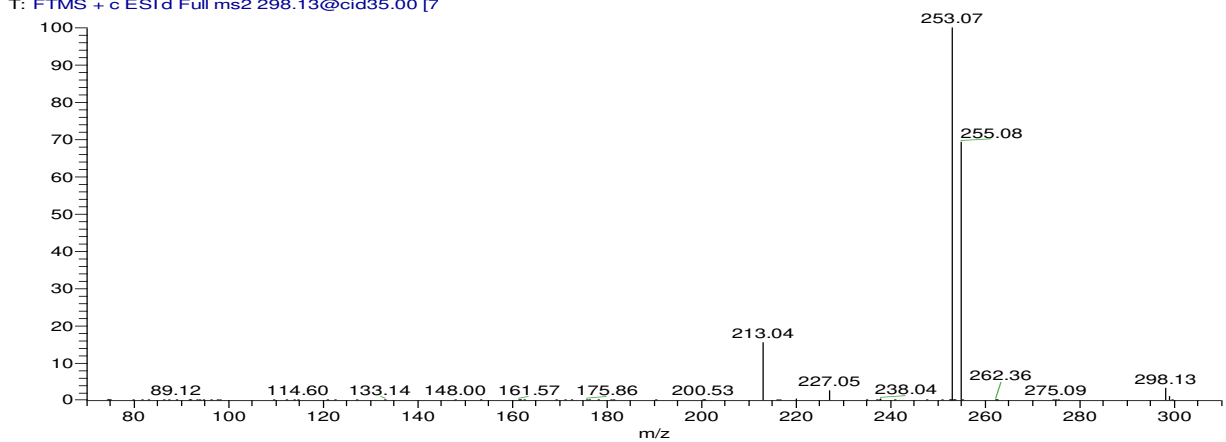


Figure S20: fragmentation pattern of PTP298 according to MSⁿ obtained from LC-HRMS

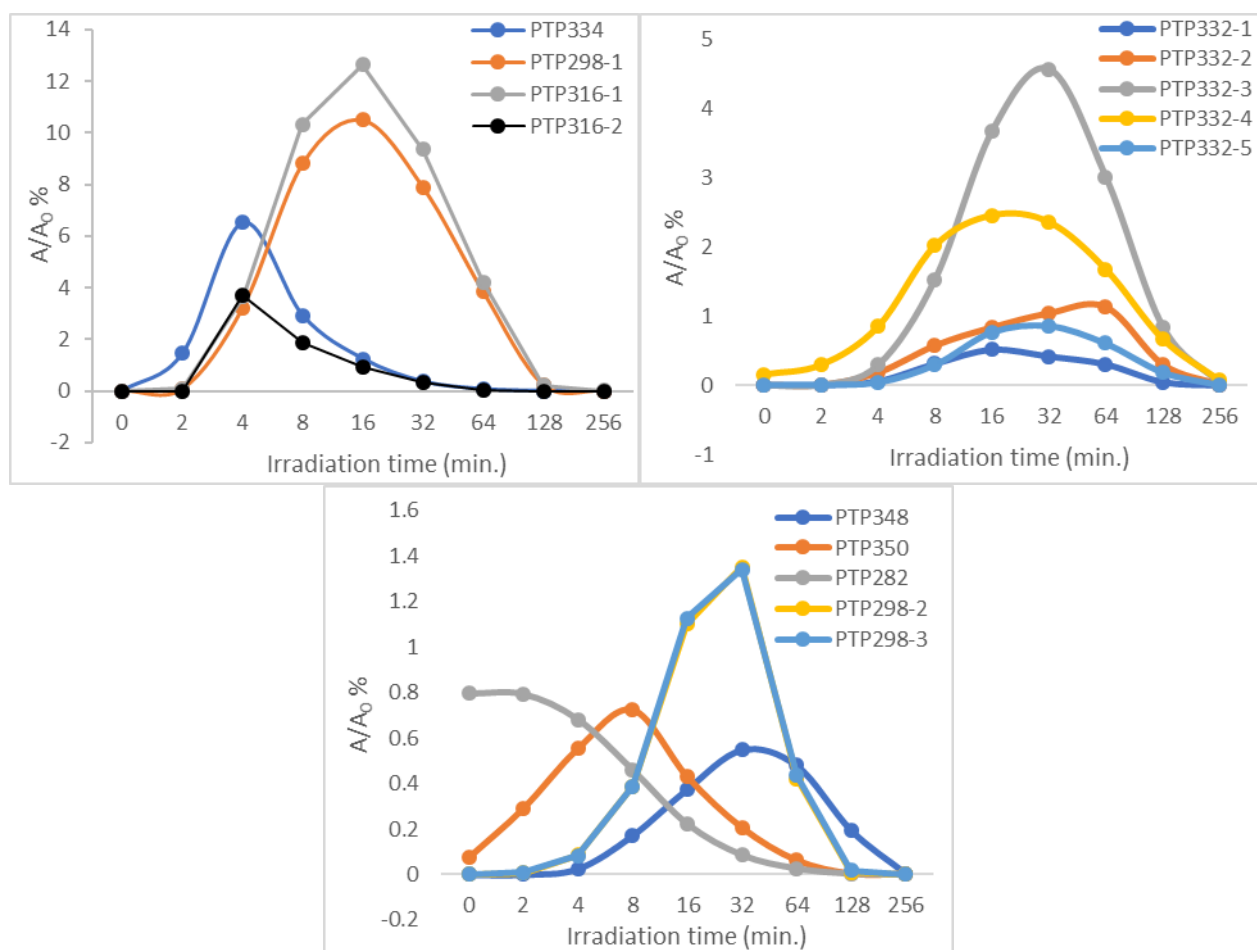
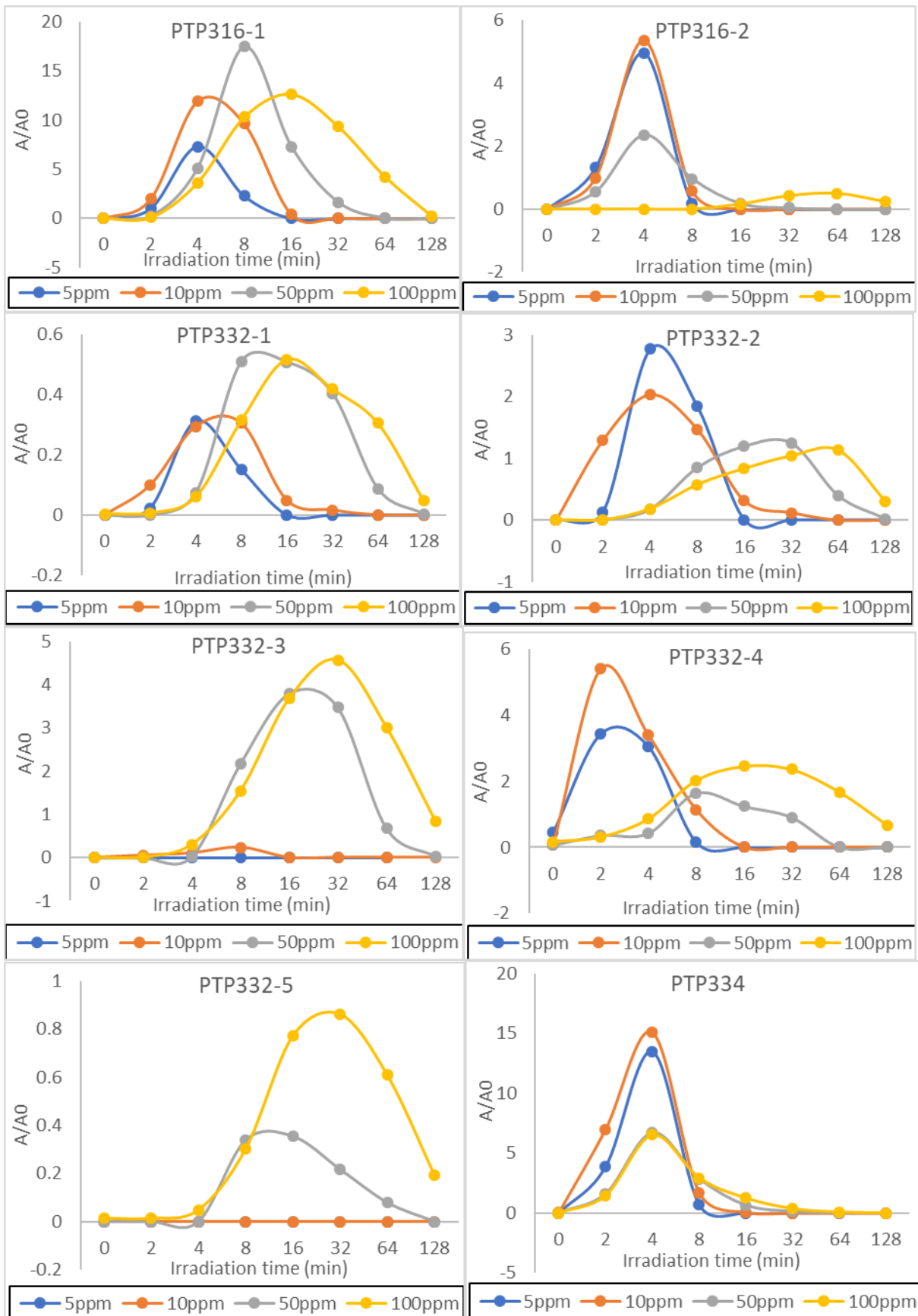


Figure S21: Time curves of the relative peak area A/A_0 (%) of the PTPs during photolysis assigned to their m/z ratio (A is the peak area of the PTP at a specific time point, A_0 is the peak area of CPTX (100 mg L^{-1}) at 0 min) ($n = 3$, with $SD < 0.27$ and $RSD < 13.6\%$)



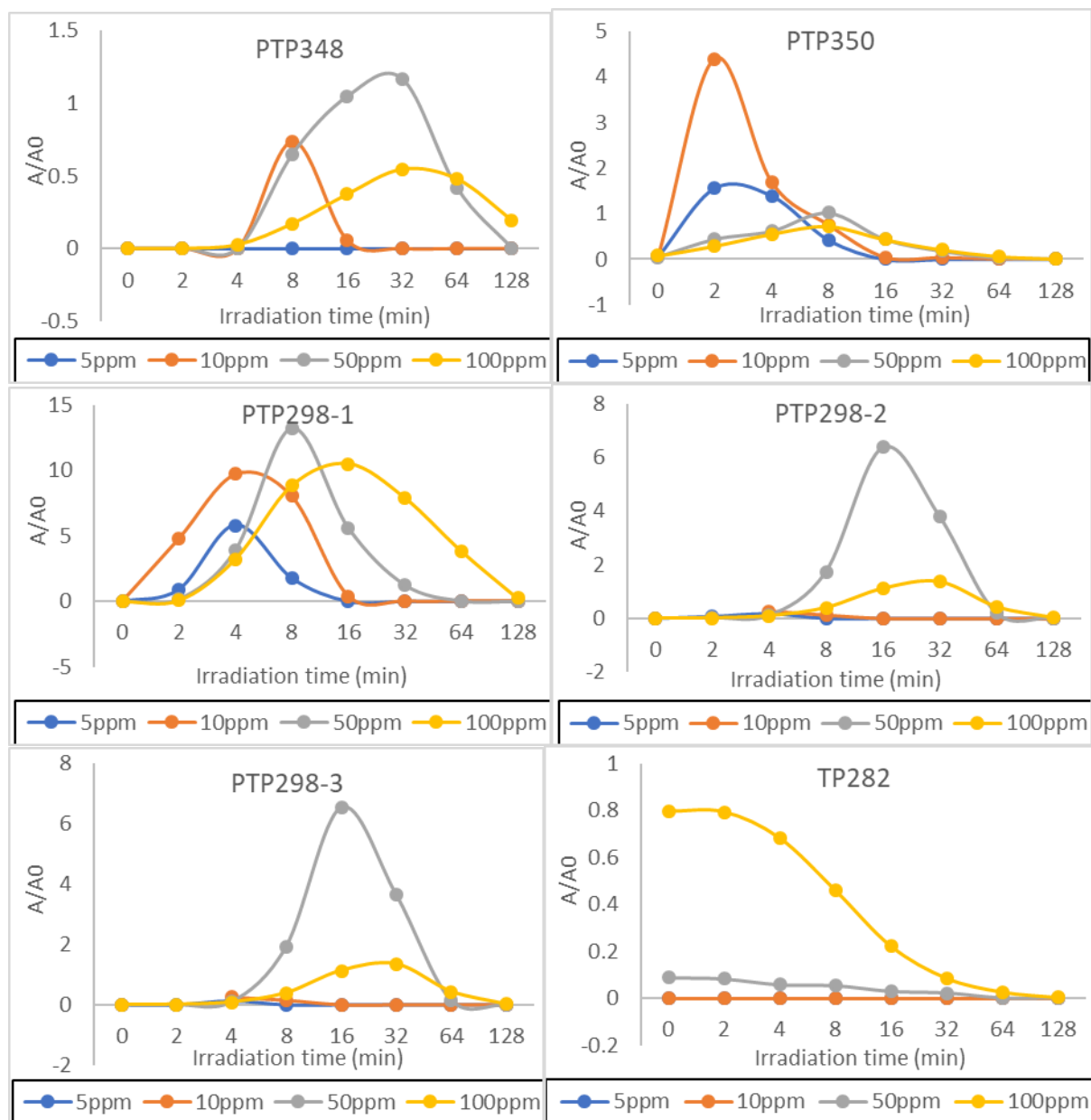
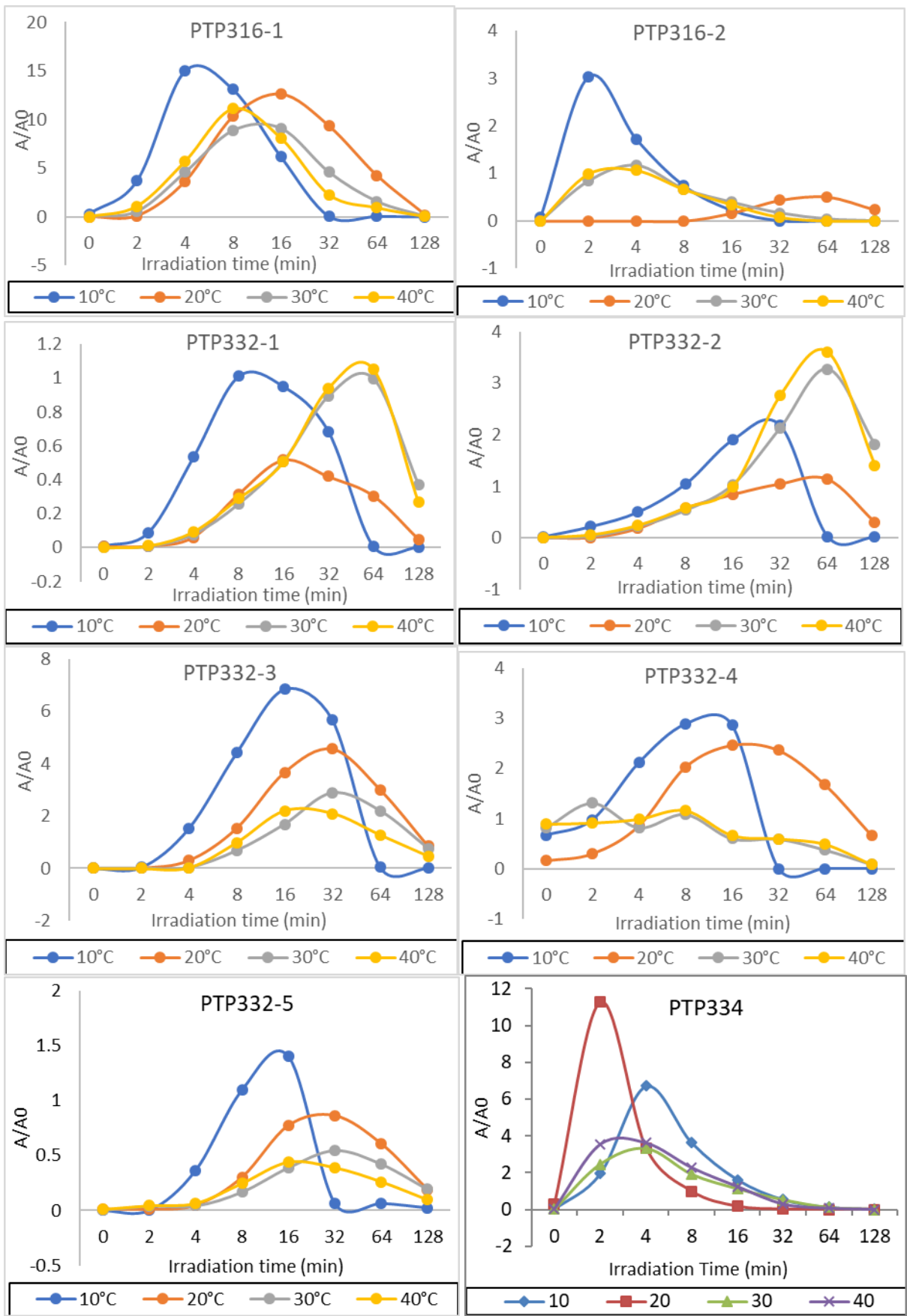


Figure S22: Time curves of the relative peak area A/A_0 (%) of CPTX PTPs during photolysis at different concentrations.



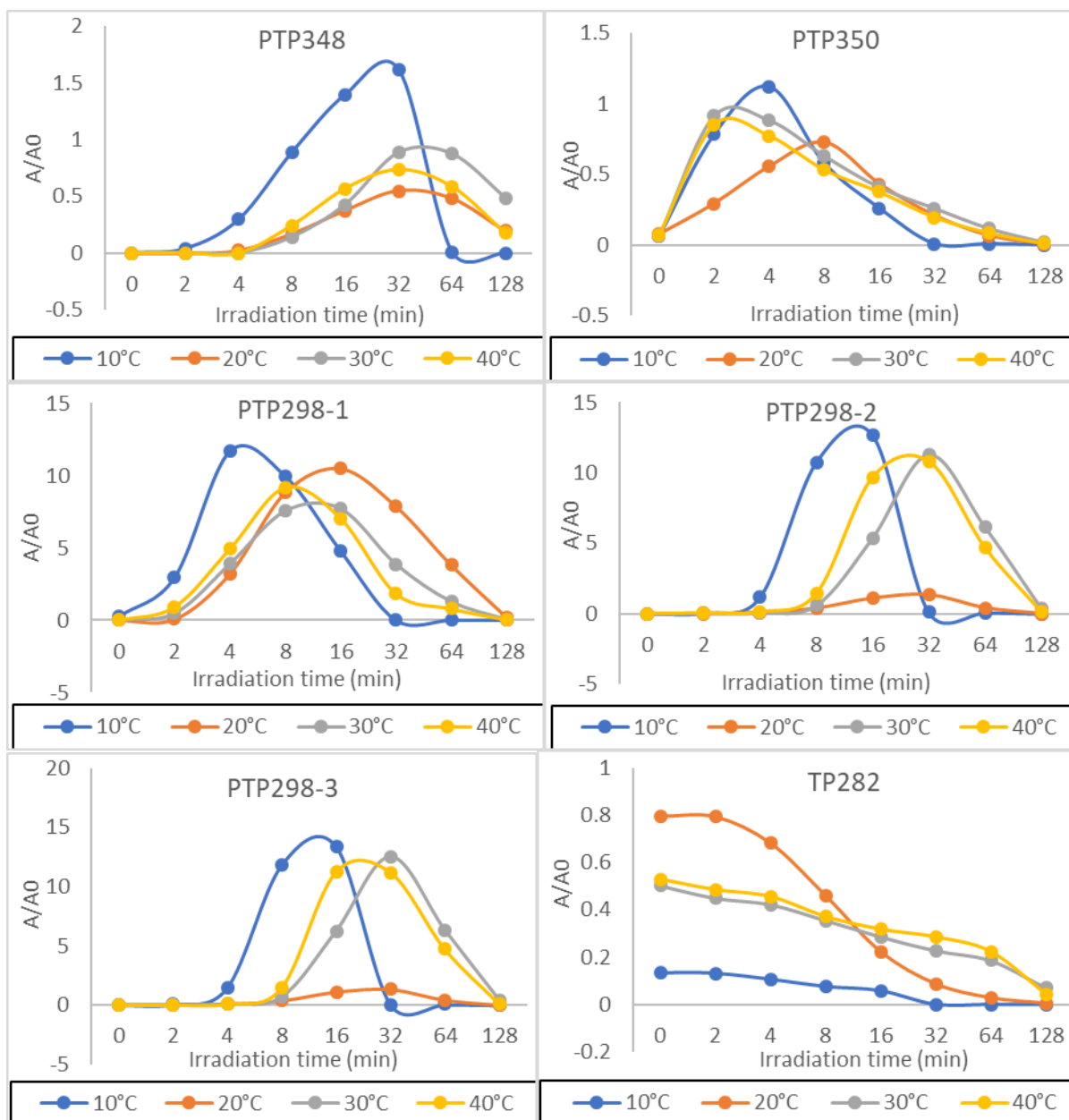
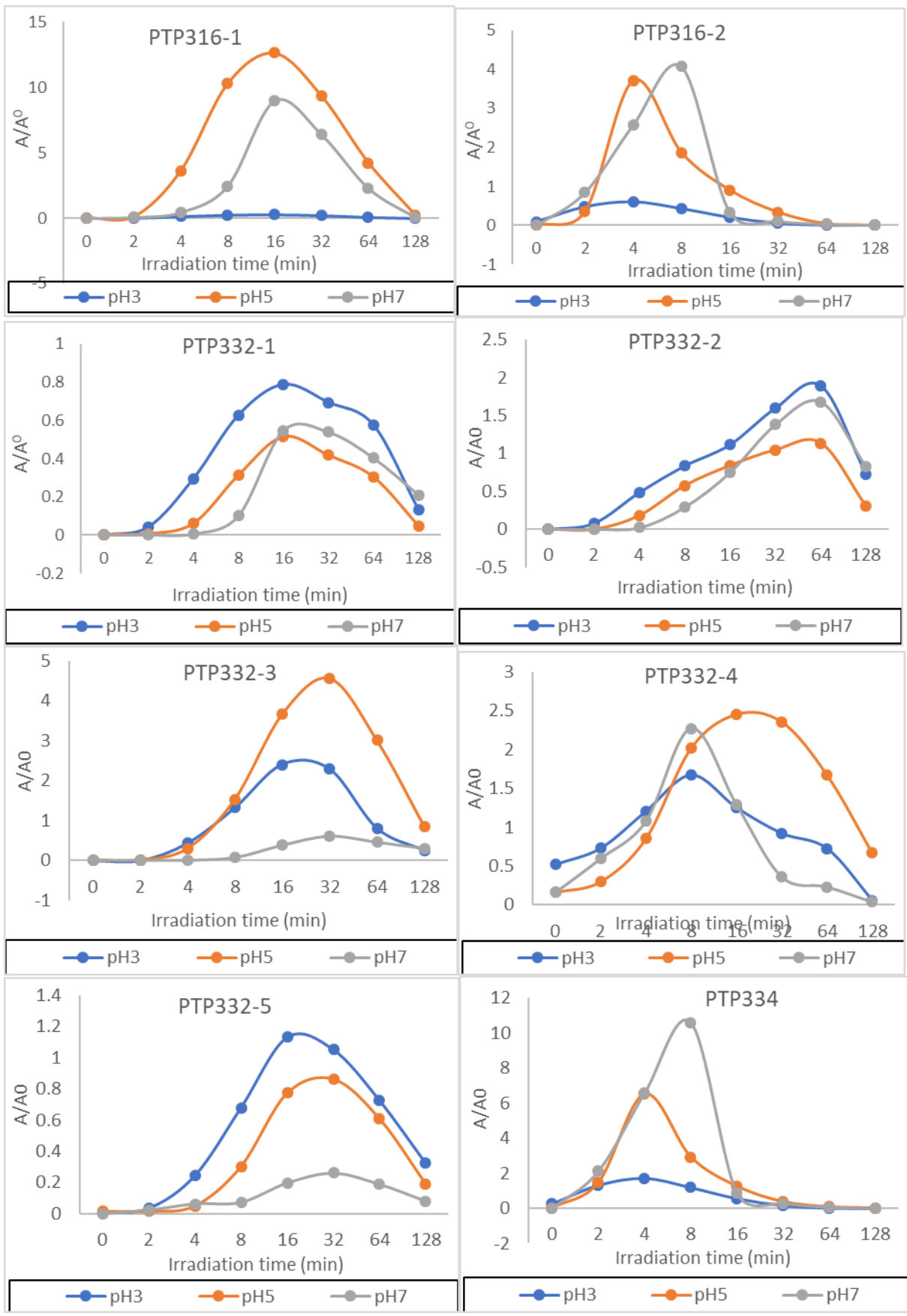


Figure S23: Time curves of the relative peak area A/A_0 (%) of CPTX PTPs during photolysis at different Temperature.



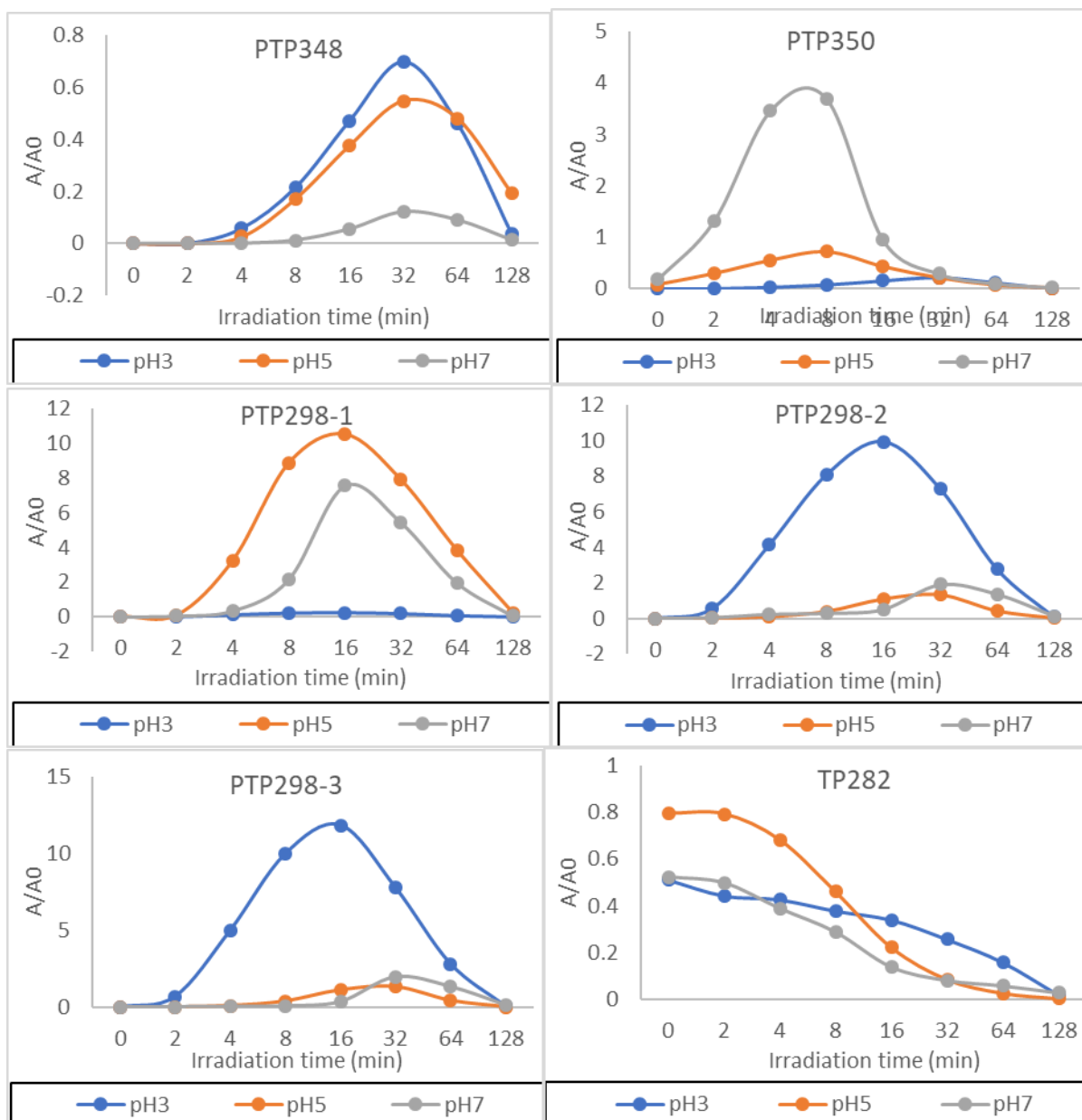
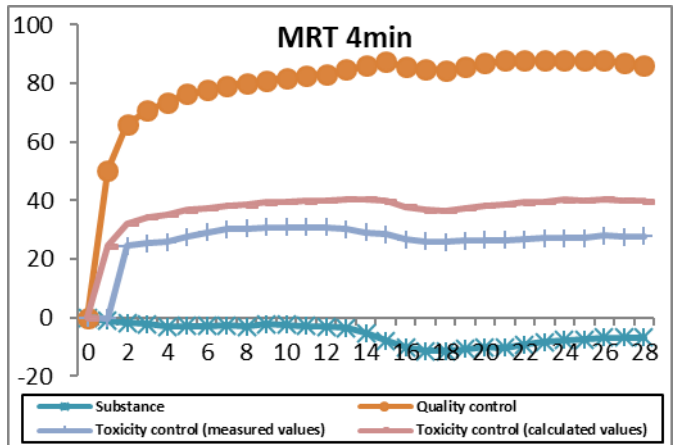
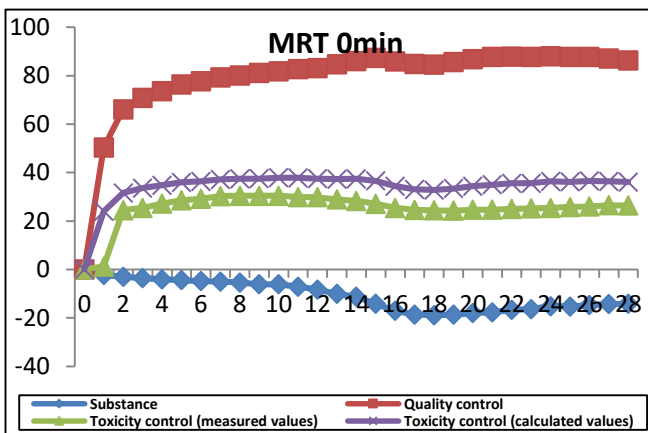
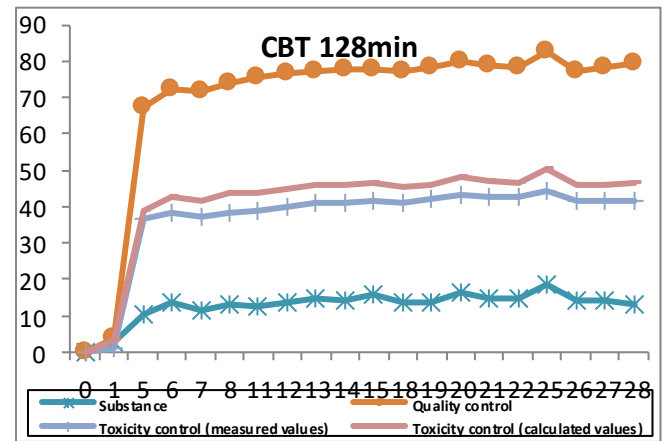
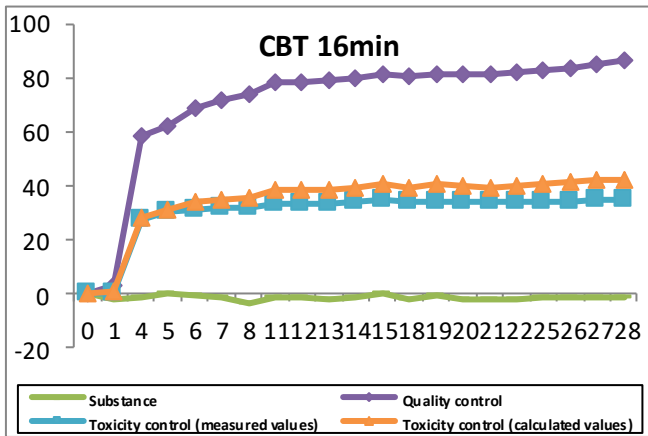
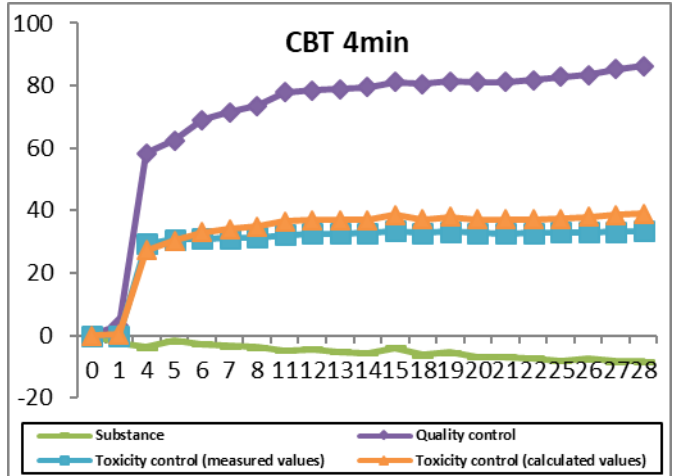
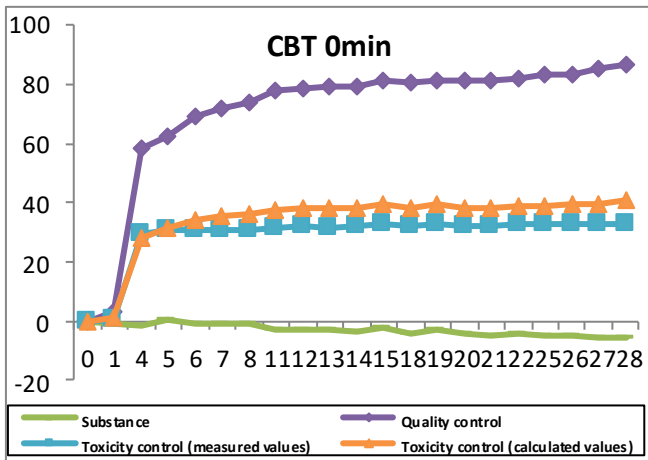


Figure S24: Time curves of the relative peak area A/A_0 (%) of CPTX PTPs during UV-photolysis at different pH values.



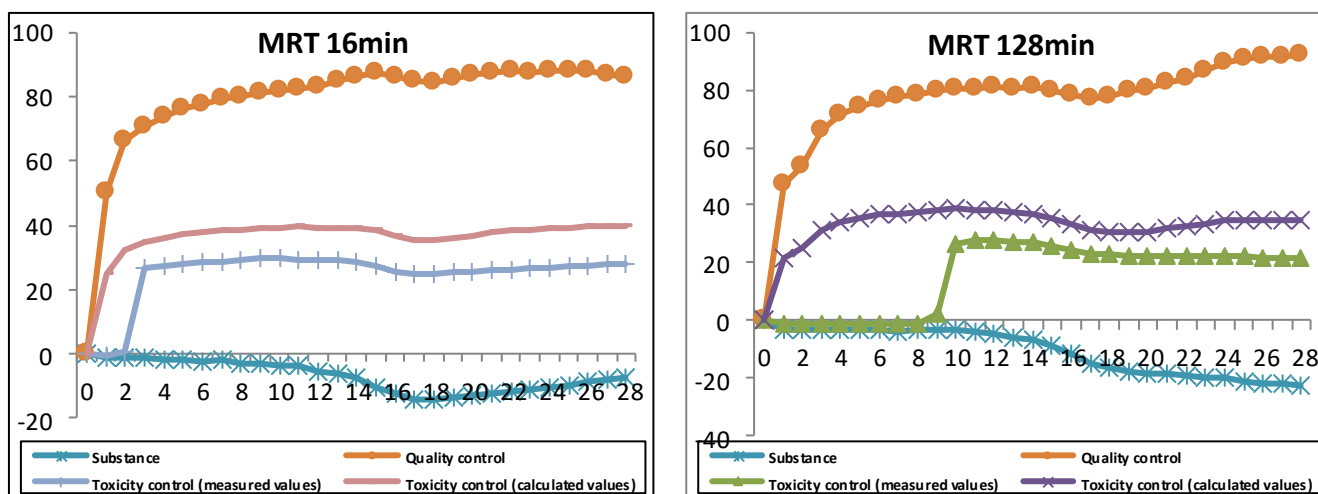


Figure S25: Closed Bottle test and Manometric Respiratory Test results of CPTX and its photolytic mixtures at different irradiation time points.

*X axis is the time in days, and Y axis is the biodegradation (%).

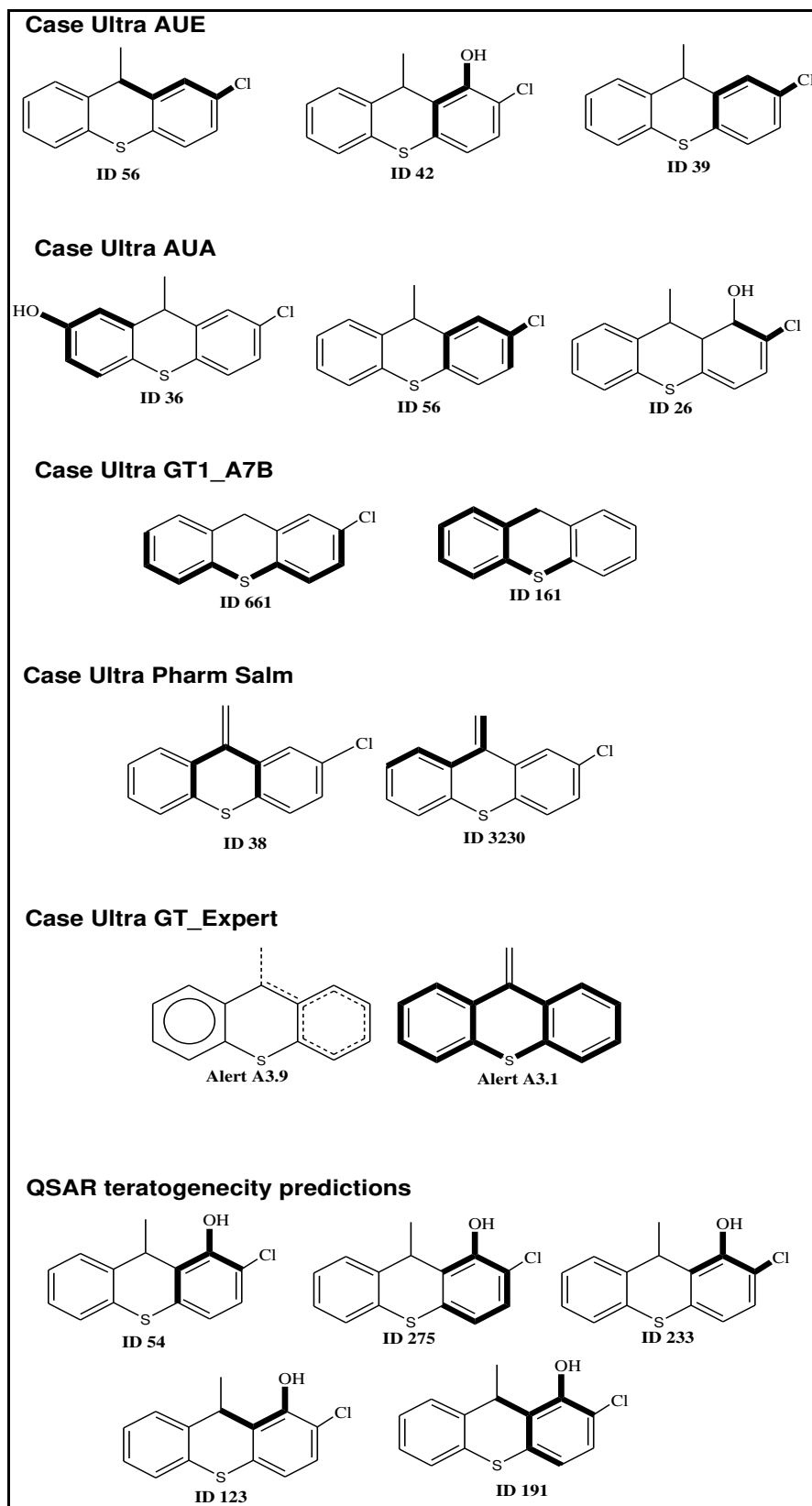


Figure S26: Structural alerts (in bold) in CPTX and its TPs for environmental toxicity by different QSAR models.

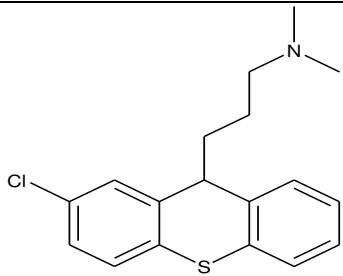
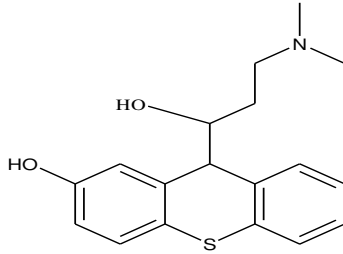
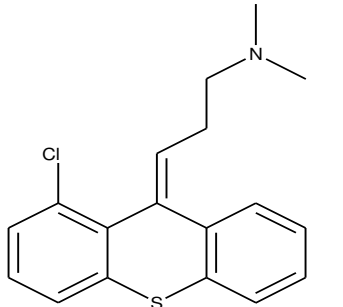
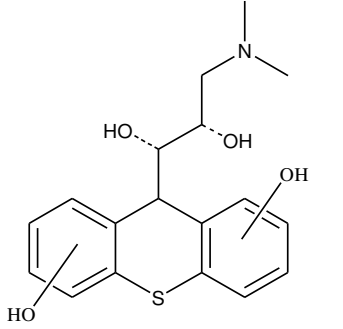
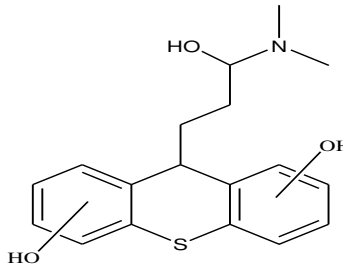
Tables

Table S1: a) Test system of the Closed Bottle test (CBT), b) Test system of the manometric respiratory test (MRT); “x” = addition, “-“ = no addition.

a	Blank	Quality control	Test	Toxicity control
Mineral medium	x	x	x	x
Inoculum (2 drops L ⁻¹)	x	x	x	x
CPTX (2.4 mg L ⁻¹ = 5 mg L ⁻¹ ThOD)	-	-	x	x
Sodium acetate (6.4 mg L ⁻¹) (ThOD = 5 mg L ⁻¹)	-	x	-	x

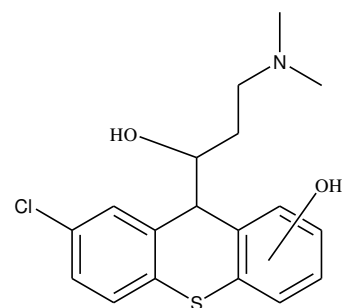
b	Blank	Quality control	Test	Toxicity control	Sterile control
Mineral medium	x	x	x	x	x
Inoculum (80 mL L ⁻¹)	x	x	x	x	-
CPTX (14.4 mg L ⁻¹ = 30 mg L ⁻¹ ThOD)	-	-	x	x	x
Sodium acetate (ThOD = 30 mg L ⁻¹) ¹⁾	-	x	-	x	x
Sodium azide (160.09 mg L ⁻¹)	-	-	-	-	x

Table S2: Accurate mass measurements of CPTX and its TPs determined by HRLCMS-LTQ Orbitrap in MS and MSⁿ mode

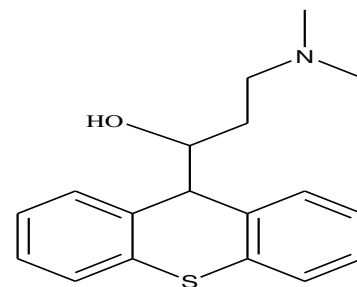
product ion (TP)	(Z/E)CPTX	15.13	316.09225	316.09212	9.5	C ₁₈ H ₁₉ NCIS	0.125	
precursor ion (MS ² :316)			271.03372	271.03428	10.5	C ₁₆ H ₁₂ ClS	-0.555	
			273.04941	273.04993	9.5	C ₁₆ H ₁₄ ClS	-0.515	
			231.00349	231.00298	9.5	C ₁₃ H ₈ ClS	0.515	
precursor ion (MS ³ :316/273)			231.00212	231.00298	9.5	C ₁₃ H ₈ ClS	-0.855	
Product ion (TP)	PTP316-1	12.21	316.13663	316.13658	8.5	C ₁₈ H ₂₂ O ₂ NS	0.054	
precursor ion (MS ² :316)			271.07843	271.07873	9.5	C ₁₆ H ₁₅ O ₂ S	-0.297	
			298.12558	298.12601	9.5	C ₁₈ H ₂₀ ONS	-0.431	
precursor ion (MS ³ :316/271)			253.06776	253.06816	10.5	C ₁₆ H ₁₃ OS	-0.402	
product ion (TP)	PTP316-2	13.33	316.09207	316.09212	9.5	C ₁₈ H ₁₉ NCIS	-0.055	
precursor ion (MS ² :316)			271.034	271.03428	10.5	C ₁₆ H ₁₂ ClS	-0.275	
			273.04932	273.04993	9.5	C ₁₆ H ₁₄ ClS	-0.605	
			245.01776	245.01917	9.5	C ₁₄ H ₁₀ ClS	-0.865	
			231.00232	231.00298	9.5	C ₁₃ H ₈ ClS	-0.655	
precursor ion (MS ³ :316/273)			231.00221	231.00298	9.5	C ₁₃ H ₈ ClS	-0.765	
product ion (TP)	PTP332-1	8.54	332.13159	332.13149	8.5	C ₁₈ H ₂₂ O ₃ NS	0.099	
precursor ion (MS ² :332)			314.12051	314.12093	9.5	C ₁₈ H ₂₀ O ₂ NS	-0.416	
			213.03616	213.03686	9.5	C ₁₃ H ₉ OS	-0.702	
			287.07367	287.07364	9.5	C ₁₆ H ₁₅ O ₃ S	0.028	
			243.04858	243.04743	9.5	C ₁₄ H ₁₁ O ₂ S	1.153	
precursor ion (MS ³ :332/314)			213.03642	213.03686	9.5	C ₁₃ H ₉ OS	-0.442	
product ion (TP)	PTP332-2	8.93	332.13153	332.13149	8.5	C ₁₈ H ₂₂ O ₃ NS	0.039	
precursor ion (MS ² :332)			314.12042	314.12093	9.5	C ₁₈ H ₂₀ O ₂ NS	-0.506	
			287.07333	287.07364	9.5	C ₁₆ H ₁₅ O ₃ S	-0.312	
			269.06284	269.06308	10.5	C ₁₆ H ₁₃ O ₂ S	-0.237	
			213.03629	213.03686	9.5	C ₁₃ H ₉ OS	-0.572	
			245.02611	245.02669	9.5	C ₁₃ H ₉ O ₃ S	-0.581	
precursor ion (MS ³ :332/287)			229.03081	229.03178	9.5	C ₁₃ H ₉ O ₂ S	-0.967	
			213.03619	213.03686	9.5	C ₁₃ H ₉ OS	-0.672	

precursor ion (MS ³ :332/314)			213.03622	213.03686	9.5	C ₁₃ H ₉ OS	-0.642	
product ion (TP)	PTP332-3	9.98	332.13144	332.13149	8.5	C ₁₈ H ₂₂ O ₃ NS	-0.051	
precursor ion (MS ² :332)			314.12045	314.12093	9.5	C ₁₈ H ₂₀ O ₂ NS	-0.476	
			287.07336	287.07364	9.5	C ₁₆ H ₁₅ O ₃ S	-0.282	
precursor ion (MS ³ :332/314)			271.07715	271.07873	9.5	C ₁₆ H ₁₅ O ₂ S	-1.577	
			243.04597	243.04743	9.5	C ₁₄ H ₁₁ O ₂ S	-1.457	
			229.03076	229.03178	9.5	C ₁₃ H ₉ O ₂ S	-1.017	
product ion (TP)	PTP332-4	11.52	332.08713	332.08704	9.5	C ₁₈ H ₁₉ ONClS	0.091	
precursor ion (MS ² :332)			257.01813	257.01863	10.5	C ₁₅ H ₁₀ ClS	-0.495	
			314.07611	314.07647	10.5	C ₁₈ H ₁₇ NCIS	-0.365	
			287.03091	287.02919	10.5	C ₁₆ H ₁₂ OCIS	1.72	
			271.03397	271.03428	10.5	C ₁₆ H ₁₂ ClS	-0.305	
product ion (TP)	PTP332-5	14.12	332.08701	332.08704	9.5	C ₁₈ H ₁₉ ONClS	-0.029	
precursor ion (MS ² :332)			314.07626	314.07647	10.5	C ₁₈ H ₁₇ NCIS	-0.215	
			289.04306	289.04484	9.5	C ₁₆ H ₁₄ OCIS	-1.78	
			287.02866	287.02919	10.5	C ₁₆ H ₁₂ OCIS	-0.53	
product ion (TP)	PTP334	13.33	334.10263	334.10269	8.5	C ₁₈ H ₂₁ ONClS	0.091	
precursor ion (MS ² :334)			316.09265	316.09212	9.5	C ₁₈ H ₁₉ NCIS	-0.515	
precursor ion (MS ³ :334/316)			273.04956	273.04993	9.5	C ₁₆ H ₁₄ ClS	-0.365	
			271.03397	271.03482	10.5	C ₁₆ H ₁₂ ClS	-0.305	
			231.00111	231.00298	9.5	C ₁₃ H ₈ ClS	-1.865	
product ion (TP)	PTP348	9.56	348.12665	348.12695	8.5	C ₁₈ H ₂₂ O ₄ NS	0.245	
precursor ion (MS ² :348)			330.11542	330.11584	9.5	C ₁₈ H ₂₀ O ₃ NS	-0.421	
			303.06873	303.06856	9.5	C ₁₆ H ₁₅ O ₄ S	0.174	
			259.08035	259.07928	8.5	C ₁₅ H ₁₅ O ₂ S	1.623	
precursor ion (MS ³ :348/330)			259.04358	259.04289	9.5	C ₁₄ H ₁₁ O ₃ S	1.239	
			245.02504	245.02669	9.5	C ₁₃ H ₉ O ₃ S	-1.651	
			213.03632	213.03686	9.5	C ₁₃ H ₉ OS	-0.542	

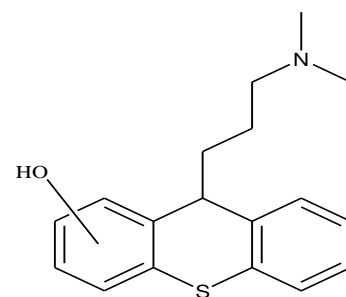
product ion (TP)	PTP350	12.24	350.09772	350.0976	8.5	C ₁₈ H ₂₁ O ₂ NCIS	0.116
precursor ion (MS ² :350)			332.08682	332.08704	9.5	C ₁₈ H ₁₉ ONCIS	-0.219
precursor ion (MS ³ :350/332)			261.01312	261.01354	9.5	C ₁₄ H ₁₀ OCIS	-0.42
			314.07678	314.07702	10.5	C ₁₈ H ₁₇ NCIS	0.305



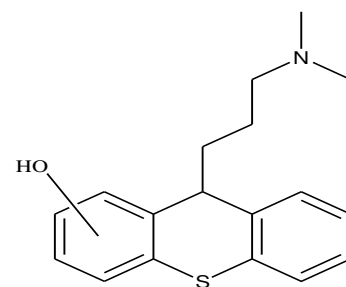
product ion (TP)	PTP298-1	11.2	298.12656	298.12601	9.5	C ₁₈ H ₂₀ ONS	0.548
precursor ion (MS ² :298)			255.08328	255.08381	9.5	C ₁₆ H ₁₅ OS	-0.532
			253.06839	253.06816	10.5	C ₁₆ H ₁₃ OS	0.228
			227.05223	227.05251	9.5	C ₁₄ H ₁₁ OS	-0.282
			213.03654	213.03686	9.5	C ₁₃ H ₉ OS	-0.322
precursor ion (MS ³ :298/253)			235.05705	235.0576	11.5	C ₁₆ H ₁₁ S	-0.548
			223.05626	223.0576	10.5	C ₁₅ H ₁₁ S	-1.338
precursor ion (MS ³ :298/255)			213.03638	213.03686	9.5	C ₁₃ H ₉ OS	-0.482



product ion (TP)	PTP298-2	12.39	298.12625	298.12601	9.5	C ₁₈ H ₂₀ ONS	0.239
precursor ion (MS ² :285)			255.08334	255.08381	9.5	C ₁₆ H ₁₅ OS	-0.472
			253.06842	253.06816	10.5	C ₁₆ H ₁₃ OS	0.258
			213.03664	213.03686	9.5	C ₁₃ H ₉ OS	-0.222
			227.05217	227.05251	9.5	C ₁₄ H ₁₁ OS	-0.342
precursor ion (MS ³ :298/253)			235.0569	235.0576	11.5	C ₁₆ H ₁₁ S	-0.698
			223.05692	223.0576	10.5	C ₁₅ H ₁₁ S	-0.678
			211.05598	211.0576	9.5	C ₁₄ H ₁₁ S	-1.618
precursor ion (MS ³ :298/255)			213.03622	213.03686	9.5	C ₁₃ H ₉ OS	-0.642



product ion (TP)	PTP298-3	12.86	298.12595	298.12601	9.5	C ₁₈ H ₂₀ ONS	-0.062
precursor ion (MS ² :285)			255.08331	255.08381	9.5	C ₁₆ H ₁₅ OS	-0.502
			253.06836	253.06816	10.5	C ₁₆ H ₁₃ OS	0.198
			227.0522	227.05251	9.5	C ₁₄ H ₁₁ OS	-0.312
			213.03656	213.03686	9.5	C ₁₃ H ₉ OS	-0.302
precursor ion (MS ³ :298/253)			235.05687	235.0576	11.5	C ₁₆ H ₁₁ S	-0.728
			225.03537	225.03686	10.5	C ₁₄ H ₉ OS	-1.492
			211.0583	211.0576	9.5	C ₁₄ H ₁₁ S	0.702



precursor ion (MS ³ :298/255)			213.03629	213.03686	9.5	C ₁₃ H ₉ OS	-0.572
product ion (TP)	PTP282	13.96	282.13083	282.1311	9.5	C ₁₈ H ₂₀ NS	-0.267
precursor ion (MS ² :282)			239.08766	239.0889	9.5	C ₁₆ H ₁₅ S	-1.238
			237.07246	237.07325	10.5	C ₁₆ H ₁₃ S	-0.788
			211.05635	211.0576	9.5	C ₁₄ H ₁₁ S	-1.248
			197.04115	197.04195	9.5	C ₁₃ H ₉ S	-0.798
precursor ion (MS ³ :282/239)			197.04115	197.04195	9.5	C ₁₃ H ₉ S	-0.798

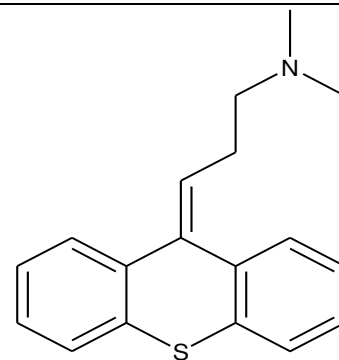


Table S3: Results of the investigated aerobic biodegradation test assays for CPTX and its photolytic mixtures.

Biodegradation test	Test sample	Biodegradation after 28 days %	Parent compound elimination %	DOC removal %
CBT				
	0 min	-5.3	4.2	
	4 min	-8.3	7.4	
	16 min	-1.4	8.2	
	128 min	3.3	9.9	
MRT				
	0 min	-14.2	0.1	2.4
	4 min	-6.7	1.2	5.1
	16 min	-7.6	2.9	14.7
	128 min	-22.8	5.9	35.5

Table S4: Q-SAR predictions for CPTX and its TPs for ready biodegradability by different models: 1: Catalogic-BOD Kinetic (OECD 301F) _v.08.09, 2. Catalogic BOD 28 days MITI (OECD 301C) _v.06.07. 3: Case Ultra, MITI Ready biodegradation (AU6), 4: MITI Biodegradation probability Biowin 5 (linear model), 5: MITI Biodegradation probability Biowin 6 (MITI non-linear model), (Positive results are red, RB: Ready Biodegradable, NRB: Non Ready Biodegradable)

Compounds	Smiles	OASIS catalogic		Case Ultra	Epi Suite		Log P
		Catalogic OECD 301F*	Catalogic OECD 301C*	AU6	Biowin 5**	Biowin 6**	
cisZCPTX	<chem>CN(C)CCC=C1c2ccccc2Sc3ccc(Cl)cc31</chem>	0.1279	0.0414	-	-0.1428	0.0028	5.18
PTP316-1	<chem>CN(C)CCCC1c2ccccc2Sc3cc(O)c(O)cc13</chem>	0.1764	0.0369	-	0.006	0.0158	3.870034
PTP316-2	<chem>CN(C)CCCC1c2ccccc2Sc3cc(O)c(O)cc13</chem>	0.1408	0.0332	-	0.006	0.0158	3.870034
PTP316-3	<chem>CN(C)C(O)CCC1c2ccccc2Sc3ccc(O)cc13</chem>	0.176	0.231	±	0.011	0.0175	3.645018
PTP316-4	<chem>CN(C)CCCC1c2ccccc2Sc3cc(O)c(O)c13</chem>	0.0761	0.0414	-	0.006	0.0158	3.870034
PTP316-5	<chem>CN(C)CCCC1c2cccc(O)c2Sc3ccc(O)cc13</chem>	0.1719	0.0322	-	0.006	0.0158	3.870034
PTP316-6	<chem>CN(C)CCCC1c2ccc(O)cc2Sc3ccc(O)cc13</chem>	0.1685	0.033	-	0.006	0.0158	3.870034
PTP316-7	<chem>CN(C)CCCC1c2cc(O)ccc2Sc3ccc(O)cc13</chem>	0.1428	0.033	-	0.006	0.0158	3.870034
PTP316-8	<chem>CN(C)CCCC1c2cc(O)ccc2Sc3cccc(O)c13</chem>	0.178	0.0324	-	0.006	0.0158	3.870034
PTP316-9	<chem>CN(C)CCC(O)C1c2ccccc2Sc3ccc(O)cc13</chem>	0.1466	0.0314	±	0.011	0.0175	3.359548
PTP316-10	<chem>CN(C)CC(O)CC1c2ccccc2Sc3ccc(O)cc13</chem>	0.1395	0.028	±	0.011	0.0175	3.359548
PTP316-11	<chem>CN(C)CCCC1c2ccccc2Sc3cc(O)cc(O)c13</chem>	0.1894	0.0333	-	0.006	0.0158	3.870034

PTP316-12	CN(C)CCCC1c2cccc2Sc3c(O)ccc(O)c13	0.202	0.0321	-	0.006	0.0158	3.870034
PTP316-13	CN(C)CCCC1c2cccc(O)c2Sc3cccc(O)c13	0.2695	0.0316	-	0.006	0.0158	3.870034
PTP316-14	CN(C)CCCC1c2ccc(O)cc2Sc3cccc(O)c13	0.2747	0.0324	-	0.006	0.0158	3.870034
PTP316-15	CN(C)CCCC1c2c(O)cccc2Sc3cccc(O)c13	0.2765	0.0317	-	0.006	0.0158	3.870034
PTP316-16	CN(C)CCC(O)C1c2cccc2Sc3cccc(O)c13	0.1953	0.0307	±	0.011	0.0175	3.359548
PTP316-17	CN(C)CC(O)CC1c2cccc2Sc3cccc(O)c13	0.1841	0.0273	±	0.011	0.0175	3.359548
PTP316-18	CN(C)C(O)CCC1c2cccc2Sc3cccc(O)c13	0.2359	0.2308	±	0.011	0.0175	3.645018
PTP316-19	CN(C)CCCC1c2cccc2Sc3c(O)c(O)ccc13	0.1975	0.0443	-	0.006	0.0158	3.870034
PTP316-20	CN(C)CCCC1c2ccc(O)cc2Sc3c(O)cccc13	0.2537	0.0336	-	0.006	0.0158	3.870034
PTP316-21	CN(C)CCCC1c2ccc(O)cc2Sc3cc(O)ccc13	0.2137	0.0341	-	0.006	0.0158	3.870034
PTP316-22	CN(C)CCC(O)C1c2cccc2Sc3cc(O)ccc13	0.1799	0.0314	±	0.011	0.0175	3.359548
PTP316-23	CN(C)CC(O)CC1c2cccc2Sc3cc(O)ccc13	0.1678	0.0285	±	0.011	0.0175	3.359548
PTP316-24	CN(C)C(O)CCC1c2cccc2Sc3cc(O)ccc13	0.2123	0.2223	±	0.011	0.0175	3.645018
PTP316-25	CN(C)CCCC1c2cccc(O)c2Sc3c(O)cccc13	0.2607	0.0331	-	0.006	0.0158	3.870034
PTP316-26	CN(C)CCC(O)C1c2cccc2Sc3c(O)cccc13	0.1861	0.0306	±	0.011	0.0175	3.359548
PTP316-27	CN(C)CC(O)CC1c2cccc2Sc3c(O)cccc13	0.1735	0.0276	±	0.011	0.0175	3.359548

PTP316-28	CN(C)C(O)CCC1c2cccc2Sc3c(O)cccc13	0.2222	0.2218	±	0.011	0.0175	3.645018
PTP316-29	CN(CO)CCCC1c2cccc2Sc3c(O)cccc13	0.3481	0.0291	+	0.1601	0.0437	3.609898
PTP316-30	CN(C)CC(O)C(O)C1c2cccc2Sc3cccc13	0.1189	0.0271	±	0.0161	0.0195	2.849061
PTP316-31	CN(C)C(O)CC(O)C1c2cccc2Sc3cccc13	0.1994	0.2098	±	0.0161	0.0195	3.134531
PTP316-32	CN(C)C(O)C(O)CC1c2cccc2Sc3cccc13	0.1209	0.143	±	0.0161	0.0195	3.134531
PTP332a-1	CN(C)CCCC1c2cccc2Sc3c(O)c(O)c(O)c13	0.1672	0.0426	-	0.0144	0.0144	3.538941
PTP332a-2	CN(C)CCCC1c2cccc2Sc3c(O)cc(O)c(O)c13	0.089	0.0403	-	0.0144	0.0144	3.538941
PTP332a-3	CN(C)CCCC1c2cccc(O)c2Sc3ccc(O)c(O)c13	0.0778	0.0415	-	0.0144	0.0144	3.538941
PTP332a-4	CN(C)CCCC1c2ccc(O)cc2Sc3ccc(O)c(O)c13	0.0778	0.0422	-	0.0144	0.0144	3.538941
PTP332a-5	CN(C)CCCC1c2cc(O)ccc2Sc3ccc(O)c(O)c13	0.0778	0.0424	-	0.0144	0.0144	3.538941
PTP332a-6	CN(C)CCCC1c2c(O)cccc2Sc3ccc(O)c(O)c13	0.0778	0.0418	-	0.0144	0.0144	3.538941
PTP332a-7	CN(C)CCC(O)C1c2cccc2Sc3ccc(O)c(O)c13	0.0778	0.0408	±	0.0194	0.016	3.028454
PTP332a-8	CN(C)CC(O)CC1c2cccc2Sc3ccc(O)c(O)c13	0.0778	0.0377	±	0.0194	0.016	3.028454
PTP332a-9	CN(C)C(O)CCC1c2cccc2Sc3ccc(O)c(O)c13	0.1993	0.2414	±	0.0194	0.016	3.313925
PTP332a-10	CN(C)CCCC1c2cccc2Sc3c(O)c(O)cc(O)c13	0.2239	0.0433	-	0.0144	0.0144	3.538941
PTP332a-11	CN(C)CCCC1c2cccc(O)c2Sc3cc(O)cc(O)c13	0.2598	0.0331	-	0.0144	0.0144	3.538941

PTP332a-12	CN(C)CCCC1c2ccc(O)cc2Sc3cc(O)cc(O)c13	0.2312	0.0341	-	0.0144	0.0144	3.538941
PTP332a-13	CN(C)CCCC1c2cc(O)ccc2Sc3cc(O)cc(O)c13	0.1724	0.0342	-	0.0144	0.0144	3.538941
PTP332a-14	CN(C)CCCC1c2c(O)cccc2Sc3cc(O)cc(O)c13	0.281	0.0336	-	0.0144	0.0144	3.538941
PTP332a-15	CN(C)CCC(O)C1c2cccc2Sc3cc(O)cc(O)c13	0.184	0.0325	±	0.0194	0.016	3.028454
PTP332a-16	CN(C)CC(O)CC1c2cccc2Sc3cc(O)cc(O)c13	0.1717	0.028	±	0.0194	0.016	3.028454
PTP332a-17	CN(C)C(O)CCC1c2cccc2Sc3cc(O)cc(O)c13	0.2172	0.2363	±	0.0194	0.016	3.313925
PTP332a-18	CN(C)CCCC1c2cccc2Sc3c(O)c(O)c(O)cc13	0.2332	0.046	-	0.0144	0.0144	3.538941
PTP332a-19	CN(C)CCCC1c2ccc(O)c2Sc3cc(O)c(O)cc13	0.1389	0.0369	-	0.0144	0.0144	3.538941
PTP332a-20	CN(C)CCCC1c2ccc(O)cc2Sc3cc(O)c(O)cc13	0.1389	0.038	-	0.0144	0.0144	3.538941
PTP332a-21	CN(C)CCCC1c2cc(O)ccc2Sc3cc(O)c(O)cc13	0.2109	0.0379	-	0.0144	0.0144	3.538941
PTP332a-22	CN(C)CCCC1c2cc(O)c(O)c2Sc3cccc(O)c13	0.1389	0.0373	-	0.0144	0.0144	3.538941
PTP332a-23	CN(C)CCC(O)C1c2cccc2Sc3cc(O)c(O)cc13	0.1753	0.0363	±	0.0194	0.016	3.028454
PTP332a-24	CN(C)CC(O)CC1c2cccc2Sc3cc(O)c(O)cc13	0.1683	0.0336	±	0.0194	0.016	3.028454
PTP332a-25	CN(C)C(O)CCC1c2cccc2Sc3cc(O)c(O)cc13	0.2399	0.2442	±	0.0194	0.016	3.313925
PTP332a-26	CN(C)CCCC1c2ccc(O)c2Sc3c(O)cc(O)cc13	0.161	0.0339	-	0.0144	0.0144	3.538941
PTP332a-27	CN(C)CCCC1c2ccc(O)cc2Sc3c(O)cc(O)cc13	0.1455	0.0351	-	0.0144	0.0144	3.538941

PTP332a-28	CN(C)CCCC1c2cc(O)ccc2Sc3c(O)cc(O)cc13	0.1378	0.0335	-	0.0144	0.0144	3.538941
PTP332a-29	CN(C)CCCC1c2cc(O)cc(O)c2Sc3cccc(O)c13	0.1729	0.0326	-	0.0144	0.0144	3.538941
PTP332a-30	CN(C)CCC(O)C1c2cccc2Sc3c(O)cc(O)cc13	0.1381	0.0324	±	0.0194	0.016	3.028454
PTP332a-31	CN(C)CC(O)CC1c2cccc2Sc3c(O)cc(O)cc13	0.13	0.0269	±	0.0194	0.016	3.028454
PTP332a-32	CN(C)C(O)CCC1c2cccc2Sc3c(O)cc(O)cc13	0.1657	0.2405	±	0.0194	0.016	3.313925
PTP332a-33	CN(C)CCCC1c2cccc(O)c2Sc3c(O)c(O)ccc13	0.1997	0.0462	-	0.0144	0.0144	3.538941
PTP332a-34	CN(C)CCCC1c2ccc(O)cc2Sc3c(O)c(O)ccc13	0.1997	0.0465	-	0.0144	0.0144	3.538941
PTP332a-35	CN(C)CCCC1c2ccc(O)c(O)c2Sc3ccc(O)cc13	0.202	0.0452	-	0.0144	0.0144	3.538941
PTP332a-36	CN(C)CCCC1c2ccc(O)c(O)c2Sc3cccc(O)c13	0.202	0.0448	-	0.0144	0.0144	3.538941
PTP332a-37	CN(C)CCC(O)C1c2cccc2Sc3c(O)c(O)ccc13	0.1873	0.0439	±	0.0194	0.016	3.028454
PTP332a-38	CN(C)CC(O)CC1c2cccc2Sc3c(O)c(O)ccc13	0.1673	0.0417	±	0.0194	0.016	3.028454
PTP332a-39	CN(C)C(O)CCC1c2cccc2Sc3c(O)c(O)ccc13	0.1813	0.2339	±	0.0194	0.016	3.313925
PTP332a-40	CN(C)CCCC1c2ccc(O)cc2Sc3c(O)ccc(O)c13	0.2232	0.0341	-	0.0144	0.0144	3.538941
PTP332a-41	CN(C)CCC(O)C1c2ccc(O)c2Sc3c(O)cccc13	0.2444	0.0328	±	0.0194	0.016	3.028454
PTP332a-42	CN(C)CC(O)CC1c2ccc(O)c2Sc3c(O)cccc13	0.2269	0.0294	±	0.0194	0.016	3.028454
PTP332a-43	CN(C)C(O)CCC1c2ccc(O)c2Sc3c(O)cccc13	0.2387	0.2315	±	0.0194	0.016	3.313925

PTP332a-44	CN(C)CCCC1c2cccc(O)c2Sc3c(O)ccc(O)c13	0.2232	0.033	-	0.0144	0.0144	3.538941
PTP332a-45	CN(C)CCC(O)C1c2cccc(O)c2Sc3c(O)cccc13	0.2516	0.0323	±	0.0194	0.016	3.028454
PTP332a-46	CN(C)CC(O)CC1c2cccc(O)c2Sc3c(O)cccc13	0.2346	0.0289	±	0.0194	0.016	3.028454
PTP332a-47	CN(C)C(O)CCC1c2cccc(O)c2Sc3c(O)cccc13	0.2459	0.2314	±	0.0194	0.016	3.313925
PTP332b-1	CN(C)CCC=C1c2cc(Cl)ccc2Sc3cccc(O)c31	0.1253	0.0464	-	-0.1344	0.0025	4.659748
PTP332b-2	CN(C)CCC=C1c2cc(O)ccc2Sc3ccc(Cl)cc31	0.1253	0.0466	-	-0.1344	0.0025	4.659748
PTP332b-3	CN(C)CCC=C1c2ccc(O)cc2Sc3ccc(Cl)cc31	0.1174	0.042	-	-0.1344	0.0025	4.659748
PTP332b-4	CN(C)CCC=C1c2cccc(O)c2Sc3ccc(Cl)cc31	0.1346	0.0417	-	-0.1344	0.0025	4.659748
PTP332b-5	CN(C)CCC=C1c2cccc2Sc3c(O)cc(Cl)cc31	0.2739	0.0467	-	-0.1344	0.0025	4.659748
PTP332b-6	CN(C)CCC=C1c2cccc2Sc3cc(O)c(Cl)cc31	0.2758	0.0472	-	-0.1344	0.0025	4.659748
PTP332b-7	CN(C)CCC=C1c2cccc2Sc3ccc(Cl)c(O)c31	0.1279	0.0473	-	-0.1344	0.0025	4.659748
PTP332b-8	CN(C)CCC(O)=C1c2cccc2Sc3ccc(Cl)cc31	0.1875	0.0277	OD	-0.0355	0.0046	4.57251
PTP332b-9	CN(C)CC(O)C=C1c2cccc2Sc3ccc(Cl)cc31	0.1325	0.0368	±	-0.1294	0.0028	4.209719
PTP332b-10	CN(C)C(O)CC=C1c2cccc2Sc3ccc(Cl)cc31	0.12	0.2313	±	-0.1294	0.0028	4.434731
PTP334b-1	CN(C)CCC(O)C1c2cccc2Sc3ccc(Cl)cc13	0.1748	0.0295	±	-0.1019	0.0051	4.335975
PTP334b-2	CN(C)CC(O)CC1c2cccc2Sc3ccc(Cl)cc13	0.1628	0.0247	±	-0.1019	0.0051	4.335975

PTP334b-3	CN(C)C(O)CCC1c2ccccc2Sc3ccc(Cl)cc13	0.2013	0.2346	±	-0.1019	0.0051	4.621445
PTP334b-4	CN(C)CCCC1c2cc(Cl)ccc2Sc3cccc(O)c13	0.2452	0.0307	-	-0.107	0.0046	4.846461
PTP334b-5	CN(C)CCCC1c2cc(O)ccc2Sc3ccc(Cl)cc13	0.1613	0.0313	-	-0.107	0.0046	4.846461
PTP334b-6	CN(C)CCCC1c2cccc(O)c2Sc3ccc(Cl)cc13	0.2286	0.0301	-	-0.107	0.0046	4.846461
PTP334b-7	CN(C)CCCC1c2ccc(O)cc2Sc3ccc(Cl)cc13	0.2064	0.0307	-	-0.107	0.0046	4.846461
PTP334b-8	CN(C)CCCC1c2ccccc2Sc3ccc(Cl)c(O)c13	0.1855	0.0367	-	-0.107	0.0046	4.846461
PTP334b-9	CN(C)CCCC1c2ccccc2Sc3ccc(O)c(Cl)cc13	0.1884	0.0326	-	-0.107	0.0046	4.846461
PTP334b-10	CN(C)CCCC1c2ccccc2Sc3ccc(O)cc(Cl)cc13	0.1874	0.0311	-	-0.107	0.0046	4.846461
PTP348a-1	CN(C)CCCC1c2ccccc2Sc3ccc(O)c(O)c(O)c(O)c13	0.0232	0.049	-	0.0228	0.0131	3.207848
PTP348a-2	CN(C)CCCC1c2cc(O)ccc2Sc3cc(O)c(O)c(O)c13	0.171	0.044	-	0.0228	0.0131	3.207848
PTP348a-3	CN(CO)CCCC1c2ccccc2Sc3cc(O)c(O)c(O)c13	0.1342	0.0405	+	0.1769	0.0365	2.947712
PTP348a-4	CN(C)CCCC1c2cccc(O)c2Sc3cc(O)c(O)c(O)c13	0.171	0.0414	-	0.0228	0.0131	3.207848
PTP348a-5	CN(C)CCCC1c2ccc(O)cc2Sc3cc(O)c(O)c(O)c13	0.171	0.042	-	0.0228	0.0131	3.207848
PTP348a-6	CN(C)CCCC1c2c(O)ccc2Sc3cc(O)c(O)c(O)c13	0.171	0.0431	-	0.0228	0.0131	3.207848
PTP348a-7	CN(C)CCC(O)C1c2ccccc2Sc3cc(O)c(O)c(O)c13	0.1637	0.0421	±	0.0278	0.0146	2.697361
PTP348a-8	CN(C)CC(O)CC1c2ccccc2Sc3cc(O)c(O)c(O)c13	0.1342	0.0377	±	0.0278	0.0146	2.697361

PTP348a-9	CN(C)C(O)CCC1c2cccc2Sc3cc(O)c(O)c(O)c13	0.2317	0.2636	±	0.0278	0.0146	2.982831
PTP348a-10	CN(C)CCCC1c2cc(O)ccc2Sc3c(O)cc(O)c(O)c13	0.091	0.0411	-	0.0228	0.0131	3.207848
PTP348a-11	CN(C)C(O)CC(O)C1c2ccc(O)cc2Sc3c(O)cccc13	0.2286	0.2144	±	0.0329	0.0162	2.472345
PTP348a-12	CN(C)CCCC1c2cccc(O)c2Sc3c(O)cc(O)c(O)c13	0.091	0.0421	-	0.0228	0.0131	3.207848
PTP348a-13	CN(C)CCCC1c2ccc(O)cc2Sc3c(O)cc(O)c(O)c13	0.091	0.0429	-	0.0228	0.0131	3.207848
PTP348a-14	CN(C)CCCC1c2c(O)cccc2Sc3c(O)cc(O)c(O)c13	0.091	0.0407	-	0.0228	0.0131	3.207848
PTP348a-15	CN(C)CCC(O)C1c2cccc2Sc3c(O)cc(O)c(O)c13	0.091	0.0398	±	0.0278	0.0146	2.697361
PTP348a-16	CN(C)CC(O)CC1c2cccc2Sc3c(O)cc(O)c(O)c13	0.091	0.0352	±	0.0278	0.0146	2.697361
PTP348a-17	CN(C)C(O)CCC1c2cccc2Sc3c(O)cc(O)c(O)c13	0.2093	0.2405	±	0.0278	0.0146	2.982831
PTP348a-18	CN(C)CCCC1c2cc(O)ccc2Sc3c(O)c(O)cc(O)c13	0.229	0.0444	-	0.0228	0.0131	3.207848
PTP348a-19	CN(C)C(O)CCC1c2cccc2Sc3c(O)c(O)c(O)cc13	0.2574	0.2539	±	0.0278	0.0146	2.982831
PTP348a-20	CN(C)CCCC1c2cccc(O)c2Sc3c(O)c(O)cc(O)c13	0.229	0.0436	-	0.0228	0.0131	3.207848
PTP348a-21	CN(C)CCCC1c2ccc(O)cc2Sc3c(O)c(O)cc(O)c13	0.229	0.0446	-	0.0228	0.0131	3.207848
PTP348a-22	CN(C)CCCC1c2c(O)cccc2Sc3c(O)c(O)cc(O)c13	0.229	0.0438	-	0.0228	0.0131	3.207848
PTP348a-23	CN(C)CCC(O)C1c2cccc2Sc3c(O)c(O)cc(O)c13	0.2217	0.0429	±	0.0278	0.0146	2.697361
PTP348a-24	CN(C)CC(O)CC1c2cccc2Sc3c(O)c(O)cc(O)c13	0.1921	0.0387	±	0.0278	0.0146	2.697361

PTP348a-25	CN(C)C(O)CCC1c2cccc2Sc3c(O)c(O)cc(O)c13	0.2779	0.2474	±	0.0278	0.0146	2.982831
PTP348a-26	CN(C)CCCC1c2ccc(O)c(O)c2Sc3c(O)cc(O)cc13	0.2043	0.0472	-	0.0228	0.0131	3.207848
PTP348a-27	CN(C)CCCC1c2ccc(O)c(O)c2Sc3cc(O)c(O)cc13	0.1422	0.051	-	0.0228	0.0131	3.207848
PTP348a-28	CN(C)CCCC1c2ccc(O)c(O)c2Sc3ccc(O)c(O)c13	0.0795	0.0554	-	0.0228	0.0131	3.207848
PTP348a-29	CN(C)CCC(O)C1c2cc(O)cc2Sc3c(O)c(O)ccc13	0.1917	0.0448	±	0.0278	0.0146	2.697361
PTP348a-30	CN(C)CC(O)CC1c2cc(O)cc2Sc3c(O)c(O)ccc13	0.1713	0.0428	±	0.0278	0.0146	2.697361
PTP348a-31	CN(C)C(O)CCC1c2ccc(O)c(O)c2Sc3ccc(O)cc13	0.1855	0.2385	±	0.0278	0.0146	2.982831
PTP348a-32	CN(C)CCCC1c2c(O)ccc(O)c2Sc3c(O)ccc(O)c13	0.5581	0.0313	-	0.0228	0.0131	3.207848
PTP348a-33	CN(C)CCCC1c2cc(O)cc(O)c2Sc3c(O)ccc(O)c13	0.1931	0.0319	-	0.0228	0.0131	3.207848
PTP348a-34	CN(C)CCCC1c2ccc(O)c(O)c2Sc3c(O)ccc(O)c13	0.2283	0.0464	-	0.0228	0.0131	3.207848
PTP348a-35	CN(C)CCC(O)C1c2cccc(O)c2Sc3c(O)ccc(O)c13	0.2234	0.0322	±	0.0278	0.0146	2.697361
PTP348a-36	CN(C)CC(O)CC1c2cccc(O)c2Sc3c(O)ccc(O)c13	0.2014	0.0284	±	0.0278	0.0146	2.697361
PTP348a-37	CN(C)C(O)CCC1c2cccc(O)c2Sc3c(O)ccc(O)c13	0.2964	0.2359	±	0.0278	0.0146	2.982831
PTP348a-38	CN(C)C(O)CCC1c2cccc(O)c2Sc3ccc(O)c(O)c13	0.2038	0.2366	±	0.0278	0.0146	2.982831
PTP348a-39	CN(C)CCC(O)C1c2cccc(O)c2Sc3ccc(O)c(O)c13	0.0795	0.041	±	0.0278	0.0146	2.697361
PTP348a-40	CN(C)CCCC1c2cc(O)c(O)c2Sc3cc(O)c(O)cc13	0.17	0.0424	-	0.0228	0.0131	3.207848

PTP348a-41	CN(C)CCC(O)C1c2ccc(O)c c2Sc3cc(O)c(O)cc13	0.137	0.0373	±	0.0278	0.0146	2.697361
PTP348a-42	CN(C)CC(O)CC1c2ccc(O)c c2Sc3cc(O)c(O)cc13	0.1294	0.0342	±	0.0278	0.0146	2.697361
PTP348a-43	CN(C)C(O)CCC1c2ccc(O)c c2Sc3cc(O)c(O)cc13	0.2457	0.2398	±	0.0278	0.0146	2.982831
PTP348a-44	CN(C)CC(O)CC1c2ccccc2S c3c(O)c(O)c(O)cc13	0.2212	0.0424	±	0.0278	0.0146	2.697361
PTP348a-45	CN(C)CCC(O)C1c2ccccc2S c3c(O)c(O)c(O)cc13	0.2311	0.0455	±	0.0278	0.0146	2.697361
PTP348a-46	CN(C)CCCC1c2cc(O)c(O)c (O)c2Sc3cccc(O)c13	0.1764	0.0465	-	0.0228	0.0131	3.207848
PTP348a-47	CN(C)CCCC1c2cc(O)ccc2S c3c(O)c(O)c(O)cc13	0.2848	0.0472	-	0.0228	0.0131	3.207848
PTP348a-48	CN(C)CCCC1c2ccc(O)cc2S c3c(O)c(O)c(O)cc13	0.1764	0.0492	-	0.0228	0.0131	3.207848
PTP348a-49	CN(C)CCCC1c2ccccc(O)c2S c3c(O)c(O)c(O)cc13	0.1764	0.0481	-	0.0228	0.0131	3.207848
PTP348a-50	CN(C)CCCC1c2c(O)cc(O)c c2Sc3ccc(O)c(O)c13	0.0795	0.0436	-	0.0228	0.0131	3.207848
PTP348a-51	CN(C)CCCC1c2c(O)cc(O)c c2Sc3cc(O)cc(O)c13	0.2493	0.0347	-	0.0228	0.0131	3.207848
PTP348a-52	CN(C)CCCC1c2c(O)cc(O)c c2Sc3c(O)ccc(O)c13	0.2283	0.0334	-	0.0228	0.0131	3.207848
PTP348a-53	CN(C)C(O)CCC1c2c(O)ccc c2Sc3cc(O)cc(O)c13	0.2673	0.2414	±	0.0278	0.0146	2.982831
PTP350-1	CN(C)CCCC1c2c(O)cccc2S c3ccc(Cl)c(O)c13	0.2681	0.0381	-	-0.0985	0.0042	4.515368
PTP350-2	CN(C)CCCC1c2cc(O)ccc2S c3ccc(Cl)c(O)c13	0.1684	0.0388	-	-0.0985	0.0042	4.515368
PTP350-3	CN(C)CCCC1c2ccccc2Sc3c (O)cc(Cl)c(O)c13	0.1908	0.0379	-	-0.0985	0.0042	4.515368

PTP350-4	CN(C)CCCC1c2cccc(O)c2Sc3ccc(Cl)c(O)c13	0.2468	0.0383	-	-0.0985	0.0042	4.515368
PTP350-5	CN(C)CCCC1c2ccc(O)cc2Sc3ccc(Cl)c(O)c13	0.2336	0.0386	-	-0.0985	0.0042	4.515368
PTP350-6	CN(C)CCCC1c2cccc2Sc3cc(O)c(Cl)c(O)c13	0.1934	0.0378	-	-0.0985	0.0042	4.515368
PTP350-7	CN(C)CCC(O)C1c2cccc2Sc3ccc(Cl)c(O)c13	0.1803	0.0361	±	-0.0935	0.0047	4.004882
PTP350-8	CN(C)CCCC1(O)c2cccc2Sc3ccc(Cl)c(O)c13	0.196	0.0345	-	-0.0772	0.0033	3.906427
PTP350-9	CN(C)C(O)CCC1c2cccc2Sc3ccc(Cl)c(O)c13	0.2098	0.2487	±	-0.0935	0.0047	4.290352
PTP350-10	CN(CO)CCCC1c2cccc2Sc3ccc(Cl)c(O)c13	0.3289	0.0344	+	0.0556	0.0119	4.255233
PTP350-11	CN(C)CCCC1c2cc(Cl)cc(O)c2Sc3cccc(O)c13	0.2717	0.0329	-	-0.0985	0.0042	4.515368
PTP350-12	CN(C)CCCC1c2cc(O)ccc2Sc3c(O)cc(Cl)cc13	0.1714	0.0315	-	-0.0985	0.0042	4.515368
PTP350-13	CN(C)CCCC1c2ccc(O)cc2Sc3c(O)cc(Cl)cc13	0.1953	0.0338	-	-0.0985	0.0042	4.515368
PTP350-14	CN(C)CCC(O)C1c2cccc2Sc3c(O)cc(Cl)cc13	0.182	0.0304	±	-0.0935	0.0047	4.004882
PTP350-15	CN(C)CC(O)CC1c2cccc2Sc3c(O)cc(Cl)cc13	0.1691	0.0268	±	-0.0935	0.0047	4.004882
PTP350-16	CN(C)C(O)CCC1c2cccc2Sc3c(O)cc(Cl)cc13	0.2123	0.2314	±	-0.0935	0.0047	4.290352
PTP350-17	CN(C)CCCC1(O)c2cccc2Sc3c(O)cc(Cl)cc13	0.1912	0.029	-	-0.0772	0.0033	3.906427
PTP350-18	CN(C)CCCC1c2cc(Cl)ccc2Sc3ccc(O)c(O)c13	0.0795	0.0408	-	-0.0985	0.0042	4.515368
PTP350-19	CN(C)CCCC1c2cc(Cl)ccc2Sc3cc(O)cc(O)c13	0.2109	0.0321	-	-0.0985	0.0042	4.515368

PTP350-20	CN(C)CCCC1c2cc(Cl)ccc2 Sc3c(O)ccc(O)c13	0.2283	0.0312	-	-0.0985	0.0042	4.515368
PTP350-21	CN(C)CCCC1(O)c2cc(Cl)cc c2Sc3cccc(O)c31	0.2639	0.0297	-	-0.0772	0.0033	3.906427
PTP350-22	CN(C)CC(O)CC1c2cc(Cl)cc c2Sc3cccc(O)c13	0.2211	0.0264	±	-0.0935	0.0047	4.004882
PTP350-23	CN(C)C(O)CCC1c2cc(Cl)cc c2Sc3cccc(O)c13	0.2315	0.2307	±	-0.0935	0.0047	4.290352
PTP350-24	CN(C)CCCC1c2cc(Cl)ccc2 Sc3cc(O)c(O)cc13	0.1377	0.0353	-	-0.0985	0.0042	4.515368
PTP350-25	CN(C)CCCC1c2cc(Cl)ccc2 Sc3c(O)cc(O)cc13	0.1413	0.0318	-	-0.0985	0.0042	4.515368
PTP350-26	CN(C)CC(O)CC1c2cc(O)cc c2Sc3ccc(Cl)cc13	0.1481	0.0272	±	-0.0935	0.0047	4.004882
PTP350-27	CN(C)C(O)CCC1c2cc(O)cc c2Sc3ccc(Cl)cc13	0.1747	0.2308	±	-0.0935	0.0047	4.290352
PTP350-28	CN(C)CCCC1(O)c2cc(O)cc c2Sc3ccc(Cl)cc31	0.166	0.0306	-	-0.0772	0.0033	3.906427
PTP350-29	CN(C)CCCC1c2cc(Cl)ccc2 Sc3c(O)c(O)ccc13	0.1953	0.0444	-	-0.0985	0.0042	4.515368
PTP350-30	CN(C)CC(O)CC1c2ccc(O)c c2Sc3ccc(Cl)cc13	0.1787	0.0266	±	-0.0935	0.0047	4.004882
PTP350-31	CN(C)C(O)CCC1c2ccc(O)c c2Sc3ccc(Cl)cc13	0.1913	0.2261	±	-0.0935	0.0047	4.290352
PTP350-32	CN(C)CCCC1(O)c2ccc(O)c c2Sc3ccc(Cl)cc31	0.2102	0.03	-	-0.0772	0.0033	3.906427
PTP350-33	CN(C)C(O)C(O)CC1c2cccc c2Sc3ccc(Cl)cc13	0.1155	0.1389	±	-0.0885	0.0052	3.779866
PTP350-34	CN(C)C(O)CCC1(O)c2cccc c2Sc3ccc(Cl)cc31	0.2086	0.2292	±	-0.0721	0.0037	3.681411
PTP298-1	CN(C)CCC(O)=C1c2cccc2 Sc3cccc31	0.1767	0.0285	OD	0.069	0.0173	3.927175

PTP298-2	<chem>CN(C)CC(O)C=C1c2ccccc2Sc3ccccc31</chem>	0.1282	0.046	±	-0.0249	0.0106	3.564384
PTP298-3	<chem>CN(C)C(O)CC=C1c2ccccc2Sc3ccccc31</chem>	0.1321	0.2286	±	-0.0249	0.0106	3.789397
PTP298-4	<chem>CN(C)CCC=C1c2ccccc2Sc3ccc(O)c31</chem>	0.117	0.0507	-	-0.0299	0.0095	4.014413
PTP298-5	<chem>CN(C)CCC=C1c2ccccc2Sc3ccc(O)cc31</chem>	0.117	0.051	-	-0.0299	0.0095	4.014413
PTP298-6	<chem>CN(C)CCC=C1c2ccccc2Sc3c(O)ccc31</chem>	0.1296	0.0481	-	-0.0299	0.0095	4.014413
PTP298-7	<chem>CN(C)CCC=C1c2ccccc2Sc3cc(O)ccc31</chem>	0.1658	0.0468	-	-0.0299	0.0095	4.014413
PTP282-1	<chem>CN(C)CCC=C1c2ccccc2Sc3ccccc31</chem>	0.1261	0.0501	-	-0.0383	0.0104	4.345506

* "100% biodegradation" was assigned a numeric value of 1 and "0% biodegradation" was assigned a numeric value of 0.

**A Probability greater than or equal to 0.5 indicates readily biodegradable substance and a probability Less than 0.5 indicates not readily biodegradable

Table S5 : QSAR toxicity predictions for CPTX and its TPs using the different models of the ICHM7 guideline conformal set from Case Ultra: (1) Salmonella mutagenicity TA 97. 98. 100. 1535–1538 (GT1 A7B). (2) A–T mutation E. coli and TA102 (GT1 AT E. coli). (3) Expert rules for genotoxicity (GT Expert). (4) E. coli mutagenicity (all strains) (Pharm E. coli). (5) Salmonella mutagenicity (TA 97. 98. 100. 1535–1538) (Pharm Salm).

Compounds	GT1_A7B	GT1_AT_ECOLI	GT_EXPERT	PHARM_ECOLI	PHARM_SALM
cisZCPT	+	-	+	-	+
PTP316-1	-	-	-	-	-
PTP316-2	-	-	-	-	-
PTP316-3	±	OD	-	OD	-
PTP316-4	±	-	-	-	-
PTP316-5	±	-	-	-	-
PTP316-6	±	-	-	-	-
PTP316-7	±	-	-	-	-
PTP316-8	±	-	-	-	-
PTP316-9	±	-	-	-	-
PTP316-10	±	-	-	-	-
PTP316-11	-	-	-	-	-
PTP316-12	-	-	-	-	-
PTP316-13	-	-	-	-	-
PTP316-14	-	-	-	-	-
PTP316-15	-	-	-	-	-
PTP316-16	-	-	-	-	-
PTP316-17	-	-	-	-	-
PTP316-18	-	OD	-	OD	-
PTP316-19	-	-	-	-	-
PTP316-20	-	-	-	-	-
PTP316-21	-	-	-	-	-
PTP316-22	-	-	-	-	-
PTP316-23	-	-	-	-	-
PTP316-24	-	OD	-	OD	-
PTP316-25	-	-	-	-	-
PTP316-26	-	-	-	-	-
PTP316-27	-	-	-	-	-
PTP316-28	-	OD	-	OD	-
PTP316-29	-	-	+	-	-
PTP316-30	-	-	-	-	-
PTP316-31	-	OD	-	OD	-
PTP316-32	-	OD	-	OD	-
PTP332a-1	-	±	-	-	-
PTP332a-2	-	-	-	-	-

PTP332a-3	±	-	-	-	-
PTP332a-4	±	-	-	-	-
PTP332a-5	±	-	-	-	-
PTP332a-6	±	-	-	-	-
PTP332a-7	±	-	-	-	-
PTP332a-8	±	-	-	-	-
PTP332a-9	±	OD	-	OD	-
PTP332a-10	-	-	-	-	-
PTP332a-11	-	-	-	-	-
PTP332a-12	-	-	-	-	-
PTP332a-13	±	-	-	-	-
PTP332a-14	-	-	-	-	-
PTP332a-15	-	-	-	-	-
PTP332a-16	-	-	-	-	-
PTP332a-17	-	OD	-	OD	-
PTP332a-18	-	±	-	-	-
PTP332a-19	-	-	-	-	-
PTP332a-20	-	-	-	-	-
PTP332a-21	±	-	-	-	-
PTP332a-22	-	-	-	-	-
PTP332a-23	-	-	-	-	-
PTP332a-24	-	-	-	-	-
PTP332a-25	-	OD	-	OD	-
PTP332a-26	-	-	-	-	-
PTP332a-27	-	-	-	-	-
PTP332a-28	±	-	-	-	-
PTP332a-29	-	-	-	-	-
PTP332a-30	-	-	-	-	-
PTP332a-31	-	-	-	-	-
PTP332a-32	-	OD	-	OD	-
PTP332a-33	-	-	-	-	-
PTP332a-34	-	-	-	-	-
PTP332a-35	±	-	-	-	-
PTP332a-36	-	-	-	-	-
PTP332a-37	-	-	-	-	-
PTP332a-38	-	-	-	-	-
PTP332a-39	-	OD	-	OD	-
PTP332a-40	-	-	-	-	-
PTP332a-41	-	-	-	-	-
PTP332a-42	-	-	-	-	-
PTP332a-43	-	OD	-	OD	-
PTP332a-44	-	-	-	-	-
PTP332a-45	-	-	-	-	-

PTP332a-46	-	-	-	-	-
PTP332a-47	-	OD	-	OD	-
PTP332b-1	±	-	+	-	+
PTP332b-2	±	-	+	-	+
PTP332b-3	±	-	+	-	+
PTP332b-4	±	-	+	-	+
PTP332b-5	-	-	+	-	+
PTP332b-6	-	-	+	-	+
PTP332b-7	+	-	+	-	+
PTP332b-8	+	-	+	-	+
PTP332b-9	+	-	+	-	+
PTP332b-10	+	OD	+	OD	+
PTP334b-1	±	-	-	-	-
PTP334b-2	±	-	-	-	-
PTP334b-3	±	OD	-	OD	-
PTP334b-4	±	-	-	-	-
PTP334b-5	±	-	-	-	-
PTP334b-6	±	-	-	-	-
PTP334b-7	±	-	-	-	-
PTP334b-8	±	-	-	-	-
PTP334b-9	-	-	-	-	-
PTP334b-10	-	-	-	-	-
PTP348a-1	-	-	-	-	-
PTP348a-2	±	±	-	-	-
PTP348a-3	-	±	+	-	-
PTP348a-4	-	±	-	-	-
PTP348a-5	-	±	-	-	-
PTP348a-6	-	±	-	-	-
PTP348a-7	-	±	-	-	-
PTP348a-8	-	±	-	-	-
PTP348a-9	-	±	-	OD	-
PTP348a-10	±	-	-	-	-
PTP348a-11	-	OD	-	OD	-
PTP348a-12	-	-	-	-	-
PTP348a-13	-	-	-	-	-
PTP348a-14	-	-	-	-	-
PTP348a-15	-	-	-	-	-
PTP348a-16	-	-	-	-	-
PTP348a-17	-	OD	-	OD	-
PTP348a-18	±	-	-	-	-
PTP348a-19	-	±	-	OD	-
PTP348a-20	-	-	-	-	-
PTP348a-21	-	-	-	-	-

PTP348a-22	-	-	-	-	-
PTP348a-23	-	-	-	-	-
PTP348a-24	-	-	-	-	-
PTP348a-25	-	OD	-	OD	-
PTP348a-26	-	-	-	-	-
PTP348a-27	-	-	-	-	-
PTP348a-28	±	-	-	-	-
PTP348a-29	±	-	-	-	-
PTP348a-30	±	-	-	-	-
PTP348a-31	±	OD	-	OD	-
PTP348a-32	-	-	-	-	-
PTP348a-33	-	-	-	-	-
PTP348a-34	-	-	-	-	-
PTP348a-35	-	-	-	-	-
PTP348a-36	-	-	-	-	-
PTP348a-37	-	OD	-	OD	-
PTP348a-38	±	OD	-	OD	-
PTP348a-39	±	-	-	-	-
PTP348a-40	-	-	-	-	-
PTP348a-41	-	-	-	-	-
PTP348a-42	-	-	-	-	-
PTP348a-43	-	OD	-	OD	-
PTP348a-44	-	±	-	-	-
PTP348a-45	-	±	-	-	-
PTP348a-46	-	±	-	-	-
PTP348a-47	±	±	-	-	-
PTP348a-48	-	±	-	-	-
PTP348a-49	-	±	-	-	-
PTP348a-50	±	-	-	-	-
PTP348a-51	-	-	-	-	-
PTP348a-52	-	-	-	-	-
PTP348a-53	-	OD	-	OD	-
PTP350-1	±	-	-	-	-
PTP350-2	±	-	-	-	-
PTP350-3	-	-	-	-	-
PTP350-4	±	-	-	-	-
PTP350-5	±	-	-	-	-
PTP350-6	-	±	-	-	-
PTP350-7	±	-	-	-	-
PTP350-8	±	-	-	-	-
PTP350-9	±	OD	-	OD	-
PTP350-10	±	-	+	-	-
PTP350-11	-	-	-	-	-

PTP350-12	±	-	-	-	-
PTP350-13	-	-	-	-	-
PTP350-14	-	-	-	-	-
PTP350-15	-	-	-	-	-
PTP350-16	-	OD	-	OD	-
PTP350-17	-	-	-	-	-
PTP350-18	±	-	-	-	-
PTP350-19	±	-	-	-	-
PTP350-20	±	-	-	-	-
PTP350-21	±	-	-	-	-
PTP350-22	±	-	-	-	-
PTP350-23	±	OD	-	OD	-
PTP350-24	±	-	-	-	-
PTP350-25	±	-	-	-	-
PTP350-26	±	-	-	-	-
PTP350-27	±	OD	-	OD	-
PTP350-28	±	-	-	-	-
PTP350-29	±	-	-	-	-
PTP350-30	±	-	-	-	-
PTP350-31	±	OD	-	OD	-
PTP350-32	±	-	-	-	-
PTP350-33	±	OD	-	OD	-
PTP350-34	±	OD	-	OD	-
PTP298-1	-	-	+	-	+
PTP298-2	-	-	+	-	+
PTP298-3	-	OD	+	OD	+
PTP298-4	-	-	+	-	+
PTP298-5	+	-	+	-	+
PTP298-6	-	-	+	-	+
PTP298-7	-	-	+	-	+
PTP282-1	-	-	+	-	+

(+) positive prediction for the respective endpoint. (-) negative prediction for the respective endpoint. inconclusive ((±). the probability of being positive is around the model's current classification threshold ± 10%). and (OD) Out of domain

Table S6: QSAR teratogenicity predictions for CPTX and its TPs by different models (Case Ultra software): A50 (Teratogenicity in Rabbits), A51 (Teratogenicity in Rats), A52 (Teratogenicity in Mouse), and A53 (Teratogenicity in misc. Mammals).

Compound	A50	A51	A52	A53
cisZCPT	-	-	-	-
PTP316-1	-	-	±	±
PTP316-2	-	-	-	-
PTP316-3	OD	-	±	-
PTP316-4	-	+	-	-
PTP316-5	-	-	-	-
PTP316-6	-	-	±	-
PTP316-7	-	-	-	-
PTP316-8	-	-	-	-
PTP316-9	-	-	-	-
PTP316-10	-	-	-	-
PTP316-11	-	-	-	-
PTP316-12	-	-	-	-
PTP316-13	-	-	-	-
PTP316-14	-	-	±	-
PTP316-15	-	-	-	-
PTP316-16	-	-	-	-
PTP316-17	-	-	-	-
PTP316-18	OD	-	±	-
PTP316-19	-	+	-	-
PTP316-20	-	-	±	-
PTP316-21	-	-	±	-
PTP316-22	-	-	±	-
PTP316-23	-	-	±	-
PTP316-24	OD	-	+	-
PTP316-25	-	-	-	-
PTP316-26	-	-	-	-
PTP316-27	-	-	-	-
PTP316-28	OD	-	±	-
PTP316-29	-	OD	OD	-
PTP316-30	-	-	-	-
PTP316-31	OD	-	±	-
PTP316-32	OD	-	-	-
PTP332a-1	-	+	-	±
PTP332a-2	-	+	-	±
PTP332a-3	-	+	-	-
PTP332a-4	-	+	±	-
PTP332a-5	-	+	-	-

PTP332a-6	-	+	-	-
PTP332a-7	-	+	-	-
PTP332a-8	-	+	-	-
PTP332a-9	OD	+	±	-
PTP332a-10	-	+	-	±
PTP332a-11	-	-	-	-
PTP332a-12	-	-	±	-
PTP332a-13	-	-	-	-
PTP332a-14	-	-	-	-
PTP332a-15	-	-	-	-
PTP332a-16	-	-	-	-
PTP332a-17	OD	-	±	-
PTP332a-18	-	+	-	±
PTP332a-19	-	-	±	±
PTP332a-20	-	-	+	±
PTP332a-21	-	-	±	±
PTP332a-22	-	-	±	±
PTP332a-23	-	-	±	±
PTP332a-24	-	-	±	±
PTP332a-25	OD	-	+	±
PTP332a-26	-	-	-	-
PTP332a-27	-	-	±	-
PTP332a-28	-	-	-	-
PTP332a-29	-	-	-	-
PTP332a-30	-	-	-	-
PTP332a-31	-	-	-	-
PTP332a-32	OD	-	±	-
PTP332a-33	-	+	-	-
PTP332a-34	-	+	±	-
PTP332a-35	-	+	-	-
PTP332a-36	-	+	-	-
PTP332a-37	-	+	-	-
PTP332a-38	-	+	-	-
PTP332a-39	OD	+	±	-
PTP332a-40	-	-	±	-
PTP332a-41	-	-	±	-
PTP332a-42	-	-	±	-
PTP332a-43	OD	-	+	-
PTP332a-44	-	-	-	-
PTP332a-45	-	-	-	-
PTP332a-46	-	-	-	-
PTP332a-47	OD	-	±	-
PTP332b-1	-	-	-	±

PTP332b-2	-	-	-	-
PTP332b-3	-	-	-	-
PTP332b-4	-	-	-	-
PTP332b-5	-	-	-	-
PTP332b-6	-	-	±	±
PTP332b-7	-	+	+	±
PTP332b-8	-	-	-	-
PTP332b-9	-	-	-	-
PTP332b-10	OD	-	±	-
PTP334b-1	-	-	-	-
PTP334b-2	-	-	-	-
PTP334b-3	OD	-	±	-
PTP334b-4	-	-	-	-
PTP334b-5	-	-	-	-
PTP334b-6	-	-	-	-
PTP334b-7	-	-	±	-
PTP334b-8	-	+	±	-
PTP334b-9	-	-	+	±
PTP334b-10	-	-	-	-
PTP348a-1	-	±	-	-
PTP348a-2	-	+	-	±
PTP348a-3	-	+	OD	±
PTP348a-4	-	+	-	±
PTP348a-5	-	+	±	±
PTP348a-6	-	+	-	±
PTP348a-7	-	+	-	±
PTP348a-8	-	+	-	±
PTP348a-9	OD	+	±	±
PTP348a-10	-	+	-	±
PTP348a-11	OD	-	+	-
PTP348a-12	-	+	-	±
PTP348a-13	-	+	±	±
PTP348a-14	-	+	-	±
PTP348a-15	-	+	-	±
PTP348a-16	-	+	-	±
PTP348a-17	OD	+	±	±
PTP348a-18	-	+	-	±
PTP348a-19	OD	+	±	±
PTP348a-20	-	+	-	±
PTP348a-21	-	+	±	±
PTP348a-22	-	+	-	±
PTP348a-23	-	+	-	±
PTP348a-24	-	+	-	±

PTP348a-25	OD	+	±	±
PTP348a-26	-	+	-	-
PTP348a-27	-	+	±	±
PTP348a-28	-	+	-	-
PTP348a-29	-	+	-	-
PTP348a-30	-	+	-	-
PTP348a-31	OD	+	±	-
PTP348a-32	-	-	-	-
PTP348a-33	-	-	-	-
PTP348a-34	-	+	-	-
PTP348a-35	-	-	-	-
PTP348a-36	-	-	-	-
PTP348a-37	OD	-	±	-
PTP348a-38	OD	+	±	-
PTP348a-39	-	+	-	-
PTP348a-40	-	-	±	±
PTP348a-41	-	-	+	±
PTP348a-42	-	-	+	±
PTP348a-43	OD	-	+	±
PTP348a-44	-	+	-	±
PTP348a-45	-	+	-	±
PTP348a-46	-	+	-	±
PTP348a-47	-	+	-	±
PTP348a-48	-	+	±	±
PTP348a-49	-	+	-	±
PTP348a-50	-	+	-	-
PTP348a-51	-	-	-	-
PTP348a-52	-	-	-	-
PTP348a-53	OD	-	±	-
PTP350-1	-	+	±	-
PTP350-2	-	+	±	-
PTP350-3	-	+	+	±
PTP350-4	-	+	±	-
PTP350-5	-	+	+	-
PTP350-6	-	±	±	-
PTP350-7	-	+	±	-
PTP350-8	-	+	±	-
PTP350-9	OD	+	+	-
PTP350-10	-	+	±	-
PTP350-11	-	-	-	-
PTP350-12	-	-	-	-
PTP350-13	-	-	±	-
PTP350-14	-	-	-	-

PTP350-15	-	-	-	-
PTP350-16	OD	-	±	-
PTP350-17	-	-	-	-
PTP350-18	-	+	-	-
PTP350-19	-	-	-	-
PTP350-20	-	-	-	-
PTP350-21	-	-	-	-
PTP350-22	-	-	-	-
PTP350-23	OD	-	±	-
PTP350-24	-	-	±	±
PTP350-25	-	-	-	-
PTP350-26	-	-	-	-
PTP350-27	OD	-	±	-
PTP350-28	-	-	-	-
PTP350-29	-	+	-	-
PTP350-30	-	-	±	-
PTP350-31	OD	-	+	-
PTP350-32	-	-	-	-
PTP350-33	OD	-	-	-
PTP350-34	OD	-	±	-
PTP298-1	-	-	-	-
PTP298-2	-	-	-	-
PTP298-3	OD	-	±	-
PTP298-4	-	-	-	±
PTP298-5	-	-	-	-
PTP298-6	-	-	-	-
PTP298-7	-	-	-	-
PTP282-1	-	-	-	-

Table S7: The predicted bacterial toxicity of CPTX and its TPs with acute toxicity models for *Vibrio fischeri* [Microtox Toxicity to Environmental Bacteria (AUA. Case Ultra) and acute toxicity *Vibrio fischeri* model (Oasis Catalogic)] + Rainbow Trout Toxicity (AUE. Case Ultra)

Compounds	AUA*	Acute tox 30min**	AUE
cisZCPTX	±	<=0.0969	OD
PTP316-1	-	<=1.7808	±
PTP316-2	-	<=1.7718	+
PTP316-3	±	<=21.8235	±
PTP316-4	-	<=1.7745	OD
PTP316-5	±	<=1.7704	+
PTP316-6	±	<=1.7729	±
PTP316-7	±	<=1.7911	±
PTP316-8	±	<=1.7783	+
PTP316-9	±	<=21.5028	+
PTP316-10	±	<=21.4627	±
PTP316-11	-	<=1.7608	OD
PTP316-12	-	<=1.7613	OD
PTP316-13	-	<=1.7607	OD
PTP316-14	±	<=1.7495	OD
PTP316-15	-	<=1.7546	OD
PTP316-16	-	<=21.2876	+
PTP316-17	-	<=21.2860	OD
PTP316-18	OD	<=21.7301	OD
PTP316-19	-	<=1.7663	OD
PTP316-20	±	<=1.7745	OD
PTP316-21	±	<=1.7594	OD
PTP316-22	±	<=21.3688	±
PTP316-23	±	<=21.4567	OD
PTP316-24	±	<=21.4876	OD
PTP316-25	-	<=1.7642	OD
PTP316-26	-	<=21.4480	+
PTP316-27	-	<=21.4265	OD
PTP316-28	OD	<=21.5656	OD
PTP316-29	OD	<=18.0545	OD
PTP316-30	-	<=100.4145	±
PTP316-31	OD	<=100.5362	±
PTP316-32	OD	<=99.7972	±
PTP332a-1	-	<=2.1244	OD
PTP332a-2	-	<=5.6926	OD
PTP332a-3	-	<=5.7557	OD
PTP332a-4	±	<=5.7458	OD

PTP332a-5	±	<=5.7803	+
PTP332a-6	-	<=5.6859	OD
PTP332a-7	-	<=69.1392	+
PTP332a-8	-	<=69.5925	OD
PTP332a-9	OD	<=70.3538	OD
PTP332a-10	-	<=5.6663	OD
PTP332a-11	-	<=5.7779	OD
PTP332a-12	±	<=5.7226	OD
PTP332a-13	±	<=5.7358	+
PTP332a-14	-	<=5.7087	OD
PTP332a-15	-	<=69.3383	+
PTP332a-16	-	<=68.8335	OD
PTP332a-17	OD	<=69.6305	OD
PTP332a-18	-	<=2.1306	+
PTP332a-19	-	<=5.7952	+
PTP332a-20	±	<=5.7201	±
PTP332a-21	±	<=5.7663	±
PTP332a-22	-	<=5.7438	+
PTP332a-23	-	<=69.3343	+
PTP332a-24	-	<=70.3268	±
PTP332a-25	OD	<=70.4120	±
PTP332a-26	-	<=5.7559	+
PTP332a-27	±	<=5.7785	+
PTP332a-28	±	<=5.8265	+
PTP332a-29	-	<=5.7337	+
PTP332a-30	-	<=69.9821	+
PTP332a-31	-	<=69.5251	+
PTP332a-32	OD	<=70.1394	+
PTP332a-33	-	<=5.6275	OD
PTP332a-34	±	<=5.7171	OD
PTP332a-35	±	<=5.7546	+
PTP332a-36	-	<=5.7565	OD
PTP332a-37	-	<=68.7623	+
PTP332a-38	-	<=69.9144	OD
PTP332a-39	OD	<=69.3683	OD
PTP332a-40	±	<=5.6615	OD
PTP332a-41	±	<=68.8469	+
PTP332a-42	±	<=69.3175	OD
PTP332a-43	±	<=69.4066	OD
PTP332a-44	-	<=5.6453	OD
PTP332a-45	-	<=69.1679	+
PTP332a-46	-	<=68.9132	OD
PTP332a-47	OD	<=70.3753	OD

PTP332b-1	±	<=0.3090	±
PTP332b-2	+	<=0.3025	OD
PTP332b-3	+	<=0.3033	OD
PTP332b-4	±	<=0.2988	±
PTP332b-5	±	<=0.2992	±
PTP332b-6	+	<=0.3038	OD
PTP332b-7	±	<=0.3006	OD
PTP332b-8	±	<=0.7821	±
PTP332b-9	±	<=3.5590	OD
PTP332b-10	±	<=3.5967	OD
PTP334b-1	±	<=1.5368	+
PTP334b-2	±	<=1.5318	+
PTP334b-3	±	<=1.5572	+
PTP334b-4	±	<=0.1337	+
PTP334b-5	+	<=0.1335	+
PTP334b-6	±	<=0.1340	+
PTP334b-7	+	<=0.1330	+
PTP334b-8	±	<=0.1322	OD
PTP334b-9	+	<=0.1327	+
PTP334b-10	±	<=0.1326	+
PTP348a-1	-	<=6.6410	OD
PTP348a-2	±	<=6.9281	+
PTP348a-3	OD	<=68.1218	OD
PTP348a-4	-	<=6.8674	OD
PTP348a-5	±	<=6.8326	OD
PTP348a-6	-	<=6.7506	OD
PTP348a-7	-	<=83.0379	+
PTP348a-8	-	<=82.8457	OD
PTP348a-9	OD	<=83.8903	OD
PTP348a-10	±	<=18.5472	+
PTP348a-11	±	<=1038.1418	+
PTP348a-12	-	<=18.2372	OD
PTP348a-13	±	<=18.5311	OD
PTP348a-14	-	<=18.7082	OD
PTP348a-15	-	<=221.7070	+
PTP348a-16	-	<=221.8801	OD
PTP348a-17	OD	<=221.2104	OD
PTP348a-18	±	<=18.4801	+
PTP348a-19	OD	<=83.6511	+
PTP348a-20	-	<=18.2414	OD
PTP348a-21	±	<=18.3948	OD
PTP348a-22	-	<=18.3139	OD
PTP348a-23	-	<=220.9815	+

PTP348a-24	-	<=222.0061	OD
PTP348a-25	OD	<=224.5013	OD
PTP348a-26	-	<=18.5252	+
PTP348a-27	-	<=18.6123	+
PTP348a-28	-	<=18.4875	OD
PTP348a-29	±	<=224.7965	+
PTP348a-30	±	<=228.8030	+
PTP348a-31	±	<=228.4364	+
PTP348a-32	-	<=18.4127	OD
PTP348a-33	-	<=18.1505	+
PTP348a-34	-	<=18.3691	OD
PTP348a-35	-	<=220.5946	+
PTP348a-36	-	<=225.9293	OD
PTP348a-37	OD	<=221.6914	OD
PTP348a-38	OD	<=225.9491	OD
PTP348a-39	-	<=227.2914	+
PTP348a-40	-	<=18.7643	±
PTP348a-41	±	<=226.3482	+
PTP348a-42	±	<=224.6811	±
PTP348a-43	±	<=227.4218	±
PTP348a-44	-	<=82.8784	+
PTP348a-45	-	<=81.4724	+
PTP348a-46	-	<=6.9069	+
PTP348a-47	±	<=6.8856	+
PTP348a-48	±	<=6.8117	+
PTP348a-49	-	<=6.7985	+
PTP348a-50	-	<=18.4634	OD
PTP348a-51	-	<=18.6182	OD
PTP348a-52	-	<=18.2641	OD
PTP348a-53	OD	<=225.8063	OD
PTP350-1	±	<=0.4166	OD
PTP350-2	+	<=0.4179	+
PTP350-3	+	<=0.4088	±
PTP350-4	±	<=0.4190	OD
PTP350-5	+	<=0.4152	OD
PTP350-6	+	<=0.4152	OD
PTP350-7	±	<=4.9335	+
PTP350-8	±	<=1.3390	OD
PTP350-9	±	<=5.0052	OD
PTP350-10	±	<=4.2056	OD
PTP350-11	±	<=0.4194	+
PTP350-12	+	<=0.4179	+
PTP350-13	+	<=0.4140	+

PTP350-14	±	<=4.9215	+
PTP350-15	±	<=4.9707	+
PTP350-16	±	<=4.9747	+
PTP350-17	±	<=1.3431	±
PTP350-18	±	<=0.4164	+
PTP350-19	±	<=0.4186	+
PTP350-20	±	<=0.4097	+
PTP350-21	±	<=1.3625	±
PTP350-22	±	<=4.9225	+
PTP350-23	±	<=5.0877	+
PTP350-24	±	<=0.4192	+
PTP350-25	±	<=0.4155	+
PTP350-26	+	<=5.0011	+
PTP350-27	+	<=5.0601	+
PTP350-28	+	<=1.3600	OD
PTP350-29	±	<=0.4118	+
PTP350-30	+	<=4.9463	+
PTP350-31	+	<=4.9896	+
PTP350-32	+	<=1.3537	OD
PTP350-33	±	<=22.9658	+
PTP350-34	±	<=6.3119	OD
PTP298-1	-	<=3.2970	OD
PTP298-2	OD	<=15.0159	OD
PTP298-3	OD	<=15.1139	OD
PTP298-4	-	<=1.2486	OD
PTP298-5	±	<=1.2567	OD
PTP298-6	-	<=1.2578	OD
PTP298-7	±	<=1.2644	OD
PTP282-1	-	<=0.3882	OD

*Positive (+). negative (-). inconclusive ((±). the probability of being positive is around 50 ± 10%). out of domain (OD).

**the toxicity value is mg/l (IC 50).